SYNTHESIS AND APPLICATION OF SOME LDH BASED NANOCOMPOSITES FOR THE TREATMENT OF SOME TOXIC AND GREEN-HOUSE GASES

Thesis Submitted to AcSIR For the Award of the Degree of

DOCTOR OF PHILOSOPHY

In

CHEMICAL SCIENCE

By

Pinky Saikia

Registration Number 10CC15J38005

Under the Guidance of

Dr. Rajib Lochan Goswamee

Senior Principal Scientist and HoD

Advanced Materials Group

Materials Science and Technology Division

CSIR–North East Institute of Science and Technology

Jorhat 785006, Assam, India

2019

CSIR-NORTH EAST INSTITUTE OF SCIENCE & TECHNOLOGY
(Formerly Regional Research Laboratory)
(A constituent establishment of Council of Scientific & Industrial Research)
Jorhat - 785 006, Assan, INDIA
Phone: 0091-376-2370012
Fax: 0091-376-2370011, 2372523, 2370115
PABX 0091-376-2370117 / 2370139-extn 2410 (off.)
E mail : director@rrljorhat.res.in
Website: http://www.rrljorhat.res.in

RIGHT TO INFORMATION

सीएसआइआर-उत्तर पूर्व विज्ञान तथा प्रौद्योगिकी संस्थान
(सी एस आई आर की अंगीभत इकाई)
जोरहाट 785 006, आसाम, भारत
फोन : 0091-376-2370012
पिएविएक्स: 0091- 376-2370117, 2370121, 2370139
फैक्स : 0091-376-2370011, 2372523, 2370115
ई-मेल : director@rrljorhat.res.in

Dr. R. L. Goswamee
Ex Alumni DAAD (Germany) and CNRS (France)
Senior Principal Scientist, Professor of AcSIR
HoD, Advanced Materials Group,
Materials Science & Technology Division

Date: 13.07.2019

CERTIFICATE

This is to certify that the work incorporated in this Ph.D. thesis entitled ***"SYNTHESIS AND APPLICATION OF SOME LDH BASED NANOCOMPOSITES FOR THE TREATMENT OF SOME TOXIC AND GREEN-HOUSE GASES"*** submitted by ***Miss Pinky Saikia*** to Academy of Scientific and Innovative Research (AcSIR) in fulfillment of the requirements for the award of the Degree of ***Doctor of Philosophy in Chemical Science***, embodies original research work under my supervision. I further certify that this work has not been submitted to any other University or Institution in part or full for the award of any degree or diploma. Research material obtained from other sources has been duly acknowledged in the thesis. Any text, illustration, table, etc., used in the thesis from other sources, have been duly cited and acknowledged.

It is also certified that this work done by the student, under my supervision, is plagiarism free.

Pinky Saikia
(Pinky Saikia)

(Dr. Rajib Lochan Goswamee)
Supervisor
Email: goswamirl@neist.res.in

Declaration

To
The AcSIR
CSIR- Human Resource Developement Centre
Sector19, Kamla Nehru Nagar,
Ghaziabad, UP 201002, INDIA

I, **Miss Pinky Saikia**, Advanced Materials Group, Materials Science and Technology Division, North East Institute of Science and Technology, Jorhat-785006, Assam, India, declare that this thesis entitled ***"SYNTHESIS AND APPLICATION OF SOME LDH BASED NANOCOMPOSITES FOR THE TREATMENT OF SOME TOXIC AND GREEN-HOUSE GASES"*** is the result of my own investigation of the subject. The research work has been carried out by me under the guidance of Dr. Rajib Lochan Goswamee, Senior Principal Scientist & Group Leader Advanced Materials Group, Materials Science and Technology Division, North East Institute of Science and Technology, Jorhat. I have fulfilled all the requirements under Ph.D. regulation of AcSIR.

Further, I declare that no part of the thesis has been submitted to any University/Institution for any other degree.

Pinky Saikia
Pinky Saikia

Place: Jorhat

Date: 13.07.2019

DEDICATED

To

My

Beloved Parents

ACKNOWLEDGEMENTS

Although, it is not possible to express my deepest thanks and gratitude in word. I would like to thank all those who have played a crucial role during my PhD years and without whom this thesis would not have been possible.

My heartfelt gratitude goes first and foremost to my PhD supervisor, Dr. Rajib Lochan Goswamee, Senior Principal Scientist & Head of the Materials Science and Technology Division, CSIR-NEIST, Jorhat, Assam, for allowing me to carry out my PhD and constant encouragement and support to get the Clearance for my Research work. It is my honor to be his student. During these years, he always supports me a very conducive environment and gives me good advices for my research. From him, I know how to carry out a good experiment and how to explain the experimental results precisely which I did not learn before. And the most important I am impressed is how enthusiastic he is in his life and work. I am grateful for what I have learnt from him.

I would like to express my sincere thanks and gratitude to Dr. D. Ramaiah, Ex-Director, CSIR-NEIST, Jorhat, for giving me the opportunity to work in this institute and making all the facilities available for my research work.

I am very much grateful to CSIR, New Delhi for providing financial support in Network Project CSC-0104 and CSIR-Senior Research Fellowship.

I would also like to express my sincere thanks to, Dr. Lakshi Saikia, Scientist, Materials Science and Technology Division, Dr. Swapnali Hazarika, Senior Scientist, Engineering Sciences and Technology Division, Dr. Ratul Saikia, Principal Scientist, Biological Sciences and Technology Division for their kind supports and valuable suggestions as well as for accepting to be members of my doctoral advisory committee.

I am also thankful to Dr. Pinaki Sengupta, Chief Scientist & former Head Materials Science and Technology Division, Dr. Biswajit Saha, Dr.Manash R. Das, Mrs Dipa

Rajbongshi Kachari, Mr. Priyam Jyoti Bora, Mr. Paran Jyoti Kalita and Mr. Krishna Prasad Sharma, all staff members of Advanced Materials Group, MSTD, for their valuable help and support. I am also thankful to Dr. Dipak Kumar Dutta, Emeritus Scientist, MSTD, for his valuable suggestions.

I would like to thank the Analytical Chemistry Division, Glass Blowing, H.R.D cell, General Stores for their invaluable support.

I express my sincere thanks to Dr. Roy Johnson, DST-ARCI, Hyderabad and their team for providing us the ceramic honeycomb monoliths for "Gas-Solid" reaction. I express my gratitude to Prof. Rupam J. Sarma of Chemistry Department, Gauhati University and Dr. S. Vasudevan, Electro Inorganic Group, CSIR-CECRI, Karaikudi, Tamilnadu for the analytical help they have provided in some important studies. Also in the same context I would like to express my gratitude to Prof. Dr. Andrew Ayral of European Institute of Membranes University of Montpellier, France for helping in some electron microscopic analysis. I am also thankful to Ranjit Sarma, Associate Professor Department of Physics and his research group, J.B. College, Jorhat for their kind help to carry out MOCVD.

I sincerely express my special thanks to Dr. Edja F. Assanvo through whom I learnt about Iso-conversional kinetics. I appreciate all the help from him. By the same occasion, I convey my heartfelt thanks and gratitude to all my teachers from primary level to Master degree level who initiated me to reach the actual goal and aroused my interest towards this exciting subject of chemistry.

I would like to express my gratitude to my fellow research scholars from my Department respectively Ms. Champa Gogoi, Ms. Susmita Sarmah, Mrs. Rakhi Paul Bhattacharya, Ms.Gitashree Darabdhara, Ms. Priyakshree Borthakur, Ms.Sukanya

Borthakur, Mr. Jitu Saikia, Dr. Allou N'guadi Blaise, Mr. Purna Kanta Boruah, Dr. Najrul Hussain, Dr. Mirnal Saikia, Dr. Diganta Bhuyan, Dr. Pallab Saikia and also my all fellow research scholars whose name are not mentioned.

From the core of my heart, I am particularly thankful to Mr. Pallab Handique, Mr. Lusan Gogoi, Mr. Nagen Gogoi and late Moneswar Saikia for their invaluable help during my Ph.D work mainly for the"Gas-Solid" reaction experiments which were carried out in the pilot plant of Materials Science and Technology Division.

Much thanks should be dedicated to my spiritual father, Jogadev Saikia and Brother Madhurya Saikia, Sanjib Bhuyan, Paban Saikia and my uncle Pabitra Saikia, Nipen Saikia, Dimbeswar Saikia and their wives for their unforgettable prayers and support.

I would wish to thank my mother Niru Saikia, Aunty Thunumai Saikia, Sister Chimpi Saikia for their unconditional support, love and encouragements during my Ph.D.

Last but not least, my sincerest thanks go to all those whom I have not mentioned and who have contributed directly or indirectly to the realization of this work.

Place: Jorhat

Date: 13.07.2019 **Pinky Saikia**

CONTENTS

LIST OF FIGURES

LIST OF TABLES

SUMMARY

The present work is aimed at the synthesis, coating, thin film formation, development of mesoporosity and green house gas reactivity of Layered Double Hydroxides (LDHs) and their several nano material based composites and derivatives. Layered Double Hydroxides (LDHs) are 2D layered material with $Mg(OH)_2$ brucite like structure in which a part of the divalent metal ion is isomorphously substituted by trivalent metal ion giving a positively charged sheet. This charge is balanced by occupying the interlayer position with different anions. Different methods were taken to synthesize Layered Double Hydroxides (LDHs) and their nano composites viz., synthesis by 'oxide hydrolysis' method, by the sol-gel based hydrolysis of different bivalent and trivalent metal acetylacetonates, by simultaneous hydrolysis of fast hydrolysing alkoxides and slow hydrolysing metal acetylacetonates to derive SiO_2-LDH non-aqueous dispersed core-shell alcogels.

Some of the main themes undertaken in the present PhD research work are-

- The synthesis of dispersed alcogels of LDHs in the form of their SiO_2 supported nano composites, characterisation of the synthesised nano composites especially from the perspectives of their flow behaviour, effect of composition on their thermal stability and mixed metal oxidic nanosheet formability, coat and thin film formation ability of these nanocomposites over solid preforms to obtain a wash coated honeycomb reactors with supported mixed metal oxidic nano sheets laid favourably in the honeycomb channels for effective gas solid reaction catalysis mainly some of the environmentally important catalysis involving toxic and global warming gases like N_2O, CO and CH_4.
- Study of the effect of different reaction conditions to hydrolyse metal acetyl

-acetonates in obtaining the LDH type structure.

- Effect of acetylacetonate ligands on perforating some of the LDH layers having ordered distribution of bi and trivalent metal ions to obtain mesoporous LDH nanosheets and their catalytic application for conversion of CO_2 to CH_4.
- And to obtain eutectic sublimable metal diketo complexes suitable for formation of mixed metal oxide thin film by Metal Organic Chemical Vapour Deposition (MOCVD) technique over the channels of ceramic honeycomb type preforms and their uses as catalyst for the abatement of toxic green house gas N_2O.

The neat LDHs, their SiO_2 supported nanocomposites and other LDH derived products were characterized by techniques powder and single crystal X-ray diffractometry, thermal analysis (TGA-DTG), FT-IR, flow behaviour study by both controlled stress rotational rheometry and oscillatory rheometry, BET surface area and pore volume analysis, surface morphology characterisation by Scanning Electron Microscopy (SEM), Energy dispersive X-ray spectroscopy (EDXA), Transmission Electron Microscopy (TEM) and Atomic Force Microscopy (AFM), surface and electronic state characterisation by X-ray Photoelectron Spectroscopy (XPS), electrokinetic mobility or zeta potential characterisation by Laser Doppler Velocimetry, particle size analysis etc. The dispersion of LDHs and their SiO_2 supports were coated over different substrates by Dip-coating with programme dipping and withdrawal sequence to get the crack free catalytic membrane type coats. The catalysts were prepared by calcination at 450 ^oC to obtain a mixed metal nano-oxide which were then further characterized by H_2-TPR analysis. Finally, the catalytic properties of the powdered as well as the coated samples were carried out over the 'Gas-Solid' reaction for the treatment of environmentally harmful gases such as N_2O, CH_4, CO_2 and CO.

CHAPTER-I

GENERAL INTRODUCTION

1. GENERAL INTRODUCTION:

Recent development in the field of material chemistry including nanoscience gives different ideas to scientists to develop various nanocomposites by combining or modifying nanomaterials with different functional molecules. The synthesised nanocomposites possessing different unique properties which attract them towards different application such as in healthcare, environmental remediation, energy storage and conversion. Due to possession of unique properties synthetic inorganic materials become a challenger for the solution of today's environmental and industrial problems and for the design of novel composites for advanced technological processes. One of such synthetic inorganic materials with well defined structural properties is Layered Double Hydroxides (LDH) also commonly known as hydrotalcites. Among different classes of lamellar solids, LDHs are particular interest as they resembles with the conventional intercalation compounds having uniform nanoscale periodicity and complete charge separation between the interlayer ions and layers which is a distinguishing feature of their structure.

1.1. Layered Double Hydroxides (LDHs):

Layered double hydroxides (LDHs) also called hydrotalcite like compounds can be represented by the general formula $[M_{1-x}^{2+}M_x^{3+}(OH)_2]^{x+}[A_{x/n}]^{n-3}$ .m H_2O, where divalent (M^{2+} ions such as Mg^{2+}, Ni^{2+}, Fe^{2+}, Co^{2+}, Cu^{2+}, Ni^{2+} or Zn^{2+}) and trivalent (M^{3+}ions such as Al^{3+}, Cr^{3+}, Ga^{3+}, In^{3+}, Mn^{3+} or Fe^{3+}) metal cations are uniformly distributed either statically or in an orderly prearranged manner in the Mg $(OH)_2$ brucite-like sheets having various charge-compensating anions (A^{n-}) (e.g. CO_3^{2-}, NO_3^{2-} ,Cl^-, SO_4^{2-} etc.) and water molecules in their interlayer spaces [1-6] (**Fig. 1.1**). Due to the presence of interlayer anions LDHs are also known as the anionic clays. The value of x is varied in between 0.2-0.33 [7,8]. Besides divalent and trivalent metal cations

monovalent M^{I} (such as Li^{I}) and tetravalent M^{IV} (such as Ti^{IV}, Si^{IV}) cations also forms LDH structure [1,2,9]. The –OH groups in the LDH layers are oriented towards the interlayer region [10]. Different guest organic, inorganic molecules and biological molecules can intercalate with LDH layers. Layered Double Hydroxides are found rarely in nature and large no of LDHs are synthetic. Layered double hydroxides (LDHs) have many similar physical and chemical properties with clay minerals. These are respectively-layered structure, variable isomorphous substitution of metal cations, variable layer charge density, ion-exchange capacities, reactive interlayer space, swelling in water, rheological and colloidal properties which made LDHs similar to clay like material [11]. Due to the atomic-scale level uniform distribution of metal cations in the brucite-like layers as well as their ability to intercalation of interlayer anions, LDHs display great potential as precursors/supports to prepare industrially and environmentally important catalysts. In such catalysts the catalytic sites can be preferentially orientated, highly dispersed and firmly stabilized to afford excellent performance and recyclability. The different important reactions where LDH is used as catalysts belong to diverse range of fields, such as organic/pharmaceutical synthesis, clean energy generation, hydrocarbon oxidation, degradation of pollutants to control environmental pollution and photochemical reactions etc.

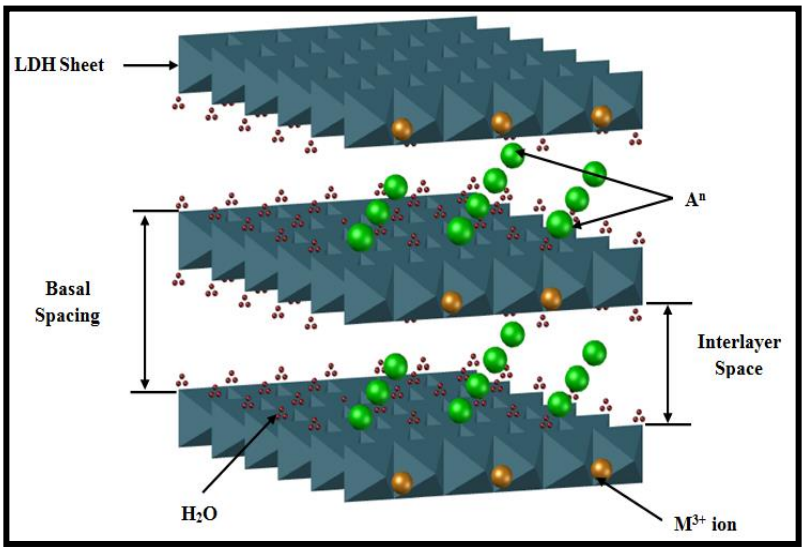

Fig. 1.1: The schematic diagram of LDH with different M^{2+}/M^{3+} molar ratios showing the metal hydroxide octahedral stacked over another, as well as water (H_2O) and interlayer anions (A^{n-}) present in the interlayer region.

1.1.1a. Structure of LDHs:

Layered double hydroxides belong to the naturally occurring minerals known as hydrotalcite family. The structure of LDHs is composed of $Mg(OH)_2$ type brucite like layers in which the divalent metal cations coordinated octahedrally by -OH groups which has been replaced by the trivalent metal cations giving the positively charged layers as shown in **Fig. 1.1**. LDHs are available both in naturally as well as synthetic. The structure of LDHs resembles with the naturally occurring mineral hydrotalcite, [$Mg_6Al_2(OH)_{16}CO_3.4H_2O$] and abbreviated as [Mg-Al-CO_3] or [Mg-Al], is hydroxi-carbonate of magnesium and aluminium, which was first discovered in Sweden around 1842 [11,12] and first prepared by Feitknecht [13,14] as a synthetic material in 1942. These occur in nature in foliated and contorted plates and/or fibrous masses. Other types of isomorphous minerals was also presented by E. Manasse, Professor of Mineralogy at the University of Florence (Italy), who also recognized the importance of carbonate ions for this type of structure [15]. All LDH minerals found in the nature

and synthesized in the laboratory have a structure similar to that of hydrotalcite or its hexagonal analogue manasseite group. The structure of LDH is built up of brucite [$Mg(OH)_2$]-like layers in which the cations are surrounded by octahedra of -OH groups. These octahedral units form infinite layers through edge-sharing and these layers are stacked over another to form the 3D structure. In LDH a fraction x of the divalent cations is isomorphously substituted by trivalent cations so that the layers acquire a positive charge which is balanced by interlayer anions. These anions are surrounded by a caging of water molecules [2,16]. The pioneering works on determination of the structure of different forms of LDH using powder XRD was carried out by Allmann and their co-workers [17], Taylor [18], Kuzel [19], Drits [20], Poppelmeir [21]. As reported by H.F.W. Taylor [18] three groups of minerals are closely associated with hydrotalcite group in nature, they are pyroaurite-sjoegrente, hydrotalcite-mannasite polytypes, reevsite-woodwardite.

LDHs can be structurally described as containing brucite [$Mg(OH)_2$]-like layers, where octahedra of Mg^{2+} (6-fold coordinated to -OH) share edges to form infinite sheets. These sheets are stacked over other and are held together by hydrogen bonding as shown in **Fig. 1.1**. When Mg^{2+} ions are substituted by a trivalent ion of similar ionic radius such as Al^{3+} a positive charge is generated in the hydroxyl sheet. This net positive charge is compensated by (e.g. CO_3^{2-}) anions, which lie in the interlayer region between the two brucite-like sheets along with the presence of water molecules in the free space of this interlayer [1]. The anions and water in the interlayer region are free to move by breaking their bonds and forming new bonds with other ions. The oxygen atoms of the water molecules and of the CO_3^{2-} groups are distributed approximately closely around the symmetry axes that pass through the hydroxyl groups (0.56 Å apart) of the adjacent brucite-like sheet. These hydroxyls are tied to the

CO_3^{2-} groups directly or via intermediate H_2O through hydrogen bridges: OH--CO_3--HO or OH--H_2O--CO_3--HO [22]. The CO_3^{2-} groups are situated flat in the interlayer and H_2O is loosely bound; they can be eliminated without destroying the structure.The divalent cations, trivalent cations, and the interlayer A^{n-} anions of LDHs together with the value of the x may be varied over a wide range, the different interesting physico-chemical properties also can be widely varied [23].

The most detailed structural investigations of LDHs were first carried out by Allmann [17,24]. Layered double hydroxides (LDHs) have a wide range of chemical compositions and depending upon the chemical composition they have different layer structures such as hydrotalcite;$[Mg_6Al_2(OH)_{16}][(CO_3).4H_2O]$ [25], pyroaurite; $[Mg_6Fe^{3+}{}_2\ (OH)_{16}][(CO_3).\ 4.5\ H_2O]$ [22], sjogrenite; $[Mg_6Fe^{3+}{}_2\ (OH)_{16}][(CO_3).4.5\ H_2O]$ [22], coalingite; $[Mg_6Fe^{3+}{}_2\ (OH)_{24}][(CO_3).\ 2\ H_2O]$ [26], takovite ;$[Ni_6Al_2(OH)_{16}][(CO_3, OH).4H_2O$ [27,28]etc. In addition to this, some other minerals are found in nature which exhibit structures similar to brucites but with an intermediate layer containing cations apart from anions. These are-Motukoreaite$[Mg_{1.82}Al_{1.12}Mn_{0.03}Zn_{0.02}(OH)_{5.15}][(Na_{0.07}K_{0.01})(CO_3)_{0.63}(SO_4)_{0.4}.2.74H_2O]$[29],Wermlandite$[Mg_7(Al_{0.57}Fe^{3+}{}_{0.43})_2(OH)_{18}][(Ca_{0.6}Mg_{0.4})(SO_4)_2.12H_2O]$[28],Mountkeithite$[(Mg_{8.15}Ni_{0.85}Cu_{0.02})(Fe^{3+}{}_{1.31}Cr_{1.02}Al_{0.65})(OH)_{24}][(CO_3)_{1.11}(SO_4)_{0.38}(Mg_{1.76}Ni_{0.18})(SO_4)_{1.94}.9.39H_2O]$[30],Hydrohonessite$[Ni^{2+}{}_{5.4}Fe^{3+}{}_{2.5}(OH)_{16}][(SO_4)_{1.28}.0.98NiSO_4.6.95H_2O]$ [31]. Most of the mineral such as Chlorite shows structural similarity with hydrotalcite type mineral where the interlayer anion is replaced by talc like alumina-silicate layers [32].

1.1.1b.Crystallographic description of the structure of LDHs Hydrotalcites):

Allmann [17,24] from single crystal data assigned the space group and unit cell data of Sjogrenite $[Mg_6Fe^{3+}{}_2(OH)_{16}][(CO_3).4H_2O]$ as- a=3.113 Å and c=15.61 Å (2H) and

Pyroaurite which is a polytype of Sjogrenite as a=3.109 Å and c=23.41 Å (3R). These two polytypes differ in stacking sequence of –OH layers with two different symmetries rhombohedral (Pyroaurite) or hexagonal (Sjogrenite). In Pyroaurite phase, the stack have the sequence BC-CA-AB-BC, of three sheets in the unit cell, or BC-CB-BC with two sheets in the unit cell with hexagonal symmetry in case of Sjogrenite the parameters of the unit cell being a and c= $2c^{/}$, where ABC stands the three-fold axis of the -OH groups in the brucite-like sheet. On the otherhand, both Pyroaurite and Hydrotalcite crystallizes in rombohedral 3R symmetry with the parameters having the unit cell of a and c= $3c^{/}$ (where, $c^{/}$ is the thickness of one layer constituted by a brucite-like sheet and one interlayer).

Apart from two polytypes of stacking sequences *viz*. two-layer hexagonal (2H) and three-layer rhombohedral sequence (3R) are also present as an intergrowth of both polytypes with a relative proportion of 3R and 2H [33]. Hydrotalcite or LDHs with rhombohedral symmetry have mainly been found in nature; the hexagonal polytype is the high temperature form of the rhombohedral one. On the otherhand, hexagonal symmetry has been discovered in the interior of some mineral crystals, while the the external part is maintained by rombohedral type; the transformation occurs only during the cooling of the mineral, but due to the energy barrier the hexagonal form can not further transform at low temperature [34]. Drits and Bookin further reported the LDH structures with one layer sequence (1H) or as a six-layer rhombohedral or hexagonal sequence (6R or 6H) [35]. Comparison of some physical and crystallographic parameters of Pyroaurite, Sjogrenite and Hydrotalcite are given in **Table 1.1.**

Table 1.1: Comparison of some physical and crystallographic parameters of Pyroaurite, Sjogrenite and Hydrotalcite

Spatial Group	Pyroaurite 3R	Sjogrenite 2H	Hydrotalcite 3R
a (Å)	3.11	3.11	3.05
c (Å)	23.41=3c/	15.61=2c/	22.81=3c/
c/(Å)	7.803	7.805	7.603
Z (mol/cell)	3/8= 3M	2/8= 2M	1/2= 3M
density (g/cm^3)	2.13	2.11	2.09
Interatomic distances, Å M-OH	2.065	2.06	2.03
OH-OH in brucite sheet	2.04	2.04	2.00
OH-H_2O	2.93	2.92	2.84

In addition to stacking variation some turbostratic distortion also have been observed in LDHs. Turbostratic disorder of LDH layer arises due to random orientation of successive layers about the stacking direction, leading to a loss in registry between successive hydroxide layers. This results in a mismatch of chemistry/geometry between hydroxide layers and interlayer anions, preventing an ideal stacking [36].

Most commonly found Hydrotalcite is $Mg_2Al(OH)_6Cl.2H_2O$ which is a common Layered Double Hydroxide having structure similar to $Mg(OH)_2$ brucite like sheet, where substitution by Al^{3+} for Mg^{2+} causes permanent positive charge development in the trioctahedral hydroxide sheet. This extra positive charge is balanced by interlayer anion such as Cl^- which is normally accompanied by water molecules [37]. By using special hydrothermal synthetic routes the Al/(Al+Mg) ratio has been raised from 0.35 to 0.44 [38,39]. In that case the unit cell 'a' dimension decreases with the increase of isomorphous substitution of Mg^{2+} by Al^{3+} below the value of 0.35 of Al/(Al+Mg) ratio. On the other hand, above the value of 0.35 of Al/(Al+Mg) ratio, the crystallographic a_o value remains constant at 3.04 Å [40]. When the value of x <0.35,each $Al(OH)_3$ is

surrounded by six $Mg(OH)_2$ octahedra and when x >0.35, $Al(OH)_3$ octahedra must be directly adjacent with each other. Therefore, Mg-Al type LDH indexed with 'a' value around 3.1 Å the overall distribution of bivalent and trivalent metal ions in the structure are random. However, in some cases, the ordering of these cations result in crystallographic 'a' value √3 times that of basic value 3.1 Å (√3×3.1 = 5.26) [40,41].

In addition to the structure of main layer, the stereochemical characteristics of various interlayer anions play vital role in the chemical and physical properties of LDHs. Particularly, the exceptional stability of CO_3^{2-} ion in the interlayer position of Mg-Al-LDH. The oxygen sites of CO_3^{2-} groups and H_2O molecules are accommodated in a single set of sites. Three oxygen sites from adjacent groups are occupied in such a way that they are in exact places to form a horizontal CO_3^{2-} ion with C atom in the center. Because of such stereochemical stability of CO_3^{2-} ion, it is very difficult to remove CO_3^{2-} from interlayer positions [42]. In some occasions, presence of CO_3^{2-} ion in the interlayer helps in formation of layered hydroxide [43]. On the other hand, if there is an oxygen atom from a water molecule, it can form reasonably good tetrahedral configuration by forming hydrogen bonds to other oxygen atoms in the interlayer and to hydroxyl groups in adjacent brucite layers.

Similar to Hydrotalcites the ordered arrangement of bivalent and trivalent ions with a larger unit cell is also found in hydrocalumite type Ca-Al LDHs. The composition of the hydrocalumite is $Ca_2Al(OH)_{6.75}(CO_3)_{0.125}(H_2O)_{2.5}$ [44]. Because of the size difference between Ca^{2+} and Al^{3+} there arises three different distortions of Portlandite $Ca(OH)_2$ layers [46]. The distortion contains three components: the OH^- ions are drawn in towards the Al^{3+} ions so that layer could alternatively be described as consisting of Ca^{2+} ions and isolated $[Al(OH)_6]^{3-}$ octahedra; these octahedra are rotated around an axis normal to the plane of the layer; and the Ca^{2+} ions are displaced parallel

to this axis, half of them in one direction and half in the other. The net result of these distortions is to render the CaO_6 octahedra very open on one side, so that H_2O molecule from the interlayer can bond to the Ca^{2+} which thus becomes seven coordinated. **Fig.1.2** shows the crystal structure of Hydrocalumite ($[Ca_2Al(OH)_6]Cl.2H_2O$ layered double hydroxides) with Cl^- ion as interlayer ion which crystallizes in rhombohedral *R-3* space group [47].

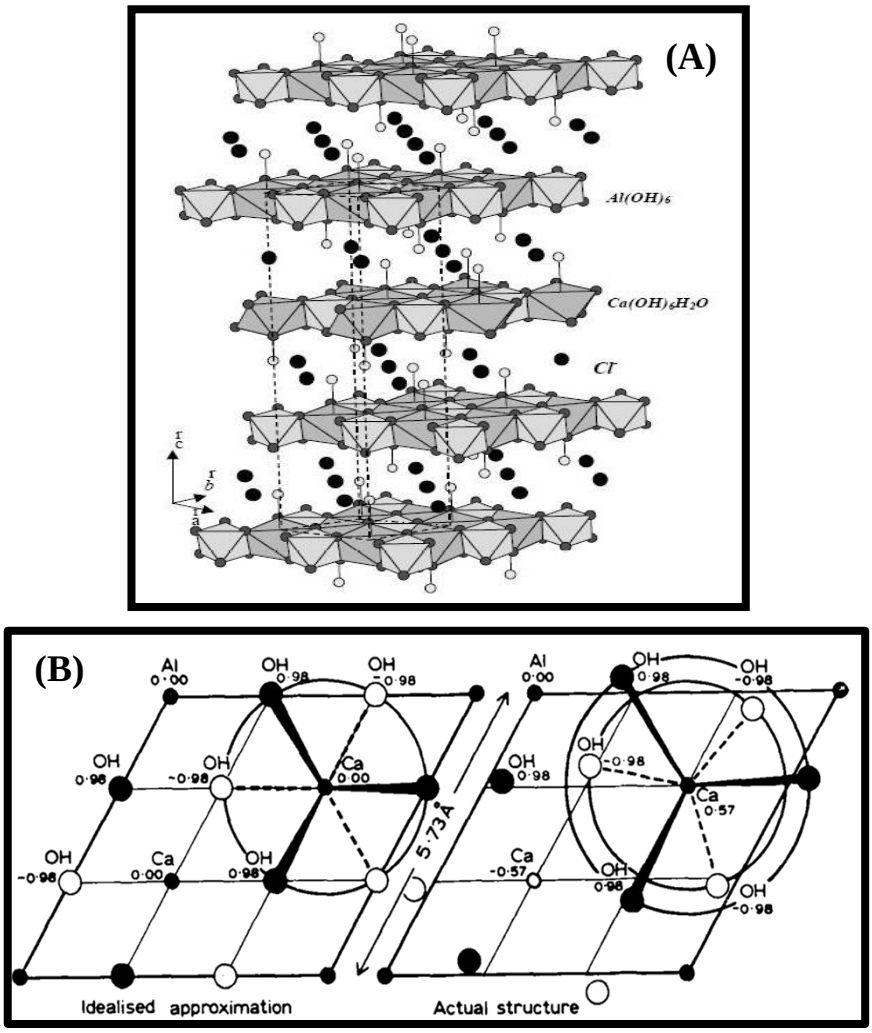

Fig. 1.2: (A) Structure of a single principal layer of composition $[Ca_2Al(OH)_6]$ in phases of the hydrocalumite group; (B) Crystal structure of $Ca_2Al(OH)_6]Cl.2H_2O$ layered double hydroxides in *R*-3 group, the cell parameter *a* = 5.7487 (5) Å and *c* = 23.492 (1) Å.

Another hydrotalcite like compound is hydrated lithium dialuminates with formula [$LiAl_2(OH)_7.2H_2O$] containing monovalent Li^+ ions in the vacancies of gibbsite like $Al(OH)_3$ octahedra, whereas the interlayer species such as Cl^- and H_2O are located disorderly over five sites midway between the $Al(OH)_3$ layers [21,48]. In addition to this another form of hydroxide layer stacking have been found and depend on the polymorph of $Al(OH)_3$ which is the rhombohedral form (*r*-$LiAl_2$) from the bayerite or nordstrandite [49]. They were initially indexed with a hexagonal cell of superlattice parameters a= 5.32 Å and c=15.24 Å indicating a cation ordered structure [50]. Later on, the unit cell were described by a C-centered monoclinic system with the cell parameters a=5.1 Å, b= 8.83 Å, c= 7.74 Å in the space group P63/mcm. The composition of this structure type is limited to $LiAl_2$ for the main layers but the interlayer chloride anions are possible to be exchanged by other inorganic and organic anion species. **Fig. 1.3** shows the structure of gibbsite and bayerite based Li-Al-Cl LDHs [51].

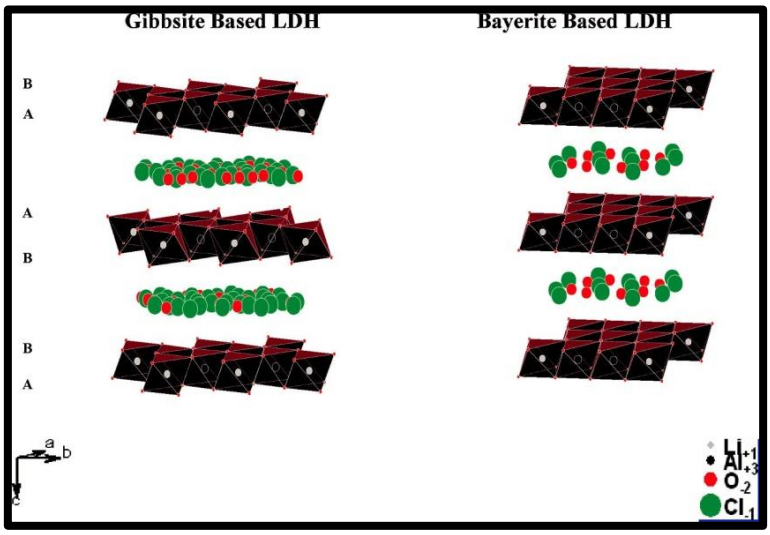

Fig. 1.3: Schematic representation of the structures of the gibbsite-based and bayerite-based Li-Al-Cl LDHs [51].

1.1.2. Types of LDHs:

Depending on structural variation Layered double hydroxides (LDHs) are classified

into three main groups-

1. The crystalline hydrated lithium aluminates with a formula $[LiAl_2(OH)_6]^+X^-.nH_2O$ where small monovalent Li^+ ions occupy the vacancies in dioctahedral positions of aluminium octahedral (bayerite) sheet [52,53]. Hydroxide ion and two water molecules present between the layers and a plane of oxygen atoms of which are stabilized by hydrogen bonding, as evidenced the increase in the bayerite lattice perpendicular to the dioctahedral layer by a 2.81 (1) Å. Crystalline hydrated lithium aluminates $[LiAl_2(OH)_6]^+X^-.nH_2O$ can be formed by the precipitation of aluminium hydroxide from the solution of aluminium salts at alkaline pH in presence of very high amount of Li^+ ion.

2. The second group is hydrocalumite $[Ca_2Al(OH)_{6.75}](CO_3)_{0.125}(H_2O)_{2.5,}$ which has the variation that the dipositive cation is Ca^{2+} or Cd^{2+} [54] and the composition is $[Ca_2M^{3+}(OH)_6]^+X^-.nH_2O$ (where M^{3+} is typically Al^{3+}; Ca^{2+}:Al^{3+} is 2:1)[18,53] which resembles more to hydrotalcite group. Many synthetic members belonging to this group are formed during hydration of Portland cement. It is formed on reaction of $CaCl_2$ with tricalcium aluminate ($3CaO.Al_2O_3$ or C_3A) which is an important component of Portland cement. Likewise tetracalcium aluminate $4CaO.Al_2O_3.xH_2O$ $[Ca_2Al(OH)_6]OH.nH_2O$ (where n=19, 13, 11 or 7) is another example of a cement hydrational phase having layered structure [18,53]. Members belonging to this group with bivalent ion other than Ca ion are also reported. The ionic radii differences of bi and trivalent metal ions in this group are larger than the same in the hydrotalcite group.

3. The third group of LDHs are the hydrotalcite type where, di and tri valent metal ions are randomly distributed in the –OH main layer with a general formula of $[M_{1-x}^{2+}M_x^{3+}(OH)_2]^{x+}[A_{x/n}]^{n-3}.m\ H_2O$. LDHs are scientifically and technologically more widely studied and used than the previous two. In nature besides the formation of

hydrotalcites in the natural process of rock and mineral weathering, authigenic formation of hydrotalcite in the sediment pore system in the lagoons of industrial waste water rich with Al^{3+}, $NaHCO_3$ and NaOH has also been reported earlier [55].

Another type of LDH is fouge`rite group of natural 'green rust' phases, $Fe_6^{3+}O_4(OH)_8[CO_3]\cdot 3H_2O$, it has a layered double hydroxide-type structure, in which brucite-like layers $[Fe_6^{3+}\ O_4(OH)_8]^{2+}$ are intercalated with CO_3^{2-} anions and water molecules [56].

1.2. Methods of synthesis of LDHs:

Layered Double Hydroxides can be synthesized by the following methods-

1.2.1. Co-precipitation method:

Co-precipiation method is the most common method of synthesis of LDHs. It is a simple and inexpensive “one pot” synthesis method [57-59]. It involves the slow addition of a mixed salts solution of divalent and trivalent metal ions in adequate proportions into a reactor containing water. The alkali solution is added in the reactor at a selected pH value, which leads to co-precipitation of the two metallic salts followed by hydrothermal treatment after filtering, washing, and drying. This method gives substantial amounts of products within a small period of time. The mechanism of this method can be explained as- firstly, condensation of hexaaqua complexes occur in solution, which build up the brucite-like layers with evenly dispersed metallic cations and with solvated interlamellar anions. The co-precipitation method offers a high degree of control for reaction parameters such as pH, temperature, aging time, mixing rate, ratio of cations and solution concentration. Depending on the control of the precipitation parameters, well-crystallized LDH phases can be obtained, properties of the LDH particles such as crystallinity, particle size, size distribution, purity and stability, can be controlled. To get well-defined phases, the operating conditions

should be optimized for each system. Four essential components are required for any co-precipitation synthesis. These are-

1. A soluble source of divalent metal cations to form the layers.

2. A soluble source of trivalent metal cations to form the layers.

3. A source of interlayer anions, usually in the form of a soluble ionic compound (e.g. sodium carbonate if carbonate is desired, sodium nitrate if nitrate is desired, etc.).

4. A strong base so as to cause precipitation of the LDH, usually sodium hydroxide. Potassium hydroxide, ammonia and urea also have been used [6,60,61].

1.2.2. Anion exchange method:

Anion exchange is another very important method to significantly modify the structure and functionality of LDH-based materials [58]. It is based on the exchange properties of the interlayer anions. Anion exchange in LDHs depends upon the electrostatic interaction between host layers and exchanged anions. Exchange is favoured for in-going anions with a high charge density. The anion-exchange method is a synthesis process in which an ion or molecule is inserted in between the layers of the crystal lattice, leaving the basic structure unchanged [62]. By comparing the equilibrium constant of exchange reactions between monovalent anions and divalent anions, Miyata proposed an order of anion selectivity - $OH^- > F^- > Cl^- > Br^- > NO_3^- > I^-$ and $CO_3^{2-} > C_{10}H_4N_2O_8S^{2-}$ (Naphthol Yellow S) > SO_4^{2-}. These results suggest that NO_3^- anions are easily displaced by OH^- anions of higher affinity towards the metal hydroxide layers [63]. Yamaoka *et al.* also gave a comparative list for divalent oxoanions: HPO_4^{2-}, $HAsO_4^{2-} > CrO_4^{2-} > SO_4^{2-} > MoO_4^{2-}$ [64]. Based on these observations, chloride and nitrate containing LDH are often used as precursors for anion exchange reactions. Several factors such as pH, the solvent and temperature influence on the anion exchange property of LDHs. Generally, higher pH (10.0-12.0)

favours the intercalation of carbonate anions while lower pH (4.5-6.0) results in the liberation of initial anion as the conjugate acid and incorporation of a less basic anion from the reaction system [65]. The lower pH results in the dissolution of LDH hydroxide layers. A suitable solvent also favours the anion-exchange process. It was found that binary solvent mixtures of alcohol and toluene prevent dissolution of the Mg_2Al-CO_3 and preserve LDH layered crystal structure during the anion-exchange reaction of aliphatic α, ω-dicarboxylate anions [66]. Similarly, ethanol/water mixture as solvent can effectively reduce the dissolution of LDH host during the intercalation of heptamolybdate ($[Mo_7O_{24}]^{6-}$)[67] and decamolybdodicobaltate (III) anions ($[H_4Co_2Mo_{10}O_{38}]^{6-}$) into Mg_RAl-LDH ($1.27 \leq R \leq 3.0$) [68]. O'Hare *et al* also found that the mixed ethanol/water solvent may also improve the crystallinity and decrease the production of $Al(OH)_3$ as an undesired product during the exchange reaction involving all isomers of both pyridine-carboxylate and toluate in $[LiAl_2(OH)_6]Cl.H_2O$ [69]. On the other hand, to some extent, higher reaction temperatures favour the exchange reaction by lowering of activation energy.

1.2.3. Hydrothermal method:

Hydrothermal method of synthesis involves the treatment of freshly precipitated mixed hydroxides or mechanical mixtures of the oxides with water in an autoclave both at high temperature (higher than 100 ^oC) and lower temperature (lower than 100 ^oC) called aging treatment [1]. This method is used to-

1) transform the small crystallites of LDHs into larger and well crystallized particles required for better characterization purposes.

2) transform amorphous precipitates into crystalline products.

At first Roy *et al*.[70] reported the synthesis of $MgAlCO_3$-HT starting from a mechanical mixture of MgO and Al_2O_3 or from a mixture obtained by decomposition

of the two nitrates by hydrothermal method. This reaction was carried out in an autoclave at temperatures lower than 598K with a total pressure ranging from 13 to 130 Mpa where the partial pressure for CO_2 varied from 0.7 to 133.3 MPa and the water pressure from 6.7 to 133 MPa.

1.2.4. Urea hydrolysis method:

Urea is one of the attractive agent for the precipitation of several metal ions into metal hydroxides from mixed solution [71,72]. Due to the unique properties such as weak Bronsted basicity (pK_b=13.8), high solubility in water and controllable hydrolysis rate it is used for the synthesis of LDHs. In presence of urea, the hydrolysis reaction progresses slowly, which results to a low degree of super saturation and better precipitation. By altering the reaction temperature, the hydrolysis rate of urea can be varied and the particle size of the LDHs can be controlled. As reported by K. Yan *et al*.[58] the urea hydrolysis method involves two steps in case of synthesis of Mg-Al-LDH-

1. The formation of ammonium cyanate (NH_4CNO) [Eqs. (1.1) and (1.2)] with subsequent fast hydrolysis of the cyanate to ammonium carbonate [Eqs. (1.2) and (1.3)] [71] which is the rate determining step-.

2. Two key intermediates, $Mg(OH)(H_2O)_{n-1}^{+}$ [Eq. (1.4)] and $Al(OH)(H_2O)_{n-1}^{2+}$ [Eq. (1.5)], are formed in weak alkaline media.

$$\mathbf{H_2N\text{-}CO\text{-}NH_2 \longrightarrow NH_4^+ + NCO^-} \quad (1.1)$$

$$\mathbf{NCO^- + 2H_2O \longrightarrow NH_4^+ + CO_3^{2-}} \quad (1.2)$$

$$\mathbf{NCO^- + 2H^+ + 2H_2O \longrightarrow NH_4^+ + H_2CO_3} \quad (1.3)$$

$$\mathbf{Mg(H_2O)_n^{2+} + H_2O \longrightarrow Mg(OH)(H_2O)_{n-1}^{+} + H_3O^+} \quad (1.4)$$

$$\mathbf{Al(OH)(H_2O)_n^{3+} + H_2O \longrightarrow Al(OH)(H_2O)_{n-1}^{2+} + H_3O^+} \quad (1.5)$$

$$Mg(OH)(H_2O)_{n-1}^{+} + Al(OH)(H_2O)_{n-1}^{2+} + OH^{-} + CO_3^{2-} \longrightarrow MgAl(OH)_3(CO_3)H_2O \quad (1.6)$$

1.2.5. Other methods:

1.2.5.1. Salt-oxide (or Hydroxide) method or acid phase synthesis from metal oxides:

The salt oxide method involves the reaction between divalent metal oxide (basic species e.g. CuO, ZnO) and trivalent metal salt (acidic species e.g. $CrCl_3$, $AlCl_3$ etc.) at acidic pH (pH = 4-5) [71]. This method is one of the pioneering works on the synthesis of LDH type hydrotalcite materials [73]. This method basically involves the reaction of a divalent metal oxide with an aqueous solution of a salt of a trivalent metal ion at low temperature. Since the pH involved in this type of synthesis is acidic whereas; hydrotalcite type LDHs are produced mainly in alkaline medium, therefore, the mechanism of formation is complicated. Divalent oxides from a local excess of -OH ions around the metal oxide surfaces in aqueous medium thereby facilitating the deposition of hydrotalcite type LDH by reaction with trivalent metal ions present in the solution phase. Although all the members of hydrotalcite type LDH can not be synthesised by this method but some important LDH like Zn-Al, Zn-Cr, Cu-Cr type can be easily synthesised by this method [74-77]. Synthesis of Ni-Al type LDH from reaction of alumina with Ni amine complexes at neutral pH also has been reported [78].

1.2.5.2. Precipitation at constant pH by induced hydrolysis:

It is the method in which LDHs are synthesised by a hydrolysis reaction involving a solution state cation and a fully hydrolysed or precipitated hydroxide cation [79]. This method is also called as induced hydrolysis because the fully hydrolysed cation causes complete hydrolysis of the second cation present in the solution state. The second

solution state cation is required to be kept at a pH slightly lower than the level at which it generally precipitates as hydroxide, e.g. $CoCl_2$ begins to precipitate at pH 7.7 as hydroxide and therefore it is kept at pH 7.4. Thus, the first cation is selected in such a way that it precipitates at a pH lower than the second cation. Since, Al^{3+} precipitates as $Al(OH)_3$ at a pH of 4.0-4.5, Co^{2+}-Al^{3+} LDH was prepared by this method from a suspension of $Al(OH)_3$ and $CoCl_2$ in aqueous medium by maintaining the pH at 7.4 for more than 7 hours. Similarly, several other LDHs involving metal ion combination like Ni^{2+}-Al^{3+}, Mg^{2+}-Al^{3+}, Co^{2+}-Al^{3+}, Co^{2+}-Fe^{3+}, Mg^{2+}-Mn^{3+} have also been synthesised by this method [80].

1.2.5.3. Synthesis from hydrolysis of alkoxides and metal acetylacetonates:

It has been reported the synthesis of Mg-Al and Li-Al LDH at room temperature at proper metal ion ratios in ionic and non ionic media. However, the products obtained sometimes contain traces of impurities like boehmite AlO(OH) [81-83]. The synthesis of LDHs by the hydrolysis of metal alkoxides and metal acetylaceonates also has been reported [84-86]. The synthesis of LDH e.g Mg-Al-LDH through hydrolysis of metal alkoxides involves the use of magnesium methoxide and Aluminium isopropoxide ($Al(OC_3H_7)_3$) in organic medium. On the other hand, the synthesis of LDH from the hydrolysis of metal acetylacetonates involves the use of different metal acetylacetonates such as $Ni(acac)_2$, $Mg(acac)_2$, $Al(acac)_3$ and $Cr(acac)_3$ in organic medium such as ethanol, acetone etc. The hydrolysis of metal alkoxides as well as metal acetylacetonates are carried out at temperature of 80 ^oC and pH ranging between 8-9 during the synthesis of LDH.

1.2.5.4. High temperature solid state reactions:

This reaction was carried out to synthesise Mg-Al, Mg-Fe, Ni-Fe, Ni-Al, Ca-Al, Cd-Al,Li-Al type LDHs [87, 88] which transforms amorphous or small crystallites of LDH

into larger and well crystallised particles.

1.2.5.5. Chimie-douce method:

Chimie-douce method also known as soft chemical method is relatively another non-classical approach used by solid state chemists to synthesise novel compounds [89]. Since oxidation-reduction process is involved in the synthesis, the metal ions taking part in Cimie-douce method are mainly transition metals as they can show multiple oxidation states. This method has advantage over other method as it can give divalent: trivalent metal ratio in a wide range which would depend upon the M^{2+}/M^{3+} solid solution range of precursor $NaM^{2+}_{1-y}M^{3+}_{y}O_2$ phase formed by high temperature solid state reaction involving Na_2O, Co_3O_4 and NiO etc. and oxidising hydrolysis of $NaM^{2+}_{1-y}M^{3+}_{y}O_2$ by selective reduction higher valent Ni to divalent state and conversion of γ-oxohydroxide formed to LDH.

1.2.5.6. Electrochemical precipitation:

In this method base is generated electrochemically over cathodic surface by reduction of anions and the metal hydroxide thus produced can either be unary or mixed-metal type hydroxide based upon the system selected. Ni-Al, Ni-Mn, Mg-Al, Mg-Cr type LDH are produced from mixtures of nitrate salt solutions of these metal ions [90, 91]. Reduction of NO_3^- to NO_2^- at the cathodic surface gives a high concentration of OH^- and H_2 gas. OH^- produced is then consumed by the corresponding metal ions to precipitate the crystalline LDH. Although, the product obtained is poorly crystalline this method can give CO_3^{2-} free LDHs, which is a serious problem in synthesis of these materials.

1.3. Methods of characterizations of LDHs:

The physicochemical characterizations of LDHs can be done by different techniques such as Powder X-ray diffraction (PXRD) analysis, Thermogravimetric analysis

(TGA), differential thermal analysis (DTA), differential scanning calorimetry (DSC), Fourier transformation infrared spectroscopy (FT-IR), Particle size analysis, Zeta-potential study, nitrogen BET surface area and pore volume analysis, X-ray photoelectron spectroscopy (XPS), Mass spectrometry analysis, Scanning electron microscopic study (SEM), Energy dispersive X-ray spectroscopy (EDX), Transmission electron microscopic study (TEM) etc. Some of the characterization techniques are discussed below-

1.3.1. Powder X-ray Diffraction (PXRD):

Powder X-ray diffraction (PXRD) is the main analytical technique for the structural characterization of LDHs and allows for the phase identification of crystalline materials [2]. The typical features of PXRD patterns of all LDH are the presence of sharp and intense lines at low angle 2θ values corresponding to the basal *00l* reflections, and less intense lines at high 2θ angle values corresponding to *002l* and *003l* reflections. When the interlayer ions are changed, a corresponding change in the highest intensity *00l* spacing are observed indicating the intercalation of new anions into the LDH layers [92,93]. On the other hand, thermally activated LDH shows different intense peaks at high 2θ angle corresponding to metal oxide formed during thermal decomposition.

1.3.2. Thermal analysis of LDHs:

The thermal stability of LDHs is determined by TGA-DTG analysis. Generally, in Thermogravimetric analysis the samples are heated up in a programmed heating rate to different temperatures and the with the increase of temperature the corresponding mass loss of the sample is recorded and plotted with temperature to get TG curve [2, 94,95]. Different types of oxidic phases are formed from LDHs after calcination such as non-stoichiometric oxides, segregated spinels, and nanometer sized oxide particles hence,

thermal study of this kind of materials get special importance. On thermal treatment during the process of heating LDHs shows different steps of weight loss and phase changes which depends upon the nature of composition of LDHs. After thermal treatment firstly, interlayer condensed water from the LDH is liberated at around 60 ^{o}C, followed by the loss of intra gallery surface water in the temperature range 120-150 ^{o}C [96,97]. This step corresponds to the shrinkage of the basal planes due to dehydration. After dehydration the next step is the dehydroxylation which occurs at around 450 ^{o}C, whereby hydroxyl groups of the framework hydroxide and interlayer anionic groups like CO_3^{2-} and Cl^- etc. begins to decompose giving rise to certain layered non-stoichiometric mixed metal oxides. Some of these oxides exhibit a rock salt like crystallographic structure [98].

1.3.3. Electron Microscopic study of LDHs:

The surface morphology of LDHs can be studied by Scanning electron microscope (SEM), Transmission electron microscope (TEM). The elemental composition of LDHs can be studied by Energy dispersive X-ray spectroscopic (EDX) analysis. LDH usually shows hexagonal platelet morphology and aggregation to form 'sand rose' motif of the hexagonal platelets as shown in **Fig. 1.4**. Similarly, TEM is also extensively used to study the exfoliated structure of LDH as well as the fringe lattices formed in the TEM gives the identification of different phases corresponding to different composition present in LDHs [99-105].

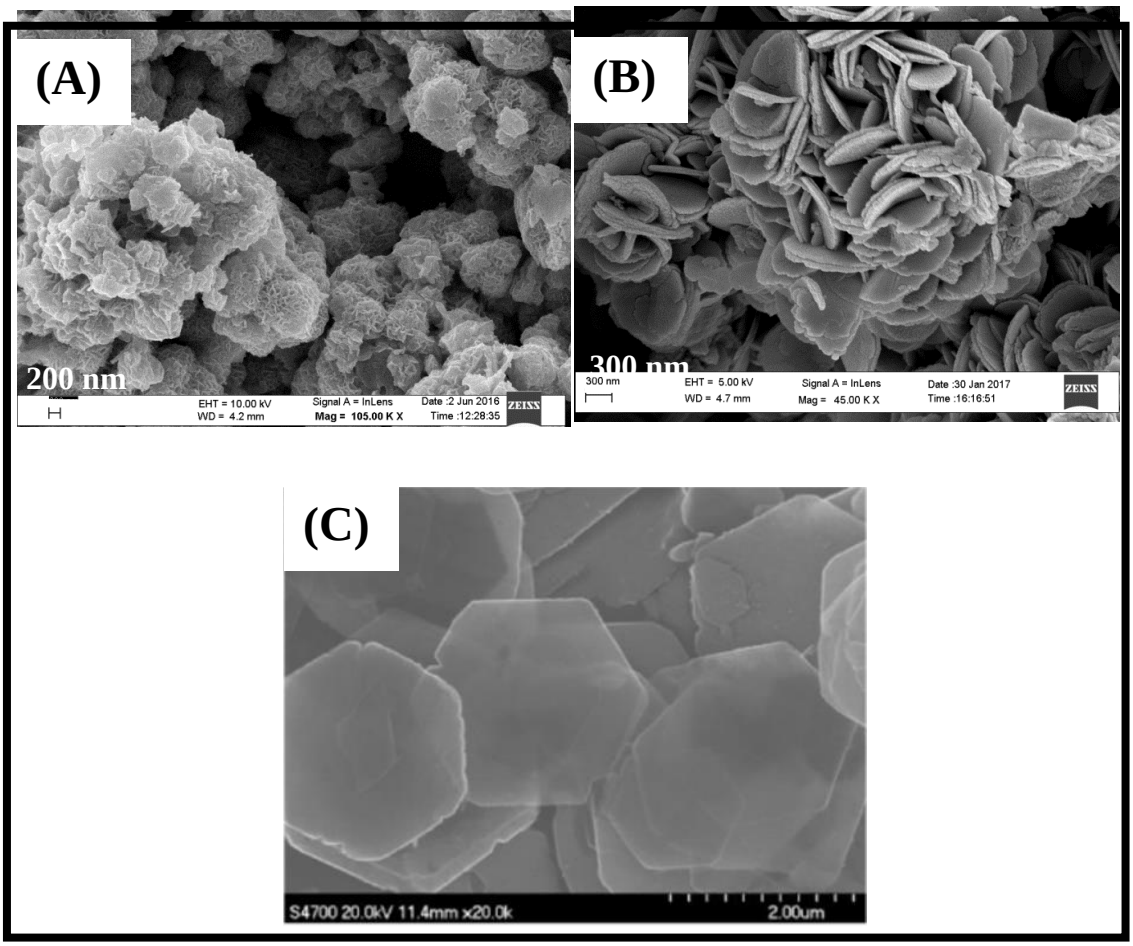

Fig. 1.4: High-magnification SEM image of a single flower-like hexagonal platelet structure of Mg/Al-CO_3 LDH (A&C) and Cu/Cr-Cl-LDH (B).

1.4. Applications of LDHs:

Layered Double Hydroxides (LDHs) also known as anionic clays find wide application prospective due to its unique properties such as anion exchange capacity, ability to capture organic and inorganic anions etc. Various mixed-metal oxides are obtained from the calcination of LDHs. Due to possession of catalytically important properties such as high surface area, uniform atomic level distribution of metal ion centers, acid-base bifunctionalitythese can be used as a catalyst with high industrial and scientific relevance including organic chemistry, environmental catalysis and natural gas conversion etc.

1.4.1. As Ion-exchanger and Adsorbent:

Due to the high surface area, high anion exchange capacities and flexible interlayer space LDHs have ability to remove negatively charged species by both surface adsorption and anion-exchange [106]. The anion-exchange capacity of LDHs is affected by the nature of the interlayer anions initially present and the layer charge density. When the layer charge density is very high the exchange reaction may become difficult. LDHs have greater affinities for multivalent anions compared with monovalent anions [63,107]. LDHs can take up anions by three different mechanisms- surface adsorption, interlayer anion-exchange and reconstruction of a calcined LDH precursor by the "memory effect". Many researchers have reported the use of LDHs for the removal of oxyanions such as - NO_3^-,SO_4^{2-}, PO_4^{3-}, AsO_4^{3-}, CrO_4^{2-}, $Cr_2O_7^{2-}$ and monoatomic anions (e.g. F^-, Cl^-, Br^-, I^-) from contaminated water [108-116]. LDHs are also promising materials as adsorbents for anionic organic contaminants *via* both ion-exchange and reconstruction reactions. There have been a large number of reports of the use of LDHs for removal of species such as aromatic carboxylic acids, phenols, pesticides, and humic or fulvic acids [106].

1.4.2. As catalyst:

Two attractive features of LDHs lead them to use as an important catalysts in different fields. Firstly, the basic sites of the brucite-like layers and secondly the atomic level uniform distribution of two or more metal ion within the brucite like layers without a segregation of ''lakes'' of separate cations, and where one of the cations is a catalytically active transition metal this can lead to high catalytic activity and selectivity [117]. Mixed-metal oxides (MMO) obtained after the calcination of LDHs have some unique properties such as high surface area and numerous Lewis base sites [118-121]. Mixed metal oxides (MMO) with a rock-salt-like structure formed by calcination of multi-component LDHs possess abundant acid and basic sites

associated with the presence of O^{2-}-Mn^{+} acid–base pairs [117]. Due to their unique ability to give Bronsted type basic sites, they are of current interest as solid base catalysts in several important organic reactions, such as Knoevenagel condensations, Michael additions, Claisen-Schmidt and aldol condensations [106].

LDHs are also used as catalyst support for many reactions such as Ziegler catalysts in the polymerization of olefins, polyethylene production [118]. Many researchers have reported the use of Mg-Al-LDH as a catalyst support for SO*x* removal from the emissions from fluidized catalytic cracking units, selective catalytic reduction (SCR) of NO by NH_3, oxidative dehydrogenation of *n*-butane and the vapor phase synthesis of isobutyraldehyde from methanol and *n*-propanol [119-128]. J. Bussi *et al*. and N. Das *et al*. [129,130] reported the use of palladium supported on Cu/Mg/Al LDHs in the liquid phase oxidation of limonene and on calcined Mg/Al LDHs for the one-pot synthesis of 4-methyl-2-pentanone (methyl isobutyl ketone) from acetone and hydrogen at atmospheric pressure.

Many researchers also have reported the use of calcined LDHs as heterogeneous catalysts in different catalytic reactions e.g. Mg/Al, Co-Mg-Al, Mg-Rh-Al, Ni/Al,Ni-Mg-Al, Ni/Al(Sn), Co/Al and Co/Al(Sn)-LDHs were tested in decomposition of N_2O, partial oxidation of CH_4, CO_2 methanation, partial oxidation of methanol (POM), steam forming of methanol (SRM) and oxidative steam reforming of methanol (OSRM) reactions, for the purpose of H_2 production for fuel cells [125-135].

1.4.3. Applications in Pharmaceutics:

LDHs have also several applications in pharmaceutics such as these were used as controlled release drug delivery system such as antacid and antipepsin agents [136,137]. Layered double hydroxides are finding unique advantages in drug delivery field because of their easy preparation, cheaper cost, better biocompatibility,

cytotoxicological benignity, and full protection of the bioactive molecule in the interlayers mainly acid buffering effect and anion exchange property [138]. It was reported that LDHs were used for the release of anti-inflammatory drugs such as ibuprofen, diclofenac, naproxen etc. Poernomo *et al*. reported the controlling rate of drug release from Mg-Al-LDH intercalated with ibuprofen [139]. Similarly, Dupin *et al*.[140] and Valeria *et al*.[141] reported the use of calcined Mg-Al-LDH for the release of diclofenac drugs via ion exchange and reconstruction methods. Wei *et al*.[142] also reported the use of Mg-Al-LDH in the release of naproxen drug. LDHs are also used for the release of antibiotic such as amoxicillin and antimicrobial molecules such as 2,4-dichlorobenzoate (BzDC) and para-hydroxybenzoate, anticancer drugs such as methotrexate [143-146]. LDHs are also used for the removal of phosphate anions from the gastrointestinal fluid with the aim of preventing hyperphosphatemia [147]. Mg-Al-LDHs has found pharmaceutical applications as an ingredient for preparing aluminum magnesium salts of antipyretic, analgesic drugs [148-150]. Recent advances in hybridization technique and increasing interest on interdisciplinary researches have brought out a strong increase in the attention to their pharmaceutical potentials. LDHs can intercalate many important biomolecules with negative charge such as oligomers, single or double stranded DNA, and simple molecules like nucleotides [151-156]. Especially, the single or double stranded DNAs have a great deal of application potentials in various fields, expanding from gene therapy to biosensing and even high density information storage. Choy *et al*. [157,158] also reported that LDHs are an efficient drug reservoir for folate derivatives.

1.4.4. Applications in Photochemistry:

LDHs can provide as novel catalyst for environmental photochemical reactions of guest molecules. LDH based photocatalysts are used in the elimination of organic

pollutants, and water reduction and water oxidation using UV or solar light as the irradiation source [118]. Due to their excellent visible light absorbing abilities, Zn-Ti-LDH and Zn-Fe-LDH afford good visible light- induced photocatalytic performance in the degradation of organic pollutants [159-164]. Zhao *et al*.[165] prepared a series of M-Cr-X-LDHs (where, M = Cu, Ni, Zn; X = NO_3^-, CO_3^{2-}) by the separate nucleation and aging steps (SNAS) method. They demonstrated that the highly dispersed Cr^{3+} ions in the octahedral sites in the LDH matrix played a significant role in the photo-excitation of electrons. They demonstrated that the highly dispersed Cr^{3+} ions in the octahedral sites in the LDH matrix played a significant role in the photo-excitation of electrons. Mohapatra *et al*. [163] reported the highest photocatalytic activity of Co^{2+} substituted Cu-Cr-LDH towards the photo degradation of organic pollutants. On the other hand, carbonate-intercalated Zn-Cr–LDH was found to be effective in the photodegradation of organic pollutants and water splitting to generate hydrogen [165-168]. Zn-Cr-LDH, Zn-Ti-LDH, Zn-Ce-LDH and Ni-Ti-LDH were reported for the use of O_2 evolution [169,170].

1.4.5. Applications in Electrochemistry:

Due to the capability of exchange of different ions LDHs are used as an electrode in electrochemistry. Layered nickel hydroxide can be used as an electrode for alkaline secondary cells. Chen *et al*. reported the electrochemical performance of Al-substituted layered α-$Ni(OH)_2$ in Nickel metal hydride batteries [171]. They have also suggested the addition of Co^{2+} and Mg^{2+} to improve the stability in alkaline solution at high temperature. Mousty *et al*. also reported the new electroactive materials derived from LDHs containing electroactive organic molecules, such as anthraquinonesulfonates, *m*-nitrobenzenesulfonate, and 2,2$^{/}$-azinobis-3-ethylbenzothiazoline-6-sulfonate [172,173]. Liao and Ye *et al*.[173] reported the synthesis of poly(ethylene oxide)/LDH

(PEO/LDH) nanocomposite polymer electrolytes for the fabrication of thin-film type Li-polymer secondary batteries. Many researchers have reported the application of organo-LDH film of Ni-Al, Zn-Cr and Zn-Al in enzyme electrode, electrocatalysis and electrochemical sensors [174]. Recently, Ruchun Li *et al*. reported the use of Ni-Co layered double hydroxides for Superior Asymmetric Electrochemical Capacitor [175].

1.4.6. Other Applications:

LDHs are used as additives in functional polymer materials. These are mainly used to stabilize polyvinyl chloride (PVC) [176-178]. Kyowa Chemical Industries (Japan) were the first to demonstrate that adding Mg/Al LDHs to PVC in combination with other additives such as zinc stearate and tin maleate leads to an enhancement in thermal stability of the resin [177]. LDHs are also used as flame retardant. Well dispersed LDH nanosheets in polymer matrices can greatly improve the flame retardancy of polymers [178-180]. Wang *et al*.[180-182] reported the synthesis of organically modified Co_2-Al–LDH polypropylene (O-Co_2-Al–LDH–PP) composites with enhanced flame retardant properties. Layered Double hyroxides as nanohybrid materials are used as cellular delivery agents, as viral carriers. Choy *et al*. reported that the use of LDH nanoparticles as delivery vectors can improve the cellular uptake of biomolecules [183]. In particular, LDH nanomaterials, because of their high positive charge and flexibility in carrying various peptides, proteins and genes show a great potential as effective cellular delivery agents. The anion exchange property of Mg-Al LDH makes it easy to directly load the biomolecules into the interlayer space. Thus, the resulting organic/inorganic nanohybrid can be directly delivered into cell [184,185].

1.4.7. Applications of LDHs in the treatment of some harmful gases:

Nitrous oxide (N_2O) is one of the most powerful greenhouse gases and it is the

largest stratospheric-ozone-depleting substance [186-190]. In particular, N_2O has a global warming potential (GWP) of approximately 310 times higher than CO_2. Due to its long lifetime of 114 years in atmosphere [191,192] it deplet the atmospheric ozone layer in the similar way to chlorofluorocarbons (CFCs). N_2O also have some toxic effect to human health. It causes megaloblastic bone-marrow depression and neurological symptoms and it inhibit the methionine synthase enzyme by interaction with vitamin B_{12} [193]. Compared to the pre-industrial period, now-a-days, due to different human activities N_2O emissions have significantly increased [194], this includes uses of chemical fertilizers, the combustion of fossil fuels and the large scale production of chemicals like nitric and adipic acid [190,195-199].

On the other hand, natural gas (NG) which is composed of primarily methane is one of the most abundant, low-cost C-containing feed stocks available in the world. Large amounts of NG emitted from refineries, chemical plants, oil wells and landfills causes pollution as it releases both CO_2 and unburnt CH_4 gases into the atmosphere [200]. **Table 1.2** shows the current concentration of three main green house gases N_2O, CO_2 and CH_4 in the atmosphere as collected by Carbon dioxide Information Analysis Center [201].

Table 1.2: Latest (2016) concentration of green house gases in relation to preindustrial period (1750)

Greenhouse gases	1750 concentration	2013 concentration	2016 Concentration [200]	Percentage increase (%)
Nitrous Oxide (N_2O)	275 ppb	326 ppb [188]	328 ppb	16
Carbon dioxide (CO_2)	280 ppm	395 ppm [188]	399.5 ppm	30
Methane (CH_4)	722 ppb	1893 ppb [199]	1894 ppb	62

Thus, from the global environment maintenance point of view the control of emission of these gases mainly N_2O emissions from combustion and chemical processes have significant importance. Different methods used to control N_2O emissions are- thermal decomposition [202], selective adsorption [202,203], decomposition by the use of plasma technology [202] and catalytic decomposition [203]. Among these methods catalytic decomposition has number of advantages for controlling N_2O emissions because of their lower energy requirements and lower cost. Whereas; further developments are needed for plasma technologies and selective adsorption before they are being used.

Similarly, the conversion of CH_4 to valuable chemicals is another challengeable work. Methane can be converted directly by a one step process or indirectly by several steps into many useful fuels and chemicals [204]. In recent years, Catalytic Partial Oxidation of methane (CPO) offers intensive attention due to its high methane conversion and high selectivity towards synthesis gas (CO and H_2) production. CPO (Eq (1.7)) gives the H_2/CO mol ratio of 2, which is favourable condition for subsequent synthesis [205]. CPO reaction is weakly exothermic therefore, energy and capital cost are very less as compared to the conventional endothermic steam reforming process.

$$CH_4 + 1/2O_2 \longrightarrow 2H_2 + CO \qquad (1.7)$$

As stated already like N_2O and CH_4, CO_2 is also a green house gas. Its present concentration in the atmosphere is 3.86×10^{-4} ppm which is far from the preindustrial level 2.8×10^{-4} ppm [206]. This drastic increase of CO_2 is the main culprit of the process of global warming. Now-a-days, CO_2 sequestration is most useful method to control its rapidly rising concentration. This method includes long time storage of CO_2 or other forms of carbon in different inorganic and biological matrix to slow down

global warming. Another important method to reduce global warming is the conversion of CO_2 to valuable feedstock by catalytic process. Among the catalytic reactions, CO_2 methanation is a promising technique for producing energy carrier or chemical [207]. Catalytic methanation of CO_2 also known as the Sabatier reaction involves the following reaction

$$CO_2 + 4H_2 \longrightarrow CH_4 + 2H_2O, \quad \Delta H_{298\,K} = -252.9 \text{ kJ/mol} \qquad (1.8)$$

The methanation of carbon dioxide is applicable for the production and purification of synthesis gas for the production of ammonia [207]. Methanation of CO_2 over different transition or non-noble metal supported, various mesoporous and LDHs based catalysts has been investigated by many researchers.

In other words, CO which is the product obtained from incomplete combustion of organic materials another toxic gas causes tissue asphyxia disease by forming carboxyhemoglobin with hemoglobin and reduces the amount of oxygen in human as well as animal health [208]. Similar to CO_2, methanation of CO is also another promising technique to reduce CO toxicity in environment [209].

1.4.7.1. LDHs as a catalyst for decomposition of toxic N_2O:

LDHs or hydrotalcite type materials after thermal decomposition or calcination at intermediate temperatures (450-600 ^oC) gives mixed metal oxide (MMO) which shows better catalytic activity due to high surface area and numerous Lewis base sites [210-213]. The use of hydrotalcite type materials of formula M-Al-CO_3-HT, where M stands for Ni, Cu and Co and their comparison to other catalysts for N_2O decomposition was reported by S. Kannan *et al*.[214]. They reported the N_2O decomposition over nickel and cobalt containing catalysts which showed highest activity even at 150 ^oC. They reported about 50 and 100 % N_2O conversion at 190 ^oC and 250 ^oC respectively, temperature of which was 100 ^oC less than the most active catalyst such as Cu-ZSM-5,

Rh-ZSM-5 and Co-ZSM-5[215]. These hydrotalcites were prepared by co-precipitation method using aqueous solutions of the metal nitrates together with Na_2CO_3 and NaOH as precipitating agents.

Similarly, Armor *et al*.[216] reported that the catalyst derived from LDH after calcination at temperature ranging from 450-500 ^oC showed maximum N_2O decomposition. Since, after calcination mixed metal oxides are formed, they reported that catalytic decomposition of N_2O over calcined Co-Al-LDH gave Co_3O_4 and $CoAl_2O_4$ phases after calcination. The N_2O decomposition over calcined $[Co_{1-x}Al_x(OH)_2[CO_3]_{x/2}.H_2O$, where x= 0.25-0.33 at different Co:Al ratios (from 2:1 to 3:1) was reported by S. Kannan *et al*.[217] in the temperature ranging from 150-280 ^oC. The Co-Al LDH was synthesized by low super saturation and sequential precipitation methods. It was observed that activity increased with increasing Co^{2+}concentration on the catalyst surface as determined by X-ray photoelectron spectroscopy. HT with Co:Al ratio 3:l obtained by low super saturation method showed 84 % N_2O conversion while $CoO-Al_2O_3$ showed only 15 % conversion at 450 ^oC under similar reaction conditions.

Perez-Ramirez *et al*. [218] proved the influence of higher Co:Al molar ratios around 1.0-3.0:1.0 on the activity for N_2O decomposition. On the other hand, according to Chang *et al*.[219] the catalytic activity depends on the molar ratio of Co:Al and it decreases with increasing cobalt concentration. The catalyst with Co:Al =1.0:1.0 showed up to 92 % N_2O conversion at 450 °C. S. Kannan [220] also reported that Mg-Co-Al-O_x with Mg:Co:Al ratio 0.94:2.0:1.0 showed about 100 % N_2O conversion with and without O_2 in the feed (2.5 % O_2 and 2.0 % H_2O) at 450 ^oC. On the other hand, Obalova *et al*.[221] reported about 80 % N_2O conversion over Mg-Co-Al-O_x with Mg:Co:Al ratio 2.0:2.0:2.0 at 450 ^oC. The catalysts containing Mg in the structure

were found to be less active catalysts compared to Mg-Co(Cu)-Al-O_x [222] catalyst which was further confirmed by Obalova *et al*.[223,224]. Due to substitution of Ni with Mg significantly decreased the catalytic activity as follows- Ni:Al (4.0:2.0) > Ni:Mg:Al (3.0:1.0:2.0 > 2.0:2.0:2.0) > Mg: Al (4.0:2.0). Ni-Al-O_x(Ni:Al= 4.0:2.0) catalyst showed about 79 % of N_2O conversion at 450 °C. After calcination of Ni-Al precursor at 450-500 °C a crystalline NiO was formed. On the other hand, the ternary mixed-metal oxides included MgO was found to be inactive in N_2O decomposition. However, according to Perez-Ramirez *et al*. [218] due to preferential adsorption of SOx on MgO presence of magnesium in Ni-Al-O and Co-Al-O catalysts prevented deactivation of the catalysts. On the other hand, the active sites remained available for N_2O reduction. According to Obalova *et al*.[225] the presence of both Ni and Mn in the systems Ni-Mn-O_x and Mg-Ni-Mn-O_x lower the decomposition of N_2O at 450 ^oC (about 20 %). The partial substitution of Mn with Al in the Co-Mn series resulted in higher activity [223] with Co:Mn:Al molar ratio 4.0:1.0:1.0. The N_2O conversion reached upto 82-97 % conversion.

About 100 % of N_2O conversion was achieved over Co-Rh-Al-O_x catalyst at temperature of 300-350 ^oC as reported by S. Kannan *et al*.[220] and K.S. Chang *et al*.[226]. The materials precursors were prepared by co-precipitation followed by calcination at 450-500 ^oC. Due to the low Rh concentration only Co_3O_4 and $CoAl_2O_4$ spinels were detected [218,220]. S. Kannan *et al*.[220] also studied the effect of rhodium loading (0.3–1.0 wt %) on the catalytic activity and reported the catalytic activity for an optimal amount of 0.7 wt % of Rh in Co-Rh-Al-O_x (Co:Al = 3:1) catalyst. As reported in several papers the dispersion of Rh influenced the catalytic acivity [225-229]. According to Parres-Esclapez *et al*.[230] besides Rh dispersion particle size also effects on the high catalytic performance.

S. Alini *et al*.[231] also studied the catalytic activity of H_2- reduced (5.0 % H_2, 750 °C) Co-Rh-Al-O_x (Co:Rh:Al=75:0.5:24.5) and Mg-Rh-Al-O_x (Mg:Rh:Al= 71:0.5:28.5, 71:1:28 or 80:1:19) at 450 °C and reported that Rh(0) dispersed homogeneously with an average particle size in the range of 1.0-3.0 nm act as the active species for N_2O decomposition. The activity of the Co-based catalysts with 2.6 % of water vapour in the feed decreased from 55 to 38 %, while the catalyst containing magnesium showed complete conversion. On the other hand, variation of the Mg:Al molar ratios in the absence of H_2O did not cause significant changes in the catalytic activity. In addition to this catalysts with higher Mg:Al ratio (Mg:Rh:Al= 80.0:1.0:19.0) deactivated faster showed in wet long-term stability tests (after 400 hours) compared to Mg:Rh:Al with a molar ratio of 71.0:1.0:28.0. This effect was due to the reoxidation of metallic rhodium. However, this deactivation in the presence of water vapour is completely reversible and increasing catalytic activity was exhibited by heating the catalysts in reducing atmosphere whereas; other reduced materials such as Mg-Rh-Pd-Al-O_x (Mg:Rh:Pd:Al=70.0:0.5:1.0:28.5 or 70.5:0.5:0.5:28.5) and Mg-Rh-La-Al (71.0:1.0:5. 0:23.0) showed lower activity in the presence of water vapour compared to Mg-Rh-Al-O_x. The lower N_2O conversion was due to the possible segregation of PdO during calcination for the samples containing palladium. This segregated PdO inhibit the synergistic interaction between both metallic rhodium and palladium. For La-containing materials, the formation of inactive Dilanthanum dioxide carbonate-II (La_2CO_5) hinders the interaction of metallic rhodium and Mg-Al-O_x, hence lower the catalytic activity. Perez-Ramirez *et al*.[218] also confirmed a promoting effect of magnesium on the structure of Co-Rh-Al-O_x. They studied the effect of 0.125 bar SO_2 and 30.0 bar O_2 in the feed for Co-Al-O_x (Co:Al = 3.0:1.0, 0.7 wt % Rh) and Mg-Co-Rh-Al-O_x (Mg:Co:Al = 1.0:3.0:1.0, 0.7 wt % Rh) catalysts. Co-Al-O_x catalyst did not

show any change in the the conversion after introducing SO_2 and O_2 into the feed at 450 °C. However, at temperatures around 325 °C the catalyst was completely deactivated. After removal of SO_2 and O_2 from the feed, the activity did not return to its previous level. Additionally, the catalyst showed a significant drop of conversion from 80 to 60 % during the first 10 hours of the stability test at 300 °C. The presence of magnesium in Co-Rh-Al-O further improved its stability in the presence of SO_2 and O_2 and reduced deactivation after 100 hours long-term stability tests. Although changes in the Mg:Al molar ratio and the basicity of the oxide matrix did not cause significant changes in the activity for N_2O decomposition of the mixed metal oxides [231] doping with some alkaline metals such as Na, Li, K and Cs significantly increased the catalytic activity [232,233]. The promoting effect of potassium on N_2O decomposition was also reported in many literatures [233-235]. In most cases, the presence of H_2O, O_2, and/or NOx (NO and NO_2) also inhibited N_2O conversion [223,236,237]. Such effects depended on the catalyst used as well as the feed composition. Deposition of small amounts of alkaline metals using an impregnation method followed by calcination did not change the structure of the support used. For example, Wu *et al*.[236] studied the catalytic property of Ni-Al-O_x (Ni:Al = 4.1:1.0) impregnated with potassium with a K:Ni molar ratio in the range of 0.05-0.2:1.0. The catalysts with K:Ni molar ratio of 0.1:1.0 and calcined at 300-400°C were the most active among the tested catalysts. Complete conversion of N_2O over these catalysts could be reached at 450°C. Catalyst with the same composition but calcined at 500 °C showed lower N_2O conversion only about 8 %. On the otherhand, the catalytic activity decreased with increasing K loading of the samples. Catalytic tests over Ni-Al-O_x and K/Ni-Al-O_x (Ni:Al = 4.1:1.0, K:Ni = 0.1:1.0) catalyst in the presence of 8.8 % H_2O and/or 4.0 % O_2 revealed that the presence of oxygen further effect on N_2O

decomposition. Although the mixture of H_2O and O_2 significantly inhibited N_2O decomposition, complete conversion of N_2O was still reached at 500 °C over the catalysts containing potassium, while N_2O conversion over undoped Ni-Al-O_x was only about 38 %. The lower catalytic activity in the presence of H_2O or O_2 was due to competitive adsorption of both these components on the same active sites responsible for N_2O decomposition. The same effect was also observed over other hydrotalcite-derived mixed metal oxides for N_2O decomposition,e.g. over K-promoted Co-Al-O_x (Co:Al=3.0:1.0, K/Co= 0.02-0.12:1.0) as studied by Cheng *et al*.[235] The relationship between catalytic performance and content of potassium was further studied by Obalova *et al*.[225,238]. Potassium deposition (0.0-3.0 wt %) on Co-Mn-Al-O_x (Co:Mn:Al= 4.0:1.0:1.0) was carried out by re-suspension of hydrotalcite-like precursors in aqueous solutions of potassium nitrate. After calcination of samples with 2.7-3.0 wt % K at 500 °C formed spinels as well as K_xMnO_2. Modification of the Co-Mn-Al-O system with different amounts of potassium significantly changed the catalytic activity. Highest activity in N_2O decomposition was observed for samples doped with both 0.9 and 1.6 wt % K. Samples modified with 4.0 % H_2O, 5.0 % O_2, 0.17 % NO and 0.1 % NO_2 were tested for N_2O decomposition under various feed compositions. The presence of H_2O and O_2 in the feed substantially decreased the catalytic activity. Therefore, the highest activity could be recovered when both components were eliminated from the feed. Additionally, the presence of NO_x influenced N_2O decomposition. The catalysts with 0.9 wt % potassium were the most active ones for feeds containing not only N_2O but also oxygen and nitrogen oxides [225]. Another series of K-doped Co-Mn-Al-O_x catalysts were obtained by impregnation of calcined hydrotalcite-like compounds or washed precipitates with an aqueous solution of KNO_3 [226]. Among the tested samples, K (1.8 wt %)/Co-Mn-Al-

O_x (Co:Mn:Al= 4:1:1) prepared by doping with potassium salt solution just after co-precipitation exhibited better activity. In the presence of 0.9 % H_2O, 5 % O_2 and 0.005 % NO, the catalyst reached 90 % conversion at 450 °C. Catalytic tests of this material in the presence of 4.0 % H_2O and 5.0 % O_2 showed only 25 % decrease in N_2O conversion during the stability test for 6 hours. In comparison, no loss in N_2O conversion was observed for a N_2O-He feed and a time-on-stream of 360 hours. The highest catalytic activity of this system confirms its great potential as an industrially relevant catalyst for N_2O abatement. Besides studies over K-doped catalysts, Xue *et al*.[239] investigated the effect of residual potassium remaining after synthesis. They reported the synthesis of Ce-Co-O_x (Ce:Co=0.21:1) which was prepared from appropriate metal nitrates with KOH as the precipitating agent, followed by calcination at 400 °C. Co_3O_4 and CeO_2 were present in the material which had a cooperative effect due to their interaction. For around 0.7 mol % potassium in the sample, decrease in the catalytic activity of around 50 °C compared to that of the catalyst without residual K was observed. Potassium-doped catalysts exhibited around 96 % conversion at 350 °C. However, no catalytic or stability tests in the presence of other components (e.g. H_2O, O_2 and NO_x) were reported. The positive effect of K was stronger compared to those of similar contents of Na. In fact, the positive effect decreased in the sequence as follows: Cs > Rb > K > Na > undoped > Li [240]. The influence of residual amount of sodium, which remained in trace amounts after washing step, was carried out by Farris *et al* [241]. Both very low (below 0.16 wt %) and very high (above 15.0 wt %) residual sodium contents caused low N_2O conversions of about 50 % and lower. Optimum sodium content in the range of 3.0-6.0 wt % in Co-Al-O_x promoted the decomposition of N_2O, exhibited over 80 % conversion at 475 °C. Doping with 1.0-2.0 wt % Na resulted in comparable results. In addition to this, deposition of residual sodium using

impregnation followed by calcination appears to be more efficient to promote the decomposition of N_2O [242]. The optimum sodium loading is dependent on the mixed metal oxides used which was proved by Xu *et al*. [242] They found that 1.5wt % of sodium as the optimum loading revealed higher activity compared to that over undoped Co-Al-O_x catalyst. A similar value (1.4wt %) was reported for Na/Co-Mn-Al-O_x as one of the most active catalysts [223]. Perez-Ramirez *et al*. [243] used Co-Rh-Al-O_x with different sodium contents ranging from 0.01 to 5.0 wt % for N_2O decomposition. Highest conversion was achieved compared to the undoped support in presence of 0.75 wt % sodium which is optimum loading for the catalyst.

A broad range of studies by Obalova *et al*.[223,240] over several alkali modified different mixed metal oxides proved that the promoting effect of alkali metals was associated with their ionization potential, the charge transfer to the catalyst and a decrease in the binding energies of all catalyst components. The sequence of the promoting effect of alkali metals was explained in terms of charge donation from the alkali metal cations to surface oxygen and further to cobalt and manganese in Co-Mn-Al-O_x [240]. Only for the system modified with Li, the N_2O conversion of Co-Mg-Al-O decreased as reported by Obalova *et al* [223-244]. On the other hand, according to A. Klyushina *et al*. [245] the synthesis methods also effect on the catalytic properties of Co-Mn-Al mixed oxides for N_2O decomposition. Three samples of mixed oxides of Co-Mn-Al with molar ratios Co:Mn:Al= 4:1:1 were prepared by three different methods (i) calcination of hydrotalcite-like precursors (Co-Mn-Al-HT-ex), (ii) calcination of corresponding nitrates (Co-Mn-Al-nitr) and (iii) calcination of the product of mechanochemical reaction of Co, Mn, Al nitrates with NH_4HCO_3 (Co-Mn-Al-carb). Different conditions of synthesis led to the formation of spinel-like phase with different structural properties leading to different catalytic activity. N_2O

conversions was found to decrease in the order of Co-Mn-Al-carb > Co-Mn-Al-HT-ex > Co-Mn-Al-nitr with decreasing surface area. The synthesis of Co-Mn-Al-LDH from carbonate precursor led to the less ordered structure and smaller crystallite size and exhibited some important properties such as - higher surface area,better reducibility and increase of mean (Co + Mn) valence. However, its highest catalyst activity was determined by the lowest bond strength of active site -oxygen while specific surface area and amount of active sites per unit surface were not decisive parameters for activities order. N_2O decomposition by using clay-supported LDH as vital component was also reported by Goswamee *et al* [246]. In this patent they used the honey comb monolith coated by clay supported LDH for the treatment of toxic N_2O. The catalytic reactions were carried out at temperatures from 400 to 600 ^oC. The coated honey comb monoliths were calcined at 450 ^oC to get mixed-metal oxide. N_2O was decomposed to N_2 and O_2 and about 90-98 % N_2O conversion was observed. Goswamee *et al.* [247] also reported the N_2O decomposition over SiO_2 supported Mg-Al LDH synthesized by sol-gel method using metal acetylacetonate as precursors. The catalytic reactions were carried out at 200-450 ^oC. It was observed that N_2O was decomposed to N_2 and O_2 at very low temperature.

In conclusion mixed-metal oxides obtained from Layered double hydroxides or Hydrotalcites appear to be efficient catalyst for N_2O decomposition and thus this type of materials can be considered as a serious candidate for the removal of N_2O.

1.4.7.2. LDHs as a catalyst for Catalytic partial oxidation of CH_4:

Oxidation of CH_4 involves two methods one is the total oxidation and another is the partial oxidation. Total oxidation of CH_4 leads to the formation of H_2 and CO_2 whereas the catalytic partial oxidation of CH_4 leads to the formation of methanol and synthesis gas (H_2/CO) etc as important feedstocks. The formation of synthesis gas (H_2/CO) from

oxidation of CH_4 also involved different methods such as-steam reforming and partial oxidation etc. The catalytic partial oxidation of CH_4 to synthesis gas (H_2/CO) is very much intensive process as compared to steam reforming ($CH_4 + H_2O \longrightarrow CO + 3H_2$, $\Delta H = +206$ kJ/mol) because of highest CH_4 conversion and high selectivity towards synthesis gas (H_2/CO) [248].

Hydrotalcite type anionic clays are also used in the catalytic partial oxidation of CH_4. The use of Rh or Ni supported catalysts obtained from Mg-Al hydrotalcite for catalytic partial oxidation of CH_4 was reported by F. Basile *et al* [249,250]. Catalytic partial oxidation of CH_4 over Ni supported Mg-Al oxide catalyst was reported by T. Shishido *et al* [251]. The catalyst was prepared by the solid phase crystallization (*spc*) method starting from Mg-Al hydrotalcite (HT) anionic clay as the precursor. The precursor $[Mg_6Al_2(OH)_{16}CO_3^{2-}]\cdot 4H_2O$ was prepared by co-precipitation method from nitrates of the metal components. The solid phase crystallized-Ni/Mg-Al showed high activity and selectivity to synthesis gas at high space velocity of 6.72×10^5 ml $h^{-1}g^{-1}cat^{-1}$. When Ni was supported by impregnating Mg-Al mixed oxide prepared from Mg-Al HT, the activity of impregnated-Ni/Mg-Al was higher than those of Ni/α-Al_2O_3 and Ni/MgO while it was close to that of *spc*-Ni/Mg-Al. This high activity of the *imp*-Ni/Mg-Al was due to the regeneration of Mg-Al HT phase from the mixed oxide during the preparation resulting in incorporation of Ni^{2+} on the Mg^{2+}sites in the HT. The partial oxidation of CH_4 over M/Mg/Al mixed oxides (where, M is Ru, Rh or Ir) was reported by F. Basile *et al* [252]. They prepared Ru and Rh containing Mg-Al mixed oxide with different compositions such as Rh/Mg/Al= 5:80:15, 5:71:24 and 5:65:30 as well as Ru/Mg/Al = 1:80:19 to 1:71:28. All of these catalysts show total oxygen conversion, high methane conversion and highest synthesis gas selectivity close to 90 %. It was observed that the catalyst with only the MgO-type phase

(Rh/Mg/Al 5:80:15) showed higher methane conversion and synthesis gas selectivity in comparison with the catalyst in which the MgO and spinel phases were present such as Rh/Mg/Al 5:71:24 and 5:65:30.

On the other hand, K.M. Lee *et al*.[253] reported the catalytic partial oxidation of CH_4 over calcined Ni-Mg/Al layered double hydroxides. It was observed that the catalyst composition and the calcination temperature effect on the catalytic properties of Ni-Mg/Al LDHs. The catalyst performance was strongly related to the Ni particle size. Ni-Mg/Al mixed oxide catalyst obtained after calcination at 1073 K with only Ni content and zero Mg/Al atomic ratio showed the better catalytic activity about 90 % CH_4 conversion due to the formation of $NiAl_2O_4$ spinels which reduced the coke deposition and deactivation of the catalyst. F. Basile *et al*.[254] also reported the catalytic partial oxidation of CH_4 over Ni/Mg/Al anionic clay derived catalysts. They reported the catalytic partial oxidation of CH_4 over four Ni based catalysts prepared through reduction of Ni/Mg/Al type hydrotalcite precursors with atomic ratios of 10:61:29, 34:37:29, 61:10:29 and 71:0:29 respectively. Z. Jiang *et al*.[255] reported the catalytic partial oxidation of CH_4 over Ni-based catalyst derived from Ni-Mg/Al ternary LDH. The ternary Ni-Mg-Al LDH was synthesized by co-precipitation method using $Mg(NO_3)_2{\cdot}6H_2O$, $Ni(NO_3)_2{\cdot}6H_2O$, and $Al(NO_3)_2{\cdot}9H_2O$ with Ni/Mg/Al molar ratios at 1:11:4, 1:11:3, 1:11:2.4, 0.4:11:2.4, 1.9:11:2.4 respectively. Different properties such as reducibility, surface basicity and catalyst reduction temperature also effect on the catalytic activity. It was observed from the results of temperature-programmed reduction and CO_2-temperature-programmed desorption that the amount of Ni-loading as well as the Mg/Al molar ratio influenced significantly on their reducibility but had little influence on the surface basicity, with the increase in Mg/Al ratio the base strength of the alkaline sites decreased. It was further observed that the

reaction temperature highly affected the reactivity of the catalysts, the catalysts reduced at high temperature led to the superior reactivity as compared to those reduced at low temperature. An in situ reduction of the catalyst had been observed in the POM reaction for catalysts reduced at low temperature. The catalysts with Ni content from 8 wt % to 15.5 wt % showed similar activity in POM reactions under the optimized reaction conditions and this activity was much higher than for catalysts with lower Ni-loading. J. Zhang *et al*.[256] reported the catalytic partial oxidation of CH_4 over fluorine modified mesoporous Ni-Mg-Al mixed oxides. Fluorine-modified Ni-Mg-Al mixed oxides was prepared by thermal decomposition of Hydrtalcite-type (HT) precursor. The results showed that fluorine was successfully introduced into Ni-Mg-Al mixed oxide *via* the high dispersion of MgF_2 which led to the formation of the periclase-type catalyst with mesoporous structure. The introduction of fluorine to the mixed oxides enhanced the basicity and nickel homogeneous distribution. Fluorine which acted as both electron and structure prompter improved the performance of Ni/Mg/AlO-F towards partial oxidation of CH_4, and the deactivation was hardly observed even after 120 hours run at 1053 K. F. Basile *et al*.[257] reported the effect of Mg/Al ratio of the hydrotalcite type precursors on the dispersion and catalytic activity of Rh and Ru catalysts. The active and stable catalyst based on Rh and Ru nanoparticles dispersed over MgO periclase or spinel matrix was prepared by calcination and reduction of M/Mg/Al Hydrotalcite-type precursors. The $MgAl_2O_4$ spinel and MgO-type phases obtained by calcination of the Rh/Mg/Al 5/71/24 sample were studied for catalytic activity. Rh was found to be more concentrated in the spinel phase whereas; the larger amount of MgO phase led to a similar amount of Rh in the two phases. The reduction of the sample led to Rh disperse particles with a maximum particle-size distribution between 2 and 3 nm, and the Rh (0) particle size supported on

the spinel was larger than that supported on the MgO phase. The change of the M^{2+}/M^{3+} ratio changes the amount of the phases and the Rh distribution. In the catalysts with the M^{2+}/M^{3+} = 80/20 the amount of spinel phase was low or absent depending on the Al/Rh concentration and the Rh was completely soluted in the MgO type phase. These phenomena led to a narrow distribution of the Rh particle size and to a high methane conversion as well as syngas selectivity. The catalyst and the particle size distribution were stable for 100 hours in hard reaction conditions. The increase of the M^{2+}/M^{3+} ratio applied to the Ru catalysts, increased the amount of Ru in the MgO structure decreasing the segregation of RuO_2 and as a result, the catalytic activity increased. Therefore, the properties and the dispersion of the active metal depend on the type of oxide in which the metal is inserted and this parameter can be tailored by varying M^{2+}/M^{3+}ratio. J. Zhang *et al*.[258] reported the partial oxidation of CH_4 over Ni/Mg/Al/La mixed oxides derived from layered double hydroxides (LDH). A series of Ni/Mg/Al/La mixed oxides prepared by thermal decomposition of layered double hydroxides. It was observed that due to larger ionic radius of La^{3+} ion only small partial La^{3+} was imported into the HT structure. In addition to this, most of lanthanum were dispersed on the surface and formed amorphous phases which existed between the crystal grains of the periclase-type solid solution. The addition of less than 6.5 % La^{3+} content gave rise to the strong basicity and high nickel dispersion with small particle sizes in the catalysts matrices, thus the corresponding mesoporous Ni/Mg/Al/La mixed oxides showed a high performance of about 99 % CH_4 conversion. Owing to the improvement of resistivity on carbon deposition and nickel sintering by La^{3+}, the catalyst deactivation was observed after 86 hours of reaction at 1053 K.

K. Takehira *et al*. [259] reported the preparation of Ni catalysts loaded in egg-shell

type by using ‘‘Memory effect’’mechanism in which Mg (Ni)-Al hydrotalcite structure was reconstituted on the catalyst surface during the preparation. Mg-Al (3:1) hydrotalcite was prepared by the co-precipitation from the nitrates of Mg(II) and Al(III), dried in air at 378 K, and calcined at 1123K for 1hour to form Mg-Al(3:1) mixed oxide. This catalyst was then used for CH_4 oxidation. It showed a high and stable activity. J. Ashok *et al*. [260] reported the CPO of CH_4 over Ni-Cu-Al catalyst. The precursors of hydrotalcite-like structures of Ni-Cu-Al catalysts derived with different Cu/Al ratios were synthesized by co-precipitation method. The CH_4 decomposition activities were studied at 600-700 ^oC and ambient pressures over calcined Ni-Cu-Al catalysts until the catalysts were deactivated completely. It was observed that addition of Cu to Ni enhanced methane decomposition activity when added in an appropriate amount. It was also observed that the Ni-Cu-Al with 60:25:15 ratio possesed higher hydrogen yields over the other compositions (60:05:35, 60:30:10, 65:00:35, 60:10:30, 60:15:25 and 60:20:20). It was further observed that among all the tested samples the Ni-Cu-Al with ratio Ni:Cu:Al 60:25:15 displayed higher activity with initial conversion of 53 % and total carbon deposition was 310 gC/g-cat over a total reaction time of 900 minutes maintained in this study. The H_2 yields increased with increase in the Cu content up to a molar composition of 60:25:15 and at above this Cu loading a rapid decrease of activity was observed. Thus, it can be revealed that a certain amount of copper can enhance methane decomposition activity of Ni.

F. Basile *et al*.[261] reported the CPO of CH_4 over Ni catalyst obtained from silicate intercalated HTlcs. Ni-containing catalysts obtained from hydrotalcite-like compounds (HTlcs) intercalated with silicate anions were prepared to get active and stable catalysts for the catalytic partial oxidation (CPO) of methane in place of conventional catalysts obtained by intercalating carbonates. The results showed that Ni catalysts

with silicate intercalated were a promising alternative to the conventional carbonate intercalated compounds. The structural and textural properties of the catalysts can be tailored by modifying the amount of silicates and then of their catalytic performances. Catalytic results showed that calcined Ni catalyst obtained from silicate intercalated HTlcs (Ni_8exHT-x, where x stands for 30 %, 20 % and stoichiometric amount) catalysts were stable with increasing the time-on-stream. Best results were observed by reducing the amount of active phase of the sample with a lower amount of silicates (stoichiometric amount). For this catalyst, the amount of magnesium available to form the MgO phase increased, thus a larger amount of Ni^{2+} species could be involved in the solid solution exhibiting highest catalytic stability.

H. Morioka *et al*.[262] reported the catalytic partial oxidation of CH_4 supported Ni catalysts prepared from Ni-Ca/Al-layered double hydroxide. They reported the synthesis of different types of Ni-M/Al-LDHs where, M=Mg, Sr and Ca respectively. The Ni-M/Al-LDHs were first synthesized by co-precipitation method and decomposed by calcination to form the precursors. The precursors were in situ reduced during the reaction to give the Ni-supported catalyst. Catalytic partial oxidation of methane was carried out in presence of Ni-Mg/Al-LDH, Ni-Sr-Al-LDH and Ni-Ca/Al-LDHs. It was observed that solid phase crystallized-Ni/Ca-Al was easily reduced to form active Ni metal particles during the reaction and showed the highest selectivity to synthesis gas production as well as the highest ability to reduce coke formation. The highest activity and the highest sustainability against coke formation of solid phase crystallized-Ni/Ca-Al were due to the stable and highly dispersed Ni metal particles on the catalyst. The highest sustainability was also partly due to the basic property of Ca-Al mixed oxide as the support. It was likely that the solid phase crystallization method starting from LDH as the precursor was effective

for the preparation of Ni supported catalyst.

D.V. Cesar *et al*.[263] reported the catalytic partial oxidation of CH_4 over Rh-Ni catalyst derived from hydrotalcite like precursors. Ni-Mg-Al and Rh-Ni-Mg-Al LDHs were first synthesized by co-precipitation methods. These were then calcined at 500 ^oC to obtain mixed metal oxide. The CPO reaction was carried out at 550 and 750 ^oC. It was observed that NiHTx catalysts with high Ni content (x=1and 5) showed high stability and high methane conversion for the partial oxidation of methane at 750 ^oC. On the other hand, catalyst with lower Ni content (x=15 and 25) exhibited low catalytic activity with low H_2/CO ratio (< 2) and showed fast deactivation. At 550 ^oC, the water gas shift reaction was highly favoured and hence increased the hydrogen yield. However, the occurrence of the Boudouard reaction produced high carbon deposition with the formation of whisker-type carbon.

In the bimetallic RhNiHT25, the Ni reducibility was increased due to the synergic effect between Rh and Ni, which increased the methane conversion and hydrogen selectivity. In addition to this, increase in stability was related to the absence of carbon deposition after 30 hours on stream at 550 and 750 ^oC respectively. These results show that the bimetallic catalyst is promising for application in membrane reactors to produce high purity hydrogen. Thus, hydrotalcites act as an active catalyst for CPO of CH_4.

1.4.7.3. CO and CO_2 methanation reaction in presence of LDH as catalyst:

Both CO and CO_2 methanation reactions are also one of the most important reactions which lead to the purification of synthesis gas for the production of ammonia and the production of syngas.

CO_2 methanation reaction over co-precipitated Ni-Alumina catalyst was reported by L.E. Alzamora *et al*.[264]. In this paper they examined the properties of the calcined

and reduced materials produced by coprecipiation method. They proposed that if a small particle size can be achieved for the nickel oxide rich phase prior to reduction; the resultant material will have high stability as well as high activity. To achieve this, the materials must be calcined under mild conditions and the reduction process must be carried out carefully, preferably with a gradual increase in reduction temperature until the desired degree of reduction is achieved. On the other hand, the effect of metal loading on the adsorption of CO_2 on Ni-Al_2O_3 catalyst was further studied by A.E. Aksoylu *et al*.[265]. They prepared a series of coprecipitated Ni-Al_2O_3 catalyst having metal loading in the range of 0-25 wt % Ni range. The effect of metal loading on CO_2 adsorption was investigated under isothermal chromatographic condition using an elution technique at temperatures ranges from 483-533 K. A.E. Aksoylu *et al*.[266] reported further the effect of structure/activity relationships in coprecipitated Ni-Al_2O_3 catalyst for CO_2 methanation. It was observed that the CO_2 methanation increased with Ni loading. A.E. Aksoylu *et al*.[267] also reported the CO_2 methanation reaction over Ni-Al_2O_3 catalyst prepared by both co-precipiated and impregnated method. They found that co-precipated catalyst had better CO_2 methanation reaction as compared to impregnated method. A. Zhao *et al*.[268] reported the CO_2 methanation raection over Ni-Al_2O_3 catalyst synthesized by solution combustion method. They prepared Ni-Al_2O_3 catalyst with varied Ni contents from 10 to 50 wt %. Ni-Al_2O_3 catalysts with Ni loading above 20 wt % showed good high temperature stability and better catalytic activity, which was due to Ni particles, scattered and spatially isolated by Al_2O_3. S. Abello *et al*.[269] reported the CO_2 hydrogenation reaction over high loaded Ni-Al mixed oxide catalyst with Ni/Al molar ratio =5 prepared by conventional co-precipitation method. Ni(Al)O_x mixed oxide with high metal loading was more active, selective and stable catalyst for carbon dioxide methanation after activation by

reduction. Co-precipitation of the metal precursors incorporates to high nickel content in the final oxide matrix which increased surface area. The amount of methane produced during carbon dioxide hydrogenation depends on temperature, pressure, H_2/CO_2 molar ratio and GHSV. Only small amounts of carbon monoxide and traces of ethane were detected as side products. Due to excessive amount of nickel resulted low dispersion and sintering which induced low catalytic activity, they reported that despite the high amount of nickel (about 70 wt %), partial reduction of the oxide also led to small metallic nickel crystallites of *ca.* 6 nm dispersed over NiO-alumina, which were active and selective for CO_2 methanation. Although, subsequent in situ reduction upon time on stream also slightly increased the Ni crystallite size, but the resulting high-loaded nickel-based catalyst displayed high stability after long time tests of around 500 hours. S. Abello *et al.*[270] also reported the CO_2 hydrogenation reaction over Takovite (Ni-Al hydrotalcites) derived mixed oxide of Ni/Al molar ratios from 1 to 3. It was observed that takovite decomposition led to the formation of a NiO phase containing Al ions and a nickel containing alumina phase (Ni-deficient spinel). The catalytic reaction was carried out at 225-400 ^{o}C. It was observed that catalyst with Ni/Al molar ratio of 2 showed better catalytic activity and was also very stable after 500 hours long time stabilty test.

CO_2 methanation reaction over Ni-Al-LDH based catalyst was reported by M. Gabrovska *et al*. [271]. Ni-Al-LDH was first synthesized by co-precipitation method by using $Ni(NO_3)_2.6H_2O$, $Al(NO_3)_3.9H_2O$ and Na_2CO_3 as precipitating agent. In this paper they reported the effect of Ni content on phase composition, physicochemical properties and activity in CO_2 hydrogenation of Ni-Al-LDH by keeping Ni^{2+}/Al^{3+} molar ratio at 0.49 (0.5NiAl), 1.48 (1.5NiAl) and 2.98 (3.0NiAl) respectively. The catalytic measurements were performed by using gaseous mixture of $CO_2/H_2/Ar$ =

0.65/34.35/65 vol % in the temperature interval 220-400 ^{o}C and GHSV from 3000 to 22,000 h^{-1}. PXRD analysis showed the formation of Ni-Al takovite like layered double hydroxides of different degree of crystallization depending on the Ni^{2+}/Al^{3+} ratio. The CO_2 methanation activity varied with the nickel content, reduction and reaction temperatures. The presence of reducible Ni^{2+}-O species as found from H_2-TPR analysis also affected on the the catalytic performance of the catalysts. The sample with high Ni content showed the highest degree of conversion after reduction at 400 and 450 ^{o}C. The large amount of nickel in the solid readily reduced to Ni^{2+}-O species after reduction and the formation of hardly reducible $NiAl_2O_4$ spinel-type phase was possible only at high temperatures than those of the reduction. The catalyst with the lowest amount of nickel (Ni^{2+}/Al^{3+}= 0.5) dominated in the methanation activity after reduction at 530 and 600 ^{o}C and reaction temperature of 260 ^{o}C due to an increase of the metallic nickel specific surface area whhich facilitated reduction of the $NiAl_2O_4$ spinel-type phase and retarding the effect of higher aluminum content on metal nickel sintering. The Ni^{2+}/Al^{3+}=1.5 catalyst showed intermediate behaviour between Ni^{2+}/Al^{3+} = 3.0 and Ni^{2+}/Al^{3+} = 0.5 often closer to Ni^{2+}/Al^{3+} = 3.0.

L. He *et al*.[272] reported the CO_2 methanation over Ni-Al hydrotalcite derived catalyst. Ni-Al hydrotalcite was prepared by co-precipitation method. In this paper they reported the use of two catalysts such as Ni-Al_2O_3-HT and Ni-Al_2O_3-IMP. It was observed that Ni-Al hydrotalcite derived catalyst (Ni-Al_2O_3-HT) exhibited a narrow Ni particle-size distribution with an average particle size of 4.0 nm and showed better methanation of CO_2 at 225 ^{o}C and reached upto 82.5 % CO_2 conversion with 99.5 % CH_4 selectivity at 350 ^{o}C, which was much better than the impregnated catalyst. The existence of large amount of strong basic sites on Ni-Al_2O_3-HT originated from the formation of Ni-O-Al structure was found from CO_2 microcalorimetry and ^{27}Al NMR

analysis. The strong basic sites present on the catalyst facilitated the activation of CO_2 and consequently promoted the activity of the catalyst. The presence of highly dispersed Ni with strong basic sites led to its unique and high efficiency for CO_2 methanation reaction.

M. V. Gabrovska *et al*.[273] reported the use of mixed-metal oxides obtained from Ni-Al LDH for CO_2 methanation reaction. They reported the effect of nickel amount on the structure, reducibility and activity of the mixed metal oxides obtained by the controlled thermal treatment of co-precipitated Ni-Al -LDH as catalyst precursor for CO_2 methanation reaction by variation of the Ni^{2+}/Al^{3+} molar ratio of Ni^{2+}/Al^{3+} = 0.5, 1.5 and 3.0 as well as the reduction and reaction temperatures. The PXRD patterns of the thermally treated samples at 200-1000 °C showed the presence of nano-sized NiO and $NiAl_2O_4$ spinel like phases in different proportion and degree of crystallinity. The Ni-Al-LDH was calcined at temperature of 500 °C due to high dispersion of the mixed oxide phases at this temperature. It was observed that after reduction at temperatures of 400, 450, 530 and 600 °C all the studied catalysts showed CO_2 hydrogenation took place effectively at reaction temperatures from 280-400 °C and GHSV between 3000 and 22000 h^{-1}. All the three catalysts showed similar activity at lower reduction and reaction temperatures towards CO_2 methanation reaction due to the formation of readily reducible Ni^{2+}-O species which produces sufficient number of Ni^0 sites which acted as active species. The catalyst with highest nickel amount regenerated the original layered structure after completion of the catalytic test. The performance of the catalyst with lowest nickel content dominates after reduction at higher temperatures due to the formation of $NiAl_2O_4$ spinel like phase which act as a reservoir and generating fresh Ni^0. The decrease of the activity in the rest of the catalysts was attributed mainly to the Ni^0 sintering.

X. Zhang *et al*.[274] reported the CO_2 methanation reaction over Ni-Mg-Al-LDHs/γ-Al_2O_3 catalyst prepared by "in situ" synthesis method. A novel Ni-Mg-Al catalyst derived from layered double hydroxides (LDHs) supported on γ-Al_2O_3 was used for catalytic reaction. They compared the catalytic activity of Ni-Mg-Al catalyst obtained in situ method with impregnated method. It showed better catalytic properties in CO_2 reforming of CH_4 during 160 hours without deactivation. The results of TEM and XRD showed that the active component nickel had small particle size and uniform dispersion which were derived from molecular-order dispersion of nickel on catalyst precursor Ni-Mg-Al-LDHs/γ-Al_2O_3. Ni-Mg-Al-LDHs/γ-Al_2O_3 catalyst possessed strong mechanical strength and high specific surface area of 200 m^2/g, since γ-Al_2O_3 plays not only as the source of trivalent cations (Al^{3+}) for synthesizing LDHs, but also as the support for LDHs grown. All of these advantages led to the resistance of carbon deposition, high catalytic activity and stability of C-LDHs/γ-Al_2O_3. On the other hand, G. Garbarino *et al*.[275] reported the CO_2 methanation reaction over Ni/Al_2O_3 catalyst at atmospheric pressure. They reported that the catalytic properties depend on the Ni content present on the catalyst. Catalytic activity of Ni/Al_2O_3 for methanation of CO_2 needed the presence of Ni metal particles which resulted due to high Ni loading. When Ni content was lower pre-reduction of the catalyst needed. The catalyst containing small Ni particles obtained by reduction of moderate loading precursor was very selective to methane without CO formation. The larger the Ni particles due to higher Ni loadings higher are the CO production.

CO_2 methanation reaction over $(Mg,Al)O_x$ supported Nickel catalyst derived from a (Ni,Mg,Al)-hydrotalcite-like precursor was reported by N. Bette *et al*.[276]. The (Ni,Mg,Al)-hydrotalcite was prepared by co-precipitation method. After reduction at 900 ^oC led to metallic Ni particles supported on a spinel type $(Mg,Al)O_x$ matrix.

Catalytic measurements carried out between 210 and 400 ^{o}C showed a reproducible CO_2 conversion into CH_4. Kinetic analysis of the data in the lower temperature range resulted in an apparent activation energy of 83.7 kJ/mol for this reaction. The catalyst showed excellent long term stability towards CO_2 methanation reaction up to 50 hours. The use of a series of Ni-Mg-La-Al hydrotalcite-derived mixed oxides obtained by thermal decomposition for CO_2 hydrogenation reaction was reported by D. Wierzbickia *et al*.[277]. The catalytic reaction was carried out at a temperature between 250-450 ^{o}C respectively. The incorporation of 2 wt % of lanthanum lead to an increase of the catalytic performance at temperatures from 250 to 300 °C towards CO_2 conversion of about 46.5-75 % and CH_4 selectivity of 98-99 % respectively. The activity was directly connected with basicity that increased with the incorporation of La into the HT-derived catalysts.

CO_2 methanation reaction over Ni-Al hydrotalcite was reported by S. Abate *et al*.[278]. Two types of Ni-Al hydrotalcite samples were synthesized by co-precipiation method at different pH such as 12 and 8.7 respectively. The catalytic activity of these samples was investigated towards hydrogenation of CO_2 at atmospheric pressure in the temperature between 250-400 °C. Their catalytic activity was then compared with alumina supported nickel-based commercial catalyst having equal nickel content which was taken as a reference sample at the temperature ranging between 250-400 ^{o}C. It was observed that their catalytic activity increased in the order of Ni-Al 12 > Ni-Al 8.7 > commercial catalyst. Hydrotalcites showed maximum CO_2 to CH_4 conversion approximately 86 % at 300 °C. The catalytic activity of the catalysts towards CO_2 conversion was related to NiO reducibility, metal surface area and Ni dispersion respectively.

M. Nizio *et al*. [279] reported the low temperature hybrid plasma-catalytic metha-

-nation over Ni-Ce-Zr hydrotalcite derived catalysts. Firstly, the Ni containing Mg-Al hydrotalcites were synthesized by co-precipitation method at constant pH and then Zirconium species were introduced into the hydrotalcite structure at this stage, using zirconium oxynitrate as zirconium source at $Al^{3+}$to Zr^{4+}molar ratio of 9:1.3 wt % aqueous solution of [Ce(EDTA)]-complexes was used for Ce-species and were introduced by ion exchange method. The resulting hydrotalcites were then calcined at 550 °C for 4 hours. The activity of Ni-Ce-Zr hydrotalcite derived catalysts was analysed in a hybrid plasma-catalytic process for the hydrogenation of CO_2 to CH_4 at low temperatures and in the presence of cold dielectric barrier discharge (DBD) plasma. It was observed that high CH_4 yields of about 80 % were measured under hybrid plasma-catalytic conditions at very low temperatures (110 °C, adiabatic conditions). On the otherhand, in the absence of plasma high CO_2 conversions and CH_4 yields were observed at temperatures higher than 330 °C. Hence, the catalytic activity was found to depend on the presence or absence of hybrid plasma. The presence of completely reduced Ni-crystallites of intermediate size present on the non-promoted catalysts was found to enhance the CO_2 methanation reaction. The addition of Ce and Zr did not result in a noticeable improvement of the catalytic activity. J. Liu *et al*.[280] reported the CO_2 methanation over alkaline-assisted Ni nano catalysts supported on Mg/Al mixed metal oxides (denoted as Ni_x/Mg_{2-x}Al-MMO) derived from Ni-Mg-Al hydrotalcite precursors. The catalytic performance toward CO_2 methanation was studied and it was observed that Ni/Mg/Al-MMO showed the best low-temperature reaction activity at 250 ^oC about 97.9 % CO_2 conversion and 97.5 % CH_4 selectivity. It was found that Ni nanoparticle and MgO basic sites at the interface served as dual active center towards CO_2 methanation and resulting in low-temperature reaction activity. It was further observed from Reflectance Fourier transform infrared

spectroscopy (in situ DRIFTS) that MgO act as the active site for CO_2 activation to give carbonate/hydrocarbonate species,while Ni provided H-species for further hydrogenation of the intermediates. Therefore, from this work it can be concluded that the influence of alkaline-assisted Ni nanoparticles on CO_2 methanation provided a promising heterogeneous catalyst. Y.Yan *et al.*[281] developed a novel W doped Ni-Mg mixed oxide catalyst. These (Ni-W-MgO_x) catalysts were prepared by homogeneous precipitation reaction. It was observed that addition of W remarkably promoted the catalytic activity towards CO_2 methanation reaction with improved stability, anti-CO-poisoning ability and resistance against coke formation as compared to the undoped Ni-MgO_x catalyst. It was identified by DRIFTS analysis that monodentate formate showed the superior reactivity towards CO_2 hydrogenation than that of bidentate formate species and the formation of more active monodentate formate species was facilitated by the addition of W to the Ni-Mg mixed oxide which leads to the greatly enhanced catalytic activity. H_2-TPR and CO_2-TPD characterization showed that doping W increased the number of stable CO_2 adsorption sites and helped in anchoring the Ni sites as a result of strengthened Ni-Mg interaction, both of which were responsible for the enhanced CO_2 methanation activity and the improved resistance against sintering. Z. Li *et al*. [282] reported the use of Ni/Mg/Al hydrotalcite for CO methanation reaction. Ni/Mg/Al layered double hydroxide was firstly prepared by co-precipitation method. The catalytic reaction was carried out at GHSV of 15000 h^{-1} and temperature of 600 ^oC respectively. After calcination Ni/Mg/Al layered double hydroxide formed $Ni_xMg_{1-x}O$ solid solution. This catalyst showed highest CO conversion in between 400-500 ^oC. Similarly, CO Methanation over bimetallic Ni-Fe catalyst derived from Ni/Fe/Mg/Al LDHs was reported by H.Tang *et al*. [209]. Ni/Fe/Mg/Al LDH was prepared by co-precipitation method. After calcination and

reduction of this LDH Ni and Fe elements were reduced and Ni-Fe alloy were highly dispersion on mixed oxide of aluminium and magnesium. This catalyst showed highest CO conversion and CH_4 selectivity at low temperature such as 250-350 ^oC. This catalyst showed about 100 % CO conversion.

Therefore, LDHs represents one of the technologically important frontline materials for different catalytic activity due to their low cost, relative ease of preparation and large number of composition/preparation variables. LDH-based catalytic materials have been rationally designed and synthesized by well-developed methodologies by taking advantage of the flexible tunability of the metal cations in the layers, and the exchangeability of the intercalated anions in interlayer galleries.

Mainly, owing to the threat of global warming, the decomposition of N_2O, catalytic partial oxidation of CH_4 and CO_2 methanation reactions are discussed here which are the most technologically important catalytic reaction now a days. We have found that LDHs plays a vital role in these catalytic reactions. After calcination and reduction of LDHs produces MMO (mixed-metal oxides) which have different properties such as high surface area, uniform atomic level distribution of metal ion centers, acid-base bifunctionality which helps to get better catalytic properties. The incorporation of La and W in the LDHs layers also increased the catalytic activity. Therefore, we believe that there remains a strong justification for the study on the application of LDH based materials in the use of the treatment of environmentally harmful greenhouse gases as well as other catalytic applications which is necessary to make further progress in this field for the ultimate benefit of mankind.

1.5. Aim of the Present work:

The aim of the present work is based on the different characteristic features of

"Layered Double Hydroxides or Mixed Metal Hydroxides" making them suitable for applications in different fields mainly in the field of environmental catalysis. It is already described that LDHs have lots of application in medical and related fields, adsorbents, toxic gas remover, catalysts and catalyst precursors, anion exchangers, clay viscosity modifier etc. The physicochemical properties of these materials are novel, flexible and exhibit a variety of important properties such as high surface area, uniform atomic level distribution of metal ion centers, acid-base bifunctionality.

To explore further developments in this area, various aspects like new synthetic routes, techniques of characterizations, solid-gas reaction for abatement of pollution from environment, rheological evaluation of dispersion or suspensions and their coating to form new catalytic device containing **Layered Double Hydroxides or Mixed Metal Hydroxides** or their derivatives is necessary to study. The present study was carried out on all these aspects mainly involving innovations in synthesis and applications.

The present study includes the synthesis of Layered Double Hydroxides and their nanocomposites by two different routes viz. Oxide hydrolysis method, non aqueous sol gel route using metal acetylacetonates as precursors and their SiO_2-LDH core shell precursors. The present study also focuses on the synthesis of sublimable mixed-metal acetylacetonates for Metal Organic Chemical Vapour Deposition (MOCVD) coating over solid preforms and mesoporosity development over the surface of LDH nanosheet by etching out of trivalent metal ion to form an active catalyst with novel characteristics for the abatement of different toxic and harmful green house gases such as N_2O, CH_4, CO and CO_2 to produce some benign gases or useful chemicals.

Various instrumental techniques such as XRD, DTA-TGA, FT-IR, Rheology, BET surface area and pore volume study, Zeta potential, Particle size analysis, Atomic

absorption spectroscopy (AAS), Mass spectrometry, SEM-EDS, TEM, Atomic Force Microscopy (AFM), X-ray Photoelectron spectroscopy (XPS), H_2-TPR etc. were used to characterize the products.

The main objectives of the present PhD work are as follows -

- Synthesis and characterizations of different types of binary and ternary LDH such as Ni-Al, Ni-Cr, Zn-Al, Mg-Cr, Ni-Mg-Cr, Ni-Mg-Al-LDH and their corresponding SiO_2 nanocomposites by sol-gel method using a combination of metal acetylacetonates and TEOS.
- Development of structured mixed metal nano oxide based catalyst from the synthesised nanocomposites and their application for direct N_2O decomposition, treatment of CO, N_2O assisted oxidation of CH_4 to H_2 and CO.
- Development of mixed metal nano oxide films over honeycomb preforms by Metal Organic Chemical Vapour Deposition (MOCVD) suitable as catalyst for direct decomposition of N_2O from selected LDH precursors derived by acid base reaction of acetylacetonate ligands with LDH.

  Development of mesoporous holey nanosheets suitable as catalyst for CO_2 hydrogenation to CH_4 from selected LDH precursors derived by acid base reaction of acetylacetonate ligands with LDH.

The contents of this thesis are distributed over seven chapters including conclusion and future prospects.

Chapter I: General Introduction

This chapter focuses the introductory overview including the background, structures, synthesis and properties of Layered double hydroxides. This chapter also explain about the motive of the present work.

This chapter also reviews the literatures related to the application of LDHs as a catalyst for the abatement of environmental pollutant such as N_2O, CH_4 and CO_2 in tune with the objective of the present PhD work.

Chapter II: Experimental

This chapter represents the experimental methods, chemicals and materials and detailed equipment used for the synthesis and characterizations of LDHs and their SiO_2 nanocomposites.

Chapter III: Synthesis and Characterizations of binary LDHs of Ni-Al, Mg-Al, Ni-Cr, Mg-Cr, Zn-Al and their SiO_2@LDH nanocomposites by non-aqueous sol-gel method and their application for N_2O decomposition and CH_4 oxidation

Both unsupported and SiO_2 supported Ni-Al, Mg-Al, Ni-Cr, Mg-Cr and Zn-Al-LDHs are synthesised by non-aqueous sol-gel method using metal acetylacetonate precursors. These are characterized by XRD, TGA, XPS, SEM-EDS, HR-TEM, FT-IR, Rheometry, Zetametry, Particle size analysis, BET surface area and H_2-TPR analysis. These nanocomposites were then coated over honey comb monolith and calcined at 450 ^oC to form as mixed-metal nanooxide which are used for the decomposition of N_2O, treatment of low ppm of CO and CO_2 gases, catalytic partial oxidation of CH_4.

This **chapter** is further classified into three parts-

Part-A: Synthesis and Characterizations of binary LDHs of Ni-Al, Mg-Al and their SiO_2@LDH nanocomposites by soft chemical sol-gel method for the treatment of N_2O, CO, CO_2 and CH_4

It includes the synthesis and characterization of Ni-Al, Mg-Al and their SiO_2 supported products. It also states about the use of these LDHs as catalyst for N_2O decomposition reaction as well as the treatment of low concentration of CO and CO_2.

Part-B: Synthesis and Characterizations of binary LDHs of Ni-Cr, Mg-Cr and their SiO_2@LDH nanocomposites by soft chemical sol-gel method for the catalytic partial oxidation of CH_4 in presence of N_2O

It includes the synthesis and characterization of Ni-Cr, Mg-Cr and their SiO_2 supported products. It states about the use of these LDHs as catalyst for catalytic partial oxidation of CH_4 in presence of N_2O.

Part-C: The effect of strength of bases and temperature on the synthesis of Zn-Al LDH by non-aqueous 'soft chemical' sol-gel method and formation of high surface area mesoporous $ZnAl_2O_4$ spinel

It states about the effect of temperature and strength of bases on the synthesis of Zn-Al-LDH. Finally the characterizations of $ZnAl_2O_4$ spinel formed from the calcination of Zn-Al-LDH.

Chapter IV: Synthesis and Characterizations of ternary LDHs of Ni-Mg-Al, Ni-Mg-Cr and their SiO_2 nanocomposites by non-aqueous sol-gel method and their application for the decomposition of N_2O and CH_4 oxidation

Ternary LDH such as Ni-Mg-Al and Ni-Mg-Cr and their SiO_2 support are synthesized by non-aqueous sol-gel method. These are characterized by XRD, TGA, XPS, SEM-EDS, HR-TEM, FT-IR, Rheometry, Zetametry, Particle size analysis, BET surface area analysis. These are used as a catalytic membrane for the decomposition of N_2O and CH_4 oxidation.

Chapter V: Synthesis of Mixed-metal acac of Cu-Cr to prepare thin film of mixed-metal nano-oxide films by MOCVD (Metal-Organic Chemical Vapour Deposition) and its application for N_2O decomposition

Mixed-metal acac of Cu-Cr is synthesized from Cu-Cr-LDH (synthesized by Oxide hydrolysis method) by the reaction with acetylacetone at room temperature. The

reaction of Cu-Cr-LDH is also carried out by varying the acetylacetone ligands. The Cu(II)/Cr(III)AcAc obtained from Cu-Cr-LDH and acetylacetone is then used as a single source precursor for the formation of nano-oxide thin film over solid preform by MOCVD technique. After that this nano-oxide thin film is used as catalyst for the decomposition of N_2O. These mixed-metal acac is characterized by PXRD, FT-IR, TGA-DTG, single crystal XRD, XPS, AFM, SEM-EDS, TEM, BET surface area and pore volume analysis.

Chapter VI: Synthesis and Characterizations of mesoporous Zn-Cr-LDH and its application for the hydrogenation of CO_2

Mesoporous Zn-Cr-LDH is synthesized by the reaction of Zn-Cr-LDH with acetylacetone and different β-diketo-ligand at different temperature conditions by etching out Cr^{3+} ion from the LDH sheet. These are then characterized by XRD, SEM-EDS, HR-TEM, XPS, FT-IR, BET surface area and pore-volume analysis. The mesoporous Zn-Cr-LDH is then used for the CO_2 hydrogenation reaction.

Chapter VII: Conclusion and Future Prospects:

This chapter highlights the salient finding of the research work along with the future scope.

Part of the work described in this thesis has been published or communicated (as detailed later).

REFERENCES:

[1] F. Cavani, F. Trifiro, A. Vaccari. *Catal. Today,* **1991**, *11*, 173-301.

[2] V. Rives. *Layered Double Hydroxides: Present and Future,* Nova Science Publishers, New York, **2001**.

[3] P. J. Sideris, U. G. Nielsen, Z. Gan, C. P. *Grey. Sci.*, **2008**, *321*,113.

[4] Q. Wang, D. O'Hare. *Chem. Rev.*, **2012**, *112*, 4124.

[5] D. G. Evans, R. C. T. Slade. *Structure and Bonding*, **2006**, *119*, 1.

[6] X. Duan, D.G. Evans. *Vol. 119, Springer-Verlag, Berlin*, **2006**.

[7] J. T. Kloprogge, D. Wharton, L. Hickey, R. L. Frost. *Am. Miner.*, **2002**, *87*, 623.

[8] R. L. Frost, K. L. Erickson, *J. Therm. Anal. Calorim.*, **2004**, *76*, 217.

[9] P.S. Braterman, Z.P. Xu, F. Yarberry, In Handbook of Layered Materials, S.M. Auerbach, K.A. Carrado and P.K. Dutta (Eds.), Marcel Dekker, New York, **2004**, 373.

[10] G. Fan, F. Li, D.G. Evans, X. Duan. *Chem. Soc. Rev*., **2014**, *43*, 7040.

[11] C. Forano, U. Costantino, V. Prevot, C. Taviot Gueho. *Layered Double Hydroxides (LDH)*. Handbook of Clay Science, **2013**, *5*, 746-771.

[12] J. He, B. Li, Y. Kang, D. G. Evans and X. Duan, *Layered Double Hydroxides*, Springer-Verlag, Germany, **2006**.

[13] F. Feitknecht. *Helv. Chim. Acta.*, **1942**, *25*, 131.

[14] F. Feitknecht. *Helv. Chim. Acta.*, **1942**, *25*, 555.

[15] E. Manasse. *Atti Sot. Toscanu SC. Nat., Proc. Verb.*, **1915**, *24*, 92.

[16] A. de Roy. Lamellar double hydroxides. *Mol. Crystal Liquid Crystal*, **1998**, *311*, 173-193.

[17] R. Allamnn. *Acta. Cryst. B.*, **1968**, *24*, 972.

[18] H. F. W. Taylor. *Miner. Mag.*, **1969**, *37*, 338-342.

[19] H.J. Kuzel, N. Jb. *Miner. Mh.*, **1976**, *5*, 319-325.

[20] V.A. Drits, T.N. Sokolova, G.V. Sokolova, V.I. Cherkashin. *Clays and Clay Miner.*,**1987**, *35 (6)*, 401-417.

[21] K.R. Poeppelmeier, S.J. Hwu. *Inorganic Chem.*, **1987**, *26*, 3297-3302.

[22] V.R. Allman. *Chimia*, **1970**, *24*, 99-108.

[23] H. Wang, X Xiang, F. Li, D.G. Evans, X. Duan. *Appl. Surf. Sci.*, **2009**, *255*, 6945-

6952.

[24] R. Allmann, H.P. Jepsen. N. Jhb. *Miner. Monat.*, **1969**, *12*, 544-551.

[25] F.A. Mumpton, H.W. Jaffe, C.S. Thomson. *Am. Miner.*, **1965**, *50*, 1893-1913.

[26] D.L. Bish, G.W. Brindley. *Am. Miner.*, **1977**, *62*, 458-464.

[27] D.L. Bish. Societe francaise de Mineralogie de Cristallographie, Orleans,18 July **1978**.

[28] G.W.Brindley. *Mineral Mag.*, **1979**, *43*, 337-340.

[29] R. Allmann, H. Maghsudnia. *Ber.Deuts.Mineral.Gesell.*, **1991**, 177.

[30] R. Allmann, J. Rius. *Z.*Fuer. *Kristall.*, **1984**, *168*, 133-144.

[31] D. L. Bish, A. Livingstone. *Miner. Mag.*, **1981**, *44*, 339-343.

[32] D. R. Hudson, M. Busell. *Miner. Mag.*, **1981**, *44*, 345-350.

[33] G. S. Thomas, M. Rajamathi, P. V. Kamath. *Clays Clay Miner.*, **2004**, *52*, 693.

[34] C. Frondel. *Am. Miner.*, **1941**, *26*, 295.

[35] V.A. Drits, A.S. Bookin, In "*Layered Double Hydroxides: Present and Future*" ed. V. Rives; Nova Science Publishers, New York, **2001**.

[36] D. G. Evans, R. C. T. Slade. *Structural Aspects of Layered Double Hydroxides.* In: Duan, X., Evans, D.G. (Ed.), *Layered Double Hydroxides.*Springer-Verlag, Berlin Heidelberg, **2005**.

[37] S. Miyata. *Clays and Clay Miner.*, **1975**, *23*, 369-375.

[38] P. Chaumette, R. Szymanski, F. Thevenot. *Clays Clay Miner.*, **1989**, *37(5)*, 396-402.

[39] S.K. Yun, T.J. Pinnavaia. *Chem. Mater.*, **1995**, *7*, 348-354.

[40] H.F.W. Taylor. *Miner. Mag.*, **1969**, *37*, 388-342.

[41] R. Allmann, H. Maghsudina. B. Deuts. *Miner. Gessell.*, **1991**, 177.

[42] A. Ennadi, M. Khaldi, A.D. Roy, J.P. Besse. *Mol. Cryst. Liq. Cryst.*, **1994**, *244*,

373.

[43] V. Rives, M. A. Ulibarri. *Coord. Chem. Rev.*, **1999**, *181*, 61.

[44] A. Terzis, S. Filippakis, H.J. Kuzel, H. Burzlaff. *Zeit Krist.*, **1987**, *181*, 29-34.

[45] I. Rousselot, C. T. Gueho, F. Leroux, P. Leone, P. Palvadeau, J. P. Besse. *J. Solid State Chem.*, **2002**, *167*, 137-144.

[46] G. Mascolo. *Miner. Petrogr. Acta.*, **1985**, *29*, 163-169.

[47] A. M. Fogg, A. J. Freij, G. M. Parkinson. *Chem. Mater.*, **2002**, *14*, 232.

[48] C.J. Serna, J.L. Rendon, J.E. Iglesias. *Clays and Clay Miner.*, **1982**, *30*, 180-184.

[49] S. Britto, P. V. Kamath. *Inorg. Chem.*, **2009**, *48*, 11646-11654; DOI:10.1021/ic9016728.

[50] M. Strokal, C. Kroeze, Cur. *Opin. Environ. Sust.*, **2014**, *9-10*, 108-121.

[51] B. A. Hungate, J. S. Dukes, M. R. Shaw, Y. Luo, C. B. Field. *Sci.*, **2003**, *302*, 1512-1513.

[52] C.J. Serna, J. L.White, S.L.Hem. *Clays Clay Miner.*, **1977**, *25*, 384.

[53] R. Fischer, H. J. Kuzel. *Cem.Concr. Res.*, **1982**, *12*, 517.

[54] S. Auer, H. Pöllmann. *J. Solid State Chem.*, **1994**, *109(1)*, 187-196.[55] M. Stoffyn, H.C. Dodge, T.F. Mackenzie. *Am. Miner.*, **1977**, *62*, 173.

[56] J.M.R. Genin, S.J. Mills, A.G. Christy, O. Gue'rin, A.J. Herbillon, E.Kuzmann, G.Ona-Nguema, C. Ruby, C. Upadhyay. *Miner. Mag.*, **2014**, *78(2)*, 447-465.

[57] W.T. Reichle. *Solid States Ionics*, **1986**, *22*, 135-141.

[58] K.Yan, G.Wu, W. Jin. *Energy Technol.*, **2016**, *4*, 354-368.

[59] F. L. Theiss, G. A. Ayoko, R. L. Frost. *Appl. Surf. Sci.*, **2016**, *383*, 200-213.

[60] H.W. Olfs, L.O. Torres-Dorante, R. Eckelt, H. Kosslick. *Appl. Clay Sci.*, **2009**, *43*, 459-464.

[61] U. Costantino, F. Marmottini, M. Nocchetti, R. Vivani. *Eur. J. Inorg. Chem.*,

1998, 1439-1446.

[62] G. R. Williams, D. O'Hare. *J. Mater. Chem.*, **2006**, *16*, 3065-3074.

[63] S. Miyata. *Clays Clay Miner.*, **1983**, *31*, 305-311.

[64] T. Yamaoka, M. Abe, M. Tsuji. *Mater. Res. Bull.*, **1989**, *24*, 1183.

[65] A. De Roy, C. Forano and J. P. Besse, in Layered Double Hydroxides: Present and Future, ed. V. Rives, Nova Science Publishers, Inc., New York, **2001**, Page no.1.

[66] J. H. Lee, S. W. Rhee, D. Y. Jung, *Chem. Mater.*, **2004**, *16*, 3774.

[67] T. Hibino, A. Tsunashima. *Chem. Mater.*, **1997**, *9*, 2082.

[68] J. Bravo-Suarez, E. A. Paez-Mozo, S. T. Oyama. *Chem. Mater.*, **2004**, *16*, 1214.

[69] L .X. Lei, R. P. Vijayan and D. O'Hare. *J. Mater. Chem.*, **2001**, *11*, 3276.

[70] D.M. Roy, R. Roy, E.F. Osbom. *Am. J. Sci.*, **1953**, *251*, 337.

[71] M. R. Othman, Z. Helwani, Martunus, W. J. N. Fernando. *Appl. Organomet.Chem.*, **2009**, *23*, 335-346.

[72] K. H. Goh, T. T. Lim, Z. Dong. *Water Res.* **2008**, *42*, 1343-1368.

[73] H. P. Boehm, J. Steinle, C. Vieweger. *Angew. Chem. Int. Ed. Engl.*, **1977**, *16*, 265

[74] W. Feitknecht, G. Fischer. *Helv. Chem. Acta.*, **1938**, *21*, 766.

[75] K. El Malki, A. De Roy, J. P. Besse. *Eur. J. Solid State Inorg. Chem.*, **1989**, *26*, 339.

[76] V.P. Danilov, E. Yu. Georgievskaya, O.N. Krasnobaeva, I.N. Lepeshkov. *Rus. J. Inorg. Chem.*, **1988**, *1*, 33.

[77] R.L. Goswamee, K.G. Bhattacharyya, H. Poellmann, D.K. Dutta. Proc.of 34th Ann. Conv. of Chemists **1997**, Univ. of Delhi, Dec 17-20, Abs No. ING (O/P) 18.

[78] O. Clause, C. Bobin, B. Rebours, J.B.C. de la d'Espinose, P. Gueroult, E. Merlen. *Appl.Clay. Sci.*, **1995**, *10*, 45.

[79] J. M. Fernandez, C. Barriga, M. A. Ulibarri, F. M. Labajos,V. Rives. *J. Mater.*

Chem.,**1994**, *4*, 1117.

[80] R. M. Taylor. *Clay Miner.*, **1982**, *17*, 369.

[81] R. M. Taylor. *Clay Miner.*, **1984**, *19*, 591.

[82] K.R. Poeppelmeier, C.K.Chiang, J.P. Thiel. *Chem. Mater.*, **1993**, *5*, 297.

[83] C.J. Serna, J.L. White, S.L. Hem. *Clays Clay Miner.*, **1977**, *25*, 384.

[84] O. Yamaguch, H. Taguchi, Y. Miyata, M. Yoshinak, K. Shimizu. *Polyhedron.*, **1987**, *6*, 1587.

[85] M. Mishra. Preparation of Composite materials containing layered double hydroxides (LDHs) and their prospective application for the treatment of some environmentally harmful gases PhD Thesis, Assam University Silchar, **2013**.

[86] M. Mishra, M.R. Das, R.L. Goswamee. *J. Sol-Gel Sci.Technol.*, **2010**, *54*, 57-61.

[87] P. Saikia, A. Gautam, R.L. Goswamee. *RSC Adv.*, **2016**, *6*, 112092-112102.

[88] S. Auer. PhD Thesis Erlangen Nuremberg University, Germany, **1992**.

[89] C. Delmas,Y. Borthomieu. *J. Solid State Chem.*, **1993**, *104*, 345.

[90] D.M. Schleich. *Solid State Ionics*, **1994**, *70/71*, 407-411.

[91] L. Indira, P.V. Kamath. *J. Mater. Chem.*, **1994**, *4*, 1487.

[92] V.P. Kamath, M. Dixit, L. Indira, A.K. Shukla, G.V. Kumar, N. Munichandraiah. *J. Electrochem. Soc.*, **1994**, *141*, 11.

[93] H. J. Spratt, S.J. Palmer, R.L. Frost. *Thermochim. Acta*, **2008**, *479(1-2)*, 1-6.

[94] J. P. Sara, A. Soisonard, R. L. Frost. *J. Colloid Interface Sci.*, **2009**, *329(2)*, 404-409.

[95] D.P. Das, J. Das, K. Parida. *J. Colloid and interface Sci.*, **2002**, *261*, 213-220.

[96] H. H. Willard, L. L. Merritt, Jr., J. A. Dean. Instrumental Methods of Analysis. Seventh edition ed., ed. J Carey, **1988**, Wadsworth Inc Belmont California.

[97] M.K. Titulaer, in “Porous structure and particle Size of Silica and Hydrotalcite

Catalyst Precursors"Chapter 9, ISSN 0072-1026; No.99, Ph.D. Dissertation Rijk universiteit Ultrecht,Nederlands.

[98] S. Miyata. *Clays Clay Miner.*, **1980**, *28(1)*, 50.

[99] M.J. Hudson, S. Carlino, D.C. Apperley. *J. Mater. Chem.*, **1995**, *5(2)*, 323.

[100] S. Vial, V. Prevot, C. Forano. *J. Phys. Chem. Solids.*, **2006**, *67*, 1048.

[101] G. Hu, D. O'Hare. *J. Am. Chem. Soc.*, **2005**, *127*, 17808.

[102] M. Adachi-Pagano, C. Forano, J. P. Besse. *J. Mater. Chem.*, **2003**, *13*, 1988.

[103] L. Z. Qiu, W. Chen, B. J. Qu. *Polymer.*, **2006**, *47*, 922.

[104] Y. Kuang, L. Zhao, S. Zhang, F. Zhang, M. Dong, S. Xu. *Mater.*, **2010**, *3*, 5220-5235; DOI:10.3390/ma3125220.

[105] M. Yang, J. Liu, Z. Chang, G.R. Williams, D. O'Hare, X. Zheng, X. Sun, X. Duan. *J. Mater. Chem.*, **2011**, *21*, 14741-14746.

[106]F. Li, X. Duan. *Structure and Bonding*, **2006**, *119*, 193-223; DOI:10.1007/430007.

[107] P.K. Dutta, M. Puri. *J. Phys. Chem.*, **1989**, *93*, 376.

[108] L Chatelet, JV Bottero, J. Yvon, A. Bouchelaghem. *Colloids Surf. A*, **1996**, *111*,167.

[109] H.S. Shin, M.J. Kim, S.Y. Nam, H.C. Moon. *Water Sci. Technol.*, **1996**, *34*, 161.

[110] L.M. Parker, N.B. Milestone, R.H. Newman. *Ind. Eng. Chem. Res.*, **1995**, *34*, 1196.

[111] R.L. Goswamee, P. Sengupta, K.G. Bhattacharyya, D.K. Dutta. *Appl. Clay Sci.*, **1998**, *13*, 21.

[112] N. Kozai, T. Ohnuki, S. Komarneni. *J. Mater. Res.*, **2002**, *17*, 2993.

[113] Y. Seida, Y. Nakano. *Water Res.*, **2002**, *36*, 1306.

[114] Y. W.You, H.T. Zhao, G. F.Vance. *Environ. Technol.*, **2001**, *22*, 1447.

[115] S. W. Rhee, M. J. Kang, H. Kim, C.H. Moon. *Environ. Technol.*, **1997**, *18*, 231.

[116] D. P. Das, J. Das, K. Parida. *J. Colloid Interface Sci.*, **2003**, *261*, 213.

[117] G. Fan, F. Li, D. G. Evans, X. Duan. *Chem. Soc. Rev.*, **2014**, *43*, 7040.

[118] D. Tichit, B. Coq. *CATTECH*, **2003**, *7*, 206.

[119] D. Tichit, D. Lutic, B. Coq, R. Durand, R. Teissier. *J. Catal.*, **2003**, *219*, 167.

[120] D. Tichit, C. Gerardin, R. Durand, B. Coq. *Top. Catal.*, **2006**, *39*, 89.

[121] Z. P. Xu, J. Zhang, M. O. Adebajo, H. Zhang, C. H. Zhou. *Appl.Clay Sci.*, **2011**, *53*, 139.

[122] H. Muller-Tamm, H. Frielingsdorf, G. Schweier, L. Reuter (**1971**) German Pat. 2,163,851 to BASF AG.

[123] A. A.Bhattacharyya, G.M. Woltermann, J.S. Yoo, A. Karch, W.E. Cormier. *Ind.Eng. Chem. Res.*, **1988**, 27, 1356

[124] J. S.Yoo, A. A. Bhattacharyya, C. A. Radlowski. *Ind. Eng. Chem. Res.*, **1991**, *30*, 1444.

[125] J. Pasel, P. Kabner, B. Montanari, M. Gazzano, A. Vaccari, W. Makowski, T. Lojewski, R. Dziembaj, H. Papp. *Appl. Catal. B:Environ.*, **1998**, *18*, 199.

[126] T. Blasco, J. M. Lopez Nieto, A. Dejoz, M.I. Vaquea. *J. Catal.*, **1995**, *157*, 271.

[127] J. M. Lopez Nieto, A. Dejoz, M. I.Vaquea. *Appl. Catal. A*, **1995**, *132*, 41.

[128] P. Dinka, K. Prandova, M. Hronec. *Appl. Clay Sci.*, **1998**, *13*, 467.

[129] J. Bussi, A. Lopez, F. Pena, P. Timbal, D. Paz, D. Lorenzo, E. Dellacasa. *Appl. Catal. A*, **2003**, *253*, 177.

[130] N. Das, D. Tichit, R. Durand, P. Graffin, B .Coq. *Catal. Lett.*, **2001**, *71*, 181.

[131] S. Kannan. *Appl. Clay Sci.*, **1998**, *13*, 347-362.

[132] R. L. Goswamee, M. Mishra, A. K. Sarma. Mixed metal oxidic nanosheets coated monolithic catalysts useful for the decomposition of N_2O and a process for the

preparation thereof. *Patent No*. WO/2014/080428.

[133] F. Basile, G. Fornasari, V. Rosetti, F. Trifiro, A.Vaccari. *Catal. Today*, **2004**, *91-92*, 293-297.

[134] J. Zhang, N. Zhao, W. Wei, Y. Sun. *Int. J.Hydrog. Energy*, **2010**, *35*, 11776-11786.

[135] D.V. Cesar, M.A.S. Baldanza, C. A. Henriques, F. Pompeo, G. Santori, J. Munera, E. Lombardo, M. Schmal, L. Cornaglia, N. Nichio. *Int. J. Hydrog. Energy*, **2013**, *38*, 5616-5626.

[136] X. Zhang, N. Wang , Y. Xu, Y.Yin , S. Shang. *Catal. Commun*., **2014**, *45*, 11-15.

[137] S. Abate, K. Barbera, E. Giglio, F. Deorsola, S. Bensaid, S. Perathoner, R. Pirone, G. Centi. *Ind. Eng. Chem. Res.*, **2016**, *55*, 8299-8308.

[138] N.G. Blaise Allou, P. Saikia, A. Borah, R. L. Goswamee. *Colloid. Polym. Sci*., **2017**;DOI:10.1007/s00396-017-4047-3.

[139] G. Poernomo, X. Rong. *J. Pharm. Sci.*, **2008**, *97*, 4367-4378.

[140] J.C. Dupin, H. Martinez, C. Guimon, E. Dumitriu, I. Fechete. *Appl. Clay Sci.*, **2004**, *27*, 95-106.

[141] A. Valeria, F. Giuseppe, G. Giuliano, P. Luana, C.T. Maria. *AAPS Pharm. Sci.Technol.*, **2002**, *3*, 1-6.

[142] M. Wei, S. Shi, J. Wang, Y. Li, X. Duan. *J. Solid State Chem.*, **2004**, *177*, 2534-2541.

[143] J. Wang, Q. Liu, G. Zhang, Z. Li, P. Yang, X. Jing, M Zhang, T. Liu, Z. Jiang. *Solid State Sci.*, **2009**, *11*, 1597-1601.

[144] B. Valeria, G. Giuliana, M. Francesca, N. Morena, T. Loredana,V. Vittoria. *Appl. Clay Sci.*, **2011**, *52*, 34-40.

[145] J. Chakraborty, S. Roychowdhury, S. Sengupta, S. Ghosh. *Mater. Sci. Eng. C*,

2013, *33*, 2168-2174.

[146] L. Yan, W. Chen, X.Y. Zhu, L.B. Huang, Z.G. Wang, G.Y. Zhu, VAL. Roy, K.N.Yu, X.F.Chen. *Chem. Commun.*, **2013**, *49*, 10938-10940.

[147] J.X. Sheng, M.N. Zhe, X. Qian, X.H. Bao, H. Jun. *J. Solid State Chem.*, **2008**, *181*,2610-2619.

[148] C. Ribeiro, GGC.Arizaga, F. Wypych, M.R. Sierakowski. *Int. J Pharm.*, **2009**, *367*, 204-210

[149] H. Zhang, K. Zou, S. Guo, X. Duan. *J. Solid State Chem.*, **2006**, *179*, 1792-1801.

[150] L. Qin, W. Wang, S. You, J. Dong, Y. Zhou, J.Wang. *Int. J. Nanomedicine*, **2014**, *9*,5701-5710.

[151] Y.Yan, Y. Dai, H. He, Y. Yu, Y.Yang. *Appl.Catal. B:Environ.*, **2016**, *196*, 108-116.

[152] J. H. Choy, S. J. Choy, J. M. Oh and T. Park. *Appl. Clay. Sci.*, **1999**, *121*, 1399.

[153] S. Miyata. US Patent 5, **1985**, 514, 389.

[154] W. Jettka, B. Gajdos, M.D. Benedikt. Eur. Patent EP 715846, to Rhone-Poulenc Rorer Gmbh, Germany, **1996**.

[155] A. Ookubo, K. Ooi, H. Hayashi. *J. Pharm. Sci.*, **1992**, *81*, 1139.

[156] L. Li, W. Gu, J. Liu, S. Yan, Z.P. Xu. *Nano Res.*, **2015**, *8*, 68.

[157] J. H. Choy, S.Y. Kwak, Y.J. Jeong, J.S. Park. *Angew. Chem. Int. Ed.*, **2000**, *39*, 4042.

[158] J. H. Choy, S.Y. Kwak, J.S. Park, Y.J. Jeong. *J. Mater. Chem.*, **2001**, *11*, 1671.

[159] Z. P. Xu, Q. H. Zeng, G. Q. (Max) Lu, A. B. Yu. *Chem. Eng. Sci.*, **2006**, *61*, 1027.

[160] N. Doi, S. Nitta, M. Kusakari, N. Takahashi. *Jpn. Kokai Tokkyo Koho* JP 60, **1984**, *225*, 719.

[161] T. Kwon, G.A. Tsigdinos, T. J. Pinnavaia. *J. Am. Chem. Soc.*, **1988**, *110*, 3653.

[162] M. Shao, J. Han, M. Wei, D. G. Evans, X. Duan. *Chem. Eng. J.*, **2011**, *168*, 519.

[163] K. M. Parida, L. Mohapatra. *Chem. Eng. J.*, **2012**, *179*, 131.

[164] Y. Zhao, S. Zhang, B. Li, H. Yan, S. He, L. Tian, W. Shi, J. Ma, M. Wei, D. G. Evans, X. Duan. *Chem. Eur. J.*, **2011**, *17*, 13175.

[165] D. G. Evans, X. Duan. *Chem. Commun.*, **2006**, 485.

[166] K. Parida, L. Mohapatra, N. Baliarsingh. *J. Phys. Chem. C*, **2012**, *116*, 22417.

[167] K. Parida, L. Mohapatra. *Dalton Trans.*, **2012**, *41*, 1173.

[168] C. G. Silva, Y. Bouizi, V. Fornes, H. Garcia. *J. Am. Chem. Soc.*, **2009**, *131*, 13833.

[169] Y. Lee, J. H. Choi, H. J. Jeon, K. M. Choi, J. W. Lee, J. K. Kang. *Energy Environ. Sci.*,**2011**, *4*, 914.

[170] H. Chen, J.M. Wang, T. Pan, Y.L. Zhao, J.Q. Zhang, C.N. Cao. *J. Electrochem. Soc.*,**2003**, *150*, 1399.

[171] C. Mousty, S. Therias, C. Forano, J.P. Besse. *J. Electroanal. Chem.*,**1994**, *63*, 374.

[172] S. Therias, C. Mousty. *Appl. Clay Sci.*, **1995**, *10*, 10.

[173] C.S. Liao, W.B. Ye. *Electrochim. Acta.*, **2004**, *49*, 4993.

[174] L.Fernandez, C. Borras, J. Mostany, B. Scharifker. Recent Advances in Electrochemical Research, **2012**, 115-140 ISBN: 978-81-7895-545-2.

[175] R. Li, Z.Hu, X. Shao, P. Cheng, S. Li, W.Yu, W. Lin, D. Yuan. *Sci. Rep.*, **2016**, *6*, 18737; DOI:10.1038/srep18737.

[176] A. Vaccari. *Catal. Today*, **1998**, *41*, 53.

[177] A. Vaccari. *Appl.Clay Sci.*, **1999**, *14*, 161.

[178] S. Miyata, M. Kuroda. US Patent 4,299, **1981**,759.

[179] L. Van Der Ven, M.L.M. Van Gemert, L.F. Batenburg, J.J. Keen, L.H. Gielgens, T.P.M. Koster, H.R. Fischer. *Appl. Clay Sci*., **2000**, *17*, 25.

[180] W. Wang, H. Pan, Y. Shi, Y. Pan, W. Yang, K. Liew, L. Song,Y. Hu. Composites, Part A, **2016**, *80*, 259-269.

[181] H. Pan, W. Wang, Q. Shen, Y. Pan, L. Song, Y. Hu, Y. Lu. *RSC Adv.*, **2016**, *6*, 111950.

[182] D.Y. Wang, A. Das, F. R. Costa, A. Leuteritz, Y.Z. Wang, U. Wagenknecht, G. Heinrich. *Langmuir*, **2010**, *26*, 14162-14169.

[183] J. H. Choy. *Solid State Phenomena*, **2006**, *111*, 1-6.

[184] Z. P. Xu, Q. H. Zeng, G. Q. (Max) Lu, A. B. Yu. *Chem. Eng. Sci.*, **2006**, *61*, 1027.

[185] P.S. Braterman, Z.P. Xu, F. Yarberry, In Handbook of Layered Materials, S.M. Auerbach, K.A. Carrado and P.K. Dutta (Eds.), Marcel Dekker, New York, **2004**, 373.

[186] B. A. Hungate, J. S. Dukes, M. R. Shaw, Y. Luo, C. B. Field. *Sci.*, **2003**, *302*, 1512-1513.

[187] J. W. Erisman, J. Galloway, S. Seitzinger, A. Bleeker, K. Butterbach-Bahl. *Cur. Opin.Environ. Sust.*, **2011**, *3*, 281-290.

[188] L. Li, J. Xu, J. Hu, Han. *Environ. Sci. Technol.*, **2014**, *48*, 5290-5297.

[189] E. A. Davidson, D. Kanter. *Environ. Res. Lett.*, **2014**, *9*, 105012.

[190] Drawing Down N_2O to Protect Climate and the Ozone Layer. AUNEP Synthesis Report. ISBN: 978-92-807-3358-7.

[191] S. Rao, K. Riahi. *Energy J.*, **2006**, *27*, 177-200.

[192] R. Ravishankara, J. S. Daniel, R. W. Portmann. *Sci.*, **2009**, *326*, 123-125.

[193] J. Weimann. Best Practice & Research Clinical Anaesthesiology, **2003**, *17*, 47-61.

[194] R. P. Wayne. Chemistry of the Atmosphere, 3rd ed; Oxford University Press: Oxford, U.K., **2000**,775.

[195] P. Wiesen, T. J. Wallington, W. Winiwarter, Reducing N_2O emissions from industry and fossil fuel combustion Drawing Down N_2O to Protect Climate and the Ozone Layer. A UNEP Synthesis Report; United Nations Environment Programme: Nairobi,**2013**. www.unep.org/pdf/UNEPN_2Oreport.pdf.

[196] S. J. Lee, I. S. Ryu, B. M. Kim, S. H. Moon. *Int. J. Green house Gas Control*, **2011**, *5*, 167-176.

[197] D.J. Wuebbles. *Mater. Sci.*, **2009**, *326*, 56-57.

[198] F. Kapteijn, J. Rodriguez-Mirasol, J. A. Moulijn. *Appl.Catal. B:Environ.*, **1996**, *9*, 25.

[199] S. A. Al-Sayari. *The Open Catal. J.*, **2013**, *6*, 17-28.

[200]T.J.Blasing. Recent Greenhouse Gas Concentrations. DOI:10.3334/ CDIAC /atg.032 Updated April **2016**.

[201] J. Wentwort, Short Lived Climate Pollutants; POST Note, POST PN 480; Parliamentary office of Science & Technology: London, U.K., October 8, **2014**.

[202] N. Russo, D. Mescia, D. Fino, G. Saracco, V. Specchia. *Ind. Eng. Chem. Res.*, **2007**, *46*, 4226-4231.

[203] M. Konsolakis. *ACS Catal.*, **2015**, *5*, 6397-6421.

[204] M. Pena, J. Gomez, J.L.G. Fierro. *Appl. Catal. A*, **1996**, *144*, 7-57.

[205] A.A. Yaremchenko, V.V. Kharton, S.A. Veniaminov, V.D. Belyaeb, V.A. Sobyanin,F.M.B. Marques. *Catal.Commun.*, **2007**, *8*, 335.

[206] S. N. Riduan, Y. G. Zhang. *Dalton Trans.*, **2010**, *39(14)*, 3347-3357.

[207] W.Wang, J.Gong. *Front. Chem. Sci. Eng.*, **2011**, *5(1)*, 2-10; DOI:10.1007/s 11705-010-0528-3.

[208] W. R. Harvey and P. Hutton. Current Anaesthesia and Critical Care, **1999**, *10*, 158-163.

[209] H. Tang, S. Li, D. Gong, Y. Guan, Y. Liu. *Front. Chem. Sci. Eng.*, **2017**; DOI:10.1007/s11705-017-1664-9.

[210] D. Tichit , B. Coq. *CATTECH*, **2003**, *7*, 206.

[211] D. Tichit, D. Lutic, B. Coq, R. Durand, R. Teissier, *J. Catal.*, **2003**, *219*, 167.

[212] D. Tichit, C. Gerardin, R. Durand, B. Coq, *Top. Catal.*, **2006**, *39*, 89.

[213] Z. P. Xu, J. Zhang, M. O. Adebajo, H. Zhang and C. H. Zhou. *Appl.Clay Sci.*, **2011**, *53*, 139.

[214] S. Kannan ,C.S. Swamy. *Appl.Catal. B:Environ.*, **1994**, *3*,109-l 16.

[215] Y Ll, J N Armor, *Appl.Catal. B:Environ.*, **1992**, *1*, L21.

[216] J. N. Armor, T. A. Braymer, T. S. Farris, Y. Li, F. P. Petrocelli, E. L. Weist, S. Kannan C. S. Swamy. *Appl.Catal. B:Environ.*, **1996**, *7*, 397.

[217] S. Kannan , C.S. Swamy. *Catal. Today*, **1999**, *53*, 725-737.

[218]J.P.Ramírez,J. Overeijnder, F. Kapteijn and J. A. Moulijn. *Appl.Catal.B: Environ.*, **1999**, *23*, 59.

[219] K. S. Chang, H. Song, Y. S. Park, J. W. Woo. *Appl.Catal. A*, **2004**, *273*, 223.

[220] S. Kannan. *App. Clay Sci.*, **1998**, *13*, 347-362.

[221] L. Obalova, K. Jiratova, F. Kovanda, K. Pacultova, Z. Lacny, Z. Mikulova. *Appl.Catal.B:Environ.*, **2005**, *60*, 289.

[222] L. Chmielarz, M. Rutkowska, P. Kuśtrowski, M. Drozdek, Z. Piwowarska, B. Dudek, R. Dziembaj, M. Michalik. *J. Therm. Anal. Calorim.*, **2011**, *105*, 161.

[223] L. Obalova, K. Jiratova, F. Kovanda, M. Valasakova, J. Balabanova, K. Pacultova. *J. Mol. Catal. A:Chem.*, **2006**, *248*, 210.

[224] L. Obalova, M. Valasakova, F. Kovanda, Z. Lacny, K. Kolinova, *Chem. Papers*,

2004, *58*, 33.

[225] L. Obalova, K. Pacultova, J. Balabanova, K. Jiratova, Z. Bastl, M. Valasakova, Z. Lacny, F. Kovanda. *Catal. Today*, **2007**, *119*, 233.

[226] K. S. Chang, X. Peng, J. *Ind. Eng. Chem.*, **2010**, *16*, 455.

[227] J. Haber, M. Nattich and T. Machej. *Appl.Catal. B:Environ.*, **2008**, *77*, 278.

[228] J. Haber, T. Machej, J. Janas and M. Nattich. *Catal. Today*, **2004**, *90*, 15.

[229] K. Yuzaki, T. Yarimizu, K. Aoyagi, S. I. Ito and K. Kunimori. *Catal. Today*, **1998**, *45*, 129.

[230] S. P. Esclapez, F. E. Lopez-Suarez, A. Bueno-Lopez, M. J. Illan-Gomez, B. Ura, J. Trawczynski, *Top. Catal.*, **2009**, *52*, 1832.

[231] S. Alini, F. Basile, A. Bologna, T. Montanari, A. Vaccari. *Stud. Surf. Sci. Catal.*, **2002**, *143*, 131.

[232] L. Obalova, K. Karaskova, K. Jiratova, F. Kovanda. *Appl. Catal. B:Environ.*, **2009**, *90*, 132.

[233] K. Karaskova, L. Obalova, K. Jiratova, F. Kovanda, *Chem. Eng. J.*, **2010**, *160*, 480.

[234] L. Chmielarz, M. Rutkowska, P. Kuśtrowski, M. Drozdek, Z. Piwowarska, B. Dudek, R. Dziembaj, M. Michalik. *J. Therm. Anal. Calorim.*, **2011**, *105*, 161.

[235] H. Cheng, Y. Huang, A. Wang, L. Li, X. Wang,T. Zhang. *Appl.Catal.B:Environ.* ,**2009**, *89*, 391.

[236] H. Wu, Z. Qian, X. Xu and X. Xu. *Ranliao Huaxue Xuebao*, **2011**, *39*, 115.

[237] L. Obalova, F. Kovanda, K. Jiratova, K. Pacultova, Z. Lacny, *Collect. Czech. Chem. Commun.*, **2008**, *73*, 1045.

[238] L. Obalova, G. Maniak, K. Karaskova, F. Kovanda, A. Kotarba. *Catal. Commun.*, **2011**, *12*, 1055.

[239] L. Xue, C. B. Zhang, H. He and Y. Teraoka. *Catal. Today*, **2007**, *126*, 449.

[240] L. Obalova, K. Karaskova, A. Wach, P. Kustrowski, K. Mamulova-Kutlakova, S. Michalik ,K. Jiratova. *Appl.Catal. A*, **2013**, *227*, 462-463.

[241] T. S. Farris, Y. Li, J. N. Armor, T. A. Braymer, US Patent, 5472677 A, **1995**.

[242] X. Xu, X. Xu, G. Zhang and X. Niu. *Ranliao Huaxue Xuebao*, **2009**, *37*, 595.

[243] J. P. Ramirez, J. M. Garcia-Cortes, F. Kapteijn, M. J. Illan-Gomez, A. Ribera, C. Salinas Martinez de Lecea, J. A. Moulijn. *Appl.Catal.B:Environ.*, **2000**, *25*, 191.

[244] K. Karaskova, L. Obalova, F. Kovanda. *Catal. Today*, **2011**, *176*, 208.

[245] A. Klyushina, K. Pacultova, K. Karaskova, K. Jiratovae, M. Ritzb, D. Fridrichova,A. Volodarskajad, L. Obalova. *J.Mol.Catal.A: Chem.*, **2016**, *425*, 237-247.

[246] R.L. Goswamee, M. Mishra, A.K. Sarma. Mixed metal oxidic nanosheets coated monolithic catalysts useful for the decomposition of N_2O and a process for the preparation thereof. *Patent No*. WO/2014/080428.

[247] R. L.Goswamee, Pinky Saikia, Angana Borah, N'Guadi Blaise Allou. A METHOD FOR THE PREPARATION OF SILICA@ Mg-Al LDH CORE SHELL DERIVED MIXED METAL OXIDE NANO-SHEET BASED COMPOSITE CATALYST FOR DECOMPOSITION OF N_2O IN SYNTHETIC AUTOMOBILE EXHAUST CONDITION".FILE NO. **201611022222.**

[248] M. Lyubovsky, S. Roychoudhury, R.L. Pierre. *Catal. Lett.*, **2005**, *99*, 113; DOI: 10.1007/s10562-005-2103-y.

[249] F. Basile, L. Basini, G. Fornasari, M. Gazzano, F. Trifir, A. Vaccaria. *Chem. Commun.*, **1996**, 2436.

[250] F. Basile, L. Basini, M. D'Amore, G. Fornasari, A. Guarinoni, D. Matteuzzi, G. DelPiero, F. Trifiro, A. Vaccari. *J. Catal.*, **1998**, *173*, 247.

[251] T.Shishido, M. Sukenobu, H. Morioka, M. Kondo, Y.Wang, K. Takaki, K.

Takehira. *Appl. Catal. A*, **2002**, *223*, 35-42.

[252] F. Basile, G. Fornasari, M. Gazzanob, A. Vaccari. *J. Mater. Chem.*, **2002**, *12*, 3296-3303.

[253] K.M. Lee, W.Y.Lee. *Catal. Lett.*, **2002**, *83*, 1-2.

[254] F. Basile, L. Basini, M. D. Amore, G. Fornasari, A. Guarinoni, D. Matteuzzi, G. Del Piero, F. Trifiro, A. Vaccari. *J. Catal.*, **1998**, *173*, 247-256.

[255] Z. Jiang, J. Su, M. O. Jones, H. Shi, T. Xiao, P.P. Edwards. *Energy & Fuels*, **2009**, *23*, 1634-1639.

[256]J. Zhang, W. Wei, Y. Sun. *Catal. Lett.*, **2010**, *135*, 321-329; DOI:10.1007/s10562-010-0268-5.

[257] F. Basile, G. Fornasari, V. Rosetti, F. Trifiro, A.Vaccari. *Catal. Today*, **2004**, *91-92*, 293-297.

[258] J. Zhang, N. Zhao, W. Wei, Y. Sun. *Int. J.Hydrog. Energy*, **2010**, *35*, 11776-11786.

[259] K. Takehira , T. Shishido , D. Shoro, K. Murakami, M. Honda, T. Kawabata, K. Takaki. *Catal. Commun.*, **2004**, *5*, 209-213.

[260] J. Ashok, M. Subrahmanyam, A.Venugopa. *Int. J. Hydrog. Energy*, **2008**, *33*, 2704 – 2713.

[261] F. Basile, P. Benito, G. Fornasari, D. Gazzoli, I. Pettiti, V. Rosetti, A.Vaccari. *Catal.Today*, **2009**, *142*, 78-84.

[262] H. Morioka, Y. Shimizu, M. Sukenobu, K. Ito, E. Tanabe, T. Shishido, K. Takehira. *Appl.Catal. A*, **2001**, *215*, 11-19.

[263] D.V. Cesar, M.A.S. Baldanza, C. A. Henriques, F. Pompeo, G. Santori, J. Munera, E. Lombardo, M. Schmal, L. Cornaglia, N. Nichio. *Int. J. Hydrog. Energy*, **2013**, *38*, 5616-5626.

[264] L. E. Alzamora, J. R. H. Ross, E. C. Kruissink, L. L.V. Reijen. *J. Chem.* Soc.*Faraday Trans.*, **1981**, *77*, 665-681.

[265] A.E. Aksoylu, A. N. Akin, S.G. Sunol, Z.I. Onsen. *Tr. J. Chem.*, **1996**, *20*, 88-94.

[266] A.E. Aksoylu, A.N. Akin, Z.I. Onsen, D.L. Trimm. *Appl. Catal. A*, **1996**, *145*, 185-193.

[267] A.E. Aksoylu, Z.I. Onsen. *Appl. Catal. A*, **1997**, *164*, 1-11.

[268] A. Zhao, W. Ying, H. Zhang, H. Ma, D. Fang. *Catal. Commun.*, **2012**, *17*, 34-38.

[269] S. Abello, C. Berrueco, D. Montane. *Fuel*, **2013**, *113*, 598-609.

[270] S. Abello, C. Berrueco, F. Gispert-Guirado, D.Montane. *Catal. Sci. Technol*., **2015**; DOI: 10.1039/c5cy01200g.

[271] M. Gabrovska, R. E. Kardjieva, D. Crisan, P. Tzvetkov, M. Shopska, I. Shtereva. *Reac. Kinet. Mech. Cat.*, **2012**, *105*, 79-99; DOI:10.1007/s11144-011-0378-0.

[272] L. He, Q. Lin, Y. Liu, Y. Huang. *J. Ener. Chem.*, **2014**, *23*, 587-592.

[273] M. V. Gabrovska, R. M. Edreva-Kardjieva, D. D. Crisan, K. K. Tenchev, D. A. Nikolova, M. Crisan. *Bulgarian Chem.Commun.*, **2013**, *45*, 617-624.

[274] X. Zhang , N.Wang , Y. Xu, Y.Yin , S. Shang. *Catal. Commun*., **2014**, *45*, 11-15.

[275] G. Garbarino, P. Riani, L. Magistri, G. Busca. *Int. J. Hydrog. Energy*, **2014**, *39*, 11557-11565.

[276] N. Bette, J. Thielemann, M. Schreiner, F. Mertens. *Chem. Cat. Chem.*, **2016**, *8*, 1-5.

[277] D. Wierzbickia, R.Debeka, M. Motaka, T. Grzybeka, M.E. Galvezb, P.D. Costab. *Catal. Commun.*, **2016**, *83*, 5-8.

[278] S. Abate, K. Barbera, E. Giglio, F. Deorsola, S. Bensaid, S. Perathoner, R. Pirone, G. Centi. *Ind. Eng. Chem. Res.*, **2016**, *55*, 8299-8308.

[279] M. Nizio, R. Benrabbah, M. Krzak, R. Debek, M. Motak, S. Cavadias, M. E. Galvez, P.D. Costa. *Catal. Commun.*, **2016**, *83*, 14-17.

[280] J. Liu, W.Bing, X. Xue, F. Wang, B. Wang, S. He,Y. Zhang, M. Wei. *Catal. Sci. Technol.*, **2016**, *6*, 3976-3983.

[281] Y. Yan, Y. Dai, H. He, Y. Yu, Y.Yang. *Appl.Catal. B:Environ.*, **2016**, *196*, 108-116.

[282] Z. Li, L. Bian, Q. Zhu,W.Wang. *Kinet.Catal.*, **2014**, *55*, 217-223.

CHAPTER-II

EXPERIMENTAL

2. EXPERIMENTAL SECTION:

2.1. Chemicals and materials:

1. Metal acetylacetonates such as $Ni(acac)_2$, $Al(acac)_3$, $Mg(acac)_2$,$Cr(acac)_3$, $Cu(acac)_2$ and $Zn(acac)_2$ were purchased from commercial suppliers like M/s Sigma Aldrich (with minimum purity 98 % or more).

2. Zinc Oxide (M/S Merck), Copper Oxide (CuO), Chromium Chloride hexahydrate (M/S Loba Chemie), sodium hydroxide (LR grade, M/S S.D. fine chem limited), were used without further purification.

3. TEOS (Tetra-ethyl-orthosilicate) from reputed suppliers like (M/s Acros Scientific, with minimum purity 98 %) were used as a SiO_2 source.

4. Solvents like ethanol and acetone (minimum purity 98 %) were used. These solvents were further distilled, dried and purified and ultra purified whenever required before using.

5. Ammonia (from M/s Merck chemicals), hydrochloric acid (A.R grade, NICE chemicals, India), were used without further purification.

6. Double-distilled water was used for preparation of solutions.

2.2. Physicochemical Characterizations and Equipment used:

2.2.1. Powder XRD analysis:

The powder XRD analysis of the products were carried out in a powder X-ray diffractometer equipment Model Rigaku Ultima IV using Cuk_{α} radiation of a wavelength of 1.54 Å at 40 mA and 40 kV X-ray generator current setting with a step size of $0.2^{o}\ 2\theta\ min^{-1}$.

2.2.2. FT-IR analysis:

Fourier Transform Infrared (FT-IR) spectra of the recrystallised products were

recorded in spectrophotometer (Perkin-Elmer 2000 System) in 4,000-400 cm^{-1} range at a spectral resolution of 4 cm^{-1} using KBr pellets. The concentration of sample in KBr pellet was kept around 0.5 % w/w.

2.2.3. Thermal analysis (TGA-DTG):

The thermo-gravimetric measurements (TGA, DTG and DTA) of dried samples were carried out in a simultaneous TG-DTA analyzer (Model SDT Q600, M/S TA Instruments, USA) using Al_2O_3 as reference at 10 ^oC/min heating rate in argon atmosphere.

The evaluation of kinetic parameters such as activation energy (E_a), pre-exponential factor (A) and reaction order (n) of some selected samples were determined for different conversions using model free iso-conversional approach which is a convenient method for determination of activation energy of conversions having multiple overlapping decompositions. Different models such as Flynn-Wall-Ozawa (FWO), Friedman, Coats-Redfern and Phadnis-Deshpande methods respectively were used for the determination of kinetic parameters.

To check coke deposition of the catalysts used after gas-solid reaction the thermogravimetric analysis were carried out under oxygen atmosphere at a heating rate of 10 ^oC/min.

2.2.4. Zeta potential analysis:

The zeta potential of the samples was measured with the Laser Doppler Velocimetry technique at 25 ^oC under a 10 Mw He-Ne laser (M/S Malvern Instruments Zetasizer Nano Z5). The particle size distribution of these nanocomposites was carried by DLS (Dynamic Light Scattering) technique in zeta sizer (M/S Malvern Instruments Zetasizer Nano Z5).

2.2.5. Brunauer, Emmett and Teller (BET) surface area measurement and pore diameter analysis:

Specific surface area of the samples was recorded *via* Nitrogen gas adsorption at 77 K applying Brunauer-Emmett-Teller (BET) calculations using Autosorb-iQ Station 1 (Quantachrome, USA). Prior to performing the experiment the samples were degassed at 100 ^{o}C for 1.5 hours.

2.2.6. Surface Morphology Study:

Surface morphology of the samples was studied by Field Emission Scanning Electron Microscope (SEM), Transmission Electron Microscope (TEM). Field Emission Scanning Electron Microscopy (FE-SEM) analysis was carried out in Carl Zeiss-Sigma VP equipment, with an accelerating voltage of 20 kV. Before the analysis the samples were dried at 40 ^{o}C in air oven for 1 week to avoid the moisture absorption. Finally, the sample surfaces were gold coated in 100 % vacuum. The chemical composition was identified by using an energy-dispersive X-ray spectroscopy (EDX) attachment present on the scanning electron microscope. The Transmission Electron Microscopy (TEM) images were recorded on a JEOL JEM-2011 electron microscope operated at an accelerating voltage of 200 kV.

2.2.7. Elemental analysis:

Micro analytical (C, H, N) data were obtained with a CHN analyser (model M/S Perkin-Elmer Model PE 2400), from CSIR-NEIST, Jorhat, India.

2.2.8. Estimation of metal ion by Atomic Absorption Spectrometry (AAS):

The estimation of metal ion of the samples was carried out by AAS analysis (model Analyst -100 Perkin Elmer) after digestion of the LDH sample in 6N HCl. The digested samples were diluted 200 times in double distilled water for estimation of

metal ion concentration like Zn^{2+}, Cu^{2+}, Cr^{3+} etc.

2.2.9. X-ray Photoelectron Spectroscopy analysis:

X-ray photoelectron spectroscopy (XPS) measurements were carried out in Thermo Scientific MULTILAB 2000 Base system with X-Ray, Auger and ISS attachments from Thermo Electron of monochromatic Al Kα X-ray source (1486.6 eV). The photoelectron spectra were calibrated in bond energy, referenced to that of the component C-C of carbon C 1s at 284.8 eV.

2.2.10. Mass Spectrometry study:

The mass spectrometry of the samples was carried out in a Trace DSQ GC-MS spectrometer.

2.2.11. Single Crystal analysis:

The single crystal XRD data of mixed-metal acetylacetonate complexes were collected by using a "Bruker Smart" diffractometer equipped with a CCD area-detector and Mo kα radiation (λ = 0.71073 Å) at 296(2) K. The data were refined by using SHELXL-97. The final R_1 = 0.0313 and wR_2 = 0.1177 with the goodness of fit on F^2 was 2.604. For analysing the details about the crystallographic data helps from Cambridge Crystallographic Data Centre software was taken.

2.2.12. Metal Organic Chemical Vapour Deposition of sublimable mixed-metal acetylacetonate complexes:

Metal Organic Chemical Vapour Deposition (MOCVD) of CCAA over honeycomb preforms (from ARCI Hyderabad, India) and glass substrate were carried out by Thermal Vacuum Deposition equipment of model HVT-2015 with voltage of 80 volt and chamber pressure 10^{-4} mbar. Thickness of the thin film deposited was measured during the evaporation of molecules from source to target under vacuum conditions at

a base pressure of 5×10^{-5} Torr with a thickness monitor (model No. DTM-10, Roorkee, India). During the process surrounding temperature was maintained at 27 ^{o}C and the input voltage at 64 volt.

2.2.13. Atomic Force Microscopy analysis of thin film:

The surface topography and root mean square (RMS) roughness of the deposited thin film were measured by atomic force microscope (AFM, Nanomagnetics Instruments, Turkey).

2.2.14. Rheological study of the nanocomposite alcogels of LDH:

Rheological properties of the nanocomposite alcogels were investigated by both rotational and oscillatory rheometer. The steady shear measurements were carried out by rotational rheometer Rheolab QC (Anton Paar) with a measuring cup C-CC27/SS/QC and measuring system CC27/P6 at 15 ^{o}C. The preliminary studies such as variation of viscosity and shear stress with shear strain and the flow modeling of these alcogels were investigated by it. The temperature of 15 ^{o}C was maintained to minimise the concentration change of dispersions by evaporation of organic solvents from the surface. The steady shear measurements were carried out in the shear rate ranging from 100-1000 s^{-1}.

For finer study involving dynamic oscillatory measurement a modular compact rheometer MCR 302 (Anton Paar) with a rough parallel plate geometry of 2.5 cm diameter and 0.1 cm gap was used at 15 ^{o}C. The sample was submitted to the parallel-plate and the amplitude of oscillation was increased up to 500 % apparent shear strain maintaining the angular frequency at 1 rad/s for the amplitude sweep test. For the frequency sweep test the shear strain was kept at 5 %. The oscillatory rheometer gave data of viscoelastic properties $G^{/}$(Storage modulus) and $G^{//}$(Loss modulus).

2.2.15. Coating of the nanocomposite alcogels over ceramic preforms:

Coating of the nanocomposite alcogels were carried out on some solid preforms like α-alumina (M/S Naskar Ceramics, Kolkata, India), honeycomb monolithic substrates like Cordierite (MgO-Al_2O_3-SiO_2, manufactured by M/S Ceramic Technology Institute, BHEL, Bangalore, India) and ZrO_2-Al_2O_3-SiO_2 (M/S SCT, France) and supplied by M/S ARCI (DST) Hyderabad. For dip coating the supports were vertically hanged and coating was done at 2.0 cm/min dipping, withdrawing rates and the substrate was kept submerged in the solution for 1 minute using a dip-coater (Model KSVD Dipcoater, Finland).

2.2.16. High Intensity Ultrasonic processor for homogenization:

The composite gels were mixed well by sonochemical shaking in high intensity ultrasonic processor (model vibracel VCX 500, Sonics and Materials Inc., USA) using solid titanium horn of length 1 inch. The operating parameters of the sonicator were 20 kHz ±50 Hz frequency at 35 % amplitude for 10 min with 4 sec pulse on and 2 sec pulse off mode at room temperature.

2.2.17. Laboratory Centrifuge:

Laboratory centrifuge (model M/S REMI R24) was used for separation of the precipitate from the prepared solutions.

2.2.18. Calcination of the samples in muffle furnace:

Before the gas-solid reaction the synthesized LDHs were calcined in an electrical muffle furnace, Model No. PID-1173D at 450 ^{o}C. The furnace was regularly calibrated by Electronics Control and Testing Services Center, Guwahati Assam under No. Department of Electronics Govt of India under calibration contract STQC Calibration F02720.

2.2.19. H_2-TPR analysis of the calcined samples:

Hydrogen temperature programmed reduction (H_2-TPR) was performed in Quantachrome ChemBET Pulsar TPR/TPD instrument in a quartz U-tube using a TCD detector. Temperature programmed reduction (TPR) of the sample was carried out by taking 90 mg of the sample. The reducing gas was a mixture of 5 vol % H_2 in N_2, at a flow rate of 80 ml/min. The temperature was increased at a rate of 20 ^oC/min from 40 ^oC to 750 ^oC.

2.2.20. Tubular furnace for gas-solid reaction:

Horizontally placed multi-segment tubular furnace (from M/S Sonnu Electrical, Kolkata) was used for Gas-Solid reactions. The temperature of the furnace for the reactivity of the catalytic/adsorptive reactivates was maintained at 200-500 ^oC in N_2O decomposition study as well as CH_4 partial oxidation reaction and CO_2 methanation reaction was carried out at 200-500 ^oC.

2.2.21. Designing of reactor containing honeycomb monoliths in tubular Stainless Steel configurations:

The stainless steel tube of length 304.8 cm and diameter 0.8 cm for the gas-solid reaction study was designed in the laboratory using ceramic wool and powdered catalysts inside it with both ends closed with rubber tubes having holes for tubing of the inlet and the outlet gases.

The stainless steel reactor was designed by the ARCI Hyderabad, India to carry out the gas-solid reaction. The stainless-steel catalytic converter has reaction area 77.8 cm^2, length 11 cm and inner diameter 0.6 cm. The honeycombs like Cordierite (MgO-Al_2O_3-SiO_2), had 360 cells per square inch and a 3.2 cm diameter (from ARCI Hyderabad, India).

2.2.22. Gas Chromatography for gas concentration study:

The Gas-solid reaction study for the decomposition/adsorption of some environmentally harmful gases like N_2O, CH_4 ,CO_2, CO were carried by Gas Chromatograph GC Chemito 1000 (from M/S Thermo-Fischer Scientific, India). The detectors used were Thermal Conductivity Detector (TCD), Electron Capture Detector (ECD) and Flame Ionization Detector (FID). The Porapak Q column for N_2O separation and a Molsieve 5A column for N_2 and O_2 separation were used. For decomposition study, the oven temperatures were maintained at 50 ^oC, at a carrier gas flow rate 25 ml/min and at 150 ^oC TCD temperature. The length of Porapak Q column was 304.8 cm in length having diameter of 0.32 cm. The concentration of CH_4 was measured by Flame Ionization Detector (FID) in GC. Calibration of GC was done from a premixed calibration standard containing N_2O, N_2 and O_2 at standard ppm with balanced Nitrogen. The product gases such as CO and CH_4 were detected by FID detector and H_2 was detected by TCD detector in a Molsieve 5A Q column by keeping the oven temperature at 50 ^oC in presence of argon as a carrier gas with flow rate of 25 ml/min and at 180 ^oC TCD temperature. The low concentration of CO_2 and CO was detected by Ni-Catalytic Reactor attachment fitted in the GC. The length of the Molsieve 5A Q column was 243.84 cm having a diameter of 0.32 cm. The product gases were collected at different interval in 1 litre capacity Tedler bags from the outlet of the SS tube. The flow rate of the gas was controlled by different types of gas flow meter obtained from M/S Gilmont, USA under atmospheric pressure. Before the catalytic reactions the catalysts were activated under a pure H_2 flow (100 ml/min flow rate) at a temperature of 500 ^oC for 2 hours. The results were estimated with standard calibration gas mixtures supplied by M/S Span Gas Mumbai, India and standard Gas

Chromatographic software IRIS-32 from M/S Thermo-Fischer India.

CHAPTER-III

SYNTHESIS AND CHARACTERIZATIONS OF BINARY LDHS OF Ni-Al, Mg-Al, Ni-Cr, Mg-Cr, Zn-Al AND THEIR SiO_2@LDH NANOCOMPOSITES BY NON-AQUEOUS SOL-GEL METHOD AND THEIR APPLICATION FOR N_2O DECOMPOSITION AND CH_4 OXIDATION

CHAPTER-III
PART-A

SYNTHESIS AND CHARACTERIZATIONS OF BINARY LDHS OF Ni-Al, Mg-Al AND THEIR SiO_2@LDH NANOCOMPOSITES BY SOFT CHEMICAL SOL-GEL METHOD FOR THE TREATMENT OF N_2O,CO,CO_2 AND CH_4

- Some part of this work has been published in ***Materials Chemistry and Physics, 186 (2017) 52-60***.

GRAPHICAL ABSTRACT

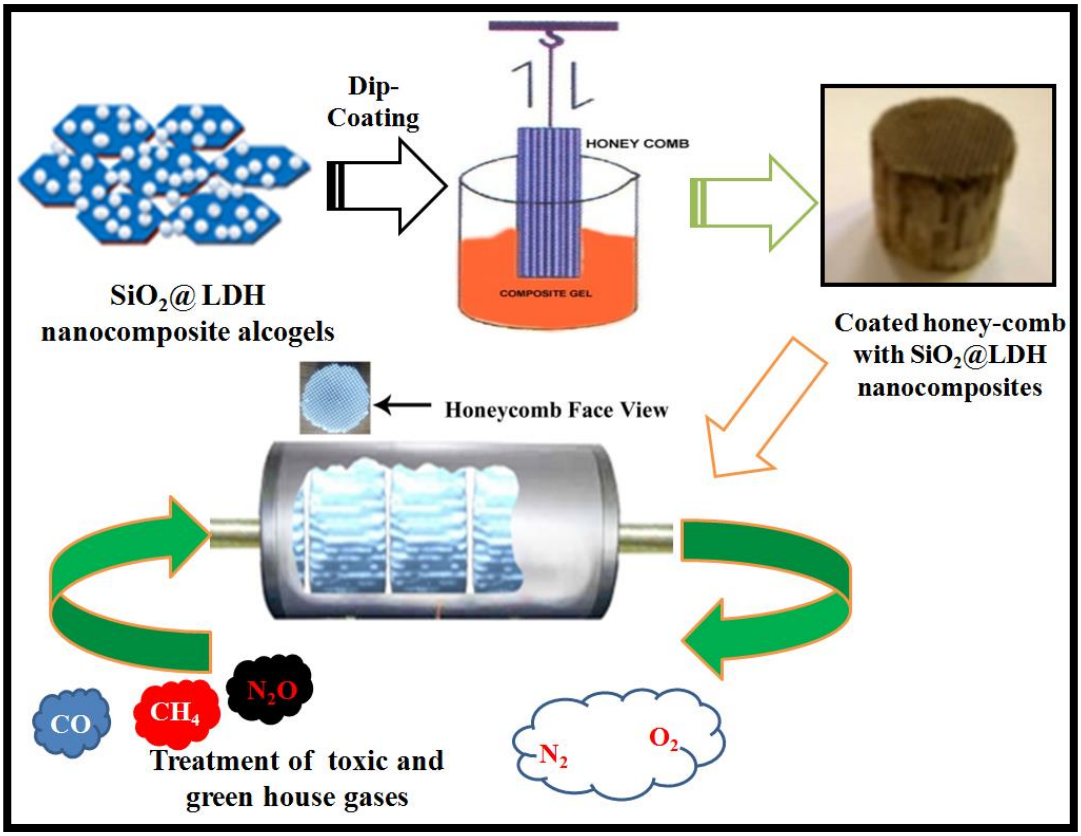

Treatment of N_2O, CO and CO_2 over SiO_2@Ni-Al-LDH/ SiO_2@Mg-Al-LDH nanocomposites coated over honeycomb monolith

ABSTRACT

This **part** describes about synthesis, characterisation and some application prospects of different binary LDHs such as Ni-Al, Mg-Al and their SiO_2 nanocomposites. These were synthesized by non-aqueous sol-gel route using different metal acetylacetonates as precursors such as $Ni(acac)_2$, $Mg(acac)_2$ and $Al(acac)_3$. These were then characterized by XRD, TGA, SEM-EDS, HR-TEM, FT-IR, Rheometry, Zetametry, Particle size analysis and BET surface area analysis. Both the unsupported and SiO_2 supported LDHs were then coated over honey comb monoliths by dip coating and calcined at 450 ^oC to form as mixed-metal nano oxide. This **part** also describes the use of both powdered as well as honey comb coated mixed metal oxide catalysts for the decomposition of N_2O and treatment of CO, CO_2 and CH_4.

3.A.1. INTRODUCTION:

Nitrous oxide (N_2O) is a powerful greenhouse gas with a global warming potential (GWP) about 300 times higher than that of CO_2. At the same time it also notably contributes to stratospheric ozone depletion [1-3]. Now-a-days, N_2O emissions have significantly increased compared to the pre-industrial period due to different human activities. This includes uses of chemical fertilizers, the combustion of fossil fuels and the large scale production of chemicals like nitric and adipic acid [1,4]. Mainly, from the global environment maintenance point of view the control of N_2O emissions from combustion and chemical processes have significant importance. A number of methods can potentially be employed to remove N_2O emissions, including: thermal decomposition [5], selective adsorption [5,6], decomposition by the use of plasma technology [5] and catalytic decomposition [5]. Catalytic decomposition offers a number of advantages over these alternative technologies for controlling N_2O emissions, including lower energy requirements and lower cost [8,9].

In earlier literatures different catalytic materials such as Fe-MFI [9-13]; LDHs [14-22]; SBA-15 based catalysts [23]; Co or Ni supported on MgO [24]; Pd-ZSM-5, Fe-ZSM-5 [11-13,25]; Mixed oxide catalysts [22]; Iron incorporated aluminophosphate molecular sieves Fe-FAPO-5 (FAPO) [26,27]; Zeolite coating on solid supports [11,28]; Rh supported on metal oxides like ZnO or CeO_2 [29]; Fe-Ferrierite catalysts [30]; Rh free Co-based ex-hydrotalcite containing Pd [19], Fe(II) [31]; Non noble metal oxide catalyst [4]; Perovskite catalyst[3]; Doubly-promoted Pt(K)/Al_2O_3-(CeO_2-La_2O_3) structured catalysts [32]; Ceria-promoted Ir/Al_2O_3 catalysts [33]; Al_2O_3 supported noble metals (Pt, Pd, Ir) [34]; RhO_x supported on metal phosphates [35]; CoO_x, CuO_x, FeO_x or MnO_x supported on ZrO_2 [36] have been reported for decomposition of N_2O gas. In all these experiments catalytic decomposition were

carried out at high temperature at above 700 ^{o}C which thus would require heating of the gas and the catalyst for effective catalytic decomposition. To replace such type of catalysts we have used mixed metal oxide nanocomposite catalyst obtained from Layered Double Hydroxides and silica supported Layered Double Hydroxides synthesized by sol-gel method which have better physico-chemical properties and were used at low temperature for the decomposition of N_2O.

Layered Double Hydroxides (LDHs) are a class of nano sheet type materials with $Mg(OH)_2$ (brucite) like layers and different intercalated anions which are presented by the general formula $[M_{1-x}{}^{2+}M_x{}^{3+}(OH)_2]^{x+}[A_{x/n}]^{n-}.m\ H_2O$, where divalent and trivalent cations may be Ni^{2+}, Zn^{2+}, Cu^{2+}, Mg^{2+}, Al^{3+}, Cr^{3+}, Ga^{3+}, Fe^{3+} and A^{n-} may be any organic or inorganic anions [37-40]. LDH can be synthesized by different methods such as co-precipitation method, hydrothermal method, oxide hydrolysis method and sol-gel hydrolysis method [41-45]. Synthesis of LDH and its different nano-composites using sol-gel route is a relatively recent approach having prospect for fabrication of multifunctional materials as it give the products in the colloidal particles range with finer particle size in a non-aqueous medium [46-50]. Having such nano-sheet type particles of catalytically important materials like LDH well distributed as a dispersion in a non aqueous solvent bear important advantages for different materials processing routes like dip and spin coating [47].

In this chapter we have also discussed about the thermal degradation kinetic study of Ni-Al-LDH synthesized by soft-chemical sol-gel method with the help of Thermogravimetry analysis. Thermogravimetry (TG) analysis has been used for the measurement of kinetics and Arrhenius parameters of the decomposition of materials. TG and DTA techniques involve the continuous measurement of physical properties such as weight and heat capacity. It is possible to calculate the kinetic parameters from

these techniques by making a number of patterns at different heating rates. Several methods are known to calculate the kinetic parameters of solid-state reactions based on Arrhenius rate law [51]. To investigate the thermal degradation kinetics the most preferably used methods are model-free iso-conversional methods namely- Flynn-Wall-Ozawa (FWO), Coats-Redfern, Kissinger-Akahira-Sunose, Friedman methods [52-58] and are convenient methods for the determination of kinetic parameters such as activation energy (E_a), pre-exponential factor (A) and reaction order (n) of conversions in a reliable way. Iso-conversional kinetic analysis involves evaluating a dependence of the effective activation energy on the conversion level or temperature and simultaneously use of this dependence for making kinetic predictions and thereby exploring the mechanisms of the thermally stimulated processes [59]. The thermal degradation kinetics of Ni-Al-LDH synthesized was investigated by using model-free iso-conversional methods such as FWO, Friedman, Coats-Redfern [60] and Phadnis-Deshpande method [61]. We have calculated from the thermo gravimetric data the kinetic parameters such as activation energy (E_a), pre-exponential factor (A) and reaction order (n) as well as the solid-state mechanism involved in the thermal degradation of Ni-Al-LDH by using these methods.

In this chapter we have used Layered Double Hydroxides (LDHs) of Ni-Al and Mg-Al and their SiO_2 supported products as catalysts for N_2O decomposition reaction at low temperature.

3.A.2. EXPERIMENTAL SECTION:

3.A.2.1. Synthesis of binary LDHs of Ni-Al and Mg-Al:

3.A.2.1.1. Ni-Al-LDH:

3.A.2.1.1a. Materials:

Metal acetylacetonates such as $Ni(acac)_2$ (Nickel acetylacetonate), $Al(acac)_3$

(Aluminium acetylacetonate) were purchased from Sigma Aldrich (98 % pure) and ammonia, ethanol, acetone from Merck chemicals (purity 98 %). Ethanol and acetone were distilled, dried and purified before using [62].

3.A.2.1.1b.Purification and distillation of Ethanol [62]**:**

Purification of ethanol involved reaction with magnesium ethoxide prepared by adding 5g of clean dry magnesium turnings and 0.5 g iodine in a 2L flask, followed by 50-75 ml absolute ethanol and warming the mixture until a vigorous reaction occurs. Heating was continued until all of the magnesium was converted to the ethoxide. Upto 1L of ethanol was added and then refluxed for 1 hour after that it was distilled off.

3.A.2.1.1c.Purification and distillation of Acetone [62]**:**

Acetone was purified from oxidizable impurities by refluxing with $KMnO_4$ until to change colourless mixture, followed by shaking with Na_2CO_3 to remove acidic impurities and distilling. 4A type Linde molecular sieve was added to the refluxing solvent to remove traces of water.

3.A.2.1.1d. Synthesis of Ni-Al-LDH by non-aqueous soft chemical sol-gel method:

Ni-Al-LDH was prepared by soft chemical method as reported in previous literature [45, 50] by the following steps; firstly, 0.02 mol $Ni(acac)_2$ was dissolved in 80 cm^3 of distilled ethanol followed by dissolution of 0.007 mol $Al(acac)_3$ in 80 cm^3 ethanol acetone (1:1) in a separate container. Mixed the both solutions at 80 ^oC and refluxed for 2 hours. Followed by, adding warm 1:2 NH_3:H_2O solutions to raise the pH of the mixture to 8-9. The resulting suspensions were continuously stirred for another 6-7 hours under a flow of Nitrogen gas. Extra care was taken to avoid the presence of unreacted $Ni(acac)_2$ in the product by carrying out the reaction at 80 ^oC for 7-8 hours, so that all the $Ni(acac)_2$ is completely hydrolysed The products of hydrolysis were separated from the suspensions by filtration, washed with hot water and dried at room

temperature in a vacuum desiccator to avoid attack by atmospheric carbon-di-oxide in the interlayer space of LDH nanosheets.

3.A.2.1.1e. Synthesis of Ni-Al-LDH by Co-precipitation method:

On the other hand, for comparison with the sol-gel products, Ni-Al LDH was also synthesised by co-precipitation method using $NiCl_2.6H_2O$ (Nickel Chloride hexahydrate), $AlCl_3.6H_2O$ (Aluminium Chloride hexahydrate), Na_2CO_3 (Sodium Carbonate) and 1M NaOH (Sodium Hydroxide) aqueous solutions as reported in the previous literature [43].

3.A.2.1.2.Mg-Al-LDH:

3.A.2.1.2a.Materials:

Metal acetylacetonates such as $Mg(acac)_2$ (Magnesium acetylacetonate), $Al(acac)_3$ (Aluminium acetylacetonate) were purchased from Sigma Aldrich (98 % pure) and ammonia, ethanol, acetone from Merck chemicals (purity 98 %). Ethanol and acetone were distilled, dried and purified before using [62] as described above.

3.A.2.1.2b. Synthesis of Mg-Al-LDH by non-aqueous soft chemical sol-gel method:

0.02 mol Magnesium acetylacetonate $Mg(acac)_2$ was dissolved in 80 cm^3 of distilled ethanol. 0.007 mol Aluminium acetylacetonate $Al(acac)_3$ was dissolved in 80 cm^3 ethanol acetone (1:1) mixture. These two solutions were mixed at 80 ^oC and after refluxing for 2 hours and raising its pH up to 10 by adding 1:2 NH_3:H_2O mixture the resulting suspensions were continuously stirred for 3-4 hours. The hydrolysis products were separated from the suspensions by filtration, washed in hot water and dried at room temperature. The yield of Sg Mg-Al LDH was ≈12 g. The products were finally washed with distilled water, dried in air oven and kept in plastic bottle.

3.A.2.2. Synthesis of SiO_2 supported nanocomposite alcogels of Ni-Al and Mg-Al LDHs:

3.A.2.2.1. Materials:

Metal acetylacetonates such as $Ni(acac)_2$, $Mg(acac)_2$ and $Al(acac)_3$ were purchased from Sigma Aldrich (98 % pure), TEOS (Tetraethyl orthosilicate from Acros Scientific, purity 98%), ethanol and acetone (from Merck chemicals, purity 98 %), ammonia were used. Ethanol and acetone were distilled, dried and purified before using [62]. Here, TEOS was used as SiO_2 source.

3.A.2.2.2. Synthesis:

It involves the following steps-

Step-1: 0.02 mol Nickel acetylacetonate ($Ni(acac)_2$)/Magnesium acetylacetonate ($Mg(acac)_2$) was dissolved in 80 cm^3 of distilled ethanol at pH 6.

Step-2:0.007 mol Aluminium acetylacetonate ($Al(acac)_3$) was dissolved in 80 cm^3 ethanol:acetone (1:1) mixture.

These two solutions were mixed at 80 ^oC by stirring for 2-3 hours. The pH of the mixture was maintained at 8-9 by adding few drops of 1:2 NH_3:H_2O mixture and finally refluxed for 6-7 hours to get Ni-Al-LDH and Mg-Al-LDH. The product obtained was then filtered and dried in air oven at 40 ^oC. 4.43 cm^3 TEOS, 0.72 cm^3 of 0.2 M aqueous HCl and 4.85 cm^3 distilled ethanol were taken and aged the mixture for 45 min in a magnetic stirrer at room temperature. The solutions of step -1 and step-2 were mixed at 80 ^oC and refluxed for 2 hours. Added hydrolysed TEOS to the mixed acetylacetonate solution and raised the pH upto 8-9 by adding 1:2 NH_3:H_2O mixture stirred continuously for another 6-7 hours to get silica supported LDH. A portion of the product was separated from the obtained free flowing gels by filtration, washed in hot water and dried at 40 ^oC in air oven. The SiO_2 supported LDHs were synthesized by

varying SiO_2 to LDH ratio. The schematic diagram is shown below-

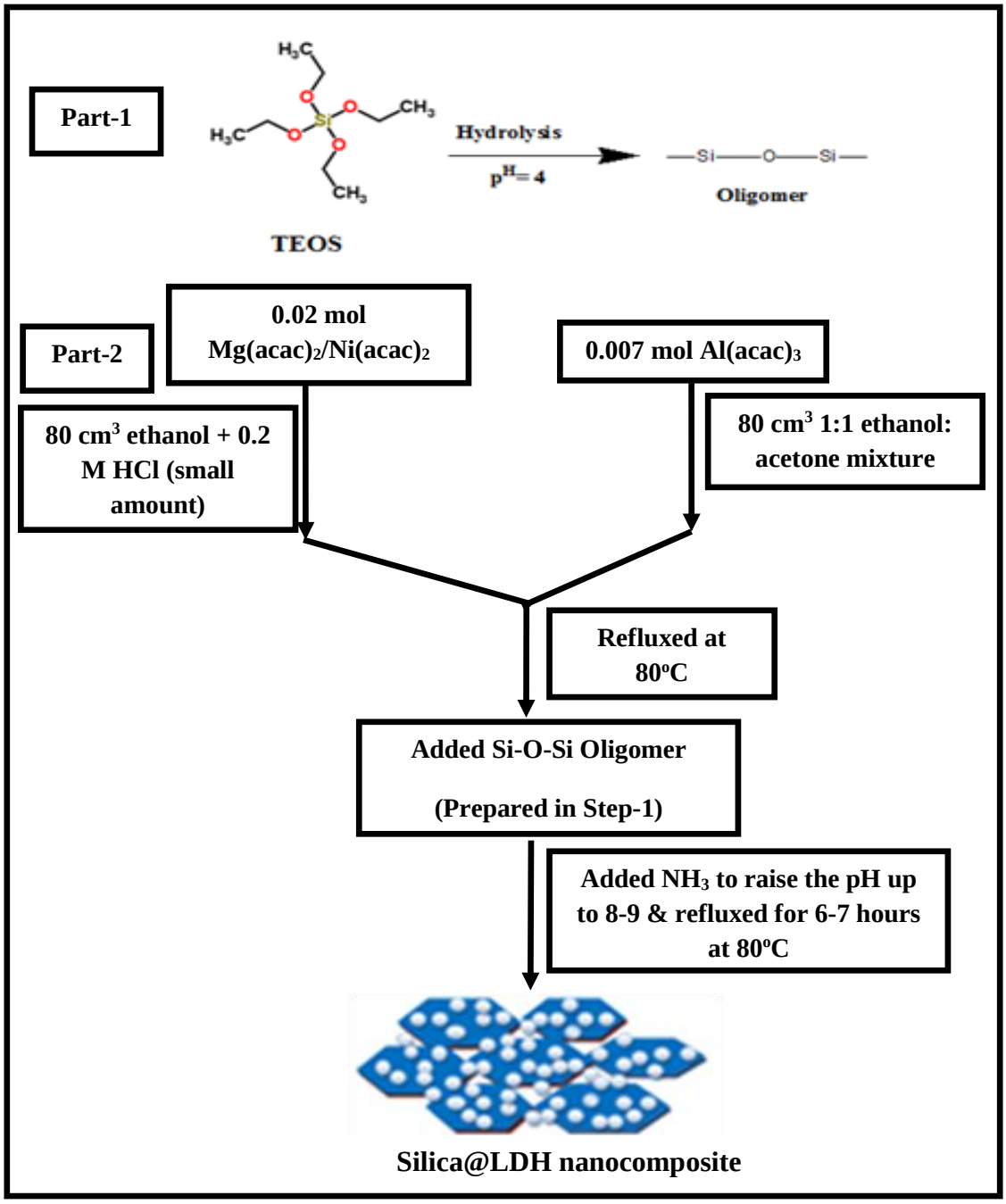

Fig. 3.A.1: Schematic diagram for the synthesis of SiO_2@LDH nanocomposite gels.

3.A.2.3. Characterizations:

3.A.2.3.1. Characterizations of unsupported Ni-Al-LDH and Mg-Al-LDH:

Powder X-Ray Diffractometric (PXRD) characterization of Ni-Al-LDH synthesised

were carried out using powder X-ray diffractometer (Model Rigaku Ultima IV) using Cuk$_\alpha$ radiation of a wavelength of 1.54 Å at 40 mA and 40 kV X-ray generator current setting with a step size of 0.2^{o}2θ min^{-1}.

Fourier Transform Infrared (FT-IR) spectra of the prepared samples were recorded in spectrophotometer (Perkin-Elmer 2000 System) in 4000-400 cm^{-1} range at a spectral resolution of 4 cm^{-1} using KBr pellets.

Scanning electron microscopy (SEM) analysis was carried out in a JEOL, JSM6390LV with an accelerating voltage of 20 kV. The samples surface for SEM was coated by Platinum. Transmission electron microscopy (TEM) images were recorded on a JEOL JEM- 2011 electron microscope operated at an accelerating voltage of 200 kV.

The thermo gravimetric measurement of the samples were carried out in a simultaneous TG-DTA analyzer (model Q-600, M/S TA Instruments) using α -Al_2O_3 as reference. Samples weighing about 10.0 mg were heated from 30 to 1000 ^{o}C at heating rate (β) of 10 ^{o}C/min in an Argon atmosphere in a non-isothermal condition. The Argon flow rate for purging was maintained at 100 ml min^{-1}.

3.A.2.3.1a. Kinetic study of Ni-Al-LDH:

The thermal degradation kinetics of Ni-Al-LDH synthesized was investigated by using model-free iso-conversional methods such as Flynn-Wall-Ozawa (FWO), Friedman, Coats-Redfern and Phadnis-Deshpande method [287-295]. Different kinetic parameters such as activation energy (E_a), pre-exponential factor (A) and reaction order (n) as well as the solid-state mechanism involved in the thermal degradation of Ni-Al-LDH by using these methods from the thermo gravimetric data.

To study the kinetic parameters of Ni-Al-LDH the thermo gravimetric measurement was carried out in a simultaneous TG-DTA analyzer (model Q-600, M/S TA

Instruments) using α -Al_2O_3 as reference. Samples weighing about 10.0 mg were heated from 30 to 1000 ^oC at various heating rates β viz. 5, 10, 15, 20 and 30 ^oC/min in an Argon atmosphere in a non-isothermal condition. The Argon flow rate for purging was maintained at 100 ml/min.

3.A.2.3.2a. Characterizations of SiO_2 supported nanocomposite alcogels of LDHs:

XRD analysis of the SiO_2 supported nanocomposite alcogels of LDHs in powdered form with different SiO_2:LDH ratios were carried out in a powder X-ray diffractometer (Model Rigaku Ultima IV) using Cuk_α radiation of a wavelength of 1.54 Å at 40 mA and 40 kV X-ray generator current setting with a step size of 0.2^o 2θ min^{-1}.

Fourier Transform Infrared (FT-IR) spectra of the prepared samples were recorded in spectrophotometer (Perkin-Elmer 2000 System) in 4,000-400cm^{-1} range at a spectral resolution of 4 cm^{-1} using KBr pellets.

Field Emission Scanning Electron Microscopy (FE-SEM) analysis was carried out in a Carl Zeiss -Sigma VP equipment, with an accelerating voltage of 20 kV. Before the analysis the gels were dried at 40 ^oC in air oven for 1 week to avoid the moisture absorption.Finally, the sample surfaces were gold coated in high vacuum. Transmission electron microscopy (TEM) images were recorded on a JEOL JEM-2011 electron microscope operated at an accelerating voltage of 200 kV. The chemical composition was identified by using an energy-dispersive X-ray spectroscopy (EDX) detector on the scanning electron microscope Model Carl Zeiss Sigma VP.

The thermogravimetric measurements were carried out in a simultaneous TG-DTA analyzer (model Q-600, M/S TA Instruments) using α -Al_2O_3 as reference. Samples weighing about 5.0 mg were heated from 30 to 700 ^oC at a rate of 10 ^oC/min in an Argon atmosphere in a non-isothermal condition.

Specific surface area of the samples was recorded *via* Nitrogen gas adsorption at 77K

applying Brunauer-Emmett-Teller (BET) calculations using Autosorb-iQ Station 1 (Quantachrome, USA). Prior to performing the experiment the samples were degassed at 100 ^{o}C for 1.5 hours.

The zeta potential of the nanocomposite alcogels were measured with the Laser Doppler Velocimetry technique at 25 ^{o}C under a 10 Mw He-Ne laser (M/S Malvern Instruments Zetasizer Nano Z5). The particle size distribution of these nanocomposites was carried by DLS (Dynamic Light Scattering) technique in zeta sizer (M/S Malvern Instruments Zetasizer Nano Z5). To carry out these studies the samples were filtered, washed with hot water and dried in air oven at 40 ^{o}C. The dried mass were ground gently in an agate mortar and redispersed in aqueous phase by shaking in an ultrasonic processor (M/S Sonics) with a 1.3 cm Ti probe for 30 minutes under 20 kHz frequency and 25 % amplitude of vibration.

3.A.2.3.2b. Rheological study of SiO_2@Ni-Al/Mg-Al nanocomposite alcogels of LDHs:

The rheological study of the nanocomposite gels with different SiO_2:LDH ratios of SiO_2@Ni-Al/Mg-Al-LDHs were carried out by rotational (Rheolab QC - Anton Paar, Austria) with a measuring cup C-CC27/SS/QC and measuring system CC27/P6 at 15 ^{o}C.

3.A.2.4. Coating of SiO_2 supported nanocomposite alcogels of LDHs over solid preforms:

Different types of SiO_2 supported nanocomposite alcogels of LDHs such as SiO_2 @Mg-Al-LDH, SiO_2@Ni-Al-LDH with different SiO_2 to LDH ratios were coated over Cordierite (MgO-Al_2O_3-SiO_2) honeycomb ceramic monolith by a dip coater (KSVD from M/S KSV Instrument, Finland) at 2 cm/min speed withdrawal and dipping rate as shown in **Fig. 3.A.2**. The honeycombs had 360 cells per square inch and a 3.2 cm

diameter. The honey comb monolithic catalysts were supplied by DST-ARCI Hyderabad, India under a collaborative agreement. Before dip-coating, the solid pre-forms were washed with distilled water and dried in air at 110 °C for 2 hours. After dip coating the coated honey comb monoliths were then withdrawn, kept hanging for few minutes.The dip-coated honey comb monoliths were dried overnight at room temperature followed by heating in air at 40°C. The thicknesses of the coats were varied by changing the SiO_2:LDH ratios.

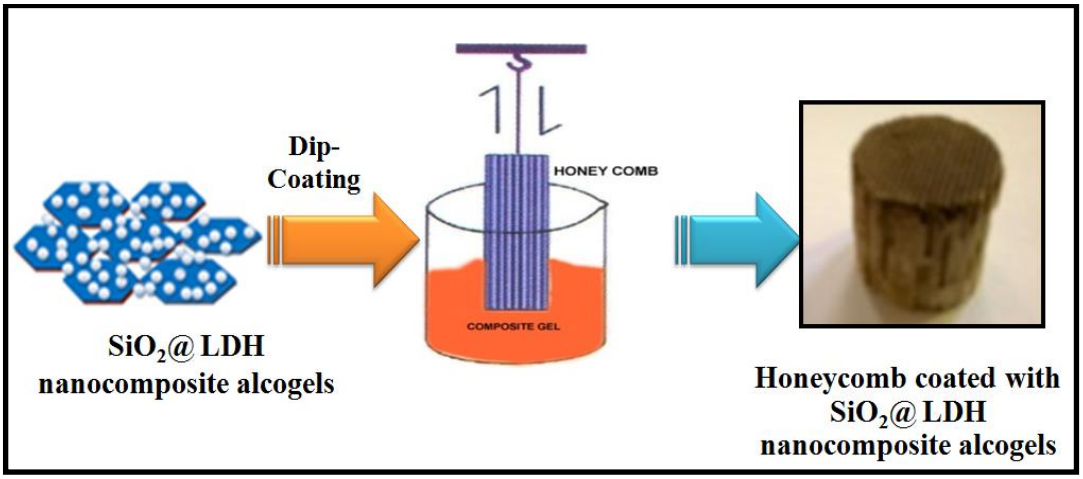

Fig. 3.A.2: Dip coating of SiO_2 supported LDH nanocomposites

3.A.2.5. Gas-solid reaction over both powder and honeycomb coated calcined SiO_2@Ni-Al-LDH and SiO_2@Mg-Al-LDHs:

3.A.2.5.1a. Preparation of the catalysts:

The catalyst were prepared by calcining both synthesized powdered and thin films of SiO_2 supported and unsupported LDHs coated over honeycomb monolithic structured catalysts in a muffle furnace under air at 450 ^oC to get mixed-metal nano-oxide. The calibration of the furnace was carried out by STQC Calibration No. F02720, Model No. PID-1173D at 450 ^oC.

3.A.2.5.1b. Characterizations of catalysts:

The calcined samples were also further characterized by PXRD, TGA-DTG, FT-IR,

SEM & EDS, BET surface area analysis etc.

3.A.2.5.2. N_2O decomposition study:

N_2O decomposition study was carried out over both in powder and honey comb coated calcined SiO_2 supported and unsupported Ni-Al-LDH and Mg-Al-LDHs.

3.A.2.5.2a. N_2O decomposition study over SiO_2@Ni-Al-LDH:

N_2O decomposition study over powdered calcined SiO_2 supported (0:1 to 1:2) and unsupported Ni-Al-LDHs were carried out at temperature 450 ^oC. The initial concentration of N_2O was maintained at 200 ppm (4.50 mmol). Before the catalytic reaction the catalyst were activated in presence of argon atmosphere in the flow rate of 100 ml/min for 2 hours at 450 ^oC. The flow rate of N_2O:Argon was maintained as 100:100 ml/min. The Gas Hourly Space Velocity (GHSV) was maintained at 8,523 h^{-1} (12,000 $cm^3g^{-1}h^{-1}$).

The catalytic reaction was carried out by packing the catalysts in a stainless steel tube (SS tube) of internal diameter 0.8 cm and length of 304.8 cm. The catalyst was kept at the middle portion of the reactor and was guarded with two glass wool plugs placed on its either sides to obtain 1.4 cm bed height. The amount of catalyst packed was about ~ 0.5 g. The catalyst packed in stainless steel reactor was fitted in a vacuum tubular furnace for the gas decomposition studies. The tubular furnace was custom built for the purpose. It had two heating zones- Segment No 1 with a maximum working temperature 900 ^oC and in Segment No 2 with a continuous working temperature upto 1250 ^oC, and maximum working temperature 1300 ^oC. The dimensions of Segment No 1 were as- diameter of 4cm, length of 100 cm and dimensions of Segment No 2 were as- length of 15cm, overall length 50 cm and diameter of hot zone 4 cm and the overall length of the furnace was 150.0 cm.

The flow of the gas was maintained by different types of flow meters. The flow rate

for N_2O decomposition reaction in presence of SiO_2@Ni-Al-LDH was maintained at 100 ml/min. The flow meters used were obtained from M/S Gilmont, USA. The furnace temperatures during the collection of decomposed gases were kept around 450 ^oC. The decomposed gases were collected in previously evacuated Tedlar bags of 1 litre capacity. The collected gases were analysed by gas chromatography (Model Chemito 1000 from M/S Thermo-Fischer, India) equipped with detectors like Thermal Conductivity Detector (TCD), Electron Capture Detector (ECD). Nickel Catalytic Reactor (NCR) using a Porapak Q column was used for N_2O separation and a Molsieve 5A column for N_2 and O_2 separation. The oven temperatures were maintained at 80 ^oC, at a carrier gas flow rate 25 ml/min and at 180 ^oC TCD temperature. The length of Porapak Q column was 304.8 cm in length having diameter of 0.32 cm.

For detection and estimation of N_2O at low concentration by ECD the oven temperature was maintained at 80 ^oC, at a carrier gas flow rate 25 ml/min and at 300 ^oC detector temperature. The length of Molsieve 5A Q column was 243.84 cm having a diameter of 0.32 cm.The results were estimated with standard calibration gas mixtures supplied by M/S Span Gas Mumbai, India and standard Gas Chromatographic software IRIS 32 from M/S Thermo-Fischer India. Calibration was done with standard calibration gas mixtures prior to estimation of the reactant as well as the product gases in both TCD and ECD of the Gas Chromatograph.

3.A.2.5.2b. N_2O decomposition study over SiO_2@Mg-Al-LDH:

N_2O decomposition study over coated honey comb monolithic support with SiO_2@ LDH ratios of 1:1, 1:2, 2:1, 1:4, 4:1 and unsupported Mg-Al-LDH in presence of mixture of CO,CO_2 and CH_4 was carried at 450 ^oC at GHSV 1,936 h^{-1} (200,000 $cm^3g^{-1}h^{-1}$). The initial concentration of N_2O was maintained at 500 ppm (11.36 mmol) and

mixture of CO, CO_2 and CH_4 were also maintained at 500 ppm (31.20 mmol CH_4, 11.36 mmol CO_2 and 17.85 mmol CO). The flow rate of N_2O:Argon was maintained as 100:250 ml/min and the mixture of CO, CO_2 and CH_4 was maintained at 100 ml/min.

The catalytic reaction over the powdered catalyst was carried out by packing the catalyst in stainless steel tube as described in the **Section 3.A.2.5.2a**.

On the other hand, the calcined coated honey comb monolithic catalysts were packed in a stainless-steel catalytic converter of reaction area 77.8 cm^2, catalyst bed length 22 cm and inner diameter 0.6 cm respectively (**Fig. 3.A.3A&B**). The detection of concentration of reactant as well as product gases were carried out in Gas chromatograph as mentioned in the **Section 3.A.2.5.2a**. The concentration of N_2O was detected in TCD and ECD. On the other hand, the concentration of CO, CO_2 and CH_4 were measured by Flame Ionization Detector (FID) in GC. The low concentration of CO and CO_2 was detected by Ni-Catalytic Reactor (methanizer at temperature 395 ^oC) attachment fitted in the GC. The product gases were collected after 30 minutes reaction time. N_2O after catalytic reaction was collected at different temperatures such as 190 ^oC, 225 ^oC and 450 ^oC respectively to check the fall in concentration of N_2O.

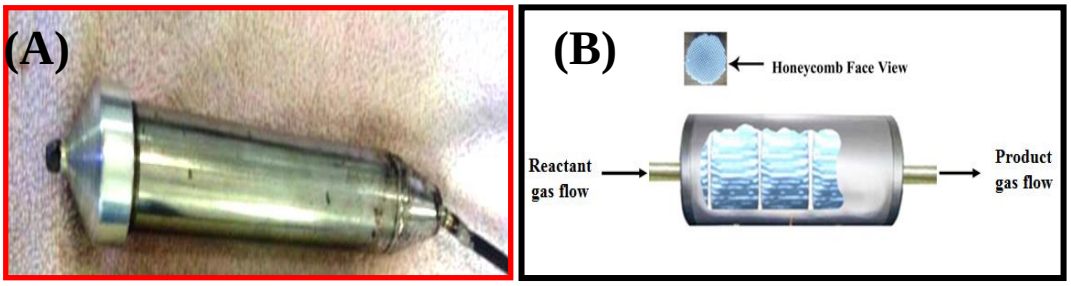

Fig. 3.A.3: (A) Stainless Steel (SS) catalytic converter containing sol-gel derived silica LDH nanocomposites coated over honeycomb monolith for the abatement of toxic green house gases (B) Schematic view of the inner side of the Stainless Steel catalytic converter packed with honey combs.

3.A.2.5.2c. Conversion expressions of N_2O decomposition study:

The percentage conversion (*X*) and percentage yield (*Y*) were calculated by the following equations [63,64] -

$$X_{N_2O} = \frac{[N_2O]_{in} - [N_2O]_{out}}{[N_2O]_{in}} \times 100 \quad (3.A.1)$$

$$Y_{O_2} = \frac{[O_2]_{out}}{[N_2O]_{in}} \times 100 \quad (3.A.2)$$

$$Y_{CO_2} = \frac{[CO_2]_{out}}{[CH_4]_{in}} \times 100 \quad (3.A.3)$$

$$Y_{CO} = \frac{[CO]_{out}}{[CH_4]_{in}} \times 100 \quad (3.A.4)$$

3.A.3. RESULTS AND DISCUSSION:

The synthesis procedure of different types of binary LDHs and their SiO_2@LDH nanocomposite alcogels are described in the **Experimental Section 3.A.2**. We synthesized binary LDHs and their SiO_2@LDH nanocomposite alcogels such as Ni-Al-LDH and Mg-Al-LDH by soft chemical sol-gel method using metal acetylacetonate as precursors in organic medium. The main advantage of using metal acetylacetonate precursors is that they undergo slow and controlled hydrolysis than the common metal alkoxides generally used in sol-gel hydrolysis reactions. This route gives a better opportunity for maintenance of desired micro-structure of hydrolysed products. However, SiO_2 component of the composite was obtained from the hydrolysis of an alkoxide precursor Tetraethyl orthosilicate (TEOS). The faster hydrolysis of TEOS than the metal acetylacetonate precursors and the oligomerisation of silicate ions in an initially maintained low pH, during the hydrolysis process helped in the formation of silica cores and associated networking to form the gels and assembling of LDH sheets

to have shells formed around the cores. They together formed the composite process of basic core-shell type soft alcogel. Such soft gels on careful drying and calcination forms an aerogel or a xerogel type catalyst having the capabilities of abatement of some of the type environmentally harmful gases at considerably lower temperatures or dielectic/super capacitor materials or filters for components of electromagnetic radiations [65,66].

This section gives interpretation of the different results obtained by the characterizations of the products as well as the gas-solid reactions carried out by different catalysts synthesised from these products.

3.A.3.1. Characterizations of binary LDHs of Ni-Al-LDH, Mg-Al-LDH and their SiO_2@LDH nanocomposite alcogels:

Binary LDHs and their SiO_2 supported products were characterized by different techniques such as PXRD, FT-IR, TGA-DTG, BET surface area and pore volume analysis, particle size analysis, zeta potential analysis, rheometric analysis, SEM and EDS, TEM analysis. These are briefly described below:

3.A.3.1.1. Powder XRD analysis:

Powder XRD analysis of binary LDHs and their SiO_2 nanocomposite alcogels was carried out using powder X-ray diffractometer (Model Rigaku Ultima IV) using Cuk_{α} radiation of a wavelength of 1.54 Å at 40 mA and 40 kV X-ray generator current setting with a step size of 0.2^{o} 2θ min^{-1}.

3.A.3.1.1.1. SiO_2@Ni-Al-LDH:

Fig. 3.A.4A & B shows the XRD patterns of the uncalcined and calcined SiO_2@Ni-Al-LDH with SiO_2:LDH ratios 0:1, 1:1, 1:2 and 2:1. The XRD pattern showed the highest intensity first *00l* reflection of LDH at 8.6^{o} 2θ with corresponding d value of 10.3Å accompanied by gradual decrease of their intensities in all the SiO_2 supported

and unsupported Ni-Al-LDH (**Fig. 3.A.4A**). The *hkl* reflections were obtained as (003), (006), (009) and (012) for LDH phase. On the other hand, in case of SiO_2@Ni-Al-LDH with SiO_2 to LDH ratios from 1:1 to 2:1 the peak due to SiO_2 were obtained at (303) and (323) respectively indicating the formation of SiO_2 supported LDH (**JCPDS PDF card no. 00-042-0022**). **Fig. 3.A.4B** shows the XRD patterns of both calcined SiO_2 supported and unsupported Ni-Al-LDHs. It showed the presence of mixed metal oxide phases after calcination at 450 ^oC. The presence of NiO and $NiAl_2O_4$ spinel type phases were observed after calcination. The peak due to NiO phases were obtained at 43.3^o (d=2.09Å), 37.3^o (d= 2.41Å), 62.9^o (d=1.48Å) 2θ values with *hkl* reflections of (012), (200), (101), (110) respectively (**JCPDS PDF card no. 00-044-1159**) in case of all these catalyst. The peak due to $NiAl_2O_4$ spinel were obtained at 45° (d= 2.013Å) and 74.4^o (d= 1.27 Å) 2θ with *hkl* reflection of (400) and (620) respectively (**JCPDS PDF card no. 00-010-0339**). The $NiAl_2O_4$ spinel phase was not observed in case of calcined SiO_2@Ni-Al-LDH with SiO_2:LDH ratio 2:1 which was due to the presence of SiO_2 which suppressed the formation of $NiAl_2O_4$ crystalline spinel. On the otherhand, the peak due to SiO_2 and Al_2O_3 were not observed in the calcined products with SiO_2 content which exists as an amorphous or poorly crystalline phase [67].

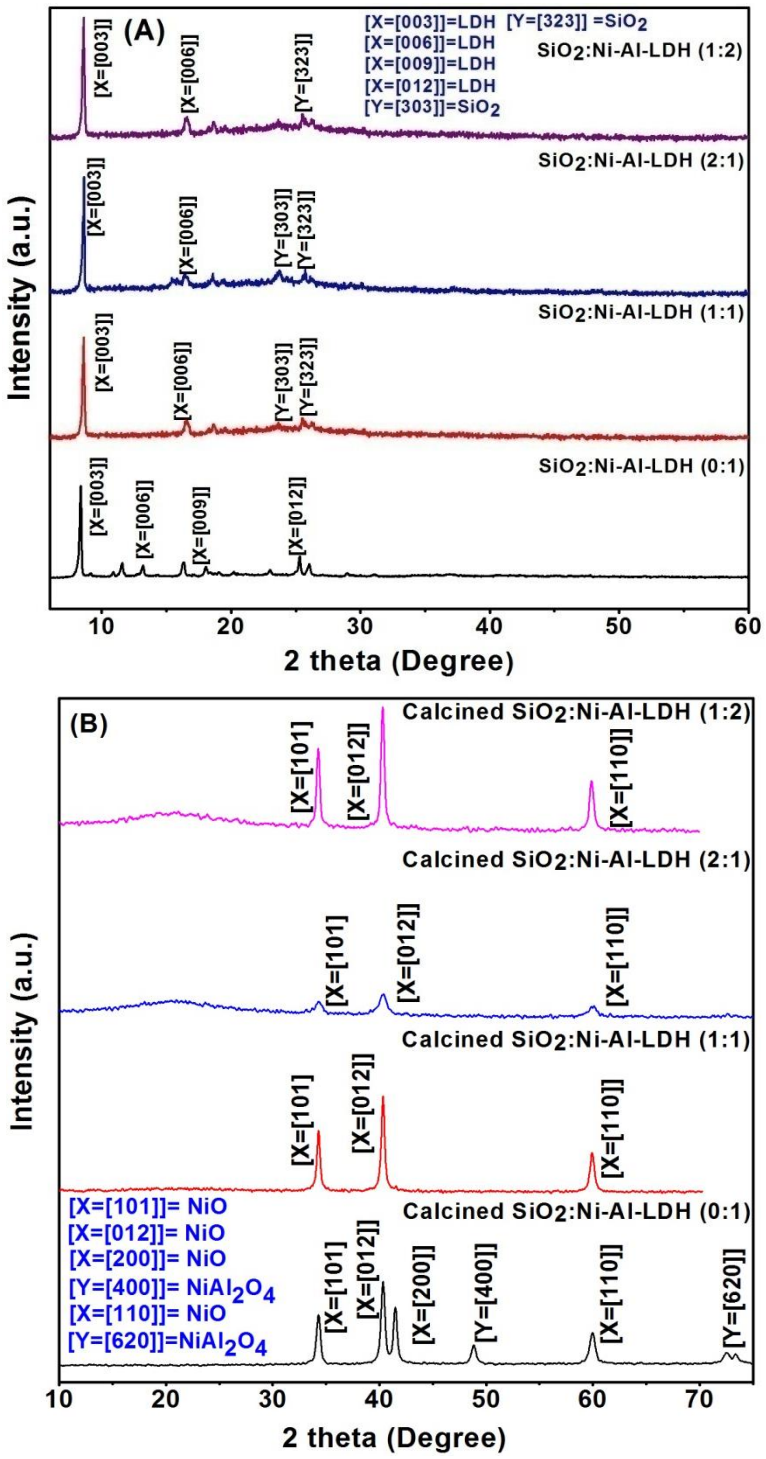

Fig. 3.A.4: XRD patterns of uncalcined (A) and calcined (B) (calcined at 450 °C) SiO_2@Ni-Al-LDH with SiO_2:LDH ratio 0:1, 1:1, 1:2 and 2:1.

3.A.3.1.1.2. SiO_2@Mg-Al-LDH:

Fig. 3.A.5A&B shows the XRD patterns of uncalcined and calcined SiO_2@Mg-Al-

LDH. **Fig. 3.A.5A** showed the presence of LDH phases of *00l* reflections with regular intervals of d-spacing in case of both SiO_2 supported and unsupported products. The peak due to LDH phases showed formation of (003), (006) and (009) planes respectively and these peaks were most prominent in case of Mg-Al-LDH with SiO_2:LDH ratios from 0:1 to 1:4. On the other hand, in case of Mg-Al-LDH with SiO_2:LDH ratios from 1:1 to 4:1 some lowest intensity peaks due to SiO_2 were obtained with *hkl* reflections (041) and (421) respectively (**JCPDS PDF card no.00-044-1394**) and the intensity of these peaks increased with the increase of SiO_2 to LDH ratios from 1:1 to 4:1.

Fig. 3.A.5B showed the presence of MgO type phases at 36.9^o (d=2.43 Å), 42.9^o (d=2.11Å) and 62.3^o 2θ (d=1.23 Å) after calcination with *hkl* reflections of (111), (200) and (220) (101) respectively (**JCPDS PDF card no. 00-045-0946**). On the other hand, in case of SiO_2 to LDH ratios 1:2, 1:3 and 1:4 some lowest intensity *00l* reflections appeared at regular interval of d-spacings indicating the reappearance of LDH structure through 'Memory effect' due to the rehydration of calcined products [68]. It was further observed that in case of calcined products with SiO_2 to LDH from 1:1 to 4:1 the peak due to SiO_2 was obtained at *hkl* reflection of (101) (**JCPDS PDF card no. 00-018-1169**).

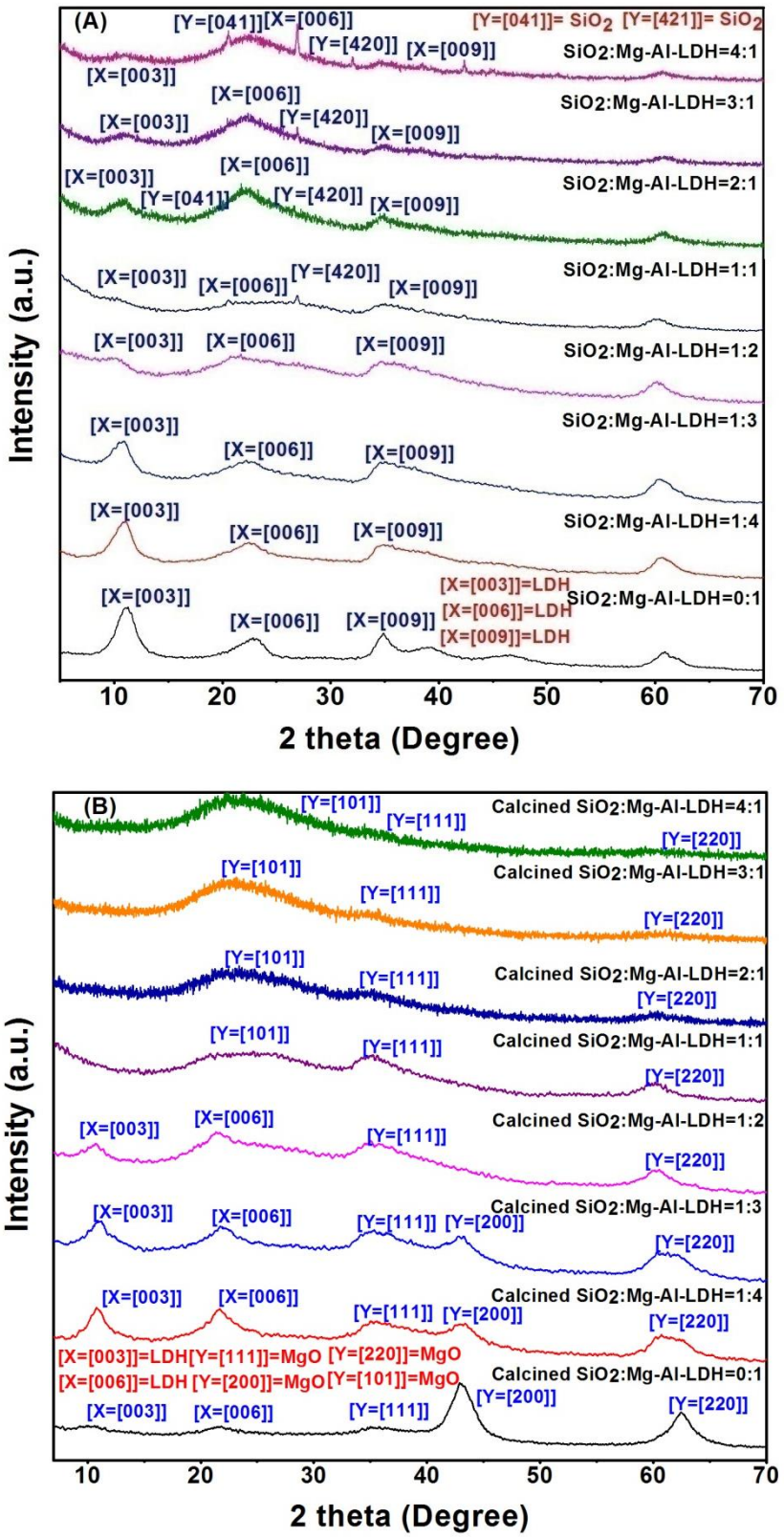

Fig. 3.A.5: XRD patterns of uncalcined (A) and calcined (B) (calcined at 450 °C) SiO_2@Mg-Al-LDH with different SiO_2 to LDH ratios.

3.A.3.1.2. FT-IR analysis of the synthesised products:

3.A.3.1.2.1. SiO_2@Ni-Al-LDH:

FT-IR of the dried powdered samples were carried out in Perkin-Elmer IR spectrometer (Model 2000) in the range 4000 to 400 cm^{-1} in the form of pressed KBr pellets with 0.8 % sample concentration.

FT-IR patterns showed the broad peak at 3432 cm^{-1} due to –OH stretching vibrations shown by both SiO_2 supported and unsupported Ni-Al-LDHs (**Fig. 3.A.6A**) [69] due to the presence of interlayer hydroxyls and H_2O molecules respectively. The peak at 1630 cm^{-1} was obtained due to strong vibration of C=O bond of enolic group of acetylacetone moiety present in the interlayers of LDH. The peak due to –C-H bending vibration was obtained at 1407 cm^{-1}. The peak at 1015-1084 cm^{-1} was due to the C-O stretching vibration. The peak at 577-797 cm^{-1} was due to the stretching vibration of M-O bond. **Fig. 3.A.6B** shows the FT-IR patterns of calcined SiO_2 supported and unsupported Ni-Al-LDH. The peak at 1630 cm^{-1} was due to the stretching vibration of -C=O group. The stretching vibration frequency due to C-O group was obtained at 1060-1070 cm^{-1}. On the other hand the peak at 790 cm^{-1} was due to stretching vibration of M-O bond present in mixed-metal oxide obtained after calcination.

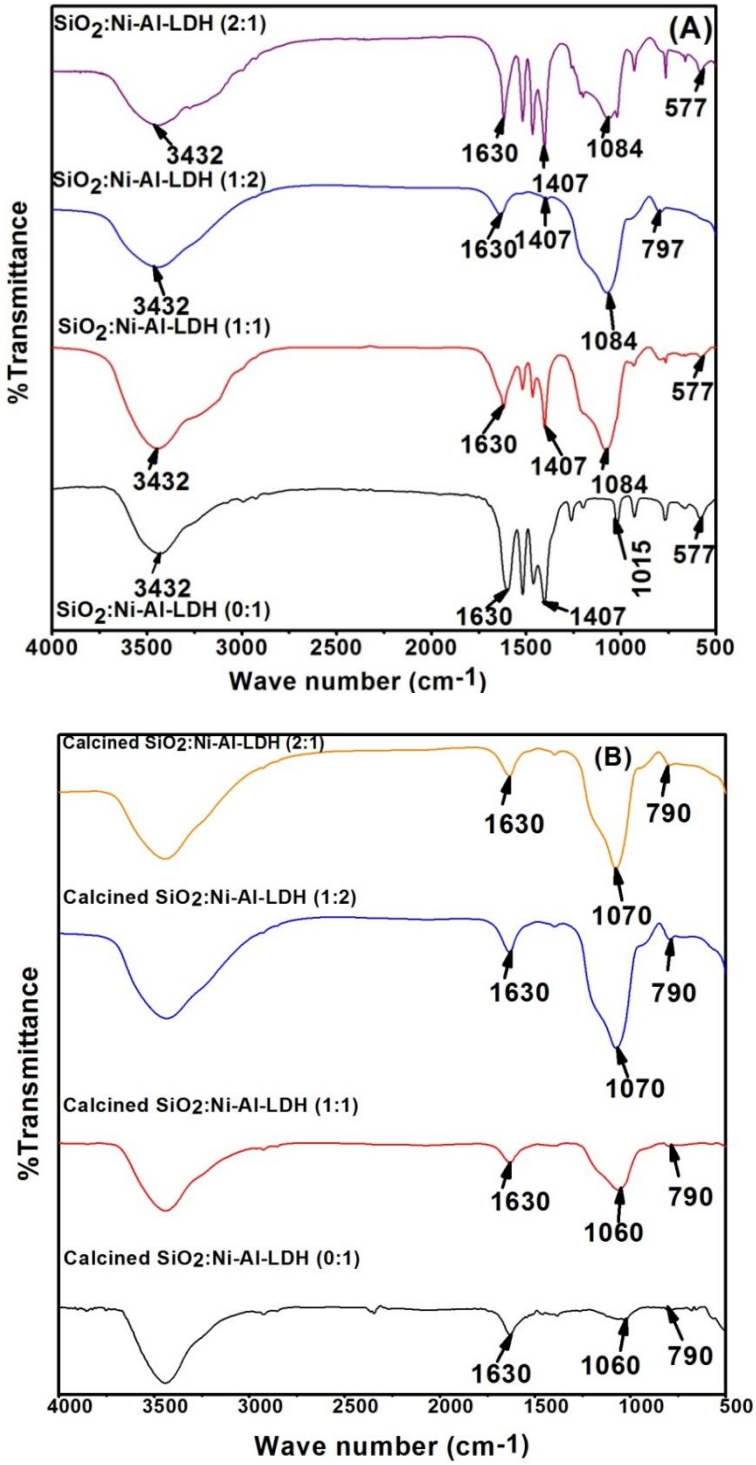

Fig. 3.A.6: FT-IR patterns of uncalcined (A) and calcined (B) (calcined at 450 ºC) SiO_2@Ni-Al-LDH with different SiO_2 to LDH ratios.

3.A.3.1.2.2. SiO_2@Mg-Al-LDH:

Fig. 3.A.7A&B shows the FT-IR patterns of uncalcined and calcined SiO_2@Mg-Al-

LDH. FT-IR patterns of uncalcined products showed (**Fig. 3.A.7A**) the broad peak at 3444 cm^{-1} due to –OH stretching vibration [70] of interlayer hydroxyls and H_2O molecules respectively. The vibrational frequency at 1638 cm^{-1} was due to stretching vibration of C=O group. The peak due to C-O stretching vibration was obtained at 1030-1086 cm^{-1}. On the other hand, the peak at 600-612 cm^{-1} was obtained due to stretching vibration of M-O bond.

Fig. 3.A.7B showed the peak at 1640 cm^{-1} due to stretching vibration of C=O group present in the acetylacetonate group in the interlayer. The peak at 1372-1400 cm^{-1} was due to –C-H bending vibration. On the otherhand, the peak due to M-O was obtained at 630-853 cm^{-1}.

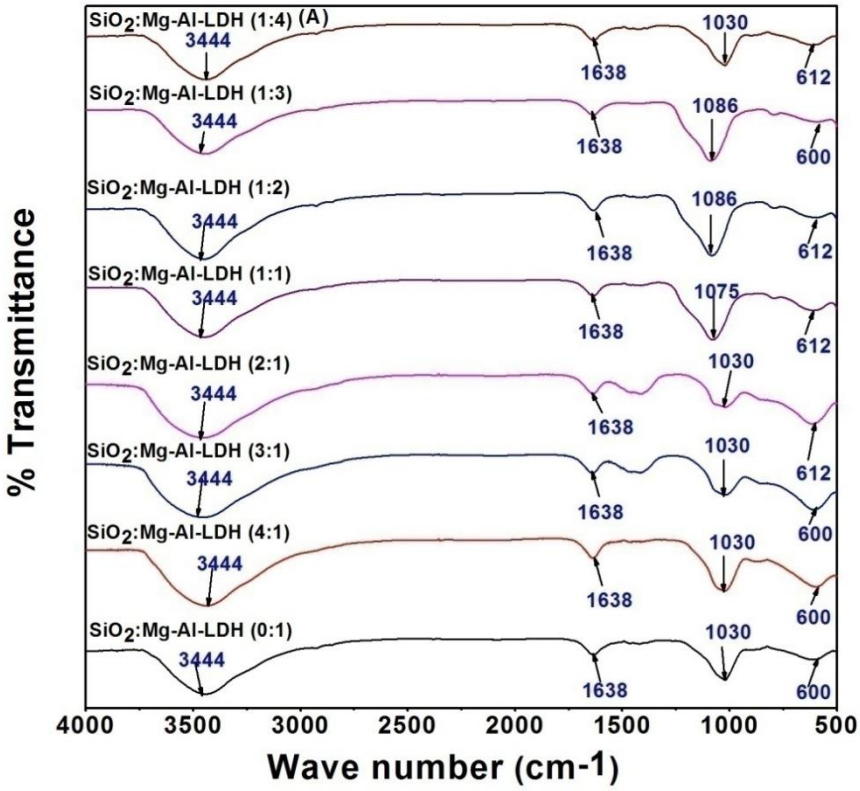

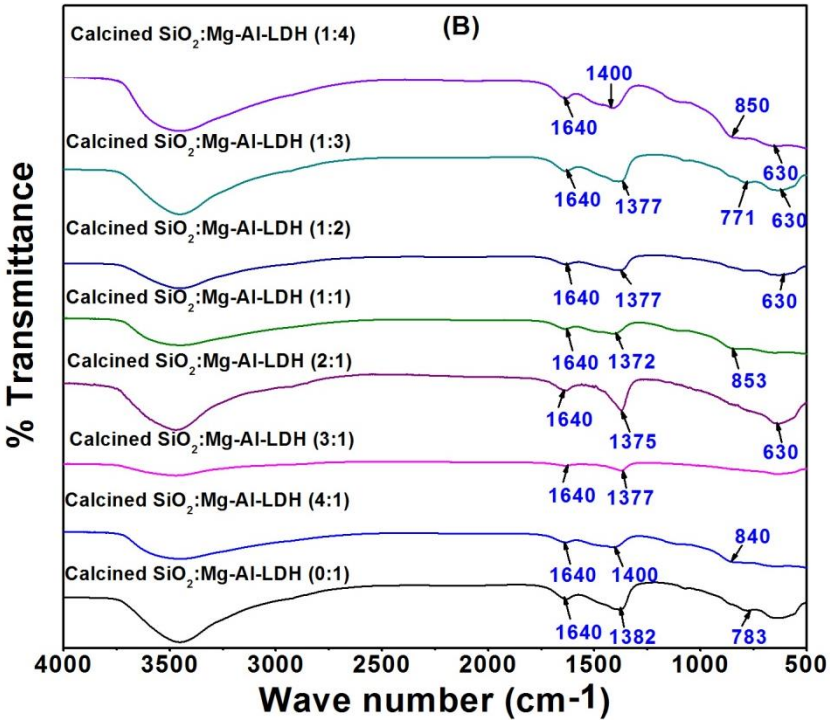

Fig. 3.A.7: FT-IR patterns of uncalcined (A) and calcined (B) (calcined at 450 °C) SiO_2@Mg-Al-LDH with different SiO_2 to LDH ratios.

3.A.3.1.3. Thermal property study (TGA-DTG analysis):

Thermogravimetric analysis of binary LDHs and their SiO_2 supported products were carried out in a simultaneous TG-DTA analyzer (Model SDT Q600, M/S TA Instruments, USA) using Al_2O_3 as reference under argon atmosphere.

3.A.3.1.3.1. Ni-Al-LDH:

3.A.3.1.3.1.1. Iso-conversional Kinetic study of thermal degradation of Ni-Al-LDH:

Iso-conversional kinetic parameters such as activation energy (E_a), pre-exponential factor (A) and reaction order (n) of Ni-Al-LDH were carried out from thermogravimetric analysis under non-isothermal condition. These kinetic parameters were determined by Flynn-Wall-Ozawa (FWO), Friedman, Coats-Redfern and Phadnis-Deshpande methods respectively. Thermogravimetric analysis was carried out

at different heating rates such as 5, 10, 15, 20 and 30 ^{o}C/min under argon atmosphere. **Fig. 3.A.8a** shows percentage weight loss and derivative weight loss *vs* temperature curves for sol-gel Ni-Al-LDH at different heating rates. TGA results showed the three step thermal degradation; first step correspond to the loss of inter-particle pore moisture [70,71], which is basically drying of unbound free water the second and third step correspond to the loss of intercalated water molecules and ions from the hydroxidic brucite like layers. The kinetic parameters were mainly studied for the second and third step weight losses which correspond to removal of hydrogen bonded surface water and structural degradation of LDH. Activation energy (E_a) was first calculated by using Flynn-Wall-Ozawa [71-74] and Friedman method [71,75]. These methods used the following equations-

Flynn-Wall-Ozawa:

$$log\beta = log\, AE_a/g(X)R - 2.315 - 0.4567E_a/RT \quad (3.A.5)$$

Thus, if a series of experiments are run at different values of heating rates(β), the apparent activation energy (E_a) can be obtained from a plot of $log\beta$ against $1/T$ for a fixed degree of decomposition (X), without having a prior knowledge of reaction order. A is the pre-exponential factor. The activation energy of Ni-Al-LDH were calculated by plotting $log\beta$ against $1000/T$ at a fixed conversion with the slope of such a line being $-0.4567E_a/RT$ for different degree of conversions (**Fig. 3.A.8b)**. The main advantage of this method is that it does not require any assumptions concerning the form of the kinetic equation other than the Arrhenius type temperature dependence.

Friedman:

$$ln\left[\beta_i\ (dX/dT)_{X,i}\right] = ln[A_X f(X)] - E_{a,X}/RT \quad (3.A.6)$$

The activation energy (E_a) can be determined from the slope of the plot of $ln[\beta_i\,(dX/dT)_{X,i}]$ *vs* $1/T_a$, at a constant X value, the subscript i is the ordinal number of an experiment performed at a given heating rate. Activation energy were obtained from the plot of $ln(\beta(dX/dT))$ against $1/T$ (Eq. 8) at constant values of X at different heating rates. A set of straight lines were obtained with the slope of $-E/R$.

To determine activation energy of the second step degradation step, X = 0.2, 0.25, 0.3, 0.35, 0.4, 0.45, 0.5, 0.55 were chosen and for the third degradation step, X= 0.7, 0.75, 0.8, 0.85, 0.9 were chosen.

The mean activation energy (E_a) obtained by FWO method were 68.06 kJ/mol and 91.28 kJ/mol for second and third step degradation respectively. The mean activation energies obtained by Friedman method were found as 68.43kJ/mol and 73.04kJ/mol for second and third step degradation, respectively. The activation energy *vs* conversion curve obtained by FWO and Friedman method are shown in **Fig. 3.A.8c**. The pre-exponential factor (A) determined by Friedman method were found as 1.43×10^2 s^{-1} and 1.82×10^2 s^{-1} for second and third step degradation. The reaction order (n) was found as 3.8 and 2.2 for second and third step degradation respectively.

On the other hand, the kinetic mechanism [76,77] for second and third step thermal degradation of Ni-Al-LDH at different heating rates such as 5, 10, 15, 20 and 30 ^oC/min were determined by Coats-Redfern and Phadnis-Deshpande methods. The equations are given below-

Coats-Redfern:

$$ln[g(X)/T^2] = ln[AR/\beta E] - E_a/RT \qquad (3.A.7)$$

The activation energy (E_a) and pre-exponential factor (A) can be obtained from a plot of $ln[g(X)/T^2]$ *vs* 1/T for different degradation step.

Phadnis-Deshpande:

$$f(X)g(X) = RT^2/E_a\,(1 - 2RT/E_a)\,dX/dT \quad (3.A.8)$$

$$F(X) = -E_a/RT \quad (3.A.9)$$

Where, *F(X)* is obtained by integrating and neglecting the small term E^2 of the equation (5) and is equal to $\int 1/\big(f(X)g(X)\big)dX$.

It was observed that the second step the and third step degradation obeyed A_3 type Avrami-Erofeev equation $(g(X) = [-ln(1-X)]^3)$ and D_4 type three dimensional diffusion mechanism with Ginstling-Brounsthein equation $F(X) = ln\ [1-(2/3)X-(1-X)^{2/3})]$ and were found to be in better agreement with FWO and Friedman method with better correlation co-efficient (*R*) (**Table 3.A.1 A,B,C&D**).

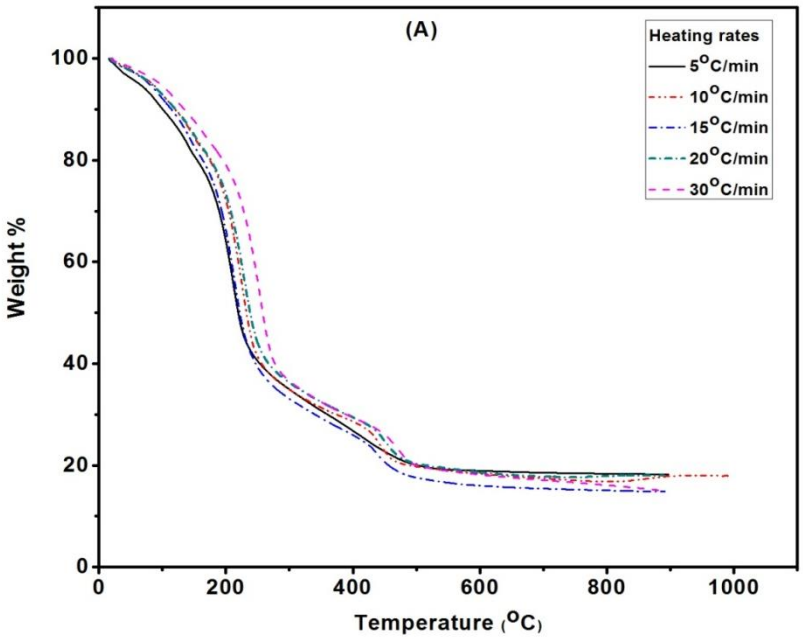

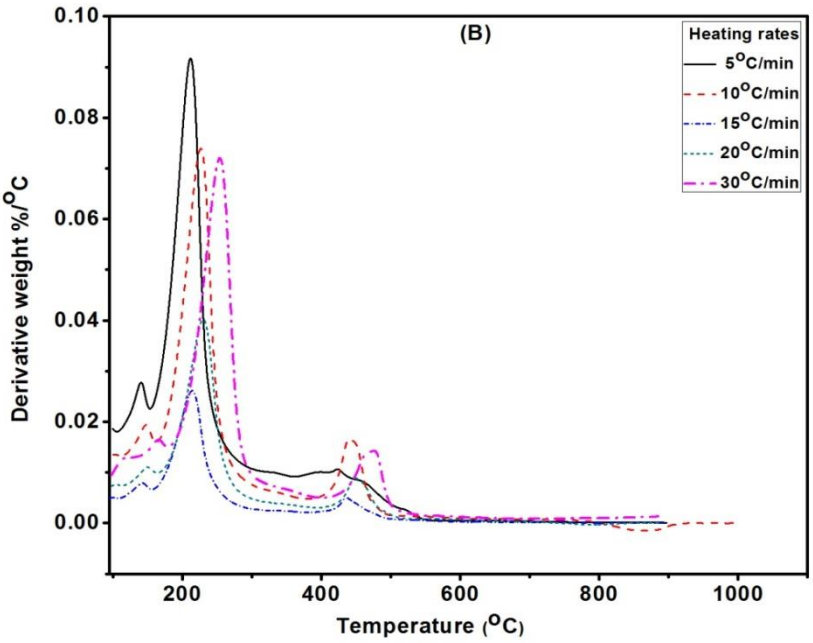

Fig. 3.A.8a: TGA patterns of Ni-Al-LDH at different heating rates (A); (B) DTG patterns of Ni-Al-LDH at different heating rates.

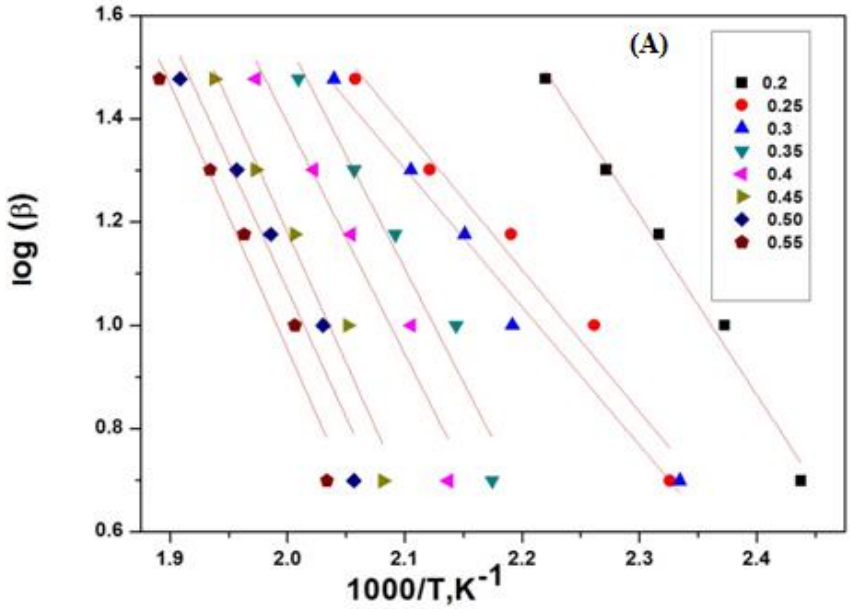

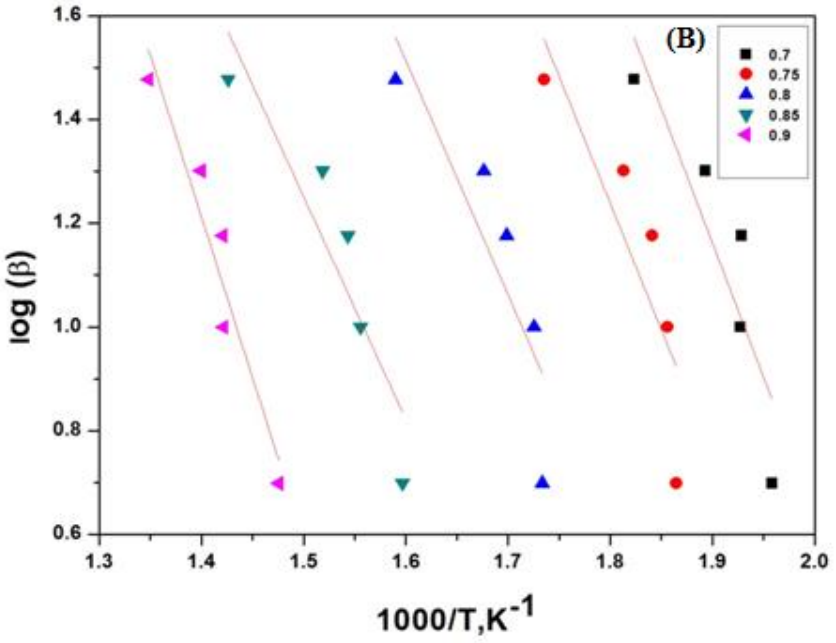

Fig. 3.A.8b: Flynn-Wall Ozawa plot of Ni-Al-LDH at varying conversion for second step degradation (A); for third step degradation (B).

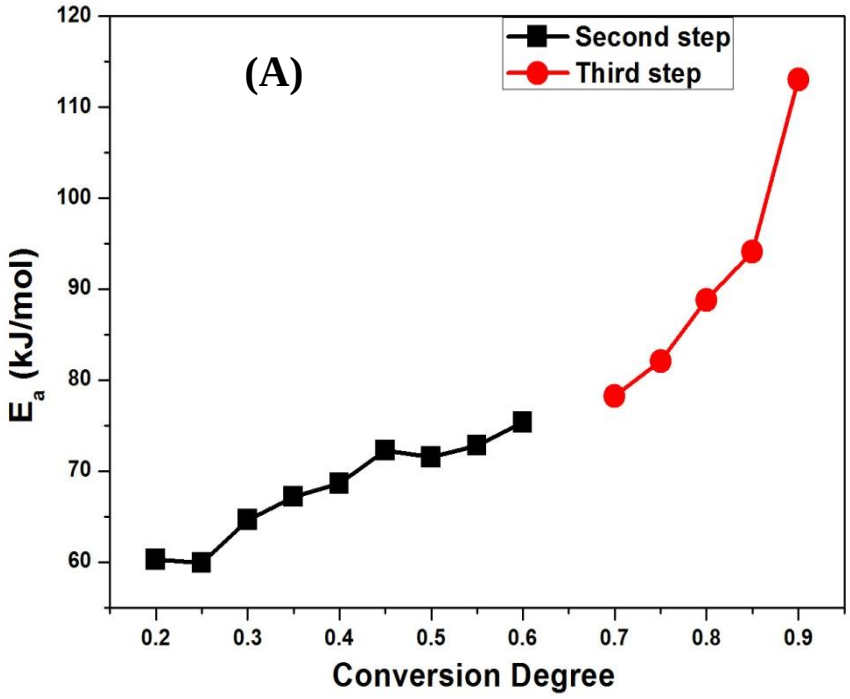

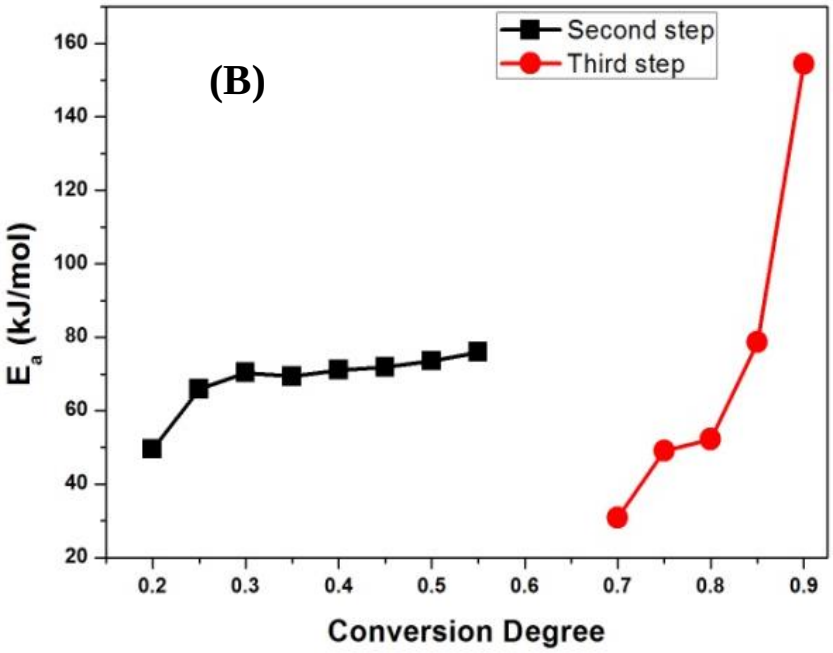

Fig. 3.A.8c: Plot of activation energies obtained by FWO method for second and third thermal degradations of Ni-Al-LDH at varying conversions (A); Plot of activation energies obtained by Friedman method for second and third thermal degradation of Ni-Al-LDH at varying conversions (B).

Table 3.A.1 (A): Activation energy calculated by using Coats-Redfern method for second step degradation at various heating rates

Heating rates (ºC/min)	Mechanism	Activation Energy (kJ/mol)	Correlation Coefficient (*R*)
5	A_2	47.64	0.99864
	A_3	63.12	0.99950
	A_4	102.68	0.99564
10	A_2	53.04	0.99786
	A_3	64.12	0.99942
	A_4	113.90	0.99614
15	A_2	55.81	0.99754
	A_3	65.52	0.99960
	A_4	119.22	0.99621
20	A_2	58.16	0.99593
	A_3	66.47	0.99958
	A_4	124.13	0.99591
30	A_2	59.47	0.99418
	A_3	67.28	0.99946
	A_4	127.12	0.99480

Table 3.A.1 (B): Activation energy calculated by Phadmis-Deshpande method for second step degradation at various heating rates

Heating rate (°C/min)	Mechanism	Activation Energy (kJ/mol)	Correlation Coefficient (*R*)
5	Power law (1)	37.75	0.96135
	Power law (2)	65.85	0.97301
	A_2	49.03	0.99439
	A_3	69.42	0.99904
10	Power law (1)	27.10	0.96697
	Power law (2)	54.21	0.96697
	A_2	43.86	0.99514
	A_3	65.93	0.99914
15	Power law (1)	26.19	0.97835
	Power law (2)	52.38	0.98763
	A_2	46.87	0.99658
	A_3	63.44	0.99978
20	Power law (1)	25.27	0.98672
	Power law (2)	50.63	0.98763
	A_2	41.64	0.99824
	A_3	60.86	0.99903
30	Power law (1)	27.77	0.97663
	Power law (2)	55.79	0.98773
	A_2	60.86	0.99527
	A_3	65.27	0.99954

Table 3.A.1 (C): Activation energies calculated by Coats-Redfern method for third step degradation at various heating rates

Heating rates (°C/min)	Mechanism	Activation Energy (kJ/mol)	Correlation Coefficient (*R*)
5	D_3	55. 38	0.99336
	D_4	78.12	0.99801
10	D_3	58.43	0.9898
	D_4	80.22	0.99877
15	D_3	58.46	0.99574
	D_4	82.30	0.99868
20	D_3	58.53	0.99758
	D_4	82.38	0.99975
30	D_3	65.40	0.99658
	D_4	91.96	0.99844

Table 3.A.1(D): Activation energies calculated by Phadnis-Deshpande method for third step degradation at various heating rates

Heating rates (°C/min)	Mechanism	Activation Energy (kJ/mol)	Correlation Coefficient (*R*)
5	D_3	41.87	0.99928
	D_4	75.14	0.99993
10	D_3	42.75	0.99029
	D_4	88.12	0.99972
15	D_3	47.09	0.99155
	D_4	83.75	0.99986
20	D_3	49.11	0.99196
	D_4	84.18	0.99871
30	D_3	57.22	0.99769
	D_4	89.04	0.99986

3.A.3.1.3.2. SiO_2@Ni-Al-LDHs:

TGA-DTG analysis of SiO_2@Ni-Al-LDH was carried out in a simultaneous TG-DTA analyzer (Model SDT Q600, M/S TA Instruments, USA) using Al_2O_3 as reference at 10 °C/min heating rate in argon atmosphere.

Fig. 3.A.9. shows the TGA-DTG patterns of SiO_2@Ni-Al-LDH with SiO_2 to LDH ratios 1:1, 1:2 and 2:1 respectively. SiO_2@Ni-Al-LDH with different SiO_2:LDH ratios also showed the three step thermal degradation first step correspond to the loss of surface and interlayer water molecules; the second and third step correspond to the loss of intercalated water molecules and acetylacetonate ion from the hydroxidic brucite like layers. First step showed the weight losses of 18.6 %,17.9 % and 11.9 % (w/w) at temperatures from 54-68 °C; second step showed the weight losses of 33 %, 32 % and 27 % (w/w) at temperatures from 209-271 °C; third step showed the weight losses of 7 %, 4 % and 3 % (w/w) respectively at temperatures from 335-499 °C (**Fig. 3.A.9A&B**) respectively.

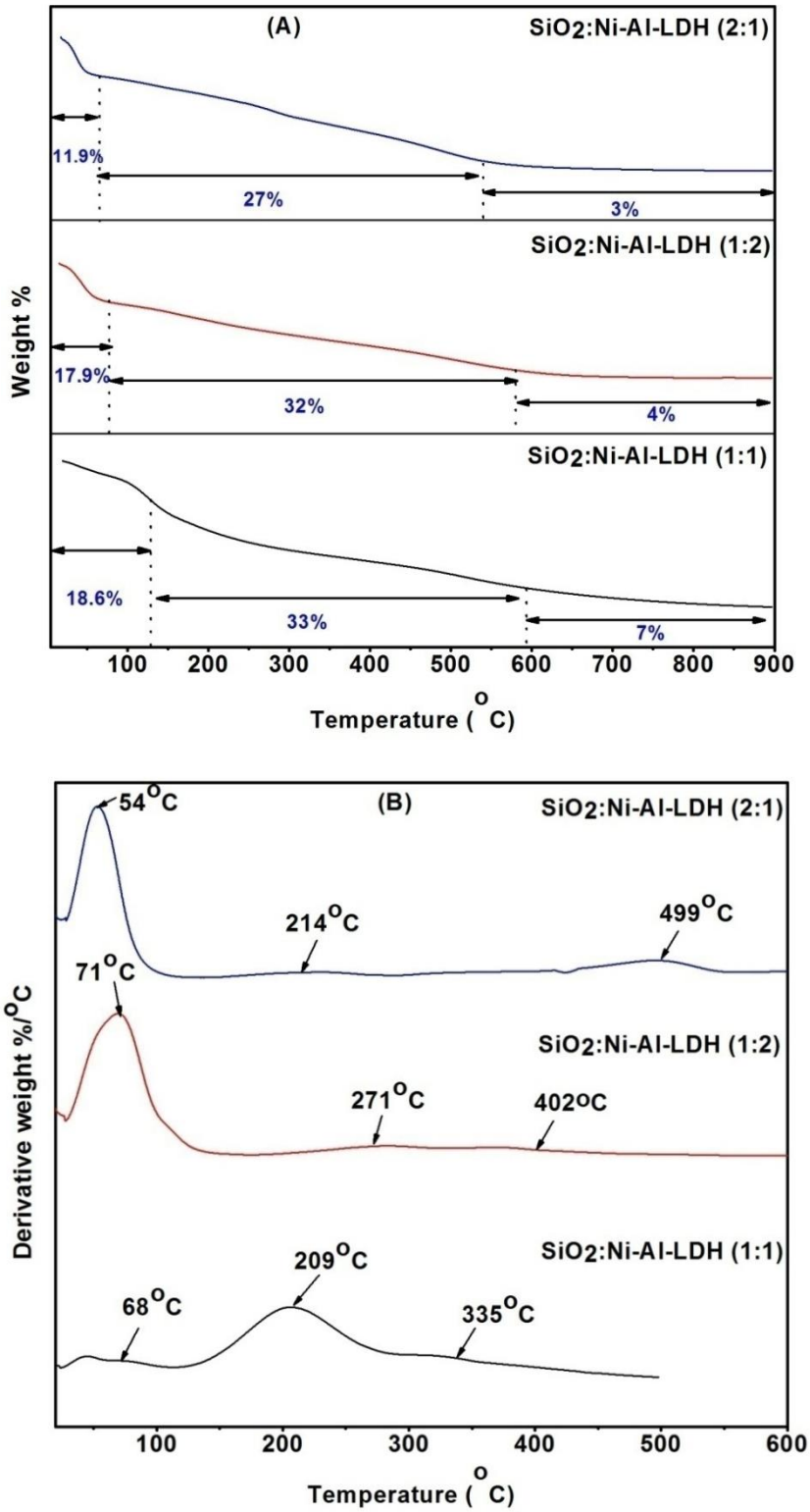

Fig. 3.A.9: TGA patterns of SiO_2@Ni-Al-LDH (A); (B) DTG patterns of SiO_2@Ni-Al-LDH.

3.A.3.1.3.3. SiO_2@Mg-Al-LDH:

Fig. 3.A.10A&B shows the TGA-DTG patterns of SiO_2@Mg-Al-LDH with SiO_2:

LDH ratios 0:1, 4:1, 3:1, 2:1, 1:1, 1:2, 1:3 and 1:4 respectively. Both SiO_2 supported and unsupported Mg-Al-LDH showed three step thermal degradation. Unsupported Mg-Al-LDH showed 13 %, 38.7 % and 8 % weight losses at temperatures 0-100 ^oC, 150-450 ^oC and 450-1000 ^oC respectively. SiO_2@Mg-Al-LDH with SiO_2 to LDH ratios 4:1, 3:1, 2:1, 1:1, 1:2, 1:3 and 1:4 showed 10.9 %, 8.4 %, 7.6 %, 18 %, 12 %, 13.1 % and 14.5 % (w/w) weight losses at temperature range of 0-100 ^oC; 14 %, 18.7 %, 18.4 %, 17 %, 21.6 %, 22.3 % and 26.7 % (w/w) weight losses at temperature range of 150-450 ^oC; 8 %, 4 %, 6.6 %, 6 %, 5%, 11.3 %, 9.2 % and 10.2 % (w/w) respectively at temperature range of 450-1000 ^oC. First step correspond to the loss of surface moisture adsorbed by the LDH samples, second and third steps correspond to the loss of interlayer water molecule as well as the interlayer ion such as acetylacetonate ion and break down of the brucite like layer.

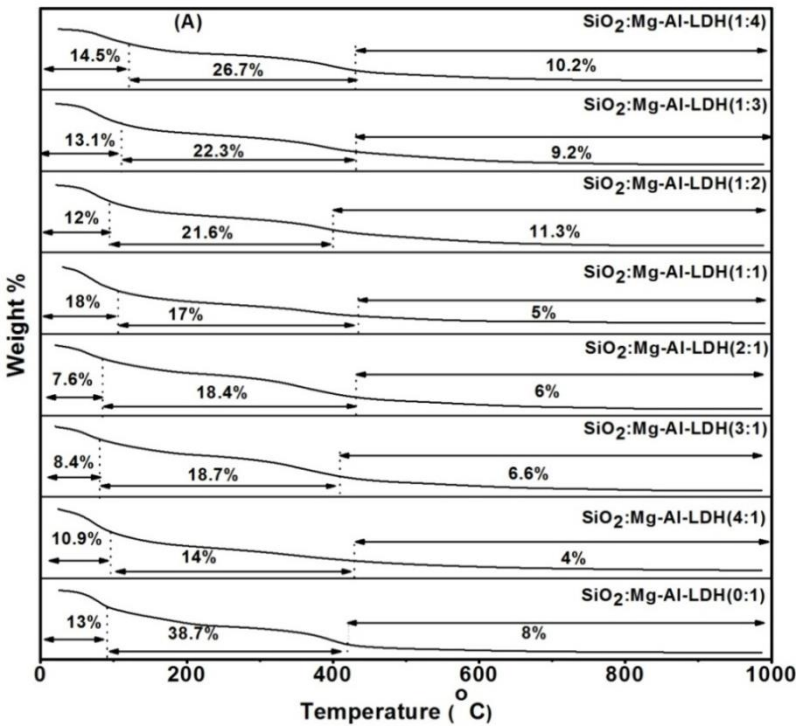

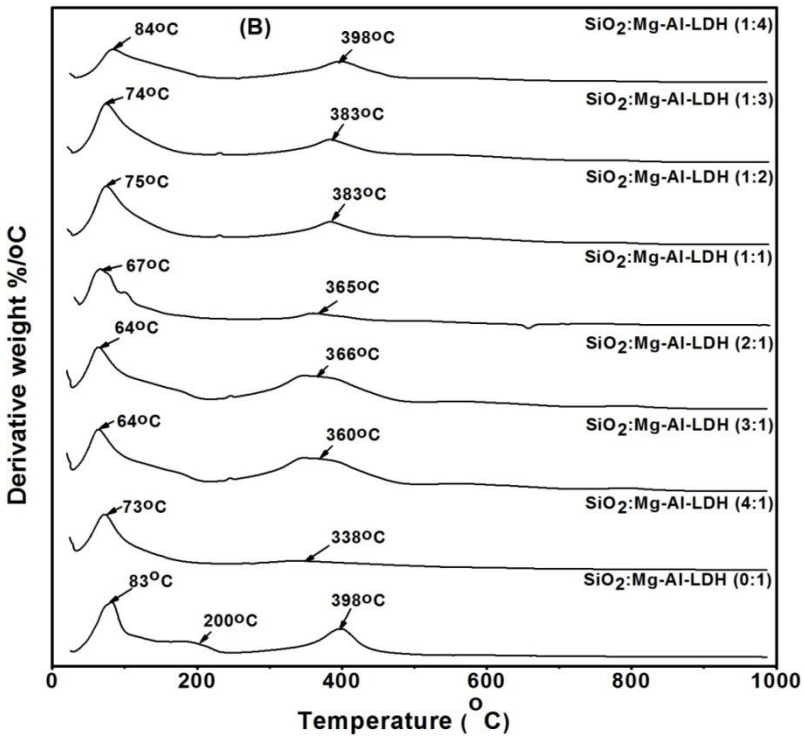

Fig. 3.A.10: (A) TGA and (B) DTG patterns of SiO_2@Mg-Al-LDH with different SiO_2 to LDH ratios.

3.A.3.1.4. Rheological study of SiO_2@LDH alcogels of binary LDHs:

To coat any dispersion over a particular solid surface by dip or spin coating technique to form a thin film the viscosity or gel strength of the dispersion plays a vital role. It affects the thickness and consequently the reproducibility and continuity of the film on drying [78].

3.A.3.1.4.1. Steady shear measurement of SiO_2@Ni-Al-LDH and SiO_2@Mg-Al-LDH:

Rheological study of SiO_2 supported and unsupported Ni-Al-LDH and Mg-Al-LDHs were carried out by using Rheolab QC (Anton Paar) with a measuring cup C-CC27/SS/QC and measuring system CC27/P6 at 15 ^oC with shear rate ranging from 100-1000s^{-1}. **Fig. 3.A.11A** shows the shear stress *vs* shear rate curves for SiO_2 supported and unsupported Ni-Al-LDH. In case of SiO_2@Ni-Al-LDH with the

increase of SiO_2 to LDH ratios from 0:1 to 2:1 shear stress increased with the increase of shear rate. These alcogels showed the non-Newtonian shear thinning behaviour and consistent to Bingham fluid [79].

Similarly, with the increase of SiO_2 to LDH ratios shear thinning properties were also found to increase indicating the increase of gelation. Similar non-Newtonian behaviour was also shown by SiO_2@Mg-Al-LDH. As the of SiO_2 content increased from 0:1 to 2:1 (SiO_2:LDH) the shear thinning property as well as the gelation property also increased (**Fig. 3.A.11B**) which helped in the coating of such alcogels over solid preforms.

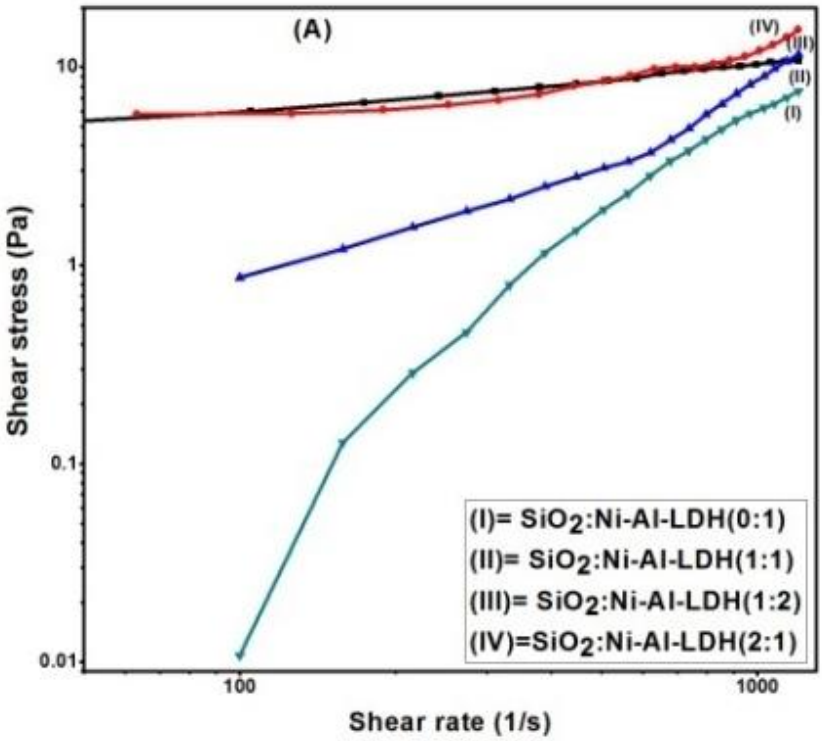

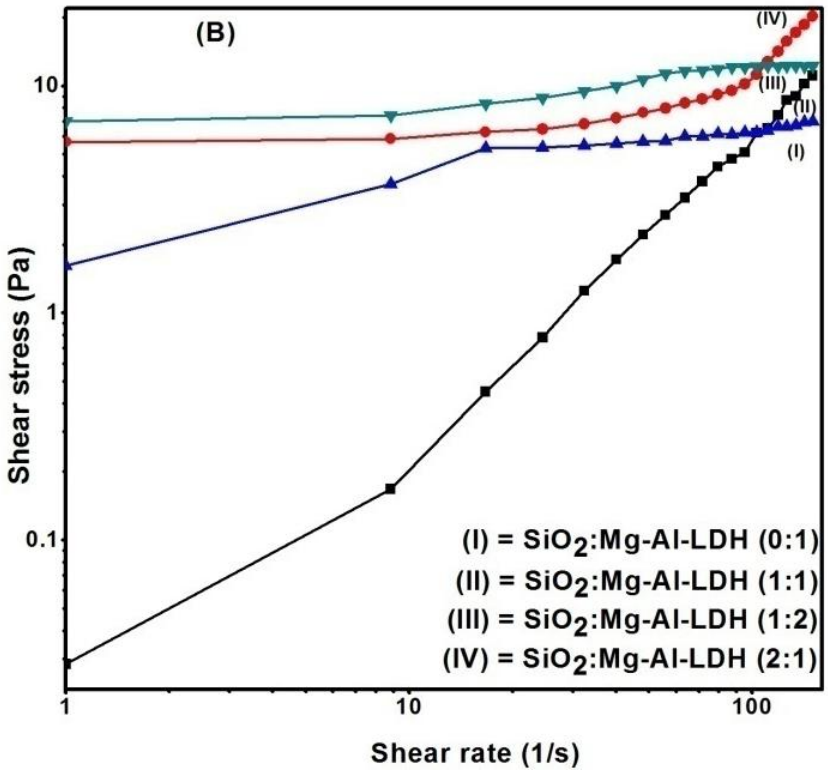

Fig. 3.A.11: Shear stress vs Shear rate curves for SiO_2@Ni-Al-LDH and Mg-Al-LDHs with varying SiO_2:LDH ratios.

3.A.3.1.5. BET Surface area and pore radius analysis:

Specific surface area of the samples was recorded *via* Nitrogen gas adsorption at 77 K applying Brunauer-Emmett-Teller (BET) calculations using Autosorb-iQ Station 1 (Quantachrome, USA). Prior to performing the experiment the samples were degassed at 100 ^{o}C for 1.5 hours.

3.A.3.1.5.1. SiO_2@Ni-Al-LDH and SiO_2@Mg-Al-LDH:

Table 3.A.2a shows the BET surface area values of SiO_2 supported and unsupported Mg-Al-LDH and Ni-Al-LDHs. It was observed that in case of SiO_2@Mg-Al-LDH with the increase of SiO_2 to LDH ratio from 0:1 to 4:1 surface area also increased from 35.4 m^2/g to 176.8 m^2/g. Similarly, in case of SiO_2@Ni-Al-LDH surface area increased from 8.5 m^2/g to 74.4 m^2/g with the increase of SiO_2 to LDH ratio from 0:1 to 2:1.

On the other hand, there was a gradual decrease of surface area in the calcined product of SiO_2@Mg-Al-LDH (**Table 3.A.2b**) which was due to the increase of crystallite size of MgO particles and shrinkage of the SiO_2 gels after calcination [80]. In case of the calcined product of SiO_2@Ni-Al-LDH there was a further increase of surface area observed from 148.5 m^2/g to 274.4 m^2/g with the increase of SiO_2 to LDH ratios from 0:1 to 2:1 indicating that the shrinkage phenomenon was not present in case SiO_2@Ni-Al-LDH as in SiO_2@Mg-Al-LDH.

Table 3.A.2a: BET Surface area of SiO_2@LDHs

Serial No.	Nanocomposites	SiO_2:LDH ratios	Surface Area (m^2/g)
1	SiO_2:Mg-Al-LDH	0:1	35.4
2	SiO_2:Mg-Al-LDH	1:1	165.8
3	SiO_2:Mg-Al-LDH	2:1	174.6
4	SiO_2:Mg-Al-LDH	1:2	158.9
5	SiO_2:Mg-Al-LDH	1:4	138.7
6	SiO_2:Mg-Al-LDH	4:1	176.8
7	SiO_2: Ni-Al-LDH	0:1	8.5
8	SiO_2:Ni-Al-LDH	1:1	45.6
9	SiO_2:Ni-Al-LDH	1:2	56.8
10	SiO_2:Ni-Al-LDH	2:1	74.4

Table 3.A.2b: BET Surface area analysis of calcined SiO_2@LDHs

Serial No.	Nanocomposites	SiO_2:LDH ratios	Surface Area (m^2/g)
1	Calcined Mg-Al-LDH	0:1	14.5
2	Calcined SiO_2:Mg-Al-LDH	1:1	53.9
3	Calcined SiO_2:Mg-Al-LDH	2:1	65.8
4	Calcined SiO_2:Mg-Al-LDH	1:2	37.7
5	Calcined SiO_2:Mg-Al-LDH	4:1	78.8
6	Calcined SiO_2:Ni-Al-LDH	0:1	148.5
7	Calcined SiO_2:Ni-Al-LDH	1:1	179.6
8	Calcined SiO_2:Ni-Al-LDH	1:2	168.8
9	Calcined SiO_2:Ni-Al-LDH	2:1	274.4

3.A.3.1.6. Zeta potential study with the variation of pH:

3.A.3.1.6.1. SiO_2@Ni-Al-LDH and SiO_2@Mg-Al-LDH:

As shown in **Table 3.A.3** the negative zeta potential of these nanocomposites after dispersion in aqueous medium increased with the increase of silica. Since, the isoelectric point of SiO_2 varies in the range 2 to 4 whereas for LDH it is 12 therefore, with the rise of SiO_2 component in the nanocomposites the magnitude of negative zeta potential increased which helped in the dispersibility of the system as well as the possibility for the formation of thin films over solid surfaces by dip-coating or spin coating.

Table 3.A.3: Zeta potential values of SiO_2@LDHs

Serial No.	Nanocomposites	SiO_2:LDH ratios	Zeta Potential (mV)	pH
1	SiO_2:Ni-Al-LDH	0:1	+30.1	8.8
2	SiO_2:Ni-Al-LDH	1:2	-22.7	8.9
3	SiO_2:Ni-Al-LDH	1:1	-20.7	8.7
4	SiO_2:Ni-Al-LDH	2:1	-21.8	9.0
5	SiO_2:Mg-Al-LDH	0:1	+27.3	7.2
6	SiO_2:Mg-Al-LDH	1:4	+22.7	9.0
7	SiO_2:Mg-Al-LDH	1:1	-30.3	8.8
8	SiO_2:Mg-Al-LDH	2:1	-26.1	8.7
9	SiO_2:Mg-Al-LDH	3:1	-24.2	8.2
10	SiO_2:Mg-Al-LDH	4:1	-16.1	6.4

3.A.3.1.7. Particle size analysis:

3.A.3.1.7.1. SiO_2@Ni-Al-LDH and SiO_2@Mg-Al-LDH:

The particle size analysis showed that sol-gel synthesis of LDH gave particles of higher size generally above 100 nm (**Fig. 3.A.12a**). It was observed that oven dried SiO_2 unsupported Ni-Al-LDH highest amount of particles were found in the range of 100-1000 nm range. On the other hand, in presence of SiO_2 the particle size further increased due to oligomerization and highest amount of particles were found in the range of 1000-10000 nm. This particle size distribution was due to the aggregated dry samples.

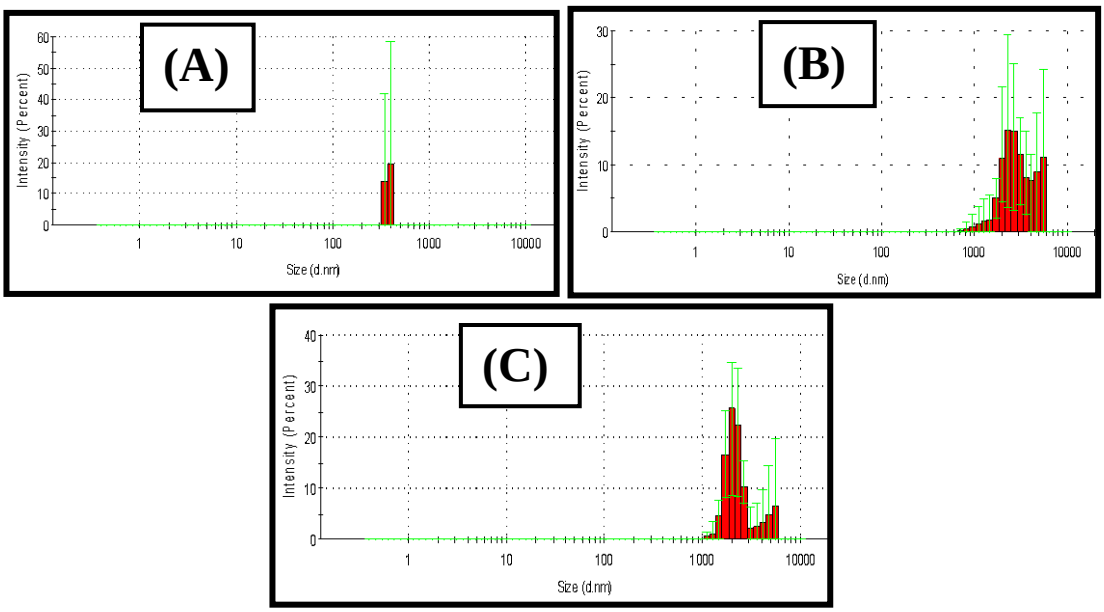

Fig. 3.A.12a: Particle size distribution curves of (A) SiO_2@Ni-Al-LDH (0:1); (B) SiO_2@Ni-Al-LDH (1:1); (C) SiO_2@Ni-Al-LDH (2:1).

Fig. 3.A.12b shows the particle size distribution curves of SiO_2@Mg-Al-LDH. It was observed that in case of SiO_2@Mg-Al-LDH with SiO_2 to LDH ratios of 1:1, 2:1 and 4:1 highest amount of particles were found in the range of 100-1000 nm.

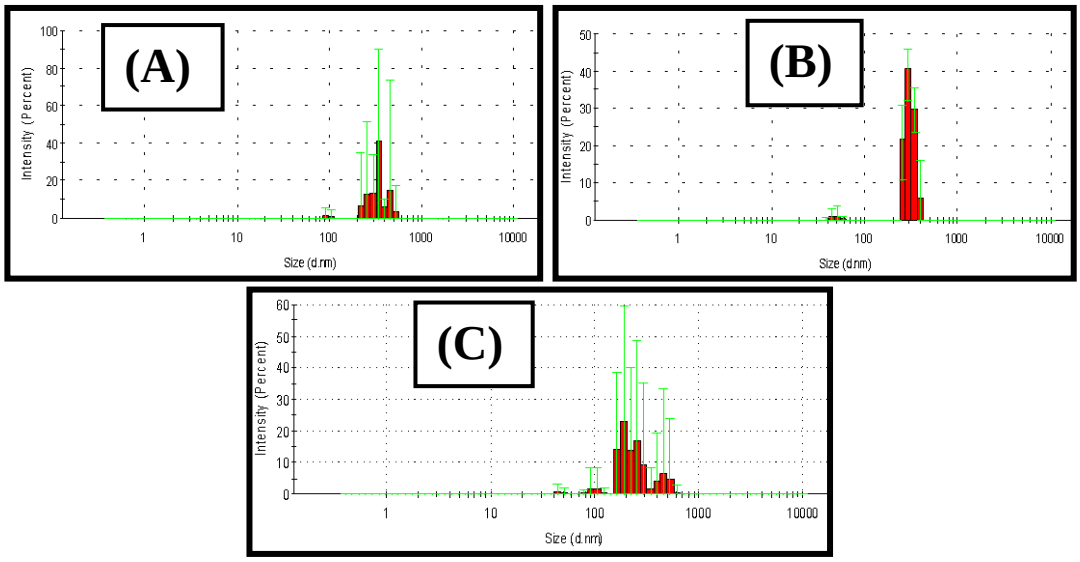

Fig. 3.A.12b: Particle size distribution curves of (A) SiO_2@Mg-Al-LDH (1:1); (B) SiO_2@Mg-Al-LDH (2:1); (C) SiO_2@Mg-Al-LDH (4:1).

3.A.3.1.8. Surface morphology study:

Surface morphology study of different binary SiO_2@LDHs were carried out by

SEM and TEM analysis the associated EDS patterns give the elemental composition of the composites.

3.A.3.1.8.1. SEM, TEM and EDS analysis:

3.A.3.1.8.1.1. SiO_2@Ni-Al-LDH and SiO_2@Mg-Al-LDH:

Fig. 3.A.13a shows SEM and TEM images of SiO_2@Ni-Al-LDH. SEM pattern (**Fig. 3.A.13a.A, B&C**) showed the platy aggregates with crumbled sides. Crumbled sides were generated during drying under high vacuum used for SEM sample preparation. However, the dried aggregates of sol-gel products have a more dispersed nature due to the extremely fine particulate origin of the former. TEM image also showed the aggregates of LDH layers with 0.245 nm lattice fringes indicating the presence of 012 plane of LDH.

On the other hand, TEM images of (**Fig. 3.A.13a.D&E**) SiO_2@Ni-Al-LDH showed that LDH layers dispersed over SiO_2 spheres where surfaces of the SiO_2 spheres were covered by LDH layers through stacking over another. **Fig.3.A.13b.A&B** shows the SEM images of calcined unsupported and SiO_2 supported Ni-Al-LDH. It was observed that the layered structure remained in the both supported and unsupported calcined Ni-Al-LDH. Only exfoliation of the layer occurred due to calcination.

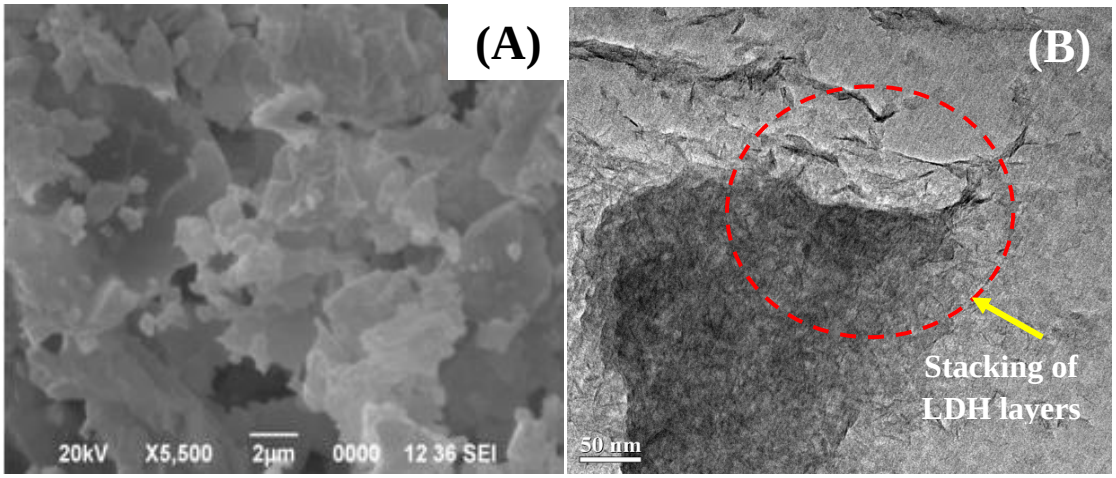

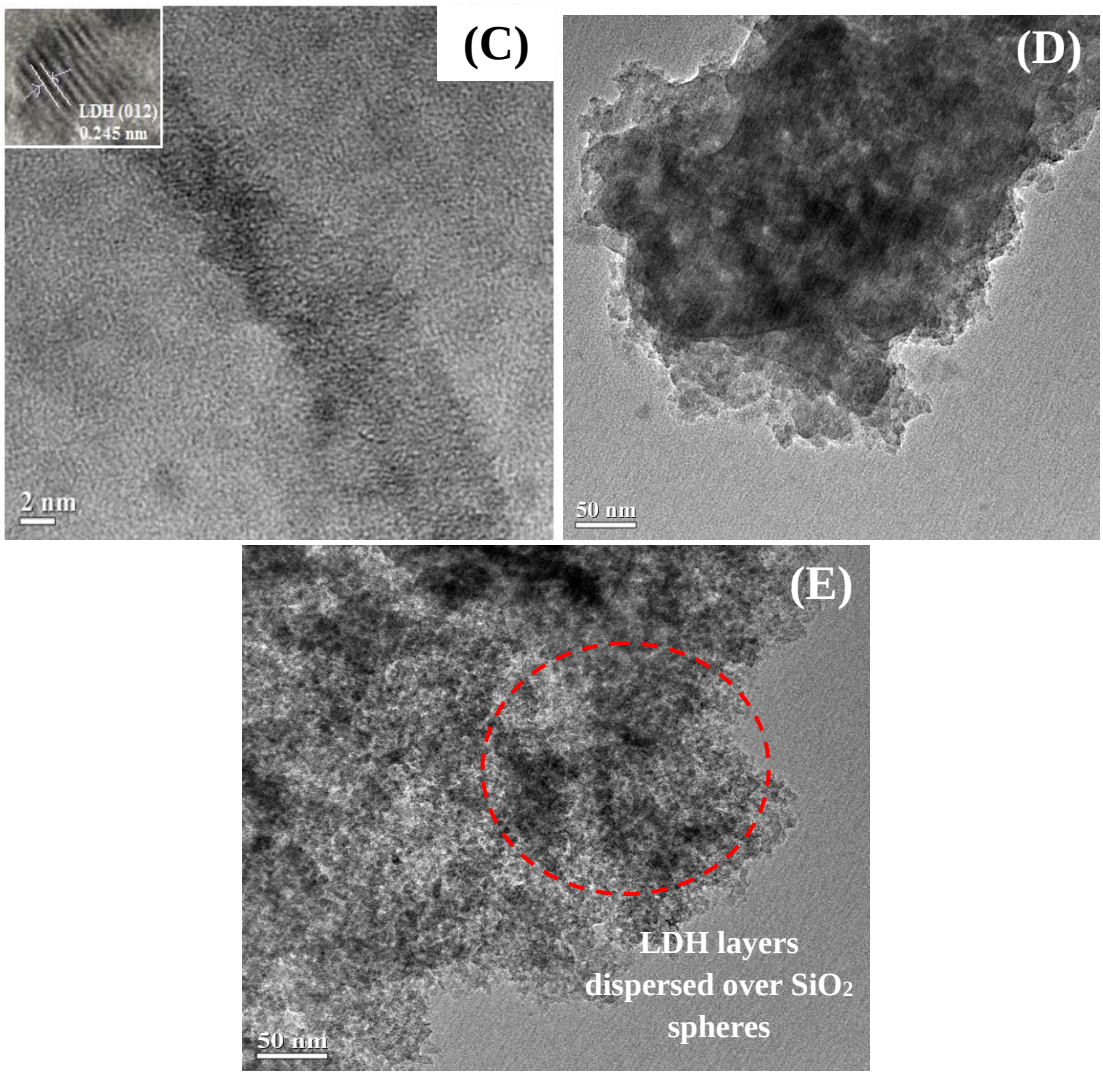

Fig. 3.A.13a: SEM and TEM images of Ni-Al-LDH (A, B&C); SiO_2@Ni-Al-LDH (2:1) (D&E).

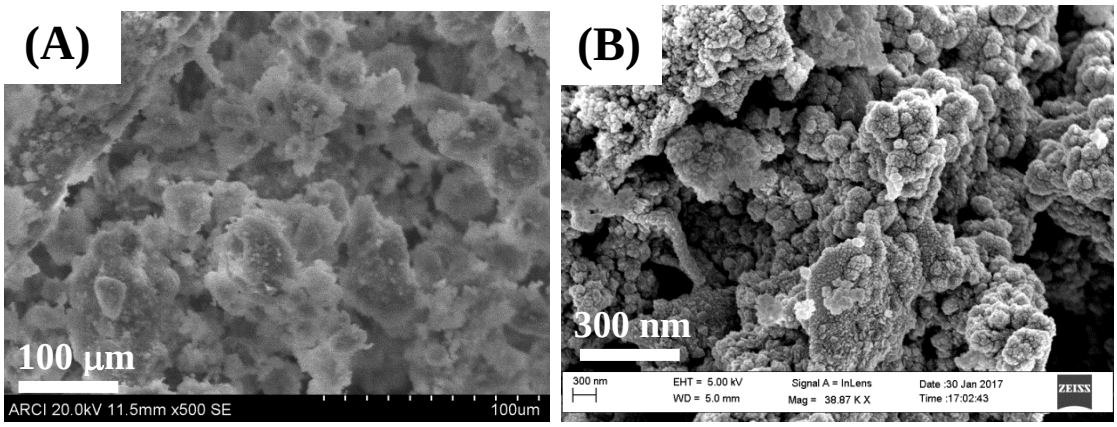

Fig. 3.A.13b: SEM images of calcined SiO_2@Ni-Al-LDH.

Fig. 3.A.13c shows SEM and TEM images of SiO_2@Mg-Al-LDHs. SEM pattern (**Fig. 3.A.13c.A**) showed the layered nature of unsupported Mg-Al-LDH. SEM patterns gave silica networking in powders from TEOS precursors over which LDH particles were present in the form of well distributed fine grains of 1-5 μm dimension (**Fig. 3.A.13c.B**). TEM images showed well grown silica cores surrounded by Mg-Al LDH nanosheet shells (**Fig. 3.A.13c.C,D&E**) which formed core-shell type structure. **Fig. 3.A.13c.E** showed the lattice fringes of (041) plane for SiO_2 which formed core part covered with LDH layers which formed the shell part. EDS pattern (**3.A.13c.F**) showed the presence of Mg, Al and O indicating the formation of Mg-Al-LDH.

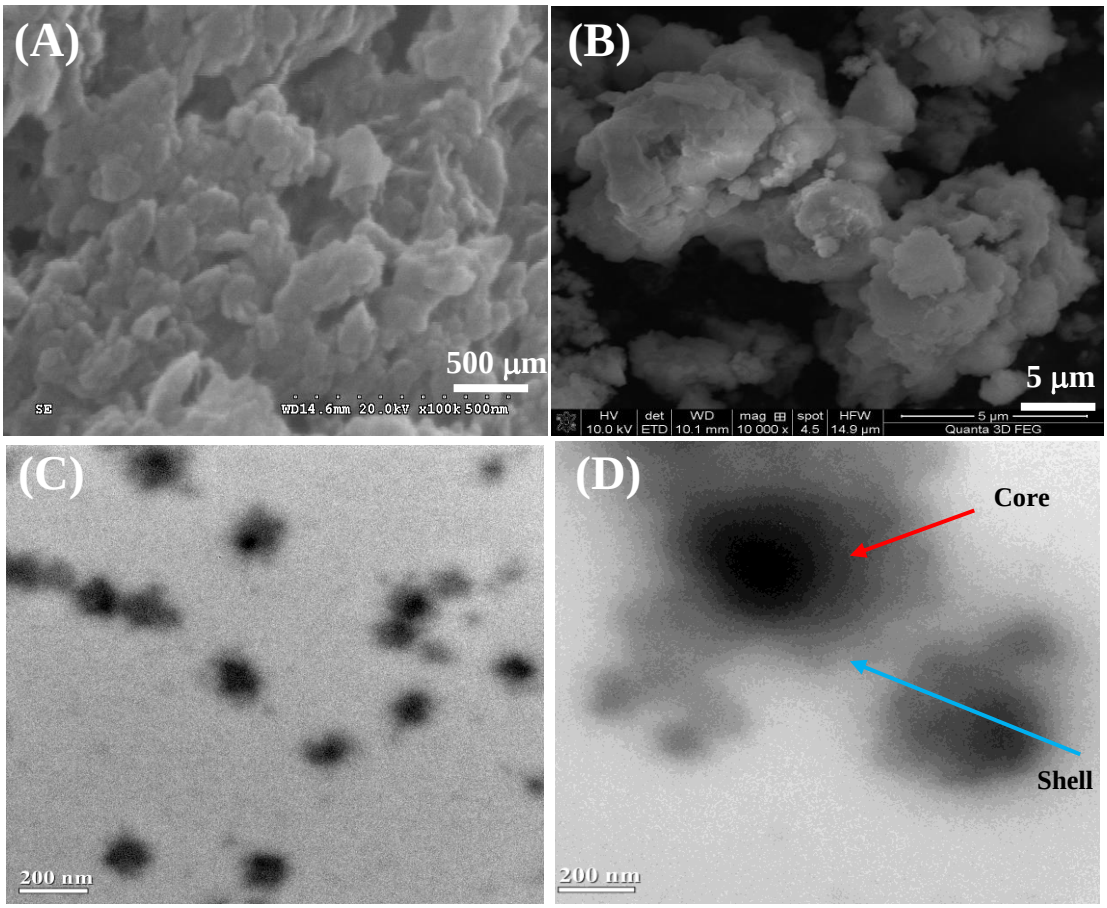

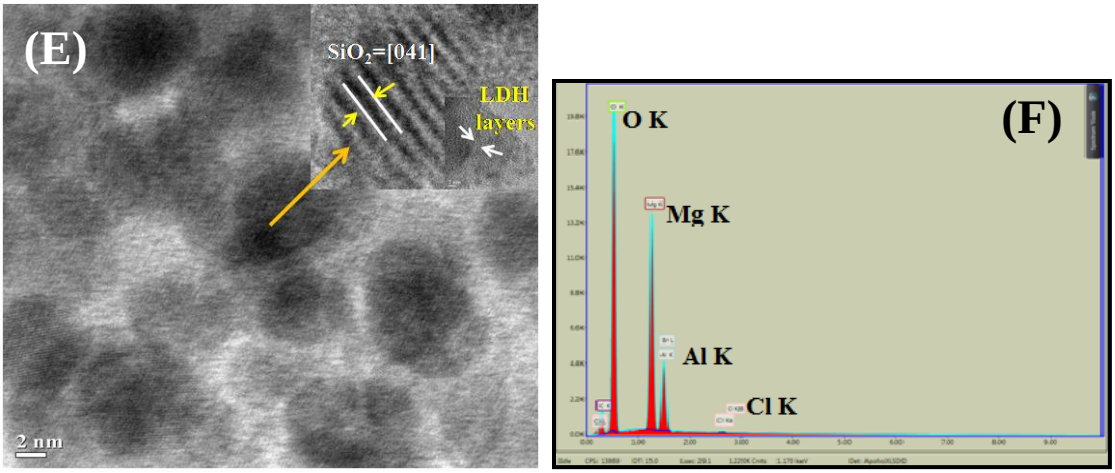

Fig. 3.A.13c: SEM image of unsupported Mg-Al-LDH (A); TEM and EDS images of SiO_2@Mg-Al-LDH with SiO_2 to LDH ratio 1:1 (B, C, D, E&F).

Fig. 3.A.13d shows the SEM pattern of calcined Mg-Al-LDH. After calcination the layered structure of Mg-Al-LDH did not change due to rehydration through 'Memory effect' of the calcined products [68] as LDH phases were observed in XRD pattern [68].

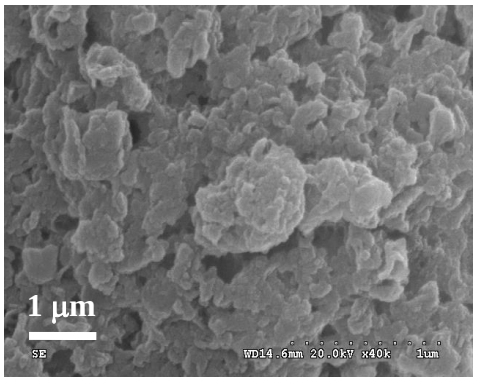

Fig. 3.A.13d: SEM image of calcined Mg-Al-LDH.

3.A.3.2. Gas-Solid reactions:

Gas-Solid reactions mainly the decomposition of toxic N_2O was carried out by using SiO_2@LDHs of Ni-Al-LDH and Mg-Al-LDH with different SiO_2:LDH ratios as catalyst. The catalytic performance was carried out over both powdered and honey comb coated catalysts. Before the gas reactions these nanocomposite alcogels were calcined at 450 ^oC to get mixed-metal nano oxide catalyst. The catalyst preparation and

catalytic performances are already described in the **Experimental Section 3.A.2**.

3.A.3.2.1. N_2O decomposition study:

3.A.3.2.1.1. N_2O decomposition over SiO_2@Mg-Al-LDH:

N_2O decomposition study over SiO_2 supported and unsupported Mg-Al-LDH was carried out in presence of low concentration of CO, CO_2 and CH_4 at 450 ^oC at Gas Hourly Space Velocity (GHSV) of 35,790 h^{-1} (200,000 $cm^3g^{-1}h^{-1}$). The flow rate of N_2O:Argon was maintained as 100:250 ml/min and the mixture of CO, CO_2 and CH_4 was maintained at 100 ml/min. The overall procedure of N_2O decomposition study over SiO_2 supported and unsupported Mg-Al-LDH has been already described in the **Experimental Section 3.A.2.6.2**. **Fig. 3.A.14a.A-G** shows the comparison of N_2O decomposition ability of hydrolysed TEOS, Mg-Al LDH alone and its silica supported composites (at various ratios of the components in the composite) in terms of Specific Decomposition Efficiencies (**SDE**). It was observed that the hydrolysed TEOS showed only 15 % N_2O conversion after 30 min reaction time (**Fig. 3.A.14a.A**). Unsupported Mg-Al-LDH showed 34 % reduction in the N_2O concentration after 30 min reaction time (**Fig. 3.A.14a.B**). It was further observed that in case of sol-gel derived silica supported Mg-Al LDH at silica to LDH ratio 1:1, there was 97 % conversion of N_2O to N_2 and O_2 after 30 min reaction time (**Fig. 3.A.14a.C**), there was 37 % conversion after 30 min in case of sol-gel derived silica supported Mg-Al LDH at silica to LDH ratio 1:2 (**Fig. 3.A.14a.D**). Sol-gel derived silica supported Mg-Al LDH at silica to LDH ratio 2:1 showed 82 % conversion after 30 min reaction time (**Fig. 3.A.14a.E**). There was 55 % conversion after 30 min in case of sol-gel derived silica supported Mg-Al LDH at silica to LDH ratio 1:4 (**Fig. 3.A.14a.F**) and 67 % conversion after 30 min in case of sol-gel derived silica supported Mg-Al LDH at silica to LDH ratio 4:1 (**Fig. 3.A.14a.G**). Therefore, it was observed that silica supported Mg-Al-LDH with

silica to LDH ratio 1:1 showed better catalytic activity towards N_2O decomposition. **Table 3.A.3** shows the Specific Decomposition Efficiency (**SDE**) in terms of LDH of these catalysts. It was observed that silica supported Mg-Al LDH at silica to LDH ratio 1:1 showed highest **SDE** value. **Fig. 3.A.14b** shows the bar diagrams for percentage N_2O decomposition in presence of SiO_2@Mg-Al-LDH catalysts with SiO_2 to LDH ratios of 1:0, 0:1, 1:1, 1:2, 2:1, 1:4 and 4:1 respectively. The fall in concentration of N_2O was detected in Thermal Conductivity Detector (TCD), Electron Capture Detector (ECD) and N_2, O_2 peak detected in Thermal Conductivity Detector (TCD) of the product gas. It was observed that initially concentration of N_2O was found as 291ppm (6.61 mmol) in TCD detector which decreased with the increase of temperature in presence of SiO_2@Mg-Al-LDH with SiO_2 to LDH ratio 1:1. The product gas was collected at various temperatures such as 190 ^oC, 225 ^oC and 450 ^oC respectively. The concentration of N_2O decreased from 291 ppm (6.61 mmol) to 0.634 ppm (0.014 mmol) as detected in ECD and showed about 97 % N_2O conversion. N_2O decomposed to N_2 and O_2 as shown in **Fig. 3.A.14b** in presence of all these catalysts and also CO, CO_2 and CH_4 concentration also decreased as shown by Gas chromatograms in **Fig. 3.A.14c.A, B&C**. The honeycomb monolith without the catalyst did not show any catalytic activity towards Gas-Solid reaction.

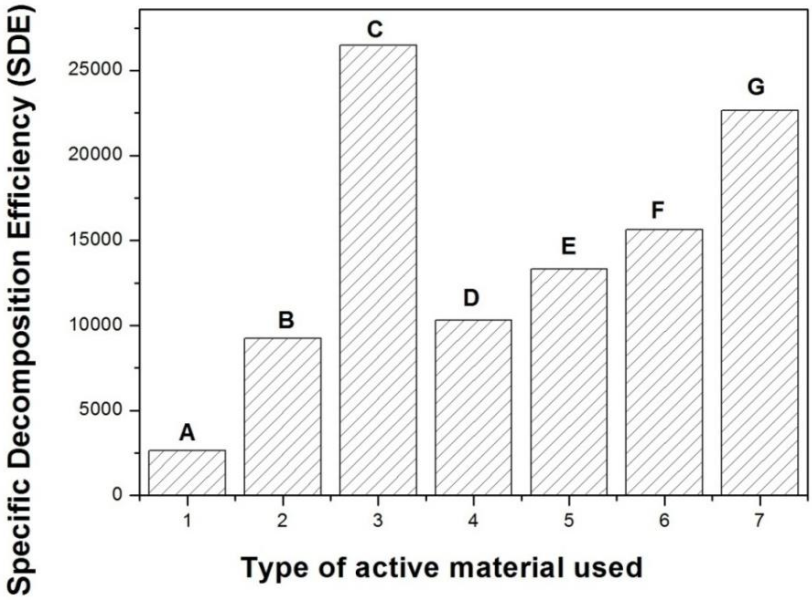

Fig. 3.A.14a: Bar Diagram of Specific N_2O Decomposition Efficiency (SDE).

Table 3.A.4: Specific Decomposition Efficiency (SDE) of the sol-gel derived hydrolysed TEOS, unsupported and silica supported materials used in Gas-Solid reactions for the decomposition of N_2O

Serial No.	SiO_2:Mg-Al LDH	% of Silica	% of Mg-Al LDH	SDE (In terms of LDH present in the composite)
1	1:0	100	0	2652 (A)
2	0:1	0	100	9248 (B)
3	1:1	50	50	26473 (C)
4	1:2	33	66	10319 (D)
5	2:1	66	33	13332 (E)
6	1:4	20	80	15646 (F)
7	4:1	80	20	22654 (G)

- *One Indian Patent is filed for the work described in the* ***Section 3.A.3.2.1.1 (File No. 201611022222).***

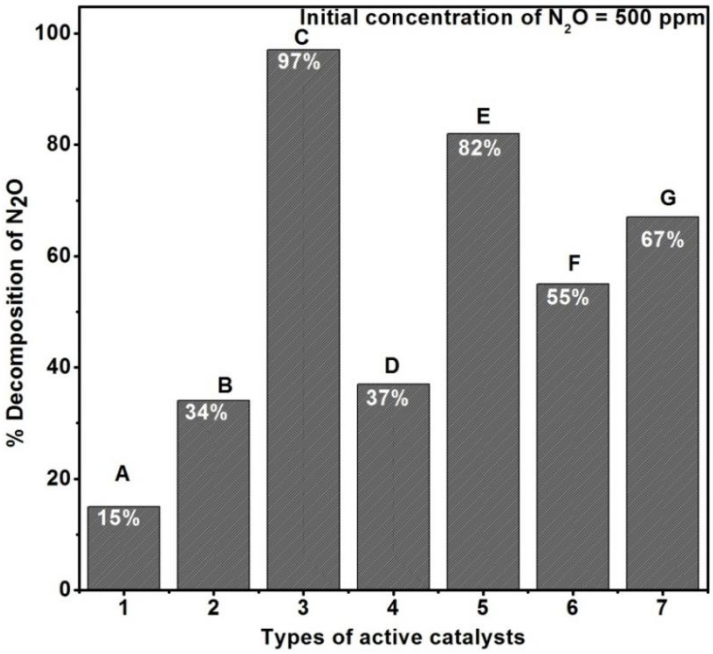

Fig. 3.A.14b: Bar diagrams for percentage decomposition of N_2O in presence of SiO_2@Mg-Al-LDH with different SiO_2 to LDH ratios.

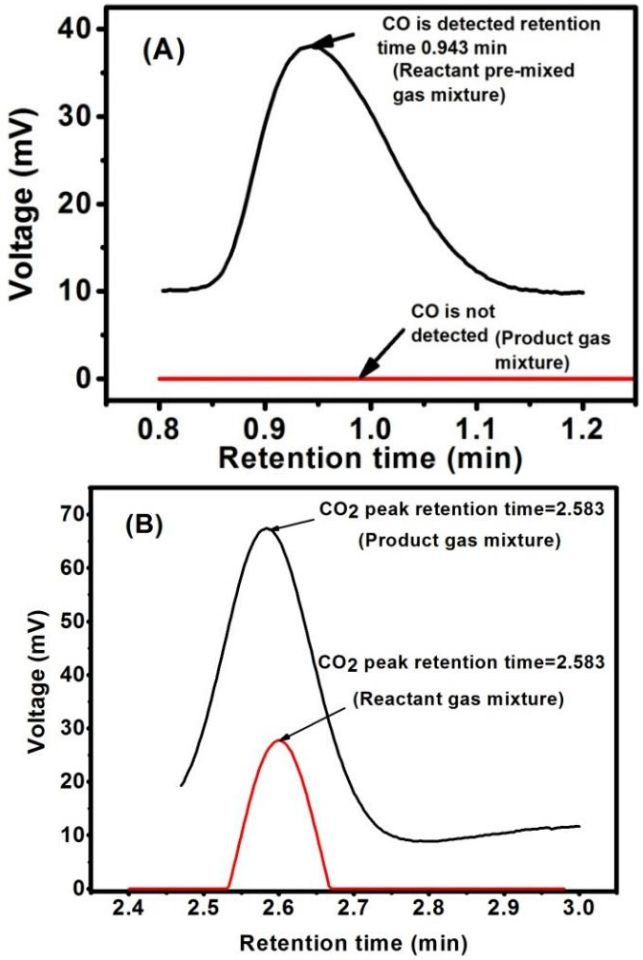

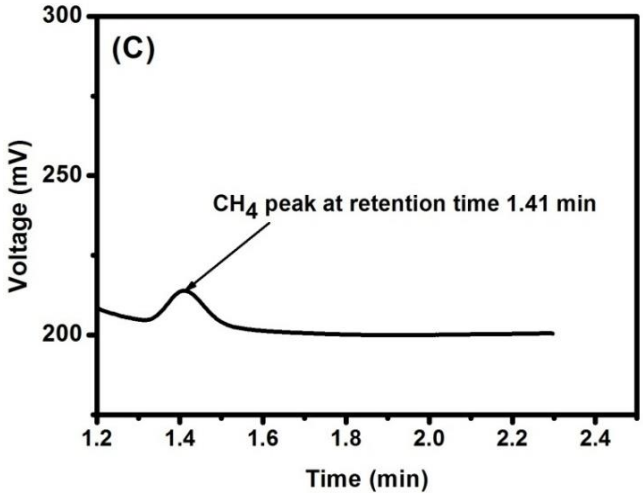

Fig. 3.A.14c: Chromatogram (FID) of reactant and product gas after passing through SiO_2@Mg-Al-LDH showing the peak due to CO, CO_2 and CH_4 (A, B&C).

3.A.3.2.1.2. N_2O decomposition over SiO_2@Ni-Al-LDH:

N_2O decomposition study over powdered SiO_2 supported and unsupported Ni-Al-LDH was carried out at 450 ^oC. Before the catalytic reaction the samples were calcined at 450 ^oC. The Argon:N_2O flow rate was maintained at 100:100 ml/min and initial concentration of N_2O was kept at 200 ppm (4.50 mmol). The Gas Hourly Space velocity (GHSV) was kept as 8,523 h^{-1} (12,000 $cm^3g^{-1}h^{-1}$). The overall procedure for the catalytic reaction has already described in the **Experimental Section 3.A.2.6.2**. **Fig. 3.A.15a** shows the percentage N_2O decomposition in presence of calcined SiO_2 supported and unsupported Ni-Al-LDH which are designated as CNA-01 (SiO_2:LDH ratio 0:1),CNA-11 (SiO_2:LDH ratio 1:1), CNA-12 (SiO_2:LDH ratio 1:2), CNA-21 (SiO_2:LDH ratio 2:1) respectively. **Table 3.A.4** shows the values of the percentage conversion of N_2O. The product gas was collected after 30 min and 60 min reaction time. It was observed that N_2O decomposed to N_2 and O_2 in presence of these catalyst. The reactivity towards N_2O decomposition of these catalyst increases in the following order CNA-01<CNA-11<CNA-12<CNA-21. CNA-01 showed about 92.3 % and 97.7

% N_2O conversion after 30 min and 60 min reaction time. CNA-11 showed about 93.9 % and 98.8 % N_2O conversion. On the other hand, CNA-12 and CNA-21 showed about 96.6 % and 99.4 % after 30 min whereas 96.8 % and 99.5 % of N_2O conversion after 60 min reaction as shown in **Fig. 3.A.15a**. It was further observed that catalyst with the highest SiO_2 to LDH 2:1 and 1:2 showed highest percentage conversion towards N_2O. Hence, it can be said that the catalytic activity depends on the SiO_2 loading and LDH loading in case Ni-Al-LDH catalyst. The mechanism for N_2O decomposition can be established as firstly N_2O was adsorbed on the catalyst surface and decomposed to N_2 and nascent oxygen and this nascent oxygen then interact with the oxygen species of the NiO catalyst as found from XRD analysis and finally formed N_2 and molecular O_2. **Fig. 3.A.15b** shows Gas Chromatograms for N_2O decomposition study over SiO_2@Ni-Al-LDH (2:1). N_2O was initially detected in Electron Capture Detector (ECD) and after 60 min reaction time no N_2O peak was observed in the product gas (**Fig. 3.A.15b.A**). On the other hand, **Fig. 3.A.15b.B** shows that N_2 and O_2 peak detected in Thermal Conductivity Detector (TCD).

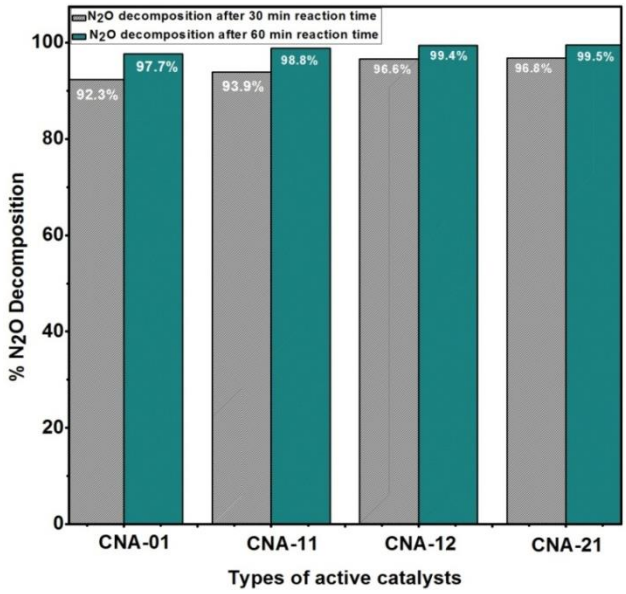

Fig. 3.A.15a: Percentage N_2O conversion in presence calcined SiO_2 unsupported and supported Ni-Al-LDH.

Table 3.A.5: N_2O Decomposition study over SiO_2@Ni-Al-LDH with different SiO_2:LDH ratios at 450 ºC

Type of active catalysts	Flow Rate (Argon:N_2O)	GHSV (Gas Hourly Space Velocity) in h^{-1}	Reactant Gas Concentration In ppm	Temperature (ºC)	Product Gas Concentration		% Decomposition	
					After 30 min	After 60 min	After 30 min	After 60 min
SiO_2:Ni-Al-LDH (0:1)	100:100 ml/min	8,523	200	450	15.34	4.56	92.3	97.7
SiO_2:Ni-Al-LDH (1:1)					12.2	2.45	93.9	98.8
SiO_2:Ni-Al-LDH (1:2)					6.87	1.13	96.6	99.4
SiO_2:Ni-Al-LDH (2:1)					6.37	1.04	96.8	99.5

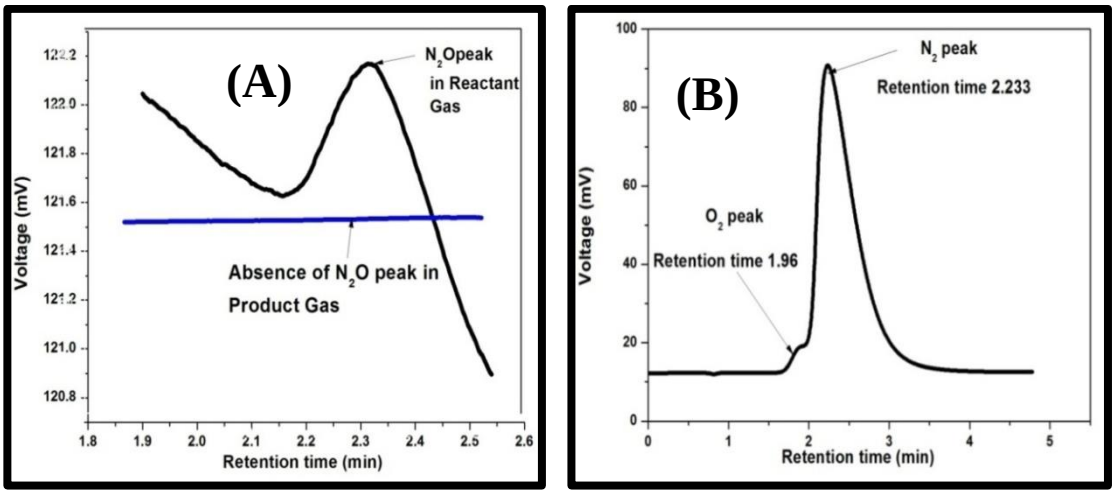

Fig. 3.A.15b: Gas Chromatograms of N_2O decomposition in presence SiO_2@Ni-Al-LDH (A) N_2O peak detected in ECD (B) N_2 and O_2 peak detected in TCD.

3.A.3.3. TGA-DTG analysis after gas reaction:

TGA-DTG analysis was carried out in TG-DTA analyzer (model Q-600, M/S TA Instruments) using α-Al_2O_3 as reference under air atmosphere to see the deposition of

coke over catalyst upto temperature 1000 ^{o}C. It was observed (**Fig. 3.A.16**) that the weight loss decreased from 6.2 % to 4 % with the increase of SiO_2 to LDH ratio from 0:1 to 2:1. Hence, coke deposition also decreased from 0:1 to 2:1 and catalyst with SiO_2 to LDH ratio 2:1 showed better catalytic activity towards N_2O decomposition due to the presence of highest amount of SiO_2. Since, coke deposition leads to deactivation of the catalyst [81]. Thus, the presence of SiO_2 in the catalysts enhanced the $NiAl_2O_4$ spinel formation and gave long life time of the catalysts [82] by reducing the deposition of coke.

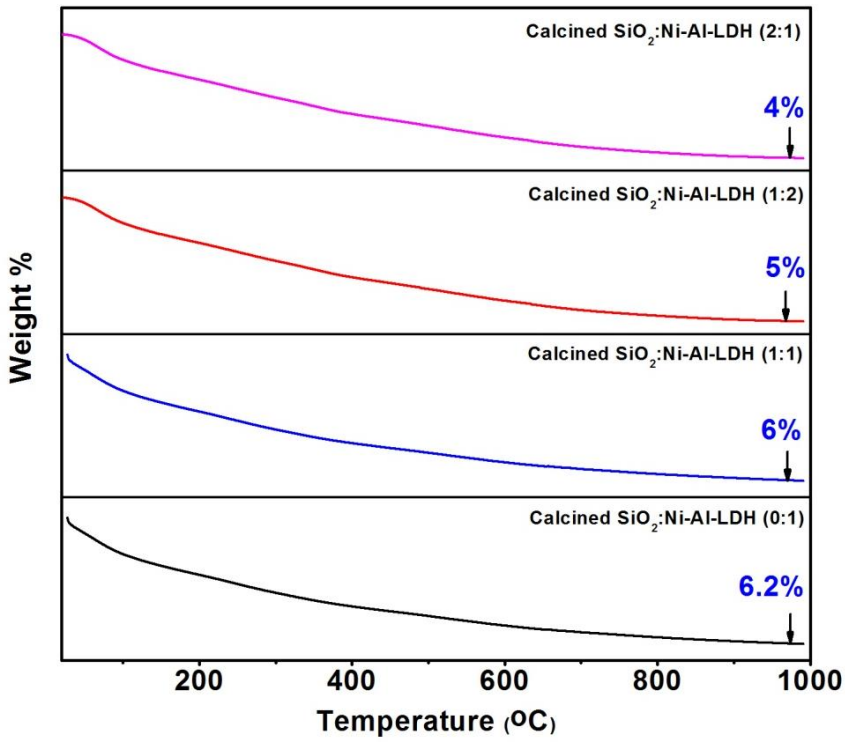

Fig. 3.A.16: TGA-DTG patterns of calcined SiO_2@Ni-Al-LDH after N_2O decomposition reaction.

3.A.4.CONCLUSIONS:

Both SiO_2@Mg-Al-LDH and SiO_2@Ni-Al-LDHs were synthesized by non-aqueous sol-gel method using metal acetylacetonate as precursors. These were then characterized by different techniques such as XRD, FT-IR, TGA-DTG, zeta potential

study, particle size analysis, rheometry, BET surface area and pore volume analysis, SEM, TEM and EDS analysis.

The kinetic parameters for the degradation of sol-gel derived Ni-Al-LDH were investigated by different methods viz. FWO, Friedman, Coats-Redfern and Phadnis-Deshpande methods. The results showed that the activation energies obtained by FWO and Friedman method for the second degradation were 68.06 kJ/mol and 68.43 kJ/mol respectively with pre-exponential factor (*A*) and reaction order (*n*) of 1.43×10^{2} s^{-1} and 3.8 respectively; for the third step degradation the activation energies were 91.28 kJ/mol and 73.04 kJ/mol with pre-exponential factor (*A*) and reaction order (*n*) of 1.82 $\times$ 10^{2} s^{-1} and 2.2 respectively. Again, the second step and third step degradation obeyed A_3 type Avrami-Erofeev equation and D_4 type three dimensional diffusion mechanism with Ginstling-Brounsthein equation and are in better agreement with FWO and Friedman method. These calculated parameters would help in future in understanding of mechanism of thermal degradation of LDH in general and sol-gel derived LDH in particular.

Zeta potential study also showed the better stability of these SiO_2@LDH nanocomposites. On the other hand, with the increase of SiO_2 to LDH ratio surface area also found to increase as well as the gel strength also increases which helps in their coating over solid preforms.

Different catalytic reactions such as N_2O decomposition reaction was carried out over mixed-metal oxides obtained from SiO_2@Mg-Al-LDH and SiO_2@Ni-Al-LDHs both in powdered and honeycomb monolithic coated form. It was observed that these catalysts showed better catalytic activity towards N_2O decomposition at 450 ^{o}C. SiO_2@Mg-Al-LDH with SiO_2 to LDH ratio 1:1 showed about 97 % conversion of N_2O to N_2 and O_2 after 30 min reaction time. On the otherhand, SiO_2@Ni-Al-LDH with

SiO_2 to LDH ratio 2:1 showed about 99.5 % N_2O conversion to N_2 and O_2. It was further observed that, in presence of SiO_2@Mg-Al-LDH not only N_2O was decomposed to N_2 and O_2 the concentration of CO and CH_4 also decreased.

REFERENCES:

[1] D.J.Wuebbles. Nitrous oxide: No laughing Matter. *Sci.*, **2009**, *326*, 56-57.

[2] F. Kapteijn, J. Rodriguez-Mirasol, J. A. Moulijn. *Appl.Catal. B:Environ.*, **1996**, *9*, 25.

[3] N. Russo, D. Mescia, D. Fino, G. Saracco, V. Specchia. *Ind. Eng. Chem. Res.*, **2007**,*46*, 4226-4231.

[4] M. Konsolakis. *ACS Catal.*, **2015**, *5*, 6397-6421.

[5] J.Wang, G. Fan, H. Wang, F. Li. *Ind. Eng. Chem. Res.*, **2011**, *50*, 13717-13726.

[6] J. C. Kramlich,W. P. Linak. *Prog. Energy Combust. Sci.*, **1994**, *20*, 149.

[7] M. A. Wojtowicz, J. R. Pels, J. A. Moulijn. *Fuel Proc. Technol.*, **1993**, *34*, 1.

[8] A. Shimizu, K.Tanaka, M. Fujimori. *Chemosphere*, **2000**, *2*, 425.

[9] G.Centi, P. Generali, L. dall'Olio, S. Perathoner, Z.Rak. *Ind. Eng. Chem. Res.*, **2000**, *39*, 131.

[10] J.P. Ramirez, G. Mul, F. Kapteijn, J. A. Moulijn. *Catal.Commun.*, **2002**, *3*, 19-23.

[11] J.P. Ramirez, F. Kapteijn, G. Mul, X. Xu, J.A. Moulijn.*Catal.Today.*, **2002**, *76*, 55-74.

[12] G. Mula, Zandbergena, F. Kapteijn, J.A. Moulijna, J.P. Ramirez. *Catal.Lett.*, **2004**, *93*, 1-2.

[13] J.P. Ramirez, G. Mul, F. Kapteijn, J. A. Moulijn. *Kinet. Catal.*, **2003**, *44*, 639-647.

[14] H. Dandl, G. Emig. *Appl.Catal. A*, **1998**, *168*, 261-268.

[15] S. Kannan, C.S.Swamy. *Appl. Catal.B:Environ.*, **1994**, *3*, 109-116.

[16] J.N. Armor, T.A. Braymer, T.S. Farris, Y. Li, F.P.Petrocelli, E.L.Weist, S.

Kannan,C.S. Swamy. *Appl.Catal.B:Environ.,* **1996**, *7*, 397-406.

[17] R S. Drago, K. Jurczyk, N. Kob. *Appl.Catal. B:Environ.,* **1997**, *13*, 69-79.

[18] K. Karaskova, L.Obalova, K. Jiratova, F. Kovanda. *Chem. Eng. J.,* **2010**, *160*, 480-487.

[19] J.P. Ramirez, F. Kapteijn, J.A.Moulijn. *Catal.Lett.,* **1999**, *60*, 133-138.

[20] S. Kannan. *Catal. Surveys from Asia,* **2006**, *10*, 117; DOI:10.1007/s10563-006-9012.

[21] S. He, Z. An, M. Wei, D.G.Evans, X. Duan. *Chem.Commun.,* **2013**, *49*, 5912.

[22] K.Galejova, L.Obalova, K.Jiratova, K.Pacultova, F. Kovanda. *Chem.Papers,* **2009**, *63(2)*, 172-179; DOI:10.2478/s11696-008-0105-0.

[23] X. Xu, H. Xu, F. Kapteijn, J.A. Moulijn. *Appl.Catal. B:Environ.,* **2004**, *53*, 265-274.

[24] Y. Izumi, T. Shimizu, T. Kobayashi, A. K-ichi. *Chem. Commun.,* **2000**, 1053-1054.

[25] I. M.Cabrera, S. Espinosa, J.C. Groen, B.Linden, F. Kapteijn, J.A. Moulijn. *J. Catal.,***2006**, *238*, 250-259.

[26] W.Wei, J.A. Moulijn, G. Mul. *J. Catal.,* **2009**, *262*, 1-8.

[27] W.Wei, J.A. Moulijn, G. Mul. *Microporous Mesoporous Mater.,* **2008**, *112*, 193-201.

[28] J.C.Jansen, H. Koegler, H. van Bekkum, H.P.A. Calis, C.M. van den Bleek, F. Kapteijn, J.A. Moulijn, E.R. Geus, N. van der Puil. *Microporous Mesoporous Mater.,* **1998**, *21*, 213-226.

[29] J. Oi, A. Obuchi, G.R. Bamwenda, A.Ogata, H. Yagita, S. Kushiyama, K.Mizuno. *Appl. Catal. B: Environ.,***1997**, *12*, 277-286.

[30] I.M.Cabrera, C. Mentruit, J.A.Z. Pieterse, R.W. van den Brink, G. Mul, F.

Kapteijn, J.A. Moulijn. *Catal.Commun.*, **2005**, *6*, 301-305.

[31] Y.D. Scherson, G.F.Wells, S.G.Woo, J. Lee, J.Park, J. Cantwell d Brian, C.S. Criddle. *Energy Environ. Sci*., **2013**, *6*, 241-248.

[32] M. Konsolakis, F. Aligizou, G. Goula, I.V.Yentekakis.*Chem.Eng. J.*, **2013**, *230*, 286-295.

[33] E. Pachatouridou, E. Papista, A. Delimitis, M.A.Vasiliades, A.M. Efstathiou, M.D. Amiridis, O.S. Alexeev, D. Bloom, G.E. Marnellos, M. Konsolakis, E. Iliopoulou. *Appl. Catal.B:Environ.*, **2016**, *187*, 259-268.

[34] E. Papista, E. Pachatouridou, E.F. Iliopoulou, A. Delimitis, G. Goula, I.V.Yentekakis, G.E. Marnellos, M. Konsolakis *13th International Conference on Clean Energy (ICCE-2014) June* **2014**,8-12.

[35] Y. Lin, T. Meng, Z. Ma. *J. Ind. Eng. Chem.*, **2015**, *28*, 138-146.

[36]D.Pietrogiacomi,M.C. Campa,L.R.Carbone,S.Tuti,M.Occhiuzzi.*Appl.Catal.B:Environ.*, **2016**, *187*, 218-227.

[37] J. S. Valente, G.R. Gattorno, M.V. Orta, E.T. Garcia. *Mater.Chem. Phys.*, **2012**, *133*, 621-629.

[38] F. Cavani, F. Trifiro, A. Vaccari. *Catal.Today*, **1991**, *11*, 173-301.

[39] V. Rives. *Nova Science Publishers, New York*, **2001**.

[40] X. Duan, D.G. Evans. *Vol. 119, Springer-Verlag, Berlin*, **2006**.

[41] Bi. Xue, F. Ting, Z. Hui. *ACS Appl. Mater. Interfaces*, **2014**, *6*, 20498-20509.

[42] M. Shao, F. Ning, J. Zhao, M. Wei, D.G. Evans, X. Duan. *J. Am. Chem. Soc.*, **2012**, *134*, 1071-1077.

[43] M. A. Aramendia, V. Borau, C. Jimenez, J.M. Marinas, J.R. Ruiz, J.F. Urbano. *J. Solid State Chem.*, **2002**, *168*, 156-161.

[44] Y. Wang , F. Li , S. Dong , X. Liu, M. Li. *J. Colloid Interface Sci*., **2016**, *467*,

28-34.

[45] M. Mishra, M.R. Das, R.L. Goswamee. *J. Sol-Gel Technol.*, **2010**, *54*, 57-61.

[46] B. M. Choudary, S. J. Vallabha, B.R. Reddy, L.K. Mannepalli, M.M. Rao, K.K. Rao, V. R. Kondapuram. United States Patent 8, 227, 046 Jul 24, **2012**.

[47] Z. Gu, J.J. Atherton, Z.P. Xu. *Chem. Commun.*, **2015**, *51*, 3024-3036.

[48] Y. Zhao, S. He, M. Wei, D.G. Evans, X. Duan. *Chem. Commun.*, **2010**, *46*, 3031-3033.

[49] J .Wang, R .Zhu, B. Gao, B. Wu, K. Li, X. Sun, H . Liu , S. Wang. *Biomater.*, **2014**, *35*, 466-478.

[50] J. Livage. *New J. Chem.*, **2001**, *25*, 1.

[51] M. Venkatesh, P. Ravi, S.P. Tewari. *J. Phys. Chem. A*, **2013**, *117*, 10162-10169.

[52] Y. He, S. Liao, Z. Chen, Y. Li, Y. Xia, W. Wu, B. Li. *Ind. Eng. Chem. Res.*, **2013**, *52*, 1870-1876.

[53] J. Cheng , Y. Pan , J. Yao , X. Wang , F. Pan. *J. Loss Prevent. in the Process Indust.*, **2016**, *40*, 139-146.

[54] A. Ghafarinazari, E. Zera, A. Lion, M. Scarpa, G.D. Soraru, G. Mariotto, N. Daldosso. *Thermochim. Acta.*, **2016**, *623*, 65-71.

[55] B. Jankovic, Z. Cupic, D. Jovanovic, M. Stankovic. *Chem. Engineer. Commun.*, **2016**, *203*, 182-199.

[56] S. C. Maiti, C. Ghoroi. *J. Therm. Anal. Calorim.*, **2015**, *12*, 1-13.

[57] Y. J. Rueda-Ordonez, K. Tannous. *Biores. Technol.*, **2015**, *196*, 136-144.

[58] J. S. Valente, E. Lima, J.A. Toledo-Antonio, M.A. Cortes-Jacome, L. Lartundo-Rojas, R. Montiel, J. Prince. *J. Phys. Chem. C*, **2010**, *114*, 2089-2099.

[59] C. Popescu. *Thermochim. Acta.*, **1996**, *285*, 309-23.

[60] A. W. Coats, J.P. Redfern. *Nature.*, **1964**, *201*, 68.

[61] A. B. Phadnis, V.V. Deshpande. *Thermochim.Acta.*, **1983**, *62*, 361-7.

[62] D. D. Perrin, W.L.F.Armarego. Purification of Labaratory Chemicals. Pergamon, Oxford, **1980**.

[63] J. Zhu, J.G. van Ommen, L. Lefferts. *Catal. Today*, **2006**, *112*, 82-85.

[64] M. Chen, J.L. Wu, Y.M. Liu, Y.Cao, K. N.Fan. *Catal.Commun.*, **2011**, *12*, 1063-1066.

[65] Z. Gu, J. J. Athertona, Z. P. Xu. *Chem. Commun.*, **2015**, *51*, 3024-3036.

[66] X. Li, D. Du, Y. Zhang, W. Xing, Q. Xue, Z. Yan. *J. Mater.Chem. A*, **2017**, *5*, 15460-15485.

[67] J. Ashok, G. Raju, P.S. Reddy, M. Subrahmanyam, A. Venugopal. *Int. J. Hydrog. Energy*, **2008**, *33*, 4809-4818.

[68] A.J. Marchi, C.R. Apestegu. *Appl.Clay Sci.*, **1998**, *13*, 35-48.

[69] F. Kovanda,V. Balek, V. Dornicak. *J. Therm. Anal. Calorim.*, **2003**, *71*, 727.

[70] S.K. Yun, T.J. Pinnavaia. *Chem. Mater.*, **1995**, *7(2)*, 348-354.

[71]Y. Hongbo, C. Meiling, W. Xu, G. Hong, Arch. *Metal. Mater.*, **2015**, *60*, 1357-1359.

[72] S. Vyazovkin, C.A. Wight. *Thermochim. Acta*, **1999**, *340*, 53-68.

[73] C. Popescu. *Thermochim. Acta*, **1996**, *285*, 309-323.

[74] T. Ozawa. *Therm. Analysis Rev. Prospect*, **2000**, *355*, 35-42.

[75] A.W. Coats, J.P. Redfern. *Nature*, **1964**, *201*, 68.

[76] A. B. Phadnis, V.V. Deshpande. *Thermochim. Acta.*, **1983**, *62*, 361-7.

[77] J. T. Sun, Y.D. Huang, G.F. Gong, H. L. Cao. *Poly. Degrad. Stab.*, **2006**, *91*, 339-346.

[78]H. Nasri, S.Khemakhem, R. B. Amar. *Per.Pol.Chem.Eng.*, **2014**, *58(2)*,171-178; DOI:10.3311/PPch.7388.

[79]X. Ji, W. Zhang, L. Shan, Y.Tian, J. Liu. *Sci. Rep.*, **2015**; DOI:10.1038/srep18367.

[80] R. Schollhorn. *Chem. Mater.*, **1996**, *8*, 1747.

[81] L. Xu, J. Zhang, F. Wang, K. Yuan, L. Wang, K. Wu, G. Xu, W. Chen. *RSC Adv.*, **2015**, *5*, 48256.

[82] R. S. Drago, K. Jurczyk, N. Kob, A. Bhattacharyya, J. Masin. *Catal. Lett.*, **1998**, *51*, 177-181.

CHAPTER-III
PART-B

SYNTHESIS AND CHARACTERIZATIONS OF BINARY LDHS OF Ni-Cr, Mg-Cr AND THEIR SiO_2@LDH NANOCOMPOSITES BY SOFT CHEMICAL SOL-GEL METHOD FOR THE CATALYTIC PARTIAL OXIDATION OF CH_4 IN PRESENCE OF N_2O

❖ Some part of this work has been published in ***RSC Advances, 6 (2016) 112092-112102.***

GRAPHICAL ABSTRACT

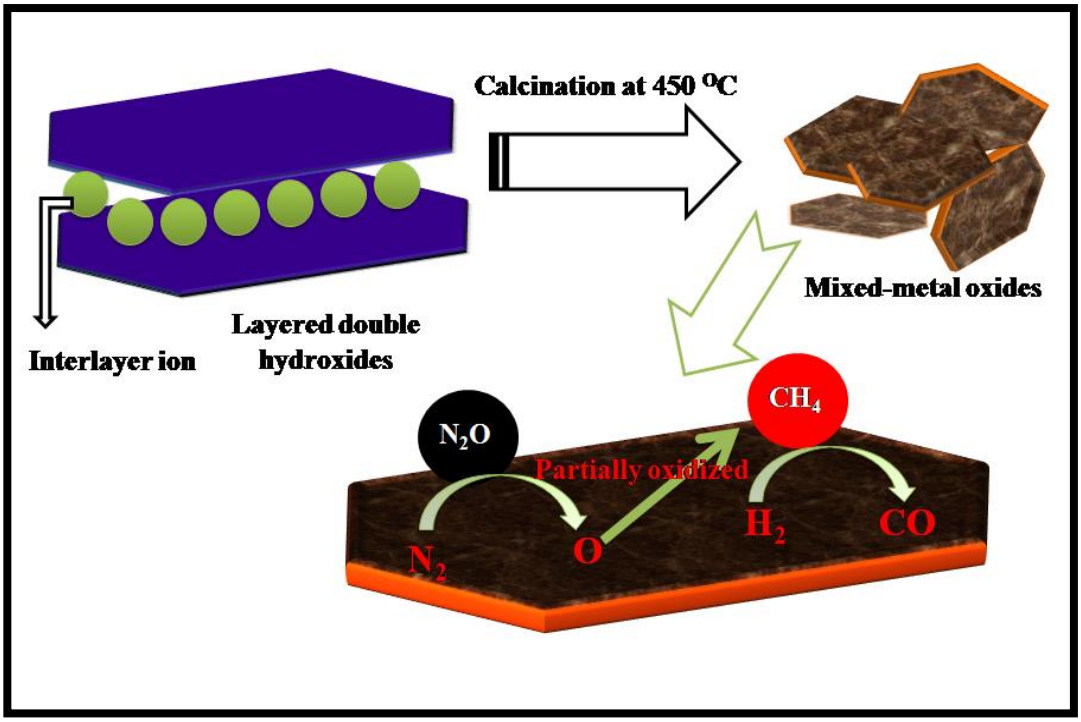

Schematic representation of catalytic partial oxidation of CH_4 in presence of N_2O by SiO_2@Ni-Cr-LDH based mixed-metal nano-oxide

ABSTRACT

This **part** describes about synthesis, characterisation and some application prospects of different binary LDHs such as Ni-Cr, Mg-Cr and their SiO_2 nanocomposites. These were synthesized by non-aqueous sol-gel route using different metal acetylacetonates as precursors such as $Ni(acac)_2$, $Mg(acac)_2$ and $Cr(acac)_3$. These were then characterized by XRD, TGA, XPS, SEM-EDS, HR-TEM, FT-IR, Rheometry, Zetametry, Particle size analysis, BET surface area analysis. Both the unsupported and SiO_2 supported LDHs were then coated over honey comb monoliths by dip coating and calcined at 450 ^{o}C to form as mixed-metal nano oxide. These mixed-metal nano oxides were further characterized by H_2-TPR, XPS analysis. This **part** also describes the use of honey comb coated mixed metal oxide catalysts for the decomposition of N_2O and Catalytic Partial Oxidation (CPO) of CH_4 to syn-gas (H_2/CO).

3.B.1. INTRODUCTION:

N_2O is the major environmental pollutant which has a global warming potential (GWP) of approximately 310 times higher than CO_2 and is the largest stratospheric ozone layer depleting substance [1-9]. Now-a-days, N_2O emission is significantly increasing due to different human activities such as application of chemical fertilizers, the combustion of fossil fuels and the large scale production of chemicals like nitric and adipic acid [10-13]. In addition to N_2O, CH_4 is also another green house gas. CH_4 is largely produced from refineries, chemical plants, oil wells and landfills [14]. Therefore, from the global environment maintenance point of view the control of N_2O and CH_4 emissions from combustion and chemical processes have significant importance. A number of methods can be employed to remove N_2O emissions, these are thermal decomposition [15,16], selective adsorption [15,17], plasma based decomposition [15] and catalytic decomposition [15]. Catalytic decomposition has advantages of lower energy requirement and lower cost over these technologies for controlling N_2O emissions.

In the similar way the conversion of CH_4 to valuable feed stocks is another ever challenging work. The direct oxidation of CH_4 in presence of O_2 has been reported by many researchers. Apart from that the catalytic partial oxidation (CPO) of CH_4 has drawn extensive attention of researchers [18]. Especially, the CH_4 present in the natural gas can be used as a valuable feed stock for the production of H_2 and other fuels [19] by this route. The CPO of CH_4 was first reported by Liander [20]. He suggested that if one O_2 molecule reacts with two molecules of CH_4 it would give H_2 and CO (synthesis gas). The partial oxidation of CH_4 involves the following reaction [18].

$$CH_4 + 1/2O_2 \longrightarrow 2H_2 + CO \qquad (3.B.1)$$

R.S. Drago *et al*.[21] reported the partial oxidation of CH_4 in presence of O_2 over NiO supported catalysts. They reported that SiO_2 supported NiO catalyst had better lifetime than NiO supported over Alumina. Although, they reported the CPO reaction at low temperature the selectivity towards H_2 and CO were obtained at 90 % and 78 %. According to them the selectivity increases only at a high temperature of above 1000 ^oC. T. Zhu *et al*.[22] reported the CPO of CH_4 to synthesis gas over Ni-CeO_2 catalyst. They had also carried out the reaction at high temperature from 500-750 ^oC and found only 86 % CO selectivity. Another work on CPO over Ni-CeO_2 catalyst at high temperature was reported by M. Peymani *et al*.[23] The CPO of CH_4 was also reported by A.C.W. Koh *et al*.[19]over Ni-cobalt catalysts. They had also reported the CPO at high temperature at about 900 ^oC. Therefore, it was found by many workers that the direct CPO of CH_4 is perhaps possible only at high temperature. On the other hand, the major problem of CPO reaction in presence of O_2 is that the molecular oxygen favours the total oxidation of CH_4 [24-27]. To overcome these problems some researcher used N_2O as oxidant for the CPO of methane. B.R.Wood *et al*.[28] reported the CPO of methane by N_2O in presence of Fe/Al-MFI catalyst. As reported by C. Mateos Pedrero *et al*.[29] the choice of N_2O as oxidant give better selectivity towards synthesis gas production. They reported the CPO of methane in presence of both O_2 and N_2O over rhodium catalysts. Although, they used N_2O as oxidant the highest selectivity towards H_2 and CO was observed only at high temperature. Another work on CPO of CH_4 was reported by C. M. Pedrero *et al*.[30] They had also reported this reaction at high temperature. The partial oxidation of CH_4 by N_2O over cobalt exchanged ZSM-5 catalyst was reported by N.A. Khan *et al*.[31] They reported this reaction at temperatures of 250-600 ^oC. In presence of these catalysts also the % CH_4 conversion did not exceed 70 %. J. Ashok *et al*.[32] have reported that the selectivity of H_2 and

CO is also dependent on the composition and preparation properties of the catalysts. Hence, development of suitable catalysts having better selectivity towards H_2 and CO especially from CPO of CH_4 by N_2O is a challenge for researchers. In such a backdrop we are reporting here the CPO of CH_4 in presence of both O_2 and N_2O over some mixed-first row transition metal sheet type nano-oxidic catalyst derived from mixed metal hydroxides or layered double hydroxides (LDHs) which are coated over honey comb monolithic supports. Where coat is constructed by dip coating of some silica-LDH based alcogels over honeycomb preforms. From the perspectives of materials designing the system have three distinct advantages - firstly while the use of core shell ultra-structure of composites provide catalytically advantageous exfoliated nanosheets of Layered Double Hydroxide precursors, silica based gelation provides non-Newtonian dispersional stability of LDH based nano-sheets and finally using alcogels or alcohols as dispersional media controls the drying and shrinkage behaviour of coated thin films of catalytically active layers over the channels of honeycomb preforms [33].

LDHs are represented by the general formula $[M_{1-x}^{2+}M_x^{3+}(OH)_2]^{x+}[A_{x/n}]^{n-3}.m\ H_2O$, where M^{2+} (e.g. Mg^{2+}, Ni^{2+}, Fe^{2+}, Co^{2+}, Cu^{2+}, Ni^{2+} or Zn^{2+}) and M^{3+} (e.g. Al^{3+}, Cr^{3+}, Ga^{3+},In^{3+}, Mn^{3+} or Fe^{3+}) where different M^{2+} and M^{3+} metal cations are uniformly and orderly distributed in the brucite-like sheets and various charge-compensating anions (A^{n-}) are present in their interlayer spaces [34-39]. LDHs have lots of applications including organic/pharmaceutical synthesis, clean energy generation, degradation of pollutants to control environmental pollution and photochemical reactions [40-45]. Mixed-metal nano-oxides are obtained from the calcination of these LDHs. Due to possession of catalytically important properties such as high surface area, uniform atomic level distribution of metal ion centers, acid-base bifunctionality these can be

used as a catalyst for various environmentally important reactions e.g. adsorption of toxic H_2S or SO_2 gas [46], the control of N_2O emission [16]. The use of Rh or Ni supported catalysts obtained from Mg-Al hydrotalcite for catalytic partial oxidation of CH_4 was reported by F. Basile *et al*.[47,48] They reported the solid phase crystallization method of synthesis of the catalysts and carried out direct CPO reaction at high temperature. J. Zhang *et al*.[49] reported the catalytic partial oxidation of CH_4 over fluorine modified mesoporous Ni-Mg-Al mixed oxides. D.V. Cesar *et al*.[50] reported the catalytic partial oxidation of CH_4 over Rh-Ni catalyst derived from hydrotalcite like precursors for which Ni-Mg-Al and Rh-Ni-Mg-Al LDHs were first synthesized by co-precipitation methods. Similarly, CPO of methane over Ni-Mg-Al spinel catalyst was reported by H. Messaoudi *et al*.[51] In all these works they reported the CPO of methane at high temperature.

In this chapter we describes the CPO of methane over mixed metal nano-oxide obtained from SiO_2@Ni-Cr-LDH and SiO_2@Mg-Cr-LDH nanocomposite alcogels with different SiO_2 to LDH ratios. The novelty of this work includes both in the synthesis procedure as well as in the use of such honey comb monolithic device to synergistically control two green house gases and to produce thereby two important clean energy component gases CO and hydrogen. In other words, we have carried out the CPO reaction in presence of low concentration of N_2O and CH_4 as well as at low temperature which also represents another novelty of the present work. The catalysts were prepared by simple sol-gel method using metal acetylacetonate of first raw transitional metal such as Ni/Mg and Cr as precursors which are not very expensive as Pd, Pt, Rh based catalyst precursors and Tetra ethyl orthosilicate (TEOS) which was used as a SiO_2 source. TEOS formed a network of distributed SiO_2 centers over which LDH were easily dispersed by forming a core-shell like structure. In terms of

performance evaluation the presence SiO_2 led to decrease in the deposition of coke over the catalyst otherwise it is a major problem of similar related heterogeneous catalysts [19].

Above these the honeycomb monolith [52,53] made from synthetic cordierite, MgO-Al_2O_3-SiO_2 are free from constraints of non-uniform access of reactants and high pressure drop in the catalytic bed which otherwise is a common problem in extruded or powder packed bed catalytic reactors. In addition the monoliths provide large external surface, uniform gas flow, low radial heat transfer, high geometric surface area, good attrition resistance and low tendency for plugging by particulates like fly ash and carbon soot generally encountered in an industrial or biological exhaust containing mixture of gases. Such mixture of gases often contains the gases of interest of the present paper viz. N_2O and CH_4. This paper also describes the effects caused by the concentration of N_2O in the feed towards the selectivity of syn gas (H_2+CO) production over these catalysts.

Such a unique combination of various favourable properties enhances scope of the present work to apply in future in areas such as combating simultaneous emission of N_2O and CH_4 from different anthropogenic sources. Emission of medley of greenhouse gases from a single source is a serious global problem in both developing and developed world. For example in a study conducted in Ghazipur, a municipal solid waste dumping site near Delhi for a period of summer months CH_4 emission ranged as 96-264 mg $m^{-2}h^{-1}$ and N_2O emission 826-1730 μg $m^{-2}h^{-1}$ [54,55]. Similarly tropical paddy fields are also reported as major source of both N_2O and CH_4 [56]. On the other hand in the developed world e.g. the United States Environmental Protection Agency also have reported simultaneous emission of both N_2O and CH_4 from hydrocarbon combustion vehicles of different types at different engine conditions.

In this chapter we have described the details of synthesis and physical properties like flow behaviour, thermal stability of the alcogels, the catalytic behaviour of calcined coated structured catalysts derived from the said core-shell type alcogels.

3.B.2. EXPERIMENTAL SECTION:

3.B.2.1. Synthesis of binary LDHs of Ni-Cr, Mg-Cr and their SiO_2 supported nanocomposites alcogels:

3.B.2.1.1. Materials:

Metal acetylacetonates such as $Ni(acac)_2$, $Mg(acac)_2$ and $Cr(acac)_3$ were purchased from Sigma Aldrich (98 % pure), ethanol and acetone (from Merck chemicals, purity 98 %), as ammonia were used. Ethanol and acetone were distilled, dried and purified before using [69]described in **Experimental Section 3.A.2.1** of **PART-A**.

3.B.2.1.2. Synthesis of Ni-Cr-LDH by non-aqueous sol-gel route:

0.02 mol Nickel acetylacetonate ($Ni(acac)_2$) was dissolved in 80 cm^3 of distilled ethanol at pH 6 by adding 0.2M HCl to dissolve $Ni(acac)_2$. 0.007 mol Chromium acetylacetonate ($Cr(acac)_3$) was dissolved in 80 cm^3 ethanol:acetone (1:1) mixture. These two solutions were mixed at 80 ^oC by stirring for 2-3 hours. The pH of the mixture was maintained at 8-9 by adding few drops of 1:2 NH_3:H_2O mixture and finally refluxed for 6-7 hours to get Ni-Cr-LDH. The product obtained was then filtered and dried in air oven at 40 ^oC.

3.B.2.1.3. Synthesis of Mg-Cr-LDH by non-aqueous sol-gel route:

0.02 mol Magnesium acetylacetonate ($Mg(acac)_2$) was dissolved in 80 cm^3 of distilled ethanol at pH 6 by adding 0.2M HCl to dissolve $Mg(acac)_2$. 0.007 mol Chromium acetylacetonate ($Cr(acac)_3$) was dissolved in 80 cm^3 ethanol:acetone (1:1) mixture. These two solutions were mixed at 80 ^oC by stirring for 2-3 hours. The pH of the mixture was maintained at 8-9 by adding few drops of 1:2 NH_3:H_2O mixture and

finally refluxed for 6-7 hours to get Mg-Cr-LDH. The product obtained was then filtered and dried in air oven at 40 ^{o}C.

3.B.2.1.4. Synthesis of SiO_2 supported nanocomposite alcogels of different LDHs:

3.B.2.1.4.1. Materials:

Metal acetylacetonates such as $Ni(acac)_2$, $Mg(acac)_2$ and $Cr(acac)_3$, were purchased from Sigma Aldrich (98 % pure), TEOS (Tetraethyl orthosilicate from Acros Scientific, purity 98 %), ethanol and acetone (from Merck chemicals, purity 98 %), ammonia were used. Ethanol and acetone were distilled, dried and purified before using [69]. Here, TEOS functioned as SiO_2 source.

3.B.2.1.4.2. Synthesis:

It involves the following steps-

Step-1: 0.02 mol Nickel acetylacetonate ($Ni(acac)_2$) / Magnesium acetylacetonate ($Mg(acac)_2$) was dissolved in 80 cm^3 of distilled ethanol at pH 6.

Step-2: 0.007 mol Chromium acetylacetonate ($Cr(acac)_3$) was dissolved in 80 cm^3 ethanol:acetone (1:1) mixture.

These two solutions were mixed at 80 ^{o}C by stirring for 2-3 hours. The pH of the mixture was maintained at 8-9 by adding few drops of 1:2 NH_3:H_2O mixture and finally refluxed for 6-7 hours to get Ni-Cr-LDH and Mg-Cr-LDH. The product obtained was then filtered and dried in air oven at 40 ^{o}C. 4.43 cm^3 TEOS, 0.72 cm^3 of 0.2 M aqueous HCl and 4.85 cm^3 distilled ethanol were taken and aged the mixture for 45 min in a magnetic stirrer at room temperature. The solutions of step -1 and step-2 were mixed at 80 ^{o}C and refluxed for 2 hours. Added hydrolysed TEOS to the mixed acetylacetonate solution and raised the pH upto 8-9 by adding 1:2 NH_3:H_2O mixture stirred continuously for another 6-7 hours to get silica supported LDH. A portion of the product was separated from the obtained free flowing gels by filtration, washed in hot

water and dried at 40 ^{o}C in air oven. The SiO_2 supported LDHs were synthesized by varying SiO_2 to LDH ratio. The schematic diagram is shown below-

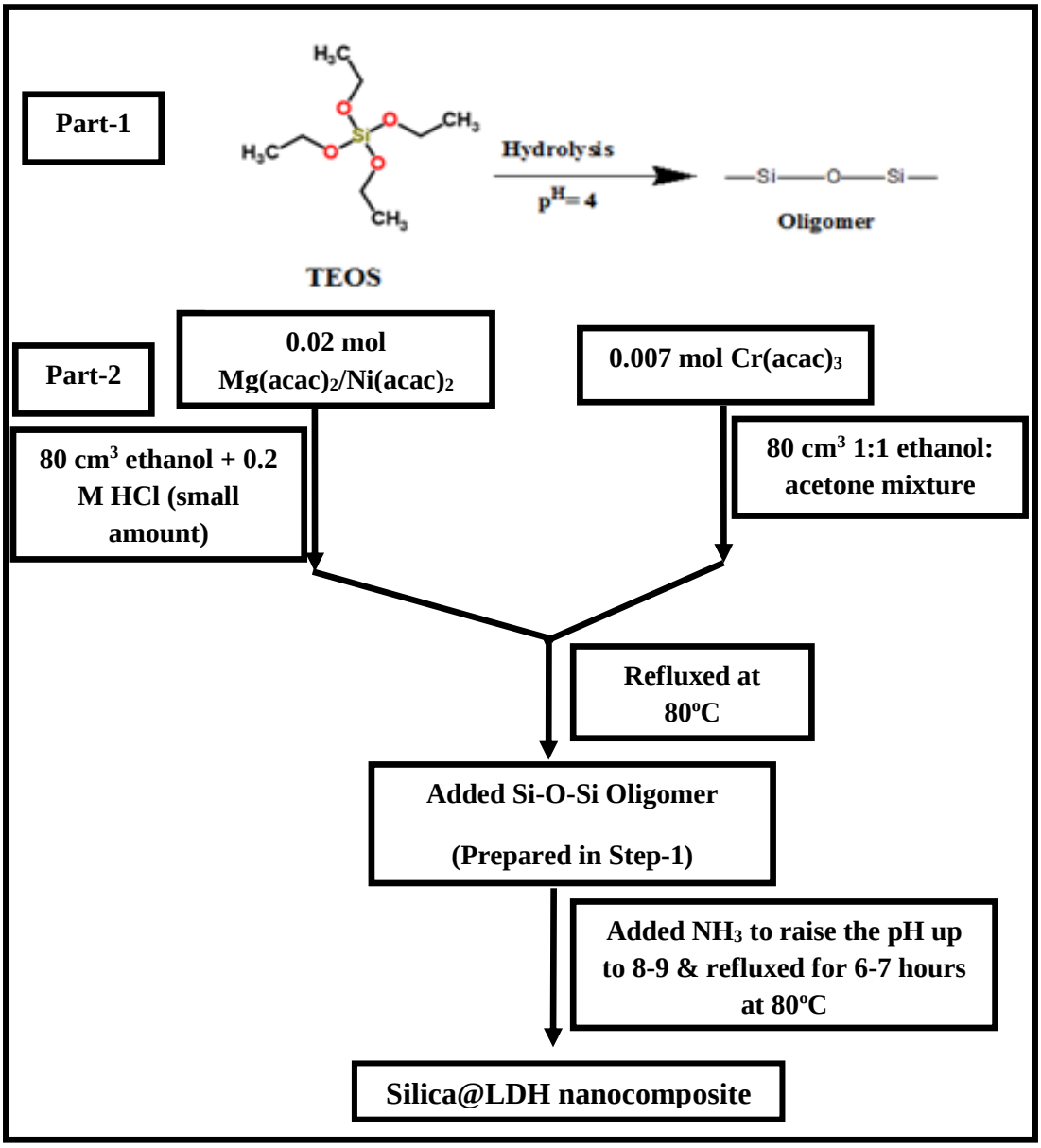

Fig. 3.B.1: Schematic diagram for the synthesis of SiO_2@LDH nanocomposite gels.

3.B.2.2. Characterizations:

Structure identification of inorganic phases formed were carried out in a powder X-ray diffractometer (Model Rigaku Ultima IV) using Cuk$_{\alpha}$ radiation of a wavelength of 1.54 Å at 40 mA and 40 kV X-ray generator current setting with a step size of 0.2^{o} 2θ

min^{-1}.

Fourier Transform Infrared (FT-IR) spectra of the prepared samples were recorded in spectrophotometer (Perkin-Elmer 2000 System) in 4,000-400 cm^{-1} range at a spectral resolution of 4 cm^{-1} using KBr pellets.

Field Emission Scanning Electron Microscopy (FE-SEM) analysis was carried out in a Carl Zeiss -Sigma VP equipment, with an accelerating voltage of 20 kV. Before the analysis the gels were dried at 40 ^{o}C in air oven for 1 week to avoid the moisture absorption. Finally, the sample surfaces were gold coated in high vacuum. Transmission electron microscopy (TEM) images were recorded on a JEOL JEM-2011 electron microscope operated at an accelerating voltage of 200 kV. The chemical composition was identified by using an energy-dispersive X-ray spectroscopy (EDX) detector on the scanning electron microscope Model Carl Zeiss Sigma VP.

The thermogravimetric measurements were carried out in a simultaneous TG-DTA analyzer (model Q-600, M/S TA Instruments) using α -Al_2O_3 as reference. Samples weighing about 5.0 mg were heated from 30 to 700 ^{o}C at a rate of 10 ^{o}C/min in an Argon atmosphere in a non-isothermal condition.

Specific surface area of the samples was recorded *via* Nitrogen gas adsorption at 77 K applying Brunauer-Emmett-Teller (BET) calculations using Autosorb-iQ Station 1 (Quantachrome, USA). Prior to performing the experiment the samples were degassed at 100 ^{o}C for 1.5 hours.

The zeta potential of the nanocomposite alcogels were measured with the Laser Doppler Velocimetry technique at 25 ^{o}C under a 10 Mw He-Ne laser (M/S Malvern Instruments Zetasizer Nano Z5). The particle size distribution of these nanocomposites were carried by DLS (Dynamic Light Scattering) technique in zeta sizer (M/S Malvern Instruments Zetasizer Nano Z5). To carry out these studies the

samples were filtered, washed with hot water and dried in air oven at 40 ^{o}C. The dried mass were ground gently in an agate mortar and redispersed in aqueous phase by shaking in an ultrasonic processor (M/S Sonics) with a 1.3 cm Ti probe for 30 minutes under 20 kHz frequency and 25 % amplitude of vibration.

3.B.2.3. Rheological study of SiO_2 supported nanocomposite alcogels of LDHs:

The rheological study of the nanocomposite gels with different SiO_2:LDH ratios were carried out by rotational (Rheolab QC - Anton Paar, Austria) with a measuring cup C-CC27/SS/QC and measuring system CC27/P6 at 15 ^{o}C.

On the other hand, the viscoelastic properties such as $G^{/}$(Storage modulus) and $G^{//}$(Loss modulus) of SiO_2@Ni-Cr-LDH and SiO_2@Mg-Cr-LDH with SiO_2:LDH ratios from 0:1 to 3:1 were studied by oscillatory rheometer (Modular compact rheometer MCR 302 Anton Paar, Austria) with a rough parallel plate geometry of 2.5 cm diameter and 0.1 cm gap was used at 15 ^{o}C. The sample was submitted to the parallel-plate and the amplitude of oscillation was increased up to 500 % apparent shear strain maintaining the angular frequency at 1 rad/s for the amplitude sweep test. For the frequency sweep test the shear strain was kept at 5 %.

3.B.2.4. Coating of SiO_2 supported nanocomposite alcogels of LDHs over solid preforms:

Different types of SiO_2 supported nanocomposite alcogels of LDHs such as SiO_2 @Mg-Al-LDH, SiO_2@Ni-Cr-LDH with different SiO_2 to LDH ratios were coated over Cordierite (MgO-Al_2O_3-SiO_2) honeycomb ceramic monolith by a dip coater (KSVD from M/S KSV Instrument, Finland) at 2 cm/min speed withdrawal and dipping rate as shown in **Fig. 3.A.2** of **PART-A** (**Experimental Section**). The honeycombs had 360 cells per square inch and a 3.2 cm diameter. The honey comb monolithic catalysts were supplied by DST-ARCI Hyderabad, India under a collaborative agreement.

Before dip-coating, the solid pre-forms were washed with distilled water and dried in air at 110°C for 2 h. After dip coating the coated honey comb monoliths were then withdrawn, kept hanging for few minutes. The dip-coated honey comb monoliths were dried overnight at room temperature followed by heating in air at 40°C. The thicknesses of the coats were varied by changing the SiO_2:LDH ratios. **Fig. 3.B.2** shows the honeycomb monoliths coated with SiO_2@Ni-Cr-LDH.

Fig. 3.B.2: Coated honeycomb monolith with SiO_2@Ni-Cr-LDH.

3.B.2.5. Gas-solid reaction over honey comb coated calcined SiO_2 supported and unsupported Ni-Cr-LDH and Mg-Cr-LDHs:

3.B.2.5.1. Catalytic partial oxidation of CH_4:

3.B.2.5.1.1. Catalytic partial oxidation of CH_4 in presence of N_2O over calcined SiO_2@Ni-Cr-LDHs (SiO_2 to LDH ratios 0:1 to 3:1):

Catalytic partial oxidation of CH_4 over honey comb monolith coated with SiO_2@Ni-Cr-LDHs with SiO_2 to LDH ratios 0:1 to 3:1was carried by the promotion of N_2O in the feed composition. In presence of these catalysts both standard partial -oxidation (SPO) in presence of O_2 and catalytic partial oxidation (CPO) of CH_4 in

presence of N_2O were carried out.

3.B.2.5.1.1a. Catalyst preparation:

The coated honeycombs were calcined at 450 ^oC in a muffle furnace for 2 hours to get mixed-metal nano-oxidic sheets supported over SiO_2. The calibration of the furnace was carried out by STQC Calibration No. F02720, Model No. PID-1173D at 450 ^oC. These mixed-metal nano-oxides are designated as CNC-01 (SiO_2:LDH ratio 0:1), CNC-11 (SiO_2:LDH ratio 1:1), CNC-21 (SiO_2:LDH ratio 2:1) and CNC-31 (SiO_2:LDH ratio 3:1) respectively. The total weight of the catalyst used as washcoat over the honecombs was about 0.4 g which was kept constant in case of all these catalysts.

3.B.2.5.1.1b Catalyst characterizations:

XRD analysis of the calcined samples were carried out in a powder X-ray diffractometer (Model Rigaku Ultima IV) using Cuk_α radiation of a wavelength of 1.54 Å at 40 mA and 40 kV X-ray generator current setting with a step size of 0.2^o 2θ min^{-1}.

The thermogravimetric measurements were carried out to check coke deposition in a simultaneous TG-DTA analyzer (model Q-600, M/S TA Instruments) using α-Al_2O_3 as reference. Samples weighing about 5.0 mg were heated from 30 to 1000 ^oC under oxygen atmosphere at a heating rate of 10 ^oC/min with flow rate of 100 ml/min in non-isothermal condition.

Temperature programmed reduction (TPR) with hydrogen was carried out in a M/S Micromeritics made instrument. About 0.0952 g of sample were pre treated at 120 ^oC in high purity helium gas (25cc/min) for 1 hour and cooled to room temperature in helium, the gas was changed to 5 % H_2/Ar (25 cc/min) at room temperature and waited till baseline is stable then TPR study was carried out from RT to 800 ^oC at 10 ^oC/min flow rate.

Field Emission Scanning Electron Microscopy (FE-SEM) analysis was carried out in a Carl Zeiss -Sigma VP equipment, at an accelerating voltage of 20 kV. Before the analysis the samples were dried at 40 ^{o}C in air oven for 1 week to avoid the moisture absorption. Finally, the sample surfaces were gold coated in 100 % vacuum. The chemical composition was identified by using an energy-dispersive X-ray spectroscopy (EDX) attachment present on the SEM. The metal ion concentration of metal acetylacetonate complexes was analysed by using AAS (Atmic absorption spectrometry) analysis (model Analyst 100 Perkin Elmer). Carbon amount was analysed by CHN analyser (model M/S Perkin-Elmer Model PE 2400), from CSIR-NEIST, Jorhat, India.

Specific surface area of the calcined samples was recorded *via* nitrogen gas adsorption at 77 K applying Brunauer-Emmett-Teller (BET) calculations using Autosorb-iQ Station 1 (Quantachrome, USA). Prior to performing the experiment the samples were degassed at 100 ^{o}C for 1.5 hours.

X-ray photoelectron spectroscopy (XPS) measurements were carried out in a Thermo Scientific MULTILAB 2000 Base system attached with X-Ray, Auger and ISS attachments having monochromatic Al K_{α} X-ray source (1486.6 eV). The photoelectron spectra were calibrated in bond energy, referenced to that of the component C-C of carbon C 1s at 284.8 eV.

3.B.2.5.1.1c. Catalytic activity in absence of N_2O: Standard catalytic partial oxidation:

The standard partial oxidation of CH_4 in the absence of N_2O was carried out over CNC-01, CNC-11, CNC-21 and CNC-31 catalysts at a temperature ranging from 200-500 ^{o}C. The feed composition for this reaction was maintained as 300 ppm CH_4 (18.70 mmol, 99.999 % pure), 150 ppm O_2 (9.37 mmol) with N_2 balanced (total flow 150

ml/min). The CH_4:O_2 mol ratio was kept as 2:1. The gas hourly space velocity was GHSV= 22,500$cm^3gcat^{-1}h^{-1}$ with respect to the weight of the catalyst in the honeycomb used as a washcoat.

3.B.2.5.1.1d. Catalytic activity in presence of N_2O:

Catalytic activity by supplying different concentration of N_2O with N_2 balanced (Supplied by M/s Eurasian Associates, Kolkata) into the feed was carried out at temperature 500 ^oC depending upon the standard partial oxidation of CH_4. The CH_4:N_2O mol ratios were kept at 2:1, 1:1 and 1:2 with 100 ppm (2.27 mmol), 300 ppm (6.8 mmol) and 500 ppm (11.36 mmol) N_2O against 70 ppm (4.36 mmol), 100 ppm (6.8 mmol) and 90 ppm (5.62 mmol) CH_4 at the same GHSV (total flow rate of 150 ml/min).

3.B.2.5.1.1e. Catalytic performance:

Catalytic performance was carried out by packing these coated honeycombs in a stainless-steel catalytic converter as described in the **Experimental Section 3.A.2.5.2** (**Fig. 3.A.3**) of **PART-A** at temperature ranging from 200-500 ^oC. The two ends of the tube were fixed with inlet and outlet tubes in a leak proof manner with rubber corks. The tube was placed inside a cylindrical furnace. The flow rate of the gas was controlled by different types of mass flow meter obtained from M/S Gilmont, USA under atmospheric pressure. Before the catalytic reactions the catalysts were activated in H_2 atmosphere (100 ml/min flow rate) at a temperature of 600 ^oC for 2 hours. The fall in concentration of N_2O and consequent increase of N_2 and O_2 in the product stream was measured by Unibead C as separating column with Thermal conductivity Detector (TCD) and Electron Capture Detector (ECD). The concentration of CH_4 was measured by Flame Ionization Detector (FID) in GC. Calibration of GC was done from a premixed calibration standard containing N_2O, N_2 and O_2 at standard ppm with

balanced Nitrogen. The product gases such as CO and CH_4 were detected by FID detector and H_2 was detected by TCD detector in a Molsieve 5A Q column by keeping the oven temperature at 50 ^oC in presence of argon as a carrier gas with flow rate of 25 ml/min and at 180 ^oC TCD temperature. The low concentration of CO was detected by Ni-Catalytic Reactor attachment fitted in the GC. The length of Molsieve 5A Q column was 243.84 cm having a diameter of 0.32 cm.The results were estimated with standard calibration gas mixtures supplied by M/S Span Gas Mumbai, India and standard Gas Chromatographic software IRIS-32 from M/S Thermo-Fischer India.

3.B.2.5.2. Catalytic partial oxidation of CH_4 by N_2O over SiO_2@Mg-Cr-LDH:

Catalytic partial oxidation of CH_4 by N_2O in presence of powdered calcined Mg-Cr-LDH at 500 ^oC. The initial concentration of N_2O and CH_4 was kept as 300 ppm (6.8 mmol) and 100 ppm (6.8 mmol).The mol ratio of N_2O:CH_4 was maintained at 1:1. The catalyst was first activated in presence of Argon in the flow rate of 150 ml/min for 2 hours. The flow rate of N_2O:CH_4 was maintained at 100:50 ml/min. The GHSV for this reaction was maintained at 12,784 h^{-1} (18,000 $cm^3g^{-1}h^{-1}$). The catalyst packing in SS tube was about ~ 0.5 g. The procedure of the catalytic reaction was same as described in the **Experimental Section 3.A.2.5.2** of **PART-A**. The product gases were collected after 30 and 60 min reaction time.

3.B.2.5.3. Conversion expressions of N_2O decomposition study and CH_4 partial oxidation:

The percentage conversion (*X*) and percentage yield (*Y*) were calculated by the following equations [57] -

$$X_{N_2O} = \frac{[N_2O]_{in} - [N_2O]_{out}}{[N_2O]_{in}} \times 100 \qquad (3.B.2)$$

$$X_{CH_4} = \frac{[CH_4]_{in} - [CH_4]_{out}}{[CH_4]_{in}} \times 100 \quad (3.B.3)$$

$$Y_{O_2} = \frac{[O_2]_{out}}{[N_2O]_{in}} \times 100 \quad (3.B.4)$$

$$Y_{H_2} = \frac{[H_2]_{out}}{2 \times [CH_4]_{in}} \times 100 \quad (3.B.5)$$

$$Y_{CO_2} = \frac{[CO_2]_{out}}{[CH_4]_{in}} \times 100 \quad (3.B.6)$$

$$Y_{CO} = \frac{[CO]_{out}}{[CH_4]_{in}} \times 100 \quad (3.B.7)$$

Turn over frequency (TOF) for this reaction was determined by using the following reaction [58]-

$$\text{TOF } (s^{-1}) = \frac{Amount\ of\ CH_4\ conversion}{Amount\ of\ Ni^0\ calculated\ based\ on\ XPS\ data} \quad (3.B.8)$$

3.B.3. RESULTS AND DISCUSSION:

The synthesis procedure of different types of binary LDHs and their SiO_2@LDH nanocomposite alcogels are described in the **Experimental Section 3.B.2**. These were synthesized by soft chemical sol-gel method using metal acetylacetonate as precursors in organic medium. The main advantage of using metal acetylacetonate precursors is that they undergo slow and controlled hydrolysis than the common metal alkoxides generally used in sol-gel hydrolysis reactions. This route gives a better opportunity for maintenance of desired micro-structure of hydrolysed products. However, SiO_2 component of the composite was obtained from the hydrolysis of an alkoxide precursor Tetraethyl orthosilicate (TEOS). The faster hydrolysis of TEOS than the metal acetylacetonate precursors and the oligomerisation of silicate ions in an initially maintained low pH, during the hydrolysis process helped in the formation of silica

cores and associated networking to form the gels and assembling of LDH sheets to have shells formed around the cores. They together formed the composite process of basic core-shell type soft alcogel. Such soft gels on careful drying and calcination forms an aerogel or a xerogel type catalyst having the capabilities of abatement of some of the environmentally harmful gases at considerably lower temperatures or dielectic/supercapacitor type materials or filters for components of electromagnetic radiations [70,71].

This section gives interpretation of the different results obtained by the characterizations of the products as well as the gas-solid reactions carried out by different catalysts synthesised from these products.

3.B.3.1. Characterizations of the binary LDHs and their SiO_2 nanocomposite alcogels:

Binary LDHs and their SiO_2 supported products were characterized by different techniques such as PXRD, FT-IR, TGA-DTG, BET surface area and pore volume analysis, particle size analysis, zeta potential analysis, rheometric analysis, SEM and EDS, TEM analysis. These are briefly described below:

3.B.3.1.1. Powder XRD analysis:

Powder XRD analysis of binary LDHs and their SiO_2 nanocomposite alcogels were carried out using powder X-ray diffractometer (Model Rigaku Ultima IV) using Cuk_{α} radiation of a wavelength of 1.54 Å at 40 mA and 40 kV X-ray generator current setting with a step size of 0.2^{o} 2θ min^{-1}.

3.B.3.1.1.1. SiO_2@Ni-Cr-LDH:

The presence of LDH phase was identified by XRD (**Fig.3.B.3**) analysis. **Fig. 3.B.3A** shows the XRD pattern of uncalcined products. XRD patterns of samples without SiO_2 component showed the peaks related to *hkl* reflections at (003), (006), (012)

originating from LDH sheet in Ni-Cr-LDH. Even with the increase of the SiO_2 component in the nanocomposites the XRD pattern invariably showed sharp *00l* reflections of the LDH phase indicating the existence of SiO_2 part in a poorly crystalline form. The position of *00l* peaks remained almost constant for each of the phases Ni-Cr indicating further the absence of intercalation of any new ions in the interlayer positions with the increase of silica content. The peaks due to SiO_2 were obtained at 18°, 22.98°, 25.94° 2θ for Cu k_α radiation with corresponding *hkl* reflections at (131), (101), (331), (300) and (350) respectively (**JCPDS PDF card no. 00-044-1394**). It was also observed that with the increase of SiO_2 content the weaker peaks due to SiO_2 became more and more intense from 1:1 to 3:1 SiO_2: LDH ratios. Also, it was observed that in case of SiO_2 bearing LDH nanocomposites additional peaks of LDH phase becomes visible, such enhancement of XRD reflections indicate a possible delaminated orientation of LDH sheets around the silica surface.

XRD analysis of the calcined SiO_2@Ni-Cr-LDH (**Fig. 3.B.3B**) showed the presence of higher intensity NiO phases with *hkl* reflection of (012) (d=2.09Å), (101) and (201) respectively and relatively lower intensity $NiCr_2O_4$ phase of *hkl* reflection (206) (**JCPDS PDF Card No.00-044-1159**) was observed in case of calcined SiO_2 unsupported product. From XRD analysis it was also found that the peaks due to $NiCr_2O_4$ phase was not observed in case of calcined products with SiO_2 to LDH ratios from 1:1 to 3:1 due to the presence of SiO_2 which suppressed the formation of spinel type phase [59]. .On the other hand, the sharp peak due to SiO_2 and Cr_2O_3 were not observed in these calcined samples which exist as amorphous or poorly crystalline SiO_2-Cr_2O_3 type phases [60]. Thus, it was observed that after calcination the LDH component of SiO_2@Ni-Cr-LDH was converted to metal oxides of Ni and Cr which

was further confirmed by SEM and EDS analysis.

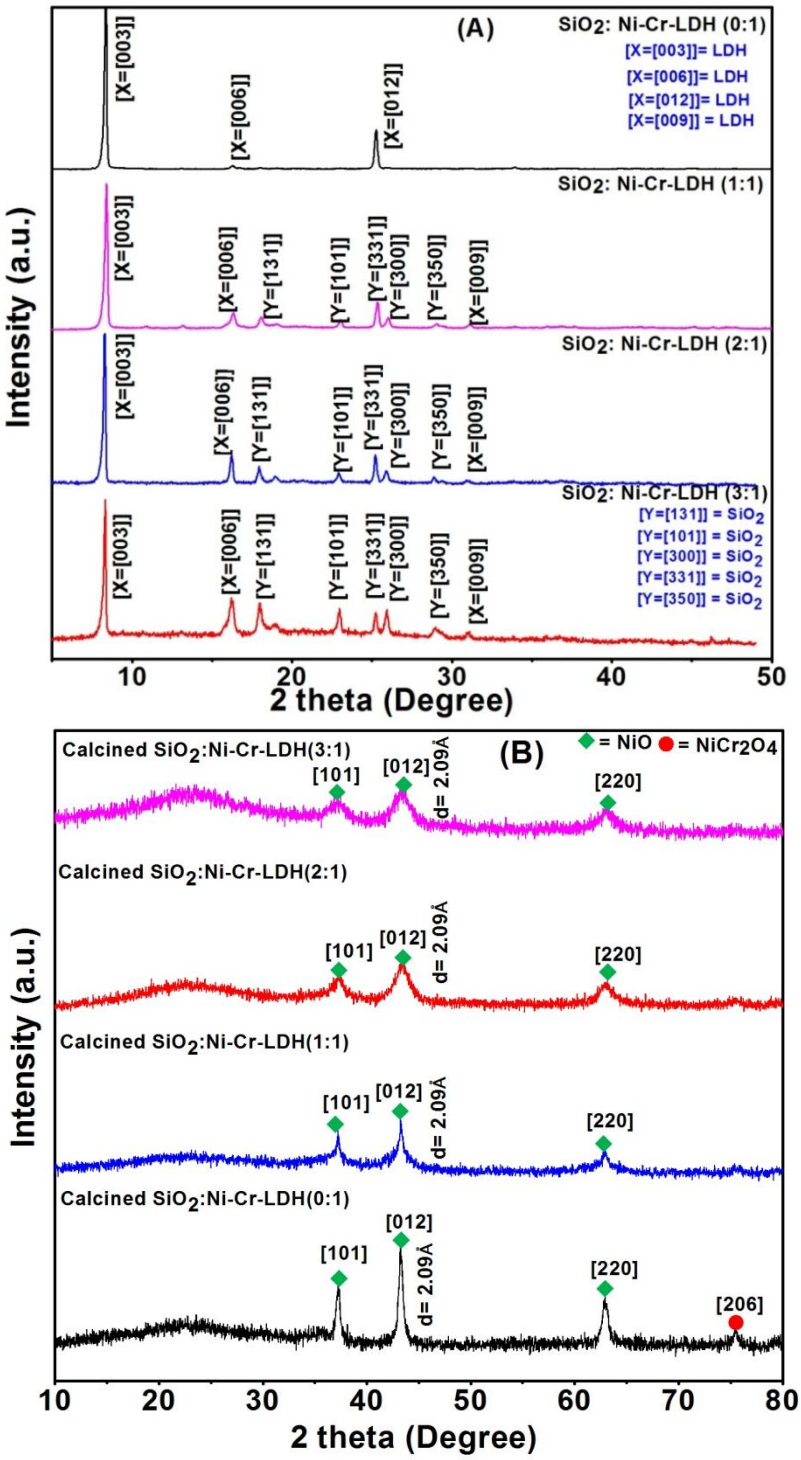

Fig. 3.B.3: XRD patterns of uncalcined (A) and calcined (B) (calcined at 450 ºC) SiO_2@Ni-Cr-LDH with different SiO_2 to LDH ratios.

3.B.3.1.1.2. SiO_2@Mg-Cr-LDH:

Fig. 3.B.4A shows the XRD patterns of unsupported and SiO_2 supported Mg-Cr-LDH

with SiO_2 to LDH ratios from 0:1 to 3:1. It showed the presence of LDH phases with *hkl* reflections of (003), (006) and (012) respectively. Like, SiO_2@Ni-Cr-LDH with the increase of the SiO_2 component SiO_2@Mg-Cr-LDH also showed sharp *00l* reflections of the LDH phase indicating the existence of SiO_2 part in a poorly crystalline form. The peaks due to SiO_2 were obtained with *hkl* reflections of (201), (331) and (220). It was further observed that with the increase of SiO_2 content the weaker peaks due to SiO_2 became more and more intense as SiO_2:LDH ratios varied from 1:1 to 3:1 [33].

Fig.3.B.4B shows the XRD pattern of calcined SiO_2@Mg-Cr-LDH with SiO_2 to LDH ratio 3:1. It was observed that XRD pattern showed the presence of MgO phases with *hkl* reflection of (211) (d= 3.05 Å) (111) and (400) (**JCPDS PDF Card No. 00-030-0794**).

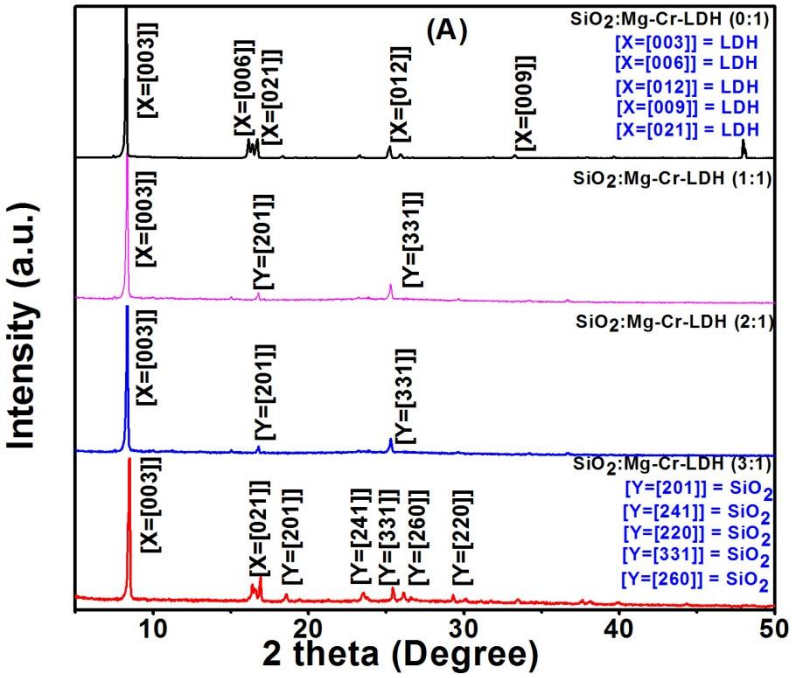

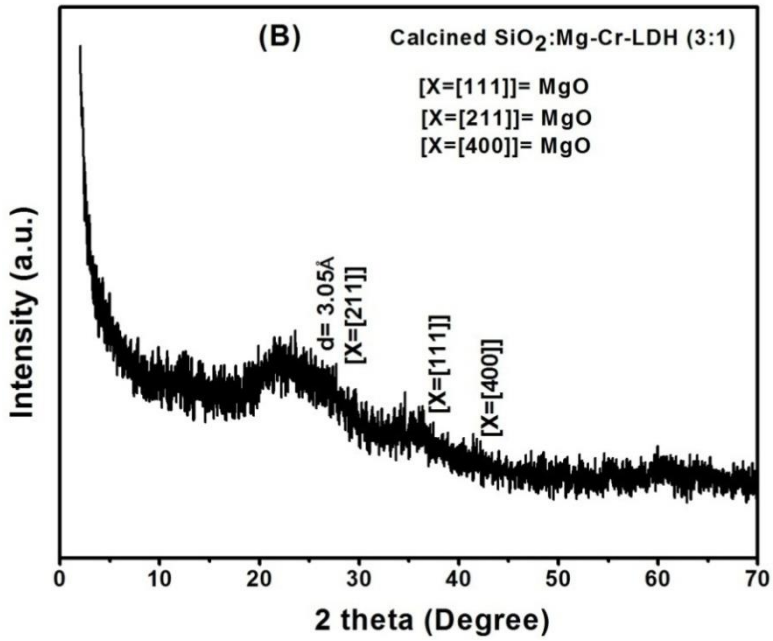

Fig. 3.B.4: XRD patterns of uncalcined SiO_2@Mg-Cr-LDH with different SiO_2 to LDH ratios (A); calcined SiO_2@Mg-Cr-LDH (SiO_2:LDH=3:1) (B).

3.B.3.1.2. FT-IR analysis of the synthesised products:

3.B.3.1.2.1. SiO_2@Ni-Cr-LDH:

FT-IR analysis (**Fig. 3.B.5A**) showed the presence of –OH stretching vibrations at around 3480-3362 cm^{-1} due to the presence of interlayer hydroxyls and H_2O molecules respectively. The peak at around 1650-1610 cm^{-1} was formed due to the C=O stretching vibrations of residual hydrolysed acetylacetonate group present in both the SiO_2 supported and unsupported Ni-Cr-LDH. The peaks at around 1022-1213 cm^{-1} was due to C-O stretching vibrations. The peaks due to C-H stretching vibration was obtained at around 2984 cm^{-1} and whereas for C-C stretching vibrations was obtained at 2332 cm^{-1} due to the presence of acetylacetone in the interlayer [33]. The peaks at around 956-921 cm^{-1} and 558-774 cm^{-1} were due to the M-O and Si-O stretching vibrations respectively [33].

Fig. 3.B.5B shows the FT-IR pattern of calcined SiO_2@Ni-Cr-LDH with the variation of SiO_2 to LDH ratios. It was observed that in these catalysts the frequency

due to stretching and bending vibrations of –OH group disappear which was found in the uncalcined products due to the conversion of metal hydroxides to metal oxides [33]. The stretching frequency due to C-O group was obtained at 1070-1095 cm^{-1}. The peak at 799 cm^{-1} and 953 cm^{-1} were due to the stretching vibration of Ni-O and Si-O bonds respectively.

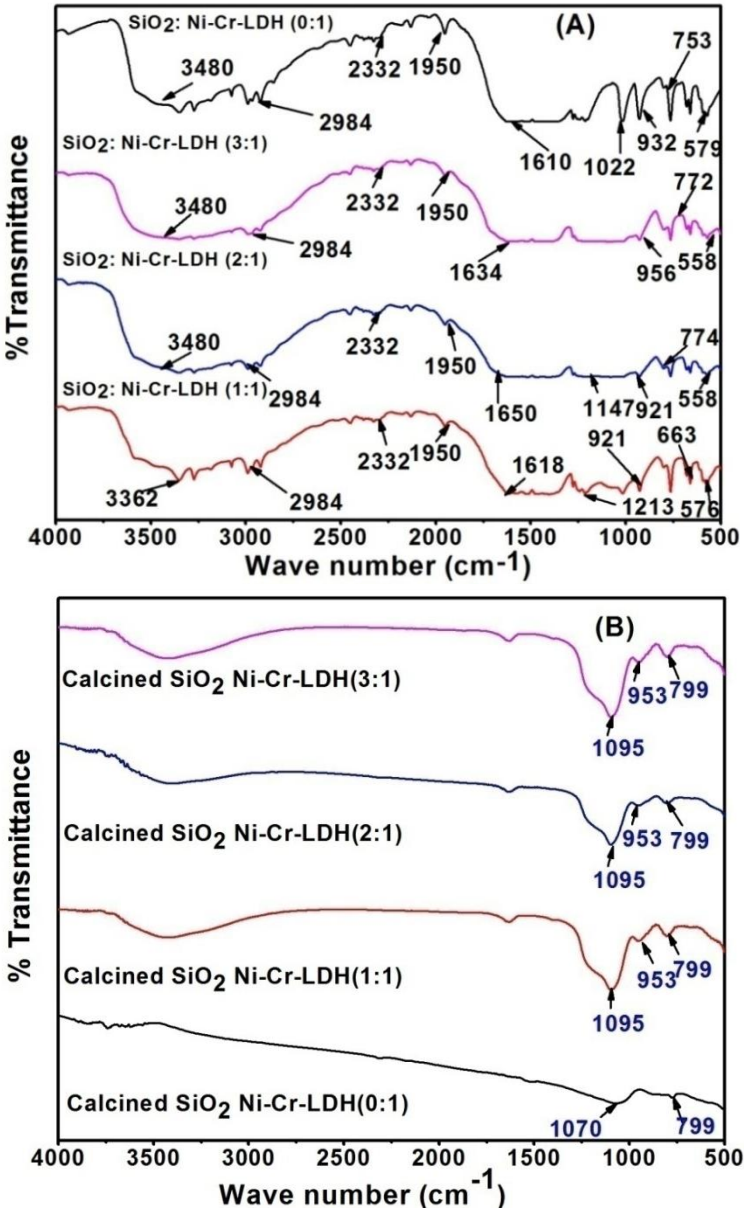

Fig. 3.B.5: FT-IR patterns of uncalcined (A) and calcined (B) (calcined at 450 ^{o}C) SiO_2@Ni-Cr-LDH with different SiO_2 to LDH ratios.

3.B.3.1.2.2. SiO_2@Mg-Cr-LDH:

FT-IR analysis (**Fig. 3.B.6**) showed the presence of –OH stretching vibrations at around 3450-3392 cm^{-1} due to the presence of interlayer hydroxyls and H_2O molecules respectively. The peaks at around 1633-1548 cm^{-1} was formed due to the -C=O stretching vibrations of residual hydrolysed acetylacetonate group present in both the SiO_2 supported and unsupported LDHs. The peaks at around 1049-1219 cm^{-1} were due to C-O stretching vibrations in both of these nanocomposites. The peaks due to C-H stretching and C-H bending vibrations were obtained at around 2966-2980 cm^{-1} and 1365-1408 cm^{-1}. The peaks at around 771-792 cm^{-1} and 447-453 cm^{-1} were due to the M-O and Si-O stretching vibrations respectively [33].

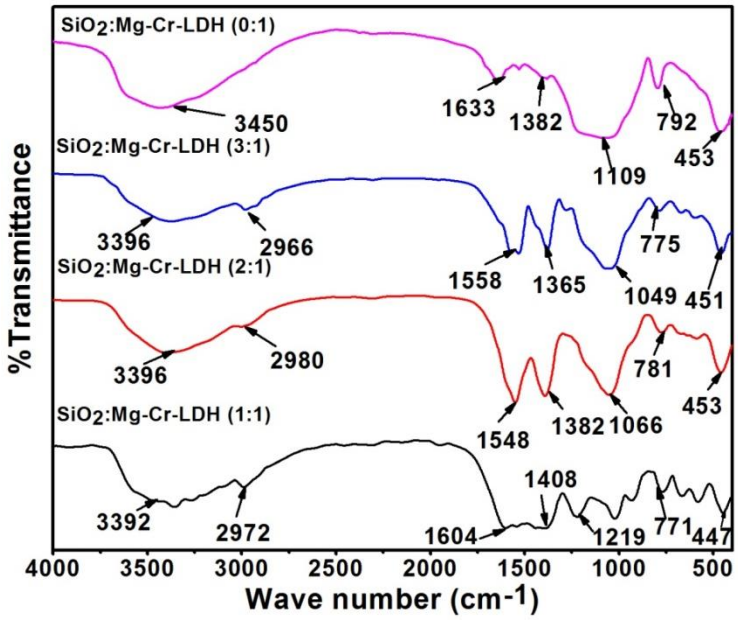

Fig. 3.B.6: FT-IR patterns of uncalcined SiO_2@Mg-Cr-LDH with different SiO_2 to LDH ratios.

3.B.3.1.3. Thermal property study (TGA-DTG analysis):

Thermogravimetric analysis of binary LDHs and their SiO_2 supported products were carried out in a simultaneous TG-DTA analyzer (Model SDT Q600, M/S TA Instruments, USA) using Al_2O_3 as reference under argon atmosphere.

3.B.3.1.3.1. SiO_2@Ni-Cr-LDH:

Fig. 3.B.7A&B shows the TGA-DTG patterns of SiO_2@Ni-Cr-LDH with different SiO_2:LDH ratios. It was observed that these nanocomposites showed different thermal changes upto 700 ^oC. Basically they undergo three step thermal degradations at temperatures around 100-160 ^oC, 200-300 ^oC and 300-700 ^oC respectively. The weight loss at around 100-160 ^oC correspond to surface solvent loss, whereas the weight loss in the temperature range 200-300 ^oC correspond to loss of pore and interlayer solvent molecules. Since, the amount of residual solvent molecule present in such a system largely depends upon various uncontrollable factors like precipitation during hydrolysis, interlayer surface exposure, oven drying time, humidity they result in the presence of varied amounts of residual solvent molecules in these nanocomposites. Therefore, a trend in the weight loss percentages in these temperature ranges with variation of composition was not observed. However, above 300^oC it was observed that with the decrease of LDH content in the system the weight loss in the temperature range 300-700 ^oC gradually decreased due to decrease of dehydroxylation. It was observed that SiO_2@Ni-Cr-LDH with SiO_2 to LDH ratios 0:1, 1:1, 2:1 and 3:1 showed 12.1 %, 11.3 %, 10.56 % and 28.12 % (w/w) weight losses at temperature ranging from 100-160 ^oC; 43.99 %, 42.07 %, 20.11 % and 21.3 % (w/w) weight losses at temperature ranging from 200-300 ^oC whereas, 18.96 %, 14.1 %, 13.34 % and 11.38 % (w/w) weight losses at temperature ranging from 300-700 ^oC respectively. At this stage the mixed metal hydroxides phase transforms to mixed metal oxides where metal ions are distributed in the same nanosheet [33,72].

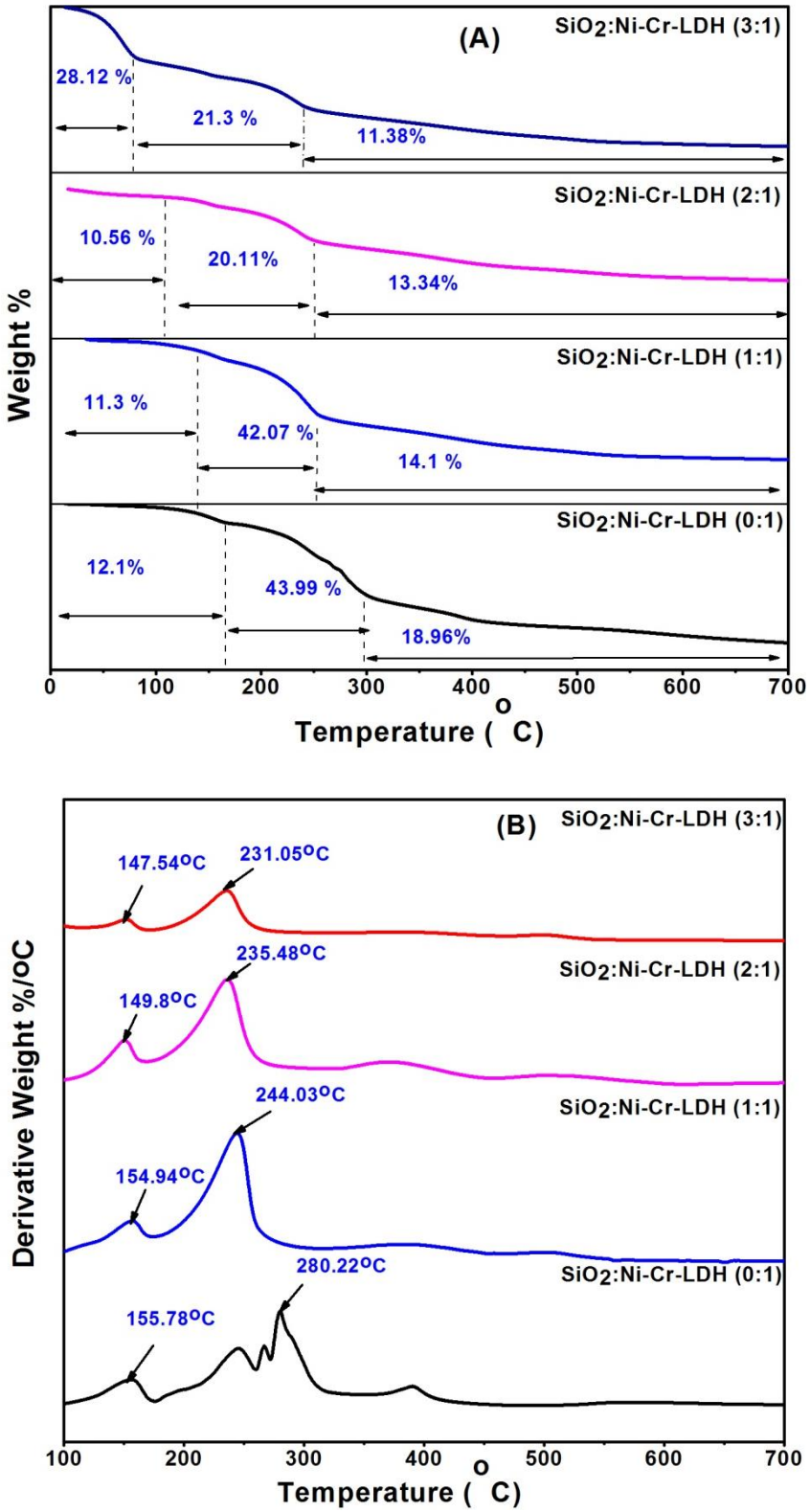

Fig. 3.B.7: TGA-DTG patterns of SiO_2@Ni-Cr-LDHs (A&B) with different SiO_2 to LDH ratios.

3.B.3.1.3.2. SiO_2@Mg-Cr-LDH:

Fig. 3.B.8 shows the TGA-DTG patterns of SiO_2 supported and unsupported Mg-Cr-LDHs. Similar to Ni-Cr-LDH, SiO_2 supported and unsupported Mg-Cr-LDHs also showed thermal changes upto 700 ^oC and three steps thermal degradation at temperatures 100-160 ^oC, 200-300 ^oC and 300-700 ^oC respectively. SiO_2@Mg-Cr-LDHs with SiO_2 to LDH ratios 0:1, 1:1, 2:1 and 3:1 showed 13.69 %, 23.78 %, 9.53 % and 9 % (w/w) weight losses at temperature range 100-160 ^oC; 43.99 %, 12.49 %, 26.78 % and 12.64 % (w/w) weight losses at temperature range 200-300 ^oC whereas 13.94 %,11.4 %, 5.56 % and 3.77 % (w/w) weight losses at temperature range 300-700 ^oC respectively. It was observed that above 300 ^oC with the decrease of LDH content in the system the weight loss in the temperature range 300-700 ^oC gradually decreased due to decrease of dehydroxylation. At this stage the mixed metal hydroxides phase transforms to mixed metal oxides where metal ions centers are dispersed in the same nanosheet [33,72].

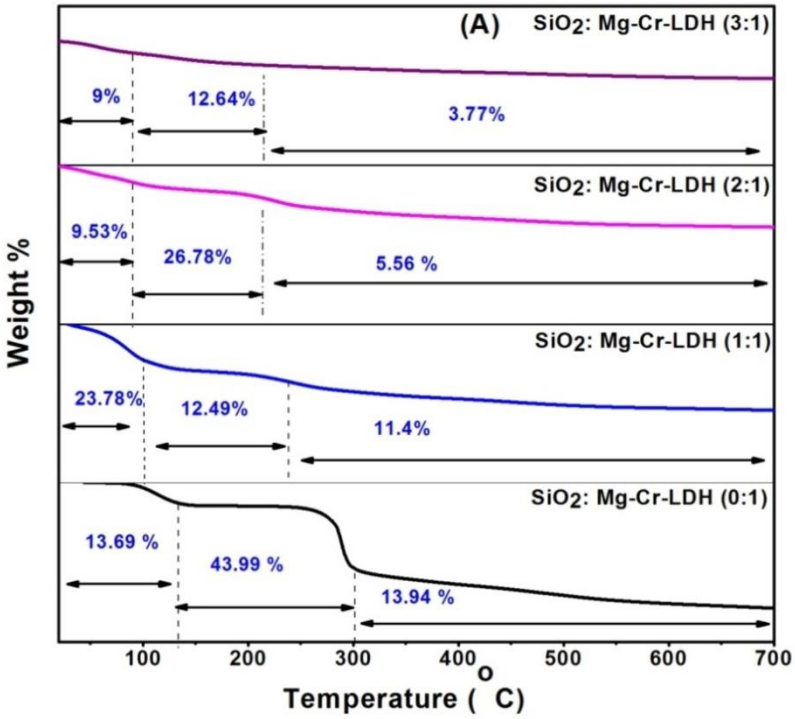

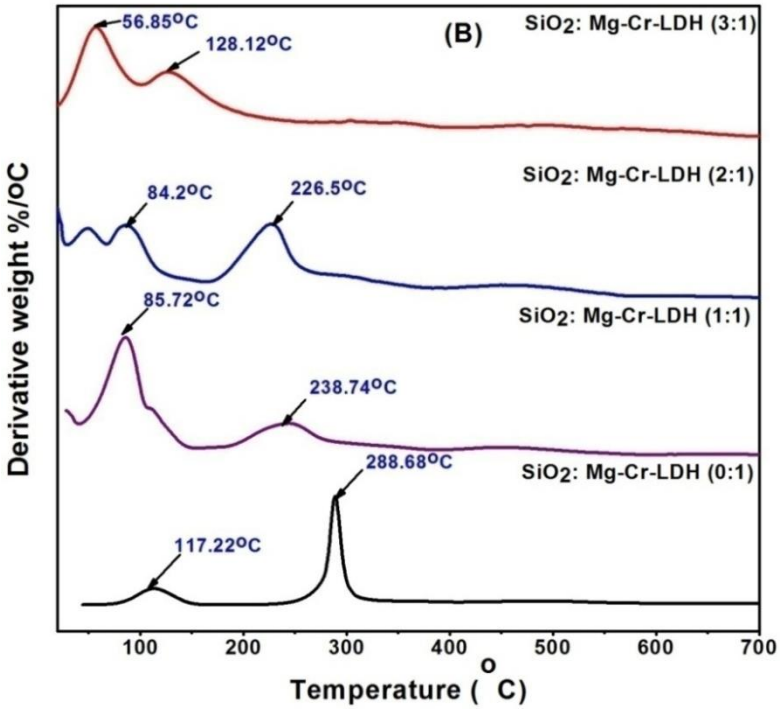

Fig. 3.B.8: TGA-DTG patterns of SiO_2 @ Mg-Cr-LDHs (A&B) with different SiO_2 to LDH ratios.

3.B.3.1.4. Rheological study of SiO_2@LDH alcogels of binary LDHs:

To coat any dispersion over a particular solid surface by dip or spin coating technique to form a thin film the viscosity or gel strength of the dispersion plays a vital role. It affects the thickness and consequently the reproducibility and continuity of the film on drying [73].

Rheological study of SiO_2@Ni-Cr-LDH and SiO_2@Mg-Cr-LDHs were carried out in both rotational viscometer (Rheolab QC, Anton Paar, with a measuring cup C-CC27/SS/QC and measuring system CC27/P6 at 15 ^oC with shear rate ranging from 100-1000 s^{-1}) and oscillatory rheometer (modular compact Rheometer MCR 302, Anton Paar) with a rough parallel plate geometry of 2.5 cm diameter and 0.1 cm gap at 15 ^oC as described in the **Experimental Section 3.B.3.1**.

3.B.3.1.4.1. Steady shear measurement:

As shown in **Fig. 3.B.9A**, **Fig. 3.B.9B**, **Fig. 3.B.9C**& **Fig. 3.B.9D** the shear stress

increased with the shear rate in both the nanocomposites which was consistent to the Bingham fluids [74] which follows the equation

$$\text{Shear stress}(\tau) = a + b.\text{Shear rate}\ (\gamma) \qquad (3.B.9)$$

Where, *a* is the Yield stress or Yield point and b is the Shear viscosity.

The Correlation ratio (*R*) was found in the range from 0.9933-0.9987 in case of SiO_2/Ni-Cr nanocomposites and 0.9883-0.9983 in case of SiO_2/Mg-Cr-LDH nanocomposites (**Table 3.B.1**). In all the rheograms it was found that the systems were basically non-Newtonian with gel strength increasing as the SiO_2 content rise. The alcogel of the LDH alone did not show much gelation despite the increasing viscosity as well as the increase of shear rate but the alcogel of SiO_2:LDH composites showed increasing gelation at low shear rate as the silica content increased. At high SiO_2:LDH ratio of 3:1 the thixotropy was found highest due to local spatial rearrangement of micro structure units in the structured gel. This was due to the breakdown of the silica network. It is responsible for the increasing gelation with increasing SiO_2 content. This behaviour helped for holding the LDH component dispersed.

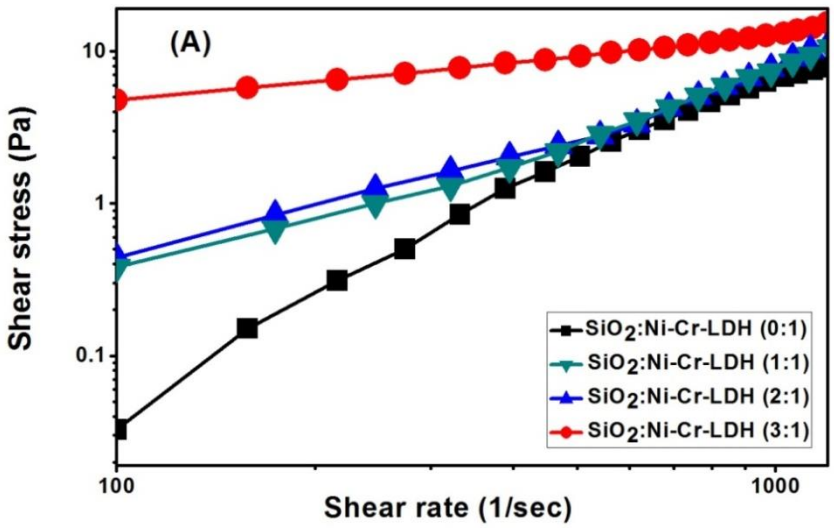

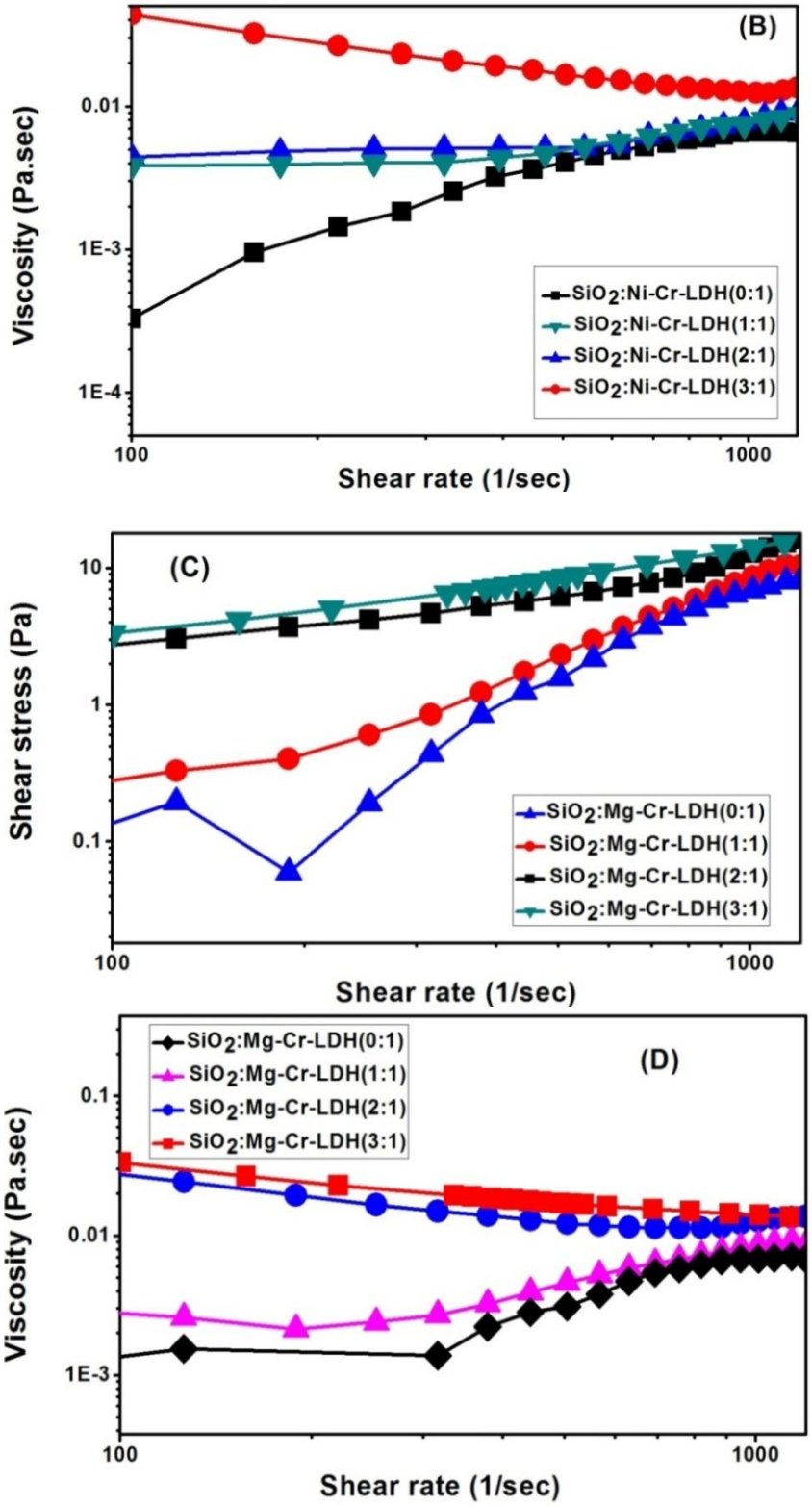

Fig. 3.B.9: Shear rate *vs* Shear stress curves (A&C) and Shear rate *vs* Viscosity (B&D) of SiO_2@Ni-Cr-LDH and SiO_2@Mg-Cr-LDH at different SiO_2 to LDH ratios.

Table 3.B.1: Yield stress and Shear viscosity values for Bingham model fitted with SiO_2@Ni-Cr and Mg-Cr-LDH nanocomposites

Nanocomposites	a (Yield Stress in Pa)	b (Shear Viscosity in Pa.s)	R (Correlation ratio)
SiO_2: Ni-Cr-LDH (0:1)	4.412	0.009	0.9933
SiO_2: Ni-Cr-LDH (1:1)	4.349	0.011	0.9975
SiO_2: Ni-Cr-LDH (2:1)	0.385	0.007	0.9987
SiO_2: Ni-Cr-LDH (3:1)	0.243	0.007	0.9987
SiO_2: Mg-Cr-LDH (0:1)	0.162	0.013	0.9883
SiO_2: Mg-Cr-LDH (1:1)	0.043	0.003	0.9916
SiO_2: Mg-Cr-LDH (2:1)	0.043	0.003	0.9916
SiO_2: Mg-Cr-LDH (3:1)	5.338	0.017	0.9983

3.B.3.1.4.2. Dynamic oscillatory shear measurements:

The viscoelastic properties of the nanocomposites were examined by oscillation measurements at constant shear stress. As shown in **Fig. 3.B.10 A&B**, the linear viscoelastic range was shown in the amplitude sweep test. The linear viscoelastic (LVE) region was found till the shear strain (γ) = 9.49% and 8.75% for SiO_2@Mg-Cr-LDH and Ni-Cr-LDH respectively. The storage modulus ($G^{/}$) represents the elastic behaviour while the loss modulus ($G^{//}$) represents the viscous behaviour in a viscoelastic material. $G^{/}$ is a measure of the deformation energy stored by a sample during the deformation process, while $G^{//}$ is a measure of the energy that is lost during the deformation process [75,76]. It was observed that, the storage modulus ($G^{/}$) was larger than the loss modulus ($G^{//}$) indicating the presence of elastic or gel like structure in these nanocomposites. After the cross over point ($G^{/} = G^{//}$, viscoelastic point) $G^{//}$ became larger than $G^{/}$ indicating the presence of liquid like structure. Beyond that critical value of shear strain both the $G^{/}$ and $G^{//}$ decreased sharply because of the break down of the structures of these nanocomposites. The cross over point in which these nanocomposites exists both as gel (elastic) and liquid (viscous) like structure are given

in **Table 3.B.2**.

The frequency sweep test for these nanocomposites was done in the linear viscoelastic region (**Fig. 3.B.11 A&B**) by keeping shear strain constant at 5 %. $G^{/}$ was found to be greater than $G^{//}$ in both of these nanocomposites indicating the elastic behaviour. The $G^{/}$ value for the SiO_2:LDH ratio at 3:1 in SiO_2@Mg-Cr-LDH and Ni-Cr-LDH was found to be higher than 0:1, 1:1 and 2:1 SiO_2:LDH ratios indicating its higher gel-like or solid-like viscoelastic behaviour. It was further observed that upto high angular frequency region $G^{/}$ remained greater than $G^{//}$ in both of these nanocomposites indicating the occurance of viscoelastic gel like structure with higher stability.

Complex viscosity (η^*) is an important parameter which describes the flow resistance of the materials in the structured state, originating as viscous or elastic flow resistance to the oscillating movement of the materials [76,77]. The mathematical expression for complex viscosity (η^*) is given below-

$$\eta^* = \frac{G^*}{\omega} \quad (3.B.10)$$

$$\omega = 2\pi f \quad (3.B.11)$$

Where, G^* is the complex shear modulus, $G^* = \sqrt{(G^{/})^2 + (G^{//})^2}$, ω is the angular frequency in rads^{-1} and f is the frequency in Hertz.

The frequency dependence of complex viscosity (η^*) of SiO_2@Ni-Cr-LDH and Mg-Cr-LDH curves showed the gradual decrease of complex viscosity with the increase of angular frequency (**Fig. 3.B.12A&B**) showing the shear thinning behaviour. The complex viscosity (η^*) was found to be dependent on SiO_2: LDH ratios. The values of complex viscosity was greater for the 3:1 SiO_2:LDH ratio. As the SiO_2 ratios increased from 0:1 to 3:1 there was a greater decrease of complex viscosity and hence showing a

good shear-thinning behaviour which is a prerequisite for dip coating.

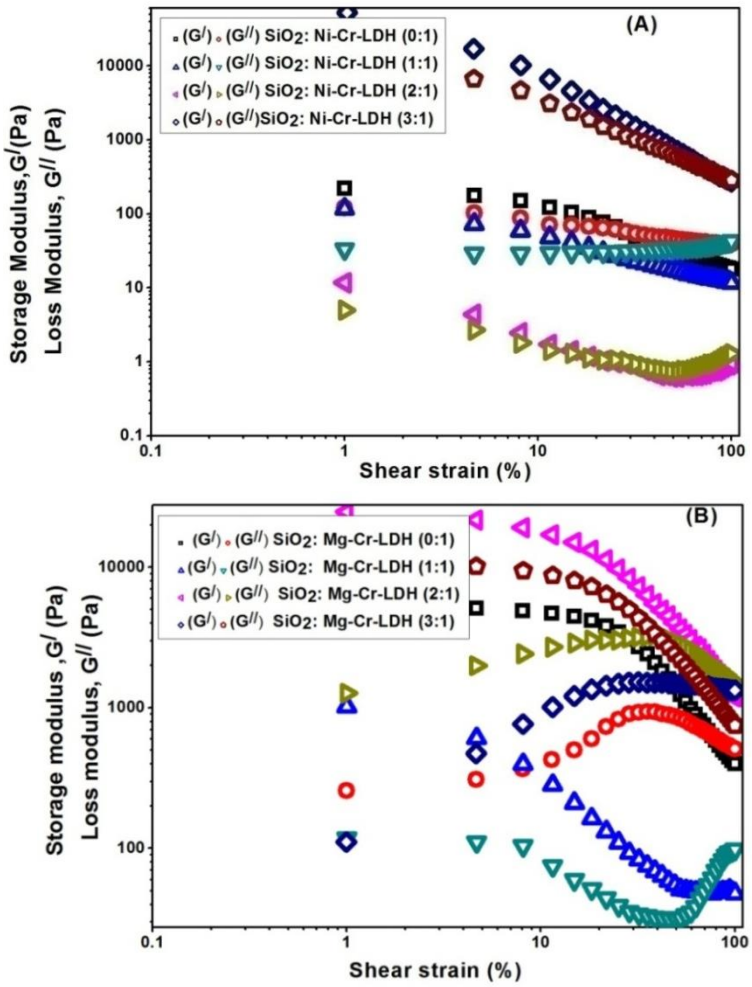

Fig. 3.B.10: Amplitude sweep for SiO_2@Ni-Cr-LDH (A) and Mg-Cr-LDH (B) at different SiO_2 to LDH ratios at 1 rad s^{-1} angular frequency.

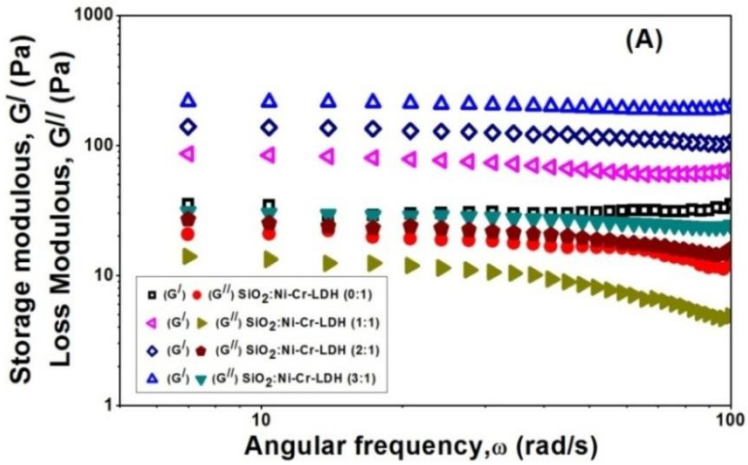

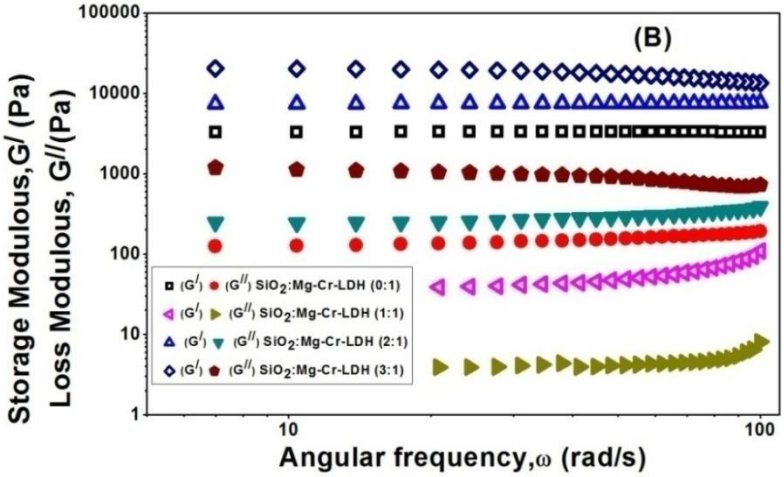

Fig. 3.B.11: Frequency sweep for SiO_2@Ni-Cr-LDH at different SiO_2 to LDH ratios at 5 % shear strain.

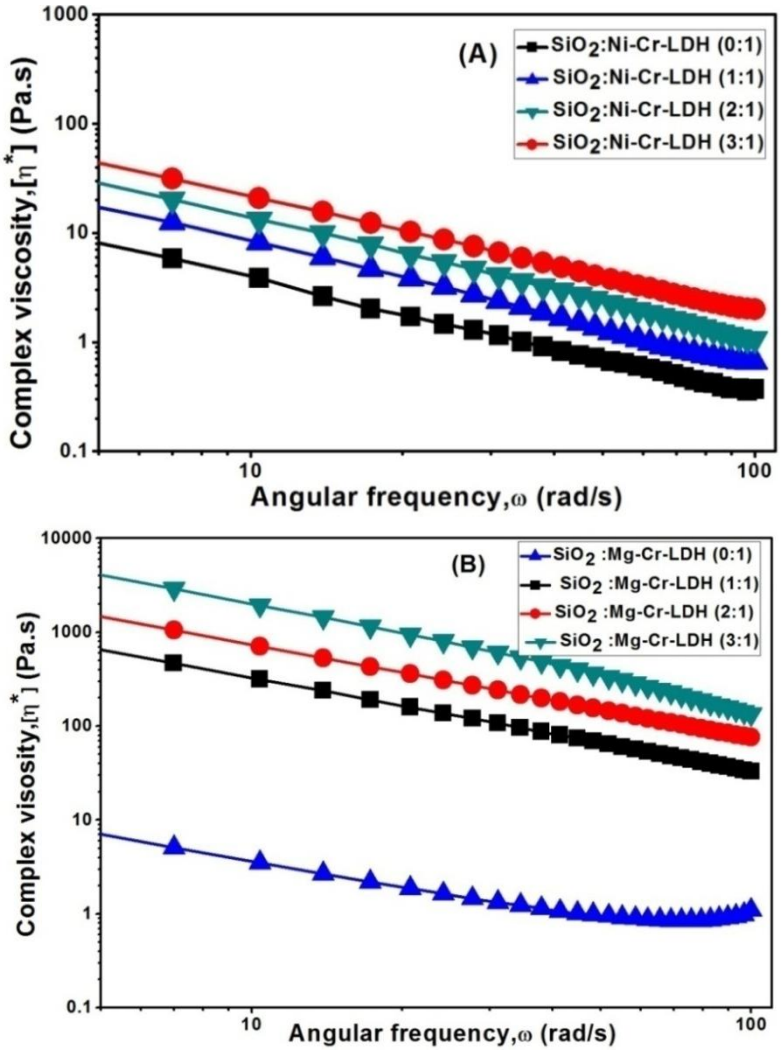

Fig. 3.B.12: Complex viscosity *vs* angular frequency curves for SiO_2@Ni-Cr-LDH (A) and Mg-Cr-LDH (B).

Table 3.B.2: Cross over point of SiO_2@Ni-Cr-LDH and Mg-Cr-LDH nanocomposites

Serial No.	Nanocomposites	Cross-over point (Pa)
1	SiO_2: Ni-Cr-LDH (0:1)	5.91×10^1
2	SiO_2: Ni-Cr-LDH (1:1)	3.06×10^1
3	SiO_2: Ni-Cr-LDH (2:1)	1.093
4	SiO_2: Ni-Cr-LDH (3:1)	3.66×10^2
5	SiO_2: Mg-Cr-LDH (0:1)	6.38×10^2
6	SiO_2: Mg-Cr-LDH (1:1)	5.02×10^1
7	SiO_2: Mg-Cr-LDH (2:1)	1.98×10^3
8	SiO_2: Mg-Cr-LDH (3:1)	1.59×10^3

3.B.3.1.5. BET surface area and pore radius analysis:

BET surface area and pore volume analysis were carried out *via* Nitrogen gas adsorption at 77 K applying Brunauer-Emmett-Teller (BET) calculations using Autosorb-iQ Station 1 (Quantachrome, USA). Prior to performing the experiment the samples were degassed at 100 ^oC for 1.5 hours.

Table 3.B.3a shows the surface area values of SiO_2 supported and unsupported Ni-Cr-LDHs. BET surface area analysis showed that with the increase of SiO_2 component from 0:1 to 3:1 SiO_2:LDH ratios in the oven dried samples the surface area also increased. In case of SiO_2@Ni-Cr-LDH the surface area increased from 13.4 m^2/g to 68.6 m^2/g and from 23.6 m^2/g to 103.6 m^2/g in case of SiO_2@Mg-Cr-LDH (**Table 3.B.3a**). On the other hand, SiO_2@Mg-Cr-LDH core shells exhibit higher surface area as compared to SiO_2@Ni-Cr-LDH core shell nanocomposites. The increase of surface area indicates their good prospects for application in different catalytic applications [78,79].

Table 3.B.3b shows the surface area values of the calcined SiO_2@Ni-Cr-LDHs. Similarly, after calcination, due to the broke down of the largely amorphous silica network surrounded by crystalline LDH structure and formation of the porous

aggregated structure the BET surface area of the calcined SiO_2@Ni-Cr-LDHs increased from 143 m^2/g to 401 m^2/g with the increase of SiO_2 to LDH ratio in the range 0:1 to 3:1. With the increase of SiO_2 to LDH from 0:1 to 3:1the pore diameter also increased from 3.2 nm to 9.6 nm in case of SiO_2@Ni-Cr-LDHs and from 3.6 nm to 7.6 nm in case of SiO_2@Mg-Cr-LDHs. Similarly, in case of calcined SiO_2@Ni-Cr-LDHs the pore diameter also increased from 3.6 nm to 9 nm. Calcined SiO_2@Mg-Cr-LDH with SiO_2 to LDH ratio 3:1 showed the surface area of 373 m^2/g and pore diameter of 4.6 nm respectively.

Table 3.B.3a: BET surface area and pore diameter of SiO_2@LDHs

Serial No.	Nanocomposites	SiO_2:LDH	Surface area (m^2/g)	Pore diameter (nm)
1	SiO_2: Ni-Cr-LDH	0:1	13.42	3.2
2	SiO_2: Ni-Cr-LDH	1:1	15.14	3.6
3	SiO_2: Ni-Cr-LDH	2:1	33.82	3.6
4	SiO_2: Ni-Cr-LDH	3:1	68.64	9.6
5	SiO_2:Mg-Cr-LDH	0:1	23.57	3.6
6	SiO_2:Mg-Cr-LDH	1:1	26.99	3.8
7	SiO_2:Mg-Cr-LDH	2:1	48.02	3.8
8	SiO_2:Mg-Cr-LDH	3:1	103.6	7.6

Table 3.B.3b: BET surface area and pore diameter of calcined SiO_2@Ni-Cr-LDH

Serial No.	Nanocomposites	SiO_2:LDH	Surface area (m^2/g)	Pore diameter (nm)
1	Calcined SiO_2:Ni-Cr-LDH	0:1	143	3.6
2	Calcined SiO_2:Ni-Cr-LDH	1:1	165	3.6
3	Calcined SiO_2:Ni-Cr-LDH	2:1	187	3.6
4	Calcined SiO_2:Ni-Cr-LDH	3:1	401	9
5	Calcined SiO_2:Mg-Cr-LDH	3:1	373	4.6

3.B.3.1.6. Zeta potential study with the variation of pH:

Similar to Ni-Al-LDH and Mg-Al-LDH in case of SiO_2@Ni-Cr-LDH and SiO_2@

Mg-Cr-LDH the negative zeta potential also increased with the increase of SiO_2 ratio indicating the better dispersibilty and stability of these nanocomposites. **Table 3.B.4** shows the zeta potential values of SiO_2@Ni-Cr-LDH and SiO_2@Mg-Cr-LDHs at different pH with the variation of SiO_2:LDH ratios.

Table 3.B.4: Zeta potential values of SiO_2@LDHs

Serial No.	Nanocomposites	SiO_2:LDH	Zeta-Potential values (mV)	pH
1	SiO_2:Mg-Cr-LDH	0:1	18.8	8.8
2	SiO_2:Mg-Cr-LDH	1:1	-16.3	8.7
3	SiO_2:Mg-Cr-LDH	2:1	-16.6	8.8
4	SiO_2:Mg-Cr-LDH	3:1	-19.5	9.0
5	SiO_2:Ni-Cr-LDH	0:1	14.9	8.8
6	SiO_2:Ni-Cr-LDH	1:1	-16.8	8.7
7	SiO_2:Ni-Cr-LDH	2:1	-17.7	8.8
8	SiO_2:Ni-Cr-LDH	3:1	-21.5	9.0

3.B.3.1.7. Particle size analysis:

Fig. 3.B.13a and **Fig. 3.B.13b** shows the particle size distribution curves of SiO_2@ Ni-Cr-LDH & Mg-Cr-LDH. It was observed that in case of both of these LDHs above 40 % of the particles were in the range of 10-100 micron which was due to the agglomerated state of the dried particles of SiO_2@LDH nanocomposites.

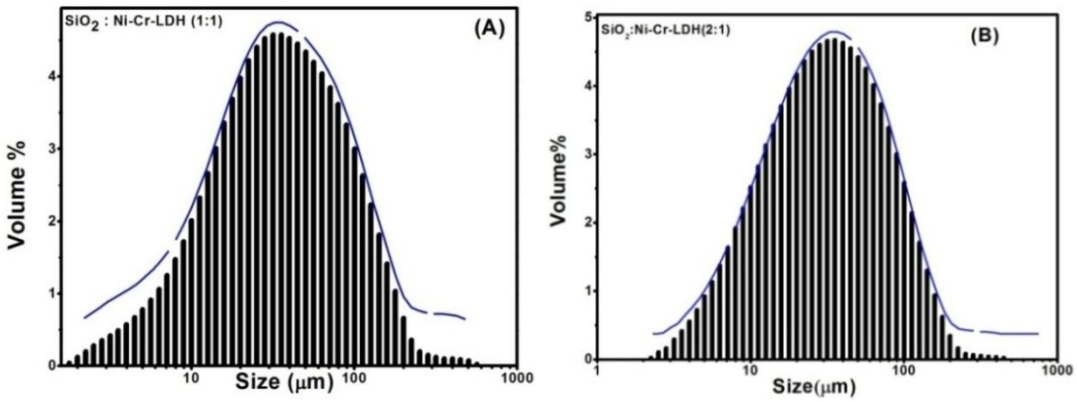

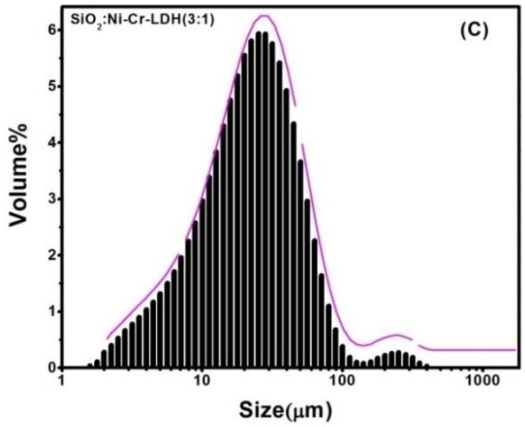

Fig.3.B.13a: Particle size distribution curves of (A) SiO_2@Ni-Cr-LDH (1:1); (B) SiO_2@Ni-Cr-LDH (2:1); (C) SiO_2@Ni-Cr-LDH (3:1).

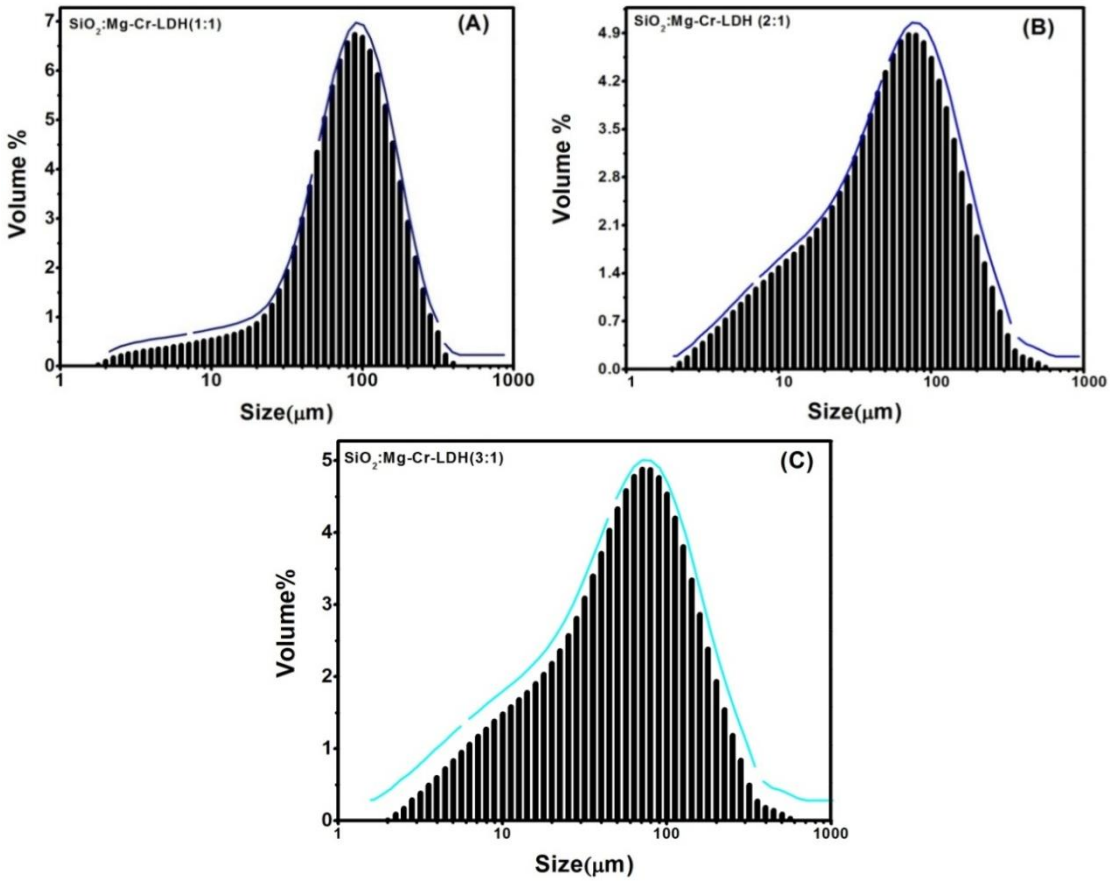

Fig. 3.B.13b: Particle size distribution curves of (A) SiO_2@Ni-Cr-LDH (1:1); (B) SiO_2@Ni-Cr-LDH (2:1); (C) SiO_2@Ni-Cr-LDH (3:1).

3.B.3.1.8. Surface morphology study:

Surface morphology study of different binary SiO_2@LDHs were carried out by SEM and TEM analysis the associated EDS patterns give the elemental composition of the

composites.

3.B.3.1.8.1. SEM, TEM and EDS analysis:

The structural morphology and elemental compositions were studied by SEM, TEM (**Fig. 3.B.14a. A, B, C, D, E & Fig. 3.B.14b. A, B, C, D&E**) and EDS (**Fig. 3.B.14b. F&G**) analysis. SEM images showed the thin platelets of Ni-Cr and Mg-Cr-LDH where the LDH sheets were arranged in nano sheets and stacked over one another (**Fig. 3.B.14a.A&D**). Similarly, TEM images (**Fig. 3.B.14a. B&C**) showed the aggregates of LDH layers of Ni-Cr-LDH with 0.243 nm lattice fringes that can be attributed to the 012 plane of Ni-Cr-LDH. TEM image (**Fig. 3.B.14a.E**) of Mg-Cr-LDH also showed the stacking of LDH layers with 57.3 nm dimension of one hexagonal plate [33].

Fig. 3.B.14b. A, B, C, D&E showed SEM and TEM images of SiO_2@Ni-Cr and Mg-Cr-LDH nanocomposites where poorly crystalline SiO_2 formed a continuous matrix on which nano-sheets of Ni-Cr and Mg-Cr-LDH were distributed. SEM and TEM images showed the hexagonal platelets of Ni-Cr-LDH which were stacked over one another and LDH layers were dispersed over SiO_2 spheres in both of these nanocomposites. **Fig. 3.B.14b.E** shows the lattice fringes with dimensions of 0.243 nm and 0.144 nm indicating the presence of (012) and (331) plane of LDH and SiO_2 respectively. The presence of Ni-Cr and Mg-Cr-LDH as well as the SiO_2 in the composites were further confirmed by selected area EDS analysis. From EDS the weight percentage of Ni and Cr in case of SiO_2@Ni-Cr-LDH were found as 13.67 % and 6.84 % whereas, the weight percentage of Mg and Cr in case SiO_2@Mg-Cr-LDH were found as 15.73 % and 7.88 % (**Fig. 3.B.14b. F&G**). The elemental mapping patterns (**Fig. 3.B.14b. H, I, J, K&L**) showed the spatial distribution of O, Si, Mg, Cr and Ni as per their synthesis ratio as well as Mg, Cr and Ni centers were uniformly

distributed around the Si centers. The presence of C and O in EDS patterns also indicated the presence of surface adsorbed acetylacetonate and alcohol molecules formed during the hydrolysis of metal acetylacetonates and alkoxide [33].

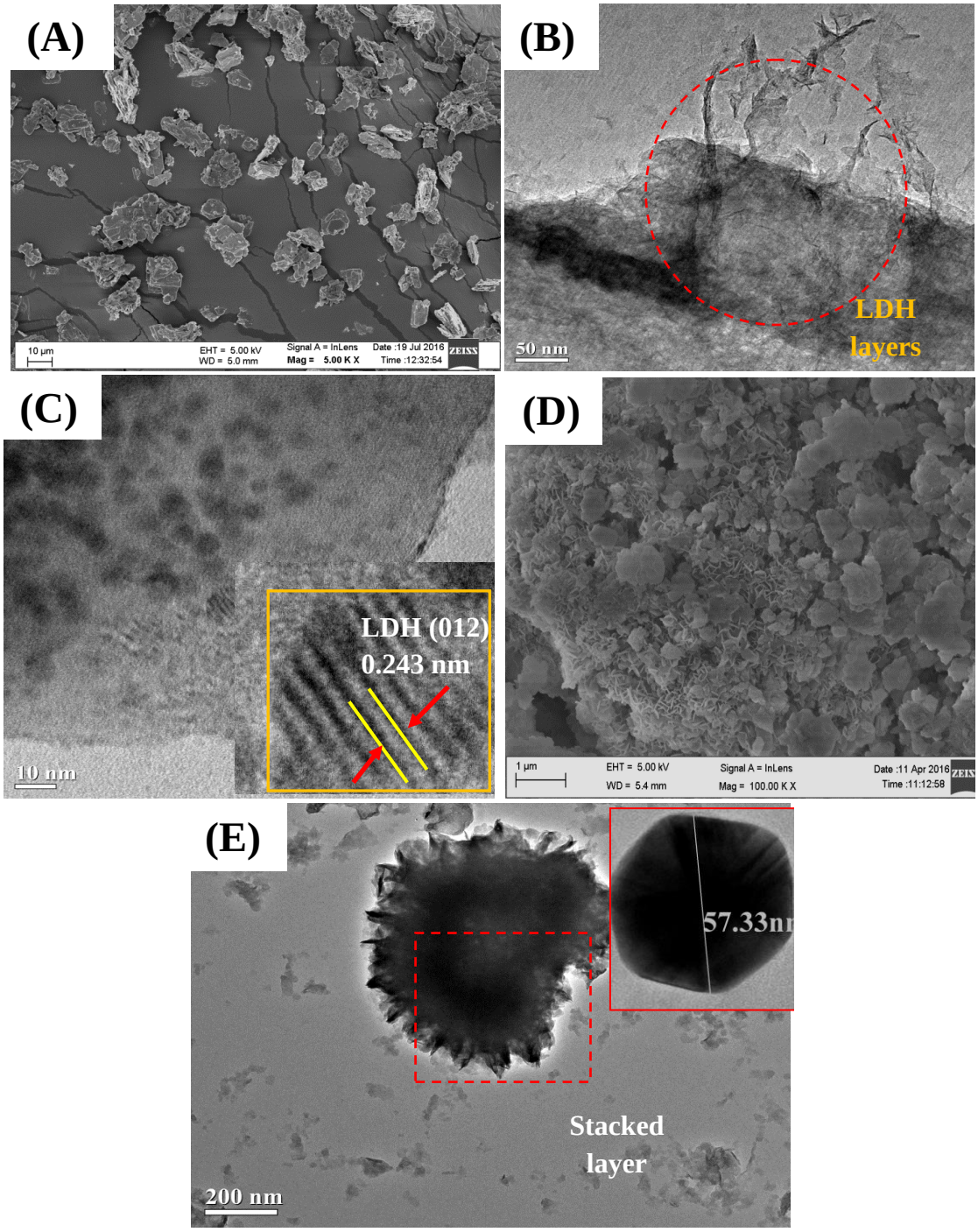

Fig.3.B.14a: SEM and TEM images of Ni-Cr-LDH (A&B); lattice fringes of Ni-Cr-LDH (C), SEM (D) and TEM images of Mg-Cr-LDH showing the stacking of layers (E).

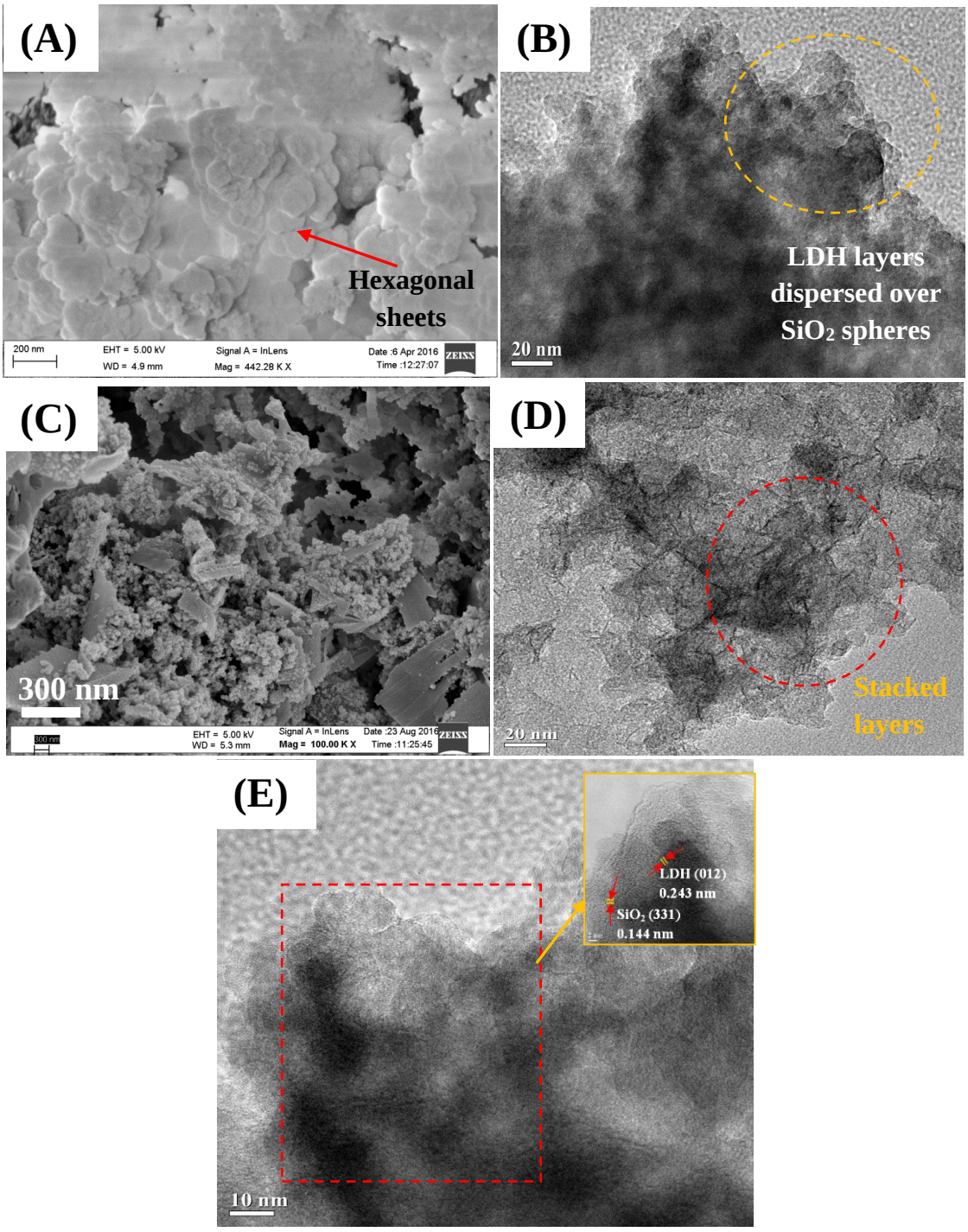

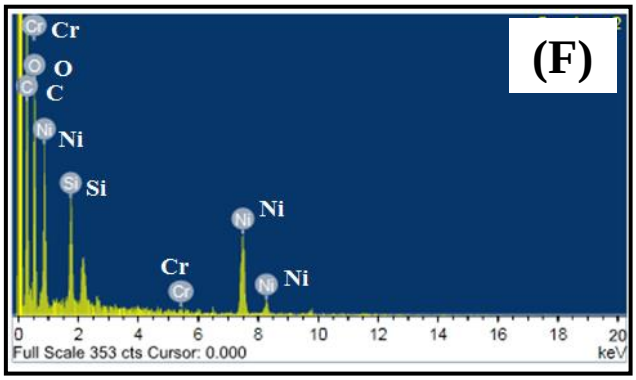

Elem...	Weight %	Atomic %
C K	42.35	62.01
O K	34.33	32.73
Si K	2.81	1.53
Cr K	6.84	0.18
Ni K	13.67	3.55
Totals	100.00	

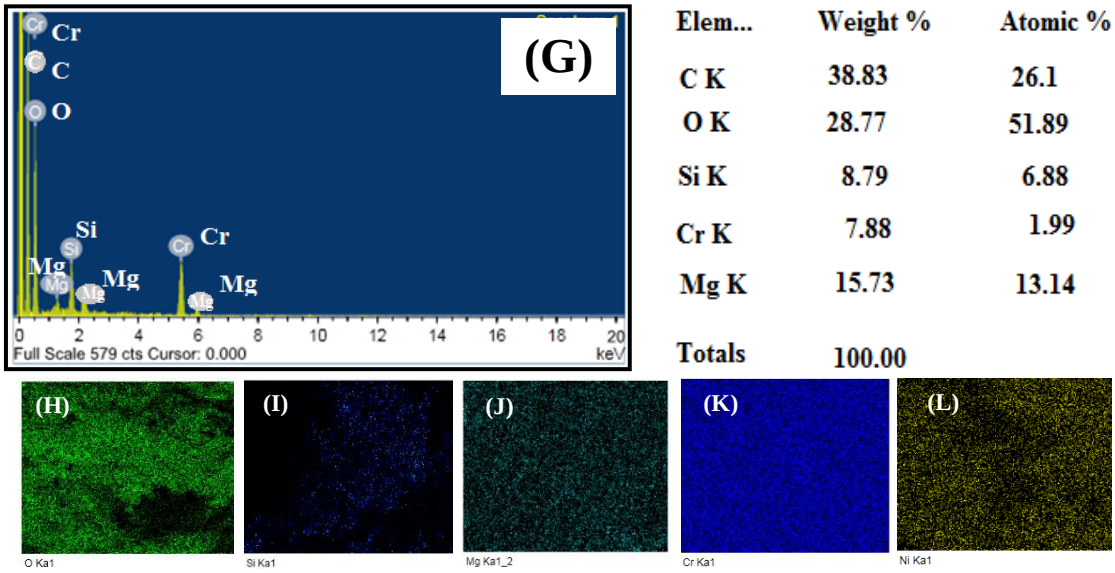

Fig. 3.B.14b: SEM and TEM images of SiO_2@Mg-Cr-LDH (A&B) and SiO_2@Ni-Cr-LDH (C&D); lattice fringes of SiO_2@Mg-Cr-LDH with 0.243 nm and 0.144 nm of 012 and 331 plane of LDH and SiO_2 (E) with SiO_2:LDH ratio 2:1 ; EDS spectra of SiO_2@Ni-Cr-LDH (F) and SiO_2@Mg-Cr-LDH (G). The elemental mapping for O (H), Si (I), Mg (J), Cr (K) and Ni (L).

SEM analysis was carried out to get the surface morphology of the calcined samples. It was observed that after calcination the layered structure of these metal oxides remained same as the parent SiO_2@Ni-Cr-LDHs. The SEM pattern showed (**Fig. 3.B.14c**) the aggregation of platy like structures which was due the presence of metal oxide nanosheet [33]. EDS analysis was carried out to get the elemental composition and it showed the presence of Ni, Cr, O and Si in these samples further confirming the formation of NiO, SiO_2-Cr_2O_3 type oxides. **Fig. 3.B.14d** shows the SEM pattern of calcined SiO_2@Mg-Cr-LDH with SiO_2:LDH ratio 3:1. It was observed that in case of this LDH also the layered structure remained after calcination.

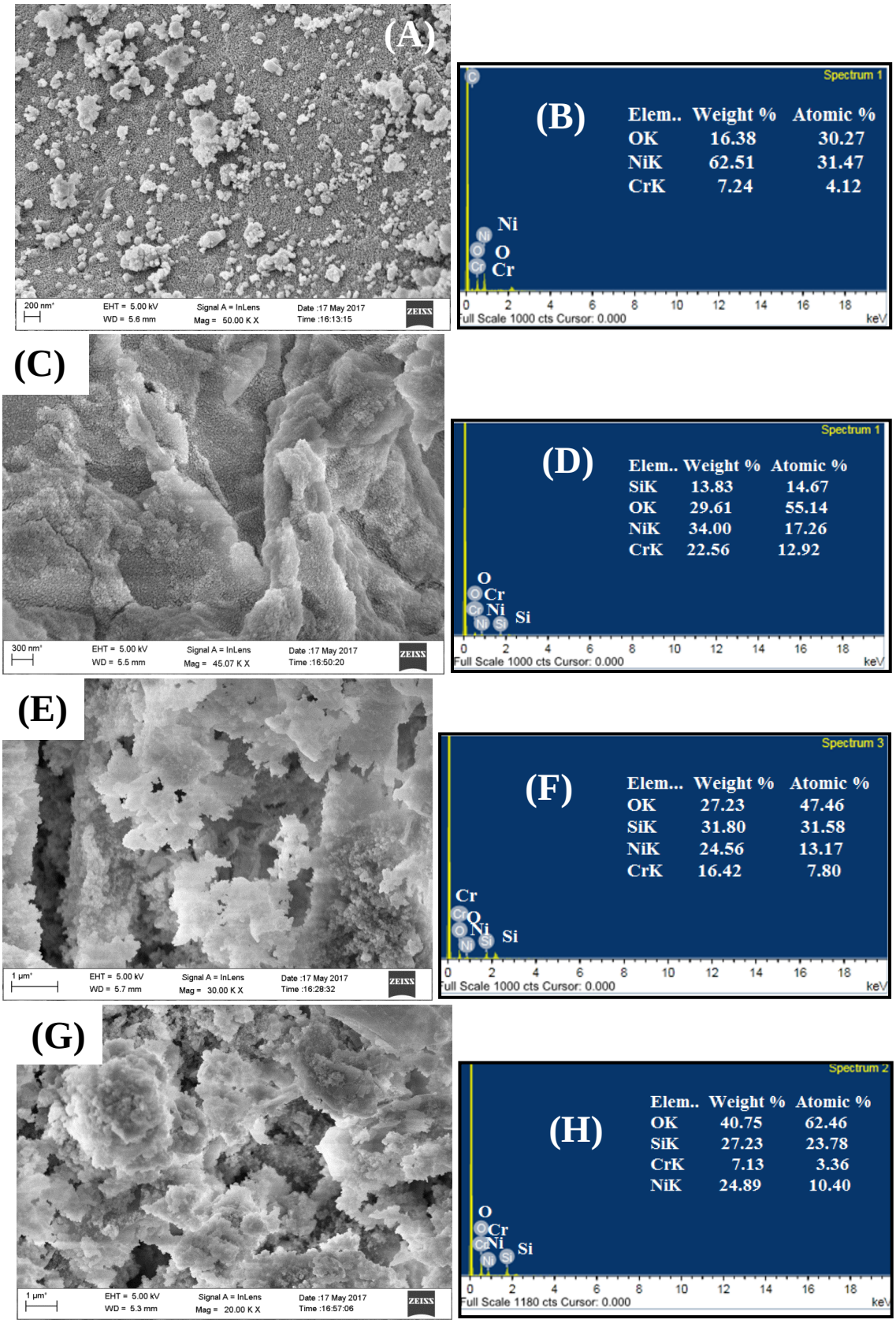

Fig. 3.B.14c: SEM and EDS patterns of calcined SiO_2@Ni-Cr-LDHs with SiO_2:LDH ratios 0:1 (A&B), 1:1 (C&D), 2:1(E&F), 3:1(G&H).

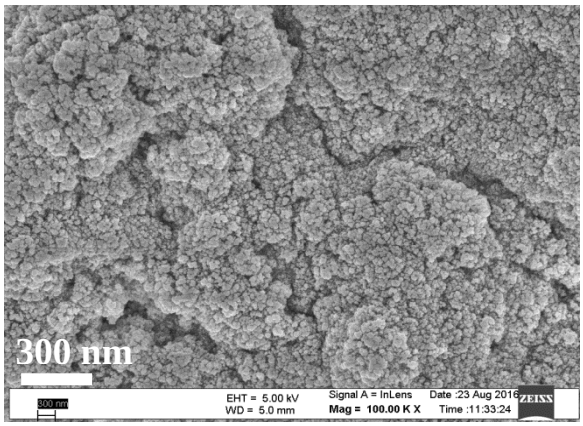

Fig. 3.B.14d: SEM pattern of calcined SiO_2@Mg-Cr-LDH with SiO_2 to LDH ratio 3:1.

3.B.3.1.9. H_2-TPR analysis:

H_2-TPR analysis of calcined SiO_2@Ni-Cr-LDHs was carried out to investigate the reducible sites as well as the T_{max} of these catalysts. H_2-TPR profiles (**Fig. 3.B.15**) shows the two step reduction for all these catalysts. The two reduction peaks for CNC-01 were obtained very distinctly at 237 ^oC corresponding to the reduction of Ni^{2+} to Ni^0 of NiO species and at high temperature of 577 ^oC corresponding to the reduction of $NiCr_2O_4$ spinel present in the catalyst also found from XRD analysis. On the other hand, CNC-11 also showed first reduction peak at 237 ^oC corresponding to the reduction of Ni^{2+} to Ni^0 of NiO species not interacting with the support whereas catalysts CNC-21 to CNC-31 showed two step reduction temperatures at 385-400 ^oC corresponding to the reduction of Ni^{2+} to Ni^0 of NiO which interact with the SiO_2 support and due to NiO-SiO_2 interaction the first reduction peak shifted to higher temperature as compared to SiO_2 unsupported catalyst due to increase of amount of SiO_2 and second reduction peak at 522 ^oC corresponding to the reduction of Ni^{2+} to Ni^0 of NiO interacting with amorphous Cr_2O_3-SiO_2 type phases [32, 60-65] probably present on the catalysts. CNC-11 showed a broad reduction peak at the T_{max} of 385 ^oC and 522 ^oC corresponding to reduction of NiO-SiO_2 and NiO-Cr_2O_3-SiO_2 type phases

that were formed due to the addition of SiO_2. It was also observed from the H_2-TPR analysis that the rate of H_2-consumption depend on the ratio of SiO_2 present on these catalyst and with the increase of SiO_2 to LDH ratio from 1:1 to 3:1 the rate of H_2-consumption also increased. **Table 3.B.5** shows the H_2-consumption in mmol/g for these catalysts at different peak temperatures and it was observed that H_2-consumption increased with temperature further indicating the strong interaction of the catalysts with SiO_2 support as a result of which $NiCr_2O_4$ spinel phase formation was not observed in CNC-11 to CNC-31 catalysts. It was further observed that Ni is in reduced state (Ni^0) in all these catalyst after H_2-pretreatment and acts as the active species which lead to the CPO of CH_4 and increased the selectivity of these catalysts towards H_2 and CO. Thus, H_2-TPR analysis further confirmed that only reducible species of these catalysts was Ni^{2+} of NiO and other species such as Cr^{3+} could not be reduced after H_2 treatment which only present as either in $NiCr_2O_4$ spinel or Cr_2O_3-SiO_2 type phases. Hence, for all these catalysts only Ni^0 took part in the catalytic activity.

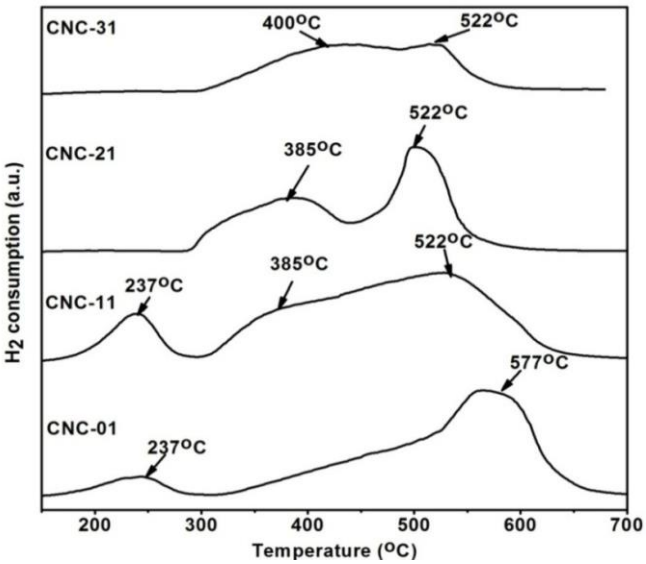

Fig. 3.B.15: H_2-TPR analysis of calcined SiO_2@Ni-Cr-LDH with different SiO_2 to LDH ratios after CPO reaction.

Table 3.B.5: H_2-consumption calculated by H_2-TPR analysis for calcined SiO_2@Ni-Cr-LDHs catalysts

Catalysts	Peak temperatures (°C)	H_2-consumption (mmol/g)
CNC-01	237	49
	577	479
CNC-11	237	39
	385	228
	522	261
CNC-21	385	278
	522	354
CNC-31	400	309
	522	434

3.B.3.2. Catalytic activity over SiO_2@Ni-Cr-LDH:

3.B.3.2.1. In absence of N_2O over structured honey comb coated catalyst (Standard partial oxidation of methane):

Standard partial oxidation of CH_4 was carried out by maintaining CH_4:O_2 mol ratio of 2:1 in presence of calcined SiO_2@Ni-Cr-LDH as catalyst with varying SiO_2 to LDH ratios at temperatures ranging from 200-500 °C. **Fig. 3.B.16** shows the percentage conversion of CH_4, O_2 and percentage yield of H_2, CO and CO_2 in presence of four different catalysts. It was observed from **Fig. 3.B.16A** that the CH_4 and O_2 conversion increased from 40 % to 85 % and 42 % to 93 % respectively with the increase of temperature from 200-500 °C in presence of CNC-01 as catalyst. The H_2 and CO yield also increased with temperature from 42 % to 75% and 40 % to 67 % respectively. On the other hand CO_2 % yield was also found to decrease from 19 % to 1.2 % with the increase of temperature. The CH_4 and O_2 conversion in presence of CNC-11 catalyst (**Fig. 3.B.16B**) increased from 50 % to 87 % and 55 % to 95 % respectively with temperature while the selectivity towards H_2 and CO increases from 53 % to 78 % and

50 % to 76 %. The CO_2 selectivity also decreased from 12.9 % to 1 % in presence of CNC-11 with the increase of temperature (**Fig. 3.B.16B**). The conversion of CH_4 and O_2 in presence of CNC-21 catalyst (**Fig. 3.B.16C**) increased from 60 % to 90 % and 64 % to 90 % respectively and yields towards H_2 and CO increased from 57 % to 83 % and 57 % to 84 % with the increase of temperature. In presence of this catalyst yields towards CO_2 further decreased from 9.8 % to 1.5 %. At 500 ^oC there is no CO_2 production observed in presence of this catalyst (**Fig. 3.B.16C**). On the other hand, CNC-31 showed better CH_4 and O_2 conversion as well as the H_2 and CO selectivity with the increase of temperature (**Fig. 3.B.16D**). It showed CH_4 and O_2 conversion from 67 % to 91 % and 75 % to 99.99 % whereas 67 % to 91 % and 62 % to 87 % H_2 and CO selectivity. The selectivity towards CO_2 in presence of this catalyst was further decreased from 7.5 % to 2.7 % only at 200 and 300 ^oC respectively (**Fig. 3.B.16D**). The overall CH_4 and O_2 percentage conversion as well as H_2, CO and CO_2 percentage yield is shown in **Table 3.B.5**. It was observed that with the increase of SiO_2 to LDH ratio from 0:1 to 3:1 the catalytic activity also increased and CNC-31 shows better catalytic activity towards standard catalytic partial oxidation of CH_4. In addition to this it was further observed that standard catalytic partial oxidation (CPO) of CH_4 also dependent on temperature and 500 ^oC temperature was found to be standard temperature for catalytic partial oxidation (CPO) of CH_4 at which all these catalysts showed highest conversion of CH_4 and O_2 and highest selectivity towards H_2 and CO.

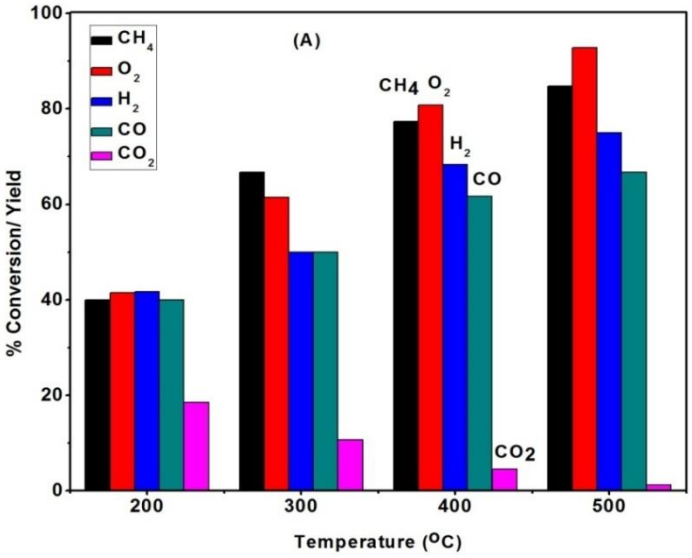
(A)
CH4
O2
H2
CO
CO2
% Conversion/ Yield
Temperature (°C)
0
20
40
60
80
100
200
300
400
500

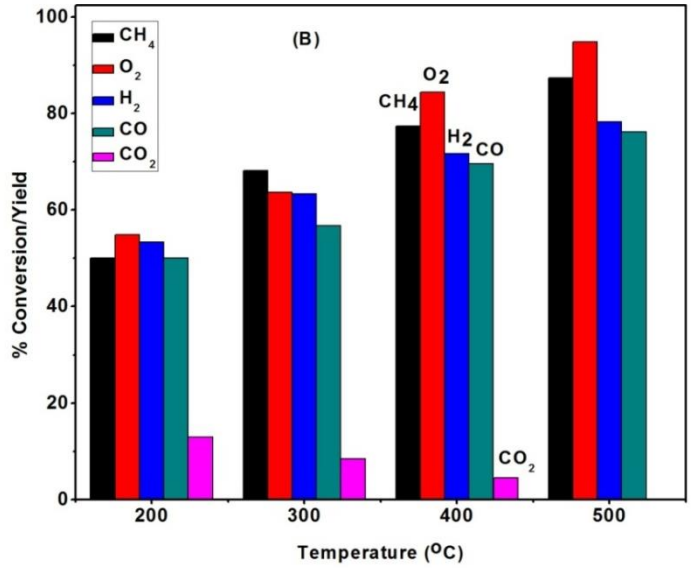
(B)
CH4
O2
H2
CO
CO2
% Conversion/Yield
Temperature (°C)
0
20
40
60
80
100
200
300
400
500

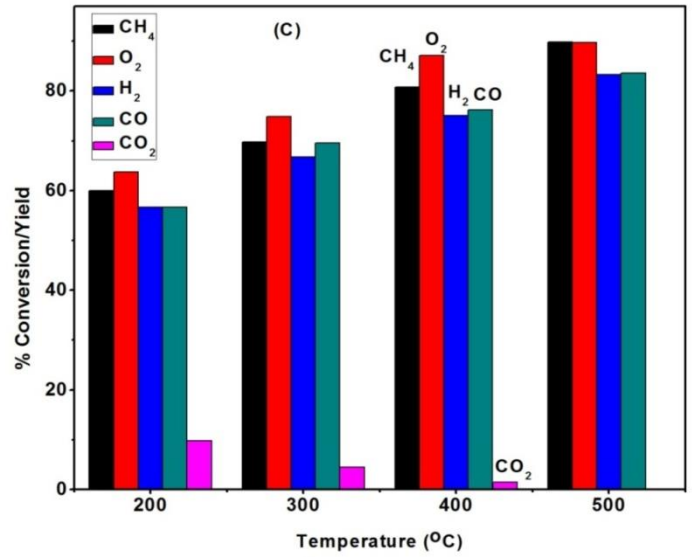
(C)
CH4
O2
H2
CO
CO2
% Conversion/Yield
Temperature (°C)
0
20
40
60
80
200
300
400
500

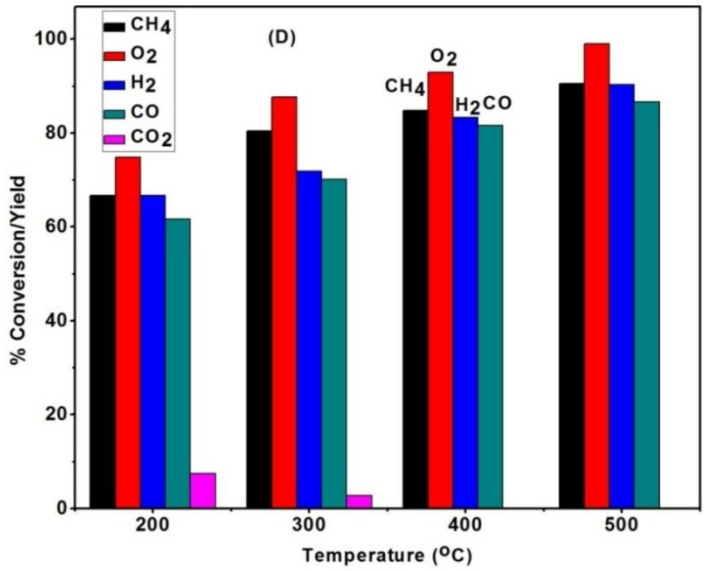

Fig. 3.B.16: Catalytic activity test : standard catalytic partial oxidation (300 ppm (18.70 mmol) CH_4 and 150 ppm (4.68 mmol) O_2 with N_2 balanced) in presence of (A) CNC-01; (B) CNC-11; (C) CNC-21 and (D) CNC-31.

Table 3.B.6: Percentage conversion and percentage yield of CH_4, O_2, H_2, CO and CO_2 in presence of calcined SiO_2@Ni-Cr-LDH with different SiO_2:LDH ratios (Total flow rate = 150 ml/min and GHSV=1,446 h^{-1} (22,500$cm^3gcat^{-1}h^{-1}$)

Type of active catalysts	(%) CH_4 Conversion				(%) O_2 Conversion				(%) H_2 Yield				(%) CO Yield			
	Temperatures (°C) (CH_4:O_2 mol ratio = 2:1)															
	200	300	400	500	200	300	400	500	200	300	400	500	200	300	400	500
CNC-01	40	67	77	85	42	62	81	93	42	50	68	75	40	50	62	67
CNC-11	50	68	77	87	55	64	84	95	53	63	72	78	50	57	70	76
CNC-21	60	70	81	90	64	75	87	90	57	67	75	83	57	70	76	84
CNC-31	67	80	85	91	75	88	93	99.99	67	72	83	91	62	70	82	87

3.B.3.2.2. Catalytic activity in presence of N_2O: Effect of N_2O in the feed (over structured honey comb coated material):

The CH_4 partial oxidation was carried out by supplying N_2O of different concentrations such as 100 ppm (2.27 mmol), 300 ppm (6.82 mmol) and 500 ppm (11.36 mmol) at the same GHSV (total flow rate of 150 ml/min) to study the effect of N_2O on the catalytic reaction. It was observed that all the catalyst showed better catalytic activity towards standard partial oxidation at 500 ^oC. Therefore, CPO of CH_4 by N_2O was carried out at 500 ^oC by varying CH_4 to N_2O ratio from 2:1, 1:1 and 1:2 respectively. **Fig. 3.B.17a** shows the percentage conversion and percentage yield of CH_4, H_2 and CO with varying N_2O concentration. It was observed that CNC-01 shows about 83.6 % and 85.8 % CH_4 conversion, 90 % and 93 % H_2, 89.9 % and 90.6 % CO selectivity at CH_4 to N_2O ratios 2:1 (100 ppm N_2O) and 1:1 (300 ppm N_2O). CNC-11 showed 93.7 % and 95.4 % CH_4 conversion and the selectivity towards H_2 and CO were observed as 94.7 %, 96.8 %, 91.6 % and 95.2 % in presence of 100 ppm and 300 ppm N_2O respectively (**Fig. 3.B.17a. A&B**). On the other hand, the percentage CH_4 conversion and percentage yield of H_2, CO were further increased from CNC-21 to CNC-31. CH_4 conversion increased from 97.1 % to 99.8 %, H_2 and CO percentage yield increases from 97.7 % to 98.7 % and 95.8 % to 98.6 % respectively in presence of 100 ppm N_2O while 98.2 % to 99.9 % CH_4 conversion, 98.9 % to 99.99 % H_2 and 97.2 % to 99.97 % CO selectivity respectively in presence of 300 ppm N_2O (**Fig. 3.B.17a.C&D**) as shown in **Table 3.B.6**. The percentage conversions of CH4 and percentage yield of H2 and CO with the active catalyst at different N2O concentrations are shown in **Fig. 3.B.17b**.

Although, the addition of 500 ppm N_2O increased the CH_4 conversion from 85 % in presence of CNC-01 to 99.9 % in presence of CNC-31, the selectivity towards H_2

and CO decreased. H_2 and CO percentage yield decreased up to 74 % and 65 % in presence of CNC-01 catalyst, whereas it showed 89.3 % H_2 conversion and 84 % in presence of CNC-31 catalyst (**Table 3.B.6**) which is due to the increase of the percentage yield of CO_2. **Fig. 3.B.17c** shows the % yield of CO_2 in presence of CNC-01 and it was observed that with the increase of concentration of N_2O % yield of CO_2 increases from 10.5 % to 23 %. This happens due to the re-oxidation of Ni catalysts from Ni^0 to Ni^{2+} which promotes the total oxidation of CH_4 and hence decreases the selectivity towards H_2 and CO. **Table 3.B.6** shows the overall percentage conversion of CH_4 and percentage yield of H_2 and CO in presence of all these catalysts.

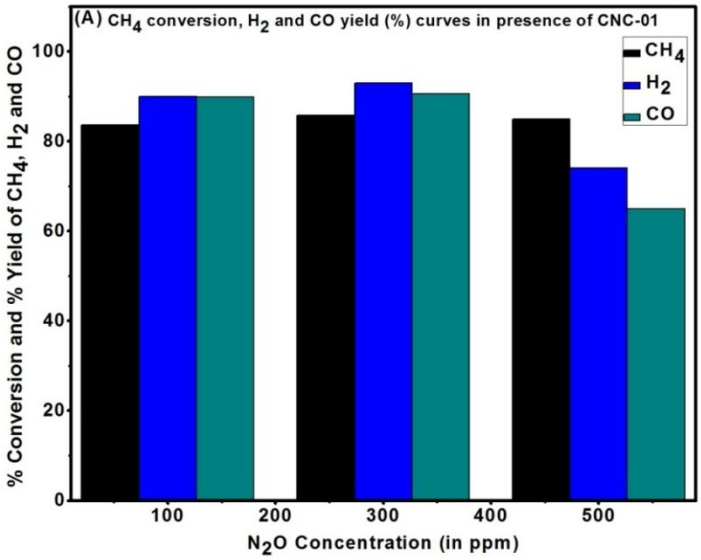

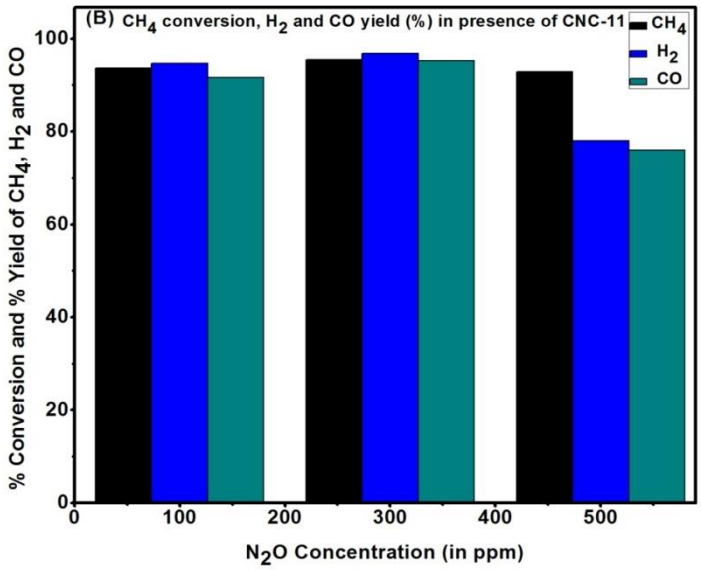

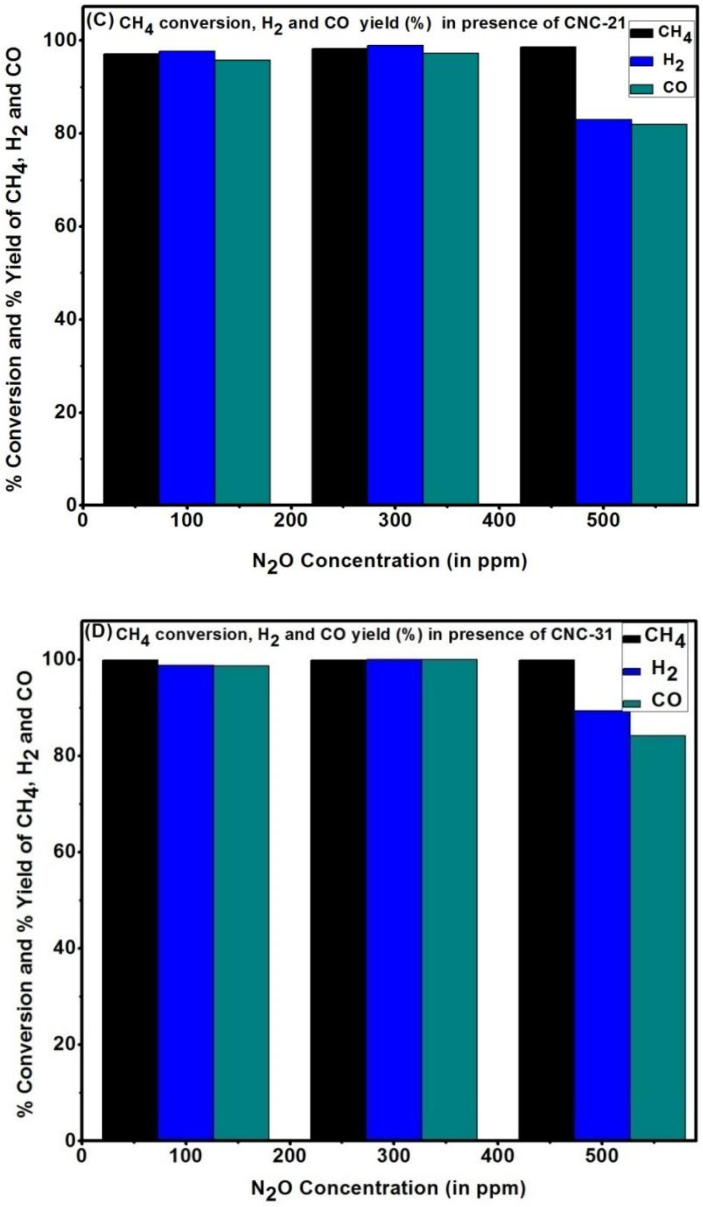

Fig. 3.B.17a: Catalytic activity test in presence of N_2O: effect of N_2O in the catalytic partial oxidation of CH_4 in presence of (A) CNC-01; (B) CNC-11; (C) CNC-21 and (D) CNC-31.

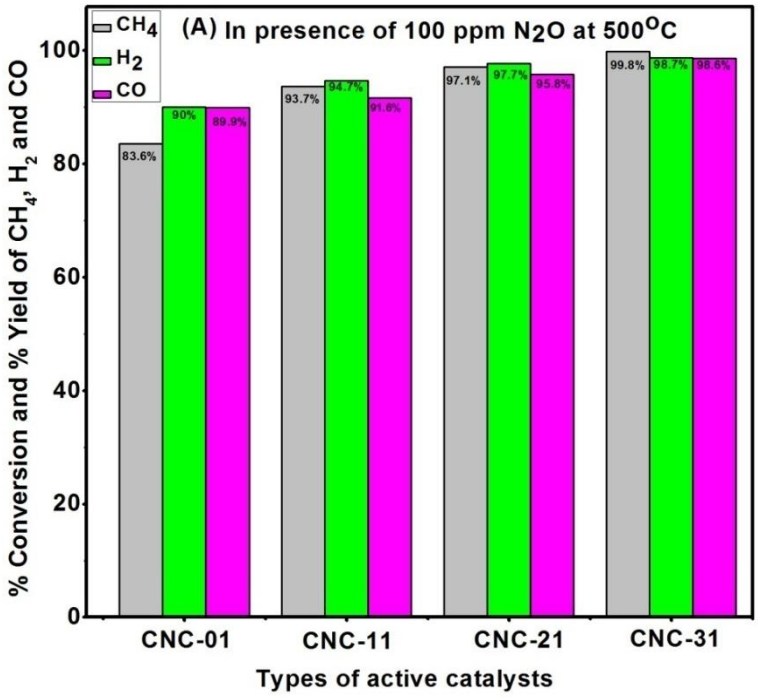
(A) In presence of 100 ppm N2O at 500°C
CH4
H2
CO
% Conversion and % Yield of CH4, H2 and CO
0
20
40
60
80
100
83.6%
90%
89.9%
93.7%
94.7%
91.6%
97.1%
97.7%
95.8%
99.8%
98.7%
98.6%
CNC-01
CNC-11
CNC-21
CNC-31
Types of active catalysts

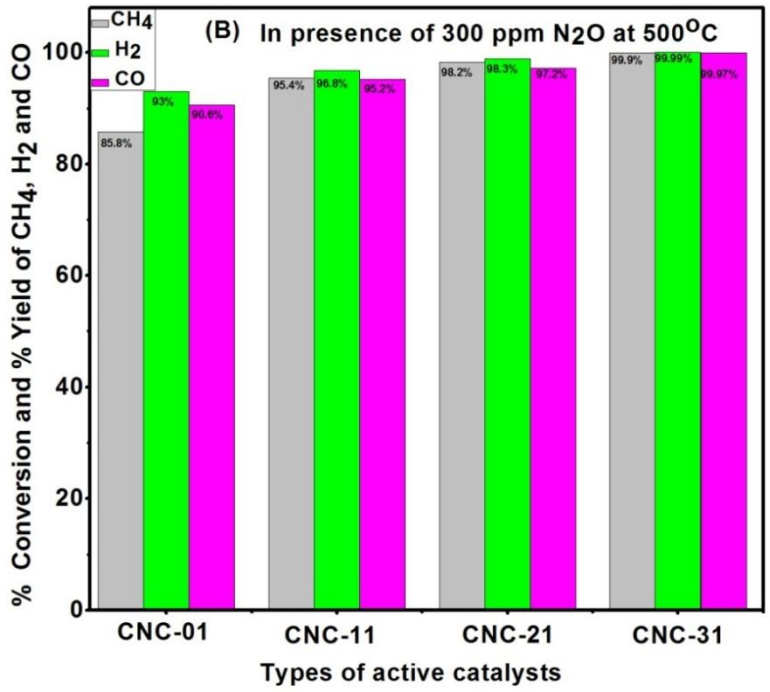
(B) In presence of 300 ppm N2O at 500°C
CH4
H2
CO
% Conversion and % Yield of CH4, H2 and CO
0
20
40
60
80
100
85.8%
93%
90.6%
95.4%
96.8%
95.2%
98.2%
98.3%
97.2%
99.9%
99.99%
99.97%
CNC-01
CNC-11
CNC-21
CNC-31
Types of active catalysts

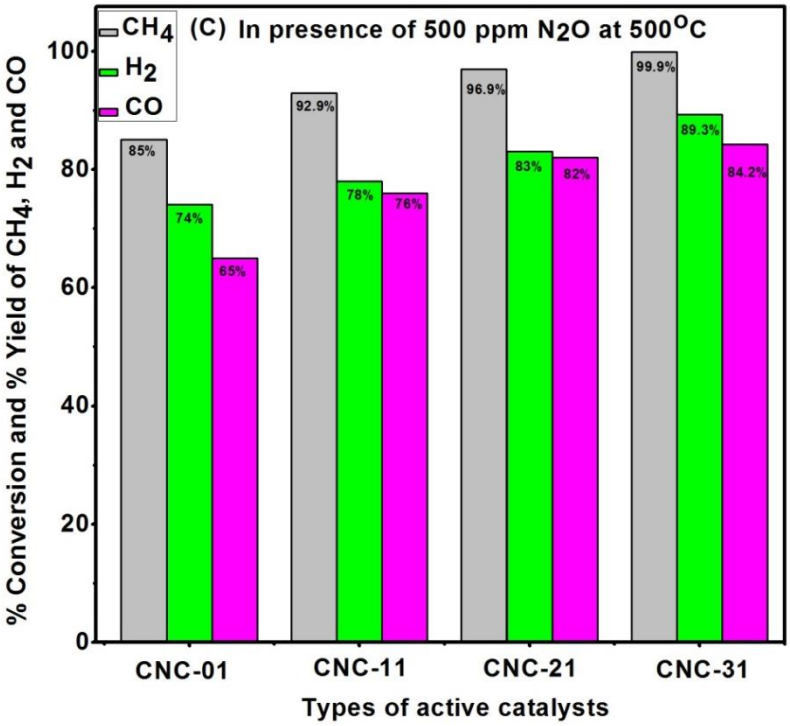

Fig. 3.B.17b: Percentage conversion of CH_4 and percentage yield of H_2 and CO in presence different N_2O concentration at 500 °C.

Table 3.B.7: Percentage conversion and selectivity of CH_4, H_2 and CO in presence of N_2O catalysed by calcined SiO_2@Ni-Cr-LDH with different SiO_2:LDH ratios at 500 °C (Total flow rate = 150 ml/min and GHSV=1,446 h^{-1} (22,500$cm^3gcat^{-1}h^{-1}$)

Type of active catalysts	(%) CH_4 conversion			(%) H_2 yield			(%) CO yield		
	CH_4:N_2O mol ratios								
	2:1 (100 ppm N_2O)	1:1 (300 ppm N_2O)	1:2 (500 ppm N_2O)	2:1 (100 ppm N_2O)	1:1 (300 ppm N_2O)	1:2 (500 ppm N_2O)	2:1 (100 ppm N_2O)	1:1 (300 ppm N_2O)	1:2 (500 ppm N_2O)
CNC-01	83.6	85.8	85	92	91.8	74	89.9	90.6	65
CNC-11	93.7	95.4	92.9	95.5	95.8	78	94.6	95.2	76
CNC-21	97.1	98.2	98.6	97.7	98.3	83	97.8	97.2	82
CNC-31	99.8	99.9	99.9	99.7	99.96	89.3	99.6	99.93	84.2

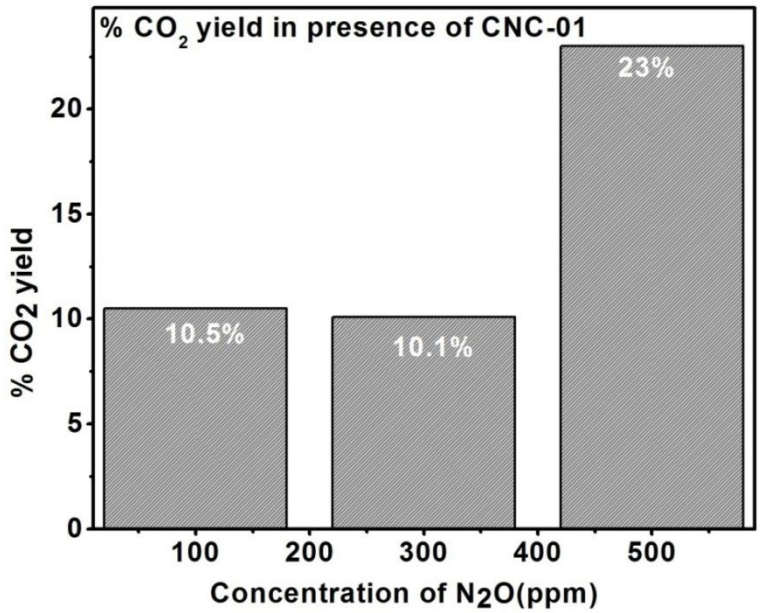

Fig. 3.B.17c: CO_2 % yield in presence of 500 ppm (11.36 mmol) N_2O at 500 °C.

3.B.3.2.3. Catalytic stability test with time:

From the above results it was observed that CNC-31 catalysts showed highest selectivity towards H_2 and CO (about 99.9 %) in presence of 100 ppm (2.27 mmol) N_2O and 300 ppm (6.82 mmol) N_2O. Depending on this the catalytic stability of this catalyst was carried out in presence of 100 ppm (2.27 mmol) N_2O and 300 ppm (6.82 mmol) N_2O at 500 °C and GHSV=1,446 h^{-1} (22,500$cm^3gcat^{-1}h^{-1}$) for 40 hour under atmospheric pressure. **Fig. 3.B.18** shows the catalytic stability test of CNC-31. It was observed that CNC-31 showed good catalytic stability upto 40 hour of reaction time.

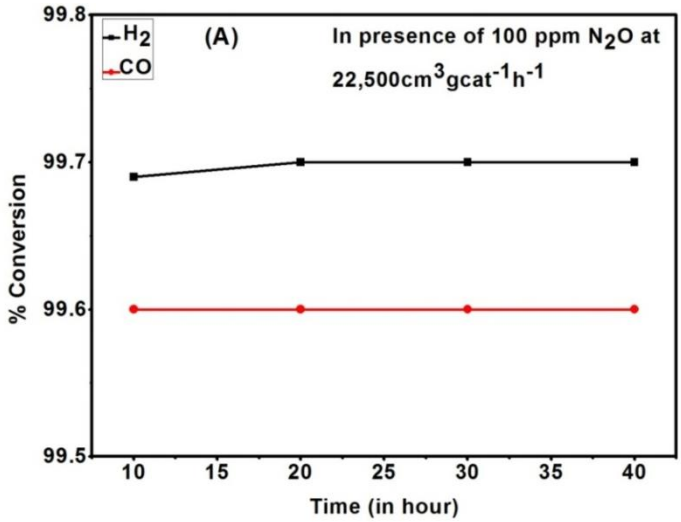

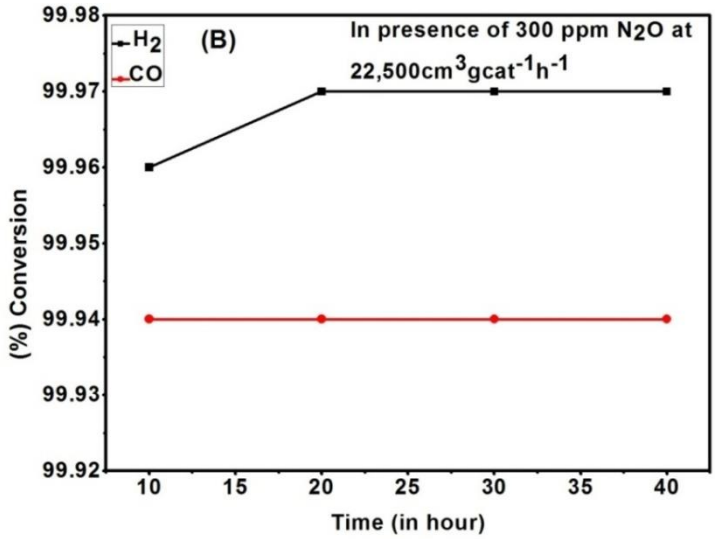

Fig. 3.B.18: Catalytic stability test of CNC-31 catalyst in presence of 100 ppm (2.27 mmol) N_2O and 300 ppm (6.82 mmol) N_2O at 500 ºC.

3.B.3.2.4. XPS analysis of the catalysts:

XPS analysis of unsupported and SiO_2 supported calcined catalysts were carried out after different catalytic reactions and were designated as CNC-01(unsupported calcined LDH with SiO_2 to LDH ratio 0:1), CNC-11 (SiO_2 supported calcined LDH with SiO_2 to LDH ratio 1:1), CNC-21 (SiO_2 supported calcined LDH with SiO_2 to LDH ratio 2:1) and CNC-31 (SiO_2 supported calcined LDH with SiO_2 to LDH ratio 3:1). XPS analysis showed the binding energy of 854.4-855.2 eV due to the presence of +2 oxidation state of $Ni2p_{3/2}$. The binding energies of 576.8-578.4 eV and 584.8-586.9 eV was attributed to the $Cr2p_{3/2}$ and $Cr2p_{1/2}$ level in all these catalyst after different catalytic reactions as shown in **Table 3.B.8a**. Si2p showed the peak at binding energy of 101-103 eV [66-68]. It was observed from the XPS analysis that Ni^0 is further oxidized to Ni^{2+} and Ni^{3+} oxidation state in all these catalysts which. After co-feeding 500 ppm N_2O, XPS analysis shows the presence of both Ni^{2+} and Ni^{3+} oxidation states of NiO species with binding energies of 855.8-856 eV and 854.4 eV indicating the further oxidation of Ni^0 to Ni^{2+} and Ni^{2+} to Ni^{3+}. Thus, the increase in

concentration of N_2O leads to decrease in the selectivity towards syngas similar to standard CPO reaction in presence of O_2. On the otherhand, Cr is present as +3 oxidation state in all these catalyst by probably forming an amorphous Cr_2O_3-SiO_2 type phase in presence of SiO_2 and acts as a support over NiO species as observed from XRD analysis. Similar formation of amorphous phase is also reported previously [60]. XPS analysis further shows the presence of C1s in all these catalyst. The binding energy value for C1s was centered at 283.3-284.6 eV after different catalytic reaction which is similar to the binding energy of adventitious carbon [30]. **Table 3.B.8b** shows the different atomic ratios of Ni/Si and C/Si in these catalysts. It was observed that the amount of SiO_2 effects on Ni dispersion and it increased with the increase of SiO_2 from CNC-01 to CNC-31. **Fig. 3.B.19** shows the XPS pattern of the catalysts after CPO reaction in presence of 500 ppm N_2O in the feed. In other words, the TOF (Turn over frequency) for all these catalysts calculated for CPO reaction with 1:1 mol ratio of N_2O:CH_4 have comparatively similar values further providing further evidence in support of Ni^0 act as the active site of these catalysts (**Table 3.B.8c**).

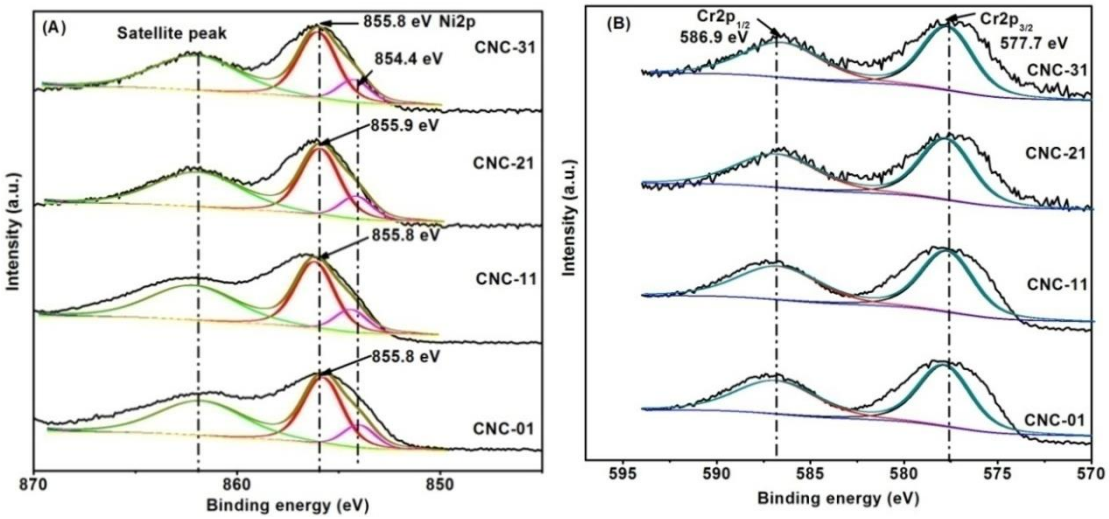

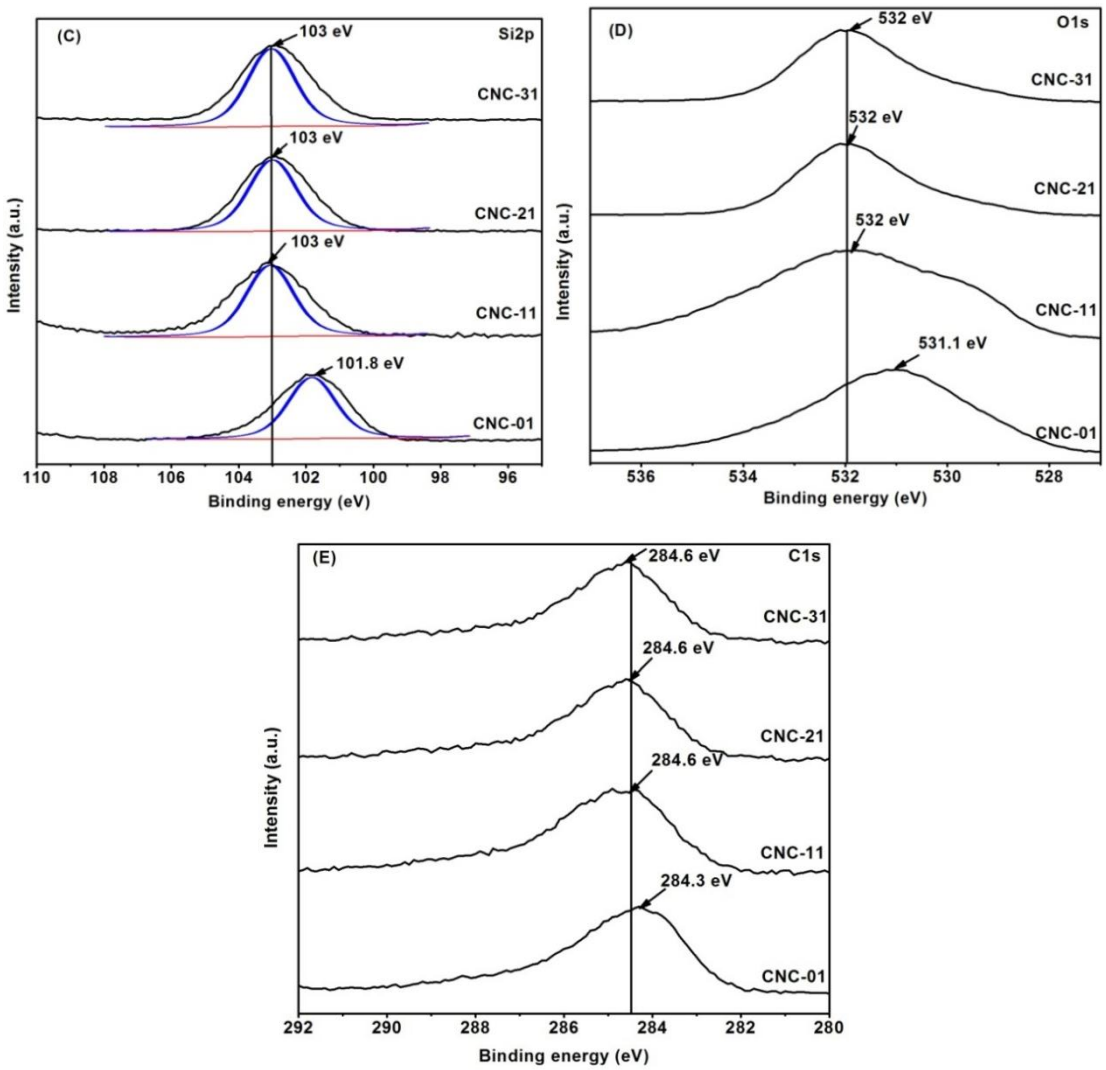

Fig. 3.B.19: XPS analysis of calcined SiO_2@Ni-Cr-LDH with different SiO_2 to LDH ratios after CPO reaction in presence of 500 ppm N_2O.

Table 3.B.8a: XPS binding energies of Ni2p and Cr2p in the calcined SiO_2@Ni-Cr-LDH catalysts having different SiO_2 to LDH ratios after different catalytic reaction

Catalyst	Ni2p (eV)				Cr2p (eV)			
	CNC-01	CNC-11	CNC-21	CNC-31	CNC-01	CNC-11	CNC-21	CNC-31
As synthesized	854.4	854.4	855.2	855.2	576.8-584.8	578.4-585.6	578.4-585.6	578.4-585.6
After H_2-pretreatment	852.8	852.7	852.8	852.7	576.8-584.8	578.4-585.6	578.4-585.6	578.4-585.6
After standard	855.8	855.8	856	856	577.7-585.6	578.4-585.6	578.4-585.6	578.4-585.6

CPO								
After CPO in presence of 300 ppm N_2O	854.3	854.4	854.5	854.5	577.7-585.6	578.4-585.6	578.4-585.6	578.4-585.6
After CPO in presence of 500 ppm N_2O	855.8	855.8	856	856	577.7-586.9	577.7-586.9	577.7-586.9	577.7-586.9

Table 3.B.8b: XPS atomic ratios of Ni/Si and C/Si in the calcined SiO_2@Ni-Cr-LDH catalysts having different SiO_2 to LDH ratios after different catalytic reaction

Catalysts after different conditions	**Ni/Si**				**C/Si**			
	CNC-01	**CNC-11**	**CNC-21**	**CNC-31**	**CNC-01**	**CNC-11**	**CNC-21**	**CNC-31**
As synthesized	**0.03**	**0.47**	**1.2**	**1.9**	**0.42**	**0.3**	**0.25**	**0.15**
After standard CPO	**0.55**	**0.64**	**0.73**	**1.2**	**3.2**	**1.3**	**0.25**	**0.15**
After CPO in presence of 300 ppm N_2O	**0.57**	**0.69**	**0.82**	**1.5**	**3.2**	**1.3**	**0.25**	**0.15**
After CPO in presence of 500 ppm N_2O	**0.59**	**0.74**	**0.85**	**1.7**	**3.2**	**1.3**	**0.25**	**0.15**

It was observed from the catalytic activity study that the selectivity towards H_2 and CO did not exceed 90 % and 86 % in the standard catalytic partial oxidation of CH_4. On the other hand, in presence of N_2O the selectivity towards H_2 and CO increased up to 99.9 %. These results can be explained on the basis of the adsorption phenomenon of O_2 and N_2O on the catalyst surfaces. Similar to the reported by C. M. Pedrero *et al.*[29] the molecular O_2 adsorbed on the catalyst surface forms an electrophilic species such as O^- or O_2^- which promotes the total oxidation instead of partial oxidation and decreases the selectivity towards H_2 and CO in presence of all these catalysts. On the otherhand, in case of CPO reaction in presence of N_2O firstly, N_2O adsorbed on the

catalyst surface decomposes to N_2 and atomic oxygen which have less oxidizing power as compared to the electrophilic species obtained from molecular O_2 [29]. Hence, the oxygen species formed by the dissociation of N_2O is most effective for the CPO of CH_4 instead of total oxidation of CH_4 and increases the selectivity of the catalysts towards H_2 and CO. The mol ratio of H_2 and CO remains as 2:1 in both of these reactions.

From the above results it was also observed that although in presence of 500 ppm N_2O the percentage conversion of CH_4 exceeded 99 % the percentage yield towards H_2 and CO decreased. This decrease was due to the re-oxidation of Ni-catalysts from Ni^0 to Ni^{2+} which favoured only the total oxidation of CH_4. Hence, the production of CO_2 was observed in presence of 500 ppm N_2O (**Fig. 3.B.16c**) with CH_4:N_2O mol ratio of 1:2. It was further observed that catalytic partial oxidation of CH_4 in presence of N_2O also depends on the mol ratio of CH_4:N_2O. Thus, highest selectivity towards syn-gas (H_2+CO) production was possible only in presence of 1:1 CH_4:N_2O mol ratio which is the equilibrium condition for CPO reaction.

The percentage conversion as well as the selectivity of CNC-01, CNC-11, CNC-21 and CNC-31 increased in the order- CNC-01< CNC-11< CNC-21< CNC-31. Thus, CNC-31was found to act as an active catalyst towards both standard CPO and catalytic partial oxidation in presence of N_2O. It showed about 99.9 % selectivity towards H_2 and CO. Although, there was a decrease of Ni loading from CNC-01 to CNC-31, the reason of the better catalytic activity was due to the increase of SiO_2:LDH ratio from 0:1 to 3:1 which increased Ni dispersion due to the presence of larger SiO_2 network over catalyst and hence increased the active sites of the catalyst. As reported by A.C.W. Koh *et al*.[19] the deposition of coke is the major problem in case of Ni-based catalyst which leads to the deactivation of the catalysts. Hence, TGA analysis was

carried out under oxygen atmosphere to check the deposition of coke after the catalytic reactions (**Fig. 3.B.20**). It was observed that the weight loss for these catalysts decreases from 8.3 % to 1% with the increase of SiO_2:LDH ratios. Thus, the presence of SiO_2 decreased the deposition of coke over these catalysts. The C/Si ratio also decreased from 3.2 to 0.15 as observed from XPS analysis after SPO and CPO in presence of N_2O with different concentration in these catalysts as shown in **Table 3.B.8b** which was further confirmed from carbon amount analysed by CHN analyzer and decreased from 1.2 % in case of fresh catalysts to 0.3 % in case of reacted catalysts. Hence, both the increase of Ni-dispersion as well as decrease in coke deposition over CNC-31 catalyst lead to it better catalytic activity towards CPO of CH_4. It showed about 99.9 % H_2 and CO selectivity at 500 ^oC and can be used as an effective catalyst for synthesis gas production at low temperature.

Table 3.B.8c: Turn over frequency of calcined SiO_2@Ni-Cr-LDH catalysts having different SiO_2 to LDH ratios at 500 ^oC

Catalysts	CNC-01	CNC-11	CNC-21	CNC-31
Amount of Ni^0 (mmol/g)	2.03	2.25	2.85	2.95
TOF (s^{-1}) $\times 10^{-3}$	1.2	1.1	0.09	0.09

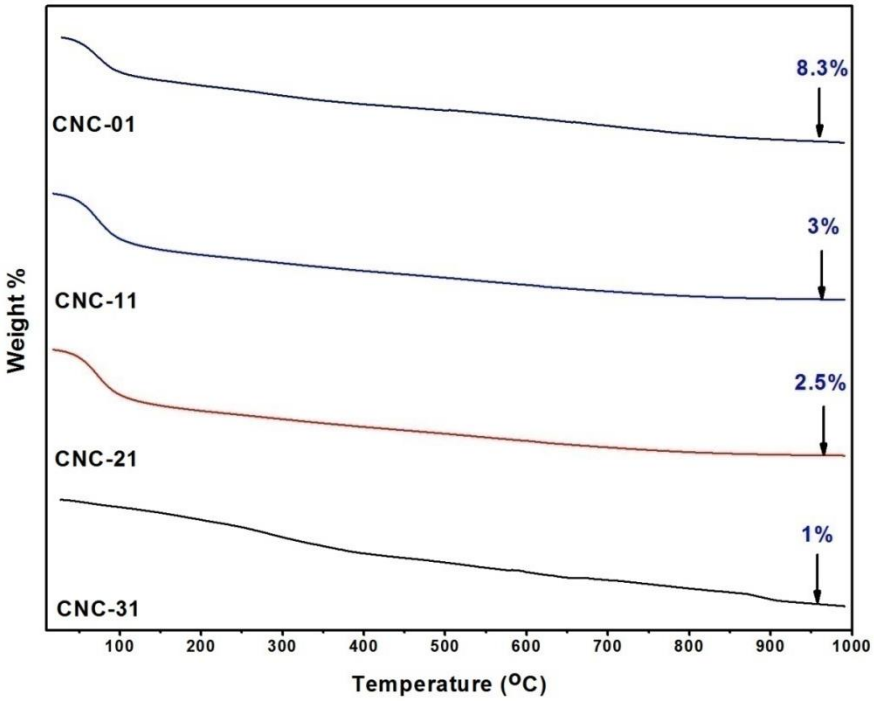

Fig. 3.B.20: TGA pattern of calcined SiO_2@Ni-Cr-LDH nanocomposites different SiO_2 to LDH ratios after gas reaction.

3.B.3.3. Catalytic partial oxidation of CH_4 by N_2O over SiO_2@Mg-Cr-LDH:

Catalytic partial oxidation of CH_4 by N_2O over SiO_2@Mg-Cr-LDH with SiO_2 to LDH ratio 3:1 was carried out at 500 ^oC based upon the catalytic behaviour of other binary LDHs. The Argon:N_2O:CH_4 flow rate was maintained at 150:100:50 ml/min. The GHSV was maintained at 12,784 h^{-1} (18,000 $cm^3g^{-1}h^{-1}$). The N_2O:CH_4 mol ratio was kept as 1:1. The product gas was collected after 30 min and 60 min reaction time. It was observed that in presence of this catalyst N_2O was first decomposed to N_2 and O_2 and this oxygen then lead to the catalytic partial oxidation of CH_4 to H_2 and CO (synthesis gas). It showed about 100 % N_2O conversion and 97.8 % CH_4 conversion after 60 min reaction time as shown in **Table 3.B.9**. It showed about 97.2 % H_2 and 96 % CO yield. **Fig. 3.B.21** shows the Gas Chromatograms for N_2O decomposition to N_2 and O_2 (**Fig. 3.B.21A** and CH_4 partial oxidation to H_2 and CO (**Fig.3.B.21B, C&D**).

Table 3.B.9: Gas-solid reaction studies for CH_4 partial oxidation by N_2O

Flow rates (Argon: N_2O:CH_4) (ml/min)	GHSV (Gas Hourly Space Velocity (h^{-1})	Reactant Gas (In ppm)		Product gas after 30 min reaction time (in ppm)		Product gas after 60 min reaction time (in ppm)		% Decomposition			
								Product gas after 30 min reaction time		Product gas after 60 min reaction time	
		N_2O	CH_4	N_2O	CH_4	N_2O	CH_4	N_2O	CH_4	N_2O	CH_4
150:100:50	12,784	300	100	12.19	16.6	-	11.43	97.6	96.8	100	97.8

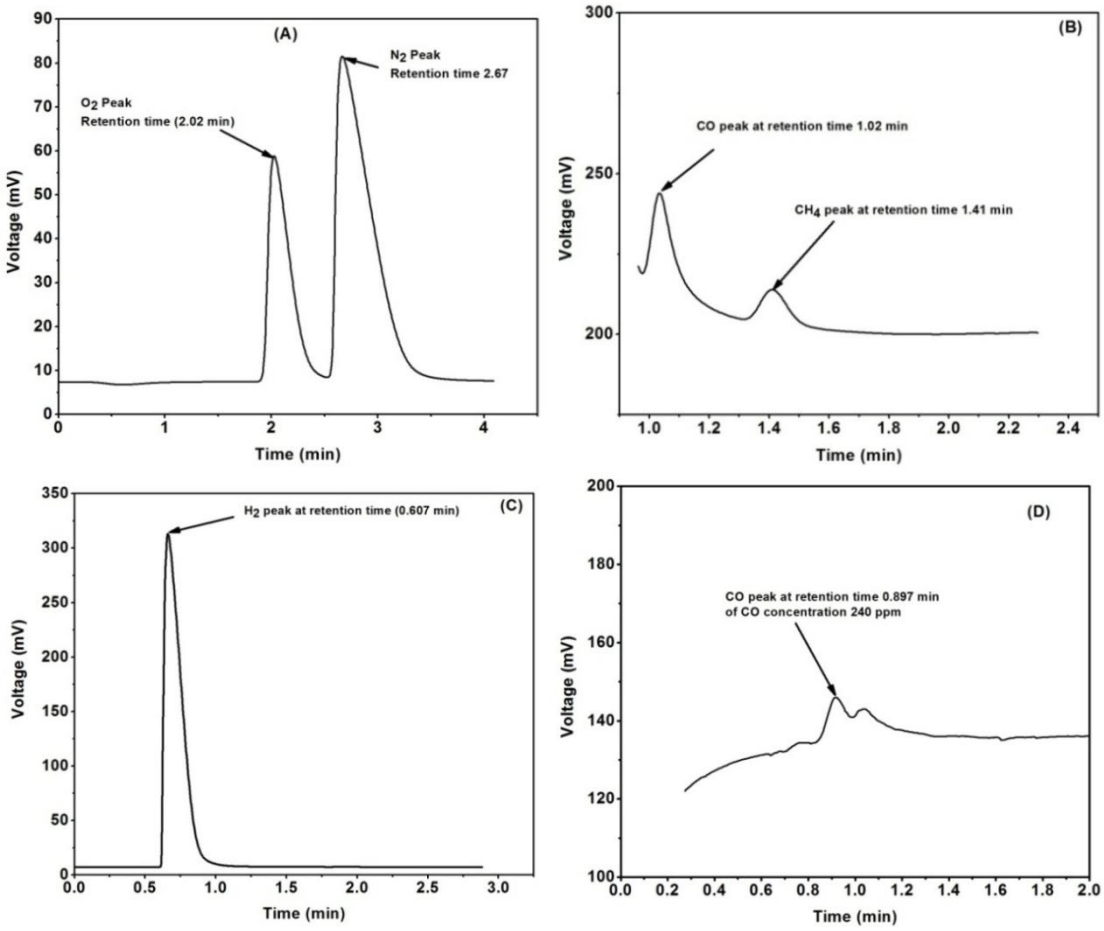

Fig. 3.B.21: Gas Chromatograms for N_2O decomposition to N_2 and O_2 (A); (B)CO and CH_4 peak detected in FID; (C) H_2 peak detected in TCD; (D) CO peak detected in FID.

- *The work described in the* ***Section*** **3.B.3.2.***has been communicated (Under Revision).*

3.B.4. CONCLUSIONS:

The SiO_2@Ni-Cr-LDH and Mg-Cr-LDH core-shell type nanocomposite alcogels were successfully synthesized by 'soft chemical' sol-gel method by using a mixed system of silicon alkoxide and metal acetylacetonate as precursors. The synthesis techniques adopted helped in dispersing otherwise difficult to exfoliate and disperse LDH nanosheets in a continuous network of silica particles. The synthesis was basically carried out in alcohol rich organic medium which bears the specific prospect of drying the gels by using specialised critical point drying techniques at low temperatures where solvents would be removed without much disturbing the microstructure of solid network. Such alcogels after normal low temperature drying when characterized by XRD, DTA-TGA, IR, zeta-potential study, particle size analysis, SEM, TEM and EDS analysis confirm the formation of nanocomposites having LDH sheets assembled around silica centers. BET surface area analysis of oven dried samples itself showed rise in surface area with the rise of silica content indicating good prospects of these materials in the field of catalysts. The flow behaviour study showed that the alcogels have Bingham fluid behaviour with a favourable shear thinning property. It was further observed that with the increase of SiO_2:LDH ratios from 0:1 to 3:1 their elastic or gel like behaviour increased with $G^{/}$ (Storage modulus) remaining greater than $G^{//}$(Loss modulus). Also, it was observed that there is a gradual decrease of complex viscosity with the increase of angular frequency showing a good shear-thinning behaviour. Simultaneously, with the increase of SiO_2 component the dispersability of these nanocomposites also kept on increasing due to which it could be easily coated over solid surface which was also observed from zeta potential analysis showing the higher negative zeta potential of SiO_2@LDH nanocomposites with 3:1 SiO_2:LDH ratio. Thus, it can be concluded that

the reported route can be a facile route for synthesis of asymmetric mesoporous membranes over solid ceramic supports. Further studies are going on the environmental catalytic application of such systems.

The standard catalytic partial oxidation and catalytic partial oxidation in presence of N_2O carried out by calcined SiO_2@Ni-Cr-LDHs coated over honey comb monoliths shows different selectivities towards H_2 and CO. For these catalysts the selectivity towards H_2 and CO does not exceed 90 % and 86 % in the standard catalytic partial oxidation of CH_4. On the other hand, the selectivity towards H_2 and CO increases in presence of N_2O. Literature says [30] in case of standard oxidation reaction the molecular oxygen adsorbed on the catalyst surface forms O^- or O_2^- electrophilic species which leads to the total oxidation of methane whereas N_2O decomposes to N_2 and atomic oxygen in presence of all these catalysts which enhance the total oxidation of methane and promotes the partial oxidation reaction due to its less reactivity. In other words selectivity towards syn-gas is highest only in presence of 1:1 CH_4:N_2O mol ratio which is the equilibrium condition for CPO reaction. Thus, it is observed that N_2O act as promoter for CPO reaction. On the other hand, at high concentration of N_2O (500 ppm) the re-oxidation of the Ni-catalysts leads to decrease of the selectivity towards H_2 and CO and which also favours total oxidation of methane and forms CO_2. It is further observed from the catalytic reaction that with the increase of SiO_2 to LDH ratios their selectivity also increases due to the increase of Ni dispersion as well as the active sites which lead to decrease in the coke deposition over the catalysts. CNC-31 shows about 99.9 % selectivity towards H_2 and CO. Hence, it can be concluded that mixed-metal nano-oxides obtained after the calcination of LDH coated over honey comb monolithic substrate act as an effective catalysts for the synthesis gas (H_2/CO) production. In presence of SiO_2 LDH form hybrid nano alcogels which helps to form a crack free

catalytic membrane as well as also increases the selectivity towards H_2 and CO by increasing the surface area. In addition to this the honey comb monoliths provide large external surface, uniform gas flow, low radial heat transfer, high geometric surface area which further increases the catalytic activity of the catalysts. The main advantage of our catalyst is that it works effectively at low temperature for the synthesis gas (H_2/CO) production without deposition of coke which is the severe problem of other reported catalyst as. Therefore, such a catalytic device obtained by coating of SiO_2@Ni-Cr-LDH nanocomposite alcogels can be effectively used for the large scale industrial level synthesis gas (H_2/CO) production.

REFERENCES:

[1] D.J. Wuebbles. *Sci.*, **2009**, *326*, 56-57.

[2] M. Strokal, C. Kroeze. *Cur.Opin. Environ. Sust.*, **2014**, *9-10*, 108-121.

[3] B. A. Hungate, J. S.Dukes, M. R. Shaw, Y. Luo, C. B. Field. *Sci.*, **2003**, *302*, 1512-1513.

[4] J. W. Erisman, J.Galloway, S. Seitzinger, A. Bleeker, K. Butterbach-Bahl. *Cur.Opin. Environ. Sust.*, **2011**, *3*, 281-290.

[5] L. Li, J. Xu, J. Hu, J. Han. *Environ. Sci. Technol.*, **2014**, *48*, 5290-5297.

[6] E. A.Davidson, D. Kanter. *Environ. Res. Lett.*, **2014**, *9*, 105012.

[7] D. Kanter, J. Alcamo, E.A. Davidson. Drawing Down N_2O to Protect Climate and the Ozone Layer. AUNEP Synthesis Report. ISBN: 978-92-807-3358-7.

[8] S. Rao, K. Riahi. *Energy J.*, **2006**, *27*, 177-200.

[9] R. Ravishankara, J. S. Daniel, R. W. Portmann. *Sci*., **2009**, *326*, 123-125.

[10] R. P. Wayne. Chemistry of the Atmosphere, 3rd ed; Oxford University Press: Oxford, U.K., **2000**, 775.

[11] P. Wiesen, T. J.Wallington, W. Winiwarter. Reducing N_2O emissions from

industry and fossil fuel combustion Drawing Down N_2O to Protect Climate and the OzoneLayer. AUNEPSynthesisReport;UnitedNationsEnvironmentProgramme:Nairobi ,**2013**.www.unep.org/pdf/UNEPN_2Oreport.pdf.

[12] S. J. Lee, I. S. Ryu, B. M. Kim, S. H. Moon. *Int. J. Green house Gas Control*, **2011**, *5*, 167-176.

[13] F. Kapteijn, J. R. Mirasol, J. A. Moulijn. *Appl.Catal. B: Environ.*, **1996**, *9*, 25-64.

[14] S. A. Al-Sayari. *The Open Catal. J.*, **2013**, *6*, 17-28.

[15] N. Russo, D. Mescia, D. Fino, G. Saracco, V. Specchia. *Ind. Eng. Chem. Res.*, **2007**, *46*, 4226-4231.

[16] R. L. Goswamee, M. Mishra, A. K. Sarma Baruah. Mixed metal oxidic nano sheets coated monolithic catalysts useful for the decomposition of toxic N_2O and a process for the preparation thereof. Patent No. US 9616412 B2, **2017**.

[17] M. Konsolakis. *ACS Catal.*, **2015**, *5*, 6397-6421.

[18] A.A. Yaremchenko, V.V. Kharton, S.A.Veniaminov, V.D. Belyaeb, V.A. Sobyanin, F.M.B. Marques. *Catal.Commun.*, **2007**, *8*, 335.

[19] A.C.W. Koh, L. Chen, W.K. Leong, B.F.G. Johnson, T. Khimyak, J. Lin. *Int. J. Hydrog. Energy*, **2007**, *32*, 725-730.

[20] H. Liander. *Trans. Faraday Soc.*, **1929**, *25*, 462-472.

[21] R.S. Drago, K. Jurczyk, N. Kob, A. Bhattacharyya, J. Masin. *Catal.Lett.*, **1998**, *51*, 177-181.

[22] T. Zhu, M. F.Stephanopoulos. *Appl.Catal. A*, **2001**, *208*, 403-417.

[23] M. Peymani, S. M. Alavi, M. Rezaei. *Int. J. Hydrog. Energy*, **2016**, *41*, 6316-6325.

[24] J. P. Ramirez, N. Blangenois, P. Ruiz. *Catal.Lett.*, **2005**, *104*, 163.

[25] F. Dury, M.A. Centeno, E.M. Gaigneaux, P. Ruiz. *Appl.Catal. A*, **2003**, *247*, 231.

[26] O. Demoulin, F. Dury, M. Navez, E.M .Gaigneaux, P. Ruiz. *Catal. Today*, **2004**, *91*, 27.

[27] O. Demoulin, I. Seunier, F. Dury, M. Navez, R. Rachwalik, B. Sulikowski, S.R. Gonzalez-Carrazan, E.M. Gaigneaux, P. Ruiz. *Catal.Today*, **2005**, *99*, 217-226.

[28] B. R.Wood, J.A. Reimer, A.T. Bell, M.T. Janicke, K.C. Ott. *J. Catal.*, **2004**, *225*, 300-306.

[29] C. M. Pedrero, B. Blerot, M.A. Soria, S.R. Gonzalez-Carrazan, P. Ruiz. *Catal.Today*, **2013**, *203*, 176-181.

[30] C. M. Pedrero, B. Blerot, M. A. Soria, S. R. Gonzalez-Carrazan, P. Ruiz. *Catal. Today*, **2013**, *213*, 155-162.

[31] N.A.Khan, E.M. Kennedy, B.Z. Dlugogorski, A.A. Adesian, M. Stockenhuber. *Catal. Commun*., **2014**, *53*, 42-46.

[32] J. Ashok, G. Raju, P.S.Reddy, M. Subrahmanyam, A. Venugopal. *Int. J. Hydrog. Energy*, **2008**, *33*, 4809-4818.

[33] P. Saikia, A. Gautam, R.L. Goswamee. *RSC Adv.*, **2016**, *6*, 112092-112102.

[34] F. Cavani, F.Trifiro, A. Vaccari. *Catal. Today*, **1991**, *11*, 173-301.

[35] V. Rives. Layered double hydroxides: present and future *Nova Science Publishers,New York*, **2001**.

[36] P. J. Sideris, U. G.Nielsen, Z. Gan, C. P. Grey. *Sci.*, **2008**, *321*, 113.

[37] Q.Wang, D. O'Hare. *Chem. Rev.*, **2012**, *112*, 4124-4155.

[38] D. G. Evans, R. C. T Slade. Layered Double Hydroxides: Structure and Bonding, **2006**, 119, 1.

[39] X. Duan, D.G. Evans. Layered Double Hydroxides. *Springer-Verlag, Berlin*, **2006**, 119.

[40] B. Xue, F.Ting, Z. Hui. *ACS Appl. Mater. Interfaces*, **2014**, *6*, 20498-20509.

[41] M. Shao, F. Ning, J. Zhao, M. Wei, D.G. Evans, X. Duan. *J. Am. Chem. Soc.*, **2012**, *134*, 1071-1077.

[42] M.A. Aramendia, V. Borau, C. Jimenez, J.M. Marinas, J.R.Ruiz, J.F. Urbano. *J. Solid State Chem.*, **2002**, *168*, 156-161.

[43] Y.Wang, F. Li, S. Dong, X. Liu, M. Li. *J. Colloid Interface Sci.*, **2016**, *467*, 28-34.

[44] M. Mishra, M.R. Das, R.L. Goswamee. *J. Sol. Gel Technol.*, **2010**, *54*, 57-61.

[45] F. Prinetto, G. Ghiotti, P. Graffin, D. Tichit. *Micrporous Mesoporous Mater.*, **2000**, *39*, 229-247.

[46] M. Mishra, R.L. Goswamee. Process for the adsorption of toxic sulphur bearing gases.Patent No. US 8,951,491 February 10, **2015**.

[47] F. Basile, L. Basini, G. Fornasari, M. Gazzano, F. Trifir, A.Vaccari. *Chem. Commun.*, **1996**, *0*, 2435-2436.

[48] F. Basile, L. Basini, M. D'Amore, G. Fornasari, A. Guarinoni, D. Matteuzzi, G.Del Piero, F. Trifiro, A. Vaccari. *J. Catal.*, **1998**, *173*, 247-256.

[49] J. Zhang, W.Wei, Y. Sun. *Catal.Lett.*, **2010**, *135*, 321-329; DOI:10.1007/s10562-010-0268-5.

[50] D.V.Cesar, M.A.S. Baldanza, C. A. Henriques, F. Pompeo, G. Santori, J. Munera, E. Lombardo, M. Schmal, L. Cornaglia, N. Nichio. *Int. J. Hydrog. Energy*, **2013**, *38*, 5616-5626.

[51] H. Messaoudi, S.Thomas, A. Djaidja, S. Slyemi, R. Chebout, S. Barama, A. Barama, F. Benaliouche. *C. R. Chimie*, **2017**, *20*, 738-746.

[52] J. L. Williams. *Catal.Today*, **2001**, *69*, 3-9.

[53] A. F. Perez-Cadenas, M. M. P. Zieverink, F. Kapteijn, J. A. Moulijn. *Catal.Today*, **2005**, *105*, 623-628.

[54] M. R. Ranjan, A. L. Ramanathan, A.Tripathi, P. K. Jha. *Int. J. Environ. Sci.*, **2014**, *4*, 919-925.

[55] A. K. Jha, C. Sharma, N. Singh, R. Ramesh, R. Purvaja, P.K. Gupta. *Chemosphere*,**2008**, *71*, 750-758.

[56] G. Saha, B. Kar, S. Karmakar. *Cur. Sci.*, **2017**, *112*, 989-995.

[57] J.J. Zhu, J.G. van Ommen, L. Lefferts. *Catal. Today*, **2006**, *112*, 82-85.

[58] M. Chen, J.L.Wu, Y.M. Liu, Y. Cao, K.N. Fan. *Catal.Commun.*, **2011**, *12*, 1063-1066.

[59] R. S. Drago, K. Jurczyk, N. Kob, A. Bhattacharyya, J. Masin. *Catal. Lett.*, **1998**, *51*, 177-181.

[60] T. Zhang, Q. Li, H. Xiao, H. Lu, Y. Zhou. *Ind. Eng. Chem. Res.*, **2012**, *51*, 11490-11498.

[61] S.R. Kirumakki, B.G. Shpeizer, G.V. Sagar, K.V.R. Chary, A. Clearfield. *J. Catal.*, **2006**,*242*, 319-331.

[62] F. M. Labajos, V. Rives. *Inorg. Chem.*, **1996**, *35*, 5313-5318.

[63] M. Gabrovska, R. Edreva-Kardjieva, G. Kadinov, M. Shopska, B. Kunev, M. Jitianu, COPRECIPITATED Ni-Cr-Al METHANATION CATALYSTS. PART- II: CHARACTERISATION OF Ni-Cr-Al MIXED OXIDES. L. Petrov, C. Bonev, G. Kadinov (Eds.), *Heterogeneous Catalysis* Proceedings of the 9th International Symposium, Varna, Bulgaria, **2000**.

[64] O.Clause, M. Gazzano, F. Trifiro, A. Vaccari, L. Zatorski. *Appl.Catal. A*, **1991**, *73*, 217-236.

[65] F. Cheng,V. Dupont, M.V. Twigg. *Appl.Catal. A*, **2016**, *527*, 1-8.

[66] H.W.Nesbitt, D. Legrand, G.M. Bancroft. *Phys. Chem. Miner.*, **2000**, *27*, 357-366.

[67] P.E. R. Blanchard, A. P. Grosvenor, R. G. Cavell, A. Mar. *J. Mater. Chem.*, **2009**,

19, 6015-6022.

[68] M.R. Alexander, R.D. Short, F.R. Jones, W. Michaeli, C.J. Blomfield. *Appl. Surf. Sci.*, **1999**, *137*, 179-183.

[69] D. D. Perrin, W.LF Armarego. Purification of Labaratory Chemicals. Pergamon, Oxford, **1980**.

[70] Z. Gu, J. J. Athertona, Z. P. Xu. *Chem. Commun.*, **2015**, *51*, 3024-3036.

[71] X. Li, D. Du, Y. Zhang, W. Xing, Q. Xue, Z. Yan. *J. Mater. Chem. A*, **2017**, *5*, 15460-15485.

[72] F. Li, J. Liu, D. G. Evans, X. Duan. *Chem. Mater.*, **2004**, *16*, 1597-1602.

[73] H. Nasri, S.Khemakhem, R. B. Amar. *Per. Pol. Chem. Eng.*, **2014**, *58(2)*, 171-178; DOI:10.3311/PPch.7388.

[74] X. Ji, W. Zhang, L. Shan, Y.Tian, J. Liu. *Sci. Rep.*, **2015**, *5*, 18367; DOI:10.1038/srep18367.

[75] M.A. Meyers, K.K. Chawla. Mechanical behavior of materials. Prentice-Hall, Upper Saddle River, NJ, **1999**, 98-103.

[76] T.G. Mezger. The Rheology Handbook, 2nd revised edition, **2006**.

[77] R. B. Bird, A. J. Giacomin. *Rheol. Acta*, **2012**, *51*, 481-486; DOI:10.1007/s00397-012-0621-2.

[78] C. Chen, R. Felton, J.C.Buffet, D. O'Hare. *Chem. Commun.*, **2015**, *51*, 3462.

[79] S.D. Jiang, Z.M. Bai, G. Tang, L. Song, A. A. Stec, T. R. Hull, Y. Hu, W.Z. Hu. *Appl. Mater. Interfaces*, **2014**, *6*, 14076-14086.

CHAPTER-III
PART-C

THE EFFECT OF STRENGTH OF BASES AND TEMPERATURE ON THE SYNTHESIS OF Zn-Al LDH BY NON-AQUEOUS 'SOFT CHEMICAL' SOL-GEL METHOD AND FORMATION OF HIGH SURFACE AREA MESOPOROUS $ZnAl_2O_4$ SPINEL

❖ This part has been published in ***Chemistry Select, 3(2018)7619-7626***.

GRAPHICAL ABSTRACT

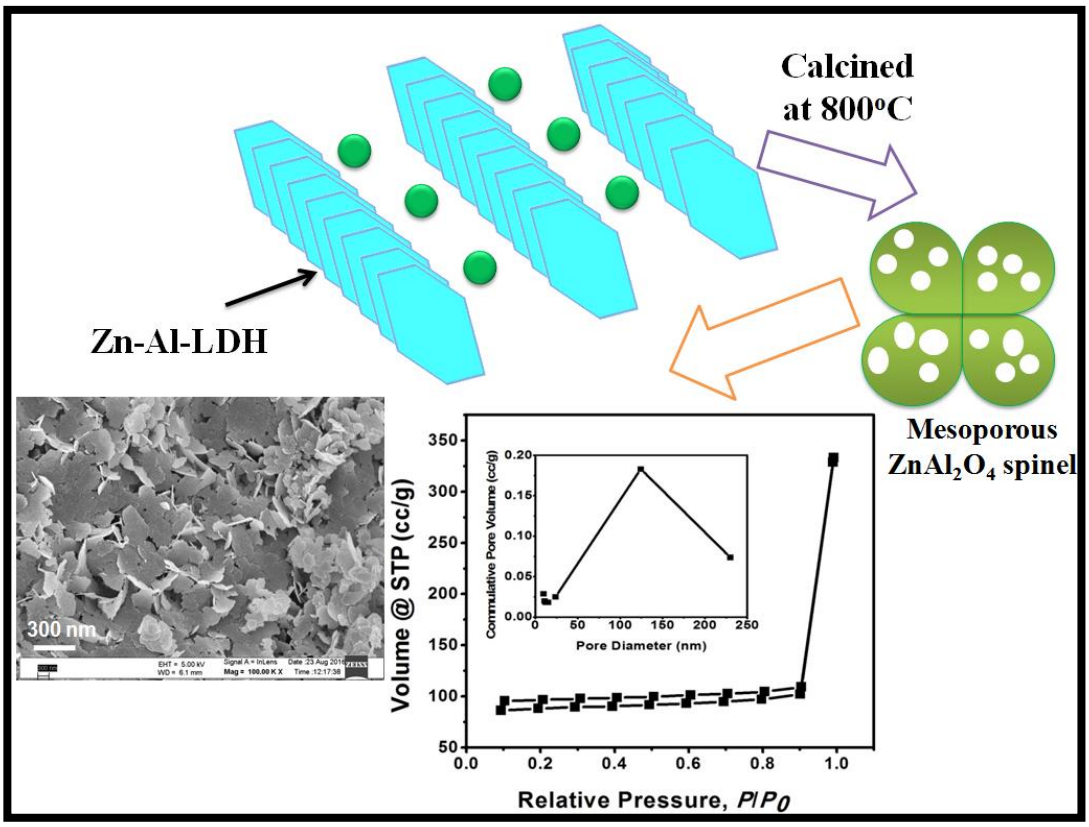

Zn-Al-LDH synthesized by soft chemical method after calcination at 800 °C formed high surface area mesoporous flower platelets like $ZnAl_2O_4$ spinel

ABSTRACT

This **part** describes about the synthesis of Zn-Al-LDH by soft-chemical sol-gel method and the effect of temperature as well as the strength of different bases. During the synthesis of Zn-Al layered double hydroxides by soft chemical non aqueous method the strength of bases as well as the temperature influences immensely the hydrolysis of $Zn(acac)_2$ and $Al(acac)_3$. Different bases such as NH_3, Diethylamine, Piperidine and NaOH was used and it was found that $Zn(acac)_2$ directly forms ZnO (Zincite) phase without reacting with $Al(acac)_3$ at temperature of around 80 ^oC. When the temperature was decreased to 0 ^oC from room temperature as well as side by side the strength of bases were increased the formation of ZnO phases reduced. Thus, Zn-Al layered double hydroxide could only be synthesized at 0 ^oC and in presence of stronger bases like NaOH and Piperidine. The XRD analysis showed the presence of low intensity ZnO phases in Zn-Al layered double hydroxide synthesized in presence of NaOH which was absent in presence of Piperidine. Zn-Al-LDH synthesized were further characterized by TGA-DTG, FT-IR, SEM-EDS, BET surface area and pore diameter analysis which showed their different characteristics as the base is changed. Zn-Al-LDH synthesized in presence of Piperidine after thermal treatment at 800 ^oC formed high surface area mesoporous flower platelet like $ZnAl_2O_4$ spinel which have surface area of 124.8 m^2/g and mesopores of dimensions about 5-20 nm respectively.

3.C.1. INTRODUCTION:

Layered double hydroxides also known as the anionic clays are represented by the general formula $[M_{1-x}^{2+}M_x^{3+}(OH)_2]^{x+}[A_{x/n}]^{n-}.m\ H_2O$ where different M^{2+} ions such as Zn^{2+}, Ni^{2+}, Mg^{2+}, Co^{2+} and M^{3+} ions such as Al^{3+}, Cr^{3+}, Ga^{3+}, In^{3+}, Mn^{3+}, Fe^{3+} are uniformly distributed and orderly prearranged in the brucite-like sheets and various charge-compensating anions (A^{n-} = CO_3^{2-}, NO_3^-, Cl^-, OH^-) are present in their interlayer spaces along with the water molecules which have attracted increasing special interest in the field of catalysis and advanced materials. Due to the atomic-scale level uniform distribution of metal cations in the brucite-like layers as well as their ability to intercalate a diverse range of interlayer anions, LDHs display great potential as precursors/supports to prepare industrially important catalysts [1-4]. After thermal treatment LDHs can be converted into well dispersed mixed-metal oxides (MMOs) with large surface area and Lewis base sites (e.g. Mg(Al)O) and also can give rise to highly dispersed metal nanoclusters [1,4-6] due to which these materials can be widely used for various applications such as anion exchanger [7], host structures for the synthesis of nano-composites materials [8]and as heterogeneous solid base catalyst in environmentally important reactions [4,9-17]. The catalytic properties of these materials depend on their crystallinity, acid-base and redox properties which can be controlled by synthesis method, composition and the thermal activation processes [5]. LDHs can be synthesized by Co-precipitation followed by hydrothermal method, micro-wave irradiation, urea hydrolysis, solvothermal, sol-gel method using inorganic precursors [18-24]. As compared to conventional co-precipitation method the LDHs obtained from sol-gel method exhibits high surface area [18,25]. The co-precipitation method yields highly crystalline materials which after calcination exhibits low surface area and low basic sites [26,27].

The study on the synthesis of Zn-Al-LDH is an important field of research due to their attractive properties such as sensors and catalysts. Many researchers reported the synthesis of Zn-Al-LDH by different methods such as co-precipitation method, sol-gel methods [29-31]. Rashad *et al*. [29] reported the synthesis of Zn-Al-LDH by co-precipitation method using $ZnCl_2$ and $AlCl_3$, K. Abderrazek *et al*.[30] also reported the synthesis of Zn-Al-LDH by co-precipitation method by using $Zn(NO_3)_2.6H_2O$ and $Al(NO_3)_3.9H_2O$. On the other hand, D.Tichit *et al*.[31] reported the synthesis of Zn-Al-LDH by sol-gel method. They did not reported clearly which precursor led to the formation of Zn-Al-LDH. They only reported that Zn-Al-LDH can be synthesized by using Zn acetate-2-hydrate ($Zn(acet)_2.2H_2O$), Zinc acetylacetonate ($Zn(acac)_2.xH_2O$), Aluminium acetylacetonate ($Al(acac)_3$), Al isopropoxide ($Al(OPr^i)_3$) precursors [28]. Zn-Al-LDH has lots of applications such as $ZnAl_2O_4$ spinels formed by the calcination of Zn-Al-LDH can be used as catalyst in organic reactions, as photocatalyst, as Li-ion battery electrodes [32-36].

In this chapter we have synthesized Zn-Al-LDH by sol-gel method using metal acetylacetonate precursors instead of alkoxides in non aqueous media. The method possesses two preliminary challenges firstly unlike the other acetylacetonates there is a basic difficulty in hydrolysing Zn acetylacetonate by weaker bases like primary and secondary amines and secondly the susceptibility of hydrolysed product $Zn(OH)_2$ to easily undergo conversion to ZnO structure. Both these factors were systematically taken care of during the study by changing the reaction temperatures and base strength. Instead of metal acetylacetonates the other practised method of synthesis of LDH in non aqueous media is the use of metal alkoxides, but it has the disadvantage that due to their fast rate of hydrolysis generally it is difficult to maintain the microstructure. The same can be better controlled by using metal acetylacetonates as their hydrolysis rate is

slow [37-39]. Basically, the sol-gel method of synthesis of hydroxides have the advantage that it gives finer particles in the colloidal range having important properties of higher dispersibility, high surface area, high thermal stability and high basic strength [40]. Such, advantages in the synthesis of LDH in aqueous media is difficult to reach [29-31,40]. Especially, these factors are important for materials to be useful for different catalytic applications. The formation of particles in the colloidal dispersible size through non-aqueous sol-gel method would help in the coating of such materials in the form crack free thin films over solid inorganic surfaces to be useful as catalytic device [42] or separation barrier. Being dispersed in organic media they have another advantage for device fabrication in material processing step as specialised drying techniques such as supercritical or hypercritical drying could be better utilized easily than in their aqueous dispersions. Report is there about the difficulty faced due to temperature sensitivity of $Zn(OH)_2$ [31,41] in the synthesis of Zn-Al-LDH at high temperature. The synthesis of Zn-Al-LDH by sol-gel method using metal acetylacetonate as precursors and the effect of temperature as well as the effect of strength of series organic bases has not been reported. Another finding of this work is that the cluster of sol-gel derived Zn-Al-LDH layered particles after calcination transforms to some high surface area mesoporous flower of $ZnAl_2O_4$ spinel which can be expected to have other application [32-36].

3.C.2. EXPERIMENTAL SECTION:

3.C.2.1. Synthesis of Zn-Al-LDH by sol-gel method [31,42]:

Zn-Al LDH was synthesized by using $Zn(acac)_2.H_2O$ and $Al(acac)_3$ (purchased from Sigma Aldrich, 98 % pure) precursors at different temperatures such as 80 ^oC, room temperature, and 0 ^oC in presence of different bases *viz*. NH_3, Diethylamine, NaOH and Piperidine. In all the cases same procedure was followed by varying the

temperature as well as the bases. 0.06 mol $Zn(acac)_2.H_2O$ was dissolved in 80 cm^3 distilled ethanol followed by the addition of required amount of HCl (Merck) for complete dissolution of $Zn(acac)_2$ and 0.02 mol $Al(acac)_3$ in 80 cm^3 ethanol and acetone mixture (1:1). Both of these solutions were mixed at different temperatures and stirred for about 3-4 hours. The pH of the solution was maintained at 9 by using NH_3, Diethylamine, NaOH and Piperidine as bases (1 M solution). The product obtained was then filtered through Whatman no. 41 filter paper and washed with ethanol and deionized water for the removal of excess amount of Cl and dried in vacuum desiccator over night. The Zn:Al ratio was kept as 3:1.

3.C.2.2. Characterizations:

Powder X-Ray Diffractometric (PXRD) analysis was carried out using powder X-ray diffractometer (Model Rigaku Ultima IV) using Cuk_α radiation of a wavelength of 1.54 Å at 40 mA and 40 kV X-ray generator current setting with a step size of $0.2^o 2\theta$ min^{-1}.

Fourier Transform Infrared (FT-IR) spectra of the prepared samples were recorded in spectrophotometer (Perkin-Elmer 2000 System) in 4,000-400cm^{-1} range at a spectral resolution of 4 cm^{-1} using KBr pellets.

Field Emission Scanning Electron Microscopy (FE-SEM) analysis was carried out in a Carl Zeiss -Sigma VP equipment, at an accelerating voltage of 20 kV. Before the analysis the samples were dried at 40 ^oC in air oven for 1 week to avoid the moisture absorption. Finally, the sample surfaces were gold coated in 100 % vacuum. The chemical composition was identified by using an energy-dispersive X-ray spectroscopy (EDX) attachment present on the scanning electron microscope. The Transmission Electron Microscopy (TEM) images were recorded on a JEOL JEM-2011 electron microscope operated at an accelerating voltage of 200 kV.

The thermogravimetric measurements were carried out in a simultaneous TG-DTA analyzer (model Q-600, M/S TA Instruments) using α-Al_2O_3 as reference. Samples weighing about 10.0 mg were heated from 30 to 1000 ^oC at 10 ^oC/min under nitrogen atmosphere in a non-isothermal condition.

Specific surface area of the samples was recorded *via* nitrogen gas adsorption at 77 K applying Brunauer-Emmett-Teller (BET) calculations using Autosorb-iQ Station 1 (Quantachrome, USA). The samples were degassed at 100 ^oC for 1.5 h prior to performing the experiment.

The Zeta potential of Zn-Al-LDH synthesized in presence of Piperidine and NaOH were measured with the Laser Doppler Velocimetry technique at 25 ^oC under a 10 Mw He-Ne laser (M/S Malvern Instruments Zetasizer Nano Z5).

3.C.3. RESULTS AND DISCUSSION:

3.C.3.1. XRD analysis:

XRD analysis of the products formed on the attempts of Zn-Al-LDH synthesis by sol-gel method was carried out to find out the presence of LDH phases (**Fig. 3.C.1**). The product obtained through hydrolysis carried out via the use of NH_3 at 80 ^oC showed the formation of ZnO (Zincite) phase with *hkl* values at (002), (100), (101), (102), (110), (103) respectively (**JCPDS PDF card no. 00-001-1136**) and LDH like phase was not identified. To further understand the mechanism the alkali was changed from NH_3 to NaOH at 80 ^oC. There also no LDH like phase could be identified. Also, the presence of low intensity unhydrolysed $Zn(acac)_2$ phase was found in NH_3 hydrolysed system (**Fig. 3.C.1A**). On the other hand, attempt to hydrolyse Zn and Al acetylacetonate in presence of NH_3 and diethylamine at 0 ^oC also showed the presence of only $Zn(acac)_2$ with high intensity *hkl* reflection of (001) having d value at 10.4 Å and (101) respectively (**JCPDS PDF card no. 00-013-0620**) in the reaction product.

As in our attempt to Zn-Al LDH through non aqueous sol-gel mediated hydrolysis of $Zn(acac)_2$ and $Al(acac)_3$ both the metal ions were supplied in the same flask therefore it was further checked whether the presence of $Al(acac)_3$ was harmful for the desired reaction especially the hydrolysis of $Zn(acac)_2$. In order to study the same hydrolysis of $Zn(acac)_2$ was carried out independently under different alkaline and temperature conditions as was performed for Zn-Al LDH synthesis. The XRD patterns of final reaction product of NH_3 mediated reaction of both 0 and 80 ^oC (**Fig. 3.C.1B**) showed the high intensity reflection with d value at 10.37 Å for $Zn(acac)_2$ indicating unsuccessful hydrolysis of $Zn(acac)_2$. However, $Zn(acac)_2$ hydrolysis at 0 ^oC in presence of both Piperdine and NaOH showed formation of $Zn(OH)_2$ but at 80 ^oC $Zn(acac)_2$ formed $Zn(OH)_2$ phases of *hkl* value at (004), (205) along with ZnO phases with *hkl* values (002), (100), (101), (102), (110), (103) and (100), (002), (101) respectively indicating temperature induced conversion of $Zn(OH)_2$ to ZnO. The presence of unreacted $Zn(acac)_2$ phase was also observed in case of hydrolysis by diethylamine at 0 ^oC of *hkl* reflections (001) along with the low intensity ZnO phase with *hkl* reflection of (100), (101) and (002) as shown in **Fig. 3.C.1B**.

Similarly, Zn-Al-LDH phase was formed only in presence of NaOH and Piperidine at 0 ^oC with *hkl* reflections of (003), (006), (009) and (012). As the temperature increased $Zn(acac)_2$ component helped in the formation of only ZnO (Zincite) phases due to the unstability of $Zn(OH)_2$ at high temperature [31, 41]. Thus, it is now further observed not only the temperature, the strength of bases also effect on the synthesis of Zn-Al-LDH. Since, the basicity of NH_3, Diethylamine and Piperidine follows the order as NH_3 < $(CH_3)_2NH$ (Diethylamine) < $C_5H_{11}N$ (Piperidine) [43] and from the XRD analysis it was found LDH phase formation occurred in presence of Piperidine mediated hydrolysis only. In presence of NaOH also the LDH phase was formed along

with the formation of some low amount of ZnO phases with *hkl* reflections of (100), (002) and (101) planes respectively. However in such sol gel mediated synthesis presence of organic Piperidine type base is preferred than a NaOH mediated system as it is easier to drive off the residual alkali from the product during post synthesis purification and conversion of LDH type hydroxides.

Didier *et al*. in the sol-gel method of synthesis of hydroxides found that the formation of alumina and ZnO phases due to the dehydration of $Zn(OH)_2$ is dependent on the reactivity of Zn and Al precursors [31]. The sols with low stability obtained by the hydrolysis of Zn and Al precursors could be stabilized by adding amines [31]. Hence, Piperidine could not only act as a strong base to facilitate hydrolysis also could readily stabilize the gel and prevent the formation of ZnO phase at 0 ^{o}C.

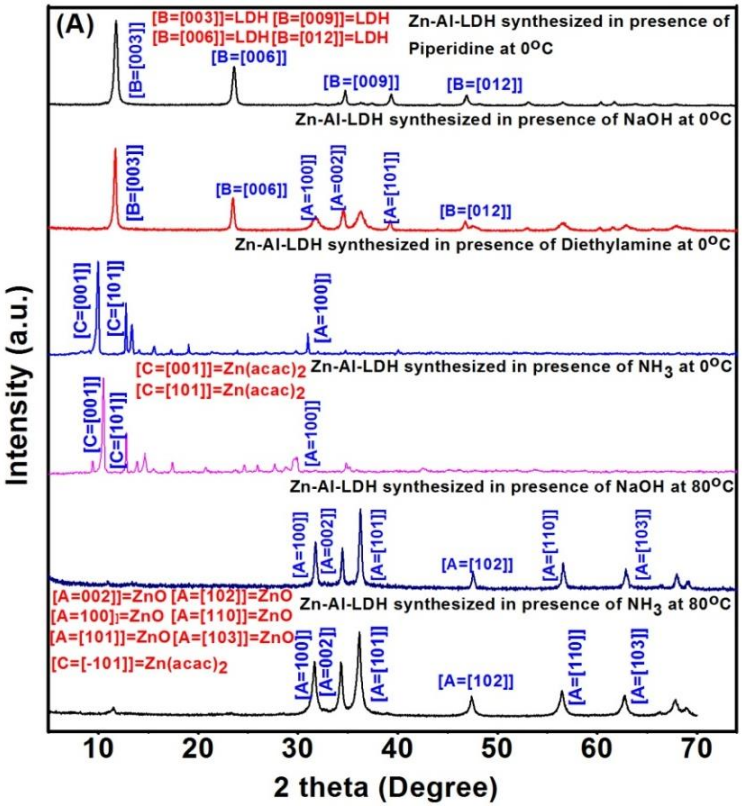

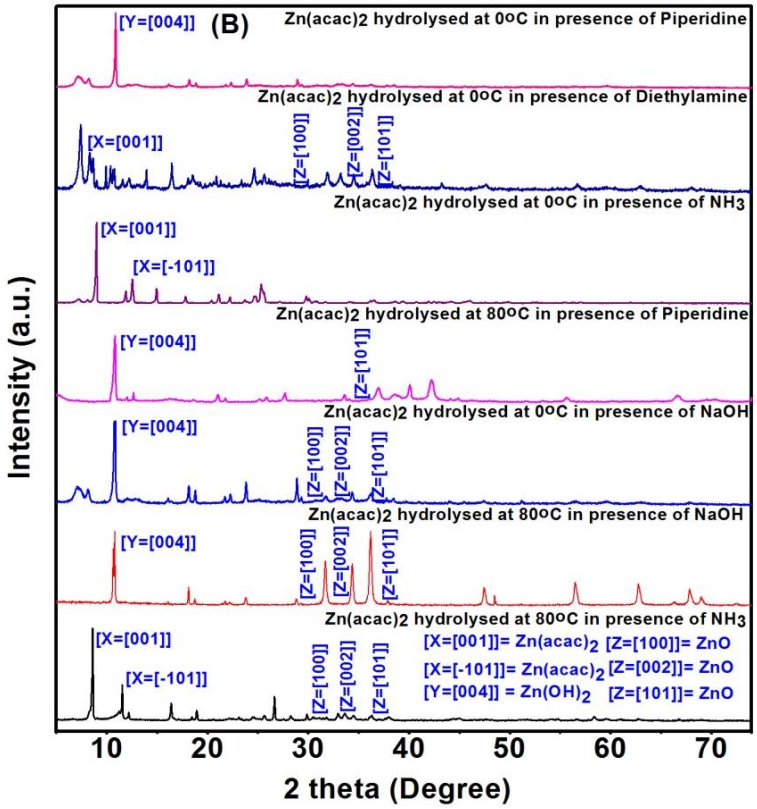

Fig. 3.C.1: (A) XRD patterns of Zn-Al-LDH synthesized by sol gel method using different bases at different temperature (0 °C and 80 °C); (B) XRD patterns of different products obtained from hydrolysis of Zn(acac)$_2$ by using different bases at different temperatures (0 °C and 80 °C).

3.C.3.2. TGA-DTG analysis:

TGA-DTG analysis showed the thermal stability of Zn-Al-LDH synthesized in presence of different bases (**Fig. 3.C.2**) at 0 °C. TGA and DTG pattern showed the 89 % of the total weight loss from the product obtained on Zn-Al-LDH synthesis carried out in presence of NH_3 in the temperature range 150-250 °C due to the removal of acetylacetonate ion of unreacted Zn(acac)$_2$ molecule. The product of Zn-Al-LDH synthesis carried out in presence of diethylamine showed two step weight loss; first step at 95.2 °C correspond to the removal of weakly adsorbed water molecule and the second step at temperature ranging from 200-300 °C with 78 % of the total weight loss correspond to the removal of acetylacetonate ion of Zn(acac)$_2$ molecule. However,

three weight losses occurred between 100 ^{o}C and 800 ^{o}C in case of product obtained on Zn-Al-LDH synthesis carried out in presence of NaOH and Piperidine. This type of weight loss is typically shown by Layered Double Hydroxides. In the temperature range 100-200 ^{o}C there are weight losses of 16 % and 15 % (w/w) corresponding to the loss of adsorbed moisture and 200-250 ^{o}C with weight losses of 14 % and 16 % corresponding to the removal of interlayer water molecules whereas in the temperature at 250-800 ^{o}C with weight losses of 7 % and 8 % corresponds to the removal of water due to the dehydroxylation of the brucite-like layers and the interlayer ions such as acetylacetonate ion [44]. In this step mixed metal hydroxides are converted to mixed metal oxides of Zn and Al.

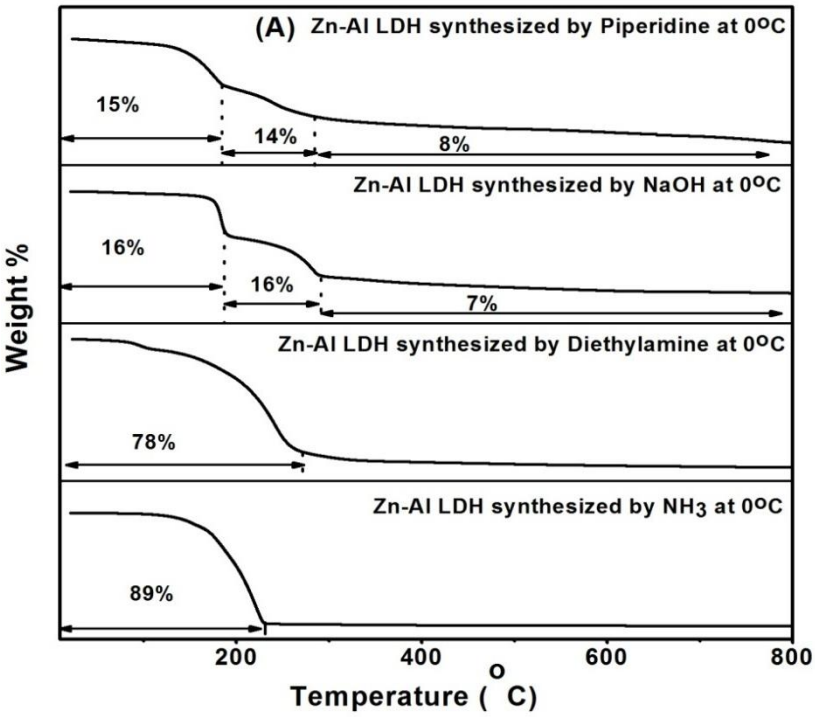

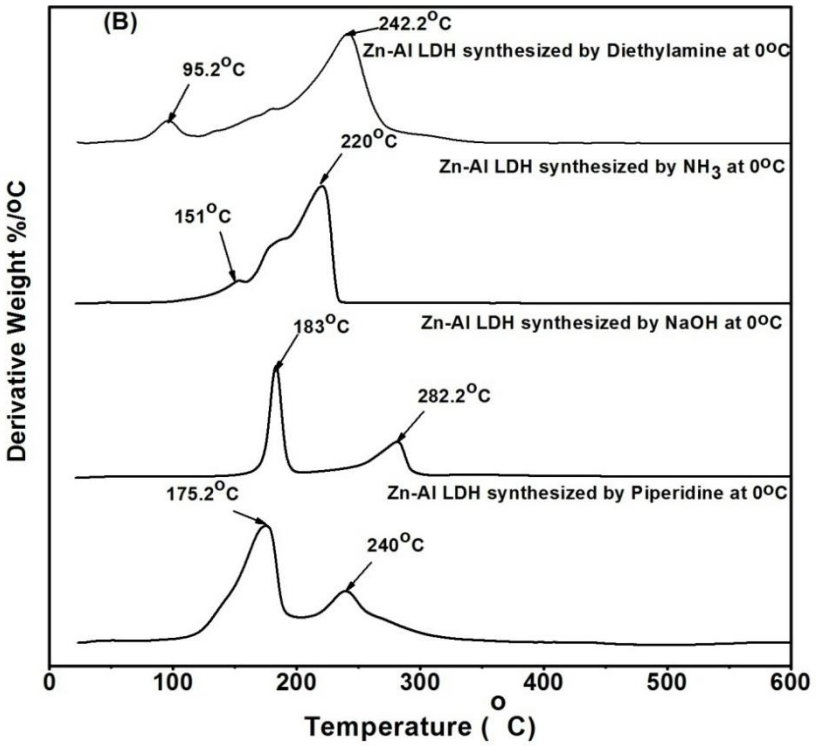

Fig. 3.C.2: TGA-DTG patterns of Zn-Al-LDH synthesized in presence of different bases (A&B).

3.C.3.3. FT-IR analysis:

FT-IR analysis (**Fig. 3.C.3**) showed that the peaks around 3387-3445 cm^{-1} were due to the –OH stretching vibration of the interlayer hydroxyls and H_2O molecules respectively in case of Zn-Al-LDH synthesized in presence of Piperdine and NaOH. The peaks at around 2984-2993 cm^{-1} were due to the C-H stretching vibration. The C=O stretching vibrations were obtained at 1517-1606 cm^{-1} due to the acetylacetonate group present in the interlayer [42]. The peaks due to M-O stretching vibrations were obtained at 771-930 cm^{-1} and 427-621cm^{-1} respectively [42].

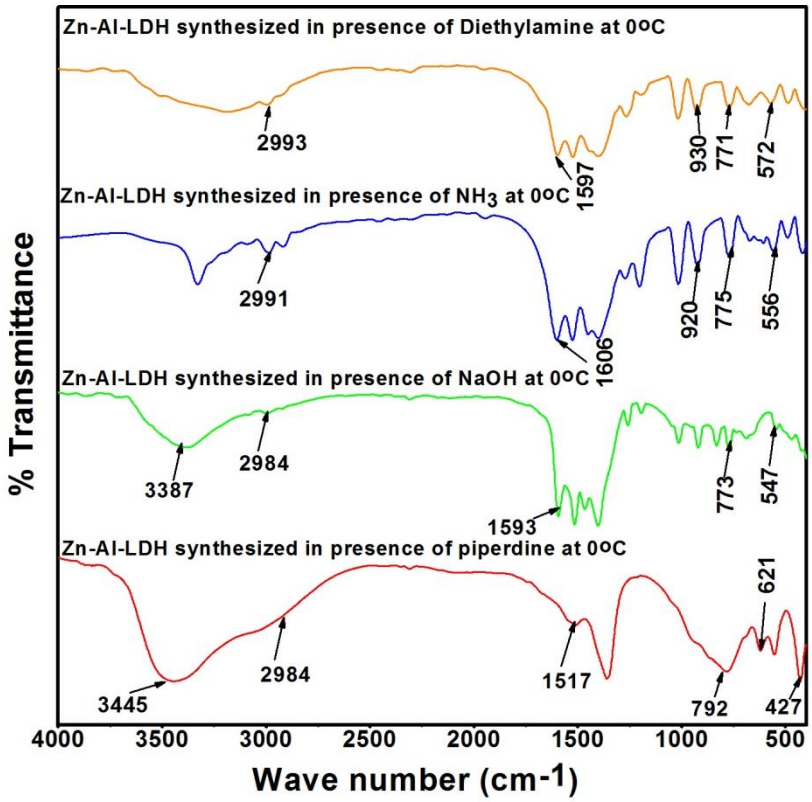

Fig. 3.C.3: FT-IR patterns of Zn-Al-LDH synthesized by sol-gel method in presence of different bases at 0 °C.

3.C.3.4. Zeta Potential study:

Zeta potential study showed that Zn-Al-LDH synthesized in presence of Piperidine had greater stability with zeta potential value 37.8 mV as compared to Zn-Al-LDH synthesized in presence of NaOH with zeta potential 14.2 mV. The low zeta potential value in Zn-Al-LDH synthesized in presence of NaOH was due to the presence of excess Na^+ ion which decreases the interelectronic repulsion between the similar charged ions and destabilises the dispersion [45]. On the other hand, in case of Zn-Al-LDH synthesized in presence of Piperidine similar behaviour was not observed which is probably due to the smaller charge to size ratio of large Piperidinum ion than Na^+ ion.

3.C.3.5. BET surface area analysis:

BET surface area analysis showed (**Table 3.C.1**) that surface area of Zn-Al-LDH

synthesized in presence of NaOH was found as 41.8 m^2/g and that of synthesized in presence of Piperidine was found as 42.6 m^2/g with pore diameter of 3.6 nm.

3.C.3.6. SEM and EDS analysis:

The surface morphology and the chemical compositions were studied by SEM and EDS analysis (**Fig. 3.C.4A, B, C&D**). in the same magnifications. The SEM images showed the presence of hexagonal platelet like structure. In case of Zn-Al-LDH synthesized by NaOH the hexagonal platelet are stacked and agglomerated whereas the hexagonal platelet of Zn-Al-LDH synthesized in presence of Piperidine were regularly dispersed and more exposed in their basal plane.

EDS analysis showed the presence of both Zn and Al (**Fig. 3.C.4C&D**). The weight percentage of Zn and Al elements were calculated to be 42.11 %, 14.3 % in case of Zn-Al-LDH synthesized in presence of NaOH and 40.72 %, 13.57 % respectively in case of Zn-Al-LDH synthesized in presence of Piperidine It was observed that Zn:Al ratio remained as 3:1 in the products also. The presence of C and O also predicted the presence of interlayer acetylacetonate group.

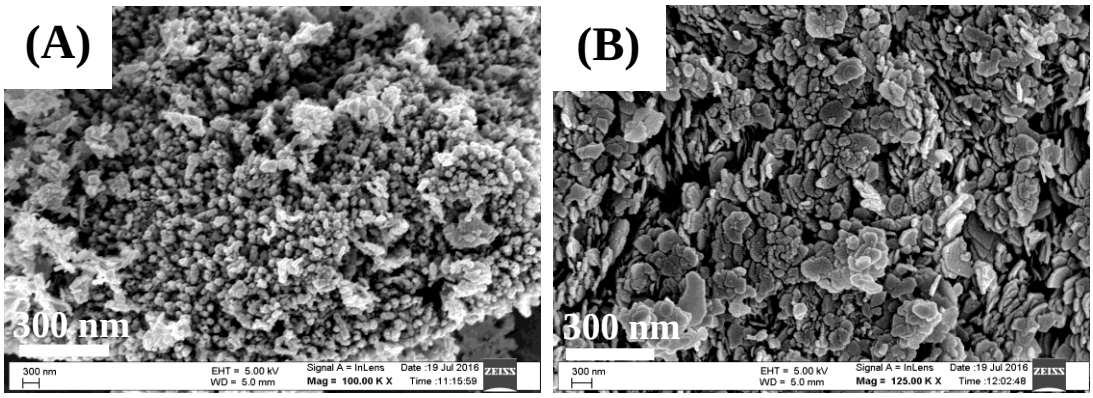

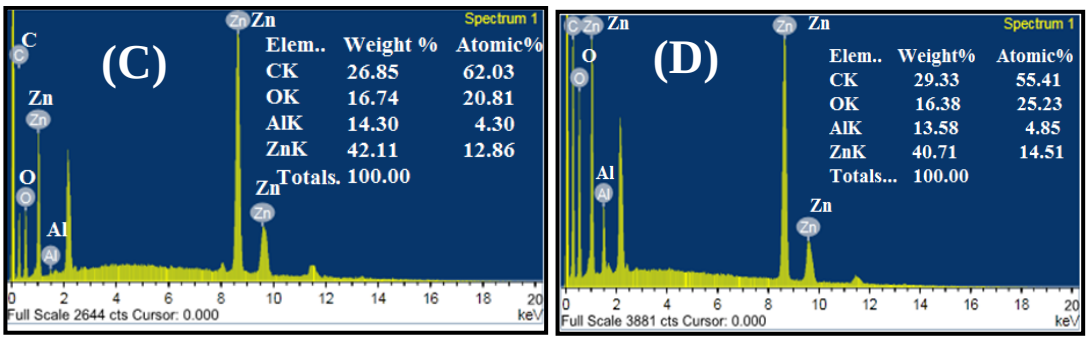

Fig. 3.C.4: SEM and EDS patterns of Zn-Al-LDH synthesized using NaOH (A&C)
and Piperidine (B&D).

3.C.3.7 Synthesis of $ZnAl_2O_4$ spinels by calcination of Zn-Al-LDH at 800 ^oC:

Zn-Al-LDH was calcined at 800 ^oC. The calcined products were characterized as follows-

3.C.3.7.1. XRD analysis:

One of the reasons for importance of LDH in different fields of materials science is the relative ease by which they can be easily converted through mild or moderate thermal degradation to nano particle or nano sheets of mixed metal oxides with high catalytic, adsorptive or photocatalytic properties. As presence of other metal ions in the medium may affect the purity and performance of the derived oxides therefore evaporable bases like ammonia or organic amine mediated synthesis is preferred during sol-gel hydrolysis of metal acetylacetonates to obtain LDH. Therefore, Zn-Al LDH synthesised through Piperidine mediated route was preferred than Zn-Al LDH synthesised through NaOH mediated route for thermal decomposition and consequent XRD characterisation to study the phases formed. The XRD pattern of Zn-Al-LDH synthesized by Piperidine after calcination at 800 ^oC (**Fig. 3.C.5**) showed the formation of $ZnAl_2O_4$ spinel with (311) (d=2.44Å), (220) and (331) *hkl* reflections (**JCPDS PDF Card no.00-003-1161**) which bear the prospects of application as important advanced materials like catalyst and catalyst support, ceramic material,

photocatalyst, optical coating, high temperature ceramic material [46-48]. The average crystallite size of $ZnAl_2O_4$ spinel was found as 10-30 nm determined by using Scherrer equation [49]. Also, the XRD pattern shows the presence of lowest intensity ZnO (Zincite) with (002) *hkl* reflection in calcined Zn-Al-LDH.

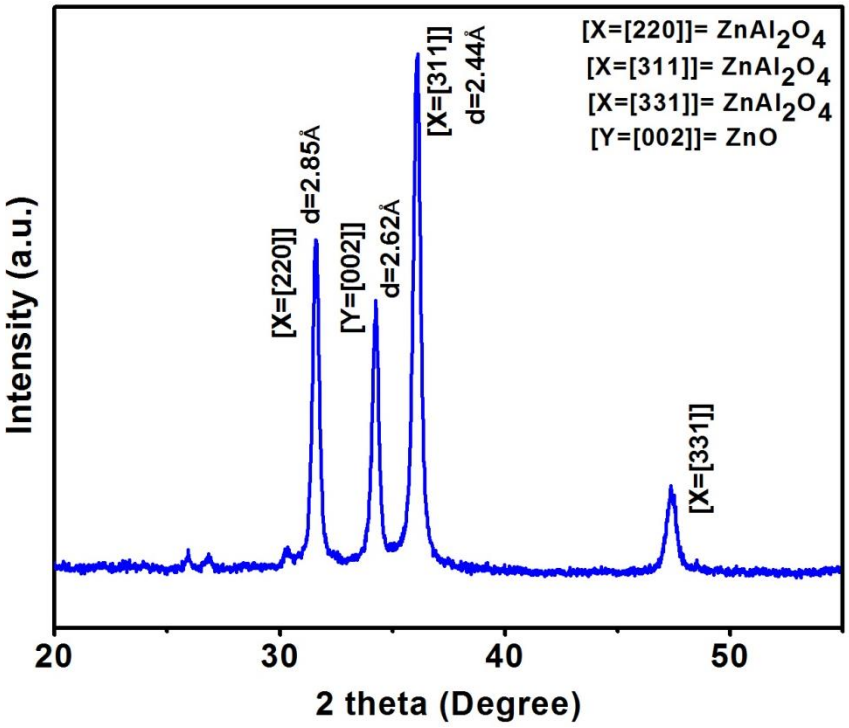

Fig. 3.C.5: XRD pattern of $ZnAl_2O_4$ spinel.

3.C.3.7.2. TGA-DTG analysis:

TGA-DTG analysis (**Fig. 3.C.6**) showed the presence of three major peaks in $ZnAl_2O_4$ spinel. The endothermic peak at 130 ^oC was due to the loss of physisorbed moisture. On the otherhand, two exothermic broad peaks one at 300-500 ^oC temperature range was due to the loss of residual organic solvents or molecules present in the interlayer as well as the conversion of hydroxide of Zn-Al to ZnO type phase whereas; the peak in the temperature ranging between 700-900 ^oC with its maximum of 809 ^oC correspond to the phase transformation of Zn-Al-LDH to $ZnAl_2O_4$ spinel [50]. TGA pattern showed only 1 % of weight loss further confirmed the formation of $ZnAl_2O_4$ spinel which was thermally stable upto the temperature of 900 ^oC.

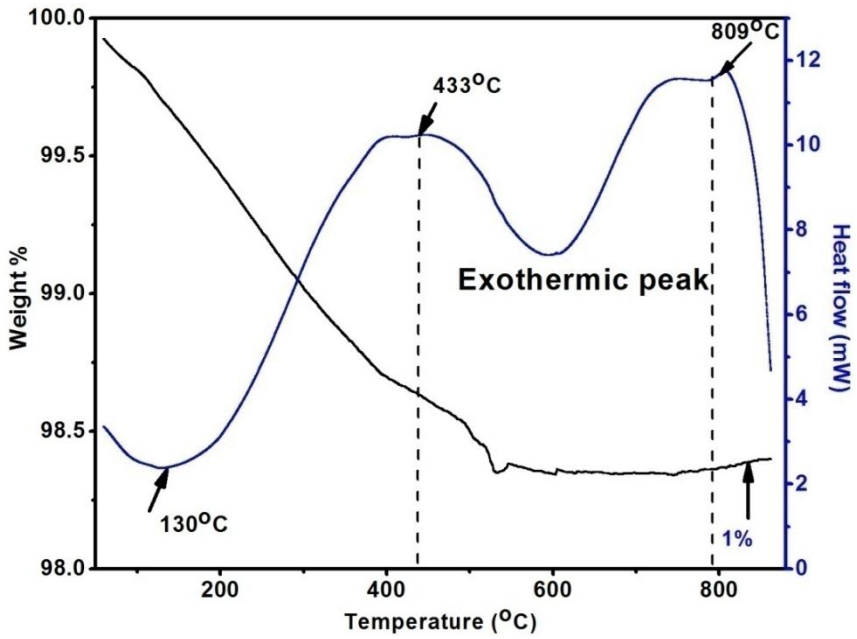

Fig. 3.C.6: TGA analysis of $ZnAl_2O_4$ spinel.

3.C.3.7.3. SEM and EDS analysis:

Fig. 3.C.7A&B shows the SEM images of $ZnAl_2O_4$ spinel. It showed the formation of some flower platelets like particles of different shapes. SEM analysis also showed the presence of mesopores of dimensions in between the range of 5-20 nm. TEM pattern (**Fig. 3.C.7C**) also showed the presence of mesopores over the platelets $ZnAl_2O_4$ spinel confirmed the formation of mesoporous $ZnAl_2O_4$ spinel. EDS analysis (**Fig. 3.C.7D**) showed the presence of Zn, Al and O in the weight % of 60.44 %, 9.42 % and 30.42 % respectively further confirmed the formation of $ZnAl_2O_4$ spinel also observed from XRD analysis.

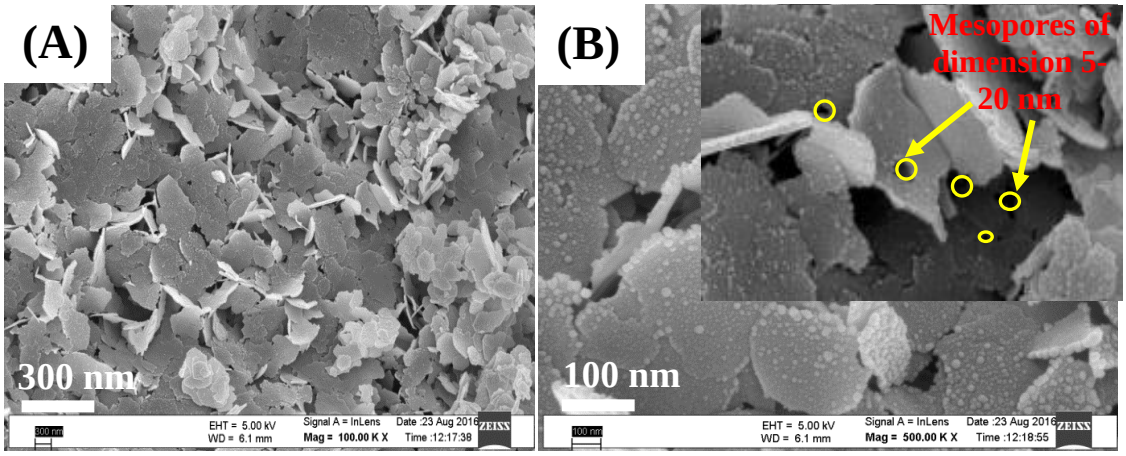

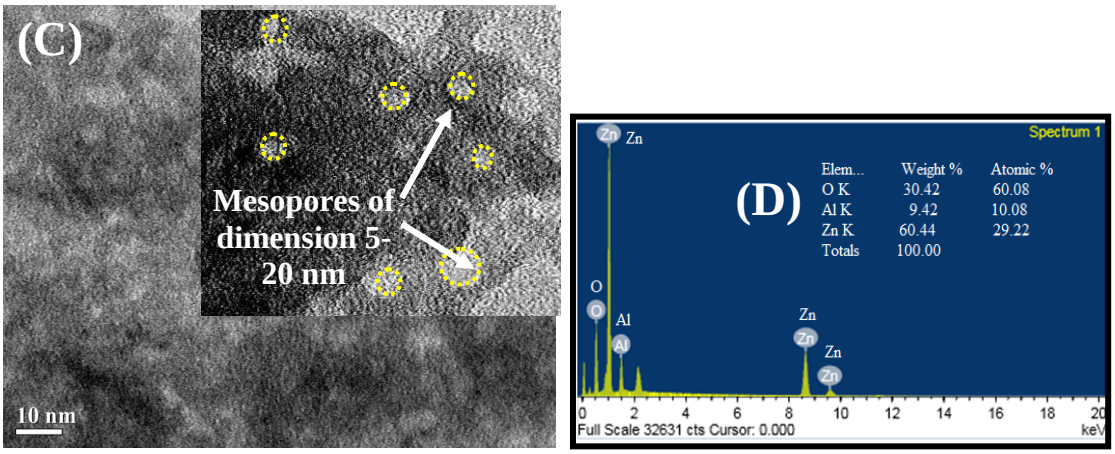

Fig. 3.C.7: SEM, TEM (A, B&C) and EDS patterns (D) of mesoporous $ZnAl_2O_4$.

3.C.3.7.4. BET surface area analysis:

The Brunauer–Emmett–Teller (BET) surface area and porosity of the $ZnAl_2O_4$ spinel was determined by N_2 adsorption-desorption isotherms of the sample at 77 K. BET surface area analysis showed that $ZnAl_2O_4$ spinel formed after the calcination of Zn-Al-LDH synthesized in presence of Piperidine possessed high surface area value of 124.8 m^2/g as compared to uncalcined products (**Table 3.C.1**). The N_2 adsorption-desorption curve (**Fig. 3.C.8**) of this material shows type-IV isotherm with mulitilayer adsorption which takes place *via* capillary condensation at high relative pressure suggesting the formation of mesoporous $ZnAl_2O_4$ spinel [51]. On the other hand, pore size distribution curve (inset) shows the average pore diameter of 9.6 nm with pore volume of 0.299 cc/g indicating the formation of mesoporous flower platelets like $ZnAl_2O_4$ spinel.

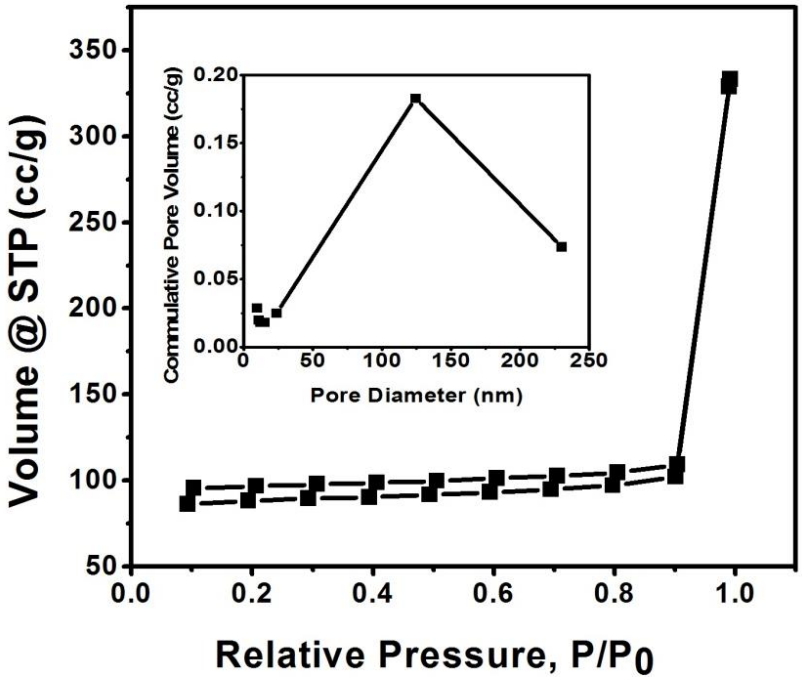

Fig. 3.C.8: N_2 adsorption-desorption curves of $ZnAl_2O_4$ spinel (inset is the pore size distribution curve).

Table 3.C.1: BET surface area values of Zn-Al-LDH synthesized in presence different bases

Serial No.	Samples	Surface area (m^2/g)	Pore diameter (nm)	Pore volume (cc/g)
1	Zn-Al-LDH synthesized in presence of NaOH	41.8	3.6	0.102
2	Zn-Al-LDH synthesized in presence of Piperidine	42.6	3.6	0.121
3	$ZnAl_2O_4$ spinel	124.8	9.6	0.299

3.C.4. CONCLUSIONS:

Both temperature as well as the strength of bases effects on the synthesis of Zn-Al-LDH. It was observed that LDH phase was formed only in presnce of NaOH and Piperdine at 0 ^oC. At high temperature such as 80 ^oC only ZnO (Zincite) phase was formed due to the unstability of $Zn(OH)_2$ at high temperature. In other words, Zn-Al-

LDH synthesized in presence of Piperdine after calcination at 800 ^{o}C formed flower platelet like high surface area mesoporous $ZnAl_2O_4$ spinel which bear the prospects of application as important advanced materials like catalyst and catalyst support, ceramic material, photocatalyst, optical coating, high temperature ceramic material [46-48] and hence expected to use as effective environmental benign catalyst in future.

REFERENCES:

[1] V. Rives. Layered double hydroxides: present and future, Nova Science Publishers, **2001**.

[2] X. Duan, D.G. Evans. Layered double hydroxides, Springer Verlag, **2006**.

[3] F. Cavani, F. Trifiro, A. Vaccari. *Catal.Today*, **1991**, *11*, 173-301.

[4] G. Fan, F. Li, D.G.Evans, X. Duan. *Chem. Soc. Rev*., **2014**, *43*, 7040.

[5] D. Tichit, B. Coq. *CATTECH*, **2003**, *7*, 206.

[6] F. Cavani, F. Trifiro, A. Vaccari. *Catal. Today.*, **1991**, *11*, 2.

[7] V. Rives, M.A. Ulibarri. *Coord. Chem. Rev.*, **1999**, *181*, 61.

[8] M.E. Moujahid, J.P. Besse, F. Leroux. *J. Mater. Chem.*, **2002**, *12*, 3324.

[9] H. Dandl, G. Emig. *Appl.Catal. A*, **1998**, 168, 261-268.

[10] S. Kannan, C.S. Swamy. *Appl.Catal. B Environ.*, **1994**, *3*, 109-116.

[11] J.N. Armor, T.A. Braymer, T.S. Farris, Y. Li, F.P. Petrocelli, E.L.Weist, S. Kannan, C.S. Swamy. *Appl.Catal. B: Environ.*, **1996**, *7*, 397-406.

[12] R S. Drago, K. Jurczyk, N. Kob. *Appl.Catal. B: Environ.*, **1997**, *13*, 69-79.

[13] K. Karaskovaa, L.Obalovaa, K. Jiratova, F. Kovanda. *Chem. Eng. J.*, **2010**, *160*, 480-487.

[14] J.P. Ramirez, F. Kapteijn, J. A. Moulijn. *Catal. Lett.*, **1999**, *60*, 133-138.

[15] S. Kannan. *Catal. Surveys from Asia.*, **2006**, *10*, 117; DOI:10.1007/s10563-006-

9012.

[16] S. He, Z. An, M.Wei, D.G. Evans, X. Duan. *Chem. Commun.*, **2013**, *49*, 5912.

[17] K. Galejova, L. Obalova, K. Jiratova, K. Pacultova, F. Kovanda. *Chem.Papers*, **2009**, *63*, 172-179; DOI:10.2478/s11696-008-0105-0.

[18] A. Maria, V. Borau, C. Jimenez, M. R. Jose, F.J. Urbano. *J. Solid State Chem.*, **2002**, *168*, 156-161; DOI:10.1006/jssc.2002.9655.

[19] D. Tichit, A. Rolland, F. Prinetto, G. Fetter, M.J. Matrinez Oritz, M.A. Valenzuela, P. Bosch. *J. Mater. Chem.*, **2002**, *12*, 3832.

[20] M. J. Climent, A. Corma, S. Iborra, K. Epping, A. Velty. *J. Catal*., **2004**, *225*, 316.

[21] S. P. Paredes, G. Fetter, P. Bosch, S. Bulbulian. *J. Mater. Sci.*, **2006**, *41*, 3377-3382.

[22] M. R. Othmana, Z. Helwania, Martunusa, W. J. N. Fernandoa. *Appl. Organometal. Chem.*, **2009**, *23*, 335-346.

[23] J. Prince, A. Montoya, G. Ferrat, J. S. Valente. *Chem. Mater*., **2009**, *21*, 5826-5835; DOI:10.1021/cm902741c.

[24] J. Song, M. Leng, X. Fu, J. Liu. *J. Alloys and Compounds*., **2012**, *543*, 142-146.

[25] F. Prinetto, G. Ghiotti, P. Graffin, D. Tichit. *Microporous Mesopororous Mater*., **2000**, *39*, 229.

[26] I. Rousselot, C. Taviot-Gueho, J.P. Besse. *Int. J. Inorg. Mater.*, **1999**, *1*, 165.

[27] S. B. Majumder, M. Jain, P.S. Dobal, R.S. Katiyar. *Mat. Sc. Eng.B*, **2003**, *103*, 16.

[28] G.M. Rashad, H.H. Someda. *Arab J. of Nucl. Sci. Appl.*, **2015**, *48*, 22-32.

[29] K. Abderrazek, N.F. Srasra, E. Srasra. *J. Chin. Chem.Soc.*,**2017**; DOI:10.1002/jccs.201600258.

[30] K. Abderrazek, F.S. Najoua, E. Srasra. *Appl. Clay Sci.*, **2016**, *119,* 229-235

[31] D. Tichit, O. Lorret, B. Coq, F. Prinetto, G. Ghiotti. *Microporous Mesopororous Mater*., **2005**, *80*, 213-220.

[32] S. Farhadi, S. Panahandehjoo. *Appl.Catal. A*, **2010**, *382*, 293-302.

[33] W. Zhang, Y. Wang, Y. Shen, M. Xie , X. Guo. *Microporous Mesopororous Mater*., **2016**, *226*, 278-283.

[34] G. Fan, J. Wang, F. Li. *Catal. Commun*., **2011**, *15*, 113-117.

[35] D. Carriazoa, M. del Arcoa, E. Garcia-Lopezb, G. Marcib, C. Martina, L. Palmisanob, V. Rives. *J. Mol.Catal. A*, **2011**, *342*, 83-90.

[36] B. J. Liu, Y. Li, X. Huang, G. Li, Z. Li. *Adv. Funct. Mater*., **2008**, *18*, 1448-1458.

[37] M. Guglielmi, G. Carturan. *J. Non-Crystalline Solids*., **1988**, *100*, 16-30.

[38] L.G. Hubert-Pfalzgraf. *Appl. Organometal. Chem*., **1992**, *6*, 627-643.

[39] A.L.Willis, Z. Chen, J. He,Y. Zhu, N. J.Turro, S. O'Brien. *J. Nanomater*., **2007**, 1-7; DOI: 10.1155/2007/14858.

[40] J. Livage. *New J. Chem*., **2001**, *25*, 1.

[41] C. G. Maier, G. S. Parks, C. T. Anderson. *J. Am. Chem. Soc.*, **1926**, *48*, 2564-2576.

[42] P. Saikia, A. Gautam, R. L. Goswamee. *RSC Adv.*, **2016**, *6*, 112092-112102.

[43] J.E. Huheey, E.A. Keiter, R.L. Keiter, O.K. Medhi. Inorganic Chemistry: *Principles of Structureand Reactivity, 4th Edition,* ISBN 006042995X/97800604299-59, **1993**.

[44] J. T. Sun, Y.D. Huang, G.F. Gong, H. L. Cao. *Poly. Degrad. Stab.*, **2006**, *91*, 339-346.

[45] P. Atkins, J.D. Paula. Physical Chemistry, Ninth Edition, Oxford University

Press, **2010**.

[46] S. Battiston, C. Rigo, E. da C. Severo, M. A. Mazutti, R.C. Kuhna, A. Gundel, E. L. Foletto. *Mater. Res.*, **2014**, *17(3)*, 734-738.

[47] C.G. Anchieta, D. Sallet, E.L. Foletto, S.S.da Silva, O.C.Filho, C.A.O.do Nascimento. *Ceramic Int.*, **2014**, *40*, 4173-4178.

[48] A. Chaudhary, A. Mohammad, S. M. Mobin. *Mater. Sci. Eng.B*, **2018**, *227*, 136-144.

[49] A. L. Patterson. *Phys. Rev.*, **1939**, *56*, 978-982.

[50] D.L. Ge, Y.J. Fan, C.L. Qi, Z. X. Sun. *J. Mater. Chem. A*, **2013**, *1*,1651.

[51] V. Kumari, A. Bhaumik. *Dalton Trans.*, **2015**, *44*, 11843.

CHAPTER-IV

SYNTHESIS AND CHARACTERIZATIONS OF TERNARY LDHS OF Ni-Mg-Al, Ni-Mg-Cr AND THEIR SiO_2 NANOCOMPOSITES BY NON-AQUEOUS SOL-GEL METHOD AND THEIR APPLICATION FOR THE DECOMPOSITION OF N_2O AND CH_4 OXIDATION

❖ This Chapter has been published in ***Catalysis Communication, 119 (2019) 1-5***.

GRAPHICAL ABSTRACT

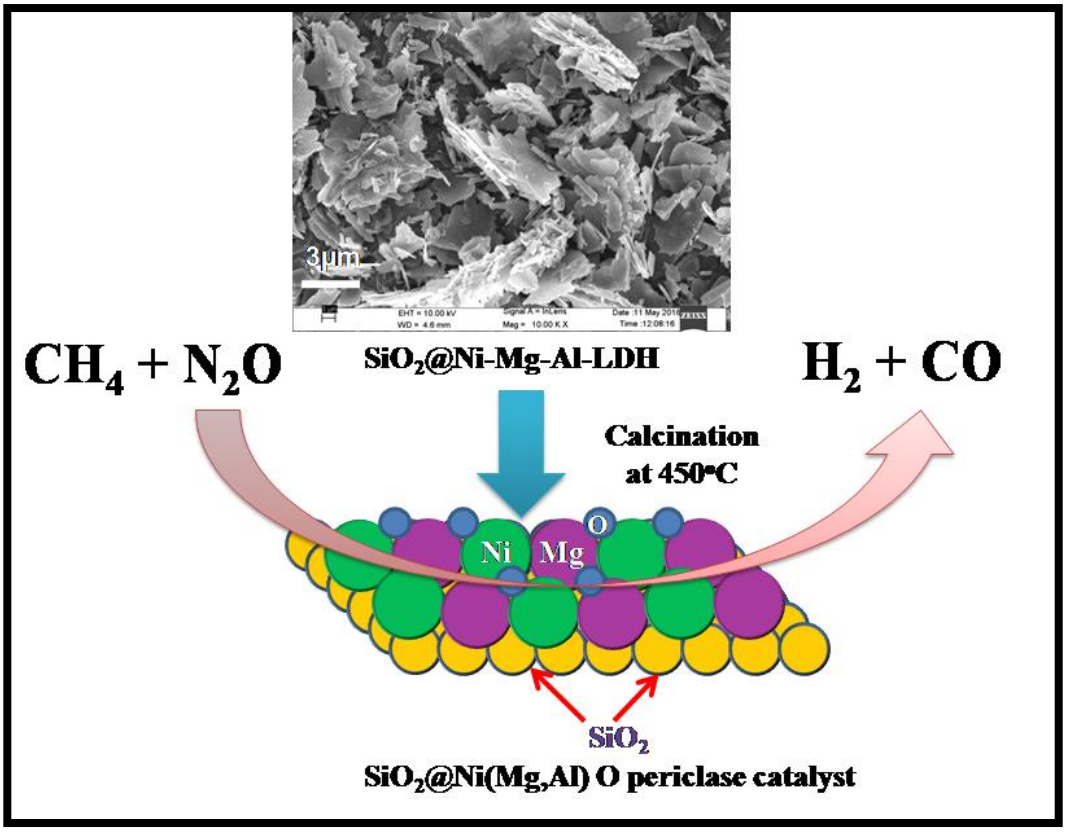

Catalytic partial oxidation of CH_4 over SiO_2@Ni(Mg,Al)O periclase type catalyst in presence of N_2O

ABSTRACT

This chapter describes about the synthesis and characterizations of ternary LDHs of SiO_2@Ni-Mg-Al and SiO_2@Ni-Mg-Cr. This chapter also describes about the catalytic behaviour of Ni(Mg,Al)O and Ni(Mg,Al)O/SiO_2 periclase type catalysts for catalytic partial oxidation of CH_4 in presence of N_2O.

The silica nanocomposites of ternary Layered Double Hydroxides (LDH) of SiO_2@Ni-Mg-Al type were synthesized at SiO_2:LDH ratios of 0:1 and 1:1 by a non aqueous sol-gel route using a combination of hydrolysis of metal acetylacetonates and alkoxides. The LDH based nanocomposites were used as catalyst for Catalytic Partial Oxidation of CH_4 in presence of N_2O. The catalysts were prepared by calcining SiO_2@Ni-Mg-Al-LDHs at 450 ^oC to get periclase type mixed-metal oxide Ni-Mg-Al-O supported over SiO_2 surface. The catalyst had surface area values of about 108.9m^2/g and 403 m^2/g at SiO_2:LDH ratios of 0:1 and 1:1 respectively which were designated as CNMA-01 (SiO_2:LDH=0:1) and CNMA-11(SiO_2:LDH=1:1) respectively. The XRD analysis showed that after calcination the Ni-Mg-Al-LDH component formed a NiO-MgO type non stoichiometric compound with periclase type structure having Ni and Al atoms well dispersed over in periclase MgO structure as a solid solution. On the other hand, the presence of SiO_2 increased the dispersion of Ni^{2+} centers over (Mg,Al)O/SiO_2 support in case of CNMA-11which helped in the reduction of Ni^{2+} to Ni^0 as observed from H_2-TPR analysis. The Ni^0 centers acted as active species for Catalytic Partial Oxidation (CPO) of CH_4 in presence of N_2O oxidant. XPS analysis also showed the presence of Ni in the +2 oxidation state in these catalysts. Although, there was a decrease of Ni mol % from CNMA-01 to CNMA-11 the low content of Ni as well as the presence SiO_2 enhanced the dispersion of Ni^{2+} over MgO periclase which also reduced the coke deposition as

well as increased the surface area of the catalyst. The catalytic partial oxidation of CH_4 in presence of N_2O was carried out by maintaining N_2O:CH_4 mol ratio of 1:1with initial concentration of N_2O and CH_4 of 300 ppm (6.8 mmol) and 100 ppm (6.8 mmol) respectively. The total flow of the reactant gas was kept at 280 ml/min and at constant Gas Hourly Space Velocity (GHSV) of 23,862 h^{-1} (56,000 $cm^3g^{-1}h^{-1}$). These catalysts showed about 99.8 % to 99.99 % H_2 and 99.5 % to 99.8 % CO yield in the temperature range of 200-500 ^oC. N_2O present on the feed acted as oxidant for CPO of CH_4 as it was first decomposed to N_2 and in the process nascent atomic oxygen is formed over LDH based catalysts. This nascent oxygen might have been adsorbed on the oxygen vacant site of the catalyst and which on desorption and consequent reaction with CH_4 led to its CPO. Due to the formation of Ni(Mg,Al)O periclase type solid solution the amount of coke deposited over the catalyst was also very low which in turn increased the catalytic activity towards *syn-gas* (H_2/CO) production.

4.1. INTRODUCTION:

Nitrous oxide (N_2O) is one of the most powerful greenhouse gas and it is the largest stratospheric-ozone-depleting substance [1-5]. N_2O has a global warming potential (GWP) of approximately 310 times higher than CO_2. Now a days, N_2O emissions have significantly increased compared to the pre-industrial period due to different human activities [6], such as uses of chemical fertilizers, the combustion of fossil fuels and the large scale production of chemicals like nitric and adipic acid [5,7-11]. N_2O also have some toxic effect to human health. It causes megaloblastic bone-marrow depression and neurological symptoms and it inhibit the methionine synthase enzyme by interaction with vitamin B_{12} [12].

Similar to N_2O, methane (CH_4) is one of the most abundant, low-cost C-containing feed stocks available in the world. Large amounts of NG are flared in refineries, chemical plants, oil wells and landfills which cause pollution [13]. The concentration of CH_4 also increases from 722 ppb in pre-industrial period to 1894 ppb and it has global warming potential (GWP) of approximately 21 times greater than CO_2 [11].

Thus, the control of emission of these gases mainly N_2O emissions from combustion and chemical processes and CH_4 emissions from refineries, chemical plants as well as landfills have significant importance. Several methods are employed for the control of N_2O and CH_4 emissions which includes – thermal decomposition [14] selective adsorption [14,15] decomposition by the use of plasma technology [14] and catalytic decomposition [15] of N_2O, steam reforming of CH_4, selective oxidation of CH_4, catalytic partial oxidation of CH_4 [16-19]. Among these catalytic decomposition of N_2O [15] and catalytic partial oxidation of CH_4 has intensive attention now-a-days [20].

Catalytic partial oxidation (CPO) of CH_4 was first reported by H. Linder in 1929[21].

The partial oxidation of CH_4 involves the following reaction-

$$CH_4 + 1/2O_2 \longrightarrow 2H_2 + CO \quad (4.1)$$

Due to high CH_4 conversion, high selectivity to syn-gas (H_2/CO), mild exothermicity as well as short time interval CPO reaction take some advantages over all other methods such as steam reforming, selective oxidation [16-21]. In other words, the use of N_2O as promoter for CPO of CH_4 to syn-gas is another profitably challangebale work for cleaner energy environment [22]. Many researchers such as Panov *et al*. [23] reported the use of N_2O as an oxidant for selective oxidations of various hydrocarbons and Wood *et al*. [24] studied the CH_4 oxidation in presence of N_2O over Fe/Al-MFI catalyst. He reported that N_2O decomposed to N_2 and nascent oxygen which forming surface methoxy groups by bonding with extraframework of Fe, which decomposed to syn-gas (H_2/CO) at elevated temperature [24].

In other words, the synthesis of some effective catalysts for CPO of CH_4 in presence of N_2O is very much necessary. The use of different types of catalysts such as noble metal like Rh, Ru based catalysts, Fe/Al-MFI catalyst, Co exchanged ZSM-5 were reported in several literatures [22,24-27]. In this paper we have reported the mixed-metal oxides derived from Layered Double Hydroxides (LDHs) are found to be most effective catalyst for CPO of CH_4 in presence of N_2O.

Layered Double Hydroxides (LDHs) also known as anionic clay have the general formula of $[M_{1-x}^{2+}M_x^{3+}(OH)_2]^{x+}[A_{x/n}]^{n-3}.m\ H_2O$, where M^{2+} (e.g. Mg^{2+}, Ni^{2+}, Fe^{2+}, Co^{2+}, Cu^{2+}, Ni^{2+} or Zn^{2+}) and M^{3+} (e.g. Al^{3+}, Cr^{3+}, Ga^{3+},In^{3+}, Mn^{3+} or Fe^{3+}). Different M^{2+} and M^{3+} metal cations are uniformly and orderly distributed in the brucite-like sheets and various charge-compensating anions (A^{n-}) are present in their interlayer spaces [28]. Due to their catalytically important properties such as high surface area, uniform atomic level distribution of metal ion centers, acid-base bifunctionality these

can be used as a catalyst in organic/pharmaceutical synthesis, clean energy generation, conversion of green house gases to useful feedstocks, degradation of pollutants to control environmental pollution and photochemical reactions [29-32]. The use of different types of LDH based catalysts for CPO of CH_4 was also reported by many researchers [33-43]. On the otherhand, the preparation of effective catalyst for CPO reaction is now becoming a challanegable work. Although, Ni-based catalyst were developed by many researcher due to its low cost, coke deposition leads to the deactivation of these catalyst [44]. Thus, the modification of Ni-based catalyst to reduce deactivation as well as to increase stability of the catalysts is another challanegable work. Hence, to overcome this problem many researchers developed some modified catalysts including the NiO-MgO solid matrix or by incorporating some specific metal or ion such as La, W, F in NiO-MgO periclase structure where, Ni^{2+} is in the dispersed state and hence increases the catalytic behaviour [33-43]. F. Basile *et al*.[33] reported the use of Ni/Mg/Al LDH based catalyst for CPO of CH_4. They reported the synthesis of Ni/Mg/Al LDH by co-precipitation method and carried out the CPO reaction of CH_4 at above 500 ^oC. T. Shishido *et al*.[34] reported the use of CPO of CH_4 in presence of Ni/Mg-Al-LDH synthesized by solid phase crystallization method. They also carried out the CPO reaction of CH_4 at high temperature. J. Zhang *et al*. [35] modified Ni/Mg/Al-LDH by addition of La for CPO reaction to increase the catalytic behaviour of these catalysts towards high syn-gas production (H_2/CO). They found only 93 % CO and 96 % H_2 yield in presence of these catalysts. On the otherhand, they carried out this reaction at high temperature and these catalysts showed highest syn-gas production at 800 ^oC. Similarly, Z. Jiang *et al*.[36] reported the use of Ni-Mg/Al-LDH bases mixed oxide for CPO reaction and they studied the effect of Mg/Al ratio on the CPO reaction. J. Zhang *et al*.[40] also reported the use of fluorine

modified mesoporous Ni/Mg/Al mixed oxide for CPO of CH_4. They also carried out the CPO reaction at high temperature about 780 ^oC. Thus, in this entire reported works the catalysts were synthesized by co-precipitation method and CPO of CH_4 was carried out at high temperature.

Hence, in this work we have described the synthesis of ternary LDHs of Ni-Mg-Al and SiO_2@Ni-Mg-Al by non-aqueous 'soft chemical' sol-gel method by using metal acetylacetonate precursors which is a different method from the previously reported methods. The novelty of our work includes both in the synthesis procedure as well as the use of SiO_2 as support and dispersant. The soft chemical sol-gel method gives finer dispersible particles [45] as a result some important properties such as surface area, thermal stability of the catalysts increases which is very necessary for an effective catalyst. In other words, the use of metal acetylaceonate helps to maintain the microstructure [46] because of their slow hydrolysis and the use of SiO_2 increases the dispersiblity of Ni^{2+} and further increase of surface area. Thus, in this manuscript we have modified the catalyst by incorporation of SiO_2 in the solid matrix which was found to be most effective in CPO reaction as it further reduces the coke deposition [47]. In this manuscript, we have also carried out the catalytic partial oxidation of CH_4 over mixed-metal oxides obtained after calcinations of theses ternary LDHs in presence of N_2O at low temperature of 200-500 ^oC respectively and at low concentration of N_2O and CH_4 which is another novelity of our work. The use of Ni(Mg,Al)O/Ni(Mg,Al)O.SiO_2 periclase type catalyst obtained from Ni/Mg/Al and SiO_2@Ni/Mg/Al Layered Double Hydroxides for CPO of CH_4 in presence of N_2O has not been reported yet. Hence, this work is expected to a future leading work and these catalysts can be used as an effective catalyst for CPO reaction.

4.2. EXPERIMENTAL SECTION:

This **Chapter** describes about the synthesis of unsupported and SiO_2 supported Ni-Mg-Al and Ni-Mg-Cr ternary LDHs by sol-gel method. This **Chapter** also describes the characterization of these LDHs by XRD, FT-IR, TGA-DTG, Rheometry, BET surface area and pore volume analysis, SEM and EDS etc. These were then used both in the powdered form and thin film coating over honey comb after calcination at 450 ^oC as a catalyst for N_2O decomposition and Catalytic Partial Oxidation (CPO) of CH_4.

4.2.1.Materials:

$Ni(acac)_2$(98%,M/SE,Merck),$Cr(acac)_3$(98%,M/S,Aldrich),$Mg(acac)_2$(98%M/S,Aldrich), $Al(acac)_3$ (98 %, M/S,Aldrich),TEOS (Tetra ethyl orthosilicate) distilled ethanol, distilled acetone, NH_4OH and HCl were used.

4.2.2. Synthesis of unsupported and SiO_2 supported Ni-Mg-Al-LDH and Ni-Mg-Cr-LDH by soft chemical sol-gel method [45,46]:

Unsupported and SiO_2 supported Ni-Mg-Al-LDH and Ni-Mg-Cr-LDH were synthesized by the following steps-

Step-1: 0.02 mol $Ni(acac)_2$/$Mg(acac)_2$ were dissolved in 80 cm^3 distilled ethanol at pH 6. Small amount of 0.2 M HCl was added to dissolve these metal acacs completely in ethanol.

Step-2: 0.007 mol $Cr(acac)_3$/$Al(acac)_3$ were dissolved in 80 cm^3 distilled ethanol:acetone (1:1) mixture.

These two solutions were mixed at 80 ^oC by stirring for 2-3 hours. The pH of the mixture was maintained at 8-9 by adding few drops of 1:2 NH_3:H_2O mixture and finally refluxed for 6-7 hours to get Ni-Mg-Al and Ni-Mg-Cr LDH. The product obtained was filtered and dried in air oven at 40 ^oC.

For the synthesis of SiO_2@Ni-Mg-Al-LDH/Ni-Mg-Cr-LDH with SiO_2:LDH ratio 1:1, TEOS was used as a source of silica. 4.43 cm^3 TEOS, 0.72 cm^3 of 0.2 M aqueous

HCl and 4.85 cm^3 distilled ethanol were taken and aged the mixture for 45 min in a magnetic stirrer at room temperature. The solutions of step-1 and step-2 were mixed at 80 ^oC and refluxed for 2 hours. Added hydrolysed TEOS to the mixed acetylacetonate solution and raised the pH up to 8-9 by adding 1:2 NH_3:H_2O mixture stirred continuously for another 6-7 hours to get silica supported LDH. A portion of the product was separated from the obtained free flowing gels by filtration, washed in hot water and dried at 40 ^oC in air oven for further characterizations like XRD, TGA-DTG, Zeta-potential study, FT-IR and BET Surface area analysis. On the other hand, the ratio of bivalent to trivalent metal was kept at 3:1. **Fig. 4.1** shows the schematic diagram of the synthesis of ternary LDHs. Bivalent to bivalent metal ion (Ni:Mg) ratio and bivalent to trivalent metal ion (Ni:Cr or Mg:Cr and Ni:Al or Mg:Al) ratio during the synthesis were maintained at 1:1and 3:1 ratio.

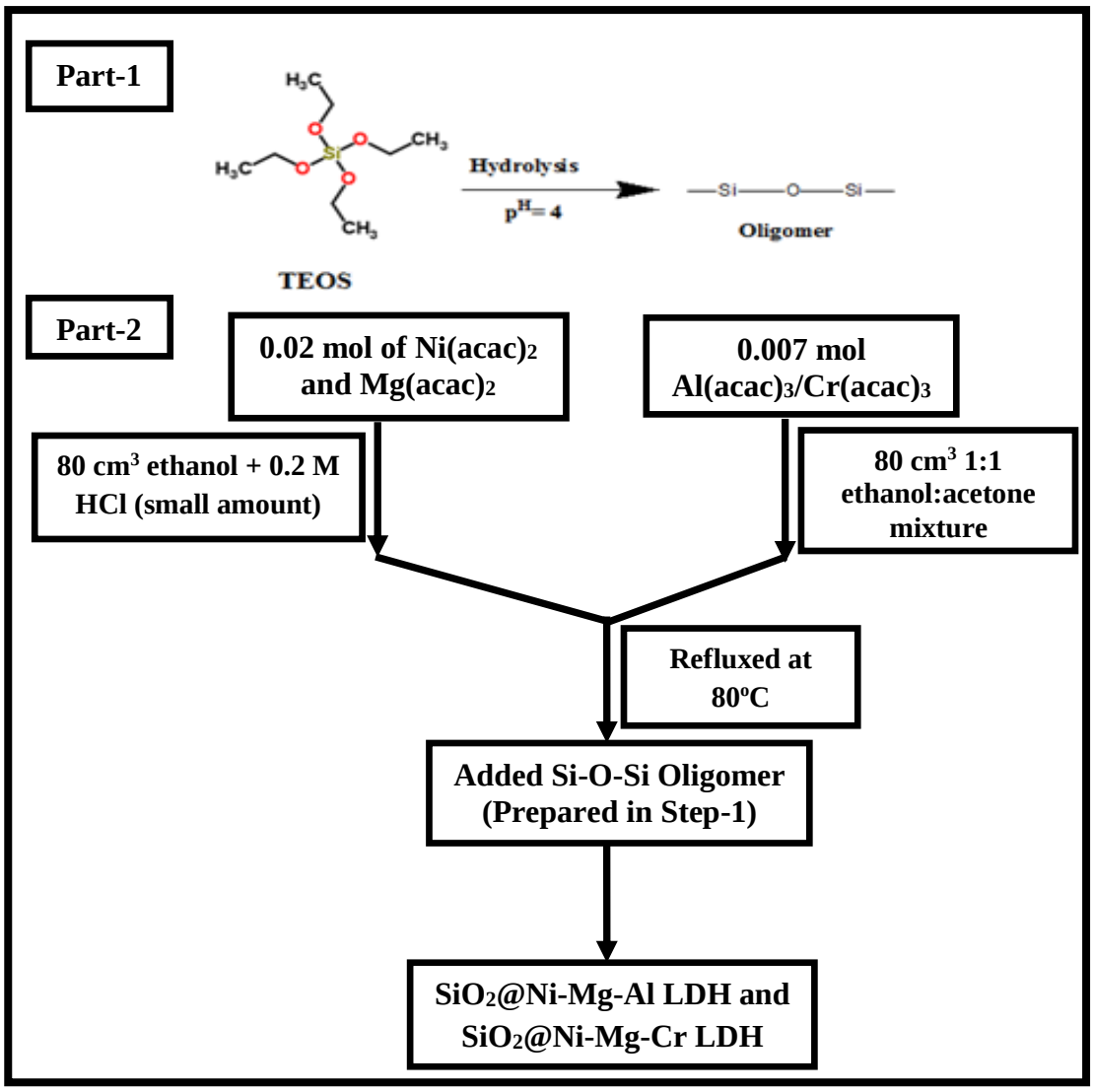

Fig. 4.1: Schematic diagram of the synthesis of SiO_2 supported ternary LDHs.

4.2.3. Characterizations:

Structure identification of inorganic phases formed were carried out in a powder X-ray diffractometer (Model Rigaku Ultima IV) using Cuk$_\alpha$ radiation of a wavelength of 1.54 Å at 40 mA and 40 kV X-ray generator current setting with a step size of 0.2° 2θ min^{-1}.

Fourier Transform Infrared (FT-IR) spectra of the prepared samples were recorded in spectrophotometer (Perkin-Elmer 2000 System) in 4,000-400cm^{-1} range at a spectral resolution of 4 cm^{-1} using KBr pellets.

Field Emission Scanning Electron Microscopy (FE-SEM) analysis was carried out in a Carl Zeiss -Sigma VP equipment, with an accelerating voltage of 20 kV. Before the analysis the gels were dried at 40 ^{o}C in air oven for 1 week to avoid the moisture absorption. Finally, the sample surfaces were gold coated in high vacuum. The chemical composition was identified by using an energy-dispersive X-ray spectroscopy (EDX) detector on the scanning electron microscope Model Carl Zeiss Sigma VP.

The thermogravimetric measurements were carried out in a simultaneous TG-DTA analyzer (model Q-600, M/S TA Instruments) using α -Al_2O_3 as reference. Samples weighing about 5.0 mg were heated from 30 to 1000 ^{o}C at a rate of 10°C min^{-1} in an Argon atmosphere in a non-isothermal condition. The deposition of coke in the catalyst was analysed by thermogravimetric measurements carried out from 30 to 1000 ^{o}C at a rate of 10 ^{o}C/min under air atmosphere.

Specific surface area of the samples was recorded *via* Nitrogen gas adsorption at 77 K applying Brunauer-Emmett-Teller (BET) calculations using Autosorb-iQ Station 1 (Quantachrome, USA). Prior to performing the experiment the samples were degassed at 100 ^{o}C for 1.5 hours.

The zeta potential of the nanocomposite alcogels were measured with the Laser Doppler Velocimetry technique at 25 ^{o}C under a 10 Mw He-Ne laser (M/S Malvern Instruments Zetasizer Nano Z5). The particle size distribution of these nanocomposites was carried by DLS (Dynamic Light Scattering) technique in zeta sizer (M/S Malvern Instruments Zetasizer Nano Z5). To carry out these studies the samples were filtered, washed with hot water and dried in air oven at 40 ^{o}C. The dried mass were ground gently in an agate mortar and redispersed in aqueous phase by shaking in an ultrasonic processor (M/S Sonics) with a 1.3 cm Ti probe for 30 minutes under 20 kHz frequency and 25 % amplitude of vibration.

Temperature programmed reduction (TPR) with hydrogen was carried out in a M/S Micromeritics made instrument. About 0.1779 g of sample were pre treated at 120 ^{o}C in high purity helium gas (25 cc/min) for 1 hour and cooled to room temperature in helium, the gas was changed to 5 % H_2/Ar (25 cc/min) at room temperature and waited till baseline is stable then TPR study was carried out from RT to 800 ^{o}C at 10 ^{o}C/min flow rate.

X-ray photoelectron spectroscopy (XPS) measurements were carried out in a Thermo Scientific MULTILAB 2000 Base system attached with X-Ray, Auger and ISS attachments having monochromatic Al K_{α} X-ray source (1486.6 eV). The photoelectron spectra were calibrated in bond energy, referenced to that of the component C-C of carbon C 1s at 284.8 eV.

Rheological properties of the nanocomposite alcogels were investigated by rotational rheometer. The steady shear measurements were carried out by rotational rheometer Rheolab QC (Anton Paar) with a measuring cup C-CC27/SS/QC and measuring system CC27/P6 at 15 ^{o}C. The preliminary studies such as variation of viscosity and shear stress with shear strain and the flow modeling of these alcogels were investigated by it. The temperature of 15 ^{o}C was maintained to minimize the concentration change of dispersions by evaporation of organic solvents from the surface. The steady shear measurements were carried out in the shear rate ranging from 100-1000 s^{-1}.

4.2.4. Catalytic activity:

4.2.4.1. Catalyst Preparation:

About 0.3g of the catalysts were packed inside a stainless steel tube of internal diameter 0.8 cm and length of 304.8 cm as described in the **Experimental Section 3.A.2.4.6.2a** of **Chapter III-PART-A**. The pack was guarded with two glass wool plugs placed on its either sides. The catalytic reactions were performed in different gas

flow rate conditions under atmospheric pressure at a temperatures range of 200-500 ^{o}C. Before the catalytic reaction LDHs were calcined at 450 ^{o}C to get mixed-metal nano-oxide. The calibration of the furnace was carried out by STQC Calibration No. F02720, Model No. PID-1173D at 450 ^{o}C.These catalysts were then designated as CNMA-01(SiO_2:LDH ratio 0:1), CNMA-11 (SiO_2:LDH ratio 1:1) and CNMC-01 (SiO_2:LDH ratio 0:1).

4.2.4.2. Catalytic partial oxidation of CH_4 by N_2O:

The catalytic reaction over ternary LDH as catalyst was carried out at temperature from 200-500 ^{o}C. The total flow rate of Argon:N_2O:CH_4 was maintained at 280 ml/min. The gas hourly space velocity was kept as GHSV= 23,862 h^{-1} (56,000$cm^3gcat^{-1}h^{-1}$) by keeping the total flow rate constant (280 ml/min). The mol ratio of CH_4: N_2O was kept at 1:1 with 300 ppm (6.8 mmol) N_2O against 100 ppm (6.8 mmol) CH_4. Before the catalytic reactions the catalysts were activated under a pure H_2 flow (100 ml/min flow rate) at a temperature of 500 ^{o}C and 850 ^{o}C for 2 hours. The reactant and product gas mixtures were collected in Tedlar bags for subsequent analysis by Gas chromatography. The overall procedure of the catalytic reaction including the use of catalytic reactor and collection as well as detection of reactant and product gas has been already described in the **Experimental Section 3.B.2.5.1.1e** of **Chapter III-PART-B**.

4.3. RESULTS AND DISCUSSION:

Ternary LDHs of Ni-Mg-Al and Ni-Mg-Cr were synthesized by non-aqueous sol-gel route using metal acetylacetonates in organic medium as described in **Experimental Section 4.2.2**. The main advantage of using metal acetylacetonate precursors is that they undergo slow and controlled hydrolysis than the common metal alkoxides generally used in sol-gel hydrolysis reactions. This route gives a better opportunity for

maintenance of desired micro-structure of hydrolysed products [46]. On the other hand, their SiO_2 supports were obtained by hydrolysis of TEOS. This nano silica forms a core network around the LDHs and forms a basic core-shell type soft alcogel which after calcination forms an aerogel or a xerogel type catalyst as already described in **Chapter-III**. The ternary LDHs of Ni-Mg-Al and Ni-Mg-Cr were characterized by XRD, FT-IR, TGA-DTG, Rheometry, BET surface area and pore volume analysis, SEM and EDS analysis.

4.3.1. Characterizations:

4.3.1.1. XRD analysis:

XRD analysis was carried out to confirm the presence of LDH phases in the ternary LDHs.

4.3.1.1.1. SiO_2@Ni-Mg-Al-LDH:

Fig. 4.2A&B shows the XRD patterns of both uncalcined and calcined SiO_2 supported and unsupported Ni-Mg-Al-LDHs. It was observed from the XRD analysis (**Fig. 4.2A**) that both unsupported and SiO_2 supported Ni-Mg-Al LDHs showed the presence of LDH phases with *hkl* reflections of (003), (006) and (009) with an usual gradual decrease of their intensities. The first sharp high intensity *00l* peak was obtained at d=10.6 Å. The peaks due to SiO_2 were obtained with *hkl* reflection of (332), (331) and (532) respectively (**JCPDS PDF Card no.00-042-0022**).

On the other hand, after calcination the layered structure of LDHs was completely destroyed and the product showed (**Fig. 4.2B**) the presence of high intensity peak with *hkl* reflection of (101), (012), (220) and (222) at about 37°,43.4°, 63°,76° and 79° 2θ respectively due to periclase like NiO-MgO solid solution (**JCPDS PDF Card no. 00-004-0835**, **JCPDS PDF Card no. 00-030-0794**) [35,43] in which the XRD peaks for NiO and with MgO were appeared in the same 2θ values. The formation of periclase

structure was further confirmed by comparing the lattice parameter of standard MgO periclase with the synthesized NiO-MgO periclase. It was observed that the lattice parameter *a* in Å for the calcined Ni-Mg-Al and SiO_2@Ni-Mg-Al-LDHs as 4.15 Å calculated by using POWD software whereas 4.21 Å for standard MgO periclase. This slight variation of lattice parameter is due to the formation of NiO-MgO type solid solution [49] where, Ni^{2+} was isomorphously substituted by Mg^{2+} and Al^{3+} was substituted by Mg^{2+} due to comparable ionic radii of 0.054 nm for Al^{3+}, 0.072 nm for Mg^{2+} and 0.069 nm for Ni^{2+} [35]. The phases due to oxides of SiO_2 such as Ni(Mg,Al)O/SiO_2 was not observed in case of CNMA-11 catalyst which may be due to the poorly crystalline nature [50,51]. On the other hand, inset of the **Fig. 4.2B** shows the presence of metallic Ni peak at 2θ value of 44.5° (d=2.04 Å) with *hkl* reflection of (111) which showed the presence of Ni^0 species (**JCPDS PDF Card no.00-001-1258**) in these catalysts.

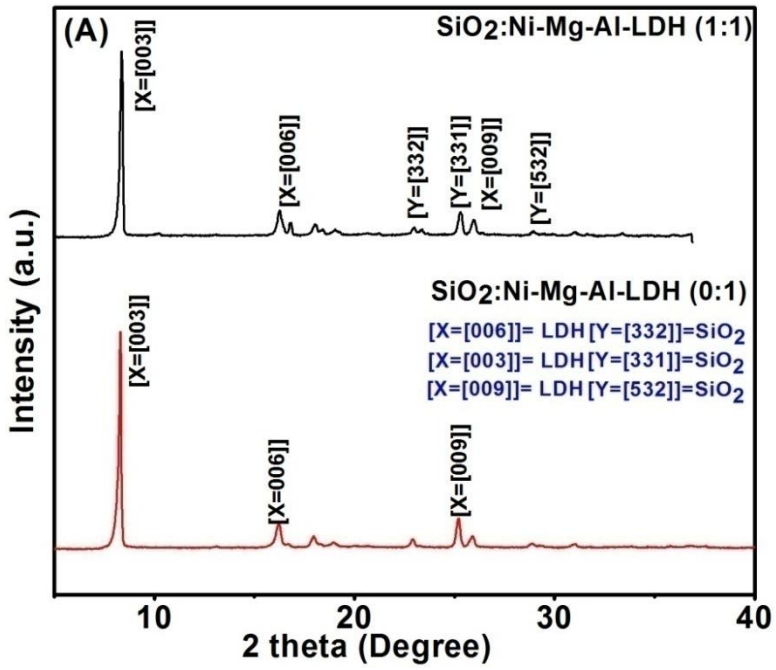

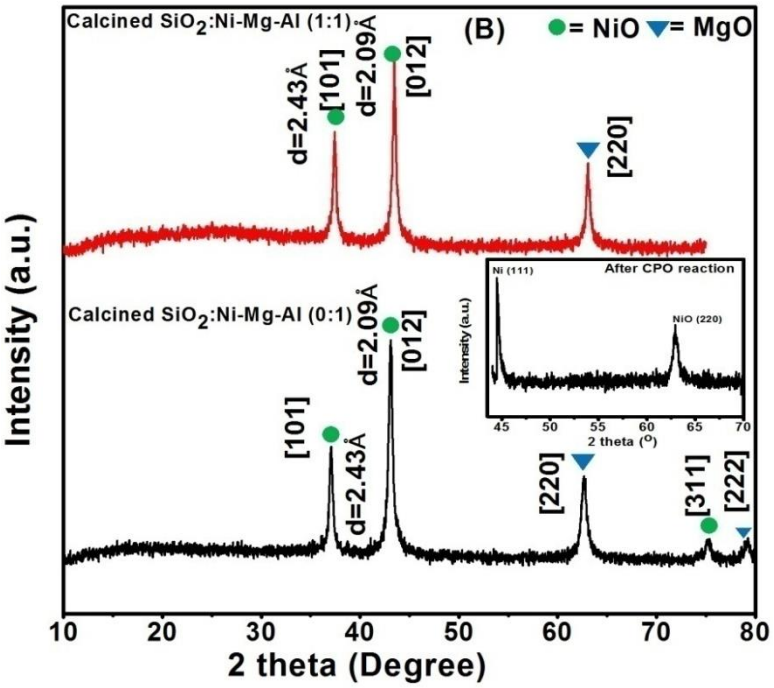

Fig. 4.2: XRD patterns of SiO_2@Ni-Mg-Al-LDH (A); Calcined SiO_2@Ni-Mg-Al-LDH (B).

4.3.1.1.2. SiO_2@Ni-Mg-Cr-LDH:

Fig. 4.3A&B shows the XRD patterns of both uncalcined and calcined SiO_2 @Ni-Mg-Cr-LDHs. It was observed (**Fig. 4.3A**) both unsupported and SiO_2 supported Ni-Mg-Cr-LDH showed the presence of LDH phases with *hkl* reflection of (003), (006), (009) and (012) respectively similar to Ni-Mg-Al-LDH. The peak due to SiO_2 were obtained with low intensity *hkl* reflection of (501), (131), (532), (305) and (512) respectively (**JCPDS PDF Card no. 00-042-0022**).

On the other hand, calcined SiO_2@Ni-Mg-Cr-LDH(**Fig. 4.3B**) also showed the presence of high intensity Ni (Mg,Cr)O periclase type phases with *hkl* reflection of (200) (d= 2.107 Å) along with the lowest intensity peak of *hkl* reflection of (101) (d= 2.43Å), (113), (202), (220) respectively (**JCPDS PDF Card no. 00-004-0835, JCPDS PDF Card no.00-030-0794**) similar to SiO_2@Ni-Mg-Al LDH [35,43].

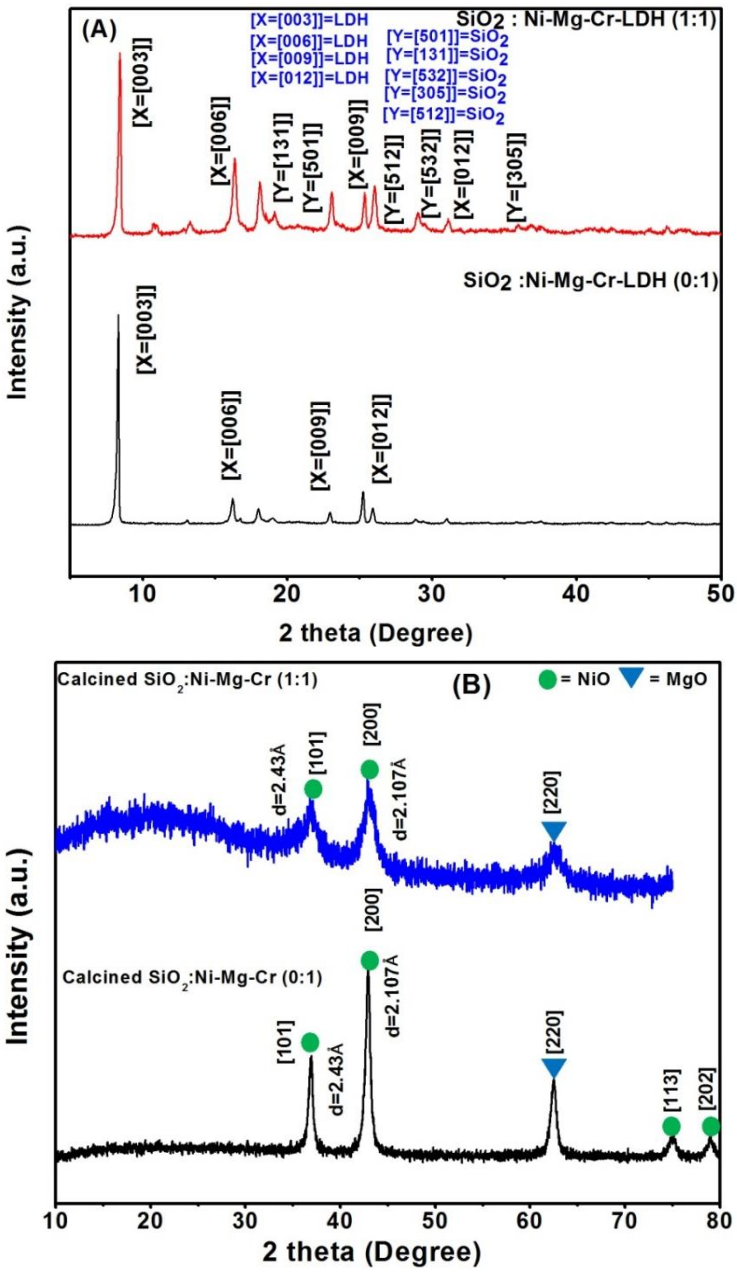

Fig. 4.3: XRD patterns of SiO_2@Ni-Mg-Cr-LDH (A); Calcined SiO_2@Ni-Mg-Cr-LDH (B).

4.3.1.2. Metal ion concentration determination by Atomic absorption spectroscopy (AAS):

Bivalent to bivalent metal ion (Ni:Mg) ratio and bivalent to trivalent metal ion (Ni:Cr or Mg:Cr and Ni:Al or Mg:Al) ratio during the synthesis were maintained at 1:1 and 3:1 ratio. The same ratio of Ni:Mg (1:1) and Ni:Cr or Mg:Cr and Ni:Al or Mg:Al (3:1)

was also found in the products as analysed by AAS analysis.

4.3.1.3. FT-IR analysis:

Fourier Transform Infrared (FT-IR) spectra of the prepared samples were recorded in spectrophotometer (Perkin-Elmer 2000 System) in 4,000-400cm^{-1} range at a spectral resolution of 4 cm^{-1} using KBr pellets.

4.3.1.3.1. SiO_2@Ni-Mg-Al-LDH:

FT-IR analysis (**Fig. 4.4A)** showed the presence of broad peak at 3431 cm^{-1} due to –OH stretching vibration. The peak at 1620 cm^{-1} was due to stretching vibration of –C=O group of acetylacetonate ion present in the interlayer. The peak due to C-O stretching vibration was obtained at 1406 cm^{-1}. The peak at 572 cm^{-1} and 763 cm^{-1} were obtained due to M-O stretching vibration [46].

On the other hand, in case of calcined products the peak due to C=O stretching vibration was obtained at 1595-1652 cm^{-1}. The peak at 1017-1076 cm^{-1} was obtained due to C-O stretching vibration and the peak due to M-O stretching vibration was obtained at 639-666 cm^{-1}.

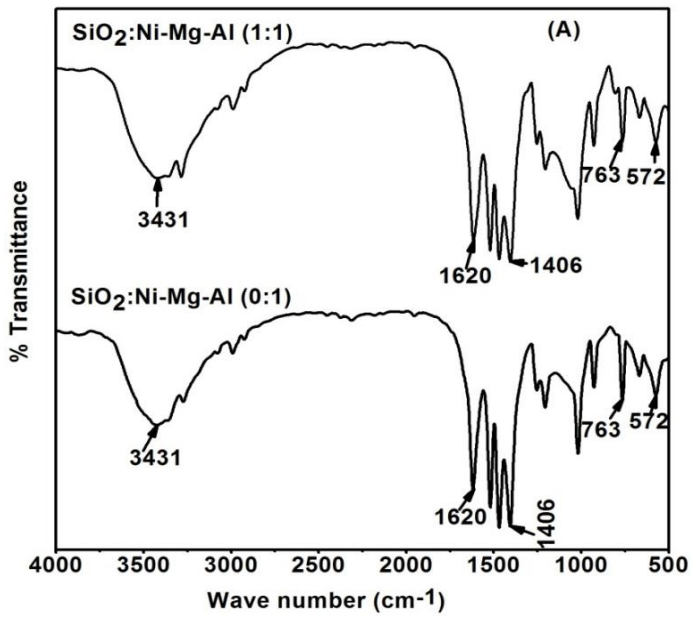

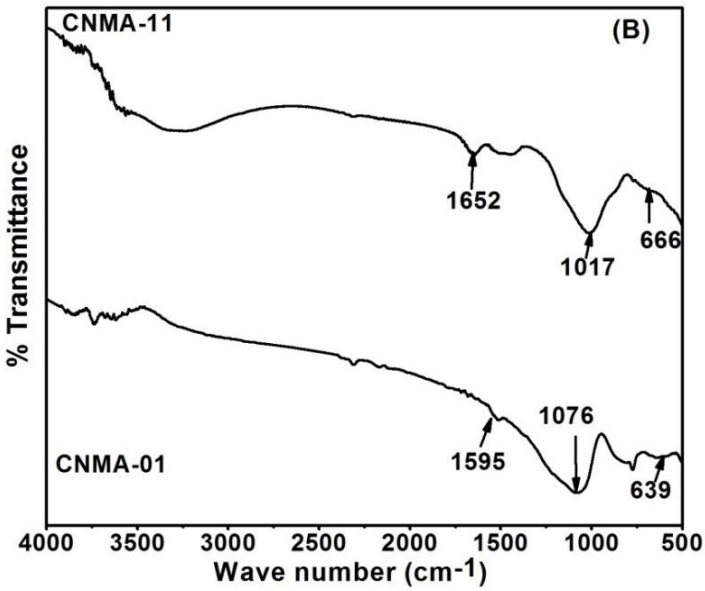

Fig. 4.4: FT-IR patterns of SiO_2@Ni-Mg-Al-LDH (A); Calcined SiO_2@Ni-Mg-Al-LDH (B).

4.3.1.3.2. SiO_2@Ni-Mg-Cr-LDH:

Fig. 4.5 A&B shows the XRD patterns of uncalcined and calcined SiO_2@Ni-Mg-Cr LDHs. The peak due to –OH stretching vibration was obtained at 3433 cm^{-1} (**Fig. 4.5A**). The peak at 1615 cm^{-1} was obtained due to C=O stretching vibration of acetylacetonate ion present in the interlayer of LDHs. The peak due to C-O and M-O stretching vibrations were obtained at 1024-1400 cm^{-1} and 570-923 cm^{-1} [46].

On the other hand, the peak due to C=O stretching vibration was obtained at 1519-1624 cm^{-1}. The peak due to C-O and M-O stretching vibrations were obtained at 1070-1420 cm^{-1} and 830-857cm^{-1} (**Fig. 4.5 B**).

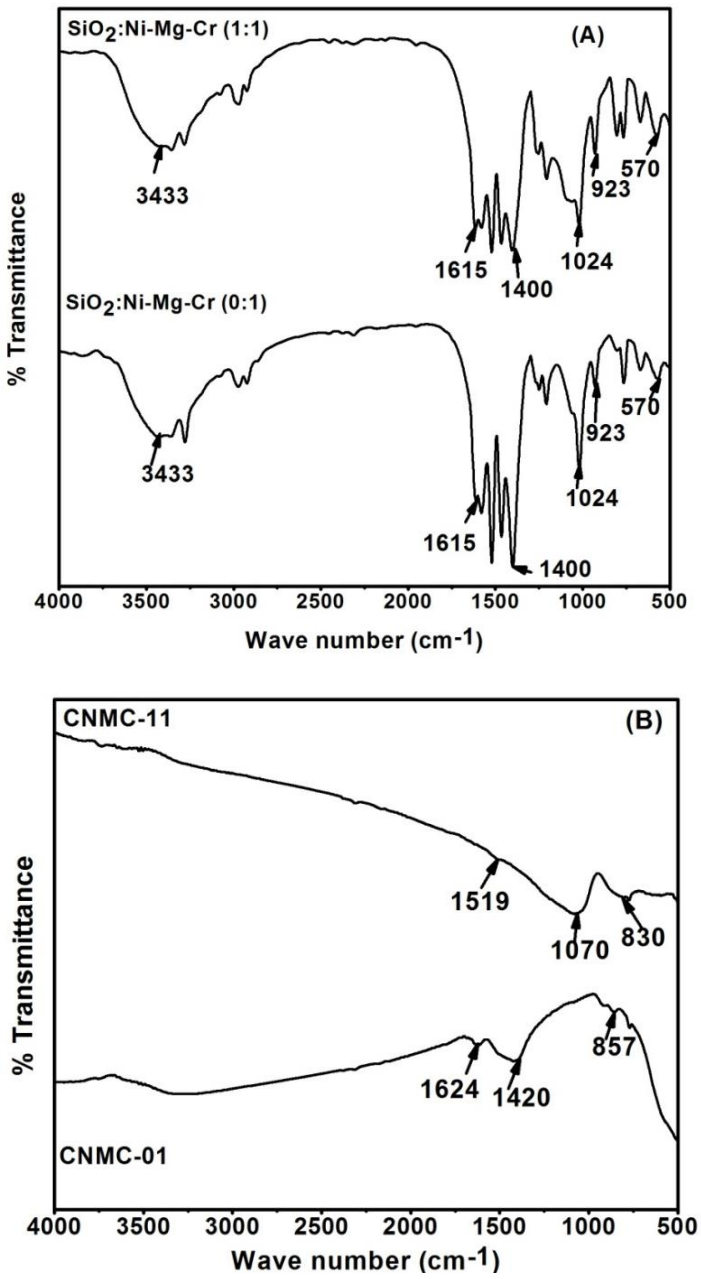

Fig. 4.5: FT-IR patterns of SiO_2@Ni-Mg-Cr-LDH (A); Calcined SiO_2@Ni-Mg-Cr-LDH (B).

4.3.1.4. TGA-DTG analysis:

4.3.1.4.1. SiO_2@Ni-Mg-Al-LDH:

TGA-DTG analysis (**Fig. 4.6A&B**) of SiO_2@Ni-Mg-Al showed the three step weight losses in both unsupported and SiO_2 supported LDHs. The first step weight loss correspond to the loss of adsorbed moisture; second step and third step correspond to

the dehydroxylation of the brucite like layer and loss of interlayer ion such as acetylacetonate ion and finally the break down of the brucite like layer [36,38]. Similar observations were also shown by DTA patterns which showed three endothermic peaks (inset of the **Fig. 4.6B**). SiO_2@Ni-Mg-Al showed the weight losses of 13.9 % and 18.6 % in the temperature range of 50-170 ^oC; 46.7 % and 49.9 % in the temperature range of 200-300 ^oC whereas 27.2 % and 13.4 % weight losses in the temperature range of 400-600 ^oC respectively. In case of SiO_2@Ni-Mg-Al (1:1), the weight loss above 400 ^oC temperature decreased as compared to SiO_2@Ni-Mg-Al (0:1) with the decrease of LDH content due to the incorporation of SiO_2. On the otherhand, the weight loss correspond to physisorbed water and dehydroxylation decreased in case of SiO_2@Ni-Mg-Al (0:1) due to increase of Mg^{2+}/Al^{3+} molar ratio in the layered structure [38].

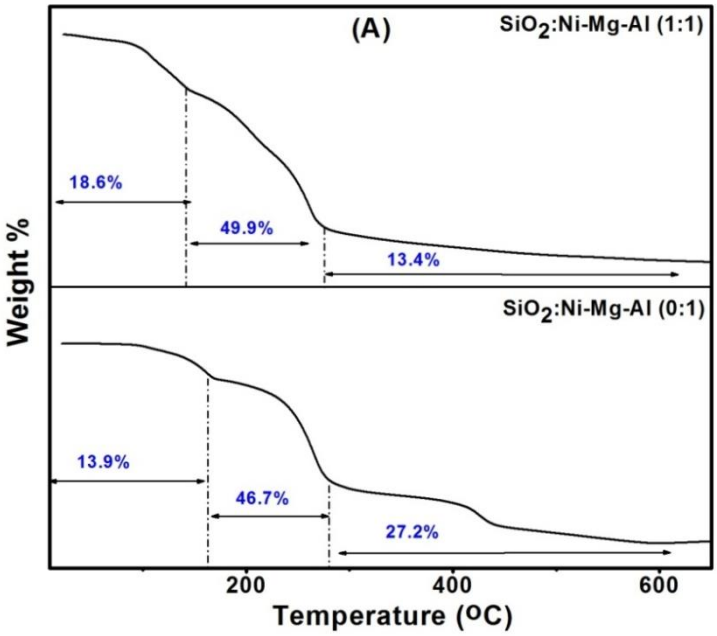

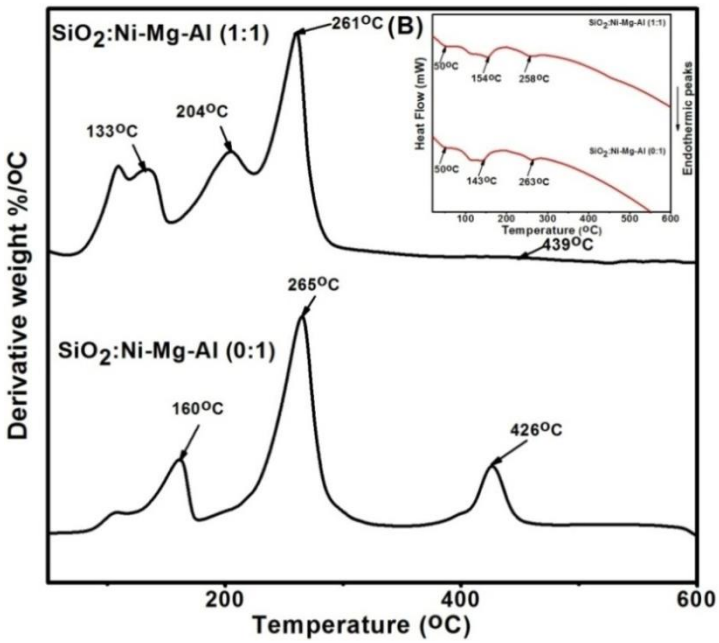

Fig. 4.6: TGA-DTG patterns of SiO_2@Ni-Mg-Al-LDH (A&B); inset is the DTA curves.

4.3.1.4.2. SiO_2@Ni-Mg-Cr-LDH:

Similar to SiO_2@Ni-Mg-Al-LDH,TGA-DTG analysis (**Fig. 4.7A&B**) also showed three steps weight losses in case of SiO_2@Ni-Mg-Cr-LDHs. It showed weight losses of 13.7 % and 14.4 % in the temperature range of 50-180 ^oC; 40 % and 42.5 % weight losses in the temperature range of 200-350 ^oC; whereas the weight losses of 23.6 % and 16.6 % weight losses in the temperature range of 350-800 ^oC. The first step correspond to the loss of adsorbed moisture, the second and third step correspond to the dehydroxylation of the brucite like layer and the loss of interlayer ion such as acetylacetonate ion present in the LDH [36,38]. DTA patterns also showed three endothermic peaks as shown in **Fig. 4.7B** (inset is the DTA curves).

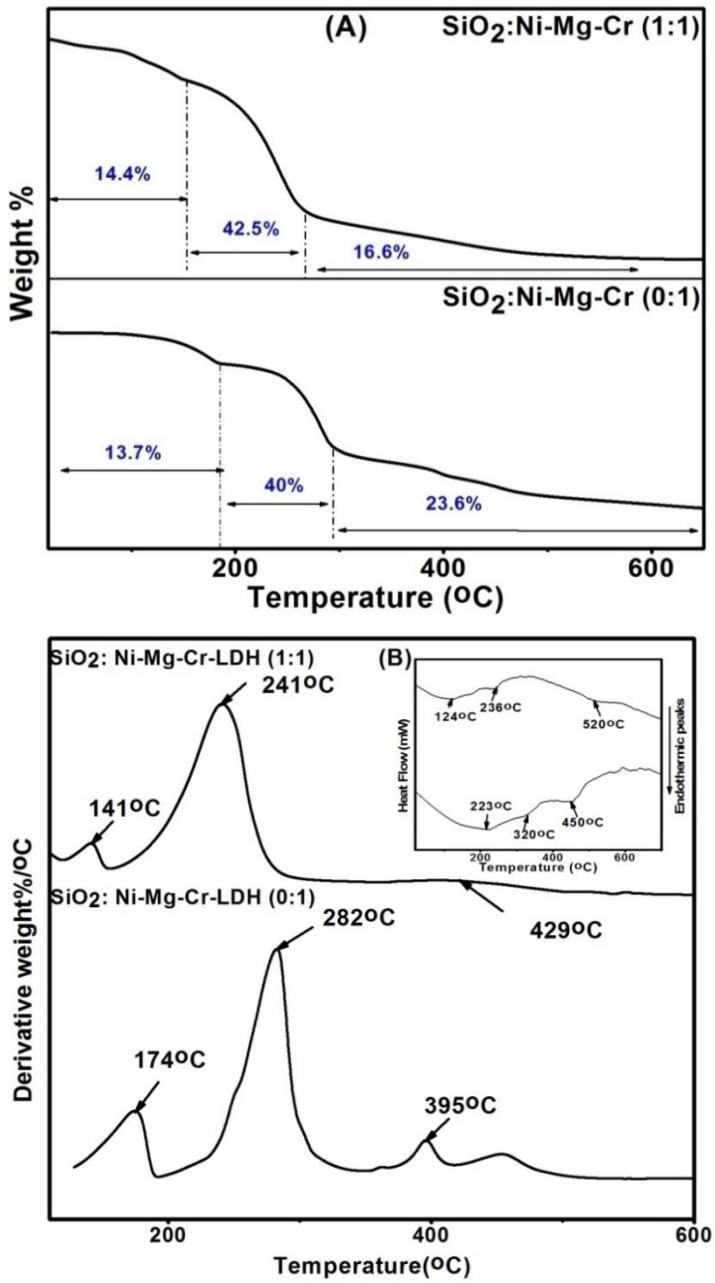

Fig. 4.7: TGA-DTG patterns of SiO_2@Ni-Mg-Cr-LDH (A&B); inset is the DTA curves.

4.3.1.5. Rheological Study:

Rheological properties of the nanocomposite alcogels were investigated by rotational rheometer. The steady shear measurements were carried out by rotational rheometer Rheolab QC (Anton Paar) with a measuring cup C-CC27/SS/QC and measuring system CC27/P6 at 15 ^{o}C as described in the **Experimental Section 4.1.3**.

Fig. 4.8A&B shows the flow curves of SiO_2@Ni-Mg-Al and SiO_2@Ni-Mg-Cr LDHs. It was observed that in case of both of these LDHs viscosity decreased with shear rate indicating the shear thinning behaviour [46]. With the increase of SiO_2 to LDH ratio the gel behaviour was found to increase in both of these LDHs.

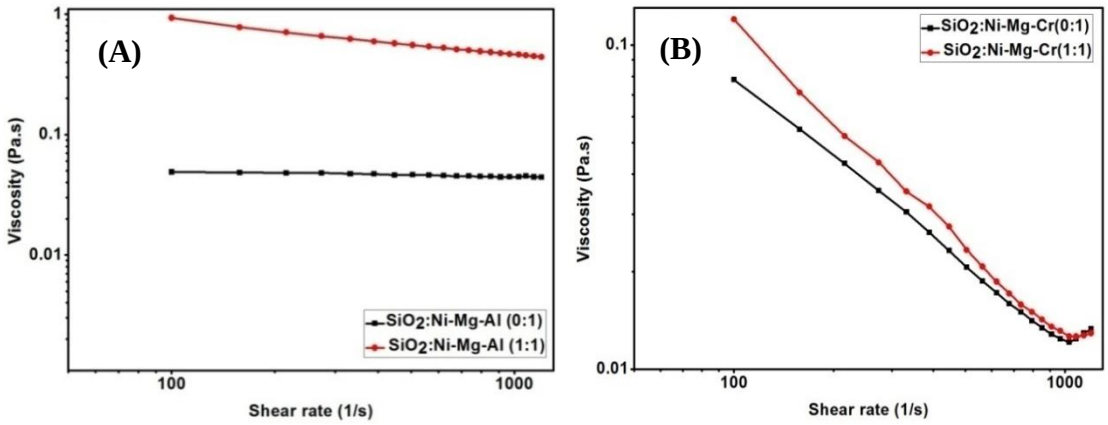

Fig. 4.8: Flow curves of SiO_2@Ni-Mg-Al-LDH (A) and SiO_2@Ni-Mg-Cr-LDH (B).

4.3.1.6. BET surface area and pore diameter analysis:

Table 4.1a and **Table 4.1b** show the surface area and pore diameter values both uncalcined and calcined SiO_2@Ni-Mg-Al and SiO_2@Ni-Mg-Cr LDHs. It was observed with the addition of SiO_2 the surface area increased from 27.3m^2/g to 38.1m^2/g in case of SiO_2@Ni-Mg-Al and from 58.5 m^2/g to 76.5 m^2/g in case of SiO_2@Ni-Mg-Cr LDH having the same pore diameter of 3.6 nm (**Table 4.1a**).

On the other hand, in case of calcined product further increase of surface area was observed with the addition of SiO_2 (**Table 4.1b**). It was observed that surface area increased from 108.9 m^2/g to 403 m^2/g in case of SiO_2@Ni-Mg-Al-LDH and from 229.5 to 446 m^2/g in case of SiO_2@Ni-Mg-Cr-LDH indicating the better catalytic properties.

Table 4.1a: BET surface area and pore radius of ternary LDHs

Serial No.	LDHs	BET surface area (m^2/g)	Pore diameter (nm)
1	SiO_2:Ni-Mg-Al-LDH (0:1)	27.3	3.6
2	SiO_2:Ni-Mg-Al-LDH (1:1)	38.1	3.6
3	SiO_2:Ni-Mg-Cr-LDH (0:1)	58.5	3.6
4	SiO_2:Ni-Mg-Cr-LDH (1:1)	76.5	3.6

Table 4.1b: BET surface area and pore radius of calcined ternary LDHs

Serial No.	LDHs	BET surface area (m^2/g)	Pore diameter (nm)
1	Calcined SiO_2:Ni-Mg-Al-LDH (0:1)	108.9	3.6
2	Calcined SiO_2:Ni-Mg-Al-LDH (1:1)	403	3.6
3	Calcined SiO_2:Ni-Mg-Cr-LDH (0:1)	229.5	3.6
4	Calcined SiO_2:Ni-Mg-Cr-LDH (1:1)	446	3.6

4.3.1.7. Zeta potential analysis:

Zeta potential analysis of ternary LDHs was carried to study their stability at different pH. It was observed that SiO_2 supported LDH showed better stability behaviour as shown in **Table 4.2**. The zeta potential value increased from 16.5 mV to 18.8 mV in case of SiO_2@Ni-Mg-Cr-LDH and from 17.8 mV to 21.9 mV in case SiO_2@Ni-Mg-Al LDH. The negative charge was due to the presence of SiO_2.

Table 4.2: Zeta potential values of ternary LDHs

Serial No	Nanocomposites	Zeta-Potential values (mV)	pH
1	SiO_2:Ni-Mg-Al-LDH (0:1)	17.8	8.8
2	SiO_2:Ni-Mg-Al-LDH (1:1)	-21.9	9.0
3	SiO_2:Ni-Mg-Cr-LDH (0:1)	16.5	8.8
4	SiO_2:Ni-Mg-Cr-LDH (1:1)	-18.8	8.7

4.3.1.8. Particle size analysis:

The particle size analysis showed that sol-gel synthesis of LDH gave particles of

higher size generally above 100 nm (**Fig. 4.9**). It was observed that oven dried SiO_2 @Ni-Mg-Al-LDH and SiO_2 @Ni-Mg-Cr-LDH highest amount of particles were found in the range of 100-1000 nm range. The increased of particle size was due to oligomerization in presence of SiO_2 .This particle size distribution was due to the aggregated dry samples.

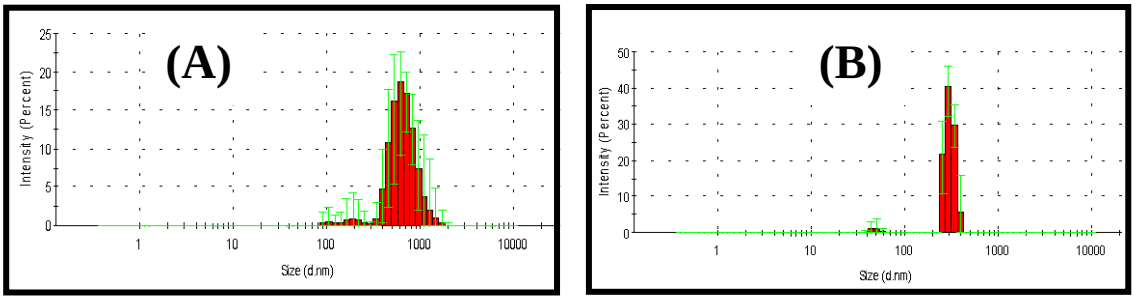

Fig. 4.9: Particle size distribution curves for SiO_2@Ni-Mg-Al-LDH (A) and SiO_2@Ni-Mg-Cr-LDH (B).

4.3.1.9. SEM and EDS analysis:

Fig. 4.10a shows SEM and EDS patterns of unsupported and SiO_2@Ni-Mg-Al (**Fig. 4.10a.A, B&E**) and Ni-Mg-Cr-LDHs (**Fig. 4.10a.C, D&F**). SEM patterns showed the presence of layered structure in both of these LDHs. Layered platelets were found to stack over another. The elemental composition were analysed by EDS analysis. It was observed that SiO_2@Ni-Mg-Al-LDH showed the weight percentage of 48.39 % C, 40.47 % O, 3.89 % Mg, 0.16 % Al, 0.48 % Si and 6.61 % Ni. On the otherhand, SiO_2@Ni-Mg-Cr-LDH showed the weight percentage of 61.76 % C, 26.14 % O, 1.22 % Mg, 0.59 % Si, 0.11 % Cr and 10.19 % Ni further confirmed the formation of ternary LDHs.

Fig. 4.10b shows the SEM patterns of calcined SiO_2@Ni-Mg-Al. SEM patterns showed the aggregation of the corrugated flaky grains during calcination due to the breakdown of LDH structure and formation of MgO like structure. EDS analysis

showed the weight percentage of 57.84% C, 27.17% O, 1.88% Mg, 0.93% Al, 3.31% Si and 8.87% Ni further confirmed the presence of Ni(Mg,Al)O/SiO_2 periclase type phases.

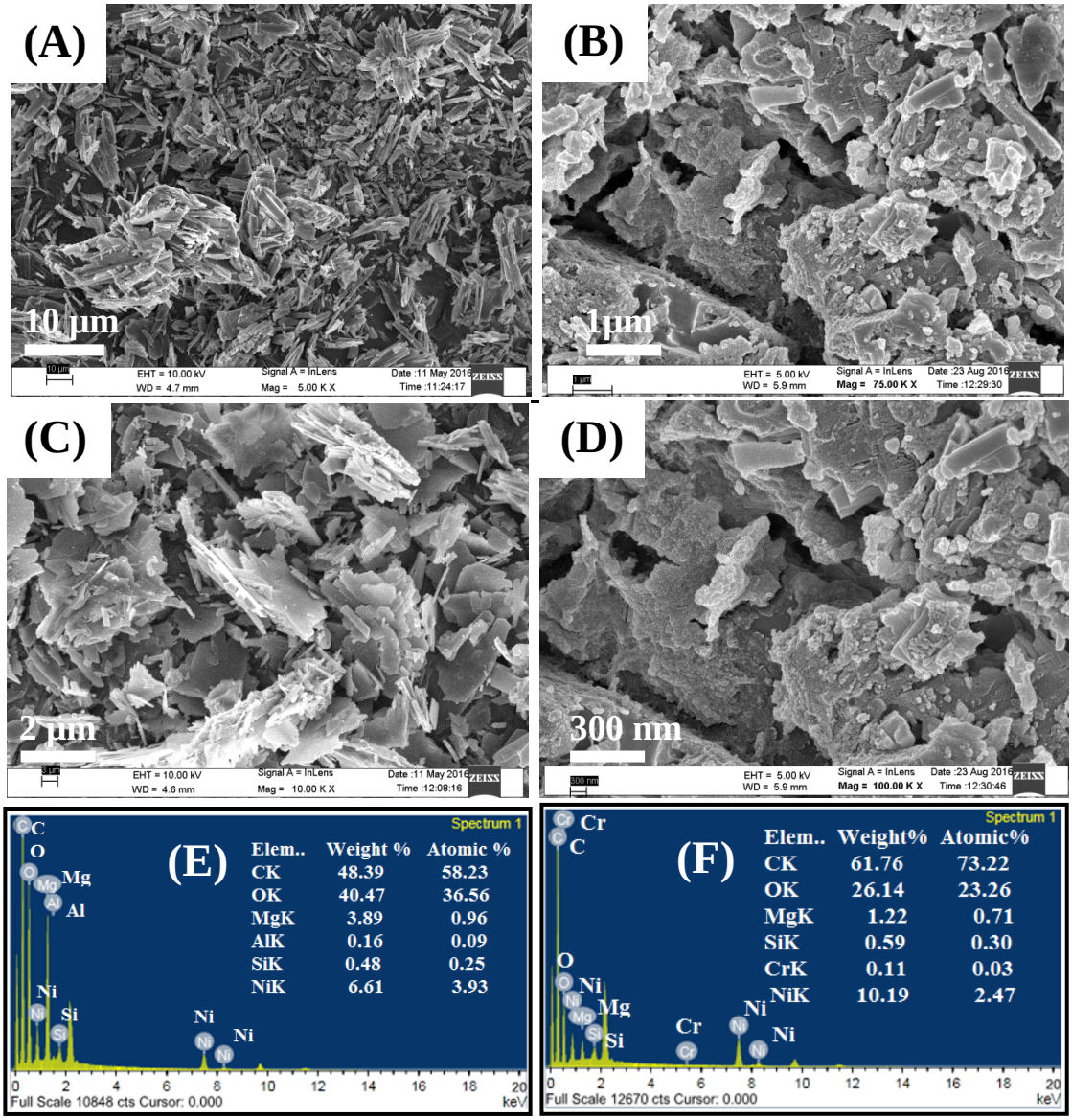

Fig. 4.10a: SEM and EDS patterns of unsupported and SiO_2@Ni-Mg-Al (A, B&E) and Ni-Mg-Cr LDHs (C,D&F).

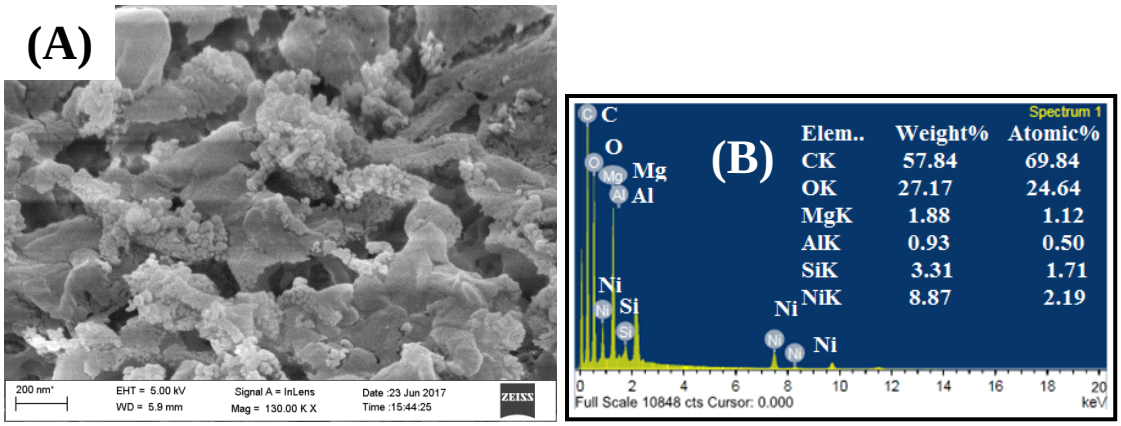

Fig. 4.10b: SEM and EDS patterns of calcined SiO_2@Ni-Mg-Al Ni-Mg-Al (A &B).

4.3.1.10. H_2-TPR analysis:

H_2-TPR analysis of the calcined products after the H_2 treatment to get the reducible sites and T_{max} of the catalysts. H_2-TPR analysis (**Fig. 4.11**) showed the high temperature reduction peak at 687 ^oC in case of CNMA-01 due to the reduction of Ni^{2+} of NiO-MgO periclase [35,42]. On the other hand, CNMA-11 showed two reduction peaks at 695 ^oC and 819^oC respectively. The peak at 695 ^oC correspond to the reduction of Ni^{2+} of NiO-MgO periclase whereas [35,42], the peak at 819 ^oC correspond to the reduction of Ni^{2+} of Mg(Ni,Al)O/SiO_2 type phases present in the catalyst. The highest reduction temperature of CNMA-11 indicating the strong interaction of Ni^{2+} with MgO periclase and (Mg,Al)O/SiO_2 which act as support for Ni dispersion [42]. These results further suggesting the better dispersibilty of Ni in case of CNMA-11 catalyst due to the presence of SiO_2 and this Ni^0 act as the active species for Catalytic partial oxidation of CH_4 in presence of N_2O.

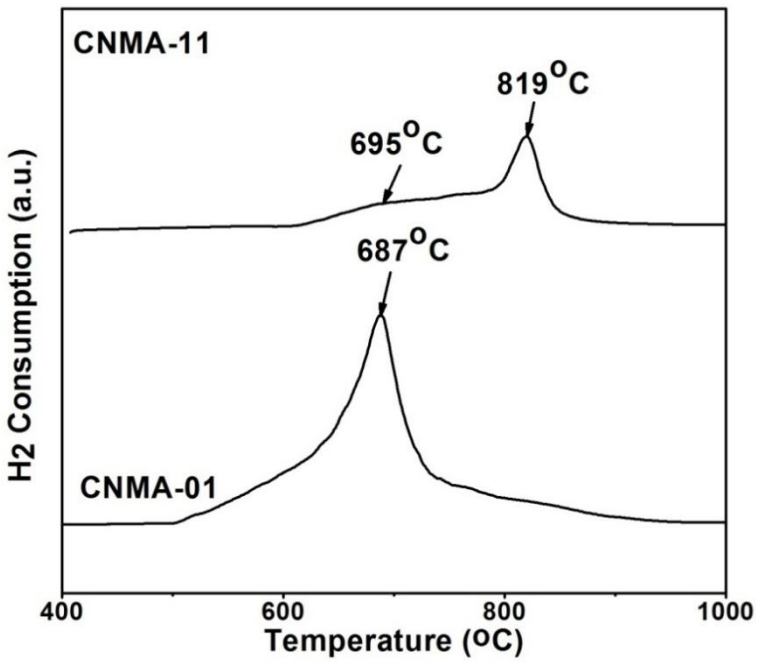

Fig. 4.11: H_2-TPR curve of calcined SiO_2@Ni-Mg-Al-LDH.

4.3.1.11. XPS analysis:

Fig. 4.12 shows the XPS pattern of the calcined SiO_2@Ni-Mg-Al-LDH after gas reaction. XPS analysis showed the presence of $Ni2p_{3/2}$ peak at binding energies of 855 eV due to Ni^{2+} species associated with NiO species before the catalytic partial oxidation reaction. On the otherhand, the binding energy of 853.2 eV due to the presence of Ni^0 species along with the satellite peak of binding energy 861.2 eV associated with the presence of Ni^{2+} as NiO-MgO periclase type phase which was also observed from XRD analysis [38, 52] which further confirmed that Ni^0 is the active site for CPO reaction. The surface Ni/(Mg+Al) atomic ratio of CNMA-01 and CNMA-11 catalysts were determined by XPS analysis and are summarized in **Table 4.3**. It was observed that with the presence of SiO_2 the surface Ni/(Mg+Al) atomic ratio increased from 0.24 to 1.35 which also increased the Ni^0 active site from 0.14 to 0.77 mmol/g of the catalyst further suggesting the presence of SiO_2 enhanced the dispersion of Ni^{2+} over NiO-MgO solid solution and also further increased the surface area [38,53].

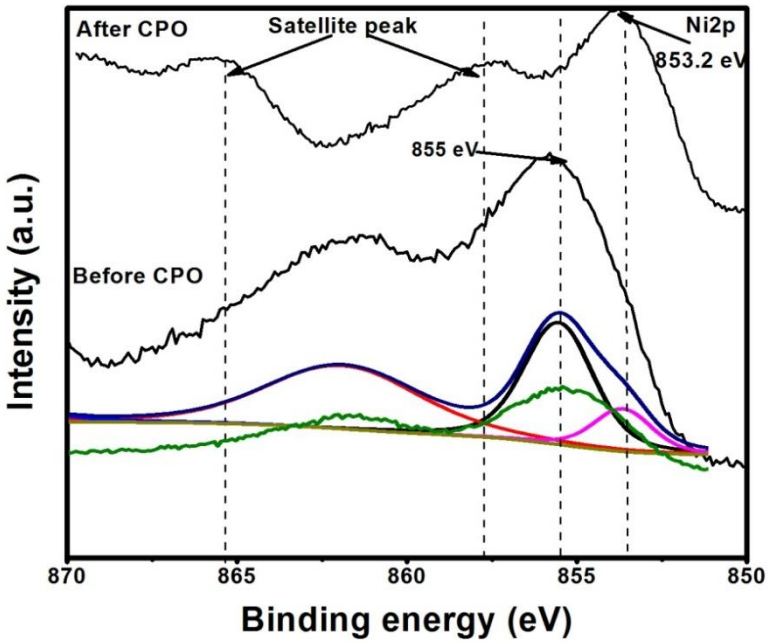

Fig. 4.12: XPS patterns of calcined SiO_2@Ni-Mg-Al-LDH.

Table 4.3: Surface element composition of Ni/Mg/Al oxide catalysts

Serial No.	Catalysts	Ni/(Mg+Al) Atomic ratio	Ni^0 (mmol/g)
1	CNMA-01	0.24	0.14
2	CNMA-11	1.35	0.77

4.3.2. Catalytic partial oxidation of CH_4 in presence of N_2O in the feed:

Catalytic partial oxidation of CH_4 by N_2O in presence of calcined SiO_2@Ni-Mg-Al was carried out at the temperature ranging from 200-500 ^oC and at GHSV of 1,542 h^{-1} (42,000 $cm^3g^{-1}h^{-1}$). Calcined SiO_2@Ni-Mg-Al and SiO_2@Ni-Mg-Cr-LDHs were designated as CNMA-01(SiO_2:LDH=0:1), CNMA-11 (SiO_2:LDH=1:1).The initial concentration of N_2O and CH_4 was maintained at 300 ppm and 100 ppm with N_2O:CH_4 mol ratio 1:1. **Fig. 4.13a.A&B** shows the percentage N_2O and CH_4 conversion in presence all these catalysts. It was observed that with the increase of percentage conversion of N_2O and CH_4 also increased. CNMA-01 showed the N_2O

conversion as 68.9 %, 74.8 %, 80.8 % and 90.4 %, CNMA-11 showed 96.7 %, 99.4 %, 99.8 % and 99.99 %.

Fig. 4.13a.B shows the percentage conversion of CH_4 in presence of all these catalysts. CNMA-01 showed 71.6 %, 80.4 %, 87.4 % and 91.2 % conversion, CNMA-11 showed 86.8 %, 97.4 %, 99.3 % and 99.99 % conversion respectively.

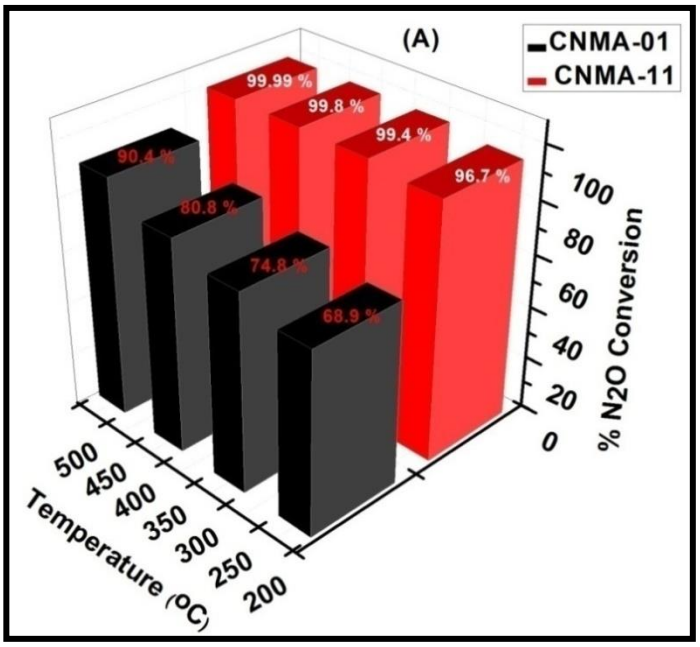

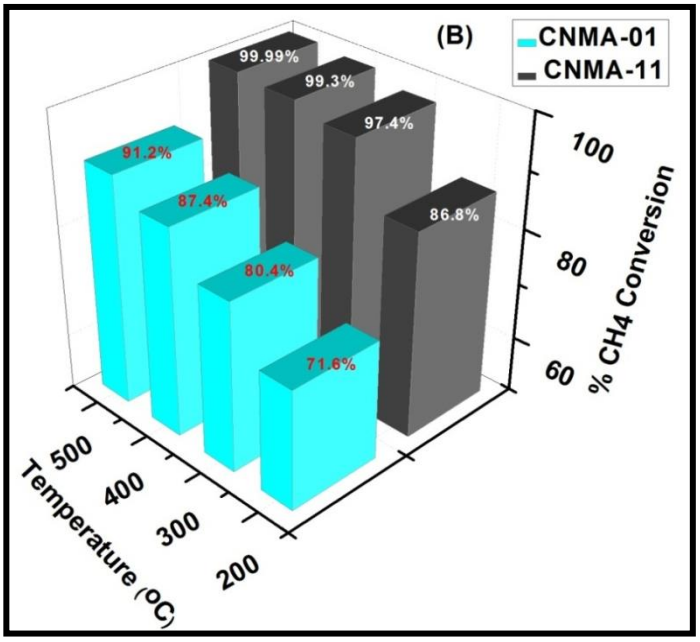

Fig. 4.13a: Percentage conversion of N_2O (A) and CH_4 (B) in presence of calcined SiO_2@Ni-Mg-Al-LDH.

Fig. 4.13b.A&B shows the percentage yield of H_2 and CO in presence of CNMA-01 and CNMA-11.With the increase of temperature from 200-500 ^oC the percentage yield of H_2 and CO increased. It was observed that CNMA-01 showed the H_2 percentage yield of 75.9 %, 82.9 %, 90.4 % and 92.5 %; CNMA-11 showed 86.8 %, 96.8 %, 99.3 % and 99.99 % yield.

On the other hand, CNMA-01 showed the percentage yield of CO about 70.2 %, 80.2 %, 88.4 % and 91.4 %; CNMA-11 showed the 84.9 %, 95.3 %, 98.7 % and 99.8 % yield. **Table 4.4** shows overall percentage conversion and percentage yield of N_2O, CH_4, H_2 and CO. The mol ratio of H_2:CO was also maintained at 2:1 in the product. The deposition of coke over the catalysts after reaction for 24 hour was analysed by TGA analysis under air atmosphere. It was observed that (**Fig. 4.13c**) CNMA-01 and CNMA-11 showed the amount of coke deposition in mg/gcat.h as 0.15 and 0.10 (**Table 4.5**) which was also confirmed from CHN analysis. CNMA-01 and CNMA-11 showed about 91.4 % and 99.99 % yield of H_2 and about 92.5 % and 99.8 % towards the yield of CO.

From the above results it was observed that the presence of SiO_2 in the catalyst plays an important rule for CPO reaction. The presence of SiO_2 led to increase of Ni dispersion in the catalyst CNMA-11 which increased the surface active site (Ni^0) of the catalyst and also negligible amount of coke deposition enhanced the selectivity towards syn-gas (H_2/CO) production (**Table 4.5**) these ternary LDHs as compared to binary LDHs as described in the **Results and Discussion Section** of **Chapter-III of PART-B**.

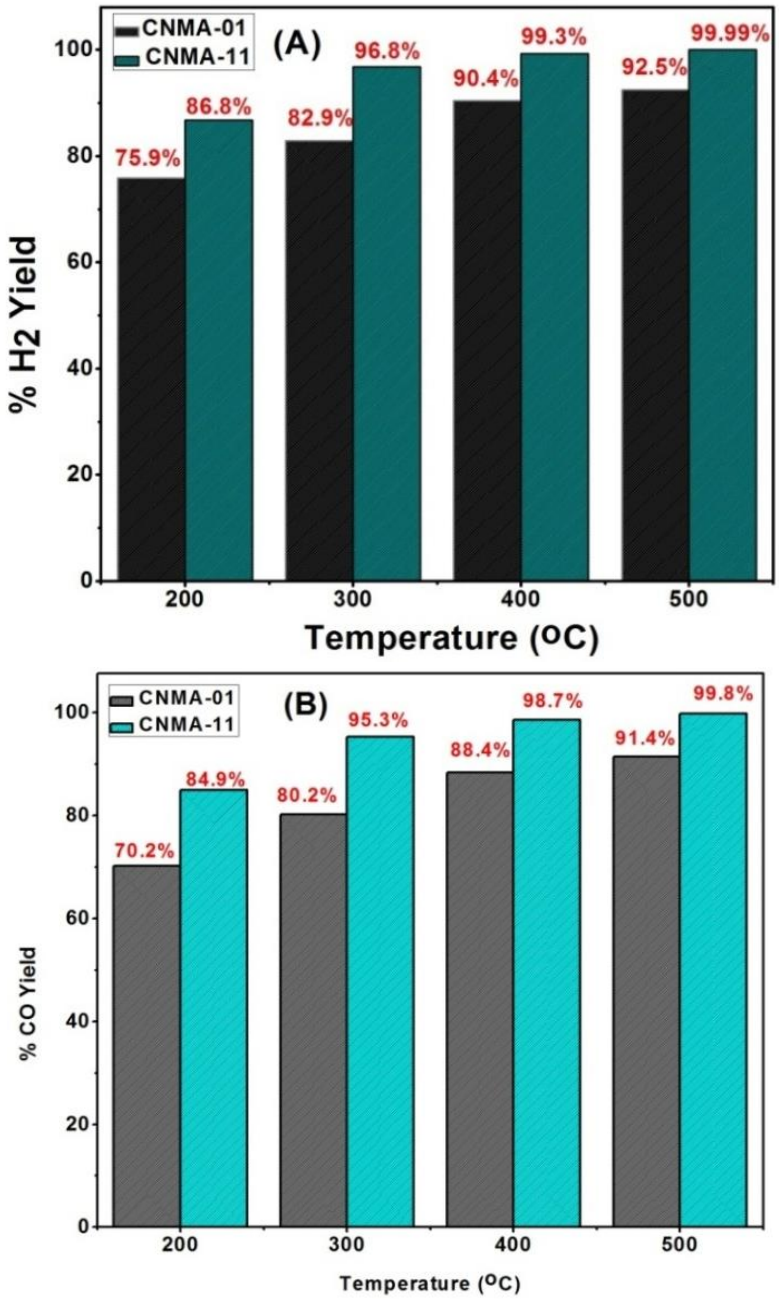

Fig. 4.13b: Percentage yield of H_2 and CO in presence of calcined SiO_2@Ni-Mg-Al-LDH (A&B).

Table 4.4: Percentage conversion and percentage yield of N_2O, CH_4, H_2 and CO in presence of both supported and unsupported ternary LDHs (Total flow rate=280 ml/min, GHSV = 1,542 h^{-1} (42,000 $cm^3g^{-1}h^{-1}$))

Type of active catalysts	(%) N_2O Conversion (Initial Concentration = 300 ppm)				(%) CH_4 Conversion (Initial Concentration = 100 ppm)				(%) H_2 Yield				(%) CO Yield			
	Temperatures (°C)															
	200	300	400	500	200	300	400	500	200	300	400	500	200	300	400	500
CNMA-01	68.9	74.8	80.8	90.4	71.6	80.4	87.4	91.2	75.9	82.9	90.4	92.5	70.2	80.2	88.4	91.4
CNMA-11	96.8	99.4	99.8	99.99	86.8	97.4	99.3	99.99	86.8	96.8	99.3	99.99	84.9	95.3	98.7	99.8

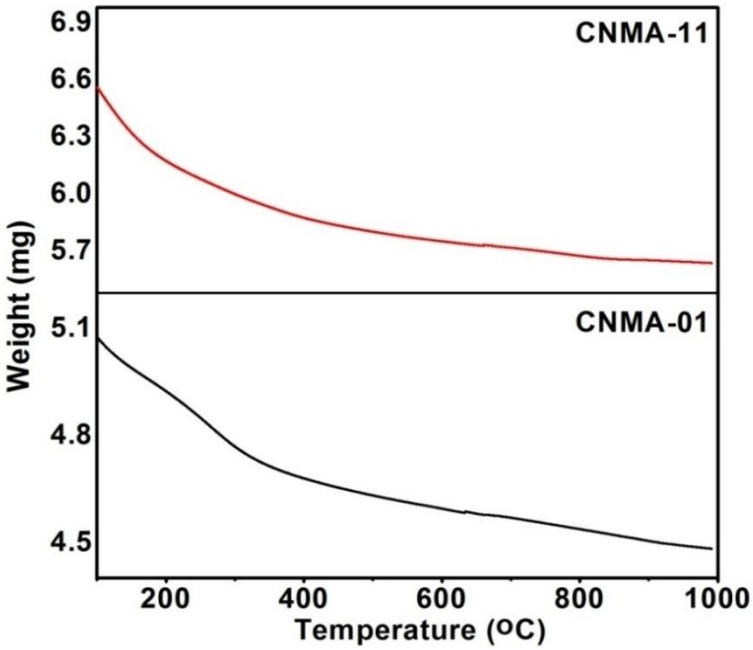

Fig. 4.13c: TGA patterns of the calcined SiO_2@Ni-Mg-Al-LDH after CPO reaction for the determination of coke.

Table 4.5: Amount of coke deposition over the calcined SiO_2@Ni-Mg-Al-LDH after CPO reaction

Types of LDHs	Coke deposition determined by TG (mg/gcat·h)
CNMA-01	0.15
CNMA-11	0.10

The mechanism involved for CPO of CH_4 in presence of N_2O over these catalyst could be explained as N_2O was first adsorbed on the oxygen vacancy sites of the catalyst and decomposed to N_2 and nascent oxygen [26,27]. This nascent oxygen was not much active to oxidize Ni^0 sites of the catalysts as XPS and H_2-TPR analysis showed the presence of Ni^{2+} in these catalyst before the CPO reaction and this nascent oxygen led to partial oxidation of CH_4 [26,27]. Thus, from the above results it was further observed that N_2O act as a promoter for partial oxidation of CH_4.

4.4. CONCLUSIONS:

Ternary LDHs of SiO_2@Ni-Mg-Al/Ni-Mg-Cr were successfully synthesized by non-aqueous sol-gel method. These were then characterized by XRD, TGA-DTG, FT-IR, Zetametry, BET surface area and pore volume analysis, SEM and EDS analysis. Mixed-metal oxides obtained after calcination of these LDHs were then used as a catalyst for catalytic partial oxidation of CH_4 in presence of N_2O. It was observed that mixed-metal oxide obtained from these LDHs possessed highest surface area values. XRD analysis showed the presence of NiO-MgO periclase type solid solution in these catalysts. The presence of SiO_2 further increased the Ni dispersion which helped in the reduction of Ni^{2+} of NiO-MgO periclase to Ni^0 as observed from H_2-TPR and XPS analysis and act as active species for Catalytic partial oxidation (CPO) of CH_4 in presence of N_2O. They showed about 91.4 % to 99.99 % H_2 and 92.5 % to 99.8 % CO yield at the temperature of 500 ^oC and CNMA-11 showed better catalytic activity as

compared to CNMA-01. N_2O present on the feed act as oxygen barrier for CPO of CH_4 as it was first decomposed to N_2 and nascent oxygen in presence of these catalyst. This nascent oxygen was not much active to oxidize Ni^0 sites of the catalysts as XPS and H_2-TPR analysis showed the presence of Ni^{2+} in these catalyst before the CPO reaction and this nascent oxygen led to partial oxidation of CH_4. Thus, these catalysts can be effectively used for the large scale industrial level synthesis gas (H_2/CO) production.

REFERENCES:

[1] B. A. Hungate, J. S. Dukes, M. R. Shaw, Y. Luo, C. B. Field. *Sci.*, **2003**, *302*, 1512-1513.

[2] J. W. Erisman, J. Galloway, S. Seitzinger, A. Bleeker, K. Butterbach-Bahl. *Cur. Opin. Environ. Sust.*, **2011**, *3*, 281-290.

[3] L. Li, J. Xu, J. Hu, Han. *Environ. Sci. Technol.*, **2014**, *48*, 5290-5297.

[4] E. A. Davidson, D. Kanter. *Environ. Res. Lett.*, **2014**, *9*, 105012.

[5] Drawing Down N_2O to Protect Climate and the Ozone Layer. AUNEP Synthesis Report. ISBN:978-92-807-3358-7.

[6] R. P. Wayne. Chemistry of the Atmosphere, 3rd ed; Oxford University Press: Oxford, U.K., **2000**,775.

[7] P. Wiesen, T. J. Wallington, W. Winiwarter, Reducing N_2O emissions from industry and fossil fuel combustion Drawing Down N_2O to Protect Climate and the Ozone Layer. A UNEP Synthesis Report; United Nations Environment Programme: Nairobi, **2013**. www.unep.org/pdf/UNEPN_2Oreport.pdf.

[8] S. J. Lee, I. S. Ryu, B. M. Kim, S. H. Moon. *Int. J. Green house Gas Control*, **2011**,*5*, 167-176.

[9] D.J. Wuebbles. *Mater. Sci.*, **2009**, *326*, 56-57.

[10] F. Kapteijn, J. R. Mirasol, J. A. Moulijn. *Appl.Catal. B: Eniron.*, **1996**, *9*, 25.

[11] S. A. Al-Sayari. *The Open Catal. J.*, **2013**, *6*,17-28.

[12] J. Weimann. Best Practice & Research Clinical Anaesthesiology, **2003**, *17*, 47-61.

[13]T.J.Blasing.Recent Greenhouse Gas Concentrations. DOI:10.3334/CDIAC/atg. 032 Updated April **2016**.

[14] N. Russo, D. Mescia, D. Fino, G. Saracco, V. Specchia. *Ind. Eng. Chem. Res.*, **2007**, *46*, 4226-4231.

[15] M. Konsolakis. *ACS Catal.*, **2015**, *5*, 6397-6421.

[16] B. C. Enger, R. Lodeng, A. Holmen. *Appl.Catal. A*, **2008**, *346*, 1-27.

[17] J. Requies,V. L. Barrio, J. F. Cambra. *Fuel*, **2008**, 87, 3223-3231.

[18] Y. B. Lin, M. R.Pillai, D. M. Bierschenk. *Catal. Lett.*, **2008**, *124*, 1-6.

[19] T. V. Choudhary,V. R. Choudhary. *Angew. Chem., Int. Ed.*, **2008**, 1828-1847.

[20] A.A. Yaremchenko, V.V. Kharton, S.A. Veniaminov, V.D. Belyaeb, V.A. Sobyanin, F.M.B. Marques. *Catal.Commun.*, **2007**, *8*, 335.

[21] H. Liander. *Trans. Faraday Soc.*, **1929**, *25*, 462-472.

[22] N.A. Khan, E.M. Kennedy, B. Z. Dlugogorski, A. A. Adesina, M. Stockenhuber. *Catal.Commun.*,**2014**, *53*, 42-46.

[23] G.I. Panov, K.A. Dubkov, E.V. Starokon. *Catal.Today*, **2006**, *117*, 148-155.

[24] B.R. Wood, J.A. Reimer, A.T. Bell, M.T. Janicke, K.C. Ott. *J. Catal.*, **2004**, *225*, 300-306.

[25] M. Peymani, S. M. Alavi, M. Rezaei. *Int. J. Hydrog. Energy*, **2016**, *41*, 6316-6325.

[26] C. M. Pedrero, B. Blerot, M.A. Soria, S.R. Gonzalez-Carrazan, P. Ruiz. *Catal.Today*, **2013**, *203*, 176-181.

[27] C. M. Pedrero, B. Blerot, M. A. Soria, S. R. Gonzalez-Carrazan, P. Ruiz. *Catal.*

Today, **2013**, *213*, 155-162.

[28] V. Rives. *Layered Double Hydroxides: Present and Future*, Nova Science Publishers, New York,**2001**.

[29] B. Xue, F. Ting, Z. Hui. *ACS Appl. Mater. Interfaces*, **2014**, *6*, 20498-20509.

[30] M. Shao, F. Ning, J. Zhao, M. Wei, D.G. Evans, X. Duan. *J. Am. Chem. Soc.*, **2012**, *134*, 1071-1077.

[31] M.A. Aramendia, V. Borau, C. Jimenez, J.M. Marinas, J.R. Ruiz, J.F. Urbano. *J.Solid State Chem.*, **2002**, *168*, 156-161.

[32] R. L. Goswamee, M. Mishra, A. K. Sarma Baruah. Mixed metal oxidic nano sheets coated monolithic catalysts useful for the decomposition of toxic N_2O and a process for the preparation thereof. Patent No. US 9616412 B2, **2017**.

[33] F. Basile, L. Basini, M. D' Amore,G. Fornasari, A. Guarinoni, D. Matteuzzi,G. Del Piero, F. Trifiro, A. Vaccari. *J. Cat.*, **1998**, *173*, 247-256.

[34] T. Shishido, M. Sukenobu, H. Morioka, M. Kondo, Y. Wang, K. Takaki, K.Takehira. *Appl.Catal. A*, **2002**, *223*, 35-42.

[35] J. Zhang, N. Zhao, W. Wei, Y. Sun. *Int. J. Hydrog. Energy*, **2010**, *35*, 11776-11786.

[36] Z. Jiang, J. Su, M.O. Jones, H. Shi, T. Xiao, P. P. Edwards. *Energy & Fuels*, **2009**, *23*, 1634-1639.

[37] A.R. Gonzalez, Y. J.O. Asencios, E. M. Assaf, J. M. Assaf. *Appl.Surf. Sci.*, **2013**, *280*, 876-887.

[38] M. Nawfal, C.Gennequin, M. Labaki, B. Nsouli, A. Aboukais, E. Abi-Aad. *Int.J. Hydrogen Energy*, **2015**, *40*, 1269-1277.

[39] F. Basile, P. Benito, G. Fornasari, D. Gazzoli, I. Pettiti, V. Rosetti, A. Vaccari. *Catal.Today*, **2009**, *142*, 78-84.

[40] J. Zhang, W. Wei, Y. Sun. *Catal. Lett.*, **2010**, *135*, 321-329; DOI:10.1007/s10562-010-0268-5.

[41] K.M. Lee, W.Y. Lee. *Catal. Lett.*, **2002**, *83*, 65-70.

[42] X. Yu, N. Wang, W. Chu, M. Liu. *Chem. Eng. J.*, **2012**, *209*, 623-632.

[43] R. Dębek, M. Motaka, D. Duraczyskac, F. Launayd, M. E. Galvez, T. Grzybeka, P. D. Costab. *Cat. Sci.Technol.*, **2016**, *00*, 1-3.

[44] R.M. Navarro, M.A. Pena, J.L.G. Fierro. *Chem. Rev.*, **2007**, *107*, 3952.

[45] J. Livage. *New J. Chem*., **2001**, *25*, 1.

[46] P. Saikia, A. Gautam, R. L. Goswamee. *RSC Adv*., **2016**, *6*, 112092-112102.

[47] A.C.W. Koh, L. Chen, W.K. Leong, B.F.G. Johnson, T. Khimyak, J. Lin. *Int. J. Hydrog.Energy*, **2007**, *32*, 725-730.

[48] J.J. Zhu, J.G. van Ommen, L. Lefferts. *Catal. Today*, **2006**, *112*, 82-85.

[49] F. Arena, F. Frusteri, A. Parrnaliana, L. Plyasova, A. N. Shmakov. *J. Chem. Soc., Faraday Trans.*, **1996**, *92(3)*, 469-471.

[50] R. S. Drago, K. Jurczyk, N. Kob, A. Bhattacharyya, J. Masin. *Catal. Lett.*, **1998**, *51*, 177-181.

[51] T. Zhang, Q. Li, H. Xiao, H. Lu, Y. Zhou. *Ind. Eng. Chem. Res.*, **2012**, 11490-11498.

[52] M.C. Biesinger, B. P. Payne, Leo W. M. Lau, A. Gerson, Roger St. C. Smart. *Surf.Inter. Anal*. **2009**, *41*, 324-332.

[53] W.S.Xia,Y.H. Hou, G. Chang, W. Z. Weng, G. B. Han, H. L. Wan. *Int. J. Hydrog. Energy*, **2012**,*37*, 8343-8353.

CHAPTER-V

SYNTHESIS OF MIXED-METAL ACAC OF Cu-Cr TO PREPARE THIN FILM OF MIXED-METAL NANO-OXIDE FILMS BY MOCVD (METAL-ORGANIC CHEMICAL VAPOUR DEPOSITION) AND THEIR APPLICATION FOR N_2O DECOMPOSITION

❖ This Chapter has been published in ***Materials Today Chemistry, 7(2018) 40-52***.

GRAPHICAL ABSTRACT

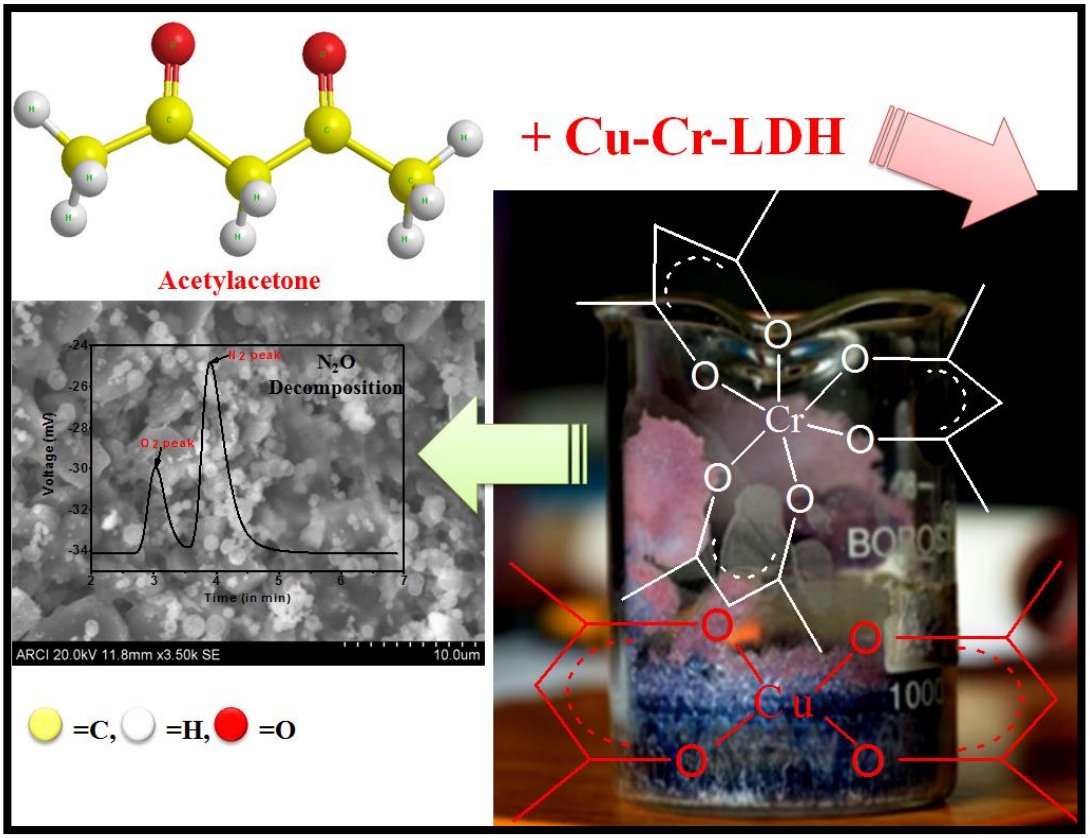

Synthesis of Cu-Cr diketo, sublimable, eutectic composite complex, rod crystals from Cu-Cr-LDH by the interaction of acetylacetone as suitable MOCVD precursor of $CuCr_2O_4$ catalysts for N_2O decomposition

ABSTRACT

Metal-acteylacetonates are important sublimable metal-organic precursors for metal-oxide thin film formation over solid preforms by MOCVD (Metal Organic Chemical Vapour Deposition) technique. Mixed-metal-acetylacetonates (MMAA) are suitable starting materials for mixed metal nano-oxidic thin film formation through such facile routes. Layered Double Hydroxides (LDH) of suitable metal ion combination can perform as appropriate starting base for neutralisation by enol form of 2,4-pentanedione or acteylacetonate tautomer ligands to obtain such MMAA. In this paper synthesis of composite crystals of Cu (II)/Cr (III) acetylacetonates (CCAA) is reported by the reaction of Cu-Cr LDH with acetylacetone. The products were characterized by various different techniques. The surface area and pore volume analysis of the crystals showed the formation of nanopores in the compound. TEM analysis confirmed that the inner core of the nanoporous crystals of $Cu(acac)_2$ was covered by coating of poorly crystallised $Cr(acac)_3$ and they together form the composite crystals, and they together form the composite crystals. Due to eutectic mixture formation the melting point of CCAA lies in between the melting points of individual components $Cu(acac)_2$ and $Cr(acac)_3$ and shows sublimability, a property important for the formation of MOCVD films. The composite was used for $CuCr_2O_4$ spinel mixed oxide films formation over solid ceramic honeycomb monolithic substrates. Application prospects of the route in the field of catalysis is high as it can directly combine the benefits of mixed metal oxide catalysis and structured supports without the involvement of a third component. In this work the performance of such a catalytic device has been tested for low temperature decomposition of high Global Warming Potential (GWP) gas N_2O to N_2 and O_2

5.1. INTRODUCTION:

The synthesis of mixed-metal organic complexes has been a subject of intensive research [1-10]. Many of these compounds have applications in the fields of ion exchange, adsorption and catalysis [11-13]. Also, some of them find use as precursor for the thin film formation by MOCVD technique [1,14-17]. Complexes of Zn (II)/Cu (II), Al (III)/Cr (III), Co (II)/Ni (II) with acetylacetonate and cubane ligands have been reported for such applications [1, 14, 18]. Due to their sublimability at low temperature solid solutions of metal acetylacetonates could be employed for the preparation of thin films [1,19-23]. These oxides form an interesting set of semiconductors with electronic and optical properties variable with the variation of their compositions [1,18].

Structurally, acetylacetone ($C_5H_8O_2$, 2,4-pentandione), is a bidentate ligand that chelates to metal atoms through two oxygen atoms in a six-membered ring [1,24-27]. In its structure there exists a keto-enol tautomerism in the carbon atom at the α-position. Factors like the solvent polarity, the nature of the substituent groups on the α and β-positions, temperature of the medium, presence of any other reactive compound in the medium can affect the tautomerism immensely. In low polarity solvents like CCl_4 the amount of enol form is higher whereas in the solvents like acetonitrile the keto form is high. The enolic protons can be removed by weak bases e.g. during reaction with metal hydroxides acetylacetone or similar diketones loses proton in the enolic –OH group [28]. In the process it forms with the common metal ions of Cu, Zn, Cr, Ni, Sc, V acetylacetonate or similar complexes [29-33]. Thus a physical mixture of such hydroxides on reaction with acetylacetonates would give mixture of unary metal acetylacetonates in the same flask.

On the other hand, synthesis and characterizations of single precursor binary metal acetylacetonate complexes of two M(II) ions and two M(III) ions by solution

chemistry routes are reported [1,2,14,18]. Rooydell *et al*.[1] reported the synthesis of bis acetylacetonate of Zn(II)/Cu(II) by a synthetic method using $Zn(acac)_2$ and $Cu(acac)_2$ in Ethanol-H_2O mixture. Gairola *et al*.[2] have reported the synthesis of tris acetylacetonate of Al (III)/Cr (III) by co-synthesis method. The syntheses of a single precursor of bis and tris mixed-metal acetylacetonates of M (II)/M (III) ions are not available in the literature. With varied prospects of application from catalysis to electronics, formation of such complexes is an interesting point to look for.

One possible way of exploring formation of such single precursor type binary mixed metal acetylacetonates is to start with well known layered double hydroxides as hydroxides for neutralising enolic acids of acetylacetone. The main advantage of such a method would be starting with a source where both bivalent and trivalent metal ions are already in the same hydroxidic nanosheet in the form of a single compound.

Layered double hydroxides (LDHs) are a class of compounds which can be represented by the general formula $[M_{1-x}^{2+}M_x^{3+}(OH)_2]^{x+}[A_{x/n}]^{n-}.mH_2O$ and they belong to highly ordered two-dimensional layered materials [34-37] where, different M^{2+} and M^{3+} metal cations, are uniformly distributed. Various well established methods are there for the synthesis of LDH [38-42]. Based upon their ionic radii difference the uniformly distributed metal ions in the unit cell level are either orderly or statistically arranged in the main hydroxidic sheets. Orderly arrangement of metal ions leads to the formation of a hydrocalumite like supercell where for every two bivalent ion one trivalent ion is present in a regular distribution. The stoichiometric shortage of hydroxides in the main sheet causes generation of positive charge over the main hydroxidic sheet which are compensated by various charge-compensating anions (A^{n-}) by occupying the interlayer spaces. These inter layers spaces also can accommodate reactant molecules to carry out reactions from its constrained space ultimately

functioning as some nanoreactors [43,44]. However, one chronic problem in introducing newer reactant molecules in the interlayers is the common presence of stereochemically favoured unexchangable CO_3^{2-} ions, which arises mainly due to very strong absorption of CO_2 from the atmosphere during their synthesis in alkaline pH. Yet, some of the LDHs like Cu-Cr-LDH can be synthesized by oxide-salt hydrolysis method [45] at acidic pH where ingress of CO_2 into the interlayers can be avoided, e.g. the inter layer species becomes Cl^- ion when $CrCl_3.6H_2O$ is taken as hydrolysing salt. Apart from that the Cu and Cr ions are distributed in this LDH in a super-cell arrangement as stated above [46,47]. Also, Cu-Cr LDH possesses a slightly different short range structure from other LDHs due to Jahn Teller distortion of $Cu^{2+}(d^9)$ ion of $Cu(OH)_6$ octahedra component [48,49] and therefore is more susceptible to chemical modification [50].

In this chapter, because of this chemical and structural uniqueness Cu-Cr-LDH was used for the synthesis of mixed-metal acac by acid-base reaction as highlighted above. It was observed these factors leads to complete destruction of LDH layered structure forming a sublimable composition which can be casted as thin film at relatively low temperature. Catalyst composition of Cu and Cr together are known for reactions like ethanol dehydrogenation, for the dehydrogenation of isoamyl alcohol to isovaleraldehyde [51,52]. Similarly, thin film of Cu-Cr LDH based composition also act as photocatalysts for reduction of organic pollutant [53-55].

The reported mixed metal β-diketonates of the present work if sublimed for the thin film formation by MOCVD technique [56] over ceramic substrates like honeycomb monoliths [57,58] or asymmetric membranes suitable multifunctional catalytic membrane reactors could be designed and prepared for environmental applications. As far as our knowledge goes no report has been so far made on the interaction of LDH

with diketones with such an application perspective in the foresight. On the otherhand, the novelity of the present work is the formation of eutectic composite crystals of Cu(II)/Cr(III) acetylacetonates from the interaction of Cu-Cr-LDH with acetylacetone. Eutectics have many applications in pharmaceuticals and materials field [59-61]. As reported by S. Cherukuvada *et al*.[59] eutectic have heterogeneous ensembled nature. The eutectic formation by Cu(II)/Cr(III) acetylacetonate crystals helped in the deposition of mixed metal oxide thin film of $CuCr_2O_4$ spinel by MOCVD technique which have many prospective applications as catalyst both in the organic reactions as well as in the clean energy production and emission control [62]. Several researchers reported the use of $CuCr_2O_4$ as a catalyst for the abatement of the green house gases. G.Comino *et al*.[63] reported the CH_4 combustion over $CuCr_2O_4$ catalyst, G. Pantaleo *et al*.[64] reported the CO oxidation. Similarly, S. Stegenga *et al*.[65] reported the NO reduction over $CuCr_2O_4$ catalyst. They also reported that $CuCr_2O_4$ based converters are superior than any other precious metal based devices. In this chapter we are reporting the use of $CuCr_2O_4$ thin film prepared by MOCVD of Cu (II)/Cr (III) acetylacetonates as a catalyst for N_2O decomposition. So far the use of $CuCr_2O_4$ thin film coated over structured honey comb monolithic catalyst for N_2O decomposition has not been reported yet.

5.2. EXPERIMENTAL SECTION:

This **Chapter** describes the synthesis of Mixed-Metal AcAc of Cu-Cr by the reaction of Cu-Cr-LDH obtained through oxide hydrolysis method with Acetylacetone (2,4-pentanedione) through acid-base neutralisation reaction. The product obtained was then characterized by PXRD, TGA-DTG, FT-IR, XPS, BET surface area and pore volume analysis, SEM, TEM and EDS analysis, XRD Single crystal analysis. This

Chapter also describes the coating of composite crystals of Cu-Cr-AcAc obtained from the reaction of Cu-Cr-LDH and Acetylacetone by MOCVD technique over solid preforms. The thin film coating was then further characterized by XRD, SEM, EDS and AFM analysis etc.

5.2.1. Synthesis:

All the chemicals used were of analytical grade, purchased from reputed suppliers like Merck, Himedia, TCI etc.

5.2.1.1. Synthesis of Cu-Cr-LDH by oxide hydrolysis method (CCL):

4 g of CuO was taken in a beaker. About 20 ml of water was added to make a paste. 1M solution of $CrCl_3.6H_2O$ was added drop wise to the paste with constant stirring. The pH of the solution was maintained at ~ 4. After addition of 20 ml of $CrCl_3.6H_2O$ the reaction mixture was placed over a magnetic stirrer and the reaction was continued for 6 hours. The temperature of the system was maintained below 40 ^oC. The supernatant liquid was decanted off after the completion of the reaction. The product washed off with hot water and dried at room temperature [45] and kept for chemical and physical chracterizations. On chemical analysis of thoroughly washed product the Cu:Cr ratio was found as 2:1.

5.2.1.2. Synthesis of Cu (II)/Cr (III) AcAc mixed metal complex (CCAA) from Cu-Cr LDH:

3g of prepared Cu-Cr-LDH (CCL) was taken in a 100 ml reactor and 72 mmol acetylacetone (7.3 ml) was added to it. For this reaction the ratio of Cu:Cr:AcAc was maintained at 2:1:6.The mixture was stirred with magnetic stirrer up to 2-3 hours at room temperature. The pH of the mixture was maintained at 4-5. The product was washed with water and filtered through Whatman- 42 filter paper. After that the product was recrystallized from different solvents such as methanol (CH_3OH), ethanol

(EtOH), acetone (CH_3COCH_3) and chloroform ($CHCl_3$). The needle like crystals were formed only after the recrystallization from $CHCl_3$ (**Fig. 5.1**).

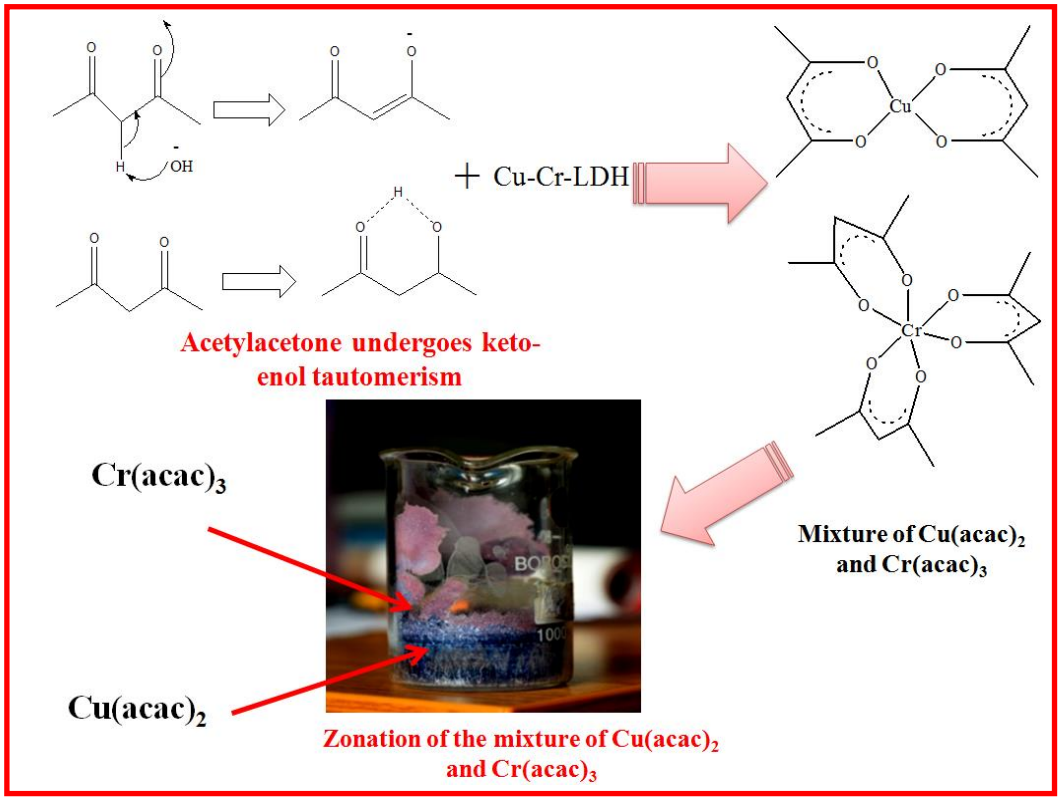

Fig. 5.1: Schematic diagram for the synthesis of mixture of $Cu(acac)_2$ and $Cr(acac)_3$.

5.2.2. Characterizations:

Powder XRD analysis were carried out using Cu k_α radiation (wavelength of ≈1.54 Å) at 40 mA and 40 kV X-ray generator current setting with a step size of 0.2°2θ min^{-1} in a Rigaku Ultima IV powder X-ray diffractometer.

The chemical composition was identified by using an energy-dispersive X-ray spectroscopy (EDX) detector on a scanning electron microscope (SU1510, Hitachi) operated at an accelerating voltage of 30 kV. The Transmission Electron Microscopy (TEM) images were recorded on a JEOL JEM-2011 electron microscope operated at an accelerating voltage of 200 kV.

X-ray Photoelectron Spectroscopy (XPS) measurements were carried out in an

ESCALAB 250 Thermo Electron equipment having monochromatic Al k_α X-ray source of energy 1486.6 eV. The photoelectron spectra were calibrated with a reference of C-C bond energy of carbon C 1s at 284.8 eV.

Fourier Transform Infrared (FT-IR) spectra of the prepared samples were recorded in spectrophotometer (Perkin-Elmer 2000 System) in 4,000-400 cm^{-1} range at a spectral resolution of 4 cm^{-1} using KBr pellets. The metal ion concentration of metal acetylacetonate complexes were analysed by using AAS spectrometry (model Analyst 100 Perkin Elmer). The mass spectrometry of Cu(II)/Cr(III)AcAc were carried out in a Trace DSQ GC-MS spectrometer.

The thermogravimetric measurements were carried out in a simultaneous TG-DTA analyzer(model Q-600, M/S TA Instruments) using α -Al_2O_3 as reference. Samples weighing about 8.0 mg were heated from 30 to 750 ^oC at various heating rates β viz. 10 ^oC/min in an Argon atmosphere under non-isothermal condition. The Argon flow rate was 100 ml/min.

The single crystal XRD data of CCAA were collected by using a "Bruker Smart" diffractometer equipped with a CCD area-detector and Mo kα radiation (λ = 0.71073 Å) at 296(2) K. The data are refined by using SHELXL-97. The final R_1 = 0.0313 and wR_2 = 0.1177 with the goodness of fit on F^2 was 2.604. For analysing the details about the crystallographic data helps from Cambridge Crystallo-graphic Data Centre software was taken.

The surface topography and root mean square (RMS) roughness of the deposited thin film were measured by atomic force microscope (AFM, M/S Nanomagnetics Instruments,Turkey).

5.2.3. Synthesis of Cu(II)/Cr(III) Oxide Thin Films over Solid Preforms:

Metal Organic Chemical Vapour Deposition (MOCVD) of CCAA over honeycomb

preforms (obtained from Advanced Research Center for Inorganics of the Department of Science and Technology Govt. of India, Hyderabad, under a mutual collaboration agreement) and glass substrate were carried out by Thermal Vacuum Deposition equipment of model HVT-2015 with voltage of 80 volt and chamber pressure 10^{-4} mbar. Before coating about 6-7 nos of honeycomb monoliths were taken and these were cleaned by boiling with oxalic acid followed by continuous washing with distilled water and then dried in an oven at 50 ^{o}C whereas, the glass substrate were cleaned with acetone. The honeycombs had 360 cells per square inch and a 3.2 cm diameter. The dimension of glass substrate was 1.9cm×1.4cm (length×breadth). The time of coating per honeycomb was about 30 min. Thickness of the thin film deposited was measured during the evaporation of molecules from source to target under vacuum conditions at a base pressure of 5×10^{-5} Torr with a thickness monitor (model No. DTM-10, Roorkee, India). During the process surrounding temperature was maintained at 27 ^{o}C and the input voltage at 64 volt.

5.2.4. Catalytic property study:

Catalytic performance study was carried out by packing these coated honeycombs in a stainless-steel (SS) cylindrical catalytic converter with 22 cm long catalyst bed and inner diameter 0.6 cm respectively at temperature 250 ^{o}C and at constant Gas Hourly Space Velocity (GHSV) of 542.4 h^{-1} (300,000 $cm^3g^{-1}h^{-1}$). The honeycomb like Cordierite ($MgO-Al_2O_3-SiO_2$) substrates had 360 cells per square inch and a 3.2 cm diameter (from ARCI Hyderabad, India). The total weight of the catalyst covered as washcoat over honeycombs was about 0.02g and kept at the middle of the reactor. The SS tube was placed inside a cylindrical furnace. The flow rate of the gas was controlled by different types of mass flow meter obtained from M/S Gilmont, USA under atmospheric pressure. Before the catalytic reactions the catalysts were activated

in argon atmosphere (100 ml/min flow rate) at temperature of 250 ^{o}C for 2 hours. The N_2O concentration was kept as 500 ppm (11.36 mmol). The fall in the concentration of N_2O and consequent increase of N_2 and O_2 in the product stream was measured by Porapak Q and Molsieve 5A as separating column with Thermal Conductivity Detector (TCD) and Electron Capture Detector (ECD). The flow rate of Argon:(N_2O+Argon) was maintained at (100:100 ml/min). The results were estimated with standard calibration gas mixtures supplied by M/S Span Gas Mumbai, India and standard Gas Chromatographic software IRIS-32 from M/S Thermo-Fischer India.

The percentage conversion (X) of N_2O and percentage yield (Y) of O_2 and N_2 were calculated by the following equation [66] –

$$X_{N_2O} = \frac{[N_2O]_{in} - [N_2O]_{out}}{[N_2O]_{in}} \times 100 \quad (5.1)$$

$$Y_{O_2} = \frac{[O_2]_{out}}{[N_2O]_{in}} \times 100 \quad (5.2)$$

$$Y_{N_2} = \frac{[N_2]_{out}}{[N_2O]_{in}} \times 100 \quad (5.3)$$

5.3. RESULTS AND DISCUSSION:

It was reported earlier that both $Cu(OH)_2$ and $Cr(OH)_3$ reacts with acetylacetones through an acid-base neutralisation reaction forming their respective metal diketo complexes [33]. It is made possible as 2,4-pentanedione or acetylacetone undergoes keto-enol tautomerism and forms the acidic –OH group in its enol form. Similar reaction of acetylacetone was expected with CCL also at room temperature through acid-base neutralization reaction resulting in the formation of a mixture of Cu(II)/Cr(III)AcAc. **Fig. 5.1** in the **Experimental Section** shows the zonation of the separation of $Cu(acac)_2$ and $Cr(acac)_3$ bluish and pink zones respectively in the glass

beaker where the crystals were allowed to dry after dissolving in chloroform ($CHCl_3$). After further recrystallization of the segregated mixture of Cu(II)/Cr(III)AcAc from chloroform new needle like bluish crystals are obtained. Similar behaviour of formation of recrystallised needle like crystals is not observed in individual products of $Cr(acac)_3$ obtained from $Cr(OH)_3$ as reported by Choudhary *et al*.[33] The crystals of $Cu(acac)_2$ obtained from $Cu(OH)_2$ have shown some needle like crystal formation behaviour on recrystallisation however their needles were shorter than crystals obtained from the reaction of Cu-Cr-LDH and acetylacetone. Thus, it may be stated that presence of second metal acetylacetonate of Cr(III) helps in the formation of needle like crystals although Cr(III) individually does not form crystals of such a shape. Similar, formation of needle like crystals in a mixed system of $Cu(acac)_2$ and $Zn(acac)_2$ has also been reported [1]. It is thus most likely that Brucite sheet like structure of parent bivalent $Cu(OH)_2$ is closely linked to the reasons for the formation of needle like crystals of mixed metal acetylacetonates. From a generalised point of view it may be stated that one of the reasons for the needle formation would be curling of the newly formed $Cu(acac)_2$ sheets with flexible metal-carbon and carbon-carbon back bones on drying of rapidly evaporating $CHCl_3$ solvent molecules, a phenomenon often observed during rapid drying of wet surfaces like paper inside an electrically heated air oven at 50-60 ^{o}C. On the other hand, it was also observed that the larger needle like crystals were formed only in presence $CHCl_3$ not in other solvents such as methanol, ethanol, acetone etc. This is due to the lower polarity of $CHCl_3$ which can not interact strongly to undergo solvation with the $Cu(acac)_2$ and $Cr(acac)_3$ of the Cu(II)/Cr(III) AcAc mixture through H-bonding as other solvent can bind through the same and hence easily evaporates to give needle like crystals [67,68].

5.3.1. Characterization of CCAA:

5.3.1.1. FT-IR Analysis:

The IR spectra of CCL, CCAA, $Cu(acac)_2$ and $Cr(acac)_3$ in the range of 4000-400 cm^{-1} are shown in **Fig. 5.2**. The FT-IR spectra showed that in case of CCL the peaks at 3745 cm^{-1} and 3832 cm^{-1} were due to the -OH stretching mode of the inter-layer hydroxyl and interlayer water molecules [69]. The sharp bending mode of water molecules at 1614 -1625 cm^{-1} in Cu-Cr-LDH was also seen in the pattern [69]. However, on examination of IR pattern of CCAA with CCL such presence of –OH group and water molecules were not observed in CCAA which indicated that the hydroxides of parent LDH had reacted with enolic acids of acetylacetone. In the FT-IR spectra of CCAA the peaks at 448, 608, 661, 774, 931, 1019, 1278, 1963, 2921, 2996 cm^{-1} present in $Cu(acac)_2$ were observed indicating the possibility of existence of $Cu(acac)_2$ molecule or similar structural component in CCAA also [1]. Almost similar behaviour of prominent IR peaks of $Cr(acac)_3$ was also seen in CCAA indicating the co-existence of $Cr(acac)_3$ components in CCAA crystals also. The assignment of some important peaks of $Cu(acac)_2$, $Cr(acac)_3$ and CCAA are shown in **Table 5.1**. The νC=O mode appeared at 1614 cm^{-1} for $Cr(acac)_3$, $Cu(acac)_2$ and CCAA respectively [1,70]. The peaks in the region 1250-1600 cm^{-1} correspond to the C-O-M bonds which caused by delocalized electrons in the C-O-M bonds. The peaks between 1000-400 cm^{-1} correspond to the stretching vibration as well as bending vibrational modes of the C-CH_3, M-O and C-H groups. The Cu-O and Cr-O bond appeared at 448 cm^{-1}, 447 cm^{-1} for $Cu(acac)_2$ and $Cr(acac)_3$ respectively whereas Cu-O and Cr-O appear at 446 cm^{-1} for CCAA. It appeared that the peaks from CCAA were contributed by both Cu and Cr with a slight shift relative to $Cu(acac)_2$, $Cr(acac)_3$. The peaks at 661 cm^{-1} corresponding ring defining +ν (M-L) also appear in CCAA [1].

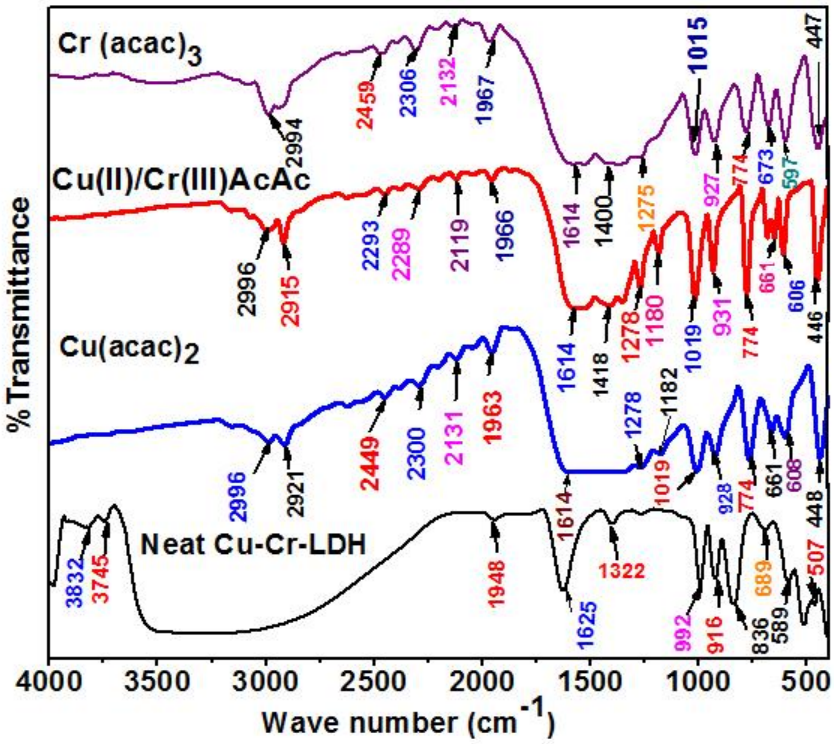

Fig. 5.2: FT-IR spectra of CCAA, Cu-Cr-LDH, Cu(acac)$_2$ and Cr(acac)$_3$

Table 5.1: Assignment of the peaks in the FT-IR spectra of Cu(acac)$_2$,Cr(acac)$_3$,and CCAA

Assignment	Cr(acac)$_3$	Cu(acac)$_2$	CCAA
ν(M-O)ring def. [1,70]	446	446	448
Ring def. +ν (M-L)	673	661	661
ν(C-CH)+ ν(C=O)	927	927	930
ν(C-C)+ ν(C=CH$_3$)	1275	1278	1278
ν(C=O)	1614	1614	1614

5.3.1.1.2. XRD analysis:

As IR analysis showed presence of peaks corresponding to both Cu(acac)$_2$ and Cr(acac)$_3$ the XRD analysis of the product of CCL and acetylacetone was carried out from the repeatedly crystallised samples obtained after dissolving the same in CHCl$_3$. The XRD patterns (**Fig. 5.3A**) shows formation of some new phases whose powder XRD pattern was different from the parent LDH for example the high basal peak of the

parent LDH at 7.77 Å corresponding to 11.38° 2Θ disappear and a new peak at 7.4 Å corresponding to 11.94° 2Θ appears. At first sight this may appear to be a 00l type high intensity basal peak of the parent LDH with a changed interlayer composition. However, absence of corresponding *00l* peaks with proportionately reduced intensities rule out such possibility of existence of LDH with modified interlayer composition. Apart from this from the solubility point also existence of LDH phase was ruled out as LDH is not soluble in $CHCl_3$ or ethanol. Thus, the highest intensity peak at 7.4 Å may correspond to $Cu(acac)_2$ with hkl reflection of (101) the same was calculated using powder data interpretational software POWD. The XRD pattern of CCAA crystals showed the presence of both $Cu(acac)_2$ and $Cr(acac)_3$ phases with hkl values (-101) (d=7.61Å) , (200) (d=5.66Å), (002) (d=5.14Å) for $Cu(acac)_2$ (**JCPDS Card No.-00-010-0736**) and (-204) (d=3.76Å), (121) (d=3.54Å) and (023) (d=3.10 Å) for $Cr(acac)_3$ (**JCPDS Card No.-00-018-1505**) of lower intensity. Therefore, from XRD pattern it can be concluded that after recrystallization $Cr(acac)_3$ and $Cu(acac)_2$ were not separated and form a composite crystals.

In order to further clarify the nature of the components in the solid product it was again dissolved in chloroform and the progress of TLC spots of the compound in ethylacetate-hexane mixture (4:1) was monitored along with standard $Cu(acac)_2$ and $Cr(acac)_3$ as reference spots side by side. It was observed that Cu-Cr-LDH derived composite product separates to two spots with R_f values equal to $Cu(acac)_2$ and $Cr(acac)_3$ respectively as shown in **Fig. 5.4A&B**. No third spot corresponding to the existence of a third phase was identified in the TLC plate. Changing the polarity of the mobile phase could not provide evidence of existence of more than two compounds in the solution stage further indicating the formation of composite crystals.

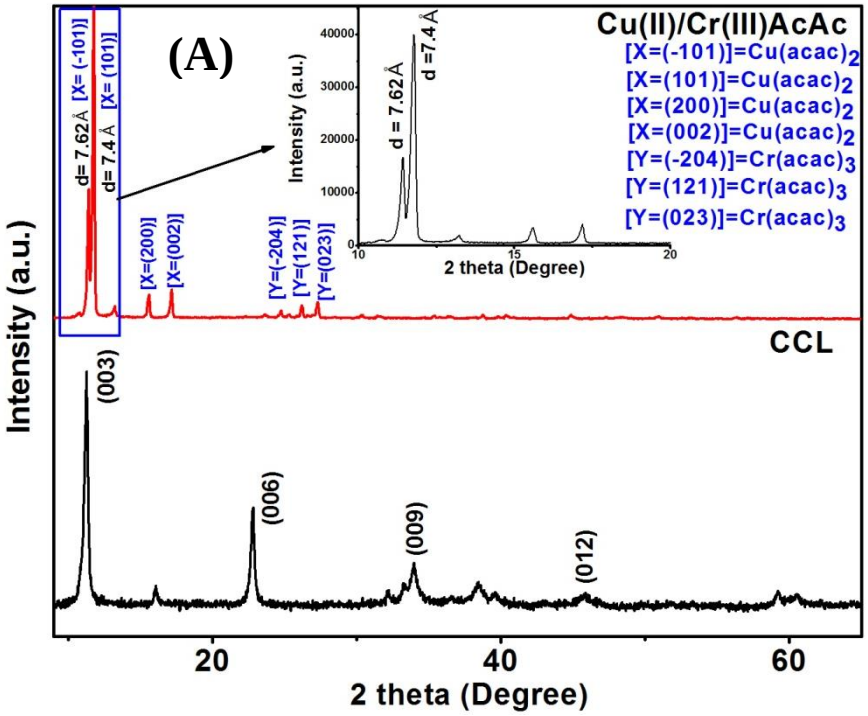

Fig. 5.3: XRD patterns of Cu-Cr-LDH (CCL) and CCAA.

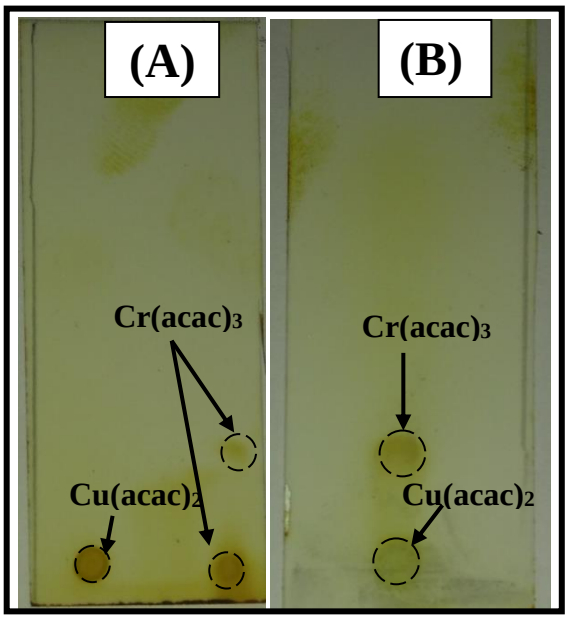

Fig. 5.4: Photograph of TLC spots- (A) standard $Cu(acac)_2$ and $Cr(acac)_3$; (B) CCAA crystals.

5.3.1.1.3. Mass spectrometric analysis:

One of the important properties of metal diketo complexes is their sublimability, literature report confirms both $Cu(acac)_2$ and $Cr(acac)_3$ as sublimable compounds.

Sublimability of the compounds makes them suitable for characterisation by mass spectroscopic analysis. Accordingly, mass spectrometric measurements were carried out with recrystallised CCAA which shows that (**Fig. 5.5**) the fragments of $Cu(acac)_2$ and $Cr(acac)_3$ were present in CCAA with mass/charge ratios (m/z) of 261 and 349 respectively. In case of CCAA, the fragments of $Cu(acac)_2$ and $Cr(acac)_3$ reduced to m/z values of 161.9 and 249 by removal of one acetylacetonate ligand from $Cu(acac)_2$ and $Cr(acac)_3$ followed by 63 m/z and 51 m/z for Cu and Cr corresponding to the removal of two molecules of acetylacetonate for Cu and three molecules of acetylacetonate for Cr. The presence of these peaks further confirmed that both $Cr(acac)_3$ and $Cu(acac)_2$ were present in CCAA in its vaporised forms.

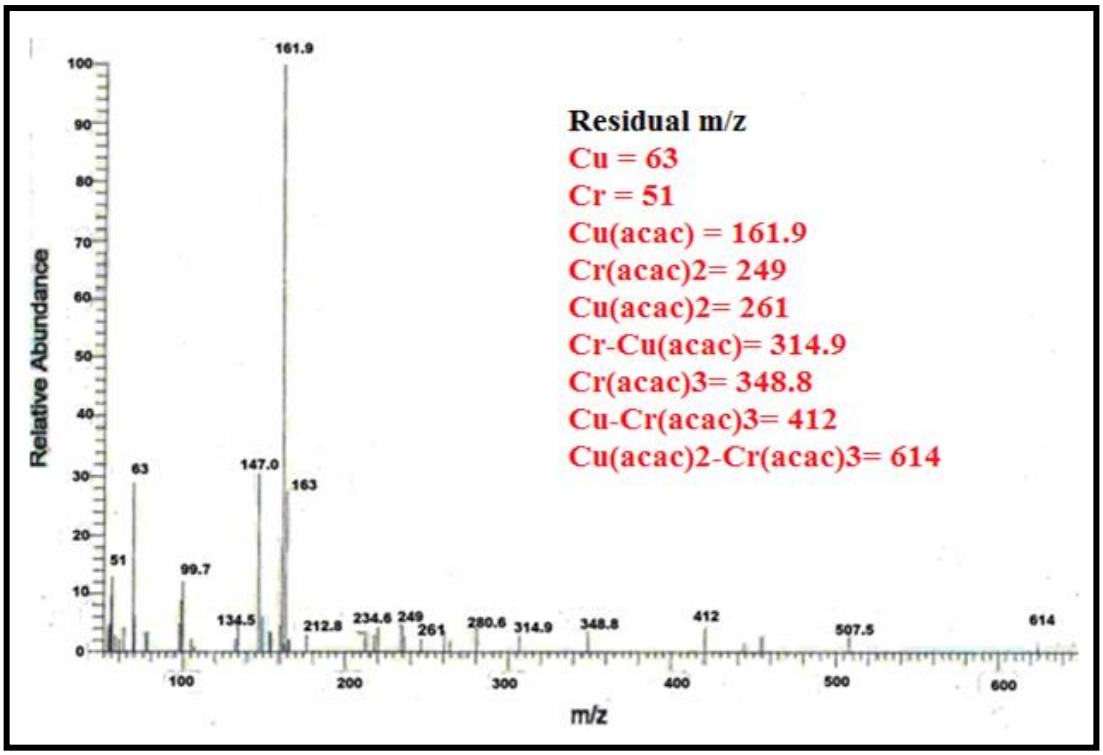

Fig. 5.5: Mass spectra of CCAA.

5.3.1.1.4. TGA-DTG analysis:

Fig. 5.6 shows the TGA patterns $Cu(acac)_2$,$Cr(acac)_3$, Cu-Cr-LDH and Cu(II)/Cr(III) AcAc crystals respectively. TGA results showed that a 95 % weight loss occurs at 266

^{o}C for CCAA crystals which was almost near to sublimation temperatures of $Cu(acac)_2$ and $Cr(acac)_3$ where around 97 % weight loss occurred at 270-275 ^{o}C. Therefore, it can be expected that CCAA can be used as a single source precursors for MOCVD application to prepare Cr dopped CuO thin films at relatively low temperatures. The melting point of CCAA (224 ^{o}C) was also found in between the range of $Cr(acac)_3$ (215 ^{o}C) and $Cu(acac)_2$ (271 ^{o}C) as measured by melting point apparatus (Model M 560). Therefore, it may be concluded that similar to the report of by C. Chandrakala *et al*.[71] due to an eutectic composition formation by $Cu(acac)_2$ and $Cr(acac)_3$ in CCAA the DTG peak also shifted to lower sublimation temperature at 266 ^{o}C as compared to individual complexes and showed a single step weight loss without the formation of much residue. Similar works on eutectic formation in metal acetylacetonate complexes were also reported by Cherukuvada *et al*.[59] and Ganduri *et al*.[60]

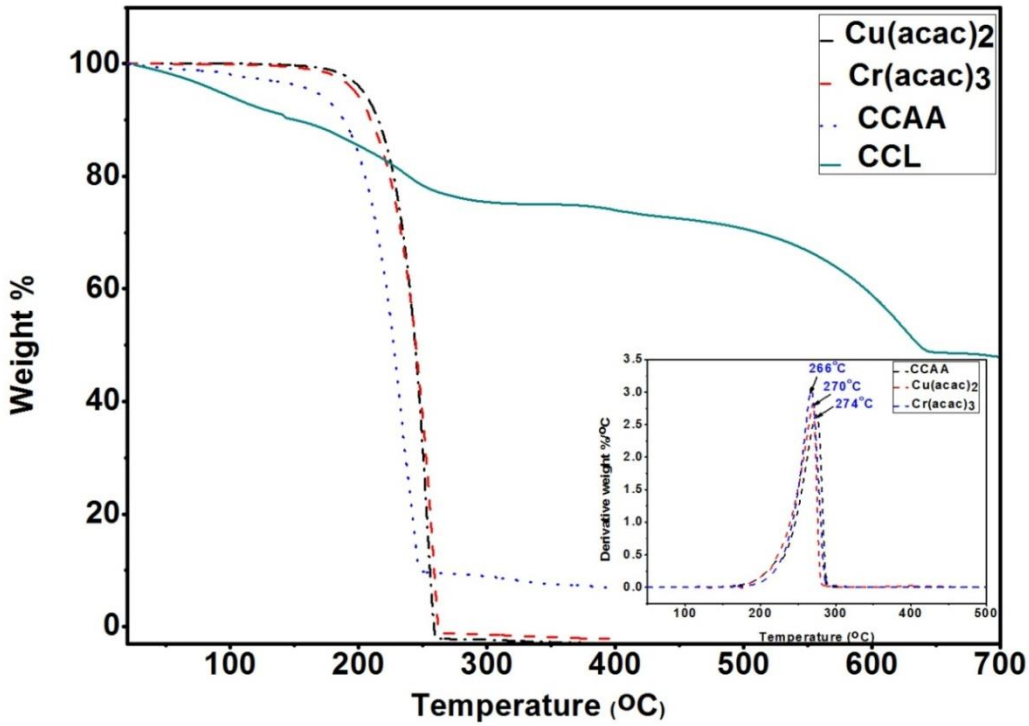

Fig. 5.6: TGA results of CCAA, $Cu(acac)_2$, $Cr(acac)_3$ and corresponding parent LDH (CCL).

5.3.1.1.5. XPS analysis:

To go further in studying the structural information about the chemical states of Cu, Cr, C and O in CCAA studies were made with XPS analysis (**Fig. 5.7**). XPS results showed peak due to C 1s (284.73 eV), O 1s (532 eV), Cu 2p (933.8-953.8 eV) and Cr 2p (571.7-587.2 eV). The C 1s spectra of CCAA crystals exhibited peaks at 284.2 eV, 284.9 eV, 285.9 eV and 287.8 eV corresponding to C-C, C=C, and C=O (**Fig. 5.7**, **Table 5.2a**) [72-75]. The Cu 2p high resolution spectra displayed two peaks corresponding to Cu $2p_{3/2}$ and Cu $2p_{1/2}$ doublet at 933.8 eV and 953.8 eV respectively, as well as peaks at 571.7 eV (Cr $2p_{3/2}$) and 587.2 eV (Cr $2p_{1/2}$) for Cr which indicated that both Cu and Cr are present in CCAA crystals [1,76-80] in their normal oxidation states. **Table 5.2b** shows the atomic percentage present in CCAA crystals, which was almost similar composition of Cu:Cr in the parent LDH.

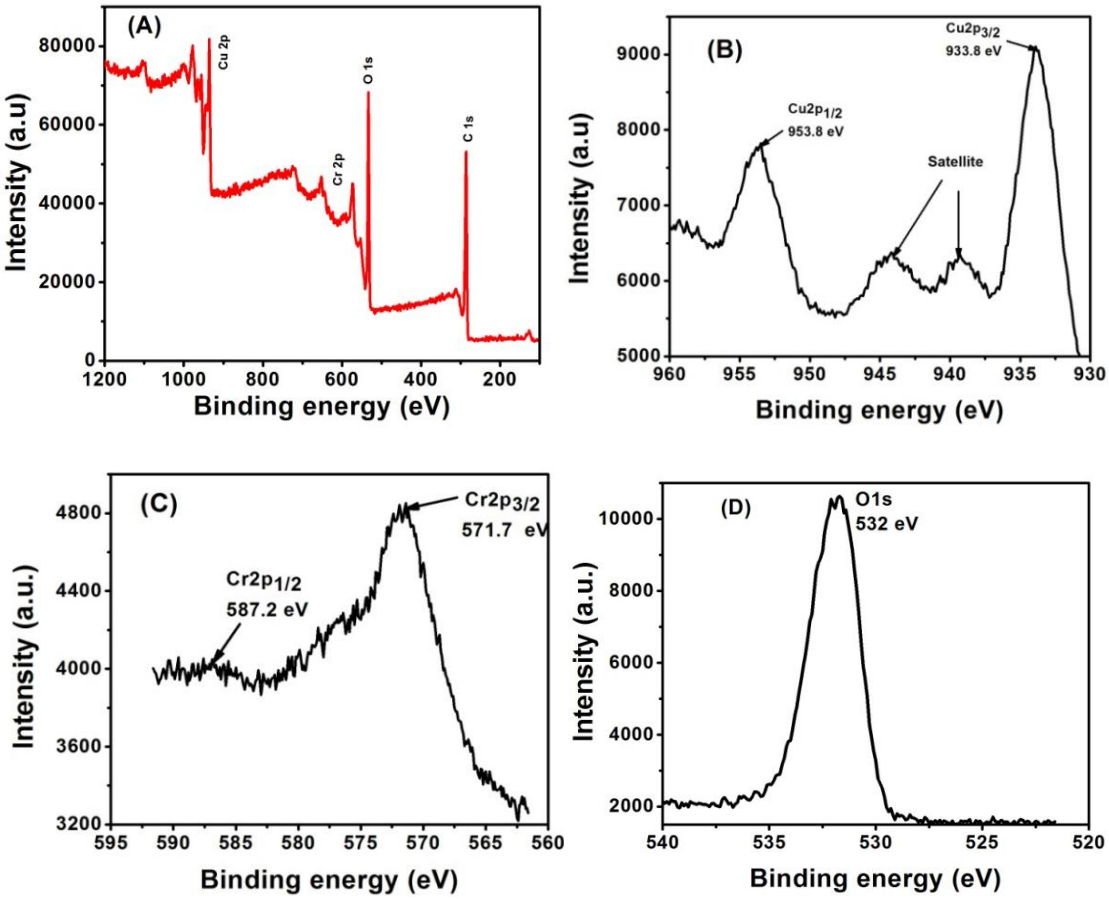

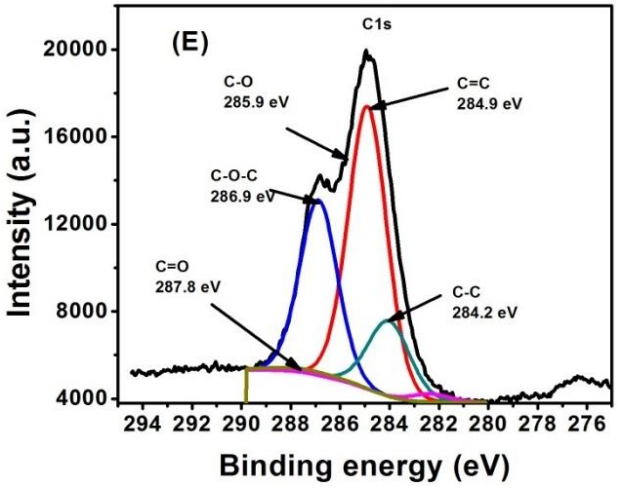

Fig. 5.7: (A) XPS survey spectra of CCAA crystals; (B) Cu 2p high resolution XPS spectra; (C) Cr2p high resolution XPS spectra, (D) O 1s high resolution XPS spectra and (E) C1s high resolution XPS spectra.

Table 5.2a: XPS results for Cu 2p, Cr 2p, C 1s and O 1s peaks of $Cu(acac)_2$, $Cr(acac)_3$ and CCAA crystals

Samples	O1s (eV)	C 1s (eV)	Cu $2p_{3/2}$, Cu $2p_{1/2}$ (eV)	Cr $2p_{3/2}$ (eV)
$Cu(acac)_2$	531.58		934.3-954.2 [1,76-78]	-
$Cr(acac)_3$			-	576.7-579.12 [79,80]
CCAA	532	284.8	933.8-953.8	571.7-587.2

Table 5.2b: Atomic percentage of C 1s, O 1s , Cu 2p and Cr 2p in CCAA crystals

Sample	C 1s	O 1s	Cu 2p	Cr 2p
CCAA	65.35	24.32	7.18	3.16

5.3.1.1.6. Optical Microscopy, SEM, EDS and TEM:

The optical microscopy (**Fig. 5.8a. A,B&C**) shows the needle like crystals of CCAA mixtures. The diameter and length of the needles were around 0.02-1.85 and 0.28-18.26 µm respectively. SEM images (**Fig. 5.8a.D**) also further confirmed the same. SEM and optical microscopic images showed that the needle like crystals possess some twisted scale like distinct edges forming rounded ripples over the needle surfaces

looking somewhat like bottom ends of sugarcane leaves forming rounded wrappings around the main body of the cane.

The formation of needle like crystals was also observed from TEM analysis (**Fig. 5.8a.A**) of CCAA crystals. **Fig. 5.8b.B** is a TEM image of a selected crystal which shows that it has two zones an inner darker core surrounded by an outer coating or shell covering the inner crystal which symmetrically covers the inner core almost from all the sides (**Fig. 5.8b.B**). Similarly, **Fig. 5.8b.C** also shows the presence of two surfaces where the inner surface is covered by an outer coating. It may be now stated that the inner dark core of Cu $(acac)_2$ is covered by a coating of $Cr(acac)_3$. The $Cu(acac)_2$ core have nanopores with dimensions higher than 3.5 nm as shown in **Fig. 5.8b.D**. The crystallite size of $Cr(acac)_3$ was also obtained from standard Scherrer equation [81] and it showed the crystallite size as 3.5 nm. These 3.5 nm size $Cr(acac)_3$ crystallites makes the coating over $Cu(acac)_2$ crystals and resulting in the formation of a larger composite crystal (**Fig. 5.8b.D**). **Fig. 5.8b.D** also shows the presence of lattice fringes with dimensions as 0.49 nm, 0.93 nm and 0.35 nm due to (200), (002) and (-101) planes of $Cu(acac)_2$ and further confirms that the inner core of $Cu(acac)_2$. This is covered by the poorly crystallised $Cr(acac)_3$ shell as shown in selected area electron diffraction (SAED) image with (023) lattice plane of $Cr(acac)_3$. Thus, the presence of both $Cu(acac)_2$ and $Cr(acac)_3$ in the composite crystal of CCAA in a core-shell arrangement is further confirmed. On the other hand, the presence of pockmark like indentations of around 3.5 nm in the $Cu(acac)_2$ core section as observed in TEM can be expected to be nanopores created by selective etching Cr^{3+} ions from the original Cu-Cr LDH structure by diketo ligand. The regularity in their distribution also could be expected because of the ordered supercell structure of parent LDH with $a=\sqrt{3}.a_o$ where a_o is the a parameter for the unit cell of Brucite like $Cu(OH)_2$. In such a cell there is one

Cr octhedra after two Cu octahedras. It had been reported that mesoporous holey nanosheets of Zinc hydroxide can be formed from Zn-Cr LDH by preferential etching of Cr (III) ions with metal diketone ligands of appropriate acid strength [28]. In case of Zn-Cr LDH, the Zn^{2+} ions instead of forming curled up or planar $Zn(acac)_2$ prefered to remain in its octahedral hydroxic configuration whereas in the present case the Cu^{2+} ion forms planar $Cu(acac)_2$ which converted to needle like curled crystals on drying out of the solvent. The formation of planar $Cu(acac)_2$ after the etching of Cr^{3+} ions by acetylacetonate ligand would naturally be favoured by inherently Jahn-Teller distorted Cu^{2+} ion where the apical atoms of the octahedra would lie at a distance higher than their distance to the -OH groups at the planar surface.

EDS analysis was carried out to get the chemical composition of atoms. EDS spectrum (**Fig. 5.8c**) shows that the atomic ratio of Cu and Cr in CCAA is 7.2:3.5. Thus, from EDS analysis it was further indicated that after recrystallization both of the acetylacetonates of Cu and Cr were not separated completely and TEM analysis showed that they formed some composite crystals as shown in **Fig. 5.8b.B&C**.

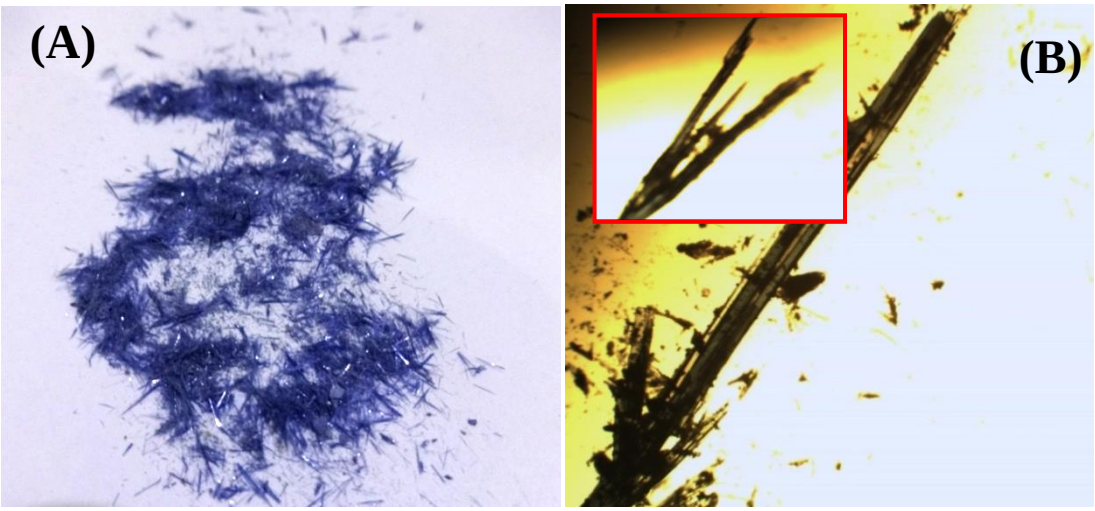

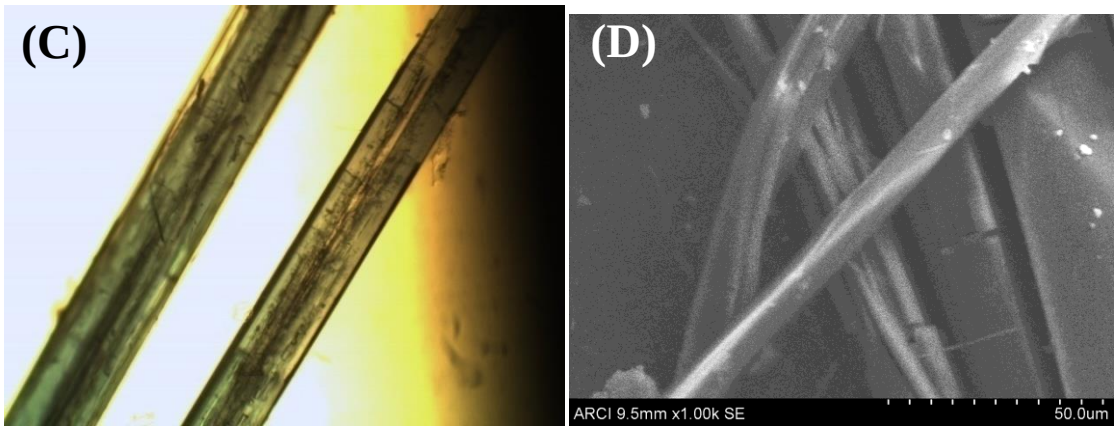

Fig. 5.8a: (A) Normal Photograph of blue coloured CCAA crystals, (B&C) Optical microscopic images and (inset) bifurcated tips of rod like crystals of CCAA (magnification 20x) &(D) SEM images of CCAA crystals at magnification 50 µm.

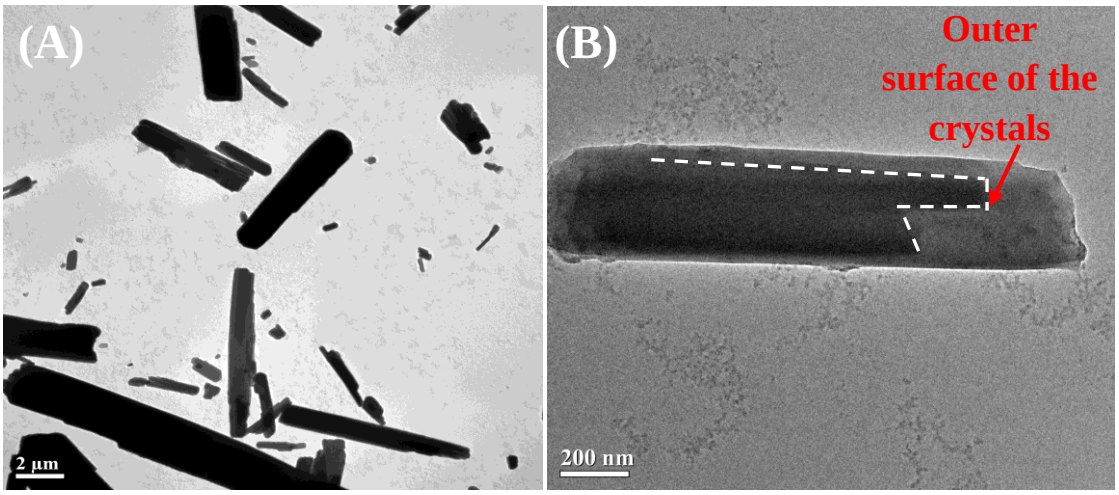

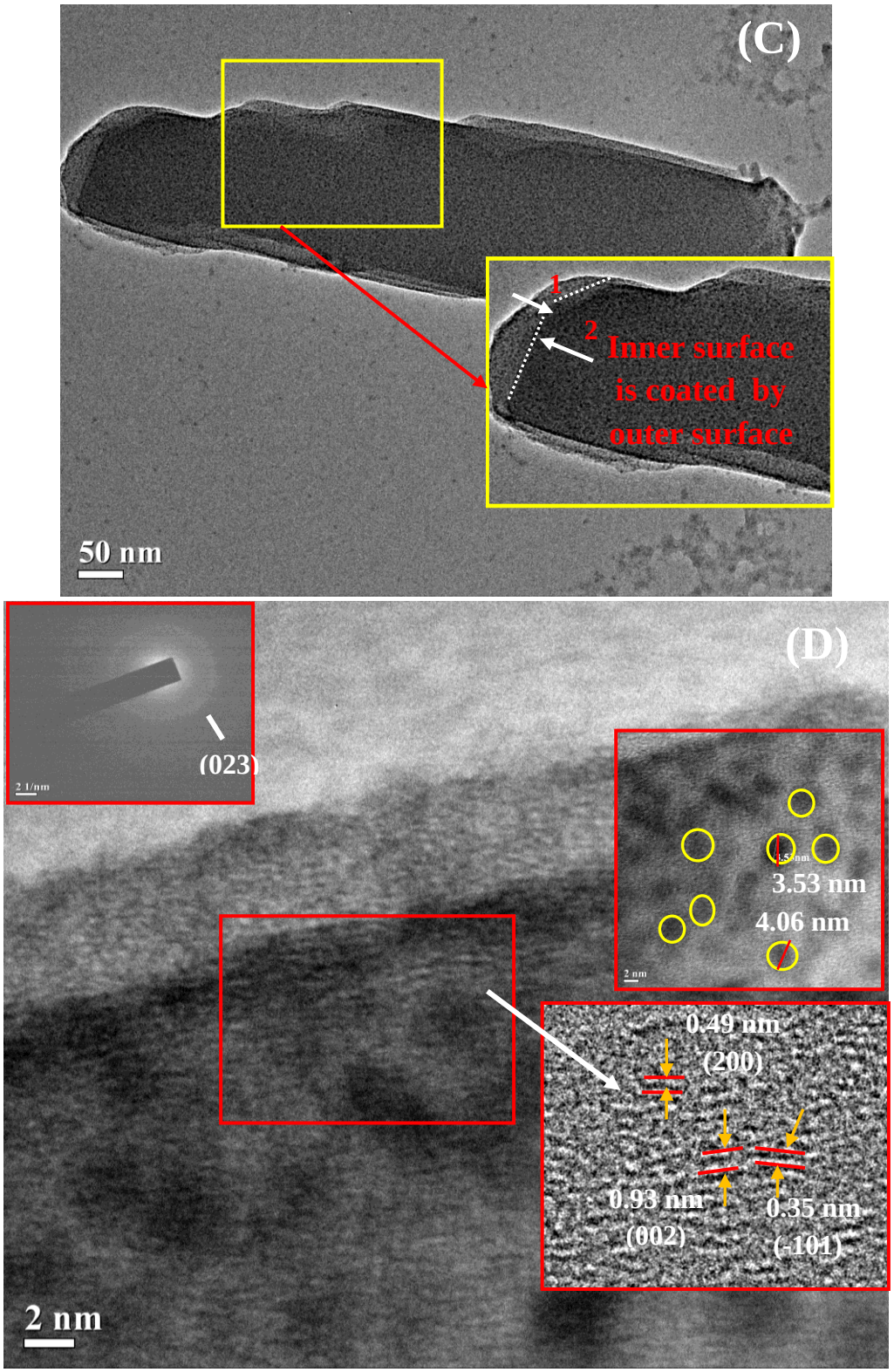

Fig. 5.8b: TEM images of CCAA crystals (A, B, C&D) showing the presence of both $Cu(acac)_2$ and $Cr(acac)_3$.

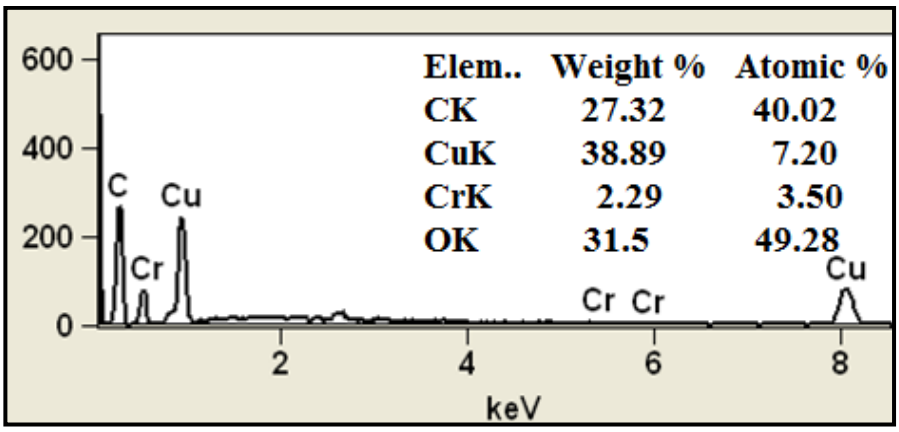

Fig. 5.8c: EDS spectra of CCAA.

5.3.1.1.7. Surface area and pore volume analysis:

As a natural corollary of the TEM findings the BET surface area and pore size analysis of the samples were carried out to know more about the nature of the pores formed on selective etching of Cr^{3+} ions from the Cu^{2+} ion backbone. It showed that in case of CCAA the BET surface area decreased slightly from 18.6 m^2/g in the parent LDH to16.8 m^2/g. However, the pore size analysis further confirming the presence of nanopores over CCAA crystals (**Table 5.3**) with an average diameter of 3.3 nm.

Table 5.3: BET surface area and pore diameter of CCL and CCAA crystals

Mixed-Metal acetylacetonates and LDH	BET area (m^2/g)	Pore diameter (nm)
CCL	18.6	3.7
CCAA	16.8	3.3

5.3.1.1.8. Single Crystal XRD analysis of CCAA crystals:

Based upon the powder XRD data single crystal XRD analysis was carried out after recrystallization from $CHCl_3$ to get the crystal structure as well as to refine the structure of CCAA crystals. Single crystal XRD analysis showed that CCAA crystals possessed square planar $Cu(acac)_2$ like structure coordinated with two acetylacetonates ligands and crystallises in monoclinic phase with space group of $P2_1/n$. The unit cell

diamensions of CCAA crystals were a=10.353 (3) Å, b=4.6978 (11) Å and c=11.387 (3) Å; angles were α= 90°, β= 91.699 (14)°and γ= 90° respectively. The volume of the crystal is 553.5 (2) $Å^3$ (**Table 5.4a**). **Table 5.4b** shows the selected bond length of CCAA crystals. **Fig. 5.9**A shows the structure of one molecule whereas **Fig. 5.9B** shows the molecular packing into unit cell containing 6 such molecules along b and **Fig. 5.9C&D** shows along c directions. **Table 5.4a** shows the bond length and bond angles of CCAA crystals. There were three types of coordinations through which the unit cells could be packed such as (C-H----O)π, (C-H----O) and (H----H) covalent bonding as shown in **Fig. 5.9C** and **Table 5.4b**. The (C-H----O) bonding was involved in the central O atom and corner C-H group. The bond length of these bonds were such as C5H5B-O2=3.485Å, C1H1C-O2=3.063 Å and C3H3B-O2=3.097 Å respectively. The another group of bonding (C-H----O)π which was also involved in the central O atom and C-H group. The bond length of these bonds were relatively shorter than (C-H----O) bonds (approximately 0.2-0.7 Å shorter) [1] such as C1H1A-O1=2.809 Å, C3H3B-O2=2.838 Å and C5H5C-O1= 2.882 Å respectively (**Fig. 5.9C**). On the other hand, the third group of (H----H) covalent bond which connected the corners of each molecule in the unit cell through H-bonding had the bond length of C5H5B-C3H3A=2.385 Å, C5H5A-C1H1B=2.537 Å, C1H1A-C1H1C=2.532 Å, C1H1C-C5H5A=2.893 Å and C5H5B-C1H1B =2.919 Å respectively [82,83] as shown in **Fig. 5.9C** and **Table 5.4b**.

Table 5.4c shows the detailed comparison of bond length and bond angles of CCAA crystals, $Cu(acac)_2$ and $Cr(acac)_3$ respectively [1,82-84]. It can be observed that although CCAA crystals possess $Cu(acac)_2$ like structure but the bond length and bond angles are relatively different from $Cu(acac)_2$. The bond length and bond angles of these crystals are also found to be different from $Cr(acac)_3$ as given in **Table 5.4c**.

Thus, it can be concluded that after recrystallization CCAA mixtures are converted into a single crystal of $Cu(acac)_2$ with the formation of some nanopores of dimension higher than 3 nm in the crystal surface which were occupied by $Cr(acac)_3$. As the most stable oxidation state of Cr is +3 [85] due to which it cannot enter into the crystal structure to form the single crystal but occupy the surface of the $Cu(acac)_2$ crystals and formed composite crystal of Cu(II)/Cr(III)AcAc. As a result of the formation of composite crystal there is some amount of distortion of individual crystal structure most probably due to steric reasons which results in variation of bond length and bond angles are from both $Cu(acac)_2$ and $Cr(acac)_3$.

(A)

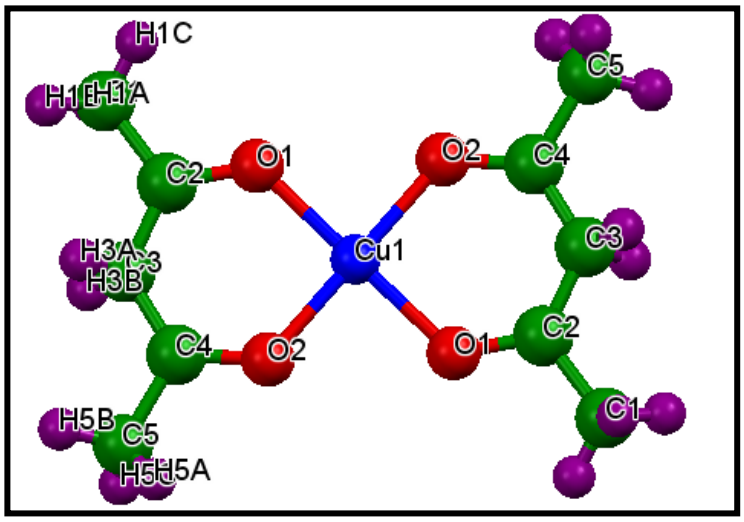

(B)

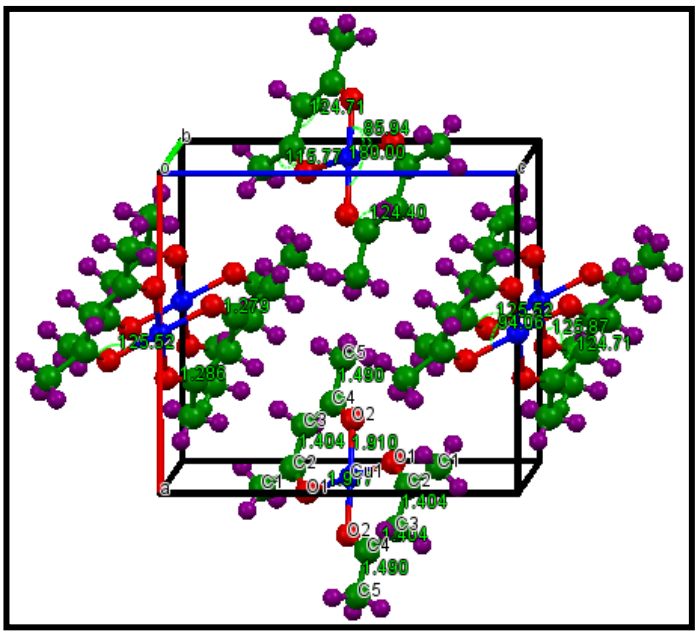

(C)

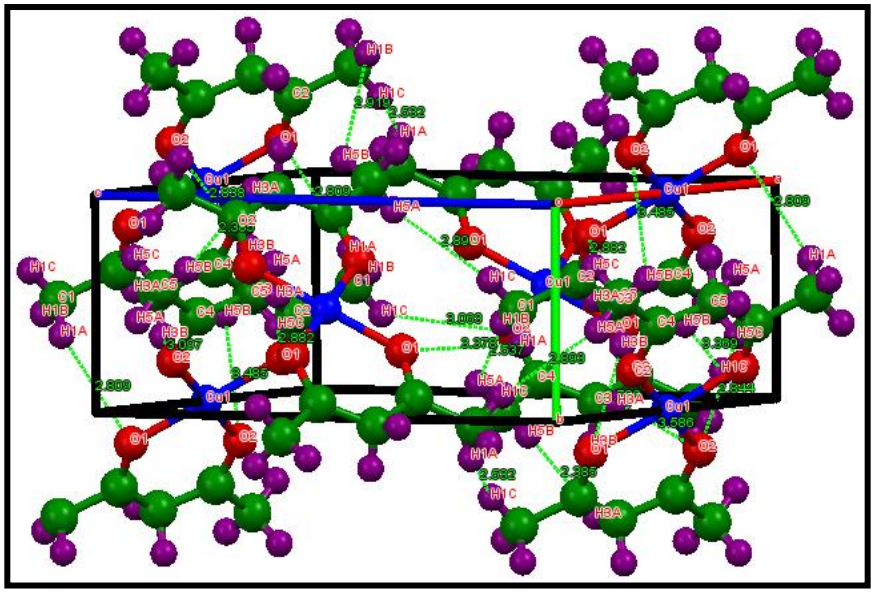

(D)

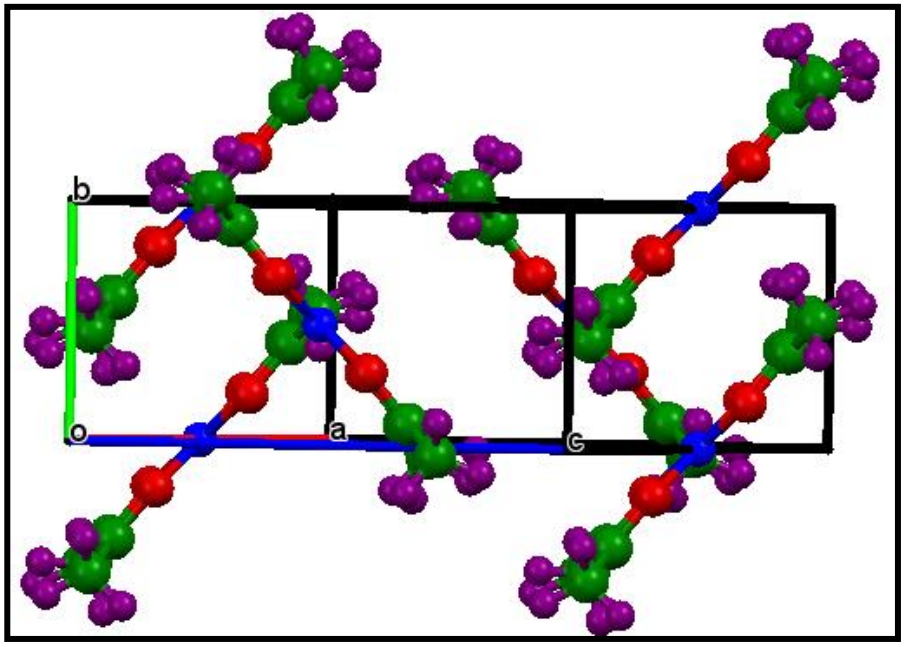

= O, = Cu, = C, = H

Fig. 5.9: Molecular packing structure of CCAA crystals; (A) Structure of single molecule; Molecular packing into unit cell along b (B) and c direction (C&D).

Table 5.4a: Crystal data of CCAA crystals

Empirical Formula	$C_{10.5}H_{14}CuO_4$
Formula weight	257.68
Temperature	296 (2) K
Diffraction Radiation wavelength	0.71073 Å
Diffraction Radiation type	Mo Kα
Crystal system	Monoclinic
Space Group	$P2_1/n$
Unit Cell dimensions	a= 10.353(3) Å, α= 90º b= 4.6978(11) Å,β= 91.699(14)º c= 11.387(3) Å,γ=90º
Volume	553.5(2)
Formula unit Z	8
Absorption Co-efficient	0.7852 cm^{-1}
Collection reflections collected	3092
Reflections no. Total	1204
Refinement method	Full-matrix least-squares on F^2
R indices (all data)	R_1= 0.0569, wR_2 = 0.1191
Absorption Correction	Semi-empirical from equivalents

Table 5.4b: Types of bonds present in the crystals obtained from CCAA crystals

Atomic bonding	Types of bonds	Bond length (Å)
C1H1A-O1	(C-H----O)π	2.809
C3H3B-O2	(C-H----O)π	2.838
C5H5C-O1	(C-H----O)π	2.882
C5H5B-O2	(C-H----O)	3.485
C1H1C-O2	(C-H----O)	3.063
C3H3B-O2	(C-H----O)	3.097
C1H1A-O1	(C-H----O)	3.378
C5H5B-C3H3A	(H----H)	2.385
C5H5A-C1H1B	(H----H)	2.537
C1H1A-C1H1C	(H----H)	2.532
C1H1C-C5H5A	(H----H)	2.893
C5H5B-C1H1B	(H----H)	2.919

Table 5.4c: Comparison of selected bond lengths and bond angles between $Cu(acac)_2$, $Cr(acac)_3$ and CCAA crystals

Bond length (Å)			
	$Cu(acac)_2$ [1]	Cu(II)/Cr(III)AcAc	$Cr(acac)_3$ [83,84]
M-O1	1.924	1.916	1.943
M-O2	1.918	1.910	1.942
C2-C3	1.385	1.403	1.393
C3-C4	1.50	1.404	1.396
C1-C2	1.385	1.481	1.530
O1-C2	1.272	1.279	1.244
O2-C4	1.272	1.286	1.255
Bond angles (º)			
O1-M-O2	93.5	94.06	91.66
O1-M-O4	86.5	85.94	-
O1-M-O3	180	179.99	-
C2-O1-M	125.4	125.5	124.69
C4-O2-M	125.37	125.8	-
O1-C2-C3	124.9	124.9	-
O2-C1-C3	125	124.4	-
O3-M-O6	-	-	90.67
O4-M-O5	-	-	90.95
C1-O1-M	-	-	126.75
O1-C1-C12	-	-	126.51
O3-C3-C36	-	-	125.7
O4-C4-C45	-	-	125.19

5.3.1.1.9. Characterizations of the thin film grown by MOCVD:

MOCVD of the CCAA crystals was carried out to get the Cu/Cr oxide thin film over the glass substrate as well as over honey comb monolith. **Fig. 5.10A&B** shows the photograph of coupons of coated honey comb and glass plate.

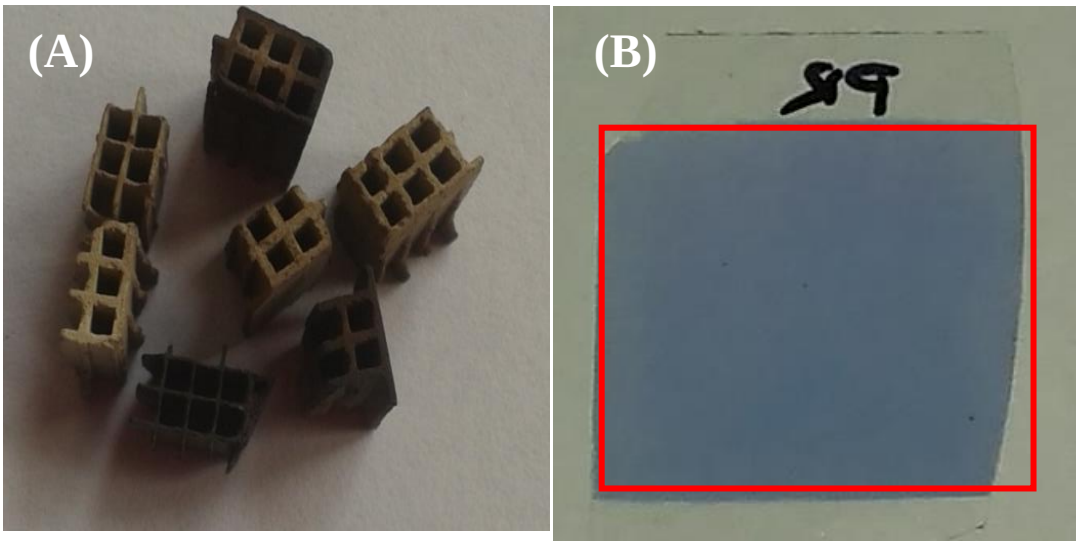

Fig. 5.10: MOCVD coating of CCAA crystals over (A) Honeycomb monolith (B) Glass plate.

The characterizations of the thin film are given below-

5.3.1.1.9.1. XRD analysis:

The structural properties of thin film deposited over glass substrate was analysed by XRD analysis. XRD analysis of CCAA thin film grown over glass substrate showed the presence of highest intensity $CuCr_2O_4$ phase with *hkl* reflection of (211) and (311) (d=2.55Å and 2.5Å) corresponding to **JCPDS Card No. 00-034-0424** and **JCPDS Card No. 00-026-0509** respectively (**Fig. 5.11**) which further confirmed the presence of $Cr(acac)_3$ over $Cu(acac)_2$ surface. As a result of which both Cu and Cr were deposited over the substrate as their corresponding oxides. On the other hand, the noise in the XRD pattern were due to the amorphous glass substrate [86,87].Therefore, this thin film of $CuCr_2O_4$ can be used as a catalyst for decomposition of environmental pollutants.

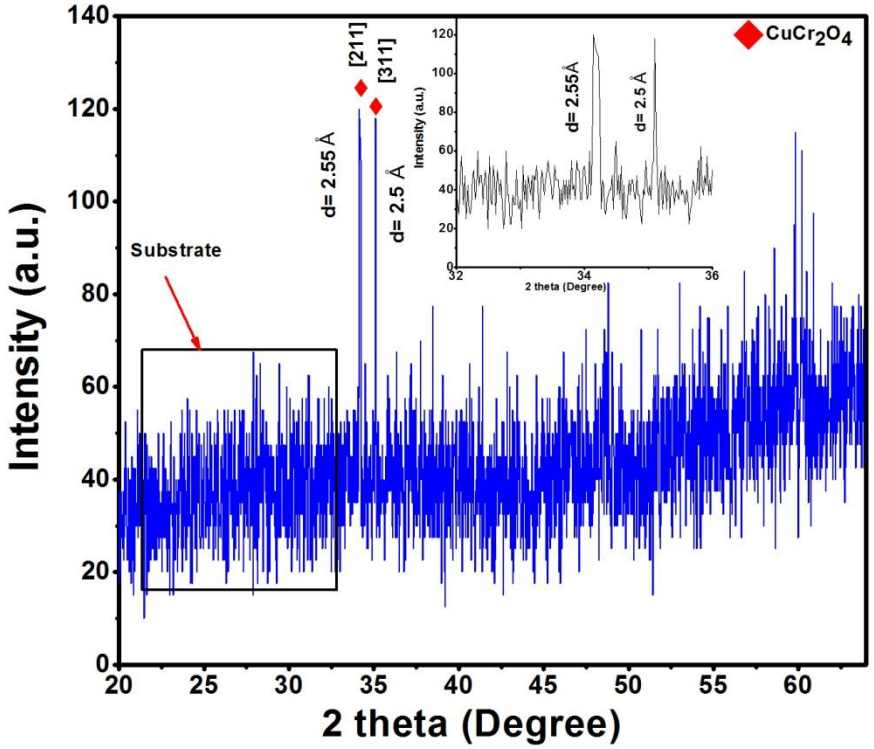

Fig. 5.11: XRD pattern of CCAA thin film grown over glass substrate.

5.3.1.1.9.2. SEM and EDS analysis:

The structural morphology of the thin film was analysed by SEM and EDS analysis (**Fig. 5.12**). From SEM analysis (**Fig. 5.12A, B&C**) it was observed the formation of some grainy structures of irregular shapes which was due to the presence of mixed phases in the thin film [88]. The thickness of the thin film deposited was 31 nm as determined by thickness measurement instrument scientific equipment and service unit (Model No. DTM-10).The formation of $CuCr_2O_4$ was further confirmed from EDS analysis which showed the presence of Cu, Cr and O with the weight % of 7.4, 2.85 and 27.5 % respectively as shown in **Fig. 5.12D**. On the other hand, the weight % of 9.85 and 52.3 corresponding to Si and Al were due to the substrate where the thin film was grown.

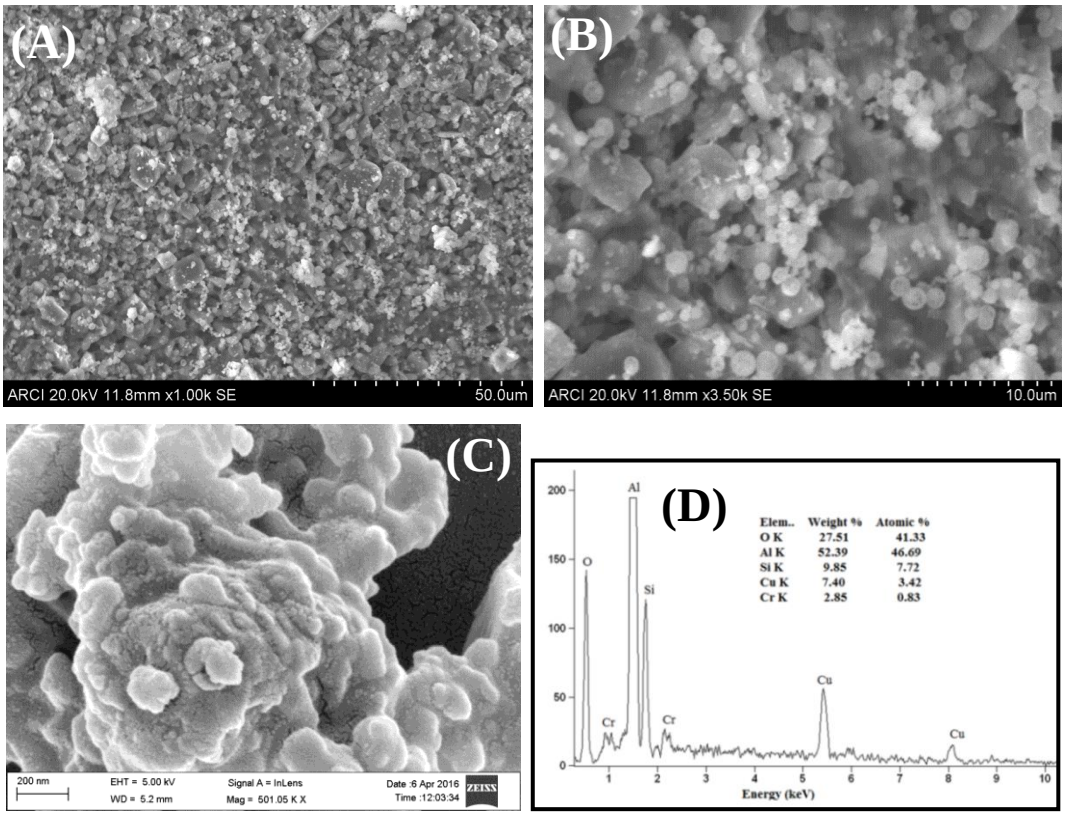

Fig. 5.12: SEM images of CCAA thin film grown on the honeycomb monolith (A&B); SEM and EDS images of CCAA thin film grown on the glass substrate (C&D) by MOCVD technique.

5.3.1.1.10. AFM analysis:

AFM images were taken to study the surface topography and root mean square (RMS) roughness of CCAA thin film deposited over glass substrate (**Fig. 5.13**). It was observed from XRD and SEM analysis that the grains of $CuCr_2O_4$ phase deposited very smoothly over glass substrate by MOCVD. The RMS roughness value of the thin film was found as 37 nm indicating the presence of larger grains which lead to the increase of surface roughness [89,90]. On the other hand, from the 3D view it was further observed that the surface of the thin film consist of different grains of different sizes as observed from SEM which may be due to the presence of mixed metal oxide of Cu/Cr as observed from XRD analysis further confirm the formation of composite crystals of CCAA.

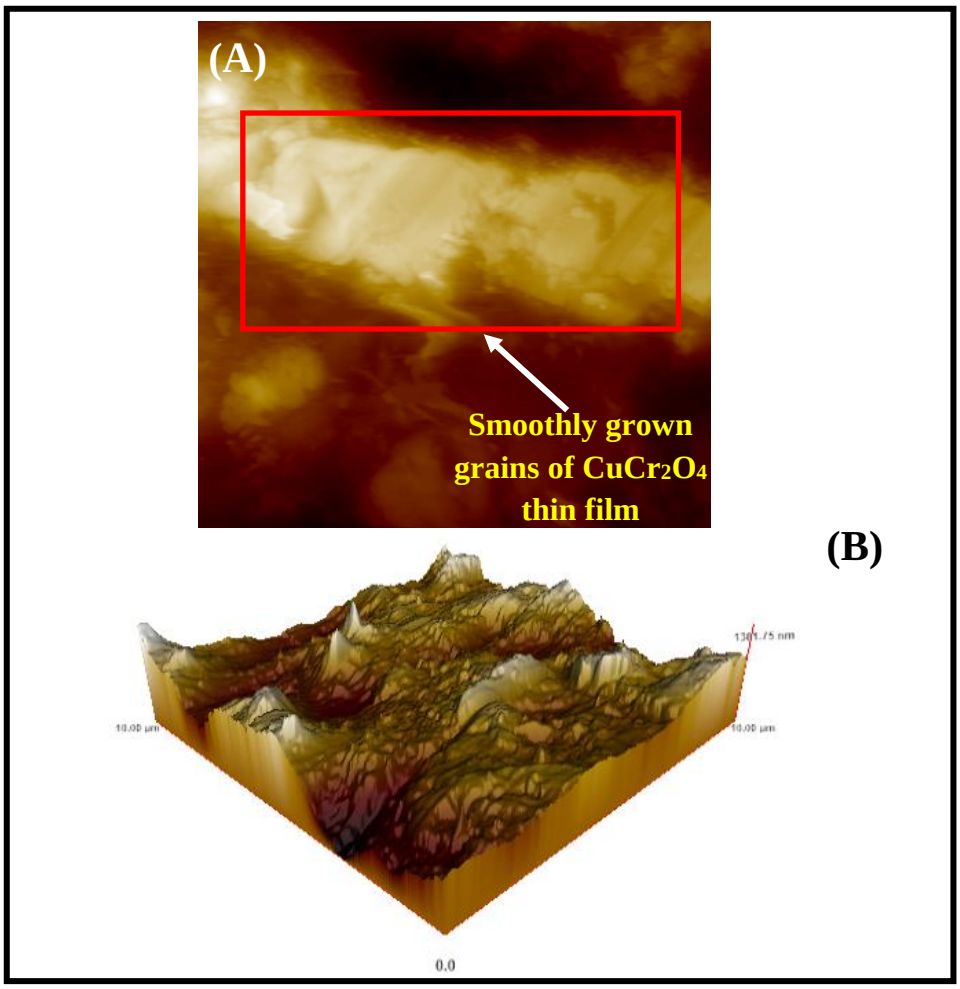

Fig. 5.13: Atomic force microscopy image of CCAA deposited over glass substrate (A) Topographic image of CCAA thin film (B) 3D view of CCAA thin film.

5.3.1.1.11. N_2O decomposition study:

N_2O decomposition study was carried over $CuCr_2O_4$ thin film coated over honey comb monolith at 250 ^oC under atmospheric pressure at constant Gas Hourly Space Velocity (GHSV) of 542.4 h^{-1} (300,000 $cm^3g^{-1}h^{-1}$). The flow rate of Argon:N_2O was maintained at 100:100 ml/min. Initial concentration of N_2O was 500 ppm (11.36 mmol). In presence of this catalyst N_2O was decomposed to N_2 and O_2 as shown in **Fig. 5.14**. The percentage decomposition of N_2O was found as about 99.8 %. It was observed that $CuCr_2O_4$ showed better catalytic activity towards N_2O reduction at low temperature.

As reported by J. Laine *et al*.[91] of $CuCr_2O_4$ catalyst due to combined presence of Cu and Cr there was prevention of the further conversion of surface Cu (II) to Cu (I) and Cu(0) and which limited the catalytic activity. According to them the activity of the catalyst depends upon the Cu-enrichment on the spinel $CuCr_2O_4$ surface which may occur due to the migration of Cu from bulk to surface and the generation of oxygen vacancies over Cu surface and on this vacant site N_2O was adsorbed and through adsorption-desorption mechanism N_2 and O_2 are formed [92,93].

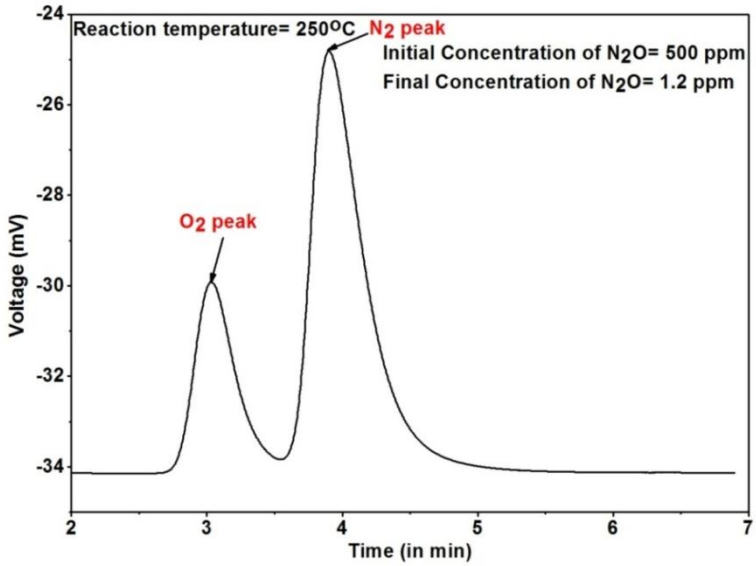

Fig. 5.14: Gas chromatograph of N_2O decomposition study over $CuCr_2O_4$.

5.4. CONCLUSIONS:

The synthesis of mixed Cu(II)/Cr(III) acetylacetonates by acid-base neutralization reaction between Cu-Cr LDH and acetylacetone at room temperature is found to be a most effective method. It is easy to carry out also and gives high yield product as well as short reaction time. From XRD analysis, the product of the CCL and acetylacetone shows the presence of both $Cu(acac)_2$ and $Cr(acac)_3$. After repeated crystallization both of these metal acetylacetonates are not separated. Although, due to the stable +3 oxidation state of Cr with an octahedral molecular configuration, $Cr(acac)_3$ can not enter into the single crystal structure basically formed by square planar configuration

of $Cu(acac)_2$ to form a $Cu/Cr(acac)_2$ mixed metal complex but they form a composite crystal with $Cr(acac)_3$ making a coat over the surface of $Cu(acac)_2$ core. Due to the formation of eutectic mixture the melting point of CCAA lies in between $Cu(acac)_2$ and $Cr(acac)_3$ and leads to the shifting of DTG peak to the sublimation temperature lower than $Cu(acac)_2$ and $Cr(acac)_3$. The TGA results show that CCAA undergoes single step weight loss (about 95 %) in a temperature of 266 ^oC without leaving much residue due to which it can be used as precursor for thin film formation by MOCVD over solid substrates at low temperature. It is also observed that CCAA deposits as thin film of $CuCr_2O_4$ which decomposes N_2O to N_2 and O_2. Thus, in future it can be proposed to be used as catalyst for further applications related to environment and synthesis.

REFERENCES:

[1] R. Rooydell, R.C. Wang, S Brahma, F. Ebrahimzadeh, C.P. Liu. *Dalton Trans.*, **2015**, *44*, 7982-7990.

[2] A. Gairola, G.V. Kunte, D. Chopra, T.N. Guru Row, A.M. Umarji, S.A. Shivashankar. *Polyhedron*, **2010**, *29*, 2680-2688.

[3] H. Xu, R. Chen, Q. Sun, W. Lai, Q. Su, W. Huang, X. Liu. *Chem. Soc. Rev.*, **2014**, *43*, 3259-3302.

[4] V. M. Manikandamathavan, T. Weyhermüller, R. P. Parameswari, M. Sathishkumar, V. Subramanian, B. U. Nair. *Dalton Trans.*, **2014**, *43*, 13018-13031.

[5] A. Ghisolfi, K. Y. Monakhov, R. Pattacini, P. Braunstein, X. Lopez, C. D. Graaf, M. Speldrich, J. V. Leusen, H. Schilder, P. Kogerler. *Dalton Trans.*, **2014**, *43*, 7847-7859.

[6] H. T. Ngo, X. Liu, K. A. Jolliffe. *Chem. Soc. Rev.*, **2012**, *41*, 4928-4965.

[7] A. Lauria, R. Bonsignore, A. Terenzi, A. Spinello, F. Giannici, A. Longo, A. M.

Almerico, G. Barone. *Dalton Trans.*, **2014**, *43*, 6108-6119.

[8] Z. Zeng, D. Matuschek, A. Studer, C. Schwickert, R. Pottgen, H. Eckert. *Dalton Trans.*, **2013**, *42*, 8585-8596.

[9] P. J. Hagrman, D. Hagrman and J. Zubieta, Angew. *Chem. Int. Ed.*, **1999**, *38*, 2638-2684.

[10] M. Baibarac, I. Baltog, I. Smaranda, M. Scocioreanu, S. Lefrant. *J. Mol. Struct.*, **2011**, *985*, 211-218.

[11] D. L. Hou, X. J. Ye, H. J. Meng, H. J. Zhou, X. L. Li, C. M. Zhen, G. D. Tang. *Appl. Phys. Lett.*, **2007**, *90*, 142502-142506.

[12] J. Kulesza, B. S. Barros, S. A. Junior. *Coord. Chem. Rev.*, **2013**, *257*, 2192-2212.

[13] M. E. Davis. *Nature*, **2002**, *417*, 813-821.

[14] A.L. Johnson, N. Hollingsworth, G. K. Kohn, K.C. Molloy. *Inorg. Chem.*, **2008**, *47*, 12040.

[15] A.P. Mllanov, R.A. Fischer, A. Devi. *Inorg. Chem.*, **2008**, *47*, 11406.

[16] H. Zhang, B. Li, J. Sun, R. Clerac, E.V. Dlkarov. *Inorg. Chem.*, **2008**, *47*, 10046.

[17] H.C. Aspinall, J.F. Bickley, J.M. Gaskell, A.C. Jones, G. Labat, P.R. Chalker, P.A. William. *Inorg. Chem.*, **2007**, *46*, 5852.

[18] A. Ghisolfi, K. Y. Monakhov, R. Pattacini, P. Braunstein, X. Lopez, C. de Graaf, M. Speldrich, J.van Leusen, H. Schilder, P. Kogerler. *Dalton Trans.*, **2014**, *43*, 7847-7859.

[19] M. S. Raghavan, P. Jaiswal, N. G. Sundaram, S. A. Shivashankar. *Polyhedron*, **2014**, *70*, 188-193.

[20] A. Gairola, A. M. Umarji, S. A. Shivashankar. *Processing and Properties of Advanced Ceramics and Composites*, ed. N. P. Bansal and J. P. Singh, Copyright © 2009 *The American Ceramic Society*, **2009**.

[21] K. Haga, P. S. Wijesena, H. Watanabe. *Appl. Surf. Sci.*, **2001**, *169-170*, 504-507.

[22] A.G. Nasibulin, E. I. Kauppinen, D. P. Brown, J. K. Jokiniemi. *J. Phys. Chem.*, **2001**, *105*, 11067-11075.

[23] A. Schejn, L. Balan, V. Falk, L. Aranda, G. Medjahdic, R. Schneider. *Cryst. Eng. Commun.*, **2014**, *16*, 4494-4500.

[24] A. M. A. Bennett, G. A. Foulds, D. A. Thornton. *Polyhedron*, **1989**, *8*, 2305-2311.

[25] R. Ferreiraa, M. Silvab, C. Freirea, B. de Castroa, J. L. Figueiredo. *Microporous Mesoporous Mater.*, **2000**, *38*, 391-401.

[26] H. F. Garces, A. E. Espinal, S. L. Suib. *J. Phys. Chem.C*, **2012**, *116*, 8465-8474.

[27] A. M. EL-Hendawy. *J. Mol. Struct.*, **2011**, *995*, 97-102.

[28] P. Saikia, J. Saikia, S. Sarmah, N. G. Allou. *J. CO_2 Utiliz.*,**2017**, *21*, 40-51; DOI: https://doi.org/10.1016/j.jcou.2017.06.017.

[29] K. Binnemans. *Rare-earth beta-diketonates in Handbook on the Physics and Chemistry of Rare Earths*, **2005**, *35 (225)*, 107-272.

[30] R.C. Mehrotra, R. Bohra, D.P. Gaur. *Metal β-Diketonates and Allied Derivatives*, Academic Press, London, **1978**, 382.

[31] I. K. Igumenov, A.E. Turgambaeva, V.V. Krisyuk, A.F. Bykov. *J. Phys IV France*, **1999**, *9*, 8-65.

[32] S. Kawaguchi.Inorg. Chem. Concepts: Variety in Coordination Modes of Ligands in Metal Complexes,Vol 11, Springer, Berlin, **1988**.

[33] B. M. Choudhary, L. K. Mannepalli, M.K. Chaudhari, S. K. Dehury, S. S. Dhar, U. Bora. *Process for the preparation of metal acetylacetonates*, WO 2004056737 A1.

[34] S.Yokota, Y. Tachi and S. Itoh. *Inorg. Chem.*, **2002**, *41*, 1342-1344.

[35] H. Ye, A. Tang, L. Huang, Y. Wang, C. Yang, Y. Hou, H. Peng, F. Zhang, F. Teng. *Langmuir*, **2013**, *29*, 8728-8735.

[36] V. Rives. *Layered Double Hydroxides: Present and Future*,Nova Science Publishers, **2001**.

[37] X. Duan, D.G. Evans. *Layered Double Hydroxides*, Springer Verlag, **2006**.

[38] F. Cavani, F. Trifiro, A. Vaccari. *Catal.Today*, **1991**, *11*, 173-301.

[39] J. Wang, G. Fan, H.Wang, F. Li. *Ind. Eng. Chem. Res.*, **2011**, *50*, 13717-13726.

[40] Bi. Xue, F. Ting, Z. Hui. *ACS Appl. Mater. Interface.* **2014**, *6*, 20498-20509.

[41] M. Shao, F. Ning, J. Zhao, M. Wei, D.G. Evans, X. Duan. *J. Am. Chem. Soc.*, **2012**, *134*, 1071-1077.

[42] M. A. Aramendia, V. Borau, C. Jimenez, J.M. Marinas, J.R. Ruiz, F. J. Urbano. *J. Solid State Chem.*, **2002**, *168*, 156-161.

[43] S. Abello, F. Medina, D. Tichit, J. P. Ramirez, J. C. Groen, J. E. Sueiras, P. Salagre,Y. Cesteros. *Chem. Eur. J.*, **2005**, *11*, 728-739; DOI:10.1002/chem.2004 00409.

[44] C.Yu, J. He. *Chem. Commun.*, **2012**, *48*, 4933-4940.

[45] Y. Wang , F. Li , S. Dong , X. Liu, M. Li. *J. Colloid and Interface Sci.*, **2016**, *467*, 28-34.

[46 H. Roussel, V. Briois, E. Elkaim, A. de Roy, J. P. Besse, J.P. Jolivet. *Chem. Mater.*, **2001**, *13*, 329-337.

[47] R.L. Goswamee, H. Poellmann, K.G. Bhattacharyya, D. K Dutta. JCPDS-PDF Card No No.51-161, **1999**.

[48] M. Mishra, M.R. Das, R.L. Goswamee. *J. Sol-Gel Tecnol.*, **2010**, *54*, 57-61.

[49] C. T. Gueho, F. Leroux, C. Payen, J.P. Besse. *App.Clay Sci.*, **2005**, *28*, 111-120.

[50] H. Roussel, V. Briois, E. Elkaim, A. de Roy, J. P. Besse. *J. Phys. Chem. B*, **2000**, *104*, 5915-5923.

[51] K. Jayanthi, P. V. Kamath. *Dalton Trans.*, **2013**, *42*, 13220-13230.

[52] G.R. Williams, A. Clout, J.C. Burley. *Phys.Chem. Chem. Phys.*, **2013**, *15*, 8616-8628.

[53] C.Y. Shiau, S. Chen, J.C. Tsai, S.I. Lin. *Appl. Catal. A*, **2000**, *198*, 95-102.

[54] C. Monica, P. Celso, F. Julio, E. Griselda, H. Eduardo, C. Sandra, R.C. Enrique. *Appl. Catal. A*, **2007**, *317*, 11-19.

[55] L.Tian, Y. Zhao, S. He, M.Wei, X. Duan. *Chem. Eng. J.*, **2012**, *184*, 261-267

[56] L.G. Hubert-Pfalzgraf. *Appl. Organometal. Chem.*, **1992**, *6*, 627-643.

[57] J. L. Williams. *Catal.Today*, **2001**, *69*, 3-9.

[58] A. F. Perez-Cadenas, M. M. P. Zieverink, F. Kapteijn, J. A. Moulijn. *Catal.Today*, **2005**, *105*, 623-628.

[59] S. Cherukuvada, A. Nangia. *Chem. Commun.*, **2014**, *50*, 906-923.

[60] R. Ganduri, S. Cherukuvada, S.Sarkar, T.N. Guru Row. *Cryst. Eng. Commun.*, **2017**, *19(7)*, 1123-1132.

[61] S. Cherukuvada, T.N. Guru Row. *Cryst.Growth Des.*, **2014**, *14*, 4187−4198

[62] R. Prasad, P.Singh. *Bull.Chem. React. Engi. Catal.*, **2011**, *6(2)*, 63-113.

[63] G. Comino, A. Gervasini, V. Ragaini. *Catal. Lett.*, **1997**, *48*, 39-46.

[64] G. Pantaleo, L.F. Liotta, A.M. Venezia, G. Deganello, E.M. Ezzo, M.A. El. Kherbawi, H. Atia. *Mater Chem Phys*., **2009**, *114*, 604-611.

[65] S. Stegenga, R.van Soest, F. Kapteijn, J.A. Moulijn. *Appl.Catal. B: Environ.*, **1993**, *2*, 257-275.

[66] J. Zhu, J. G. van Ommen, L. Lefferts. *Catal. Today*, **2006**, *112*, 82-85.

[67] R. A. Keraliya, T.G. Soni, V. T. Thakkar, T. R. Gandhi. *Diss. Technol.*, **2010**, *2*, 16-21.

[68] T. S. Davis, J. P. Fackler. *Inor. Chem.*, **1966**, *5*, 242-245.

[69] G. R. Williams, A.Clout, J. C. Burley. *Phys.Chem. Chem. Phys.*, **2013**, *15*, 8616-

8628.

[70] B.M.Weckhuysen, R.R. Rao, J. Pelgrims, R.A. Schoonheydt, P. Bodart, G. Bebras, O. Collart, P.V.D. Voort, E.F. Vansant. *Chem. Eur. J.*, **2000**, *6*, 2960-2970.

[71] C. Chandrakala, P. Sravanthi, K. S. Nagaraja, B. Jeyaraj. *Int.J. Chem.Tech. Res.*, **2015**, *7(6)*, 2711-2722.

[72] Y.L. Huang, H.W. Tien, C.C. M. Ma, S.Y. Yang, S.Y. Wu, H.Y. Liub, Y.W. Mai. *J. Mater. Chem.*, **2011**, *21*, 18236.

[73] A.P. Dementjev, U, A. de Graaf, M.C.M. van de Sanden, K.I. Maslakov, A.V. Naumkin, A.A. Serov. *Diamond and Related Mater*. **2000**, *9*, 1904-1907.

[74] M.Wojtoniszak, E.Mijowska.J.Nanopart.Res.,**2012**,*14(11)*,1-7; DOI: 10.1007 /s110510121248z.

[75] P. Rajasekar, P. Chakraborty, S. K. Bandyopadhyay, P. Barat, Pintu Sen, A. Adnot, E. Knystautas. *J. Korean Phys. Soc.*, **1998**, *32*, 365-367.

[76] M. C. Biesinger, B. P. Payne, A. P. Grosvenor, L.W.M. Lau, A. R. Gerson, R.St.C. Smart. *Appl. Surf. Sci.*, **2011**, *257*, 2717-2730.

[77] J. Park, K. Lim, R.D. Ramsier, Y.C. Kang. *Bull. Korean Chem. Soc.*, **2011**, *32*, 3395.

[78] M. C. Biesinger, L. W.M. Lau, A. R. Gerson, R. St.C. Smart. *App.Surf. Sci.*, **2010**, *257*, 887-898.

[79] C. C. Chusuei, M. A. Brookshier, D. W. Goodman. *Langmuir*, **1999**, *15*, 2806-2808.

[80] Y.F. Huang, M. Liu, Y.Q.Wang,Y. Li, J. M. Zhang, S. H. Huo. *RSC Adv.*, **2016**, *6*, 15362-15369; DOI:10.1039/C5RA23132A.

[81] A. Patterson. *Phys. Rev.*, **1939**, *56 (10)*, 978-982; DOI:10.1103/PhysRev.56.978.

[82] A. M. A. Bennett, G. A. Foulds, D. A. Thornton. *Polyhedron*, **1939**, *8*, 2305-2311.

[83] F. A. Cotton, G. Wilkinson. *Adv. Inorganic Chem.*, John Wiley and Sons: New York, (1st ed. 1962, 6th ed. **1999**). ISBN 978-0-471-19957-1.

[84] Y. Harada, G.S. Girolami. *Polyhedron*, **2007**, *26*, 1758-1762.

[85] M.A.Hameed. *J. Phys. Vapor Deposition Sci. Technol.*, **2015**, *9*, 451-454.

[86] D. Sola, J. Martinez de Mendibil, J.R. Vazquez de Aldana, G. Lifante, R. Balda, A.H. de Aza, P. Pena, J. Fernandez. *Appl.Surf. Sci.*, **2013**, *278*, 289-294.

[87] B. Morosin. *Acta Cryst.*, **1965**, *19*, 131.

[88] T. S. Tripathi, J. P. Niemela, M. Karppinen. *J. Mater. Chem. C*, **2015**, *3*, 8364-8370.

[89] T. S. Tripathi, C. S. Yadav, M. Karppinen. *Appl. Mater.*, **2016**, *4*, 1-7.

[90] R. A. Hammoodi, A. K. Abbas, A. K.Elttayef. *Int. J. Appl. Innov. Engi. Manag.*, **2014**, *3*, 1-7.

[91] J. Laine, J. Brito, F. Severino. *Catal. Lett.*, **1990**, *5*, 45-54.

[92] F. Kapteijn, J. Rodriguez-Mirasol, J. A. Moulijn. *Appl.Catal. B: Environ.*, **1996**, *9*, 25-64.

[93] E. R. S. Winter. *J. Catal.*, **1974**, *34*, 431-439.

CHAPTER-VI

SYNTHESIS AND CHARACTERIZATIONS OF MESOPOROUS Zn-Cr-LDH AND ITS APPLICATION FOR THE HYDROGENATION OF CO_2

❖ This Chapter has been published in ***Journal of CO_2 Utilization, 21 (2017) 40-51***.

GRAPHICAL ABSTRACT

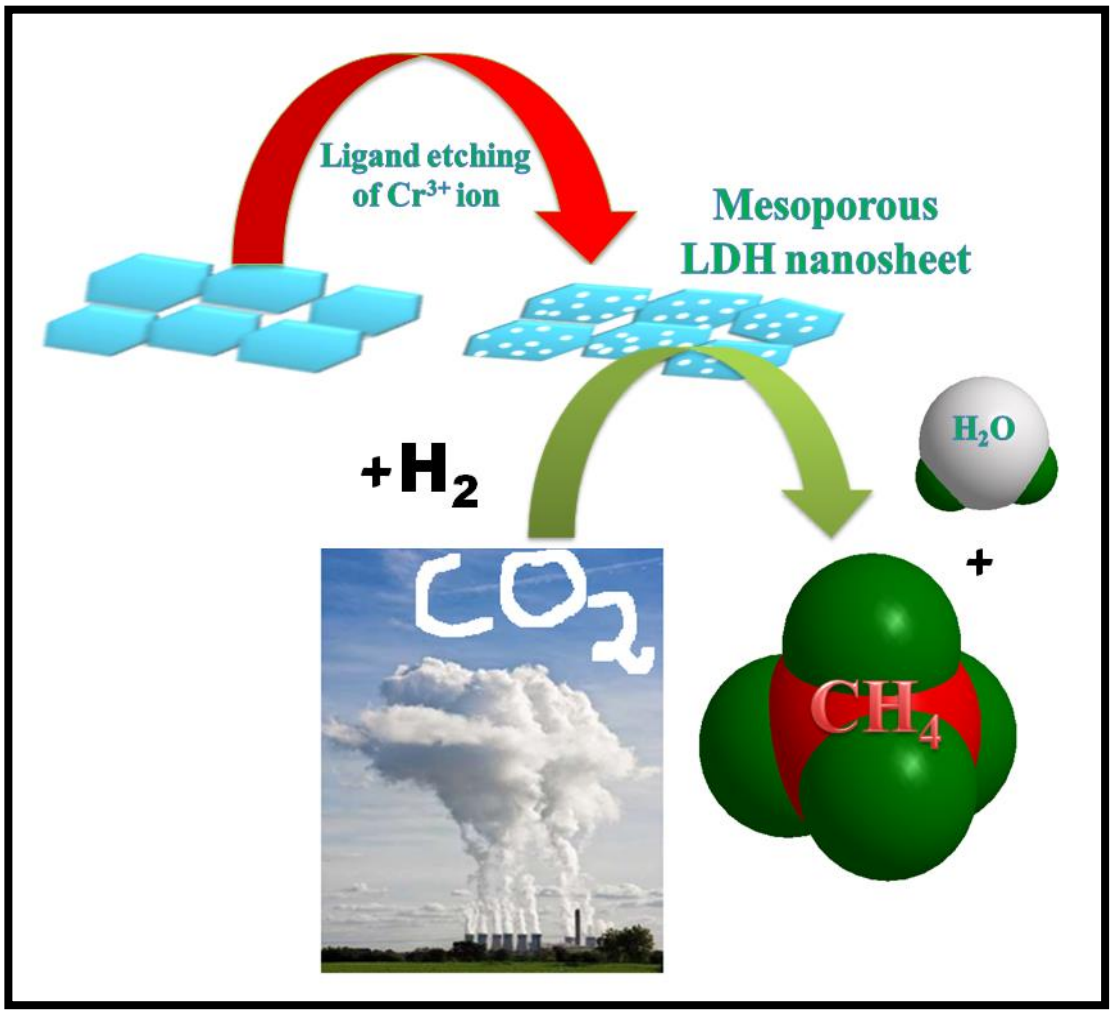

Mesoporous LDH nanosheets obtained by ligand etching as a catalyst for CO_2 hydrogenation to CH_4 and H_2O

ABSTRACT

High surface area mesoporous holey hydroxidic nanosheets were synthesised by reacting Zn-Cr-LDH with β-diketonate ligands. The different β-diketonate ligands having keto-enol tautomeric behaviour and the strength of enolic acids increasing in the order 1-phenyl-1,3-butanedione < 2,4-pentanedione < 1,1,1-trifloro-2,4-pentanedione were reacted with Zn-Cr-LDH. Strong 1,1,1-trifluoro-2,4-pentanedione reacted with Zn-Cr-LDH at room temperature itself and broken the layered structure of LDH forming a segregated Cr^{3+} stable diketo complex. On the other hand, 2,4-pentanedione and 1-phenyl-1,3-butanedione reacted with Zn-Cr-LDH at temperatures 45 and 65 ^{o}C respectively. 2,4-pentanedione preferentially etched out Cr^{3+} ion by leaving behind the LDH like structure with mesoporous holes. 1-phenyl-1,3-butanedione due to its still weaker acid strength could not etch out Cr^{3+} ion. The pores obtained in the LDH nanosheets from the reaction with 2,4-pentanedione were found within a narrow size range of 2-10 nm. Also, their BET surface area was higher. The calcined form of this mesoporous material was used as a catalyst for the hydrogenation of CO_2. The catalytic reactions carried out at temperature 200-400 ^{o}C showed approximately 100 % selectivity towards CH_4 with a small amount of H_2O as a by-product without the deposition of coke and formation of additional CO. Thus, by virtue of its improved performance at lower temperatures it is expected to have an advantage over many existing similar CO_2 hydrogenation catalysts.

6.1. INTRODUCTION:

Presently, CO_2 is considered as the most dreaded green house gas with a massive environmental threat. The CO_2 concentration in the environment has risen from a pre-industrial level of 2.8×10^{-4} ppm to a present level of 3.86×10^{-4} ppm [1-4]. Sequestration of CO_2 is considered as an immediate remedy to control its rapidly rising concentration. Another important strategy to reduce global warming is the conversion of CO_2 to valuable feedstock like methane by Sabatier reaction [3,5-7] -

$$CO_2 + 4H_2 \longrightarrow CH_4 + 2H_2O, \qquad \Delta H_{298\,K} = -\,252.9\ \text{kJ/mol} \qquad (6.1)$$

Due to its high calorific value and environmental friendliness CH_4 is considered as a highly efficient future energy carrier [8]. Conversion of CO_2 to CH_4 over different transition or non-noble metal supported, various mesoporous and LDHs based catalysts has been investigated by many researchers [1-20]. This reaction is accompanied by two side reactions one is CH_4 decomposition and another is Boudouard reaction of disproportionation of CO_2 [16] .Coke formed in these side reactions suppresses the catalytic activity [16]. Therefore, the formation of CH_4 from CO_2 by controlling such type of side reactions is one of the most important areas of research.

Different catalysts like nickel-based $Ce_xZr_{1-x}O_2$ catalyst, Co-Fe bimetallic catalyst, Manganese complexes, Ni-Al-LDH, W-doped Ni-Mg mixed oxide for the hydrogenation of CO_2 has been reported (R. Razzaq *et al*.[8], M.K. Gnanamani *et al*.[9], K. S. Rawat *et al*.[2], S. Abate *et al*.[17] and Y.Yan *et al*.[21]). Although, all these catalysts acted positively in the methanation reactions at low temperatures but some higher hydrocarbons and some additional CO are also formed as by product due to which the selectivity towards CH_4 decreases. Also, in case of some of these catalysts the coke deposition causes further decrease of catalytic activity.

Reports are there about the use of some mesoporous catalysts which have reduced coke deposition property and high CO_2 selectivity. It is reported that, due to the high surface area, enhanced yields, selectivity and ability to control the pore structures mesoporous materials are advantageous over other catalysts (N. Linares *et al*.[22]). L. Xu *et al*.[16,23] has reported the CO_2 methanation over mesoporous $CoAl_2O_4$ and $NiO-Al_2O_3$ type mixed oxide spinels. Similarly, Nannan *et al*.[24] has reported about the use of mesoporous $Ni-CaO-ZrO_2$ based catalysts for conversion of CO_2 and CH_4 to CO and H_2 or dry reformation without any formation of carbon deposits. Apart from these, several other mesoporous catalysts for CO_2 methanation reaction like ZSM5, mesoporous Co/KIT-6 and Ni-MCM-41 catalyst are also reported (L.P. Teh *et al*.[13], G. Zhou *et al*.[15], Guoan Du *et al*.[20]). Although, these catalysts act effectively for the CO_2 methanation reaction at low temperature without deposition of coke, the hydrothermal instability of the mesoporous framework of these catalysts deactivates them easily.

In this chapter, we are reporting the CO_2 methanation reaction in presence of mesoporous catalysts derived from Zn-Cr Layered Double Hydroxide (LDH) precursor. LDHs have the general formula $[M_{1-x}^{2+}M_x^{3+}(OH)_2]^{x+}[A_{x/n}]^{n-}$ .m H_2O where, M^{2+} = Zn^{2+}, Ni^{2+}, Mg^{2+}, Cu^{2+} ions etc. and M^{3+}= Cr^{3+}, Al^{3+}, Co^{3+} ions etc. with A^{n-} as different intercalated anions [25-28]. LDHs are used in many environmentally important reactions such as control of N_2O emission, hydrogenation of CO_2, catalytic partial oxidation of CH_4 to syngas. Due to various catalytically important properties such as high surface area, uniform atomic level distribution of metal ions in the same nano-sheet, compositional diversity, acid-base bifunctionality LDH can be used to synthesise new structured and novel supported catalysts [17-19, 29-38]. The use of Zn-Cr-LDH as catalyst in hydrogen production has been reported by D. Li *et al*.[39]

In this work report is made about the synthesis of mesoporous Zn-bearing-LDH like nanosheets by the interaction of Zn-Cr-LDH with some β-diketonate ligands. Generally, β-diketonate ligands are bidentate ligands which undergo keto-enol tautomerism and reacts with metal hydroxides by acid-base neutralization reactions through their enolic tautomer [40-45] In the process in many cases with metal ions like Zn^{2+}, Cr^{3+} and Cu^{2+}, they also form sublimable metal β-diketonates which have important applications as Chemical Vapour Deposition film growth precursors.

The synthesis of mesoporous Co-Al-LDH by alkali etching of Al^{3+} ion was also reported by Zhiyi Lu *et al*.[46] Radha *et al*.[47] have reported preferential leaching out of Cr(III) ion from Zn-Cr LDH structure by alkaline hypochlorite solution, however, the $Zn(OH)_2$ formed had a structure different from the parent LDH. Similar synthesis of mesoporous holey nanosheets with in plane pores from another synthetic layered material MnO_2 by selective leaching of some Mn^{4+} ion centers through some oxidation reduction reaction involving surface adsorbed Fe^{3+} ions has also been reported by G. Zhang *et al*.[48]

The method we present is a simple low cost, soft chemical method of development of holey mesoporosity in layered oxidic nanosheets and for that matter in their layered hydroxidic precursor. The method adopted here is different from the mesoporosity development in layered materials by intercalation of some active metal or metal oxide pillars inside LDH nanosheets. The present work also reports the effect of acid strength of β-diketonate ligands on their reaction with Zn-Cr-LDH. To the best of our knowledge synthesis of the mesoporous LDH by preferential etching out of constituent metal ion by some organic ligands and use of their calcined product in CO_2 hydrogenation reactions as catalyst has not been reported yet.

6.2. EXPERIMENTAL SECTION:

This **chapter** describes about the synthesis of mesoporous Zn-Cr-LDH by etching out of Cr^{3+} ion using different types of β-diketonate ligands such as 2,4-Pentanedione (acetylacetone)1,1,1-Trifluoro-2,4-pentanedione and 1-Phenyl-1,3-butanedione at different temperatures. This **Chapter** also describes the effect of strength of different types of β-diketonate ligands on the synthesis of mesoporous Zn-Cr-LDH. Mesoporous Zn-Cr-LDH synthesized was then characterized by XRD, FT-IR, TGA-DTG, BET surface area and pore volume analysis, XPS SEM, TEM and EDS analysis. The mesoporous Zn-Cr-LDH was then used as a catalyst for hydrogenation of CO_2. This Chapter also describes the preparation of catalyst and it was further characterized by H_2-TPR analysis.

6.2.1. Synthesis of Zn-Cr-LDH (ZCL):

ZCL was synthesized by oxide hydrolysis method using Zinc Oxide (ZnO, Merck, 99 %) and 1M Chromium trichloride hexahydrate ($CrCl_3.6H_2O$, Loba Chemie, 93 %). About 7 g of Zinc oxide (ZnO, Merck, 99 %) was taken in a beaker. A little amount of water was added to make a paste. 1M solution of Chromium trichloride hexahydrate ($CrCl_3.6H_2O$, Loba Chemie, 93 %) was added dropwise to the paste with constant stirring. The pH of the solution was maintained at 4 to avoid the entering atmospheric CO_2 [49,50]. After addition of about 20 ml of $CrCl_3$.$6H_2O$ the reaction mixture was stirred for 6 hours. The temperature of the system was maintained in the range of 50-60 ^oC. The Zn-Cr-LDH formed this way is free from the presence of CO_3^{2-} ion in the interlayers as overall acidic pH of the system prevents atmospheric CO_2 to attack the interlayer positions. After the completion of the reaction as seen by the formation of pink product in the bottom the supernatant was decanted off. The product was filtered with Whatman No. 42 and washed with hot water for the removal of excess Cl^- ion. The decanted product was then dried in air oven at 40 ^oC.

6.2.1.1. Reaction between Zn-Cr-LDH and different β-diketonate ligands:

About 2 g of Zn-Cr-LDH was taken in a 50 ml reactor and 50 mmol of 2,4 pentanedione (Acetylacetone (AcAc); from M/s TCI, 99 % purity) was added to it. The mixture was then stirred in magnetic stirrer for 3-5 hours at 45 ^{o}C. Finally, the product obtained was filtered with Whatman No. 42 filter paper and washed with deionized water. Same procedure was also followed in the reaction of Zn-Cr-LDH and 1-phenyl 1,3-butanedione (Benzoylacetone or BzAc from M/s Alfa Aesar, 98 % purity) and 1,1,1-trifloro 2,4 pentanedione (TFAcAc, from M/s Alfa Aesar, 98 % purity). The reactivity of these β-diketonate ligands with metal hydroxides depend on their enolic acid strengths and follows the order 1-Phenyl-1,3-butanedione < 2,4-Pentanedione < 1,1,1-Trifluoro-2,4-pentanedione. Depending upon their acid strength the reaction between ZCL and these β-diketonate ligands were carried out at 45 ^{o}C with AcAc, at 65 ^{o}C with BzAc and at room temperature with TFAcAc respectively. The molar ratio of ligand to LDH was maintained at 3:1. The products obtained were filtered and washed with deionized water. The products obtained were then recrystallised from $CHCl_3$. After recrystallisation the residue and filtrate fractions were separated out by filtration in cold condition in an ice bath. After washing and recrystallisation the residue and filtrate fractions were further characterized by various instrumental techniques.

6.2.2. Preparation of catalyst:

The mesoporous ZCL (m-ZCL-AcAc) obtained after the reaction with 2,4-Pentanedione (Acetylacetone) was further calcined at 450 ^{o}C in air for 5 hours. The calcined material, which was also a mesoporous metal oxide powder (cm-ZCL-AcAc) was then used for CO_2 hydrogenation reaction.

6.2.2.1. Catalyst activity test:

About 0.3g of cm-ZCL-AcAc was packed inside a stainless steel tube of inner diameter 0.8 cm and length of 304.8 cm. The pack was guarded with two glass wool plugs placed on its either sides. The catalytic reactions were performed in different gas flow rate conditions under atmospheric pressure at a temperatures range of 200-400 ^{o}C. The flow meters (M/S Gilmont, USA) used were calibrated at different flow rates by common water displacement technique. Before the catalytic reaction, the catalyst was first activated at 400 ^{o}C for 2 hours in a 99.999 % pure Argon atmosphere at a 150 ml/min flow rate. For the catalytic reaction the feed gases of 500 ppm H_2 with Argon balance and 200 ppm CO_2 with Argon balanced at were introduced in a total flow rate of 150 ml/min in presence of 99.999 % pure Argon which was also maintained at a flow rate of 150 ml/min. The H_2:CO_2 mol ratio was maintained at 4:1 for the reaction. The whole reaction was carried out at a Gas Hourly Space Velocity (GHSV) of 29,831 h^{-1} (30,000 $cm^3g^{-1}h^{-1}$). The product gases were collected after 20 min time interval in 1 litre capacity Tedler bags from the outlet of the SS tube and analysed by Gas Chromatograph (Chemito GC1000 from M/S Thermo Fisher, India). The GC was equipped with detectors like Thermal Conductivity Detector (TCD) and Flame Ionization Detector (FID). Low concentration of CO_2 was measured by Ni-Catalytic Reactor attachment fitted in the GC. The product gases such as CO_2 and H_2 were detected by TCD detector and CH_4 was detected by FID detector. H_2 was separated in a Molsieve 5A Q column by keeping the oven temperature at 50 ^{o}C in presence of Argon as a carrier gas with flow rate of 25 ml/min and at 180 ^{o}C TCD temperature. The length of the Molsieve 5A Q column was 240 cm with a diameter of 0.35 cm. The results were estimated with standard calibration gas mixtures of H_2 with Argon balanced = 500 ppm (250 mmol), CO_2 with Argon balanced = 200 ppm (4.5 mmol) and CH_4 with Argon balanced = 527 ppm (32mmol) and supplied by M/S Span Gas

Mumbai, India and standard Gas Chromatographic software IRIS-32 from M/S Thermo-Fischer India.

The product selectivity of CH_4 formation (S_{CH4}) and percentage conversion of CO_2 and H_2 were calculated by using the following equations [8,9] –

CO_2 (%) conversion

$$X_{CO_2}\ (\%) = \left(\frac{[M_{CO_2}]_{in} - [M_{CO_2}]_{out}}{[M_{CO_2}]_{in}}\right) \times 100 \qquad (6.2)$$

CH_4 (%) selectivity

$$S_{CH_4}\ (\%) = \left(\frac{[M_{CH_4}]_{in} - [M_{CH_4}]_{out}}{[M_{CO_2}]_{in} - [M_{CO_2}]_{out}}\right) \times 100 \qquad (6.3)$$

Where, M is the molar concentration of the inlet and outlet gases and S is the CH_4 selectivity with respect to CO_2.

6.2.3. Characterizations:

Structure identification of the recrystallised products were carried out in a powder X-ray diffractometer (Model Rigaku Ultima IV) using Cuk$_\alpha$ radiation of a wavelength of 1.54 Å at 40 mA and 40 kV X-ray generator current setting with a step size of 0.2^o 2θ min^{-1}.

Fourier Transform Infrared (FT-IR) spectra of the recrystallised products were recorded in spectrophotometer (Perkin-Elmer 2000 System) in 4,000-400 cm^{-1} range at a spectral resolution of 4 cm^{-1} using KBr pellets. The concentration of sample in KBr pellet was kept around 0.5 % w/w.

Field Emission Scanning Electron Microscopy (FE-SEM) analysis was carried out in a Carl Zeiss -Sigma VP equipment, at an accelerating voltage of 20 kV. Before the analysis the samples were dried at 40 ^{o}C in air oven for 1 week to avoid the moisture absorption. Finally, the sample surfaces were gold coated in 100 % vacuum. The

chemical composition was identified by using an energy-dispersive X-ray spectroscopy (EDX) attachment present on the scanning electron microscope which was further confirmed from AAS analysis (model Analyst 100 Perkin Elmer). The Transmission Electron Microscopy (TEM) images were recorded on a JEOL JEM-2011 electron microscope operated at an accelerating voltage of 200 kV.

The thermogravimetric measurements were carried out in a simultaneous TG-DTA analyzer (model Q-600, M/S TA Instruments) using α -Al_2O_3 as reference. Samples weighing about 5.0 mg were heated from 30 to 700 ^oC at a rate of 10 ^oC/min under Nitrogen atmosphere with flow rate of 100 ml/min in non-isothermal condition. To check coke deposition the thermogravimetric analysis of calcined m-AcAc-ZCL was carried out under oxygen atmosphere at a heating rate of 10 ^oC/min.

Specific surface area of the samples were recorded *via* Nitrogen gas adsorption at 77 K applying Brunauer-Emmett-Teller (BET) calculations using Autosorb-iQ Station 1 (Quantachrome, USA). Prior to performing the experiment the samples were degassed at 100 ^oC for 1.5 hours.

X-ray photoelectron spectroscopy (XPS) measurements were carried out in Thermo Scientific MULTILAB 2000 Base system with X-Ray, Auger and ISS attachments from Thermo Electron of monochromatic Al Kα X-ray source (1486.6 eV). The photoelectron spectra were calibrated in bond energy, referenced to that of the component C-C of carbon C 1s at 284.8 eV.

Hydrogen temperature programmed reduction (H_2-TPR) was performed in Quanta -chromeChemBET Pulsar TPR/TPD instrument in a quartz U-tube using a TCD detector. Temperature programmed reduction (TPR) of the sample was carried out by taking 90 mg of the sample. The reducing gas was a mixture of 5 vol % H_2 in N_2, at a flow rate of 80 ml/min. The temperature was increased at a rate of 20 ^oC/min from 40

^{o}C to 750 ^{o}C.

6.3. RESULTS AND DISCUSSION:

It is known that β-diketonate ligands undergo keto-enol tautomerism as shown in **Fig. 6.1**. These ligands can easily bind with metal hydroxides by acid-base neutralization reaction and forms metal β-diketonate complexes [45]. Accordingly, depending on this reaction mechanism different β-diketonate ligands with varied acid strengths were used to react with ZCL. The acid strength of the β-diketonate ligands used increases in the order as 1-Phenyl-1,3-butanedione < 2,4-Pentanedione < 1,1,1-Trifluoro-2,4-pentanedione. Phenyl and -CH_3 groups are electron donating groups which causes a considerable decrease in the enol content and destabilize their conjugate bases [51,52]. The effect is higher in case of phenyl group then in case of –CH_3 group. Therefore, BzAc did not react with hydroxides of ZCL while AcAc could react with resulting in etching out of some of the Cr^{3+} ion from ZCL nanosheets producing the formation of mesoporous nanosheets without the breakage of LDH type layered structure.

In his much cited classic work [53]on the structure of Pyroaurite and Sjoegrenite minerals von Allmann have drawn similarity of the structure of the main hydroxidic layer of LDHs with an ideal solid solution of otherwise two immiscible trioctahedral $M(OH)_2$ and dioctahedral $M(OH)_3$ type structures. In actuality the crystal structure of LDH is based on the stacking of parent $M^{II}(OH)_2$ brucite like layers where the small fraction of x is replaced by trivalent cation. In case of Zn-Cr LDH the parent brucite like layers are formed by Zn^{2+} octahedra. As compared to other LDHs another important property of Zn-Cr-LDH is that it can be formed with the ratio of Zn/Cr =2. Due to this Zn^{2+} and Cr^{3+} ions are orderly arranged inside the LDH layers as well as the Zn^{2+} and Cr^{3+} octahedra are alternate with each other [53-59]. In such a situation,

according to hard-soft acid base concept the conjugate base $AcAc^-$ of 2,4-Pentanedione acts as a hard base and preferentially etches out Cr^{3+} which by virtue of its ionic radii and charge is a more harder acid than Zn^{2+}which is a borderline acid [56,60,61] and resulting in the formation of mesoporous ZCL (**Fig. 6.1**).

On the other hand, $-CF_3$ group is an electron withdrawing group and both inductive effect and resonance effect causes the stabilization of its conjugate base. Since, higher is the stability of conjugate base the conjugate acid will more readily deprotonate [61-64]. Due to this conjugate base $TFAcAc^-$ of TFAcAc which also acts as more harder base bind easily with Cr^{3+} of ZCL at room temperature and easily formed corresponding Cr(III) β-diketonate [47].

Before the catalytic reaction the product obtained after the reaction of ZCL and AcAc was characterized by XRD, TGA-DTG, FT-IR, BET surface area analysis. These characterizations are described in the following section. The mesoporous ZCL formed by the reaction of ZCL and AcAc formed at 45 ^oC was further characterized by XPS and H_2-TPR analysis.

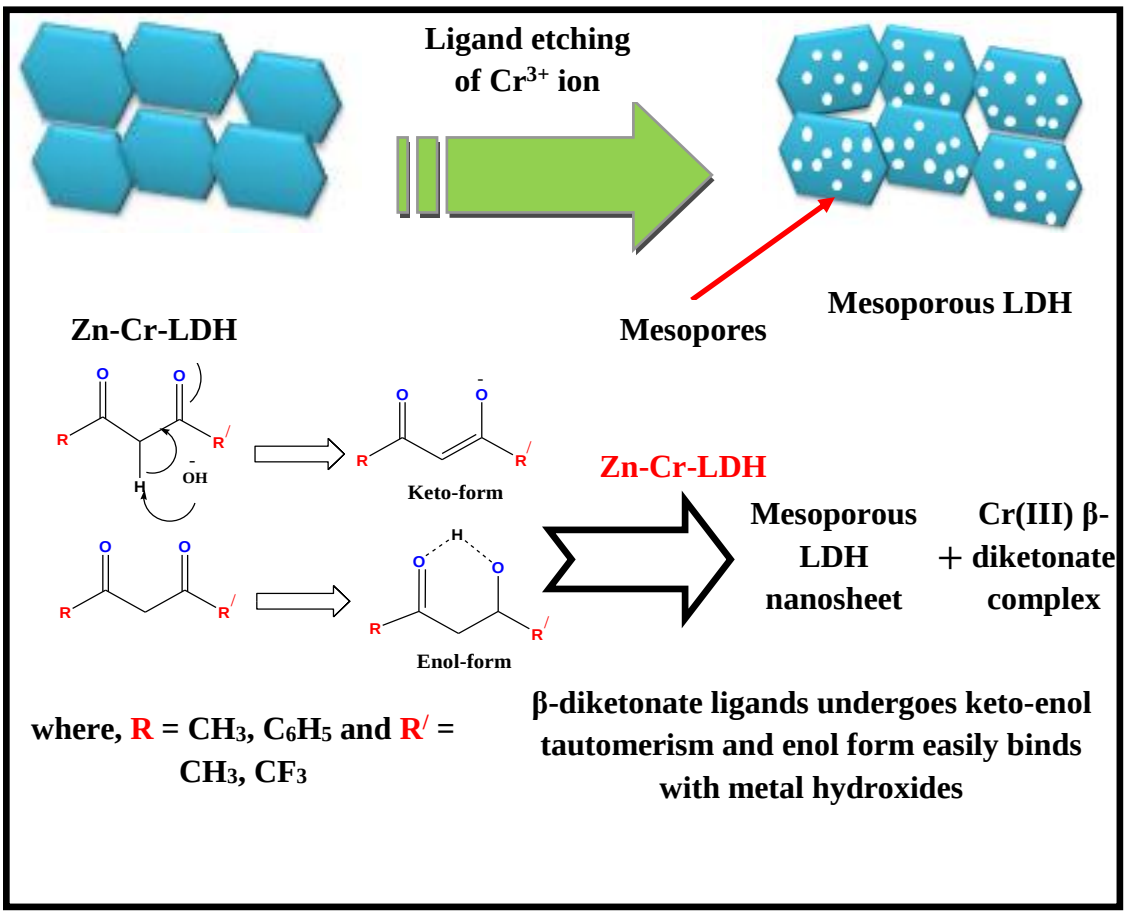

Fig. 6.1: Mechanism of the formation of mesoporous LDH by keto-enol tautomerism of β-diketonate ligands.

6.3.1. Characterizations:

6.3.1.1. PXRD analysis:

The XRD pattern of ZCL (**Fig. 6.2a.A**) showed the peaks with *hkl* reflections of (003), (006), (009) and (012) respectively originating from LDH phase. **Fig. 6.2a.B&C** shows XRD patterns of the product obtained after the reaction of ZCL and AcAc and BzAc respectively it was observed that attempt of the etching out of Cr^{3+} ion by AcAc from ZCL did not cause significant changes in the layered material like crystal structure [46]. The characteristic *00l* basal reflections of these materials remained unchanged. Similar, retention of the parent layered structure after etching out of metal ions through in plane pore formation has been reported in case of layered

MnO_2 structure also [48]. **Fig. 6.2b.** showed the XRD pattern of the dried portion of the filtrate fraction of ZCL and AcAc reacted product. It was observed that the Cr^{3+} ion etched out as $Cr(acac)_3$ after the reaction with AcAc which showed the highest intensity peak with *hkl* reflection of (200) along with the low intensity *hkl* reflections of (002), (011), (212), (-204) and (121) respectively in XRD (**JCPDS Card No.- 00-018-1505**).

On the other hand, the recrystallised product obtained from ZCL and TFAcAc reaction (**Fig. 6.2a.D**) showed the highest intensity peak (d = 4.03Å) with *hkl* reflection of (223) along with other low intensity *hkl* reflections such as (201), (211) respectively due to the formation of $Cr(TFAcAc)_3$ (**JCPDS Card No.- 00-044-1590**). Along with this Cr(III) complex the formation of $Zn(OH)_2$ phase was also evidenced from the XRD pattern which had *hkl* reflections (202), (111), (101), (212) and (115) respectively (**JCPDS Card No.- 00-020-1436**, **Fig. 6.2a.D**). Although, the reaction product of ZCL-TFAcAc was washed in ice cold $CHCl_3$ and from it by XRD solid phases due to $Cr(TFAcAc)_3$ and $Zn(OH)_2$ was identified, however, a diketo complex of Zn like $Zn(TFAcAc)_2$ could not be separated. Probably, if formed this diketo complex decomposed in the solution state due to unstable soft-hard interaction of Zn^{2+} and $TFAcAc^-$ and reverted to $Zn(OH)_2$. Since, it was formed through recrystallisation therefore unlike in AcAc-ZCL case, it acquired a new structure different from the original LDH. Similar reformation of $Zn(OH)_2$ structure after leaching of Cr^{3+} ion in strong reaction conditions has been reported by Kamath and Radha [47].

The XRD pattern of 450 ^oC calcined phase of the reaction product of ZCL and AcAc reacted at 45 ^oC (cm-ZCL-AcAc, **Fig. 6.2a.E**) showed that even after calcination the LDH like structure with remains of basal peaks was not erased off completely and (003) reflection appeared at d= 7.92 Å. However, along with it the XRD pattern

showed the formation of ZnO phase having reflection of (101),(100) and (002) planes along with some low intensity reflections corresponding to $ZnCr_2O_4$ spinel phase showing *hkl* reflection of (440) plane (**JCPDS Card No. 00-001-1123**).

Since, the main objective of this **Chapter** is synthesis and characterizations of mesoporous Zn-Cr-LDH and mesoporous Zn-Cr-LDH was found only in presence of AcAc ligand hence, further characterizations of reacted products obtained in presence of TFAcAc and BzAcAc were not reported in this **Chapter**.

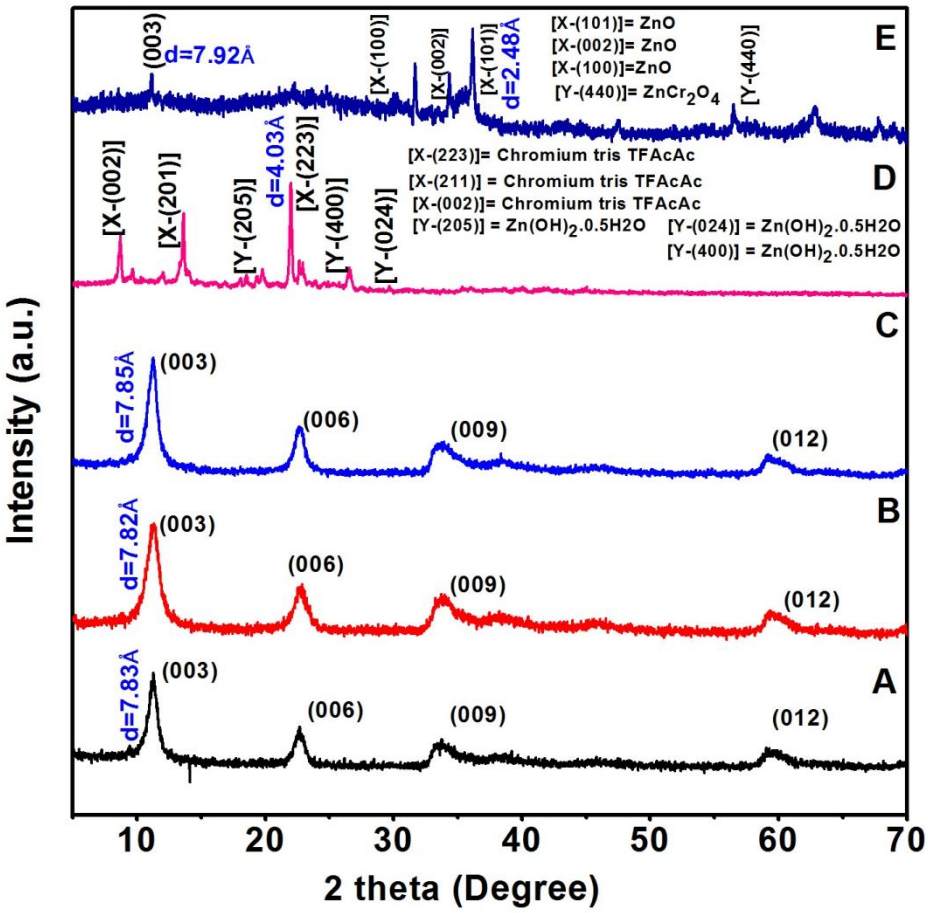

Fig.6.2a : XRD patterns of (A) ZCL , (B) product of reaction of ZCL with AcAc at 45 ºC (m-ZCL- AcAc); (C) ZCL with BzAc at 65 ºC ; (D) ZCL with TFAcAc at room temperature and (E) Calcined mesoporous ZCL (cm-ZCL-AcAc).

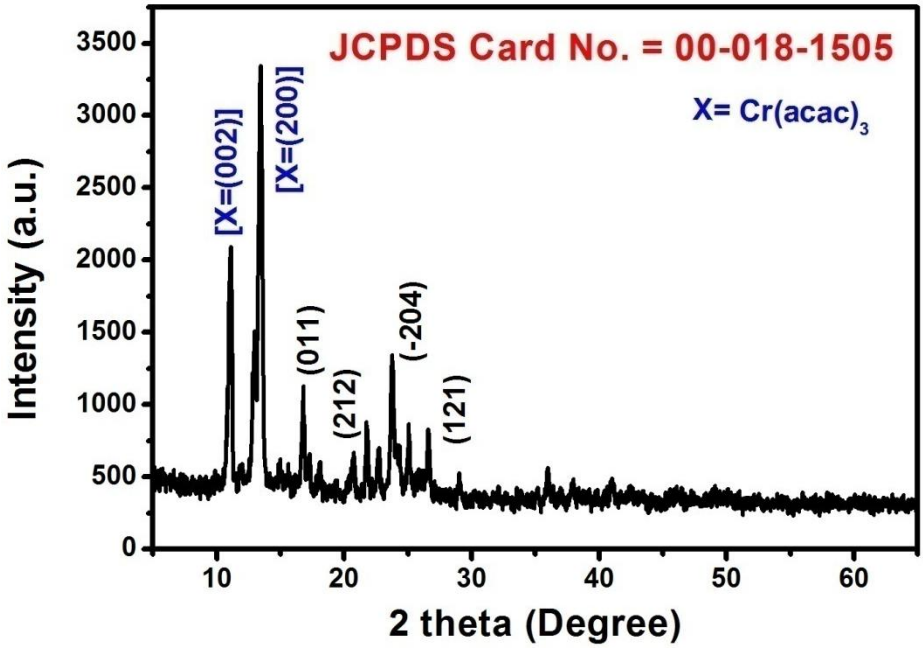

Fig. 6.2b: XRD pattern of the recrystallised product from the filtrate fraction of the ZCL-AcAc reacted product at 45 ºC.

6.3.1.2. TGA-DTG analysis:

The TGA-DTG analysis was carried out under Nitrogen atmosphere to know the thermal stability of the prepared samples. It showed (**Fig. 6.3A**) the three step thermal degradation of ZCL; where the first step of temperature around 50-150 ºC with 15.16 % weight loss corresponds to the removal of surface adsorbed moisture, second step of temperature range around 250-350 ºC with 11.82 % weight loss correspond to the loss of interlayer solvent molecules as well as the interlayer ions and the third step of temperature around 450-600 ºC with 10.4 % weight loss correspond to the dehydroxylation step appearing due to breakdown of brucite like layer [65]. It was observed that due to the etching out of Cr^{3+} ion from ZCL by AcAc ligand the weight loss in the TGA pattern about the breakage of hydroxidic backbone is slightly lower, also it affected on the maximum decomposition temperatures. Side by side as the trivalent Cr^{3+} ion is etched out from the main layer in the second weight loss zone

corresponding to loss of interlayer species. The weight loss in this region is 16.95 % in case of m-AcAc-ZCL and 11.82 % in case of ZCL. The removal of trivalent ion from the main layer leads to decrease in the charge over the main hydroxidic layer resulting in weaker interaction between the interlayer species and the main layer as a result there is greater weight loss from the interlayers m-AcAc-ZCL than in ZCL As, due to etching out of Cr^{3+} ion by AcAc ligand some mesopores were developed resulting in the development of void space inside the hydroxidic nano sheets there is a decrease of the maximum decomposition temperature corresponding to their second and third step degradations from 333.2 ^{o}C and 475.7 ^{o}C in ZCL to 273.2 ^{o}C and 459.31 ^{o}C in ZCL-AcAc. The DTG pattern of cm-ZCL-AcAc (**Fig. 6.3B**) showed the thermal degradation of temperature around 100-120 ^{o}C corresponding to the loss of surface adsorbed moisture and temperature around 150-200 ^{o}C correspond to the loss of traces of moisture bound in the interlayers or pores. There was no further changes in the weight due to the prior conversion of metal hydroxides present to mixed metal oxides. The DSC pattern showed one non weight loss exothermic peak at 430 ^{o}C which could correspond to the segregation of mixed metal oxides to ZnO and traces of $ZnCr_2O_4$ spinel [66].

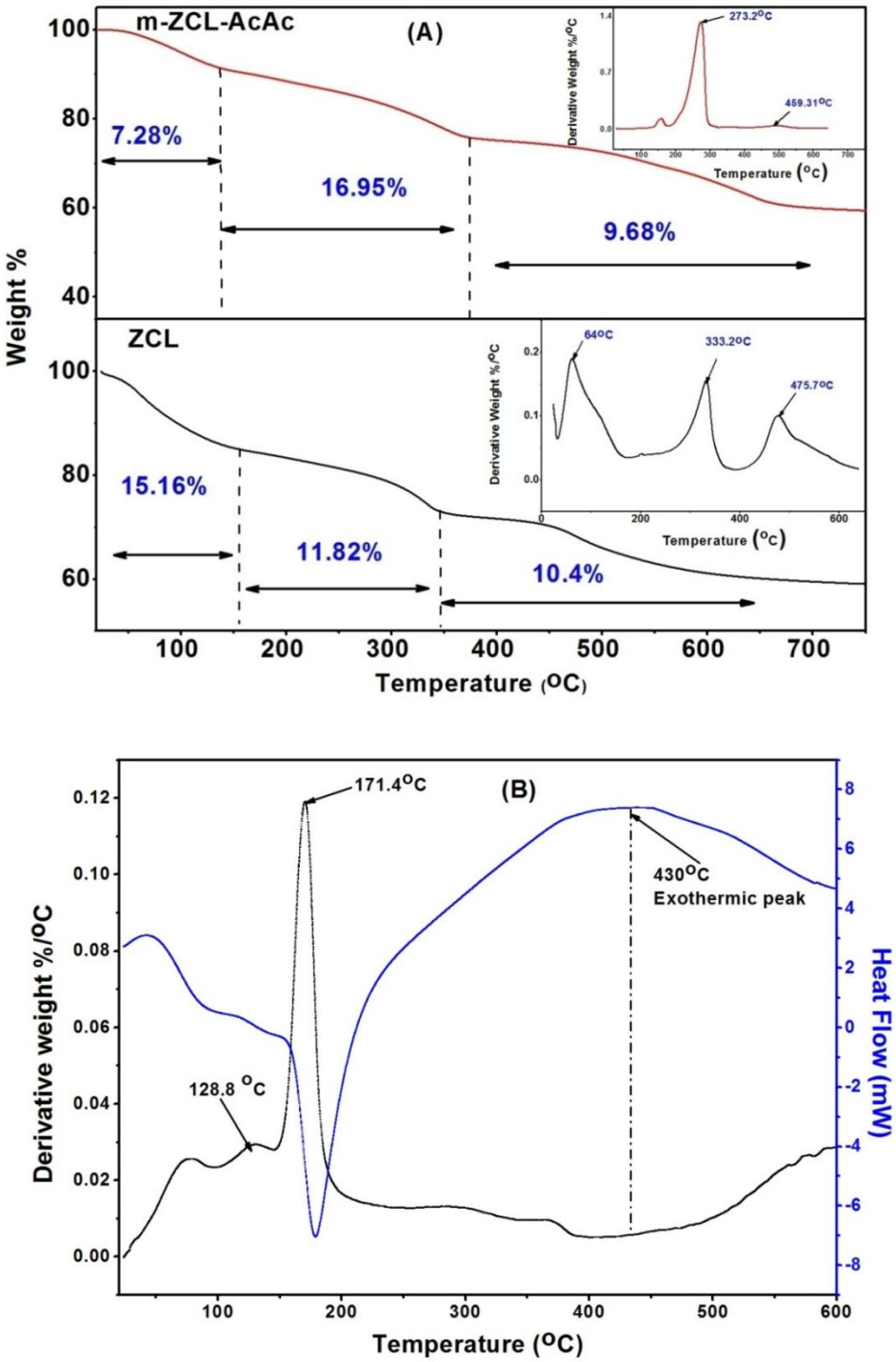

Fig. 6.3: TGA-DTG analysis of ZCL and m-ZCL-AcAc (A) and the calcined mesoporous ZCL (B) (cm-ZCL-AcAc).

6.3.1.3. FT-IR analysis:

The chemical structure of mesoporous LDH synthesized from ZCL was further examined by FT-IR analysis (**Fig. 6.4**). It was observed that etching by AcAc did not

effect much on the positions of the hydroxy groups remaining in the LDH type structure. The –OH stretching band was also obtained at 3439 cm^{-1} in both ZCL and ZCL-AcAc reacted product as the parent ZCL (**Fig. 6.4**). It was observed that ZCL phase showed a broad peak due to the –OH stretching at 3439 cm^{-1}, the peak due to bending mode of –OH group was obtained at 1630 cm^{-1}. The M-O stretching band was obtained at 565 cm^{-1} and 675 cm^{-1} respectively. The –OH stretching band in case of ZCL-AcAc reacted product were also obtained at 3439 cm^{-1}, similarly the –OH bending mode of vibrations were obtained at 1630 cm^{-1} respectively. The M-O stretching vibrations of these products were obtained at around 565 cm^{-1} and 675 cm^{-1} respectively. It was observed that etching by AcAc did not affect much on the positions of the hydroxy groups remaining in the LDH type structure. The M-O stretching vibrations in case of this product were obtained at 527-596 cm^{-1}, 731-790 cm^{-1} and 864-947 cm^{-1} respectively.

In case of calcined mesoporous ZCL (cm-ZCL-AcAc) the some weak –OH stretching vibration was obtained at 2855 cm^{-1} and 2922 cm^{-1} respectively. The bending mode of vibration of –OH was obtained at 1630 cm^{-1} which indicates that at 450 ^{o}C calcination the LDH structure was not completely free from hydroxides some of these are from traces of H_2O adsorbed from the surrounding. The peak for Zn-O and Cr-O stretching vibrations due to ZnO and $ZnCr_2O_4$ phases were obtained at 464 cm^{-1} and 629 cm^{-1} respectively.

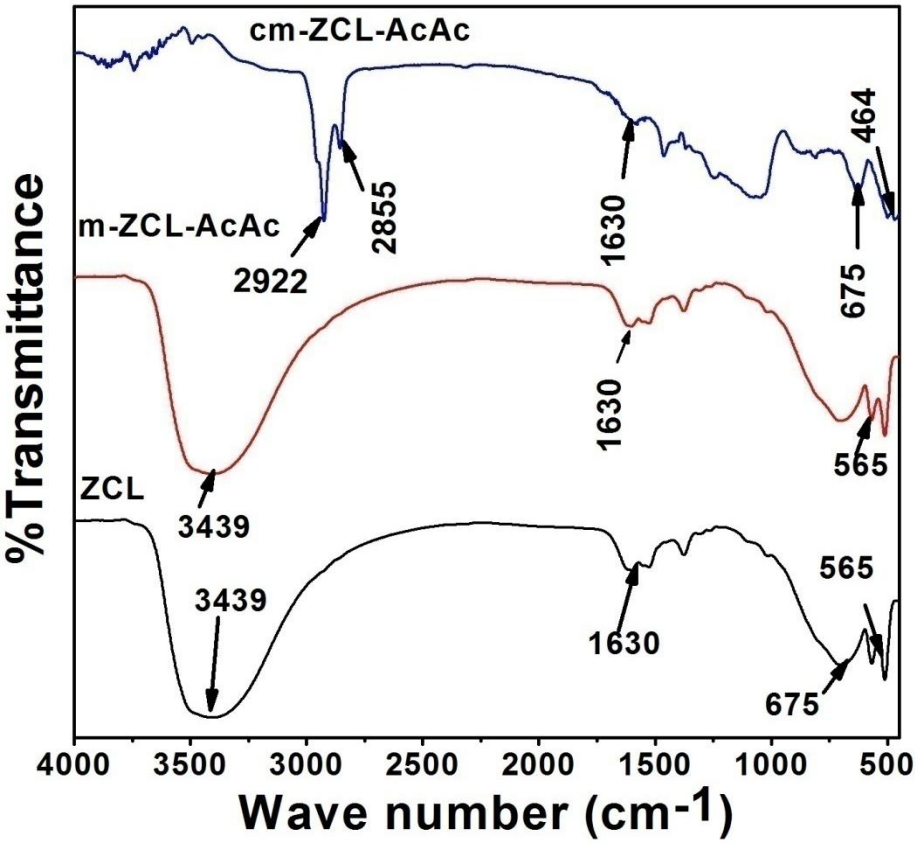

Fig. 6.4: FT-IR patterns of Zn-Cr-LDH (ZCL), product of ZCL and AcAc at 45 ºC (m-ZCL-AcAc) and calcined mesoporous ZCL (cm-ZCL-AcAc).

6.3.1.4. BET surface area and pore diameter:

BET surface area analysis showed that AcAc formed a high surface area mesoporous ZCL (m-ZCL-AcAc) by reacting with ZCL at 45 ºC with average pore diameter of 5.3 nm (**Table 6.1**). The surface area of parent LDH was found as 26.6 m^2/g which increased to 89.5 m^2/g in case of AcAc reacted product (m-ZCL-AcAc). After calcination of m-ZCL-AcAc at 450 ºC in air atmosphere the surface area was further increased to120.6 m^2/gm (cm-ZCL-AcAc) with a slight increase of pore diameter from 5.3 nm to 5.4 nm due to the conversion of mesoporous mixed metal hydroxide to mesoporous mixed metal oxide. **Fig. 6.5A&B** shows the nitrogen adsorption and desorption isotherms (A) and pore size distribution curves (B) for these products, where around 5nm porosity is prominently shown by m-ZCL-AcAc.

Since, from the perspectives of heterogenous catalysis higher is the surface area better is the catalytic activity, therefore mesoporous ZCL (m-ZCL-AcAc) or its calcined mesoporous product (cm-ZCL-AcAc) can be expected to be better catalyst for suitable reactions involving gas phase reactions. Accordingly, the same was selected as a catalyst for an environmentally important reaction hydrogenation of CO_2.

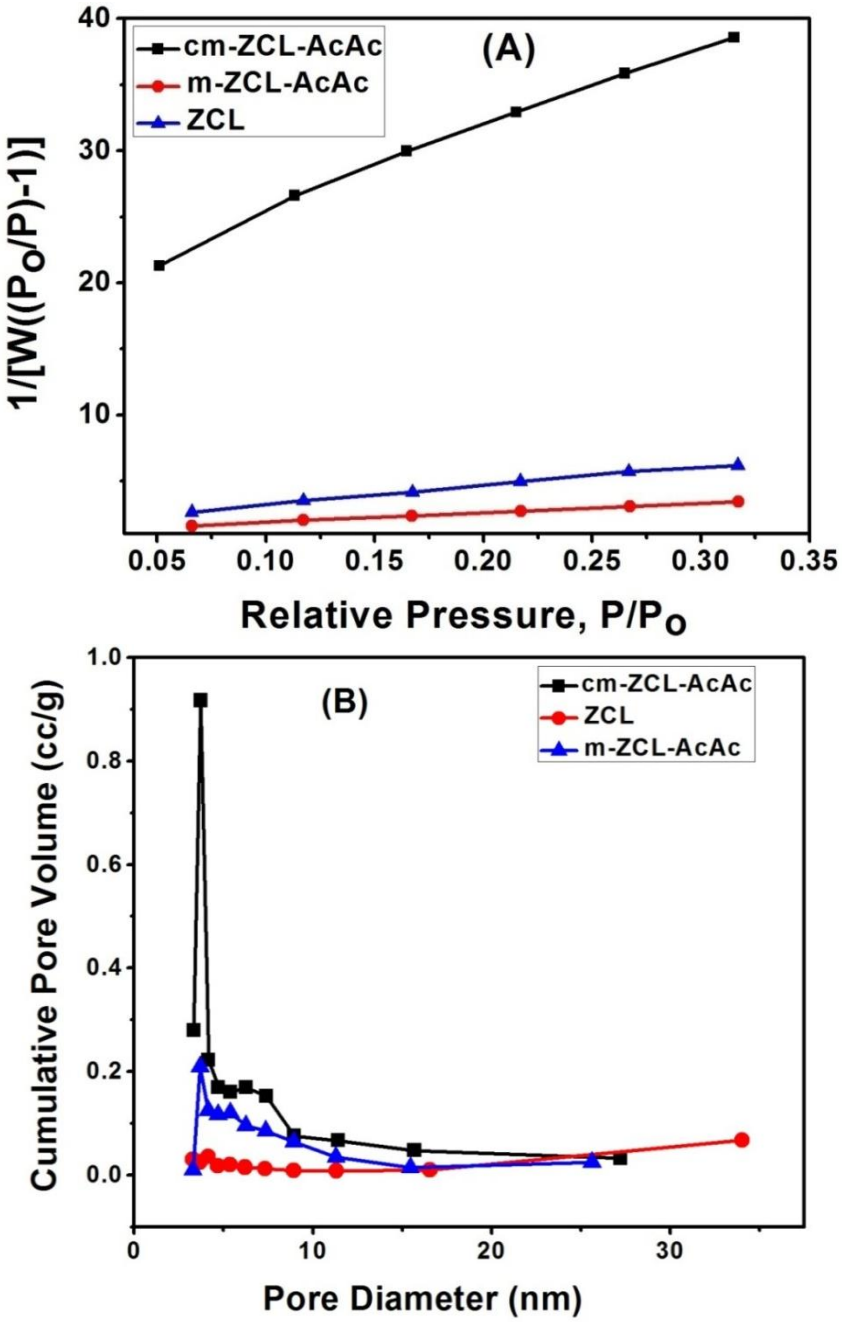

Fig. 6.5: BET plot (A) and pore size distribution (B) curves for the product obtained from ZCL and AcAc at 45 °C.

Table 6.1: Surface area and pore radius of Zn-Cr-LDH and the product of the reaction between Zn-Cr-LDH and AcAc

Serial No.	Samples	BET surface area (m^2/g)	Pore diameter (nm)
1	ZCL	26.6	3.6
2	ZCL with AcAc at 45 ºC (m-ZCL-AcAc	89.5	5.3
3	Calcined mesoporous from ZCL-AcAc (cm-ZCL-AcAc)	120.6	5.4

6.3.1.5. XPS analysis:

The chemical state of Zn, Cr and O in uncalcined mesoporous ZCL (m-ZCL-AcAc) was analysed by XPS analysis (**Fig. 6.6**). XPS analysis showed the peak due to O1s (531.85 eV), Zn 2p (1021.79 eV and 1044.8 eV) and Cr 2p (577.5 eV and 587.3 eV) (**Table 6.2**). XPS spectra of Zn2p showed the binding energy of 1021.79 eV for $Zn2p_{3/2}$ and 1044.8 eV for $Zn2p_{1/2}$ (**Fig. 6.6B**) whereas XPS spectra of Cr2p showed the binding energy of 577.5 eV for $Cr2p_{3/2}$ and 587.3 eV for $Cr2p_{1/2}$ (**Fig. 6.6C**) which indicated the presence of both $Zn^{2+}$and Cr^{3+}states in ZCL [67-69]. XPS spectra of O1s showed the peak at binding energy of 531.85 eV indicated the presence of OH group [70] (**Fig. 6.6D**). It was thus confirmed from XPS that the small amount of Cr ion in m-ZCL-AcAc was present in Cr^{3+} oxidation state, which perhaps is responsible for existence of some LDH like structure even after etching of major amount of Cr by AcAc.

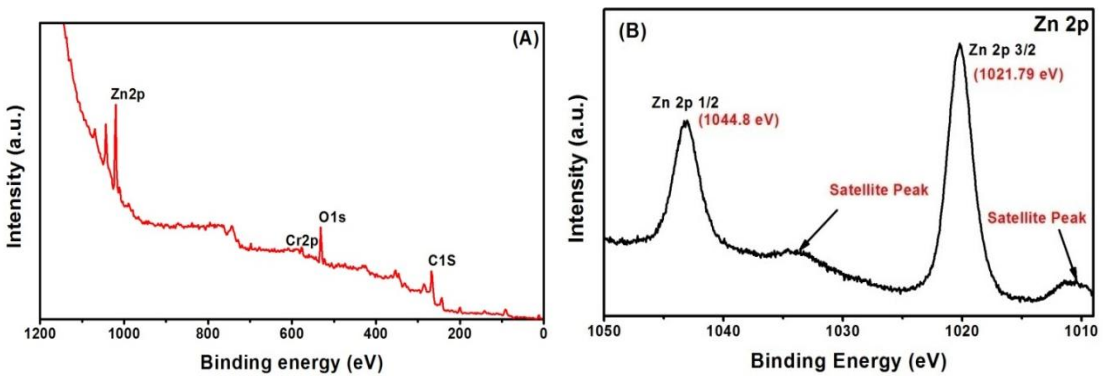

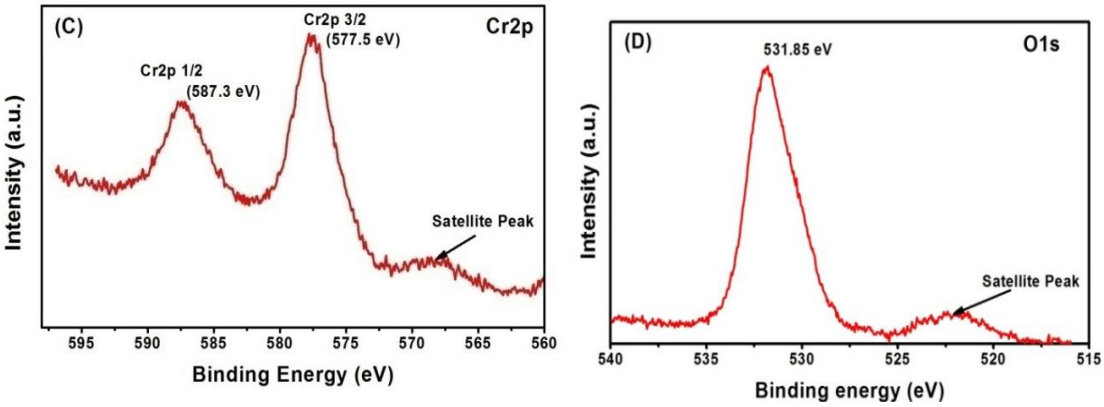

Fig. 6.6: XPS survey (A) spectra of Zn2p (B) and Cr2p (C) scan for mesoporous ZCL (m-ZCL- AcAc).

6.2: XPS results of Zn 2p, Cr 2P and O 1s peaks of mesoporous ZCL (m-ZCL-AcAc)

Sample	Zn $2p_{3/2}$, Zn $2p_{1/2}$ (eV)	Cr $2p_{3/2}$, Cr $2p_{1/2}$ (eV)	O1s (eV)
Mesoporous ZCL (m-ZCL-AcAc)	**1015-1045**	**570-590**	**525-535**

6.3.1.6. SEM, EDS and TEM analysis:

Fig. 6.7A&B showed the SEM and EDS patterns of ZCL. SEM images of ZCL showed the flower like hexagonal platelet characteristic of LDH structure. The elemental composition of ZCL as analysed by EDS analysis showed the presence of Zn, Cr, Cl and O with weight percentage of 48.83 %, 24.15 %, 8.77 % and 18.25 % respectively. The Zn/Cr ratio in ZCL was found as 2:1. SEM pattern of mesoporous m-ZCL-AcAc (**Fig. 6.7C**) showed the same morphology of layered hexagonal platelet as of parent ZCL nanosheets which are generally shown by LDH type crystals. The length of the hexagonal plates was about 0.2-1 µm and thickness of 10-50 nm respectively (**Fig. 6.7E**). Preferential etching of Cr^{3+} by AcAc and consequent formation of meso pores in these nano sheets were further observed from the EDS

pattern of m-ZCL-AcAc (**Fig. 6.7D**) where the Zn/Cr ratio decreased to 48.83:1.03 weight % which was also obtained from AAS based elemental analysis. **Fig. 6.7F** showed the SEM image of calcined mesoporous ZCL. It was observed that after calcination also the external morphology of the nanocrystals remained similar to parent hexagonal LDH crystals. **Fig. 6.7G-L** showed the elemental mapping of Cr, Zn, O and C respectively which also confirmed the etching out of Cr^{3+} ion as the elemental composition of Cr was found to decrease.

The formation of mesoporous LDH was further analysed by TEM analysis (**Fig. 6.8**). TEM image of mesoporous LDH (**Fig. 6.8A**) showed that the LDH layers were stacked over the other. **Fig. 6.8B** showed the lattice fringes with 0.263 nm and 0.113 nm dimensions indicating the presence of (003) and (009) plane of LDH. Due to preferential etching out of Cr^{3+} ion some pores were developed which were found to have dimension of 2-10 nm in TEM analysis (**Fig. 6.8C&D**).

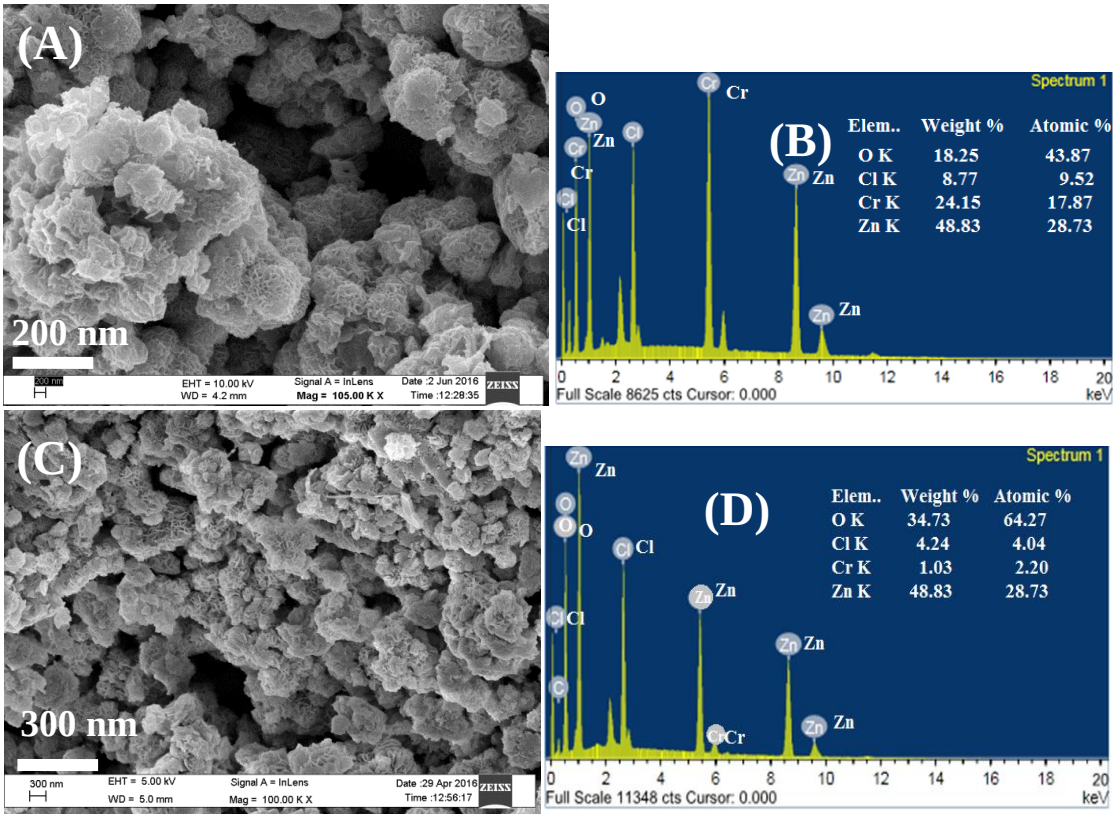

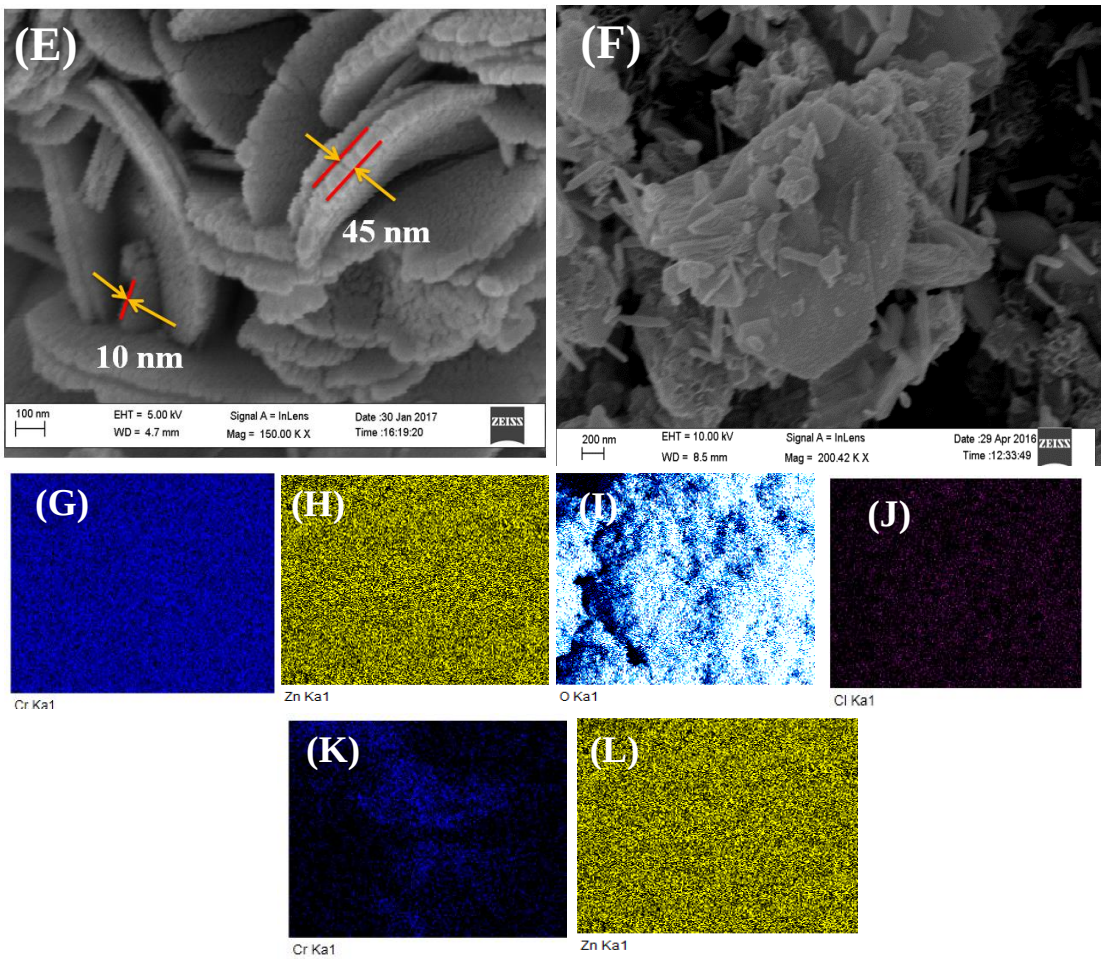

Fig. 6.7: SEM and EDS patterns of ZCL (A&B), mesoporous ZCL (m-ZCL-AcAc) showing the thickness of LDH layers (C, D&E), calcined mesoporous ZCL (cm-ZCL-AcAc) (F) ; elemental mapping of ZCL and mesoporous ZCL (m-ZCL-AcAc) for Cr (G&K), Zn (H&L), O (I), Cl (J).

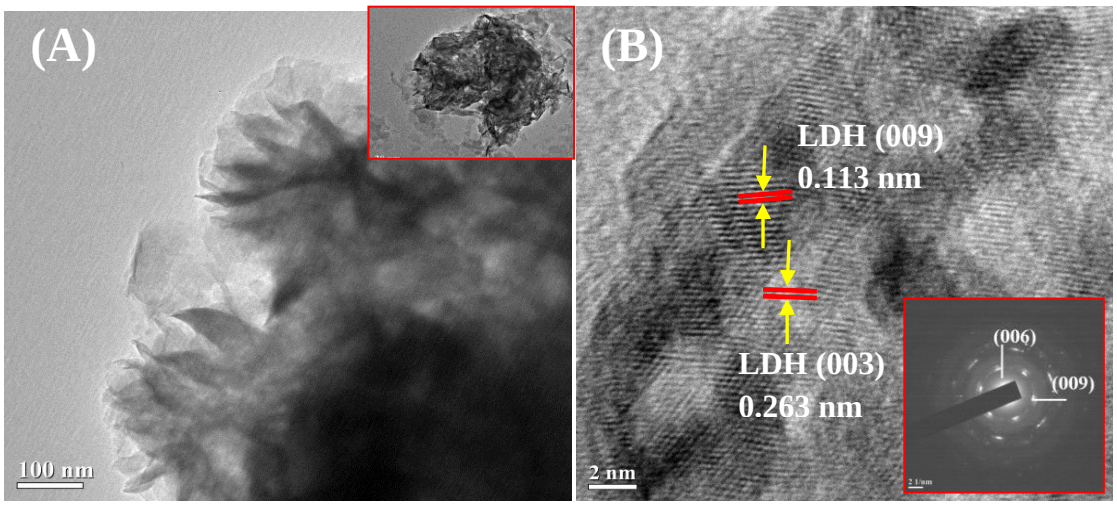

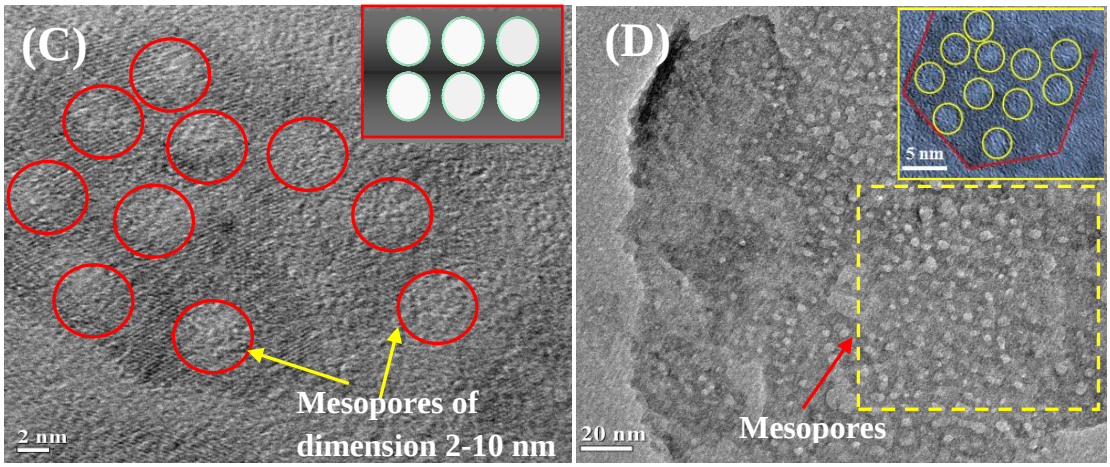

Fig. 6.8: TEM images of mesoporous ZCL (m-ZCL-AcAc) (A, C&D); lattice fringes of mesoporous ZCL (m-ZCL-AcAc) (B) with 0.263 nm and 0.113 nm dimension along with SAED image.

6.3.1.7. H_2-TPR analysis:

The H_2-TPR analysis of calcined mesoporous ZCL (cm-ZCL-AcAc) was carried out to investigate the reducibility of the catalyst. It showed two reduction peaks at temperatures 450 and 550 ^oC respectively (**Fig. 6.9**). The peak at 450 ^oC was due to the reduction of ZnO to free state Zn and at 550 ^oC was due to the formation of $ZnCr_2O_4$ spinel [66,71] which was observed in XRD analysis also. The broad reduction peak obtained after H_2 adsorption at temperatures ranging from 300-500 ^oC was due to the presence of excess Zn active site. Since, higher is the reducibility of ZnO to free state Zn better is the catalytic activity [71,72]. Hence, this catalyst showed better catalytic activity which was due to Cr^{3+} depletion and through that enrichment of free state Zn as well as mesoporosity development.

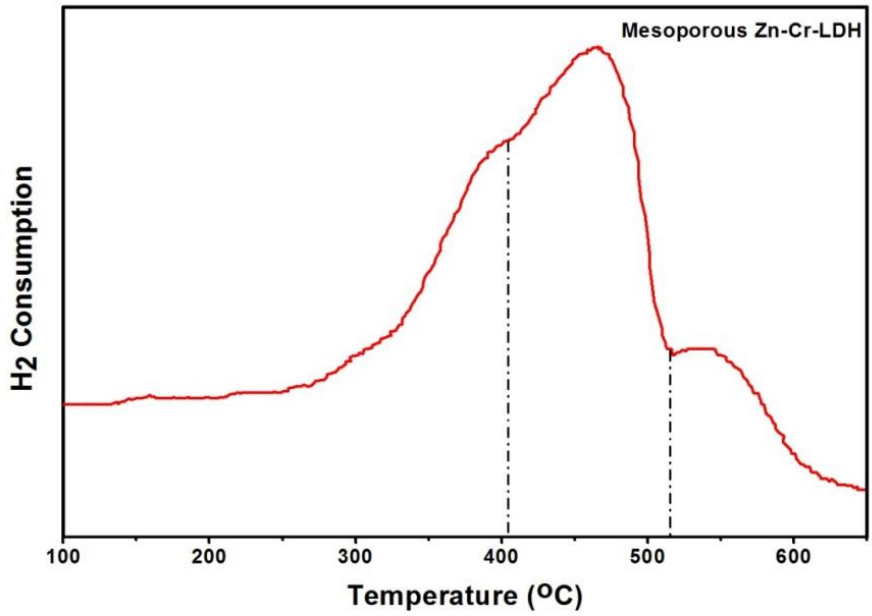

Fig. 6.9: H_2-TPR profile of calcined mesoporous ZCL (cm-ZCL-AcAc) catalyst.

6.3.1.8. Catalytic activity of Mesoporous Zn-Cr-LDH (cm-ZCL-AcAc):

6.3.1.8.1. Effect of temperature on catalytic activity:

The conversion of CO_2 and H_2 in presence of mesoporous calcined ZCL was carried out at temperature ranging from 200-400 °C and Gas Hourly Space Velocity (GHSV) of 29,831 h^{-1} under atmospheric pressure. **Fig. 6.10a.A&B** showed the CO_2 and H_2 conversion curves respectively with temperature (**Fig. 6.10b.A&B**). It was observed that with the increase of temperature the degree of conversion also increased. At temperature 200 °C, the percentage conversion of CO_2 was about 78.11 % which increased upto 99.8 % conversion at 400 °C. Similarly, the percentage conversion of H_2 was observed as 70.24 % at 200 °C which increased upto 99.1 % at 400 °C (**Table 6.3**).

Fig. 6.10a.C showed the CH_4 (%) selectivity curve with temperature (**Fig. 6.10b.C**). It was observed that mesoporous ZCL showed good catalytic activity within temperature of 200-400 °C. Initially, CH_4 selectivity at temperature 200 °C was about 31.47 %, which was found to increase with temperature. At 400 °C the CH_4 selectivity

was found as high as 99.9 %. The results are shown in (**Table 6.3**). As reported in earlier literature mesostructure could promote catalytic activity due to large surface area, large pore volume and more barrier free pore channels [16,73,74]. Mesoporous ZCL with pore diameter of 2-10 nm showed better CH_4 selectivity due to its high surface active sites availabilty and narrow pore radius. Since, the kinetic diameter of H_2, CH_4 and CO_2 are 0.3 nm, 0.4 nm and 0.33nm respectively [22,75] hence, mesoporous ZCL adsorbed H_2 and CO_2 in their active sites and formed CH_4 and H_2O as product which is shown in the following equation –

$$CO_2 + 4H_2 \longrightarrow CH_4 + 2H_2O \qquad (6.4)$$

6.3.1.8.2. Catalytic stability test with time:

Catalytic stability was analysed at different temperature from 200-400 ^oC for 40 hours with GHSV of 29,831 h^{-1} (30,000 $cm^3g^{-1}h^{-1}$) under atmospheric pressure. **Fig. 6.11** showed the catalytic stability curves for mesoporous ZCL catalyst. It was observed that, this catalyst showed high catalytic activity and good catalytic stability during the 40 hours reaction time. It was further observed that with the increase of time the percentage conversion of CO_2 and H_2 as well as the CH_4 formation also increased in the temperature range of both 200-300 ^oC as well as 350-400 ^oC. Finally at 350-400 ^oC it showed complete conversion of CO_2 to CH_4 from 95.7 % to 99.9 %. This effect we ascribe as due to the stability of the mesoporous structure of ZCL nanosheets with depleted Cr content and enriched Zn content.

It was further observed that there was no coke deposited on this catalyst as analysed by TGA-DTG (**Fig. 6.11**) after 40 hours long term stability test under oxygen atmosphere which showed only 1 % weight loss. Due to which this catalyst could actively promote the catalytic activity without the formation of additional CO as intermediate. Besides, it produced only small amount of H_2O as by product. In

comparison to other mesoporous catalyst used in hydrogenation reaction [3,10-23] it showed better catalytic activity with 99.9 % CH_4 formation at low temperature below 400 ^oC.

It is reported by L. Xu *et al*.[16] that mesoporous catalyst helps in low carbon deposition during hydrogenation reactions. Thus, the mesoporous ZCL based catalyst described in this chapter helped in the methanation of CO_2 without carbon deposition and hence, it is proposed as a useful catalyst for methanation of CO_2 and is capable of showing enhanced stability even at low temperature.

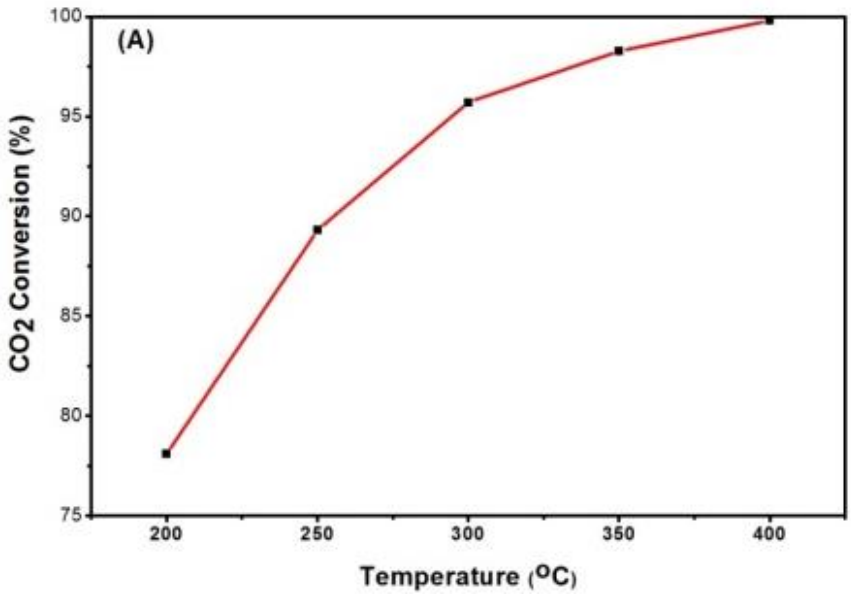

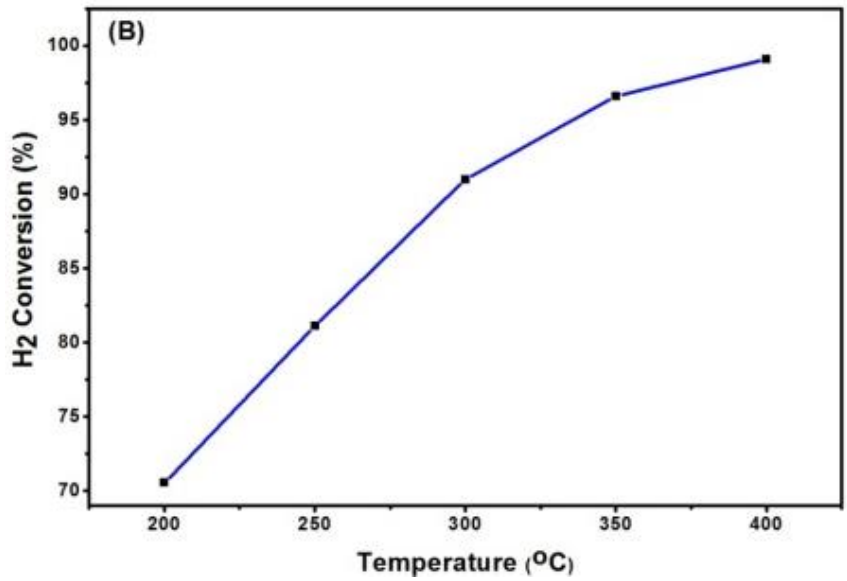

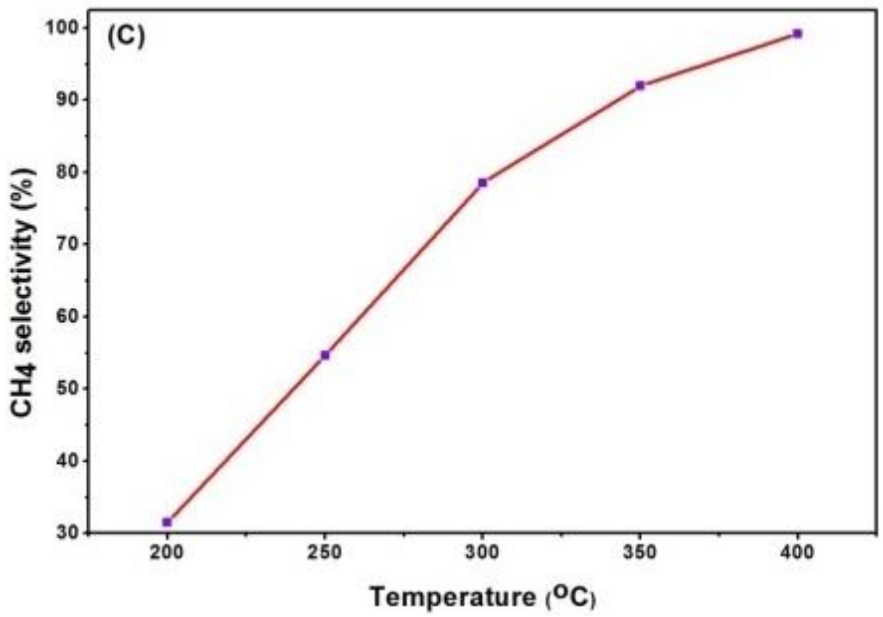

Fig. 6.10a: Catalytic activity of mesoporous ZCL (cm-ZCL-AcAc) showing (A) percentage conversion of CO_2 with temperature ; (B) percentage conversion of H_2 with temperature and (C) CH_4 selectivity with temperature.

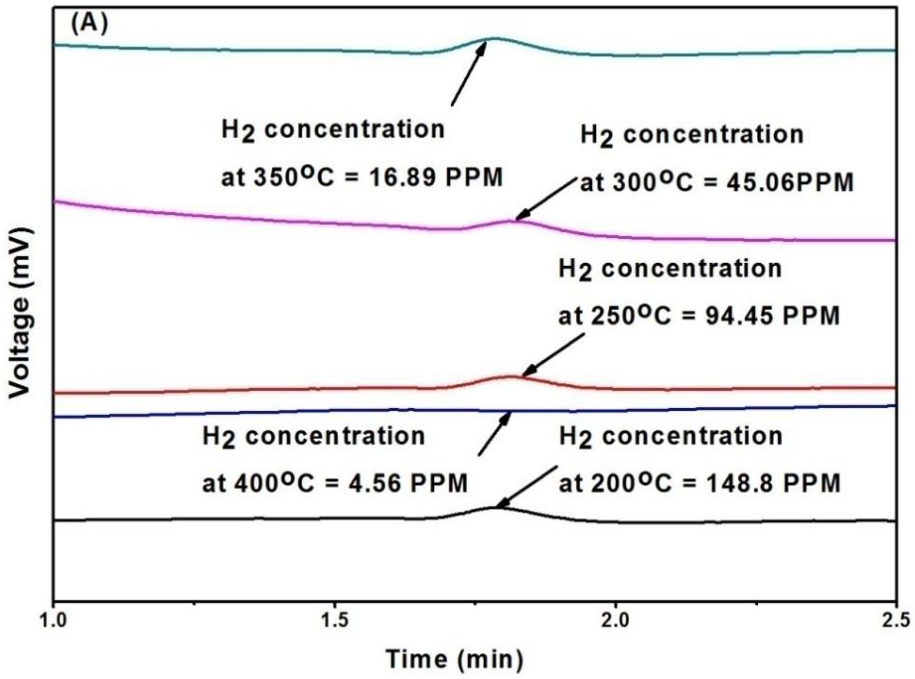

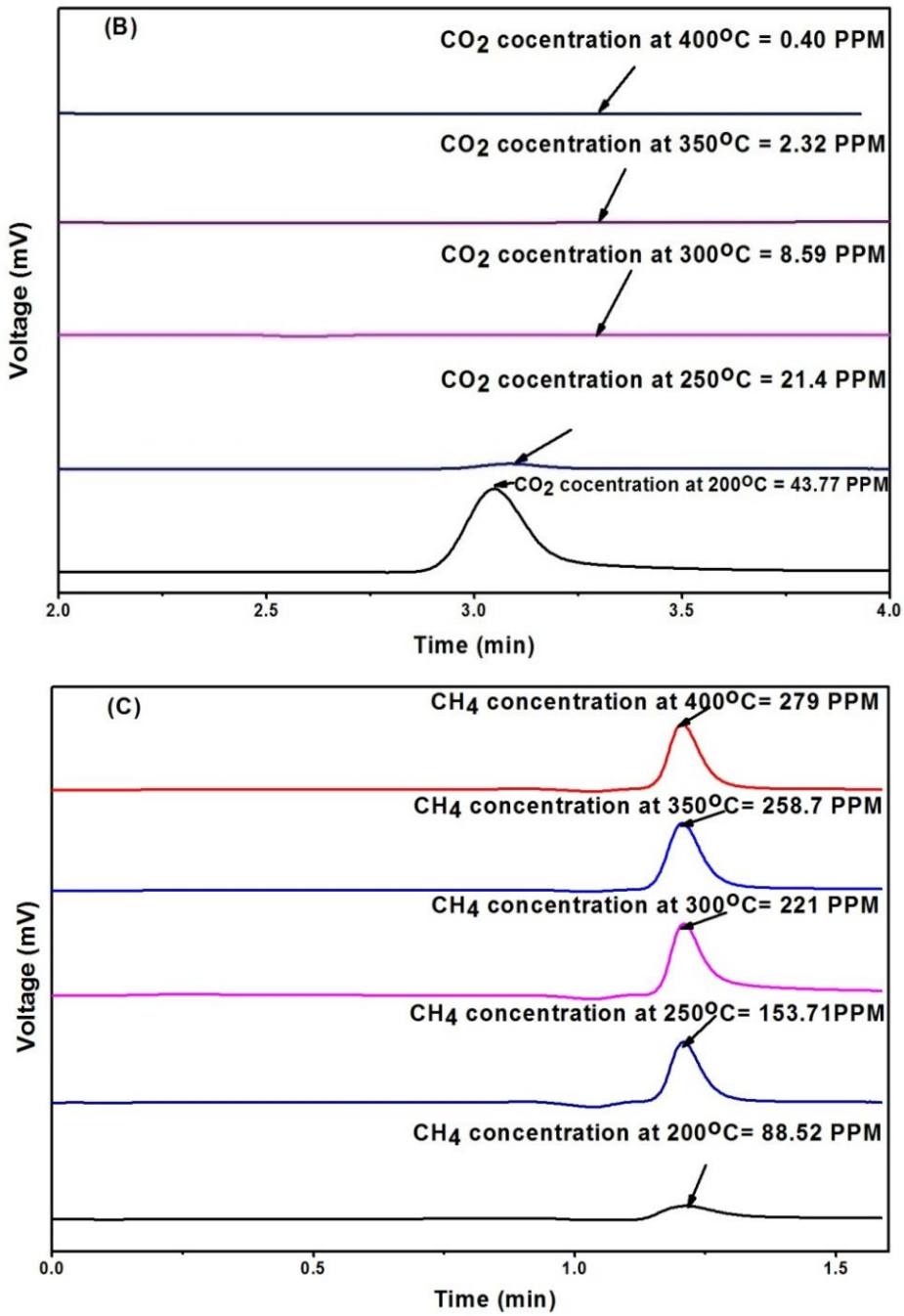

Fig. 6.10b: Gas Chromatograms for CO_2 hydrogenation reaction showing the concentration of H_2 (A), CO_2 (B) & CH_4(C) at temperatures ranging from 200-400 °C.

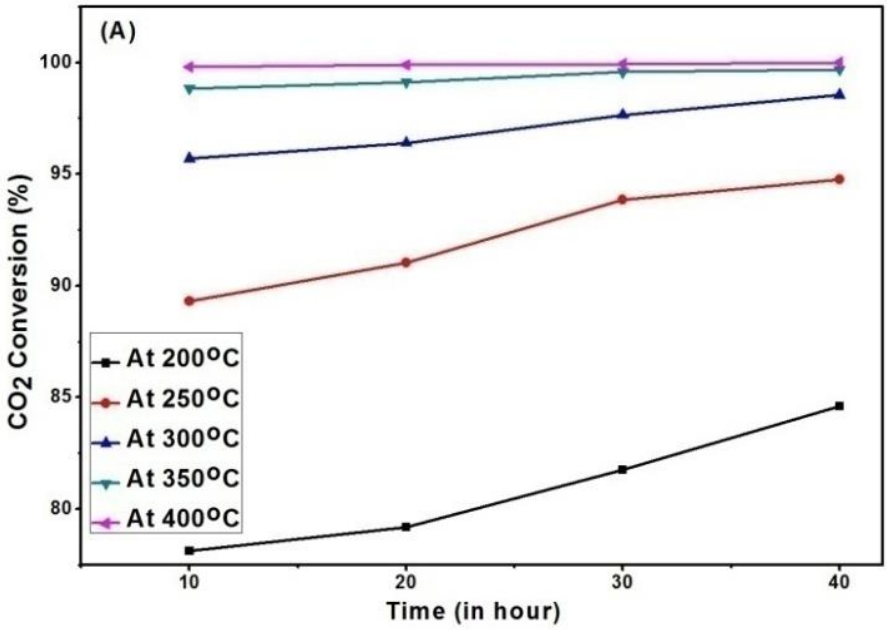
(A)
100
95
90
85
80
CO_2 Conversion (%)
At 200°C
At 250°C
At 300°C
At 350°C
At 400°C
10
20
30
40
Time (in hour)

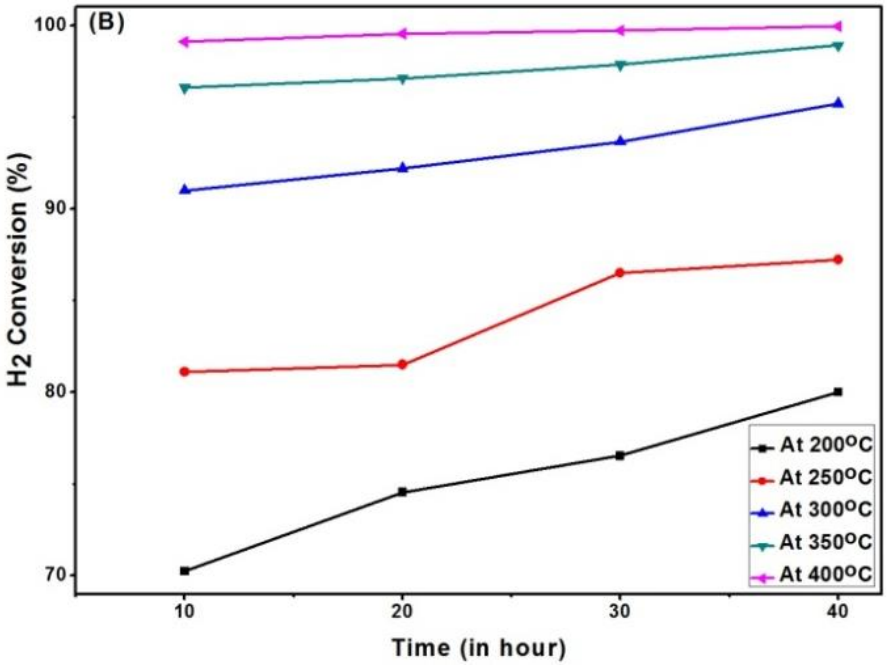
(B)
100
90
80
70
H_2 Conversion (%)
At 200°C
At 250°C
At 300°C
At 350°C
At 400°C
10
20
30
40
Time (in hour)

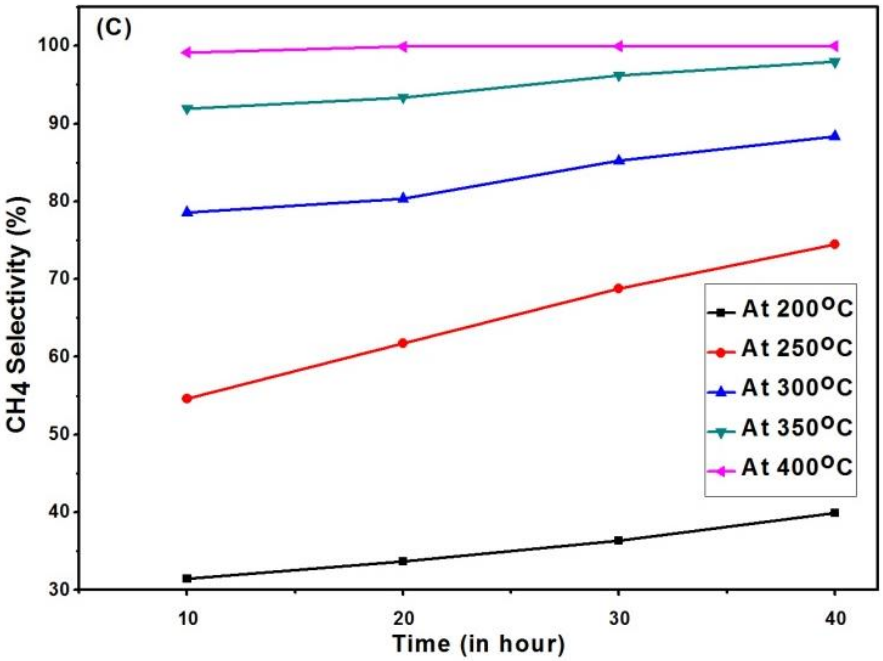

Fig. 6.11: Catalytic activity of mesoporous ZCL (cm-ZCL-AcAc): (A) percentage conversion of CO_2 with time; (B) percentage conversion of H_2 with time and (C) CH_4 selectivity with time.

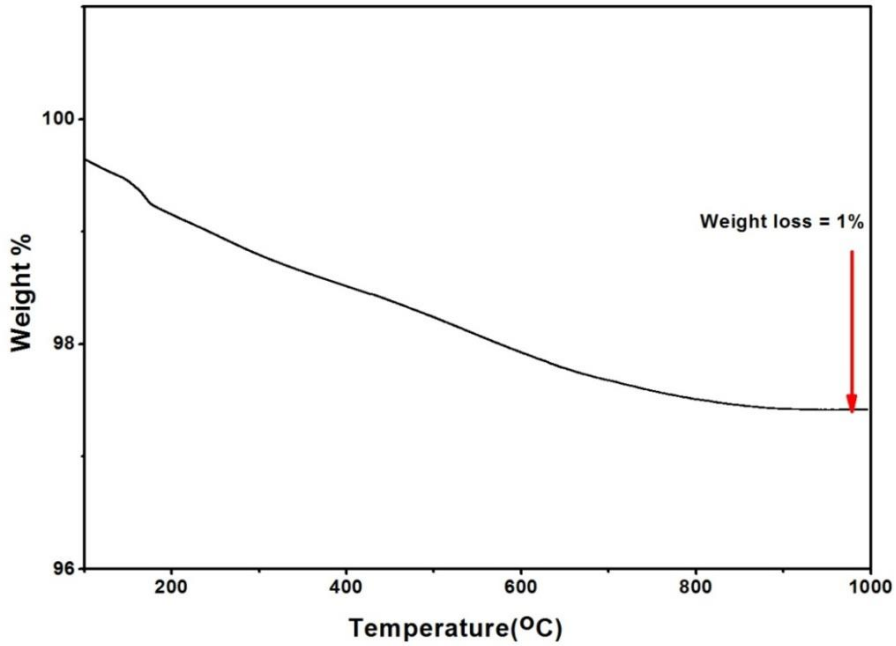

Fig. 6.12: TGA pattern of calcined mesoporous ZCL (cm-ZCL-AcAc) after 40 hour long term stability test.

Table 6.3: Catalytic percentage conversion of CO_2, H_2 and percentage yield of CH_4 in presence of mesoporous ZCL (cm-ZCL-AcAc)

Type of Active Catalyst	Flow Rate ($Ar:N_2+H_2:N_2+CO_2$ flow rate)	GHSV (Gas Hourly Space Velocity) in h^{-1}	Reactant Gas Concentration in ppm		Temperature (° C)	CO_2 % Conversion	H_2 % Conversion	% yield of CH_4
			H_2	CO_2				
Mesoporous Zn-Cr-LDH (cm-ZCL-AcAc)	150:100:50 ml/min	29,831	500	200	200	78.11	70.24	31.47
					250	89.31	81.11	54.64
					300	95.70	90.99	78.56
					350	98.84	96.6	91.96
					400	99.8	99.09	99.9

6.4. CONCLUSIONS:

High surface area mesoporous low Cr and Zn rich LDH was synthesized by the reaction of Zn-Cr-LDH and 2,4 pentanedione at 45 °C (**Table 6.1**). It was observed that Zn-Cr-LDH reacted with β-diketonate ligands through acid base reaction due to keto-enol tautomerism. Preferential etching out of metal ions leads to the formation of mesopores in the Zn-Cr LDH nano sheets. The electron withdrawing properties of any substituent groups present in the β-diketonate ligands profoundly affect their acid strength which in turn affects the preferential etching of the Cr^{3+} ion from the LDH structure. The calcined product of mesoporous Zn-Cr-LDH formed in the process showed good catalytic activity towards the methanation of CO_2 at temperature 200-400 °C. By drawing analogy with previous reported work the main active sites of this catalyst is expected to be the free Zn^{2+} ion formed from ZnO like structural units formed in the mesoporous ZCL after calcination. It formed CH_4 as the major product

with small amount of H_2O as by product without coke deposition as well as the formation of additional CO as intermediate. It showed 99.9 % CH_4 selectivity at temperature 400 ^oC. Although, many researchers reported the use of various mesoporous catalyst for the methanation reaction, the main advantage of our catalyst is that it act as an active catalyst at temperatures below 350 ^oC and showed a 40 hours long term stability at all the temperatures ranging from 200-400 ^oC. Thus, it has a prospect to replace all other catalyst which is used for the methanation of CO_2 especially at temperatures above 400 ^oC and those catalysts whose catalytic activity is suppressed due to coke deposition. Therefore, there is a scope to study this LDH activation process for future large-scale industrial level CO_2 hydrogenation reactions.

REFERENCES:

[1] W. Wang, S. Wang, X. Ma, J. Gong. *Chem. Soc. Rev.*, **2011**, *19*, 3703-3727.

[2] K. S. Rawat, A. Mahata, I. Choudhuri, B. Pathak. *J. Phys.Chem.C*, **2016**, *120*, 16478-16488; DOI:10.1021/acs.jpcc.6b05065.

[3] W. Wang, J. Gong. *Front. Chem. Sci. Eng.*, **2011**, *5*, 2-10; DOI:10.1007/s11705-010-0528-3.

[4] S. N. Riduan, Y.G. Zhang. *Dalton Trans.*, **2010**, *39*, 3347-3357.

[5] V. Deerattrakul, P. Dittanet, M. Sawangphruk, P. Kongkachuichay. *J. CO_2 Utiliz.*, **2016**, *16*, 104-113.

[6] M.D. Porosoff, B.Yan, J.G. Chen. *Energy Environ. Sci.*, **2016**, *9*, 62; DOI:10.1039/c5ee02657a.

[7] G.Centi, S. Perathoner. *Catal.Today*, **2009**, *148*, 191-205.

[8] R. Razzaq, C. Li, N. Amin, S. Zhang, K. Suzuki. *Energy & Fuels*, **2013**, *27*, 6955-6961; DOI: 10.1021/ef401049v.

[9] M.K. Gnanamani, G. Jacobs, H.H. Hamdeh, W. D.Shafer, F. Liu, S. D. Hopps,

G.A.Thomas,B.H.Davis.*ACSCatal.*, **2016**, *6*, 913-927; DOI:10.1021/acscatal.5b01346.

[10] H. Liu, Y. Lin, Z. Ma. *Chin. J. Catal.*, **2016**, *37*, 73-82.

[11] M.A.A. Aziz, A.A. Jalil, S. Triwahyono, R.R. Mukti, Y.H. Taufiq-Yap, M.R. Sazegar. *Appl. Catal.B: Environ.*, **2014**, *147*, 359-368.

[12] L. Xu, H. Song, L. Chou. *Appl.Catal.B: Environ.*, **2011**, *108-109*, 177-190.

[13] C.S. Budi, H.C. Wu, C.S. Chen, D. Saikia, H.M. Kao. *Chem. Sus. Chem.*, **2016**, *9*, 1-7; DOI: 10.1002/cssc.201600710.

[14] L.P. Teh, S. Triwahyono, A.A. Jalil, R.R. Mukti, M.A.A. Aziz, V. Shishido. *Chem. Eng. J.*, **2015**, *270*, 196-204.

[15] G. Zhou, T. Wu, H. Zhang, H. Xie, V. Feng. *Chem. Eng. Commun.*, **2014**, *201*, 233-240.

[16] L. Xu, J. Zhang, F. Wang, K. Yuan, L. Wang, K.Wu, G. Xu, W. Chen. *RSC Adv.*, **2015**, *5*, 48256.

[17] S. Abate, K. Barbera, E. Giglio, F. Deorsola, S. Bensaid, S. Perathoner, R. Pirone, G.Centi. *Ind. Eng. Chem. Res.*, **2016**, *55*, 8299-8308; DOI:10.1021/acs.iecr.6b01581.

[18] M. Gabrovska, R. E. Kardjieva, D. Crisan, P. Tzvetkov, M. Shopska, I. Shtereva. *Reac. Kinet. Mech. Cat.*, **2012**, *105*, 79-99; DOI:10.1007/s11144-011-0378-0.

[19] D. Wierzbicki, R. Debek, M. Motak, T. Grzybek, M. E. Galvez, P.D. Costa. *Catal. Commun*., **2016**, *83*, 5-8.

[20] G. Du, S. Lim, Y. Yang, C. Wang, L. Pfefferle, G. L. Haller. *J. Catal.*, **2007**, *249*, 370-379.

[21] Y. Yan, Y. Dai, H. He,Y. Yu, Y. Yang. *Appl.Catal. B: Environ.*, **2016**, *196*, 108-116.

[22] N. Linares, A.M. Silvestre-Albero, E. Serrano, J. Silvestre-Albero, J. Garcia-Martinez. *Chem. Soc. Rev.*, **2014**, *43*, 7681-7717.

[23] L. Xu, F. Wang, M. Chen, J. Zhang, K.Yuan, L.Wang, K.Wu, G. Xu, W. Chen. *RSC Adv.*, **2016**, *6*, 28489-28499.

[24] S. Nannan, X. Wen, F. Wang, W. Wei, Y. Sun. *Energy Environ. Sci.*, **2010**, *3*, 366-369.

[25] V. Rives. *Layered double hydroxides: present and future*, Nova Science Publishers, **2001**.

[26] X. Duan, D.G. Evans. *Layered double hydroxides*, Springer Verlag, **2006**.

[27] F. Cavani, F. Trifiro, A. Vaccari. *Catal.Today*, **1991**, *11*, 173-301.

[28] T. Hibino, W. Jones. *J. Mater. Chem.*, **2001**, *11*, 1321-1323.

[29] H. Dandl, G. Emig. *Appl.Catal. A*, **1998**, *168*, 261-268.

[30] S. Kannan, C.S. Swamy. *Appl. Catal. B: Environ.*, **1994**, *3*, 109-116.

[31] J.N. Armor, T.A. Braymer, T.S. Li, Y. Farris, F.P. Petrocelli, E.L. Weist, S. Kannan, C.S. Swamy. *Appl.Catal. B: Environ.*, **1996**, *7*, 397- 406.

[32] R. S. Drago, K. Jurczyk, N. Kob. *Appl.Catal. B: Environ.*, **1997**, *13*, 69-79.

[33] K. Karaskovaa, L. Obalovaa, K. Jiratova, F. Kovanda. *Chem. Eng. J.*, **2010**, *160*, 480-487.

[34] J.P. Ramirez, F. Kapteijn, J. A. Moulijn. *Catal. Lett.*, 1999, 60, 133-138.

[35] S. Kannan. *Catal. Surv. from Asia*, **2006**, *10*, 117-137; DOI:10.1007/s10563-006-9012.

[36] S. He, Z. An, M. Wei, D. G. Evans, X. Duan. *Chem. Commun.*, **2013**, *49*, 5912-5920.

[37] K. Galejova, L. Obalova, K. Jiratova, K. Pacultova, F. Kovanda. *Chem. Papers*, **2009**, *63*, 172-179; DOI:10.2478/s11696-008-0105-0.

[38] J. Feng, Y. He, Y. Liu, Y. Du, D. Li. *Chem. Soc. Rev.*,**2015**, *44*, 5291-5319; DOI:10.1039/C5CS00268K.

[39] D. Li, Y. Cai, Y. Ding, R. Li, M. Lu, L. Jiang. *Int. J. Hydrog. Energy,* **2015**, *40*, 10016-10025.

[40] F. A. Cotton, G. Wilkinson. *Adv. Inorganic Chem.* John Wiley and Sons: New York, (1st ed. **1962**, 6th ed. **1999**). ISBN 978-0-471-19957-1.

[41] R.C. Mehrotra, R. Bohra, D.P. Gaur. In Metal β-Diketonates and Allied Derivatives, Academic Press, London, **1978**, 382.

[42] I.K. Igumenov, A.E. Turgambaeva, V.V. Krisyuk, A.F. Bykov. J. Phys IV France, **1999**, *9*, 8-65.

[43] S. Kawaguchi. *Inorganic Chemistry Concepts: Variety in Coordination Modes of Ligands in Metal Complexes*, 11, Springer, Berlin, **1988**.

[44] L.G. Hubert-Pfalzgraf. *Appl.Organomet. Chem.*, **1992**, *6*, 627-643.

[45] B. M. Choudhary, L. K. Mannepalli, M.K. Chaudhari, S. K. Dehury, S. S. Dhar, U. Bora. *Process for the preparation of metal acetylacetonates*, US 7,282,573 B2, **2007**.

[46] Z. Lu, W. Zhu, X. Lei, G.R.Williams, D. O'Hare, Z. Chang, X. Sun, X. Duan. *Nanoscale*, **2012**, *4*, 3640-3643.

[47] A.V. Radha, P.V. Kamath. *Bull. Mater. Sci.*, **2004**, *27*, 355-360.

[48] G. Zhang, L. Ren, Z.Yan, L. Kang, Z. Lei, H. Xu, F. Shi, Z.H.Liu. *Chem. Commun.*, **2017**, *53*, 2950; DOI:10.1039/c6cc10250f.

[49] H.P. Boehm, J. Steinle, C. Vieweger. *Angew.Chem. Int. Ed.*, **1977**, *16*, 265-266.

[50] P. Bharali, R. Saikia, R. K. Boruah, R. L. Goswamee. *J. Thermal Anal. Calorim.*, **2004**, *78*, 831-838.

[51] V. Rives, M.A. Ulibarri. *Coord. Chem. Rev.*, **1999**, *181*, 61.

[52] J.W. Boclair, P.S. Braterman. *Chem. Mater.*, **1998**, *10*, 2050.

[53] V.R. Allman. *Chimia*, **1970**, *24*, 99-108.

[54] D.W. Bruce, D. O'Hare. Inorganic Materials,Wiley, Chichester, **1997**.

[55] H.F.W. Taylor. *Miner. Mag*., **1969**, *37*, 338-342.

[56] V. Rives, M.A. Ulibarri. *Coord. Chem. Rev*., **1999**, *181*, 61.

[57] J.W. Boclair, P.S. Braterman. *Chem. Mater*., **1998**, *10*, 2050.

[58] N. Guttmann, B. Muller. *J.Solid State Chem*., **1996**, *122*, 214.

[59] R. R. Delgado, M. A. Vidaurre, C.P. De Pauli, M.A. Ulibarri, M.J. Avena. *J. Colloid and Interface Sci.*, **2004**, *280*, 431-441.

[60] H. Roussel, V. Briois, E. Elkaim, A. de Roy, J. P. Besse. *J. Phys. Chem. B*, **2000**, *104*, 5915-5923.

[61] J.E. Huheey, E.A. Keiter, R.L. Keiter, O.K. Medhi. Inorganic Chemistry: *Principles of Structure and Reactivity, 4th Edition*, ISBN006042995X/9780060429959, **1993**.

[62] W.U. Malik, G.D. Tuli, G.D. Madan. Selected Topics In Inorganic Chemistry, First Edition, ISBN 81-219-0600-8, **1976**.

[63] J. Toullec. Keto-enol equilibrium constant. In The chemistry of enols, Z. Rappoport, Editor. **1990**, John Willey: Chichester, England, 323-398.

[64] E. Iglesias. *Cur. Org. Chem.*, **2004**, *8*, 1-24.

[65] P. Alcais, P. Brouillard. *Chem. Soc. Perk. T.*, **1976**, *2*, 257-258.

[66] P. Saikia, B.N'G. Allou, A.Borah, R.L. Goswamee. *Mater.Chem. Phys.*, **2017**, *186*, 52-60.

[67] H. Tajizadegan, A. Heidary, O.Torabi, M.H. Golabgir, A. Jamshidi. *Int. J. Appl. Ceram. Technol.*, **2016**, *13*, 289-294; DOI:10.1111/ijac.12440.

[68] D. Xue, D. Fan, W. Shen. *Nanoscale Res. Lett.*, **2013**, *8*, 46

[69] H.Ye, A.Tang, L. Huang, Y.Wang, C. Yang, Y. Hou, H. Peng, F. Zhang, F. Teng. *Langmuir*, **2013**, *29*, 8728-8735; DOI:10.1021/la401707u.

[70] E.Unveren, E. Kemnitz, S. Hutton, A. Lippitz, W. E. S. Unger. *Surf. Interface Anal.*, **2004**, *36*, 92-95.

[71] M. Richetta, L. Digiamberardino, A. Mattoccia, P. G. Medaglia, R. Montanari, R. Pizzoferrato, D. Scarpellini, A. Varone, S. Kaciulis, A. Mezzi, P. Soltania, A. Orsini. *Surf.Interface Anal.*, **2016**, *48*, 514-518.

[72] B. Fubini, E. Giamllo, F. Trifiro, A. Vaccari. *Therm. Acta*, **1988**, *133*, 155-161.

[73] L. Tan, G.Yang, G. Yoneyama, Y. Kou, Y. Tan, T. Vitidsant, N. Tsubaki. *Appl.Catal. A*, **2015**, *505*, 141-149.

[74] J. Su, J.S. Chen. *Microporous Mesoporous Mater.*, **2017**, *237*, 246-259.

[75] A. Galve, D. Sieffert, E.Vispe, C. Tellez, J.Coronas, C. Staudt. *J. Membrane Sci.*, **2011**, *370*, 131-140.

[77] J. Duan, M. Higuchi, R. Krishna, T. Kiyonaga, Y. Tsutsumi, Y. Sato, Y. Kubota, M. Takatae, S. Kitagawa. *Chem. Sci.*, **2014**, *5*, 660-666.

CHAPTER-VII

CONCLUSION
AND
FUTURE PROSPECTS

7. CONCLUSION AND FUTURE PROSPECTS:

During the course of this work different types of binary LDHs such as Ni-Al, Mg-Al, Ni-Cr, Mg-Cr, Zn-Al and ternary LDHs such as Ni-Mg-Al and Ni-Mg-Cr as well as their SiO_2 supported core shell type nanocomposites in the form of alcogel based dispersions were synthesized by non-aqueous soft chemical sol-gel method by starting with different metal acetylacetonates as precursors whose details are described in the **Chapter-III and IV**. This method of synthesis of LDH had the inherent advantages like the advantage of alcogel formation than hydrogel formation, where the former has the advantages of facile drying without stress induced cracks in thin films formed on solid substrates, free from carbonate introduction to the interlayers through dissolution of carbon dioxide in water medium, dispersible smaller size of LDH nanosheets. These were characterized in the dried powdered form by different techniques such as PXRD, TGA-DTG, FT-IR, zeta potential, particle size analysis, BET surface area and pore volume analysis, SEM, TEM and EDS analysis etc. Since, the knowledge of flow properties are essential for coating any gel by dip coating over solid preforms the nanocomposite alcogels were further characterized in the liquid form by Rheometric analysis to study their flow behaviour. These nanocomposite alcogels were then used as catalyst after calcination for two different environmental application viz. N_2O direct decomposition and catalytic partial oxidation of CH_4 by N_2O and Oxygen. To obtain the information on role played by specific metal centers on these reactions the catalyst obtained after calcination were also further characterized by H_2-TPR and XPS analysis.

It was observed that sol-gel method by using metal acetylacetonate as precursors gave LDHs with finer particles. In case of Ni-Al, Mg-Al, Ni-Cr, Mg-Cr and Zn-Al combinations and as synthesized by sol-gel method XRD analysis showed the presence

of LDH phases. TGA analysis also showed the three step thermal degradation for these LDHs. The thermal degradation kinetic of Ni-Al-LDH was studied by Flynn-Wall-Ozawa (FWO), Friedman, Coats-Redfern, Phadnis-Deshpande methods. The kinetic parameters such as activation energy (E_a), reaction order (n), pre-exponential factor (A) were calculated by using these methods. The kinetic parameters for the degradation of sol-gel derived Ni-Al-LDH were investigated by different methods viz. FWO, Friedman, Coats-Redfern and Phadnis-Deshpande methods. The results showed that the activation energies obtained by FWO and Friedman method for the second degradation were 68.06 kJ/mol and 68.43 kJ/mol respectively with pre-exponential factor (*A*) and reaction order (*n*) of 1.43×10^2 s^{-1} and 3.8 respectively; for the third step degradation the activation energies were 91.28 kJ/mol and 73.04 kJ/mol with pre-exponential factor (*A*) and reaction order (*n*) of 1.82×10^2 s^{-1} and 2.2 respectively. Again, the second step and third step degradation obeyed A_3 type Avrami-Erofeev equation and D_4 type three dimensional diffusion mechanisms with Ginstling-Brounsthein equation and are in better agreement with FWO and Friedman method. These calculated parameters would help in future in understanding of mechanism of thermal degradation of LDH in general and sol-gel derived LDH in particular as described in the **Results and Discussion Section of Chapter-III-PART-A**.

On the other hand, silica supported LDH nanocomposite alcogels were synthesized by 'soft chemical' non-aqueous sol-gel route using a mixture of metal acetylacetonate and Tetraethylorthosilicate (TEOS) precursors. The synthesis was designed on the basis of differences of rate of hydrolysis and metal acetylacetonates. Faster hydrolysis of the alkoxide than the metal acetylacetonates precursors gives an inner SiO_2 core around which crystalline LDH sheets are dispersed to give one gel network in an organic medium. The LDH-SiO_2 gels were highly stable dispersions where LDH

particles, which are otherwise non-dispersible due to bigger crystalline sizes irrespective of whether synthesised in aqueous medium or in non-aqueous medium, were uniformly distributed in the gel. They formed a Bingham type fluid and in the Linear Viscoelastic region they have G' bigger than G" indicating more gel like behaviour (**Results and Discussion Section of Chapter-III-PART-B**).With the increase of SiO_2 to LDH ratios their other properties such as surface area and zeta-potential also increased indicating their good prospects as catalysts for suitable reactions. The-SiO_2 gels were coated over solid preforms by dip coating technique. The coats when dried and calcined formed good thin films of mixed metal oxides. The calcined products showed the presence of NiO, $NiAl_2O_4$, MgO and $MgCrO_4$ type phases. These thin films of mixed metal nano oxides over honeycomb as well as in the powder formed were then used as environmental catalyst for direct decomposition of N_2O and Catalytic Partial Oxidation (CPO) of CH_4 in presence of N_2O and Oxygen. It was observed that all these catalysts showed better catalytic activity towards N_2O decomposition as well as CPO of CH_4. Both Ni-Al-LDH and Mg-Al-LDH showed about 99.5 % and 97 % N_2O conversion to N_2 and O_2. On the other hand, both Ni-Cr and Mg-Cr-LDHs showed better catalytic activity towards CPO of CH_4 to syn gas (H_2/CO) production as described in the **Results and Discussion Section 3.B.3.2** and **3.B.3.3 of Chapter-III-PART-B**. The standard catalytic oxidation and catalytic partial oxidation in presence of N_2O carried out by calcined SiO_2@Ni-Cr-LDHs coated over honey comb monoliths showed different selectivities towards H_2 and CO. For these catalysts the selectivity towards H_2 and CO did not exceed 90 % and 86 % in the standard catalytic partial oxidation of CH_4. On the other hand, the selectivity towards H_2 and CO increased in presence of N_2O. In case of standard oxidation reaction the molecular oxygen adsorbed on the catalyst surface formed O^- or O_2^- electrophilic

species which leads to the total oxidation of methane whereas N_2O decomposed to N_2 and oxygen electrophilic species in presence of all these catalysts. The oxygen electrophilic species was less reactive and and promoted the partial oxidation reaction. In addition to this, Ni^{2+} of NiO active species was further oxidized to Ni^{3+} in presence of O_2 which promoted the total oxidation reaction. Thus, it was observed that N_2O act as promoter for CPO reaction. Similarly, at high concentration about 500 ppm (11.36 mmol) of N_2O the re-oxidation of the Ni-catalysts lead to decrease of the selectivity towards H_2 and CO and which also favoured total oxidation of methane and formed CO_2. It was further observed from the catalytic reaction that with the increase of SiO_2 to LDH ratios their selectivity also increased due to the increase of the active sites with Ni dispersion as well as no coke deposition on the catalysts. CNC -31 showed about 99.9 % selectivity towards H_2 and CO. From these results it can be concluded that, mixed-metal nano-oxides obtained after the calcination of LDH coated over honey comb monolithic substrate act as an effective catalysts for the syn-gas (H_2/CO) production. In presence of SiO_2, LDH form hybrid nano alcogels which helps to form a crack free catalytic membrane as well as also increases the selectivity towards H_2 and CO by increasing the surface area. In addition to this the honey comb monoliths provide large external surface, uniform gas flow, low radial heat transfer, high geometric surface area which further increases the catalytic activity of the catalysts. The main advantage of our catalyst is that it works effectively at low temperature for the synthesis gas (H_2/CO) production without deposition of coke which is the severe problem of other reported catalysts. Therefore, such a catalytic device obtained by coating of SiO_2@Ni-Cr-LDH nanocomposite alcogels can be effectively used for the large scale industrial level synthesis gas (H_2/CO) production. Similarly, calcined SiO_2@Mg-Cr-LDH with SiO_2 to LDH ratio 3:1 showed better catalytic activity

towards syn gas (H_2/CO) production about 97.2 % H_2 and 96 % CO yield. It showed about 100 % N_2O and 97.8 % CH_4 conversion (**Section 3.10.2.9.3.**).

On the other hand, in case of synthesis of Zn-Al-LDH by sol-gel method using metal acetylacetonates there was observed a drastic effect of base and temperature (**Section 3.C.2** of **Chapter-III-PART-C**). It is observed that by starting from metal acetylacetonates for the synthesis of Zn-Al-LDH the hydrolysis of $Zn(acac)_2$ is possible in presence of strong bases such as Piperidine and NaOH only. The XRD patterns of Zn-Al-LDH phases further showed that not only the strong bases the reaction can be performed only at 0 ^oC. It is not possible to carry out the reaction at high temperature because at high temperature it leads to the formation of ZnO (Zincite-a Wurtzite type structure). Zn-Al-LDH synthesized in presence of Piperidine at 0 ^oC in organic solvent after calcination at 800 ^oC gave $ZnAl_2O_4$ spinel which can be used as catalyst in many prospective applications.

As described in the **Chapter-IV** of **Section 4.3.1.** XRD analysis also showed the presence of LDHs phases with *hkl* reflection of (003), (006), (009) and (012) with corresponding gradual decrease of intensity in case of Ni-Mg-Al and Ni-Mg-Cr-LDHs as well as their SiO_2 supported products. TGA patterns of Ni-Mg-Al and Ni-Mg-Cr showed the three step thermal degradation as binary LDHs. The presence of Ni, Mg, Cr and Al in these LDHs was further confirmed from EDS analysis. SEM patterns showed the presence of larger platelet of ternary LDHs. Ternary LDHs also formed stable dispersion in presence of SiO_2 as they showed better zeta potential values at different pH. It was observed that mixed-metal oxide obtained from these LDHs possessed highest surface area values. XRD analysis showed the presence of NiO-MgO periclase type solid solution in these catalysts. The presence of SiO_2 further increased the Ni dispersion which helped in the reduction of Ni^{2+} of NiO-MgO

periclase to Ni^0 as observed from H_2-TPR analysis and act as active species for Catalytic partial oxidation (CPO) of CH_4 in presence of N_2O. SiO_2@ Ni-Mg-Al (1:1) showed better catalytic activity towards CPO of CH_4 between the temperatures of 200-500 ^oC. It showed about 99.99 % CH_4 conversion as well as about 99.99 % H_2 yield and 99.8 % CO yield.

As described in the **Chapter-V** mixed metal acetylacetonate of Cu(II)/Cr(III) was synthesized by the reaction of Cu-Cr-LDH and β-diketonate ligand such as acetylacetone through acid-base neutralization reaction. The parent LDH was first synthesized by oxide hydrolysis method. The Cu(II)/Cr(III)AcAc composite crystals obtained was then characterized by PXRD, FT-IR, TGA-DTG, Mass spectrometry, Atomic Absorption analysis (AAS), SEM, TEM and EDS analysis, Single crystal analysis etc. These composite crystals were then used as a single source precursor for the thin film formation by Metal Organic Chemical Vapour Deposition (MOCVD) technique. This thin film was then further characterized by XRD, SEM and EDS, AFM analysis and used as a catalyst for N_2O decomposition. LDH and acac reacts with each other by an acid base reaction due to keto-enol tautomerism of acac. There is a differential reactivity of acac and different metal ions that form the LDH. The synthesis of mixed Cu(II)/Cr(III)AcAc by acid-base neutralization reaction between Cu-Cr LDH and acac at room temperature was found to be a most effective method. It was easy to carry out also and gave high yield product as well as short reaction time. From XRD analysis, the product of the CCL and AcAc showed the presence of both $Cu(acac)_2$ and $Cr(acac)_3$. After repeated recrystallization both of these acacs were not separated. Although, due to the stable +3 oxidation state of Cr with an octahedral molecular cofiguration, $Cr(acac)_3$ could not enter into the single crystal structure basically formed by square planar configuration of $Cu(acac)_2$ to form a $Cu/Cr(acac)_2$

mixed metal complex but they formed a composite crystal with $Cr(acac)_3$ making a coat over the surface of $Cu(acac)_2$ core. Due to the formation of eutectic mixture the melting point of CCAA lay in between $Cu(acac)_2$ and $Cr(acac)_3$ and lead to the shifting of DTG peak to the sublimation temperature lower than $Cu(acac)_2$ and $Cr(acac)_3$. The TGA results showed that CCAA undergo single step weight loss (about 95 %) in a temperature of 266 ^oC without leaving much residue due to which it could be used as precursor for thin film formation by MOCVD over solid substrates at low temperature. It was also observed that CCAA deposited as thin film of $CuCr_2O_4$ which decomposed N_2O to N_2 and O_2 as described in the **Section 5.3.1.1.11** of **Chapter-V**. In future it can be used a catalyst for further application related to environment.

Mesoporous Zn-Cr-LDH was synthesized by the reaction of Zn-Cr-LDH with the β-diketonate ligand such as acetylacetone through acid base neutralization reaction. The effect of strength of β-diketonate ligand during the synthesis was also studied by using different types of β-diketonate ligands such as Acetylacetone (2,4 pentanedione), 1,1,1-Trifluoro-2,4-pentanedione, Benzoylacetone as described in the **Chapter-VI**. The parent LDH was first synthesized by oxide hydrolysis method. The products obtained were then characterized by PXRD, TGA-DTG, FT-IR, BET surface area and pore volume analysis, XPS, SEM, TEM and EDS analysis. The mesoporous Zn-Cr-LDH was then used as a catalyst for CO_2 hydrogenation reaction. Before the catalytic reaction the mesoporous Zn-Cr-LDH was calcined and further characterized by H_2-TPR analysis. High surface area mesoporous low Cr and Zn rich LDH was synthesized by the reaction of Zn-Cr-LDH and 2,4 pentanedione at 45 ^oC. It was observed that Zn-Cr-LDH reacts with β-diketonate ligands through acid base reaction due to keto-enol tautomerism. Preferential etching out of metal ions leads to the formation of mesopores in the Zn-Cr LDH nano sheets. The electron withdrawing properties of any

substituent groups present in the β-diketonate ligands profoundly affect their acid strength which in turn affects the preferential etching of the Cr^{3+} ion from the LDH structure. The calcined product of mesoporous Zn-Cr-LDH formed in the process showed good catalytic activity towards the methanation of CO_2 at temperature 200-400 ^oC. By drawing analogy with previous reported work the main active sites of this catalyst is expected to be the free Zn^{2+} ion formed from ZnO like structural units formed in the mesoporous ZCL after calcination. It formed CH_4 as the major product with small amount of H_2O as by product without coke deposition as well as the formation of additional CO as intermediate. It showed 99.9 % CH_4 selectivity at temperature 400 ^oC. Although, many researchers reported the use of various mesoporous catalyst for the methanation reaction, the main advantage of our catalyst is that it acts as an active catalyst at temperatures below 350 ^oC and showed a 40 hours long term stability at all the temperatures ranging from 200-400 ^oC as described in the **Section 6.3.1.8** of **Chapter-VI**. Thus, it has a prospect to replace many other catalysts which is used for the methanation of CO_2 especially at temperatures above 400 ^oC and those catalysts whose catalytic activity is suppressed due to coke deposition. Therefore, there is a scope to study this LDH activation process for future large-scale industrial level CO_2 hydrogenation reactions.

Thus, it can be understood from various descriptions given above, in future the different works carried out in this thesis have the potential to become source of directional light for development of novel multifunctional inorganic catalytic membrane reactors, a device which can function both as a catalyst and membrane barrier for catalytic conversion of toxic gaseous emissions especially those obtained during hydrocarbon based fuel oxidation into benign gases at very low temperature specifically by using different above explained low cost non-noble metal based

supported mixed metal nano-oxides obtained from nano sheets of Layered Double Hydroxides.

The works related to eutectic Cu(II)/Cr(III)AcAc composite crystals can be expected to the use as a single source precursor for the formation of nanooxide thin film by MOCVD technique at low temperature and provide further future insight to use as a catalyst for the control of emission of other green house gases.

The works related to mesoporous LDH obtained by etching out of one of the metal ion can also be expected for the use as a catalyst in CPO of CH_4 and N_2O decomposition to useful chemicals in future which are emitted from combustion of hydrocarbons as well as from Municipal solid waste (MSW) dump sites which is the major problem of environmental pollution now-a-days.

Finally the work and the results of the present work can be highlighted in the following sentences-

1. Metal acetylacetonates can be used for non-aqueous sol-gel hydrolysis of LDH nano-sheets.
2. Some of the metal acetylacetonates e.g. $Zn(acac)_2$ undergoes hydrolysis only in low temperature and in presence of strong bases like Piperidine and NaOH to obtain LDH.
3. Differential rate of hydrolysis of metal acetylacetonates and TEOS can be used to design synthesis of silica-LDH core shell based alcogels.
4. Above alcogels can be used to fabricate nano material based catalytic devices for fabrication of coated honeycomb monolithic reactors for control of toxic and environmental harmful gases like N_2O, CO, CH_4 and CO_2.
5. However, the reaction of Cu-Cr LDH with acetylacetones forms some well grown eutectic mixed-metal acetylacetonate crystals suitable for MOCVD over

solid substrates.

6. These mixed metal acetylacetonate crystals deposites as mixed-metal oxide thin film of $CuCr_2O_4$ over honeycomb monolithic support and shows better catalytic activity towards decomposition of toxic gas N_2O to N_2 and O_2.
7. Excess acetylacetonate in presence of Zn-Cr type LDH forms some holey nano-sheets having high mesoporosity by etching out of Cr^{3+} ion.
8. This mesoporous Zn-Cr-LDH shows better catalytic activity towards CO_2 hydrogenation reaction without deposition of coke.

Appendix-I

List of Publications and Seminars/Conferences attended

LIST OF PUBLISHED AND COMMUNICATED PAPERS/PATENTS

1.“Iso-conversional kinetics study on thermal degradation of Ni-Al layered double hydroxide synthesized by ‘soft chemical’ sol-gel method’’ by **Pinky Saikia**, N’Guadi Blaise Allou, Angana Borah, R.L.Goswamee. ***Materials Chemistry and Physics***, 186 (2017) 52-60. (**IF=2.21**)

2.“Synthesis of nanohybrid alcogels of SiO_2 and Ni-Cr/Mg-Cr-LDH:study of their rheological and dipcoating properties” by **Pinky Saikia**, Arvind Gautam, R.L. Goswamee. ***RSC Advances***, 6 (2016) 112092-112102. (**IF=2.936**)

3. “Hybrid Nanocomposites of Layered Double Hydroxides: An Update on their Biological Applications and Future Prospects”, N’guadi Blaise Allou, **Pinky Saikia**, Angana Borah and Rajib Lochan Goswamee. ***Colloid and Polymer Science***, 295 (2017) 725-747. (**IF=1.723**)

4. “Synthesis of high surface area mesoporous hydroxidic nanosheet through preferential etching out of Cr^{3+} by β-diketonate ligands from Zn-Cr LDH structure and their use as catalyst for CO_2 hydrogenation” by **Pinky Saikia**, Jitu Saikia, Susmita Sarmah, N’Guadi Blaise Allou, R.L. Goswamee. ***Journal of CO_2 Utiliation***, 21 (2017) 40-51. (**IF=5.503**)

5. “Synthesis of Polyacrylamide/Layered Double Hydroxides Hybrid Composite Gel via *in situ* Polymerization and Study of its Rheological and Thermal Behavior”, N’guadi Blaise Allou, **Pinky Saikia**, Edja Florentin Assanvo and Rajib Lochan Goswamee. ***Polymer Composite***, DOI: 10.1002/pc.24524. (**IF=1.943**)

6. “Synthesis of Cu-Cr diketo, sublimable, eutectic composite complex, rod crystals from LDH as suitable MOCVD precursor of $CuCr_2O_4$ catalysts upon ceramic preforms for N_2O decomposition” by **Pinky Saikia**, S. Vasudevan, Rupam J. Sarma, Rajib

Lochan Goswamee. ***Materials Today Chemistry***, 7(2018) 40-52. (**IF=Pending**)

7. "The effect of strength of bases and temperature on the synthesis of Zn-Al LDH by non-aqueous 'soft chemical' sol-gel method and formation of high surface area mesoporous $ZnAl_2O_4$ spinel" by **Pinky Saikia**, Rajib Lochan Goswamee. ***Chemistry Select***, 3 (2018)7619-7626. (**IF=1.505**)

8."Catalytic Conversion of CH_4 to *Syn-Gas* (H_2/CO) by N_2O promotion over Ceramic Honeycomb Channels Coated with SiO_2@Ni-Cr-LDH Nanohybrid Alcogels"by **Pinky Saikia**, Champa Gogoi, Paran Jyoti Kalita, Rajib Lochan Goswamee (**Under revision**).

9. "Catalytic partial oxidation of CH_4 to *syn gas* (H_2/CO) in presence of N_2O over periclase type Ni(Mg,Al)O@SiO_2 catalyst obtained by non aqueous route" by **Pinky Saikia** and Rajib Lochan Goswamee. ***Catalysis Communication***, 119 (2019) 1-5. (**IF=3.463**)

10. "Harmful weed to prospective adsorbent: low-temperature–carbonized Ipomoea carnea stem carbon coated with aluminum oxyhydroxide nanoparticles for defluoridation'' by Jitu Saikia, Susmita Sarmah, **Pinky Saikia**, Rajib Lochan Goswamee. **Environmental Science and Pollution Research,** 2018. DOI: 10.1007/ s11356-018-3572-z. (**IF=2.8**)

11. "Adsorptive removal of fluoride upon alumina activated potter's clay and its sludge management'' by Susmita Sarmah, Jitu Saikia, **Pinky Saikia**, Champa Gogoi and Rajib Lochan Goswamee (**Under revision**).

12. One Patent is filed on "A method for the preparation of Silica@Mg-Al LDH core shell derived mixed metal oxide nano-sheet based composite catalyst for decomposition of N_2O in synthetic automobile exhaust condition" by **Pinky Saikia**, Angana Borah, N'Guadi Blaise Allou, Rajib Lochan Goswamee. File no. **201611022222** (**Indian Patent**).

Book Chapters

1. **"Synthesis and Application of Hydrotalcite based 2D mixed-oxide nanosheets for CO_2 hydrogenation"** by **Pinky Saikia** and Rajib Lochan Goswamee in "Research Trends in Natural Resource (Volume-01). AkiNik Publications New Delhi,Printing Press License No.: F.1 (A-4) press 2016.

2. **"Recent advances in the synthesis and application of transition metal Hydrotalcite based catalysts for the conversion of two high GWP gases N_2O and CH_4"** by **Pinky Saikia** and Rajib Lochan Goswamee in Air Pollution and Control

CH_4" by **Pinky Saikia** and Rajib Lochan Goswamee in Air Pollution and Control Technologies (Volume-01). ENVBOOKS series (**Under Review**).

LIST OF PRESENTED PAPERS

1. **Oral poster presentation** on "Studies on Thermal Decomposition of Some Common Transition Metal Acetylacetonates" by **Pinky Saikia** and R.L.Goswamee on "8 th Mid-Year CRSI National Symposium in Chemistry" from 10-12th July, 2014 on CSIR-NEIST, Jorhat, Assam.

2. **Oral poster presentation** on "INTERACTION OF METAL-β-DIKETONATES WITH LAYERED DOUBLE HYDROXIDES" by **Pinky Saikia** and R.L.Goswamee in Material Research Society of India (MRSI-2016) symposium on "Advanced Materials for Sustainable Applications''and 27th Annual General Meeting from 18-21 February, 2016 on CSIR-NEIST, Jorhat, Assam.

3. **Oral presentation** on "Synthesis of high surface area mesoporous Zn-Cr-LDH nano-sheet by preferential etching out of Cr^{3+} ions in presence of β-diketonate ligands" by **Pinky Saikia** and R.L.Goswamee in the 4th international conference ICAMMP-IV in IIT-Kharagpur, 2016.

4. **Oral poster presentation** on "Catalytic partial oxidation of CH_4 by N_2O to synthesis gas (H_2/CO) in presence of SiO_2/Ni-Cr-LDH nanohybrids as catalyst" by **Pinky Saikia** and Rajib Lochan Goswamee in a national seminar on "Recent developments in synthesis and catalysis sponsored by UGC from 10-11th march in Chemistry Department, Dibrugarh University.

5. **Oral presentation** on "Synthesis of sublimable Cu-Cr diketo complex eutectic composite rod crystals from LDH as suitable MOCVD precursor of $CuCr_2O_4$ catalysts upon ceramic preforms for N_2O decomposition" by **Pinky Saikia** and Rajib Lochan Goswamee in national seminar "Recent Trends in Environment Responsive Chemical Processes (**RTERCP-2017)**" on held in 22nd & 23rd September' 2017 in D.R. College, Golaghat.

6. **Oral poster presentation** on "Synthesis of sublimable diketo eutectic composite crystals from mixed-metal hydroxides as precursor for MOCVD upon ceramic preforms" by **Pinky Saikia** and Rajib Lochan Goswamee in Material Research Society of India (MRSI) 2018 North East Chapter conference on "The Frontiers on Chemical Biology" held on 26-28th June 2018 in CSIR-NEIST, Jorhat, Assam.

7. Oral presentation on "Catalytic partial oxidation of CH_4 to *syn gas* (H_2/CO) in presence of N_2O over periclase type SiO_2@Ni(Mg,Al)O catalyst synthesised by non aqueous route" by **Pinky Saikia** and Rajib Lochan Goswamee in National Seminar on Chemistry in Interdisciplinary Research (NSCIR-2018) held on 9-10th November 2018 in Department of Chemistry, Nagaland University.

Appendix-II

REPRINT OF PUBLISHED PAPERS